



***AN EMPIRICAL FEASIBILITY ASSESSMENT FOR INCREMENTAL  
SHEET FORMING***

by

***Muftooh Ur Rehman Siddiqi***

A thesis presented in fulfillment of the requirements for the degree of

**Doctorate in Engineering (EngD)**

Advanced Forming Research Center  
Department of Design, Manufacture & Engineering Management  
University of Strathclyde  
Glasgow, Scotland, UK

### **Declaration of Author's Rights**

“The copyright of this thesis belongs to the author under the terms of the United Kingdom Copyright Acts as qualified by the University of Strathclyde Regulation 3.51. Due acknowledgement must always be made of the use of any material contained in, or derived from, this dissertation. Any correspondence concerning this service should be sent to mechovator@gmail.com.”

## ***Dedication***

*This thesis is dedicated to my parents Mr. and Mrs. Mujeeb Ur Rehman Siddiqi. Without whom none of this was possible.*

## **Acknowledgement**

First and foremost, I would like to thank God Almighty for giving me the strength, knowledge, ability and opportunity to undertake this research study and to persevere and complete it satisfactorily. Without his blessings, this achievement would not have been possible.

I will like to thank Prof. Jonathan Corney and Dr. Giribaskar Sivaswamy for their supervision and guidance throughout the work. Author would also like to thank Dr. Amir Siddiq, Dr. Rahul and Dr. Dorothy for their help and efforts.

I would like to acknowledge the support from the Department of Design, Manufacture and Engineering Management.

I would like to express the deepest gratitude for my friends and family specially Engr. Shahana Mujeeb Siddiqi, Engr. Fatima tu Zuhra Siddiqi, Hina Mujeeb Siddiqi and Dina Mujeeb Siddiqi for their encouragement and support.

I would not be who I am today without you all.

## **A**bstract

Many sheet forming processes such as hammering and spinning, have been used in the manufacturing industry for decades and consequently have strengths and weakness that are well known. In contrast, Incremental Sheet Forming (ISF) is an emerging type of forming process whose capabilities are not yet fully understood. So while it is clear that ISF processes have several advantages, such as low cost and good surface finish. It has proved difficult to define the limits of the process in terms of macro-parameters such as deformation and sheet thickness. So whereas the capabilities of many sheet metal manufacturing processes are effectively characterized by forming limit curves this has not been possible with ISF. In other words, there is a lack of methodologies for assessing the feasibility of using ISF for particular components.

This thesis investigates several aspects of the ISF process and develops a quantitative methodology that allows a first approximation of the feasibility of component manufacturing using the ISF process in terms of deflection and thickness reduction. It was found that thickness reduction can be accurately modeled in terms of analytical model developed for sheet metal forming.

The predictions of the method are assessed and found to give a good correspondence with measured data for the range of wall angles, materials and geometries assessed.

The parameters of the proposed methodology have been determined by experimental studies of commercially pure Titanium Grade 4 (CpTi), Aluminium alloys (AA1050-H-14, AA2024-O and AA7075-O) and Stainless Steel (SS304-L) to understand the process of incremental sheet forming and its impact on the final properties of the sheet metal. The proposed method called “ISF-FCheck” uses two charts to quantify maximum strain in relation to the depth and thickness reduction. Discussion of these results has also supported the development of a more detailed understanding of the interaction of the process parameters and lead to a new theoretical and graphical representation of the ISF process.

# Contents

<b>1. Introduction</b>	<b>2</b>
<b>1.1 Process overview</b>	<b>2</b>
<b>1.2 Applications and advantages</b>	<b>4</b>
<b>1.3 Component properties</b>	<b>6</b>
<b>1.4 Research gap</b>	<b>8</b>
1.4.1 Towards a design check method for ISF	11
1.4.2 Proposed model	14
<b>1.5 Aim</b>	<b>16</b>
<b>1.6 Objectives</b>	<b>16</b>
<b>1.7 Overview</b>	<b>19</b>
<b>1.8 Summary</b>	<b>22</b>
<b>2. Literature review</b>	<b>24</b>
<b>2.1 Evolution of ISF process</b>	<b>24</b>
<b>2.2 Sheet Metal forming processes</b>	<b>25</b>
2.2.1 Hammering	25
2.2.2 Spinning	26
2.2.3 Stamping	27
<b>2.3 Incremental sheet forming</b>	<b>27</b>
2.3.1 General ISF	27
2.3.2 Applications and geometries	28
<b>2.4 Researched Geometries</b>	<b>31</b>
<b>2.5 Forming Equipment Design</b>	<b>32</b>
2.5.1 Purpose built ISF machines	33
2.5.2 Adapting CNC milling machines for ISF	33
2.5.3 Robotic ISF systems	33
2.5.4 ISF tools	35

<b>2.6</b>	<b>Manufacturing Parameters .....</b>	<b>36</b>
2.6.1	Forming Tool path .....	36
2.6.2	Forming Angle.....	37
2.6.3	Tool Size .....	38
2.6.4	Step Size.....	39
2.6.5	Forming Speeds .....	39
2.6.6	Lubrication.....	40
<b>2.7</b>	<b>Mechanics and Materials .....</b>	<b>40</b>
2.7.1	Materials.....	40
2.7.2	Forces .....	41
2.7.3	Deformation and strains.....	42
2.7.4	Stress .....	42
2.7.5	Thickness reduction .....	42
2.7.6	Surface roughness .....	42
2.7.7	Material characterization .....	44
2.7.8	Failure .....	44
<b>2.8</b>	<b>Process accuracy .....</b>	<b>46</b>
2.8.1	Springback .....	47
2.8.2	Toolpath compensation.....	47
<b>2.9</b>	<b>Numerical Modeling.....</b>	<b>47</b>
<b>2.10</b>	<b>Research classification .....</b>	<b>48</b>
<b>2.11</b>	<b>Economics .....</b>	<b>49</b>
2.11.1	Economic Analysis.....	49
2.11.2	Break Even Analysis .....	50
2.11.3	Cost comparison .....	51
<b>2.12</b>	<b>Advantages and disadvantages of ISF .....</b>	<b>51</b>
<b>2.13</b>	<b>Formability .....</b>	<b>53</b>
<b>2.14</b>	<b>Research gap summary .....</b>	<b>55</b>

2.15	Summary .....	55
<b>3.</b>	<b>Methodology.....</b>	<b>57</b>
3.1	Research model selection.....	57
3.2	Defining the experimental process .....	58
3.3	Test components .....	62
3.4	Summary .....	63
<b>4.</b>	<b>ISF parameters for spherical geometry.....</b>	<b>64</b>
4.1	Formed dome geometry.....	65
4.1.1	Thickness and profile .....	65
4.1.2	Strains .....	67
4.2	Influence of tool size .....	69
4.2.1	Thickness and Profile .....	69
4.2.2	Major and Minor Strains.....	70
4.2.3	Surface roughness .....	72
4.3	Symmetric and asymmetric shape comparison .....	73
4.3.1	Part thickness and profile .....	74
4.3.2	Strain.....	77
4.4	Summary .....	80
<b>5.</b>	<b>ISF parameters for angular geometry .....</b>	<b>81</b>
5.1	Accuracy.....	82
5.2	Thickness.....	89
5.3	Major and Minor Strain.....	97
5.4	Von Mises strains.....	101
5.5	Surface roughness.....	112
5.6	Summary .....	117
<b>6.</b>	<b>Validation of ISF-FCheck .....</b>	<b>118</b>



6.1	Manufacturing .....	119
6.2	Profile and accuracy .....	120
6.3	Thickness reduction .....	125
6.4	Major and Minor Strain.....	127
6.5	Von Mises strain .....	130
6.6	Surface roughness.....	132
6.7	Summary .....	134
<b>7.</b>	<b><i>Discussion and conclusion</i></b> .....	<b>135</b>
7.1	Aims and Objectives.....	135
7.2	The deformation process.....	135
7.2.1	Cellular model.....	136
7.2.2	Internal mechanics of the deformation process.....	139
7.3	Qualitative model .....	140
7.4	Quantitative results .....	143
7.5	Quantitative design check .....	145
7.6	Limitations.....	147
7.7	Future work.....	148
7.8	Conclusion .....	149
7.9	Summary .....	149
	<b><i>References</i></b> .....	<b>151</b>
<b>8.</b>	<b><i>Appendix A -Initial scoping experiments</i></b> .....	<b>160</b>
8.1	Tensile testing and modeling.....	160
8.2	Manufacturing .....	163
8.2.1	Etching .....	163
8.2.2	Parameters .....	164
8.3	3D Scanning .....	165

8.3.1	Major and Minor strain .....	166
8.3.2	Springback .....	167
8.3.3	Thickness and profile .....	167
<b>8.4</b>	<b>Material Characterization.....</b>	<b>169</b>
8.4.1	Sample preparation .....	169
8.4.2	Microstructure .....	171
<b>8.5</b>	<b>Summary .....</b>	<b>173</b>
<b>9.</b>	<b><i>Appendix B - Material testing and data acquisition .....</i></b>	<b><i>175</i></b>
9.1	Material selection .....	175
9.2	Material composition.....	176
9.3	Tensile tests.....	177
9.3.1	Critical material properties.....	182
9.4	Nakajima Test.....	183
9.5	Surface roughness.....	186
9.6	Microstructural characterization and Fractography.....	188
9.7	Summary .....	190
<b>10.</b>	<b><i>Appendix C - Design and implementation of equipment and geometries.....</i></b>	<b><i>192</i></b>
10.1	Design and manufacturing of the tool.....	192
10.1.1	Design of the tool.....	193
10.1.2	Manufacturing of Tool .....	196
10.2	Design and manufacturing of fixture.....	198
10.2.1	Methodology.....	199
10.2.2	Fixture Design Methodology.....	200
10.2.3	Fixture Requirements: Deformation forces and forming depth .....	200
10.2.4	Fixture Design Concepts .....	201
10.2.5	Prototype assessment.....	206
10.2.6	Detailed design and validation.....	207

10.2.7	Kinematic assessment.....	208
10.2.8	Mechanical Assessment.....	208
<b>10.3</b>	<b>Design and implementation of experimental geometry.....</b>	<b>210</b>
10.3.1	Multi-slope.....	211
10.3.2	Double sided .....	216
<b>10.4</b>	<b>Data acquisition equipment .....</b>	<b>216</b>
10.4.1	3D Scanning .....	216
10.4.2	Surface Strains .....	218
10.4.3	Surface roughness.....	219
<b>10.5</b>	<b>Summary .....</b>	<b>220</b>
<b>11.</b>	<b><i>Appendix D – Multi-slope geometry results .....</i></b>	<b>221</b>
	<b>SS304L Results .....</b>	<b>221</b>
	<b>AA1050H Results.....</b>	<b>228</b>
	<b>AA2024 Results.....</b>	<b>264</b>
	<b>AA7075 Results.....</b>	<b>292</b>
<b>12.</b>	<b><i>Appendix E – Hardware, Software &amp; Conclusions.....</i></b>	<b>320</b>
<b>13.</b>	<b><i>Appendix F - Work summary .....</i></b>	<b>323</b>
13.1	Summary with respect to aims and objectives .....	323
13.2	Chapter wise: Discussion and summary .....	324
13.3	Overall conclusions .....	327

## List of Figures

Figure 1-1 ISF process schematics. ....	3
Figure 1-2 ISF of sheet metal blanks; (a) pre-cut concentric hole, (b) conventional(C) Schematic representation of the experimental setup [13].....	4
Figure 1-3 Applications in aerospace industry (Hydraulic access door of Airbus A320 aircraft).....	5
Figure 1-4 Applications in automotive industry. ....	6
Figure 1-5 Applications in biomedical industry. ....	6
Figure 1-6 Input and output parameters of the ISF process.....	12
Figure 1-7 Prediction of formed component's output parameters. ....	13
Figure 1-8 Thickness profile; (a)Sine law [62], (b) Reality.....	14
Figure 1-9 ISF-FCheck process. ....	15
Figure 1-10 Two feasibility charts.....	15
Figure 1-11 Methodology. ....	18
Figure 1-12 Thesis roadmap. ....	23
Figure 2-1 Hammering [2].....	26
Figure 2-2 Spinning; (a) Conventional, (b)Shear[81].....	26
Figure 2-3 Stamping process [82].....	27
Figure 2-4 ISF of sheet metal blanks; (a) pre-cut concentric hole, (b) conventional(C) Schematic representation of the experimental setup [13].....	28
Figure 2-5 Reflexive surface for headlights [86].....	29
Figure 2-6 Automotive heat/vibration shield [87]. ....	29
Figure 2-7 Scaled model of a train[57]. ....	30
Figure 2-8 Cranial implants formed through ISF process [89].....	30

Figure 2-9 Relation of depth with wall thickness [13] .....	31
Figure 2-10 Test shape toolpath (cone, hyperbola and flower) [92].....	32
Figure 2-11: Fixture Design; (a) Purpose built [17], (b) purpose built AISF machine [106], (c) for CNC milling machine, [99], (d) Robots [105].....	34
Figure 2-12 Sine law [62] .....	38
Figure 2-13 Surface roughness. ....	44
Figure 2-14 Crack propagation in ISF;(a) Scheme,(b) Zigzag,(c) Straight,(d) Straight (part obtained by conventional forming) [137]. ....	45
Figure 2-15 Deformation, failure and plastic deformation during ISF; (a)In-plane stretching, (b) plastic deformation,(c) Failure by cracking[13].....	46
Figure 2-16 Accuracy of the formed component [61]. ....	47
Figure 2-17 Comparison of calculated and measured part geometry[142].....	48
Figure 2-18 Schematic of breakeven point [146]. ....	50
Figure 2-19 Conventional vs SPIF [146].....	52
Figure 2-20Cost comparison; (a) Car hood, (b) Oil tank cover, (c) Pyramid [146]. ....	53
Figure 2-21 FLC and FFL for commercial sheets of Aluminum (AA1050-H111) [13] .....	54
Figure 2-22 ISF-FCheck process. ....	55
Figure 3-1 Research pathway [149].....	58
Figure 3-2 Research Mapping.....	60
Figure 4-1 Tool path of ISF Process; (a) tool path over a die, (b) Milling process simulation. .....	64
Figure 4-2 3D scanning; (a) Formed part in scanning frame, (b) Part being scanned, (c) Scanned geometry centered. ....	65
Figure 4-3 Formed part; (a) Sheet, (b)Thickness profile, (c) Percentage thickness reduction, (d) Profile.....	66
Figure 4-4 (a) Location of photos, (b) Grid over formed surface through ARGUS.....	67
Figure 4-5 (a) Major strain, (b) Mises Strain, (c) Major and Minor strain, (d) Minor strain.	68
Figure 4-6 (a) Formed parts, (b) Thickness profile.....	70

Figure 4-7 Major and Minor strain; (a) On sheet, (b)Plot.....	71
Figure 4-8 Surface roughness of tool A; (a) surface 2D profile, (b) 3D contour. ....	72
Figure 4-9 Surface roughness profile of tool B .....	73
Figure 4-10: Final Aluminum sheets; (a) case A, (b) case B, (c) case C.....	73
Figure 4-11: Thickness profiles of the sheet for; (a) case A, (b) case B, (c) case C.....	75
Figure 4-12 Geometric profiles of the sheet; (a) case A, (b) case B, (c) case C, (d) 3D scan of case B with section lines. ....	76
Figure 4-13: Thickness reduction % of the sheet; (a) case A, (b) case B, (c) case C. ....	76
Figure 4-14 (a) Location of photos, (b) Formed surface through ARGUS. ....	77
Figure 4-15: Major strain profile in the sheets; (a) case A, (b) case B, (c) case C. ....	78
Figure 4-16: Minor strain profile in the sheets; (a) case A, (b) case B, (c) case C.....	79
Figure 4-17: Von Mises strain profile in the sheets; (a) case A, (b) case B, (c) case C. ....	79
Figure 4-18: Von Mises strain % vs thickness reduction %. ....	80
Figure 5-1 Multi-slope geometry AA1050°H; (a) without BSP SS1, (b) with BSP SS2, (c) with BSP SS3.....	83
Figure 5-2 Section X; (a) SS1, (b) SS2 (with BSP), (c) SS3 (with BSP). ....	84
Figure 5-3 Section Y; (a) SS1, (b) SS2 (with BSP), (c) SS3 (with BSP). ....	85
Figure 5-4 Qualitative CAD comparison; top and isometric view; (a) SS1, (b) SS3. ....	86
Figure 5-5 Qualitative CAD comparison; top and side views; (a) SS1, (b) SS3. ....	87
Figure 5-6 Quantitative CAD comparison; top and isometric view; (a) SS1, (b) SS2.....	88
Figure 5-7 Quantitative CAD comparison; top and side views; (a) SS1, (b) SS2. ....	89
Figure 5-8 Thickness profile SS2; top and isometric view.....	90
Figure 5-9 Thickness profile SS2; Top and side views. ....	90
Figure 5-10 Thickness vs Depth SS2; (a) 60°, (b) 50°, (c) Curve 50°, (d) 40°, (e) Wall angle Comparison. ....	94
Figure 5-11 Thickness reduction of SS2 specimen; top and isometric view.....	95
Figure 5-12 Thickness reduction of SS2 specimen; top and side views.....	95

Figure 5-13 Thickness reduction% vs Depth Stainless Steel of SS specimens; (a) 60°, (b) 50°, (c) Curve 50°, (d) 40°, (e) Wall angle Comparison. ....	97
Figure 5-14 Minor strain of SS2 specimen; top and isometric view. ....	97
Figure 5-15 Minor strain of SS2 specimen; top and side views. ....	98
Figure 5-16 Major strain; top and isometric view. ....	98
Figure 5-17 Major strain of SS2 specimen; top and side views. ....	99
Figure 5-18 Major strains plotted on formed SS304L component. ....	100
Figure 5-19 Major and minor strain graph.....	101
Figure 5-20 Von Mises strains, top and isometric view SS2.....	101
Figure 5-21 Von Mises strains, top and side view SS2. ....	102
Figure 5-22 Von Mises Strain% vs Depth Stainless Steel; (a) 60°, (b) 50°, (c) 40°, (d) SS2 Wall angle Comparison.....	104
Figure 5-23 Thickness reduction% vs Von Mises Strain%; (a) SS2, (b) AA1-2. ....	105
Figure 5-24 Thickness reduction% vs Von Mises Strain% for SS2 and AA1-2, combined.	106
Figure 5-25 Principal strains in elements deformed during (a) Tensile test, (b) Plane strain [151].....	107
Figure 5-26 Principal element of unit side representing the force acting on a face and small deformation. ....	108
Figure 5-27 Von Mises assumption for value of $\beta$ for wall and corner feature. ....	110
Figure 5-28 Thickness reduction% vs Von Mises Strain% for SS2 and AA1-2, combined, Empirical vs Analytical.....	111
Figure 5-29 Maximum Von Mises Strain% at maximum depths for all Aluminum Alloys.	112
Figure 5-30 Surface view through Alicona.....	113
Figure 5-31 Surface roughness profiles of the straight wall feature; (a) As received, (b) 40°, (c) 50°, (d) 60°. ....	115
Figure 5-32 Surface roughness profiles of the curved wall feature; (a) 50°, (b) 60°.....	115
Figure 5-33 Surface roughness with respect to the wall angle. ....	116
Figure 6-1 Double sided geometry. ....	118

Figure 6-2 Scanned CAD model with sections.....	120
Figure 6-3 Section profile (45); (a) Case A, (b) Case B. ....	121
Figure 6-4 Section profile (45); (a) Case A, (b) Case B. ....	121
Figure 6-5 CAD comparison; (a) Case A, (b) Case B. ....	123
Figure 6-6 Quantitative CAD comparison; (a) Case A, (b) Case B.....	124
Figure 6-7 Thickness comparison; (a) Case A, (b) Case B.....	126
Figure 6-8 Thickness reduction comparison; (a) Case A, (b) Case B. ....	127
Figure 6-9 Thickness reduction % plotted on the component. ....	127
Figure 6-10 Major strain comparison; (a) Case A, (b) Case B. ....	128
Figure 6-11 Major strain plotted on the component. ....	128
Figure 6-12 Minor strain comparison; (a) Case A, (b) Case B.....	129
Figure 6-13 Major and minor strain.....	130
Figure 6-14 Von Mises strain comparison; (a) Case A, (b) Case B. ....	131
Figure 6-15 Von Mises strain plotted on component.....	131
Figure 6-16 Thickness reduction% vs Von Mises Strain% for Basin and Cross features....	132
Figure 6-17 Surface view through Alicona.....	133
Figure 6-18 Surface roughness profiles; (a) 50° wall, (b) Cross feature. ....	133
Figure 7-1 ISF process schematics. ....	136
Figure 7-2 Cellular visualisation of deformation process.....	138
Figure 7-3 Internal loading on material. ....	139
Figure 7-4 ISF formability. ....	140
Figure 7-5 Qualitative ISF parameter relationships.....	142
Figure 7-6 Qualitative model for thickness. ....	143
Figure 7-7 (a) Maximum Von Mises Strain% at maximum depths for all Aluminum (b)Thickness reduction% vs Von Mises Strain% for SS2 and AA1-2, combined.....	144
Figure 7-8 Thickness reduction% vs Von Mises Strain% for Basin and Cross features for double sided sheet forming. ....	145



Figure 7-9 ISF-FCheck process. ....	146
Figure 7-10 Application of cellular model for quantitative design check. ....	146
Figure 7-11 Assessment methodology.....	148
Figure 8-1 Tensile tests CPTi; (a)Stress-Strain curve, (b)Rolling angle to strength. ....	161
Figure 8-2 3D scan results of tensile testing.....	162
Figure 8-3 Validation of Numerical Model of UTM specimen.....	163
Figure 8-4 Etched part with markers .....	164
Figure 8-5 ISF rig, hole flanging [13].....	164
Figure 8-6 3D scan of manufactured part .....	166
Figure 8-7 Major and Minor strain. ....	167
Figure 8-8 Springback.....	167
Figure 8-9 (a) Wall angle[153], (b) Thickness profile.....	168
Figure 8-10 Deformation profile; (a) 10mm, (b) 17mm.....	169
Figure 8-11 Samples taken out from ISF sheet.....	170
Figure 8-12 Microstructure of undeformed sheet at different magnifications; (a) 1000X, (b) 3000X.....	171
Figure 8-13 Microstructure of deformed sheet; (a) 1000 x, (b)2000x.....	172
Figure 8-14 Fractography (a) 100X, (b) 500X.....	173
Figure 9-1 Specimen preparation; (a) Waterjet cutting, (b) Samples on the sheet metal, (c) Samples at 0°, 45° ad 90° RD.....	178
Figure 9-2 Equipment used for Tensile tests and data acquisition; (a) UTM, (b) micrometer, vernier-calipers and scale.....	179
Figure 9-3 Stress-strain graphs, AvsB; (a) 0RD, (b) 45RD, (c) 90RD.....	180
Figure 9-4 Stress-strain graphs at different rolling directions; (a) strain rate A, (b) strain rate B.....	181
Figure 9-5 FLC test preparation; (a) Specimen, (b) Lubricant. ....	184
Figure 9-6 FLC; (a) Test arrangement, (b) Measurement setup, (c) Durig the process. ....	185

Figure 9-7 Forming Limit Curve AA1050H.....	186
Figure 9-8 Surface roughness of tensile specimens; (a) 0A, (b) 0B, (c) 45A, (d) 45B, (e) 90A, (f) 90B.....	187
Figure 9-9 Sample preparation and mounting; (a) Electropolishing machine, (b) Sample mounted after polishing, (c) Sample mounted on SEM/EBSD, (d) Sample tilted for EBSD. ....	189
Figure 9-10 Ductile fracture SS304L, ORD-A; (a) 1000X, (b) 3000X.....	191
Figure 10-1 Tool conceptual designs; (a) Concept 1, (b) Concept 2A, (c) Concept 2B.....	194
Figure 10-2 3D models; (a) Exploded assembly view of concept 3, (b) Concept 4, (c) Concept 5.....	195
Figure 10-3 Manufacturing and commissioning of tool; (a) Block, (b) Thrust bearings in the tool, (c) Hemispherical tool, (d) Tool while performing ISf process, (e) Wooden die. ....	197
Figure 10-4 Types of Incremental Sheet Forming Fixtures; (a) Positive, (b) Negative. ....	199
Figure 10-5: Conceptual design 1 .....	202
Figure 10-6: Conceptual design 2.....	203
Figure 10-7: Conceptual design 3.....	204
Figure 10-8 3D CAD of fixture concepts; (a) Concept 4: scissors, (b) Concept 5: 3 pillars. ....	206
Figure 10-9 Scissor concept prototype at different levels (a) lowest, (b) highest. ....	206
Figure 10-10 Testing on polymer sheet; (a) Start, (b) Finish, (c) Wooden die.....	208
Figure 10-11 ISF equipment; (a) CAD model of rotating tool (4.5mm Dia), (b) Rotating tool (16.5mm Dia), (c) Equipment mounted on CNC, (d) Nylon bushes and wooden Dies. ....	209
Figure 10-12 Complex geometries formed through ISF.....	210
Figure 10-13 Reflexive surface for headlights [49].....	210
Figure 10-14 Automotive heat/vibration shield [87]. ....	211
Figure 10-15 CAD model of the designed shape (a) Isometric view, (b) Drawing details. ....	212
Figure 10-16 Manufacturing of backsupporting plate; (a) Water jet cutting, (b) Smoothing. ....	214

Figure 10-17 Setup of system with guages; (a) X and Y (lateral), (b) Z (depth).....	214
Figure 10-18 Setup of system with guages; (a) X and Y (lateral), (b) Z (depth).....	215
Figure 10-19 ISF process for Multi-slope geometry; (a) Start, (b) Tool path generated in Alphacam, (c) Tool forming the sheet metal. ....	215
Figure 10-20 Double sided geometry. ....	216
Figure 10-21 ATOS 3D scanner; (a) Tritop scale bars and reference markers, (b) While scanning, (c) Focus at the center (d) CAD comparison. ....	217
Figure 10-22 Surface strain equipment; (a) EU classic electrolyte system, (b) Roller submerged in Electrolyte, (c) Marking sheet, (c) Marked Sheet, (d) Nikon Camera. ....	218
Figure 10-23 Surface roughness; (a) Gel gun, (b) Alicona infinite focus. ....	219
Figure 10-24 Aligning geometries with software co-ordinates ....	219
Figure 11-1 Ductile fracture SS304L, ORD-A at 2000X. ....	221
Figure 11-2 Ductile fracture SS304L, 45RD-A; (a) 1000X, (b) 2000X , (c) 3000X.....	224
Figure 11-3 Ductile fracture SS304L, 9ORD-A; (a) 1000X, (b) 2000X , (c) 3000X.....	227
Figure 11-4 Forming Limit Curve AA1050.....	228
Figure 11-5 Multi-slope geometry AA1050°H; (a) without BSP, (b) with BSP.....	229
Figure 11-6 Section X; (a) AA1-1050H, (b) AA2-1050H (c) AA3-1050H. ....	230
Figure 11-7 Section Y; (a) AA1-1050H, (b) AA2-1050H (c) AA3-1050H. ....	230
Figure 11-8 Qualitative CAD comparison; top and isometric view; (a) AA1-1050H, (b) AA2-1050H (c) AA3-1050H. ....	231
Figure 11-9 Qualitative CAD comparison; top and side views; (a) AA1-1050H, (b) AA2-1050H (c) AA3-1050H. ....	232
Figure 11-10 Quantitative CAD comparison; top and isometric view; (a) AA1-1050H, (b) AA2-1050H (c) AA3-1050H. ....	233
Figure 11-11 Quantitative CAD comparison; top and side views; (a) AA1-1050H, (b) AA2-1050H (c) AA3-1050H. ....	234
Figure 11-12 Thickness profile, top and isometric view; (a) AA1-1050H, (b) AA2-1050H (c) AA3-1050H.....	235

Figure 11-13 Thickness profile top and side views; (a) AA1-1050H, (b) AA2-1050H, (c) AA3-1050H.....	236
Figure 11-14 Thickness vs Depth AA1-7075 AA2-7075 & AA3-1050H; (a) 60°, (b) 50°, (c) Curve 50°, (d) 40°, (e) Wall angle Comparison AA1-1050H, (f) Wall angle Comparison AA2-1050H, (g) Wall angle Comparison AA3-1050H.....	240
Figure 11-15 Thickness reduction; top and isometric view , (a) AA1-1050H, (b) AA2-1050H (c) AA3-1050H.....	241
Figure 11-16 Thickness reduction; top and side views, (a) AA1-1050H, (b) AA2-1050H (c) AA3-1050H.....	242
Figure 11-17 Thickness reduction% vs Depth AA1-1050H AA2-1050H & AA3-1050H; (a) 60°, (b) 50°, (c) 40°, (d) Curve 50°, (e) Wall angle Comparison AA1-1050H, (f) Wall angle Comparison AA2-1050H, (g) Wall angle Comparison AA3-1050H .....	246
Figure 11-18 Minor strain; top and isometric view (a) AA1-1050H, (b) AA2-1050H (c) AA3-1050H.....	247
Figure 11-19 Minor strain; top and side views (a) AA1-1050H (b) AA2-1050H (c) AA3-1050H.....	248
Figure 11-20 Major strain; top and isometric view (a) AA1-1050H, (b) AA2-1050H (c) AA3-1050H.....	249
Figure 11-21 Major strain; top and side views (a) AA1-1050H, (b) AA2-1050H, (c) AA3-1050H.....	250
Figure 11-22 a) Major strains plotted on formed AA1-1050H, (b) Major strains plotted on formed AA2-1050H component (c) Major strains plotted on formed AA3-1050H component.....	252
Figure 11-23 Major and minor strain graph AA1-1050H.....	252
Figure 11-24 Major and minor strain graph AA2-1050H.....	253
Figure 11-25 Major and minor strain graph AA3-1050H.....	253
Figure 11-26 Von Mises strains, top and isometric view; (a) AA1-1050, (b) AA2-1050, (c) AA3-1050. ....	254

Figure 11-27 Von Mises strains, top and side view; (a) AA1-1050, (b) AA2-1050, (c) AA3-1050.....	255
Figure 11-28 Von Mises Strain% vs Depth AA1-1050 AA2-1050H & AA3-1050H; (a) 60°, (b) 50°, (c) 40°, (d) c50° (e) Wall angle Comparison AA1-1050H, (f) Wall angle Comparison AA2-1050H (g) Wall angle Comparison AA3-1050H. ....	259
Figure 11-29 Thickness reduction% vs Von Mises Strain%; (a) AA1-1050H, (b) AA2-1050H.....	260
Figure 11-30 Thickness reduction% vs Von Mises Strain% for AA1-1050H and AA2-1050H, combined.....	260
Figure 11-31 Surface roughness profiles of the straight wall feature; (a) As received, (b) 50°, (c) 60°, .....	261
Figure 11-32 Surface roughness profiles of the curved wall feature; (a) 50°, (b) 60°,.....	262
Figure 11-33 Surface roughness with respect to the wall angle. ....	262
Figure 11-34 Forming Limit Curve AA2024.....	264
Figure 11-35 Multi-slope geometry; (a) AA1-2024, (b) AA2-2024.....	265
Figure 11-36 Section X; (a) AA1-2024, (b) AA2-2024. ....	266
Figure 11-37 Section Y; (a) AA1-2024, (b) AA2-2024. ....	266
Figure 11-38 Qualitative CAD comparison; top and isometric view; (a) AA1-2024, (b) AA2-2024.....	267
Figure 11-39 Qualitative CAD comparison; top and side views; (a) AA1-2024, (b) AA2-2024.....	268
Figure 11-40Quantitative CAD comparison; top and isometric view; (a) AA1-2024, (b) AA2-2024. ....	269
Figure 11-41Quantitative CAD comparison; top and side views; (a) AA1-2024, (b) AA2-2024.....	270
Figure 11-42 Thickness profile, top and isometric view; (a) AA1-2024, (b) AA2-2024.....	271
b) Figure 11-43Thickness profile top and side views; (a) AA1-2024, (b) AA2-2024. ....	272
Figure 11-44 Thickness vs Depth AA1-2024 & AA2-2024; (a) 60°, (b) 50°, (c) Curve 50°, (d) 40°, (e) Wall angle Comparison AA1-2024, (f) Wall angle Comparison AA2-2024 ....	275

Figure 11-45 Thickness reduction% vs Depth AA1-2024 & AA2-2024; (a) 60°, (b) 50°, (c) Curve 50°, (d) 40°, (e) Wall angle Comparison AA1-2024, (f) Wall angle Comparison AA2-2024 .....	277
Figure 11-46 Thickness reduction; top and isometric view , (a) AA1-2024, (b) AA2-2024	278
Figure 11-47 Thickness reduction; top and side views, (a) AA1-2024, (b) AA2-2024. ....	279
Figure 11-48 Minor strain; top and isometric view (a) AA1-2024, (b) AA2-2024.....	280
Figure 11-49 Minor strain; top and side views (a) AA1-2024 (b) AA2-2024.....	281
Figure 11-50 Major strain; top and isometric view (a) AA1-2024, (b) AA2-2024. ....	282
Figure 11-51 Major strain; top and side views; (a) AA1-2024, (b) AA2-2024.....	283
Figure 11-52 Surface roughness- 2024.....	284
Figure 11-53 a) Major strains plotted on formed component; (a) AA1-2024, (b) AA2-2024. ....	285
Figure 11-54 Major and minor strain graph AA1-2024.....	286
Figure 11-55 Major and minor strain graph AA2-2024.....	286
Figure 11-56 Von Mises Strain% vs Depth AA1-2024 & AA2-2024; (a) 60°, (b) 50°, (c) 40°, (d) c50° (e) Wall angle Comparison AA1-2024, (f) Wall angle Comparison AA2-2024. ....	289
Figure 11-57 Surface roughness profiles of the straight wall feature 2024; (a) 40°, (b) 50°, (c) 60°.....	290
Figure 11-58 Surface roughness- 2024.....	291
Figure 11-59 Forming Limit Curve AA7075.....	292
Figure 11-60 Multi-slope geometry; (a) AA1-7075, (b) AA2-7075.....	293
Figure 11-61 Section X; (a) AA1-7075, (b) AA2-7075. ....	294
Figure 11-62 Section Y; (a) AA1-7075, (b) AA2-7075. ....	294
Figure 11-63 Qualitative CAD comparison; top and isometric view; (a) AA1-7075, (b) AA2-7075.....	295
Figure 11-64 Qualitative CAD comparison; top and side views; (a) AA1-7075, (b) AA2-7075.....	296

Figure 11-65 Quantitative CAD comparison; top and isometric view; (a) AA1-7075, (b) AA2-7075. ....	297
Figure 11-66 Quantitative CAD comparison; top and side views; (a) AA1-7075, (b) AA2-7075.....	298
Figure 11-67 Thickness profile, top and isometric view; (a) AA1-7075, (b) AA2-7075....	299
Figure 11-68 Thickness profile top and side views; (a) AA1-7075, (b) AA2-7075.....	300
Figure 11-69 Thickness vs Depth AA1-7075 & AA2-7075; (a) 60°, (b) 50°, (c) Curve 50°, (d) 40°, (e) Wall angle Comparison AA1-7075, (f) Wall angle Comparison AA2-7075....	303
Figure 11-70 Thickness reduction; top and isometric view , (a) AA1-7075, (b) AA2-7075. ....	304
Figure 11-71 Thickness reduction; top and side views, (a) AA1-7075, (b) AA2-7075. ....	305
Figure 11-72 Thickness reduction% vs Depth AA1-7075 & AA2-7075; (a) 60°, (b) 50°, (c) 40°, (d) Curve 50°, (e) Wall angle Comparison AA1-7075, (f) Wall angle Comparison AA2-7075.....	308
Figure 11-73 Minor strain; top and isometric view (a) AA1-7075, (b) AA2-7075.....	309
Figure 11-74 Minor strain; top and side views (a) AA1-7075 (b) AA2-7075.....	310
Figure 11-75 Major strain; top and isometric view (a) AA1-7075, (b) AA2-7075. ....	311
Figure 11-76 Major strain; top and side views (a) AA1-7075, (b) AA2-7075.....	312
Figure 11-77 a) Major strains plotted on formed AA1-7075, (b) Major strains plotted on formed AA2-7075 component. ....	313
Figure 11-78 Major and minor strain graph AA1-2024.....	314
Figure 11-79 Major and minor strain graph AA2-2024.....	314
Figure 11-80 Von Mises Strain% vs Depth AA1-7075 & AA2-7075; (a) 60°, (b) 50°, (c) 40°, (d) c50° (e) Wall angle Comparison AA1-7075, (f) Wall angle Comparison AA2-7075. ....	317
Figure 11-81 Surface roughness profiles of the straight wall feature; (a) 40°, (b) 50°, (c) 60°. ....	318
Figure 11-82 Surface roughness- 7075 .....	319

## List of Tables

Table 1-1 Research questions answered in results chapters. ....	21
Table 2-1: Reported ISF Machines. ....	35
Table 3-1 Experiments performed. ....	61
Table 3-2 Test components. ....	62
Table 5-1 Experiments performed. ....	81
Table 5-2 Surface roughness measurements. ....	116
Table 6-1 Surface roughness measurements. ....	134
Table 7-1 Dependent Inputs and outputs of ISF process. ....	142
Table 8-1 Tensile tests CPTi. ....	162
Table 9-1 Material Composition. ....	176
Table 9-2 Physical and mechanical properties. ....	177
Table 9-3 Tensile specimen details. ....	177
Table 9-4 Material properties. ....	183
Table 9-5 FLC specimen data. ....	185
Table 9-6 Surface roughness of tensile specimens. ....	188
Table 10-1 Design selection matrix. ....	196
Table 10-2 Concept selection matrix. ....	205
Table 11-1 Surface roughness measurements. ....	263
Table 11-2 Surface roughness- 2024 ....	284
Table 11-3 Surface roughness- 2024 ....	291
Table 11-4 Surface roughness- 7075 ....	319
Table 12-1 List of hardware used in the project. ....	320
Table 12-2 List of software used in the project. ....	322



## Nomenclature

Unless stated explicitly, the following abbreviations and symbols are used in this thesis, with their meaning listed below.

<i>Abbreviations</i>	<i>Description</i>
®	Registered trademark
°	Degree (Unit of angle)
μ	Micro
3D	Three dimensional
AA	Aluminum alloy
AA1-1050H	AA1050H without backsupporting plate 0RD and low feedrate
AA1-2024	AA2024 without crack
AA1-7075	AA7075 without crack
AA2-1050H	AA1050H without backsupporting plate 90RD and high feedrate
AA2-2024	AA2024 formed up till crack
AA2-7075	AA2024 formed up till crack
AA3-1050H	AA1050H with backsupporting plate 0RD and high feedrate
AFRC	Advanced Forming Research Centre
AISF	Asymmetric Incremental Sheet Forming
Al	Aluminum
ASTM	American Society for Testing and Materials
BSP	Back supporting plate
CAD	Computer Aided Design
CAM	Computer Aided Manufacturing
CGA	Circular grid analysis
CNC	Computer Numerically Controlled
CpTi	Commercially Pure Titanium
D	Tool diameter
Double Sided	Name of a geometry with multiple side forming
ε	Strain
EBSD	Electron backscatter diffraction (crystallographic characterisation technique)
eq	Equivalent
FC	Fixed cost
FE	Finite Element
FLC	Forming Limit Curve
FLCF	Forming limit curves at fracture

---

FLD	Forming limit diagram
fr	Fracture
HCP	Hexagonal Closed Pack (Crystal Structure)
ISF	Incremental Sheet Forming
K	Strength coefficient
L	Length
Markers	Reference points for metrology data
MPa	Mega Pascal
Multi-slope	Name of a geometry with multiple wall angles
n	Strain hardening coefficient
P	Grinding paper, ISO/FEPA Grit designation
R	Tool radius
R'	Average Lankford coefficient (plastic anisotropy)
Ra	Average surface roughness (ASME B46.1)
RD	Rolling Direction
SEM	Scanning Electron Microscope
S-N Curve	Stress against number of cycles to failure
SPIF	Single point incremental (sheet) forming
SS	Stainless Steel
SS1	SS304L without backsupporting plate 0RD and low feedrate
SS2	SS304L with backsupporting plate 0RD and high federate
SS3	SS304L with backsupporting plate 90RD and high federate
TC	Total cost
tf	Final thickness of the sheet
Ti	Titanium
to	Initial thickness of the sheet
TPIF	Two point incremental forming
TR	Total revenue
TVC	Total variable cost
UTM	Universal testing machine
UTS	Ultimate Tensile Strength
X	Magnification
$\alpha$	Wall angle
N	Poisson's ratio
$\Sigma$	Stress
$\sigma_y$	Yield strength
$\beta$	Strain ratio

---



# 1. Introduction

Metal products are the backbone of the manufacturing industry. While the value metal products contribute to help the economy is largely hidden, its importance cannot be ignored. Around 11000 companies are linked to the UK metal industry and provide over a million jobs, which makes a contribution of £400bn of the UK's GDP [1]. Thus sheet metal forming is a major component of an industrial sector (aerospace, automotive etc.) worth billions to the economy. This activity is associated with industrial sectors that range from automotive to aerospace. Within these industries a range of manufacturing processes are employed to transform the shape and properties of metallic sheet in to engineering components. However in the majority of processes (e.g. pressing, hydroforming, superplastic forming) a tool (i.e. mold) has to be created to define the shape of the deformed part. Because the tooling is usually expensive and time consuming to develop there is ongoing interest in alternative processes that use either no tooling or only light tooling (which can be cheaply produced).

This research investigates the application of one of the alternative sheet forming processes, Incremental Sheet Forming (ISF), to the manufacturing of components from aerospace alloys. Although the ISF process is easily described in qualitative terms the interaction between process parameters and the characteristics of the resulting part are still unclear. This thesis investigates a number of relationships between process parameters and functional properties with the objective of enabling better quality parts.

## 1.1 Process overview

Incremental Sheet Forming (ISF) is a process where the movement of a hemispherical tool causes highly localized deformation of the sheet metal [Figure 1-1]. Initially, the undeformed metal sheet is clamped between the top and the bottom plate. The spherical tool is controlled through a program and is fixed in a numerically controlled machine. It moves along a spiral (helical) toolpath with a defined pitch, feedrate and rotation. When the tool comes in contact with the sheet metal, a pointed load is applied by the tool on a small area of the sheet metal. Sheet metal is hanging freely in the air and is not supported, thus it deforms when the tool forces the material in the downward direction. As the tool follows a contour path it basically deforms several small areas of the sheet metal continuously and thus a large

deformation is seen in the final part. The thickness of the metal sheet reduces as it is being formed (intermediate stage), till the sheet reaches its final form.

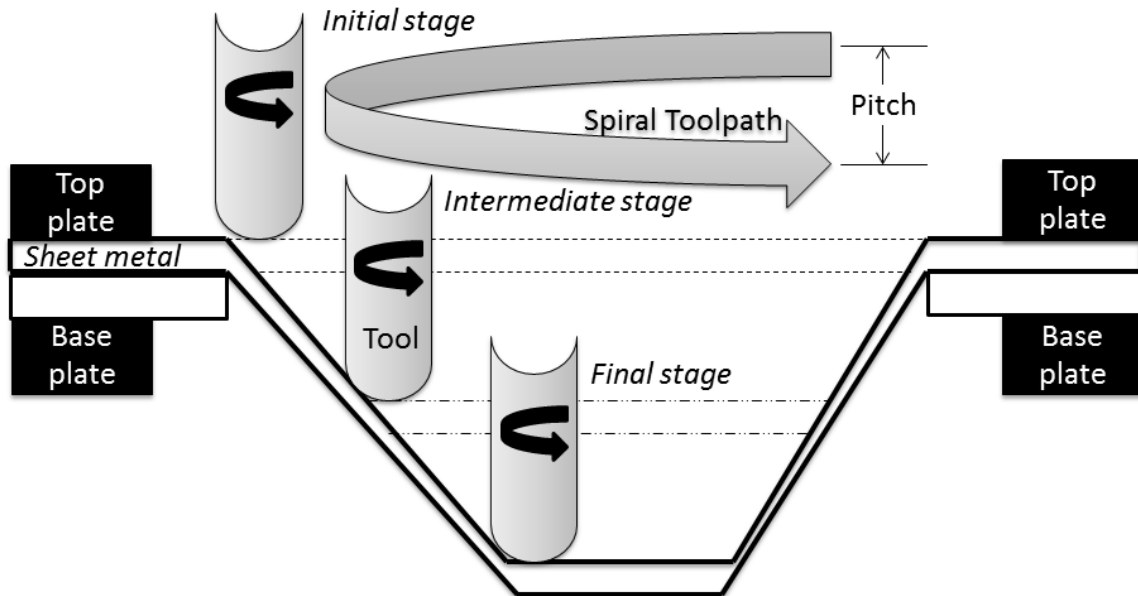


Figure 1-1 ISF process schematics.

Typically a multi-axis CNC machine with a hemispherically tipped tool and sheet clamber is used for ISF [2]. Incremental Sheet Forming is a family of processes where the movement of a spherical tool causes highly localized deformation of material in the surrounding area [3]. Although frequently referred to as being a die-less process [4] such configurations are the exception rather than the rule [5]. More generally dies are used and ISF process can be categorized by the convexity of tooling used [Figure 1-2 ] [6]. In contrast to other sheet forming processes (e.g. spinning and shear forming) ISF can create both symmetric and asymmetric shapes [7]. ISF is not limited to one-offs, but can also be regarded as a low volume production method [8] whose productivity and cycle time are affected by the size of the forming tool [9], the geometry of the part being formed [10] and the type of surface finish that is desired [11].

Frequently ISF capability is determined by the size of the fixture that can be mounted on the worktable of the CNC milling machine (the most common arrangement) [12]. The fixture is usually composed of a base plate and a top plate, which clamps the sheet using a series of threaded fasteners [13]. Forming is caused by the pressure created by the forming tool as it follows a path generated by CAM software [14] that generates localized stresses that cause

the material to yield and deform [7]. A basic setup of a forming rig is shown in Figure 1-2 with all the components listed.

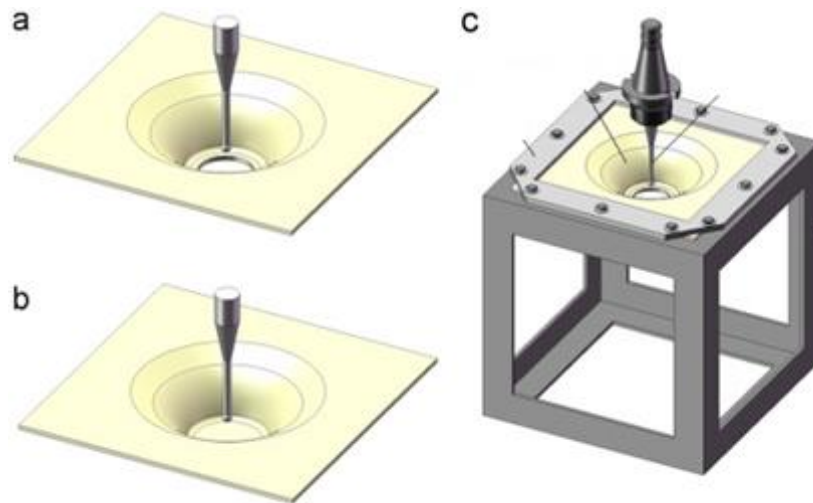


Figure 1-2 ISF of sheet metal blanks; (a) pre-cut concentric hole, (b) conventional (c) Schematic representation of the experimental setup [13]

## 1.2 Applications and advantages

Many components used in aerospace, automotive and biomedical are made with Titanium, Aluminum or Steel sheet metal using conventional forming processes [15], and researchers have reported the development of equipment (fixture and tool) to make these parts through ISF process [16-20]. Manufacturing parameters are being optimized to reduce cost and increase production rate of the process [21]. Geometries for most of these components are derived from basic geometrical features such as curve, straight wall, cone, cup or combination of these features. In this study, we have experimented with all these shapes and their interaction between each other. Real life component will have several geometrical features interacting with each other; some examples of the geometry are given in the following text.

- **Aerospace:** Aerospace parts for internal and external use [Figure 1-3] can be easily made using ISF process. For instance, external parts are fuselage, wing covers and aileron cover while internal parts are air ducts, doors, wash basins and storage

compartments. The fuselage, wash basin and storage compartments have wall feature only while door, wing and aileron cover have curved features. These components are made of titanium, aluminum or composite materials.

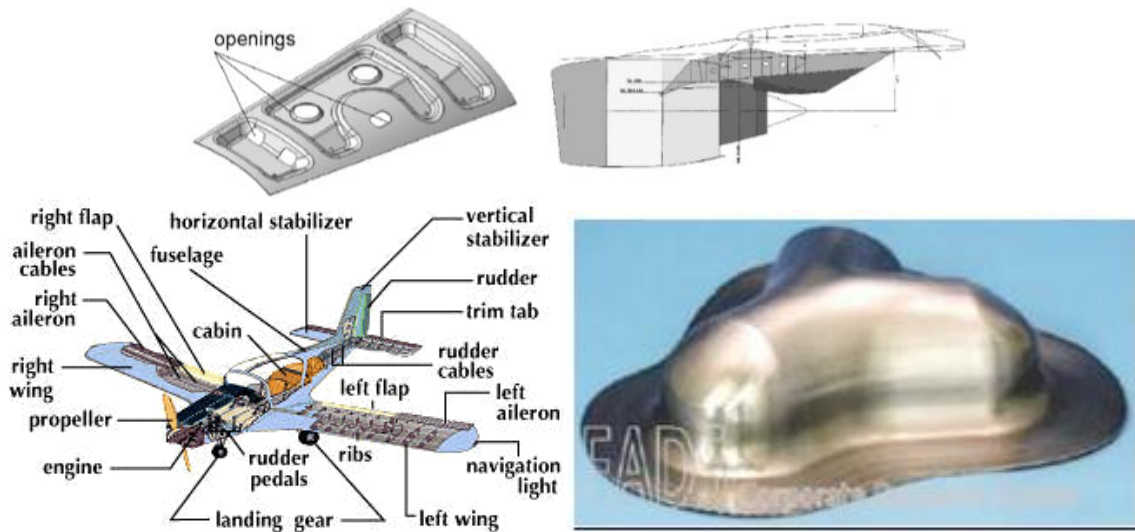


Figure 1-3 Applications in aerospace industry (Hydraulic access door of Airbus A320 aircraft).

- Automotive:** Wall feature at various angles interacting with each could be seen in this Multi-slope concept of Ashton Martin ®. Multi-slope concept has three straight walls and a curve. It can easily be observed in the figure that different sheets of metal are joined together through rivets, welding, nuts and bolts. This complete structure could be made with a single sheet using ISF process. This not only decreases production time, cost, CO<sup>2</sup> emissions, and energy usage but also gives final product a better and glamorous look. In current study, three different wall features connected to a curved feature is also researched. Figure 1-4 also shows front wing of the car has a formed semicircle. These components are generally made of steel or aluminum.

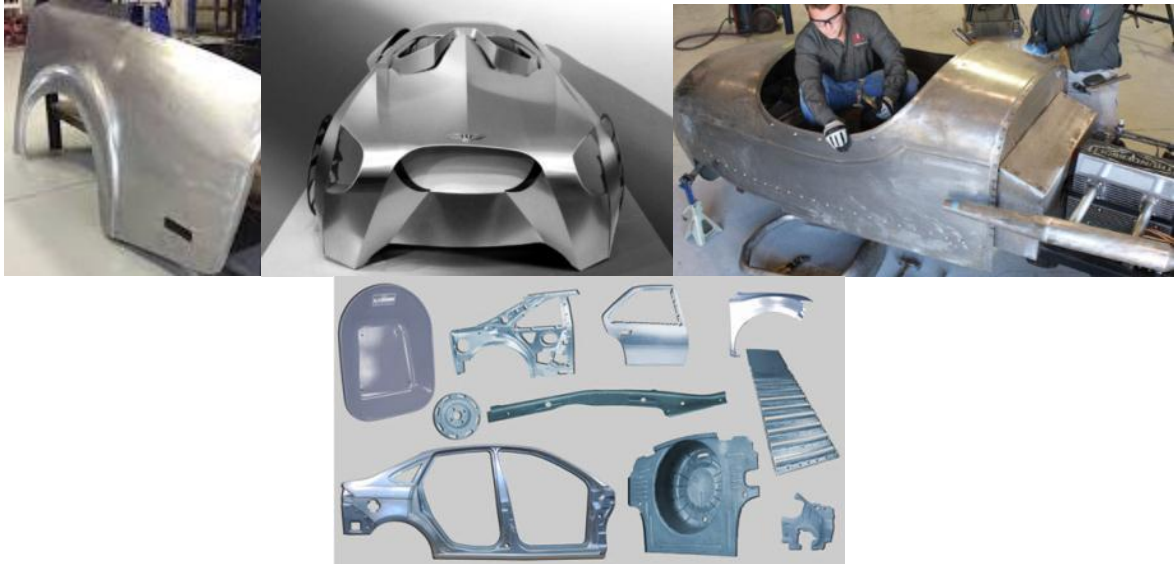


Figure 1-4 Applications in automotive industry.

- **Biomedical:** Cranial, facial and ankle surgeries are very common with biomedical practitioners [Figure 1-5]. Currently, it is very costly and time-consuming to make these components and patients have to go through a waiting list to receive components. These components are mostly made from Titanium and could easily be formed using ISF within minutes.



Figure 1-5 Applications in biomedical industry.

### 1.3 Component properties

Although ISF is highly applicable in aerospace, automotive and biomedical industries, the process cannot become established in these industries till information regarding the process capability is clearly understood and can be applied rapidly at industrial scale. If the limits of



the ISF process under various conditions and materials were clearly understood; the number of applications would increase [4].

Forming limit curve (FLC) is generally used to predict sheet forming process. Both the literature and authors own work suggest that ISF capabilities cannot be characterized by FLC curves [22]. This might be due to the repetitive load applied on the sheet metal which changes the material properties at every pass of the tool during the forming process. Knowledge of material properties and microstructural behavior of the post and pre-formed sheet metal are very important, as they will be used in practical applications in different industries. In current study, FLC tests and tensile tests were performed on the steel sheet material. FLC results were plotted with major and minor strain results of the formed component. The microstructural behavior of pre and post formed sheet metal was acquired and the difference in microstructure was reported. Microstructure and material properties change due to dislocation movement in the crystal structure because of the applied strain on the sheet metal. Thickness reduction is directly proportional to the strain applied at a particular wall angle. As failure criteria in the industry are based on strain and components formed through ISF generally fail due to thinning of sheet metal; failure prediction and component stability is discussed with respect to these two parameters.

The surface texture is a very important parameter in sheet metal components. In conventional processes, surface texture is dependent upon the die, workpiece and forming parameters. It is very important to mention here that cost of manufacturing increases directly with the surface finish as processes such as grinding etc require time and equipment. The increased cost of the final product is justified through added value in terms of longer lifespan, aesthetics or better function. Parts with sliding contacts with other metals or fluids for instance air have increased lifespan and function better if they have good surface finish. The surface finish also influences crack initiation in components under fatigue loading. Surface finish depends upon surface lay, residual stress and surface roughness. Currently, the effect of residual stress is not quantified in stress analysis, thus engineers use surface roughness values to evaluate fatigue limit in mechanical engineering design problems [23]. Several researchers evaluated the influence of surface roughness on the life of component through S-N curves [24]. Researchers have divided life of component into fatigue crack initiation life and the fatigue crack growth life and they have concluded that the influence of roughness on the fatigue strength is only influencing initiation stage. It is important to

mention here that fatigue crack initiation life predominantly determines the total fatigue life of a machine element [25, 26]. Hagan et. al. performed a surface roughness analysis on Al 3003 [11]. Due to the importance of surface roughness because of reasons mentioned above, in current study surface roughness for formed and unformed are measured for different materials and geometrical features.

Although the properties such as microstructure and surface finish are important, they are secondary in term of feasibility if the component could be formed with a given set of input and output parameters, for instance, the thickness of the formed component.

#### 1.4 Research gap

The reported research (detailed in chapter 2) has brought ISF technology a long way since its inception, however, researchers have also identified research challenges along with their results;

1. “There is a **lack of a unified theory** for the **failure** in SPIF. Thus, it is highly desirable that a **new theoretical model** can be constructed to predict fracture in SPIF using a wide range of **process variables**, such as **wall angle**, step size, **tool rotation** and **feed rate**.” [22, 27]
2. “Many parameters have a big effect on the wall angle, e.g. **tool diameter** and tool path, and future work is needed to quantify the effects on the **wall angle** such as the step size and feed rate.” [22, 28]
3. “Future work on the effect of **tool rotation** may be made in the following areas. Firstly, the effect of **tool rotation** on ISF **formability** and its effect on **sheet metal type** should be studied; secondly, there should be a focus on finding a relationship between **tool rotation** and **feed rate**; finally, a **table** of suitable **tool rotations** and **feed rates** may be developed as a guide for some important materials used in ISF

processes.” [22, 29]

4. “A table of suitable **tool rotations** and **feed rates** may be developed as a guide for some **important materials** used in ISF processes.” [22, 29, 30]
- 5  
“A study on the effect of **material anisotropy** on the **location of fracture** in SPIF is recommended.” [22, 31]
- 6  
“There are two important questions which need to be clarified in the FLCF of SPIF. The first is whether the **Nakajima test** is able to capture the fracture occurrence in the SPIF, or if a SPIF test should be used to establish FLCF. The second is whether the **FLCF** is a straight line in all types of materials or there are some materials which have the FLCF as a curve.” [22, 32]
- 7  
“Further investigation should be carried out into the effect of **initial sheet thickness to tool radius** ratio (to/R) on the FLCF, and whether it is enough to describe FLCF in SPIF.” [22, 32, 33]
- 8  
“The **surface finish** and **dimensional accuracy** of an ISF part could be improved.” [22, 34, 35]

Although the above problems are general issues, in practice manufacturing engineers are interested in solutions for specific materials. For example, the main issue for the aerospace industry is the production rate, the accuracy of the process, surface roughness and formability of materials such as CpTi, AA7075 and AA2024 under this process. Although some automotive industries have implemented ISF on small scale, its implementation on an industrial level is hindered by production rate, accuracy and formability of complicated

shapes using SS304L, AA2024 and AA1050H. In summary, the following research problems exist

1. **Geometric accuracy** is of vital importance in ISF process [6] and several researchers have discussed its importance. [36]. Ambrogio et. al. emphasizes that more research efforts should be made in order to improve geometric accuracy as this will industrialize the ISF process rapidly [37]. Lendel et. al. reported that the main disadvantages of SPIF technology are related to low dimensional and shape accuracy [12]. Meier et. al. concludes that the deviation of the formed profile from the required one cannot be neglected and necessary means should be applied to improve the accuracy of the final part, which might be effected by several factors. [38]. Kurra et al. suggests that the advantages of ISF get overshadowed by its inability to form geometry accurately. [39]. The dimensional accuracy research is very important and can lead to several applications of the process.[40]. Bpsetti et. al. blames the poor geometric accuracy of the process for its limited applications and aimed at improving the forming accuracy.[41]. Pohlak et. al. blames the elastic nature of the material and shows serious concern that large components will have higher deviation. He also states that geometrical features (curve, wall, wall angle) and forming depth might have an effect on the accuracy [42]. Malhotra et. al. suggests that ISF has embedded geometric inaccuracy due to springback [6]. Alwood et. al. used cut out blanks [43] and multi-staged forming with closed-loop feedback control system [44] to improve geometric accuracy but was not satisfied with the results.
2. **Production time and good surface finish** are the most important requirements for high productivity and low manufacturing cost [39]. Production time and surface finish are dependent upon several factors, namely, feed rate, wall angle, tool size, pitch and lubrication [39]. Lendel et. al. suggests that long processing time is one of the main disadvantages of the ISF process [12]. During ISF one side of the metal develops a rough surface called an orange peel effect. It is important to know surface roughness of the formed parts [11]. Jeswiet et. al. gave multiple examples, explaining the importance of surface roughness in ISF process [45]. Although literature about surface roughness is available for conventional machining and

forming processes [46-49], however, research studies on the surface roughness of ISF parts are limited [39].

3. **Formability of the material** is the deciding factor about its usage to form a component through ISF process. [42]. The FLC is different for ISF compared to conventional forming processes (e.g. deep drawing). [50-54]. Generally, higher strains can be achieved during ISF process [50]. Researchers have different viewpoints to why does FLC for ISF behave differently compared to conventional forming [15]. Some researchers think it is due to localization of strains [55, 56], while other think it is because of through-thickness shear [56, 57]. Although several researchers have reported a straight line with negative slope yet there are no existing standards or procedures to determine formability of the components. Experimental and theoretical research is being performed on this topic [53, 58]. Formability in ISF process is affected by various factors [3]. Some of the important factors are material type [2], sheet metal thickness [59, 60], forming tool size [9], geometry of the component [61], deformation mechanism [6] and pitch [62]; the response to the factors is maximum forming angle [63] and depth. Malhotra et. al suggests that specialized methodology of FLC is required [12].

#### **1.4.1 Towards a design check method for ISF**

This thesis is focused on this third problem; the early assessment of feasibility. The ISF research area has opportunities to develop detailed knowledge of the field through empirical and numerical studies. Figure 1-6 shows inputs and outputs of the ISF process but does not establish any relationship between these parameters. Previous studies were focused on basic (cone, pyramid etc) or commercial geometries with an aim to incorporate accuracy through multistage toolpath and control feedback systems, which are expensive and does not solve industrial issues of having accurate asymmetric complex shaped product, manufactured with easily formable materials (SS304L, AA1050H) or high strength, lightweight, hard-to-deform materials (AA2024, AA7075, CpTi), with high production rate, good finish and low-cost. **Amino states that although ISF process has a lot of potential yet it's in depth knowledge is not at a mature stage and needs immense improvement for industrial applications** [4]. This is further emphasized by Pohlak et. al. [42] and Nam et. al. [64]. From

a practical perspective implementation of ISF in the industry is still at a very early stage and only a hand full of market leaders (Boeing, Honda, Ford, Amino) are putting their effort in research and development of the process. Remainder of the sheet forming industry still has limited understanding and the process needs to be exposed to them. Therefore, it is highly desirable to identify low-cost equipment, tests and techniques to develop knowledge and frameworks for further development and commercialization of the process. Through a better understanding of the ISF process, models and frameworks could be developed which will facilitate the researchers, design and manufacturing engineers and technicians in the careful design, planning and control of the parameters that are required to overcome challenges of accuracy, production rate, finishing and formability.

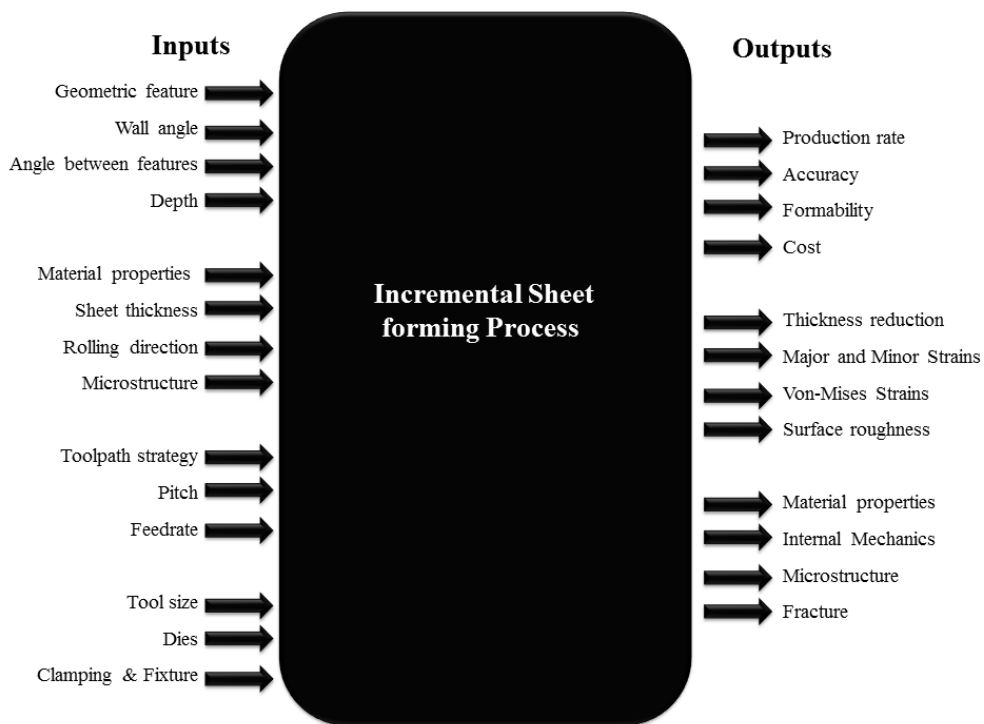


Figure 1-6 Input and output parameters of the ISF process.

Given this challenge, this thesis is focused on the exploration and development of equipment, test geometries, manufacturing parameters feasibility and decisions to help aid researchers, design and manufacturing engineers in the design and implementation of the ISF process on commercial products when faced with this uncertainty. Factors effecting formability of the sheet metal under ISF process are also explored [Figure 1-7]. The overall

aim is: “...to explore how researchers, design and manufacturing engineers can effectively plan, design, implement and control the ISF process to help facilitate forming of the sheet metal parts through ISF and enhance competitiveness.”

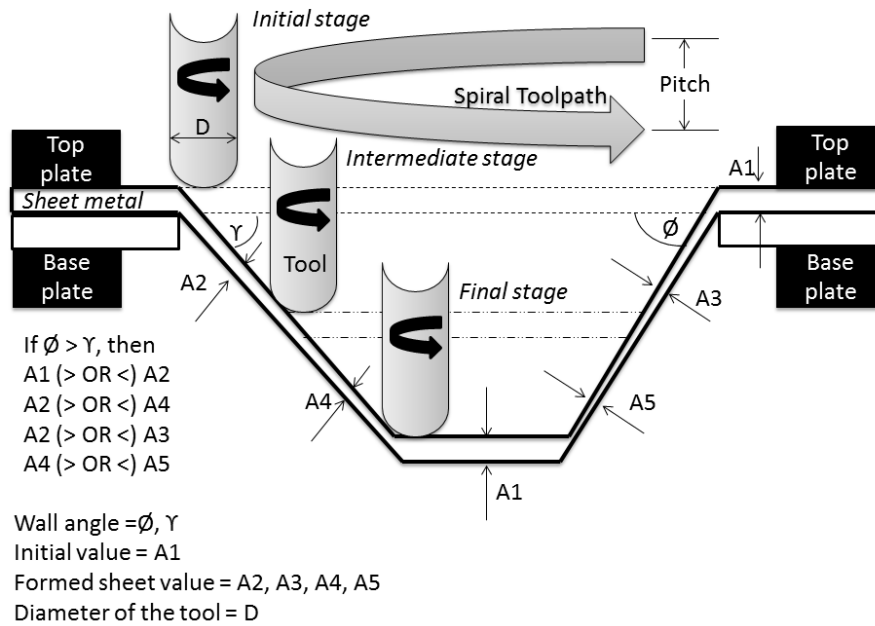


Figure 1-7 Prediction of formed component’s output parameters.

To do this, the author identified that a greater understanding of the decision-making practices in the planning, design, implementation and control of ISF process was required. Figure 1-7 shows uncertainty about a formed component’s output parameters (thickness, strain, grain elongation, material properties, internal mechanism, and behavior) at different locations with respect to the input values and strategies. In the next chapter, a methodology is presented that enhances the understanding of the ISF process.

Currently, there is no effective qualitative test to assess the formability of the component (without resorting to a complex FEA simulation). A first approximation of the relationship between sheet thickness and wall angle is offered by the sine law [62].

$$t_f = t_0 \cdot \sin \alpha \dots\dots\dots \text{Equation 1-1}$$

Where, final thickness is  $t_f$ , initial thickness is  $t_0$  and  $\alpha$  is the wall angle. According to sine law, final thickness would be zero if the forming angle is equal to 90 degree.

The forming thickness of the formed part can be calculated using Sine Law.  $\alpha$  is the angle of between horizontal and the sheet. According to Sine Law, it is impossible to make parts with wall angles equal to or more than 90 degrees. It is given by the equation [62] and shown in Figure 1-8a. It is evident that in reality the sheet metal thickness is different from the results predicted by sine law and highly non-uniform throughout the depth of the part [Figure 1-8b].

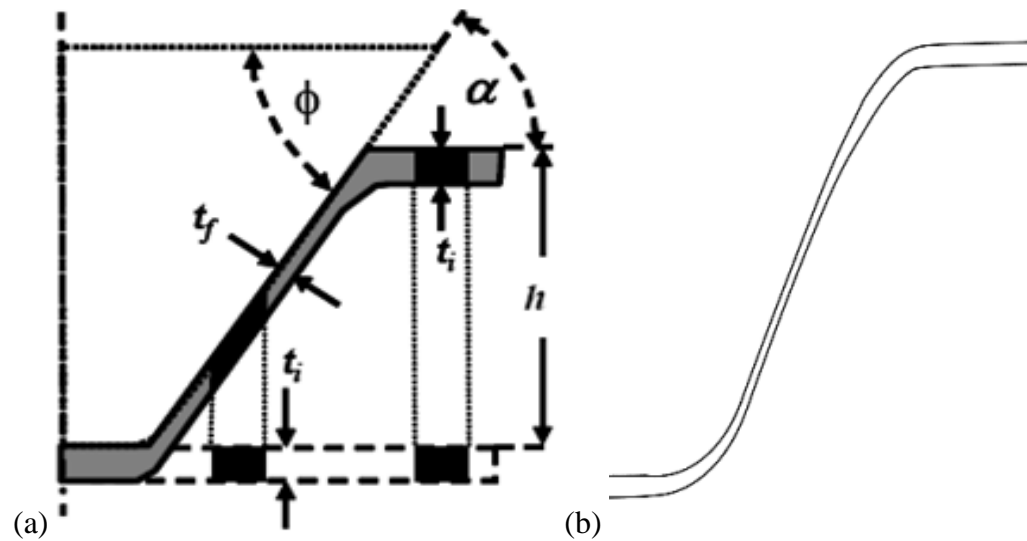


Figure 1-8 Thickness profile; (a)Sine law [62], (b) Reality.

Consequently, the limitations of the sine law have been frequently stated:

“The sine law provided an **inaccurate prediction** of the formed thickness in ISF process. Therefore, it leads to unsatisfactory **geometric accuracy** during process.” [62]

### 1.4.2 Proposed model

The review of the literature (chapter 2) and the author’s experience of the ISF process (Appendix- A) lead to the proposal of the following procedure [Figure 1-9] for an easy assessment method by which design and production engineering can determine the feasibility of a given component.



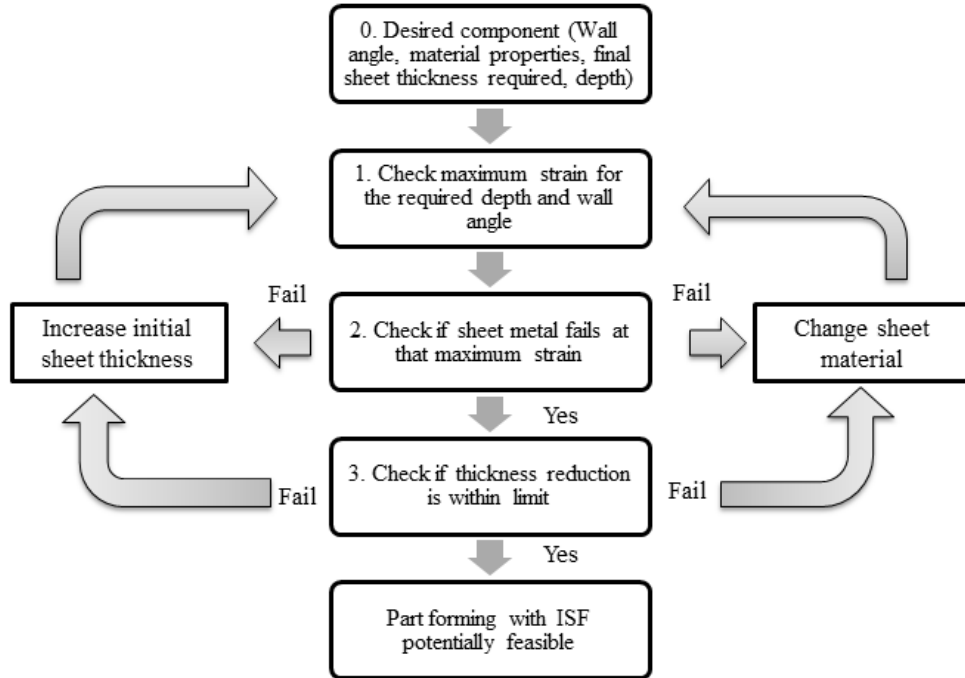


Figure 1-9 ISF-FCheck process.

Literature and initial experiments also suggest that the graphs for steps 1 and 3 will have the general form shown in Figure 1-10. However, questions arise about their form and sensitivity.

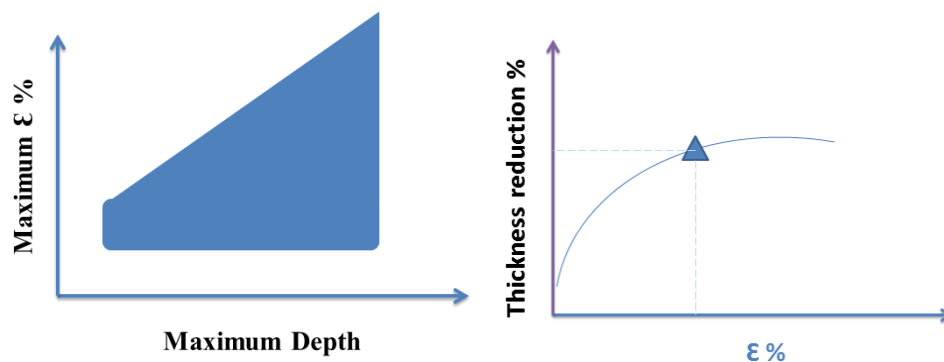


Figure 1-10 Two feasibility charts.

However to enable steps 1, 2, and 3 for materials of interest, following questions and research gaps were identified. For a given material:

1. What is the relationship between maximum strain % and maximum depth? How does it vary with
  - a. Material type

- b. Wall angle
  - c. Feedrate
  - d. Rolling direction
  - e. Clamping
  - f. Geometry
  
2. What is the relationship between thickness reduction % and maximum strain? How does it vary with
  - a. Material type
  - b. Wall angle
  - c. Feedrate
  - d. Rolling direction
  - e. Clamping
  - f. Geometry
  
3. Can simple procedure feasibility predict the ISF process?

Following aims and objectives were derived from these research questions and research gaps.

### **1.5 Aim**

- Understanding the interaction of geometric, material and manufacturing ISF process parameters with resulting properties such as quality, production, mechanics and materials.
- Creation of easy and quick assessment method by which design and production engineering can determine the feasibility of ISF for a given component.

### **1.6 Objectives**

- Through literature review, identify a possible methodology for feasibility assessment.
- Identify and perform experiments to determine the parameter for a feasibility methodology (e.g. different materials, geometries, feedrates, production rate,

accuracy, the effect of rolling direction, thickness, surface roughness, strains and material properties).

- Analysis of results and detail the feasibility assessment methodology's strengths and limitations.

Following is the methodology [Figure 1-11] applied to achieve these aims and objectives. FLC, tensile tests, material characterization, strains, thickness reduction, surface roughness analysis were performed to evaluate the difference of these parameters between pre and post formed components. This data will further help in usability and commercial applicability of the ISF process.

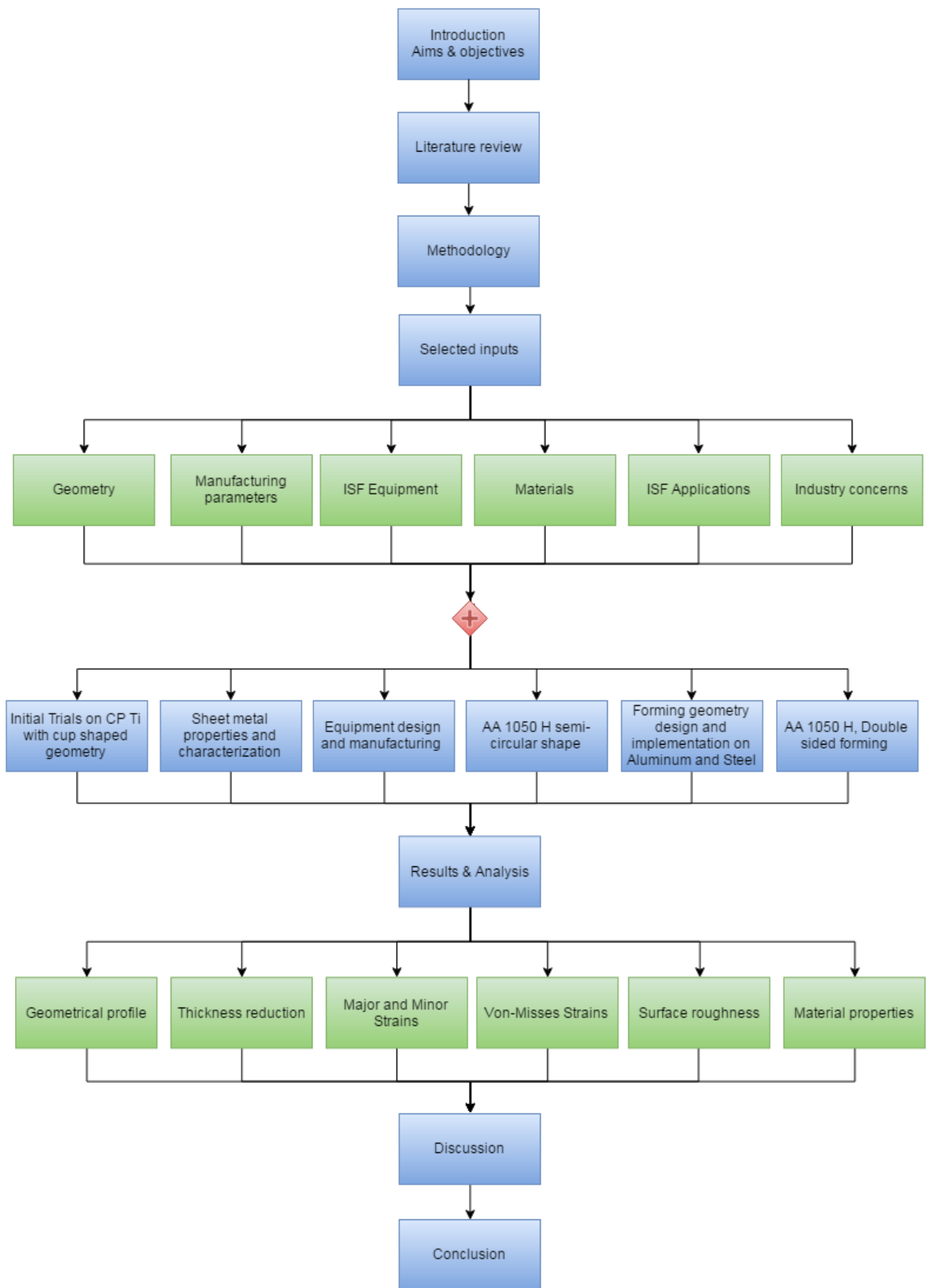


Figure 1-11 Methodology.

## 1.7 Overview

Chapter 1 introduces the concept of Incremental Sheet Forming describes the limitation and the aims and objectives. It summarizes the thesis and how it is divided into various sections and sub-sections.

Chapter 2 constitutes detailed literature review. It starts by discussing the general forming processes used in the industry such as hammering, spinning etc. and focuses down to Incremental Sheet Forming (ISF) detailing its advantages, disadvantages and current areas of research. Important issues like internal mechanics, process accuracy, numerical modeling, material, manufacturing parameters, geometries manufactured, applications, failure modes and cost viability of the process are discussed in detail. By studying different aspects of the process it is concluded that there is a knowledge gap in accuracy, thickness reduction, formability, ISF- FCheck metod, material characterization and surface roughness.

Chapter 3 illustrates research model selection, the methodology applied and techniques selected to acquire aims and objectives of the project. It also gives a brief summary of the research road mapping and the steps take to acquire this data. Experiments are tabulated and discussed. Limitations of the current study are reported.

Chapter 4 demonstrates successful tests, to form sheet metal using different tool sizes, symmetric and asymmetric dome shaped geometries. Spiral tool path was generated with CAM software for tool movement to form the geometry. After which results such as thickness reduction, profile changes, major and minor strains and Von Mises strains were acquired from these sheets using circular grid analysis, 3D scanning and other state of the art methods. All the parts were formed up to their failing point, despite which significant symmetry and evenness of distribution in formed parts was achieved.

Chapter 5 discusses 0.6mm thick, SS304L and 2mm thick, AA1050H, AA2024 and AA7075, sheet metal used to form Multi-slope geometry with variable depths. Ten tests were performed using different rolling directions and feedrates. Part profiles of the

components with and without Backsupporting-Plate were discussed and compared. Results such as thickness reduction, major and minor strains, Von Mises strains and surface roughness were discussed and the equation was presented. Effect of wall angle on these parameters and critical geometric features were discussed.

Chapter 6 discusses if a multiaxis ISF process has different relationship between parameters. Some components are formed in both positive and negative direction with respect to the sheet. Conventional forming processes can easily form parts in both directions of the initial sheet metal. ISF is at its infant stage most of the researchers generally form parts in one direction. Different geometries were conceptualized for this purpose and one of them was finalized due to its versatility and application in aerospace industry. Final conceptual geometry has two features (basin, cross) in both directions. Both these features were formed using different sizes of tools and different methodologies. AA 1050H sheet metal was used to make this part. Results such as thickness reduction, major and minor strains, Von Mises strains and surface roughness were discussed.

Chapter 7 discusses results from all the experiments in terms of objectives of the research. A model for ISF process is also developed through careful analysis of the relationship between the input and output parameters. Based on the discussion of the results and the model internal mechanics of the ISF process were explained. Limitations of the current work and future directions of research are explained. Conclusions were given at the end.

Appendix- A summarizes initial scoping of the ISF process. The author discusses several tests performed to understand the material and its properties in depth. Empirical and modeling results of Titanium tensile testing are given at the start. Manufacturing parameters used to get required shape and their effects on part are elaborated. Springback, profile shape, thickness and other results acquired by 3D scanning are discussed and analyzed. Microstructure and fractography are discussed at the end. The chapter is closed with proposed methodology and future work to be performed.

Appendix- B discusses the material properties and data acquisition systems used to gather data. Tensile tests at three different rolling directions and two strain rates were performed. Stress-strain graphs and other critical material properties were reported. Fractography, surface roughness analysis and strain thickness analysis was performed for these specimens. Nakajima test was performed to acquire forming limit curve data for the sheet metal.

Appendix- C discusses design and implementation of equipment and geometries. A Multi-slope tool for ISF process was successfully designed, manufactured and commissioned. The tool is able to rotate relative to the surface and thus friction is reduced between tool and sheet surface. The author created several concepts and evaluated against the design specifications of Incremental Sheet Forming Process. 3D modeling, visualization and finite element analysis and functional prototypes were assessed before manufacturing the flexible fixture with nylon bushes. Flexible fixture moves as the sheet is being formed. The results suggested that the Scissors design did not have sufficient lateral (i.e. horizontal) stiffness so consequently a 3 pillars concept with nylon bushes was selected as the final design. Polymer sheet with the industrial heater was used to check the functionality and the large vertical movement of the fixture during ISF process. Two new geometries “Multi-slope” and “Double sided” were designed and modeled after analyzing several geometric features. Data acquisition equipment for 3D scanning, surface roughness and surface strains were reported.

Appendix- D incorporates results from chapter 5. Table 1-1 gives research questions answered by individual chapters and Figure 1-12 shows the roadmap of the thesis.

Appendix- E lists hardware and software which enabled this research.

Appendix- F lists overall conclusions and summary of the chapters.

Table 1-1 Research questions answered in results chapters.

<b>Chapter</b>	<b>Q1</b>	<b>Q2</b>	<b>Q3</b>
<b>4</b>		✓	
<b>5</b>	✓	✓	✓
<b>6</b>		✓	✓
<b>7</b>	✓	✓	✓

## **1.8 Summary**

ISF is a process with lots of potential but uncertainty about its process window hamper its widespread adoption. To reduce this problem a design feasibility method is proposed. The subsequent chapters investigate the feasibility and limitations of implementing the proposal method.



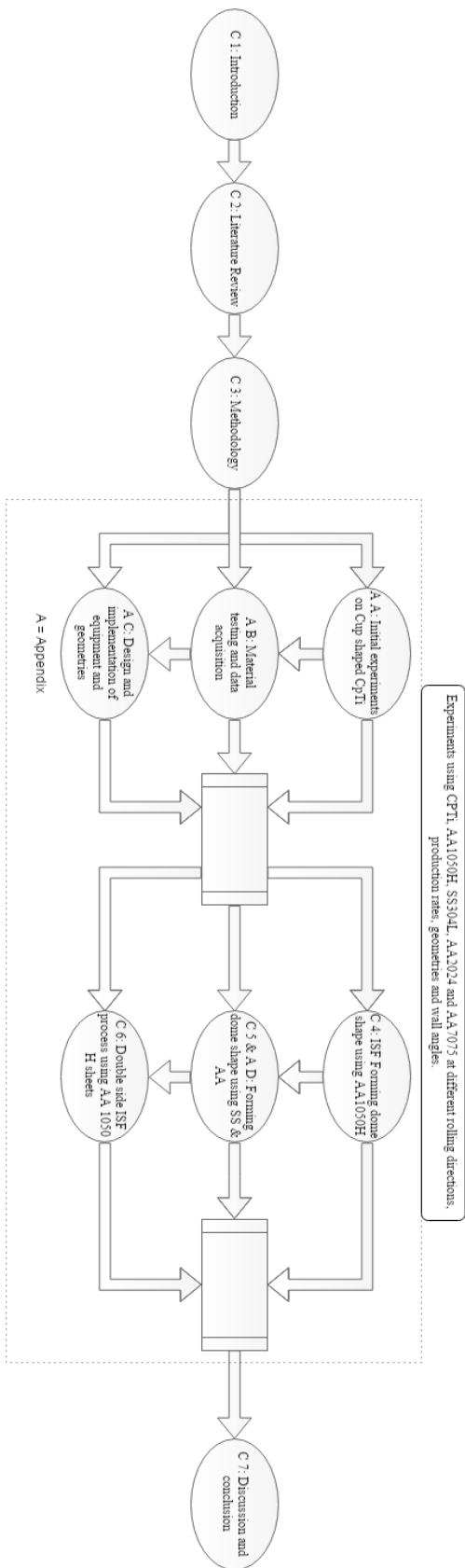


Figure 1-12 Thesis roadmap.

## 2. Literature review

The literature review starts by summarizing the emergence and evolution of the ISF process. After which general forming processes such as hammering, spinning are discussed and before Incremental Sheet Forming (ISF) is described and its advantages, disadvantages and current areas of research outlined. Important issues like internal mechanics, process accuracy, numerical modeling, material, manufacturing parameters, geometric limitations, applications, failure modes and cost viability of the process are discussed in detail. At the end of literature review, research gaps are identified.

### 2.1 Evolution of ISF process

The emergence and evolution of the modern ISF process can be summarized as occurring in three distinct stages [65]:

**Stage 1 Emergence:** The historical origins of modern ISF systems progress from the automation of artisan ‘panel beating’ processes to CNC system over a period between 1700 and 1996. During this period several companies were involved in developing various single point sheet forming technologies. Initial the focus was on variations of spinning processes (see Berghahn [66] and Leszak [67] 1967 patents) however in 1978 Mason’s published a paper which is widely regarded as the origin of the modern ISF process. Mason analyzed different forming processes and identified the processes which are most suitable for low volume batches. He also clearly describes the fundamentals of the ISF process in which a tool follows the contours of the geometry in three-dimensional space [68]. The large contribution of Japanese researchers to ISF started with the work of Iseki et. al [69] during 1989 when (aware of Mason’s work) he developed a sheet manufacturing system using a contour following tool.

**Stage 2 Fundamentals:** Most of the early research into the fundamental engineering science of the ISF process was done by Japanese automotive companies who filed several significant patents between 1993 and 2000. For example Matsubara [70] patented both Two-Point

Incremental forming in 1994 and an extension describing the downward movement of an inclined blank in 1997.

**Stage 3 Development:** From 2000 onward interest and knowledge of the ISF process spread beyond the Japanese automotive industry. Motivated by the simplicity of the ISF process researchers in Europe and American started reporting significant work in areas such as wall angles [71], feed rates [52], path optimization [21], process simulation [72], microstructure [37], springback [61], accuracy [73], applications [74, 75] and equipment design [17]. Interest from the aerospace industry resulted in several well-funded research programs and in 2003 Jeswiet et. al published a comprehensive review of ISF technology [3]. Since 2000 researchers have reported using an increasing range of different methods and technologies for ISF process [10, 15, 76-80].

However despite significant academic work compared to other sheet forming technologies (e.g. spinning, shear forming), the study of incremental sheet forming process is at a much earlier stage and the process's behavior still needs accurate mathematical models for different conditions and specific materials to be developed [17]. Before considering ISF in more detail, the technology can be put in context by considering its relationship with other sheet metal forming processes.

## **2.2 Sheet Metal forming processes**

Following are commonly used sheet forming processes in automotive and aerospace industries.

### **2.2.1 Hammering**

One of the oldest forming techniques is known as hammering. It was initially done manually but the advent of CNC's and robotics has enabled effective automation. Currently, hammering is done with robotic arms whose movements are controlled to follow predefined tool paths. The sheet is clamped in the support frame and the tool punches the sheet to manufacture the required shape as shown in Figure 2-1 [2].

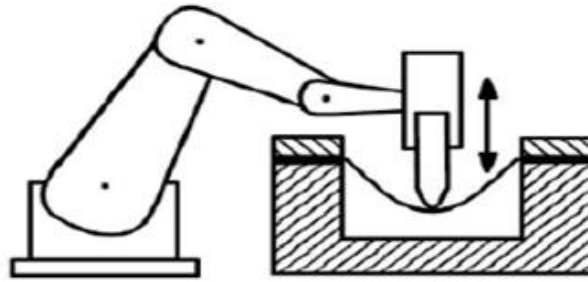


Figure 2-1 Hammering [2].

### 2.2.2 Spinning

Spinning is divided into two types [Figure 2-2]:

- Conventional spinning
- Shear spinning

During Conventional Spinning a rounded tool, or roller, is used to gradually form a sheet over a mandrel. Equipment used for spinning is quite similar to a lathe where the sheet is clamped on the center of a mandrel and tool applies a localized pressure to deform the sheet by axial and radial forces over the surface of the sheet. The tool can be actuated manually or mechanically and mostly it is suitable for producing parts which require only a limited number of step changes in diameter to be manufactured. The difference between Shear Spinning and Conventional Spinning is that in the latter stretching force is applied instead of bending. This influences variation of thickness along the wall following the sine law[81].

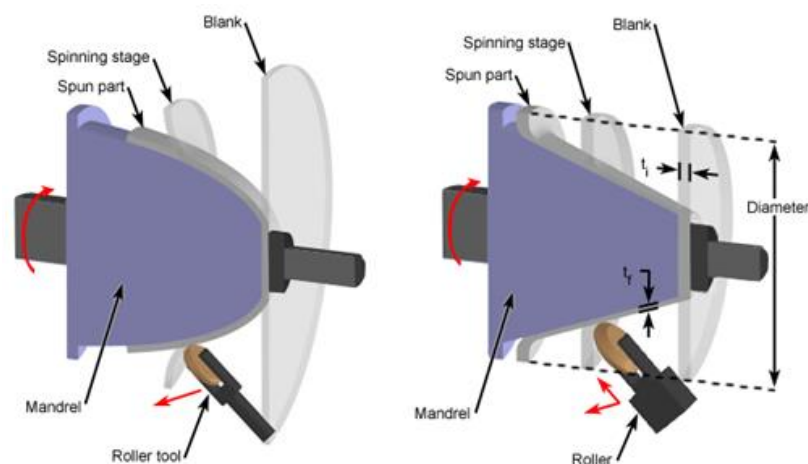


Figure 2-2 Spinning; (a) Conventional, (b)Shear[81].

### 2.2.3 Stamping

Hard tools are used to perform Stamping processes. These processes are used to manufacture a high volume of parts using a single, or multiple, die station. Stamping equipment is categorized into two types: mechanical or hydraulic presses. A flywheel is often used to store and transfer energy to the punch in mechanical presses, while hydraulic presses use pumps to generate a forming force [Figure 2-3]. Size ranges from 20 -10,000 tons, strokes range from 5-500 mm and speeds from 20-1500 strokes per minute. Mechanical presses are used for high-speed blanking, shallow drawing and for making precision parts. Hydraulic presses are suitable for deep-drawing, blanking and coining. Strokes can vary from 10-800 mm. However, despite offer high speed and precision, the process is also associated with high tooling cost (the main disadvantage of this process) [82].

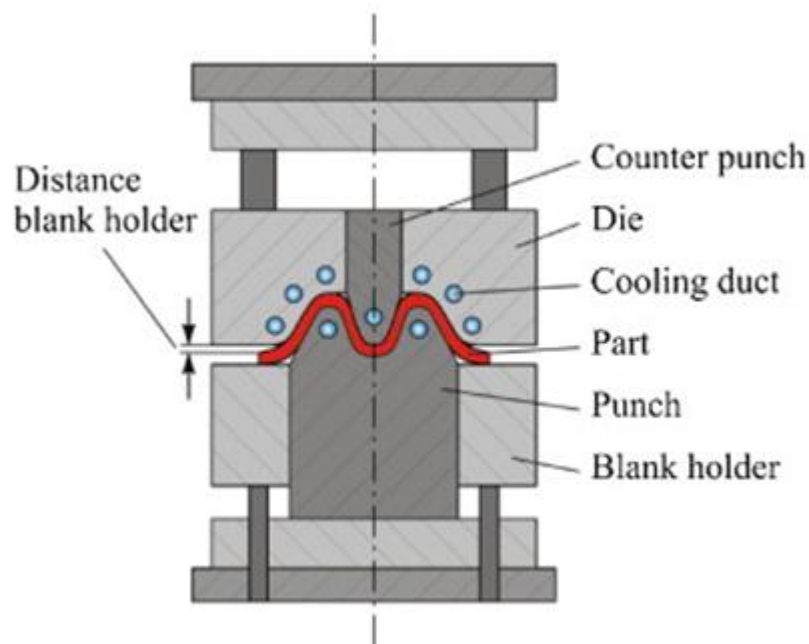


Figure 2-3 Stamping process [82]

## 2.3 Incremental sheet forming

### 2.3.1 General ISF

In contrast to these established forming methods, incremental sheet forming (ISF) is an emerging sheet metal forming process and offers more flexibility in forming capabilities

with low operating costs. It does not require any dedicated dies and it is ideal for rapid prototyping and low production volume operations. Multi-axis CNC machine tools with a hemispherical tip tool and sheet clasper can be used for ISF. In contrast, spinning and shear forming, ISF can form both symmetric and asymmetric shapes. There are various advantages of ISF including flexibility. Flexibility is due to its ability to form parts without dies using only a simple fixture and hemispherical forming tool. It is important to mention here that ISF is low volume production methods with its productivity i.e. cycle time being affected by the size of both the forming tool and the part being formed as well as the type of surface finish that is desired. ISF feasibility is also dependent upon the shape of manufactured part. A basic setup of a forming rig is shown in Figure 2-4 . The fixture is mounted on the worktable of the CNC milling machine and is composed of a base plate and a top plate, which restrict sheet with nuts and bolts. The forming region is defined by tool path generated from the CAM software that in turn creates the localized stresses and force the sheet to deform [2, 13, 83]. Water jet is also used to perform ISF process [84].

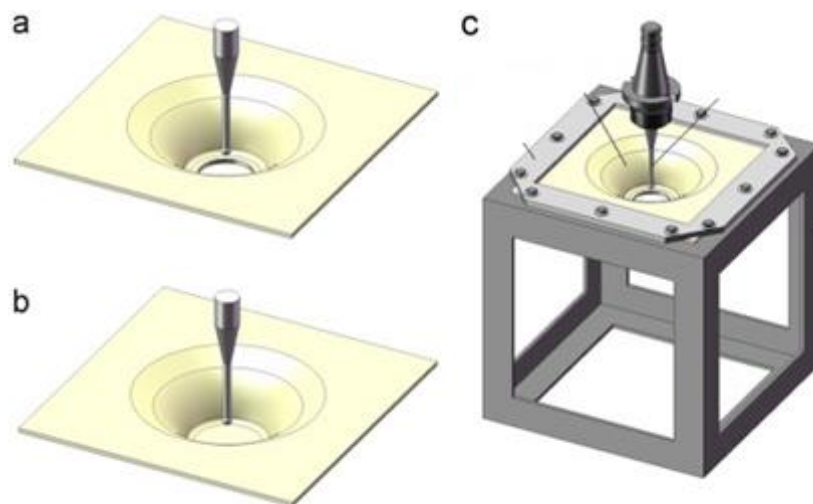


Figure 2-4 ISF of sheet metal blanks; (a) pre-cut concentric hole, (b) conventional (c) Schematic representation of the experimental setup [13]

### 2.3.2 Applications and geometries

ISF was initially developed for the automotive industry but now it is applied in biomedical applications, aerospace industry and the manufacturer of the domestic appliance.

The ISF applications can be separated into several areas i.e. rapid prototyping for the automotive industry, for example reflexive surfaces for headlights, a heat/vibration shield, or scale model of a train represented shown in Figure 2-5, Figure 2-6 and Figure 2-7 respectively. All above-mentioned geometries are formed through ISF process. Researchers have also tried using the process for remaking sheet metal parts for end of life vehicles [85].



Figure 2-5 Reflexive surface for headlights [86].



Figure 2-6 Automotive heat/vibration shield [87].



Figure 2-7 Scaled model of a train[57].

The medical field represents one of these cases which require high customization, in order to assure the best possible performance of the product. Cranial and facial surgeries are very common with biomedical practitioners. Currently, it is very costly and time-consuming to make these components and patients have to go through a waiting list to receive components. These components could easily be formed using ISF within minutes as shown in Figure 2-8. Another example is of manufacturing an ankle support, which is a copy of patient's ankle shape. To ensure the best correspondence between the obtained support and the patient body, reverse engineering approach has been implemented during manufacturing to get the proper fit of equipment on patient's ankle. Some other possible fields of application for ISF are home appliances and marine industry [88]. This not only decreases production time, cost, CO<sup>2</sup> emissions, and energy usage but also gives final product a better and glamorous look.

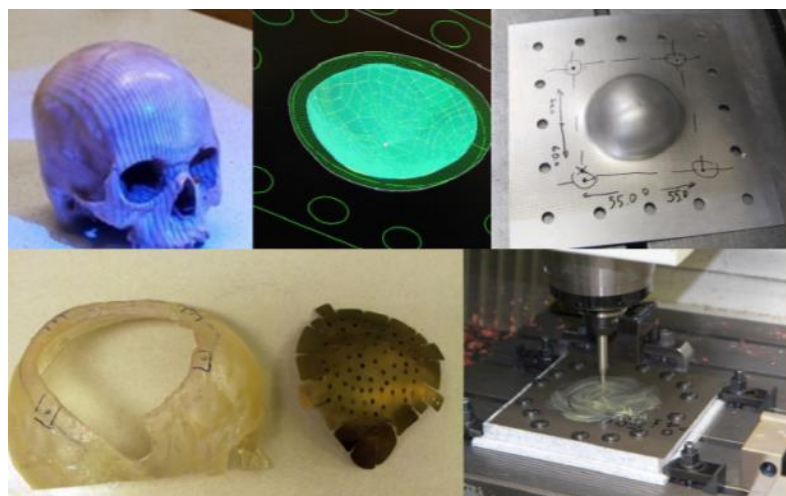


Figure 2-8 Cranial implants formed through ISF process [89].



## 2.4 Researched Geometries

Researchers worked on several geometries which include cones, pyramids, cups and spheres. The size of the part depends on machine capability. Deformation is localized so virtually any part can be manufactured. The geometric shapes that can be formed have a large effect on the forming forces and time depending on complexity. According to the sine law, vertical walls are not possible with this process because it would result in a zero final sheet thickness. Several techniques have been used to improve this limitation including localized heating using laser and multi-pass forming [90],[91]. Hole in the geometry also changes thickness with depth and is different from truncated cone without a hole as shown in Figure 2-9 [13]. The multi-pass method involves forming a part with more than one forming pass. Parts are formed from shallow to increasing angles at each pass until the desired shape is achieved. Forming in multiple steps allows strains within the part to be applied gradually rather than in a single increment. Experimentally, higher accuracies and formability are seen with this method with better thickness distribution.

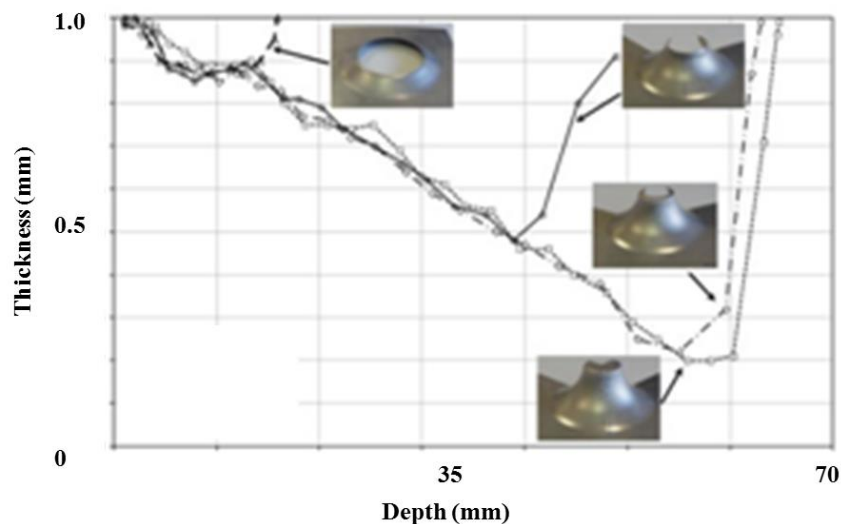


Figure 2-9 Relation of depth with wall thickness [13]

Following is the comparison of different geometries [92].

1. Truncated cone: Experiments have been made for several wall angles starting from  $45^\circ$  up to  $65^\circ$  (every  $5^\circ$ ) and with a forming depth of 30 mm. The step-down is kept at a constant value of 1 mm. The tests performed have shown that rupture occurs at a wall angle of  $65^\circ$  and at a forming depth of 24 mm.

2. Hyperbola: In the performed experiments the step-down is varied from 1 mm down to 0.2 mm similar to the IBT (Bending test). Here it is also observed that the range of strains increases with the decrease of the step-down. For a step-down of 1 mm, rupture occurs at 23 mm.

3. Flower: Experiments have been performed with varying geometrical parameters such as the degree of concavity and the degree of steepness (wall angle). The dependence of the strain range on these two parameters has been thoroughly studied using FE calculations. The numerical analysis has shown that the range of obtained strains widens with increasing concavity and wall angle. The influence of the step-down size has been studied as well. The geometric shapes analyzed yield strains for SS DC04 as shown in the diagrams.

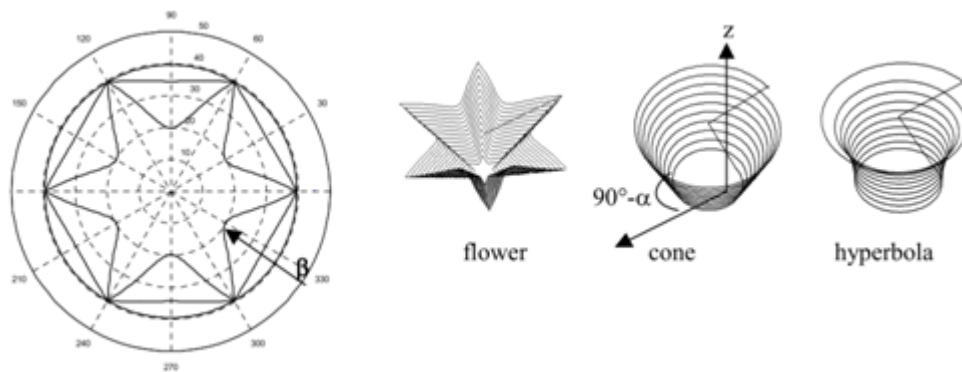


Figure 2-10 Test shape toolpath (cone, hyperbola and flower) [92]

## 2.5 Forming Equipment Design

A list of the types of machines available to do incremental forming is:

- CNC milling machines
- Purpose-built machines
- Robots, Stewart platforms and Hexapods

There are several different aspects of ISF technology being researched by different groups around the world. One of these research areas is the design of equipment to perform ISF processes. Broadly speaking incremental sheet forming processes can be classified as one of the following: bespoke purpose-built machines, adapted CNC machine tools and adapted robots [18]. The following sections describe each of these categories:

### **2.5.1 Purpose built ISF machines**

Several groups have created dedicated ISF machines. For example, Powell created a machine to support experimental work on titanium sheet [93]. Similarly, Allwood et al [17] reported the design of a machine, at Cambridge University, specifically for ISF process research that incorporates load cells to acquire forming force data as the tool moved in X, Y and Z axis. Matsubara [16, 70] further contributed to bespoke ISF equipment with several patents which described fixtures for single point incremental sheet forming that incorporates guiding and supporting bars for used with CNC machines. The vertical movement in Matsubara's fixture was actuated with two servo motors. Kitazawa reported work carried out on a rotating blank using a CNC machine [94]. Motivated by the needs of automotive manufacturers Amino's [4] company developed a commercial system for ISF. Another specialist machine for the ISF process was built for University of Saarbrücken by a Japanese company [95, 96].

### **2.5.2 Adapting CNC milling machines for ISF**

However dedicated machines are the exception rather than the rule and most research on ISF has been performed using conventional CNC machines [19, 97-100] adapted with suitable tools and fixtures [99]. Use of CNC machines is an attractive approach because of their availability and low cost (compared to other methods). A good example of this approach is the system reported by Thibaud et al. that consist of a fixed die support, a modular die, a sheet holder and attachment screws. The ISF tool is mounted on the CNC machine and a 4-axis dynamometer is used to find forces and torque during the process [101]. Similar equipment has been used by both Ambrogio et al. [102] and Duflou et al. [103]. Although the vertical movement of positive ISF fixtures is easily illustrated schematically its implementation is challenging because of the need to create a structure that is both rigid (i.e. does not tilt horizontally) and compliant (i.e. free to move vertically as the sheet deforms).

### **2.5.3 Robotic ISF systems**

Rather than moving a forming tool with a CNC machine other researchers have used multi-axis robots to generate forces and paths. Meier et al, for example, reports the use of industrial robots, shown in Figure 2-10d to form rectangular sheets into standard geometries

(cones, hemispherical, pyramids). The system supported the forming 200X200mm sheets (with a thickness between 0.5 and 1 mm). The machine consists of fix clasper, a forming tool and a supporting tool. Both tools are mounted on industrial robots which move through a programmed series of movements [18]. KU Leuven and IWU Fraunhofer Institute of Machine Tools and Forming Technology designed and manufactured a vertical table with clamping system for use in robot based ISF process [104]. A coolant supply was integrated with a 6-axis robot that was used to perform an ISF process (a similar arrangement is described by Callegari et.al [20]). Imre Paniti used FANUC S430-iF type industrial robot while describing how ISF can be provided as a flexible manufacturing service [105] . A summary of the ISF systems reported in the literature is shown in Table 2-1.

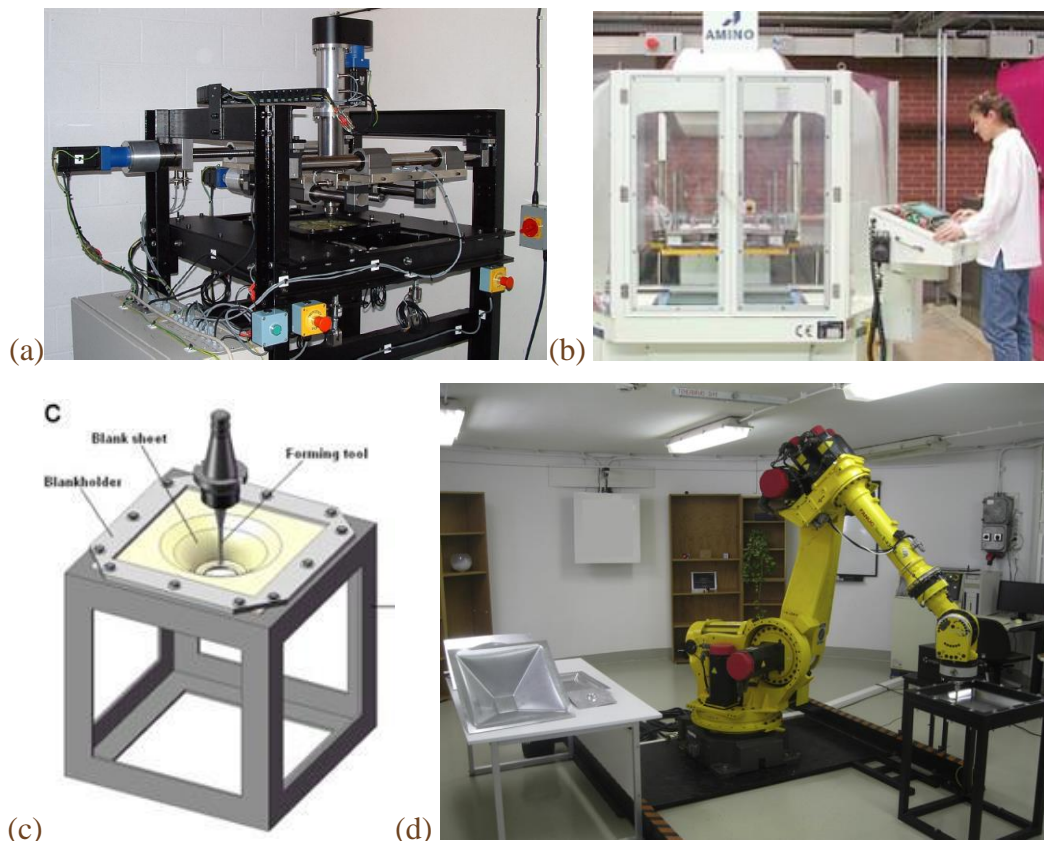


Figure 2-11: Fixture Design; (a) Purpose built [17], (b) purpose built AISF machine [106], (c) for CNC milling machine, [99], (d) Robots [105].

Table 2-1: Reported ISF Machines.

<b>Machine Type</b>	<b>Work piece area (mm)</b>	<b>Comment</b>	<b>System</b>
<b>Custom made</b>	300x300	Force sensors on tool	Allwood [17]
	Variable Custom made	Commercial system	Amino [4]
<b>Industrial Robot</b>	200x200	Supporting die feature	Meier [18]
	Not provided	Sheet clamped & formed with robotic arm	Leuven and IWU [104]
	180x180		Callegari [20]
	500 X 500		Imre Paniti[105]
<b>CNC Machine</b>	300x300	Conventional ISF process	Jesweit [7]
	34x34	Micro forming	Thibaud [101]

#### 2.5.4 ISF tools

Following literature was reviewed to identify specific research questions regarding tool design and performance:

Li used static (i.e. non-rotational) tools of two sizes i.e. 20mm and 10mm to perform an ISF process with a support die on an Aluminum sheet. Both lubricant (to decrease friction) and a two-stage forming strategy were used to manufacture the test component, however despite this serious cracks were reported [107]. Kim et. al used two different types of tools i.e. hemispherical and a ball tool. It was observed that the sum of major and minor strains increased for both types of tools when lubrication was not used and was fractionally more for a ball tool compared to a hemispherical one [52]. Liu et al used a spiral tool path to connect the contours of the formed shape [108]. Ham et al., concluded that step size has an insignificant influence on formability [109]. While Hagan et al states formability increase with speed but there are several tradeoffs including higher surface roughness, increased tool wear rates and surface defects [11]. Forming at high rotational speeds also increases the probability of tool chatter and contour trace marks on the surface [7] . Researchers have performed experiments by forming sheets into different shapes and sizes [92]. Peteket. et al reported the maximum force under 2kN to form steel DC05 [110]. Li et. al reported different forces at different wall angles for Al7075, with the maximum value of 2.5KN for 1.6mm thick sheet [111]. Mecanica et. al. said in her study that higher formability can be achieved through smaller tool radius. She argued that due to small tool size frictional heating is localized and high in magnitude. [112]. Although the literature suggests rotating tools could (in theory) produce benefits from reduced friction little work has been reported to establish how the rotating ISF tools influence thickness, strain and surface roughness.

## **2.6 Manufacturing Parameters**

Forming angle, step size, tool path, forming speeds (feed rate), tool size, shape, lubrication, and sheet material are important process parameters of ISF. These parameters are explained below to evaluate their influences on forming parameters and the formed part.

### **2.6.1 Forming Tool path**

Toolpath is generated after making a CAD model. Spiral or step transition method is used to connect tool contours. Tool path does effects thickness and formability [6]. Researchers are studying toolpath compensation [113], enhancement of accuracy through toolpath [14] and toolpath optimization through programming [21]. Figure 2-10 shows toolpath generated by

CAM software [92]. Blaga et. al. reported spiral tool path is the most optimum one. He further added that it reduces 18% major and minor strain and 13.5% thickness reduction compared to step tool path [59]. Paniti et. al. put forward a new tool path calculation approach for the double sided ISF process [114]. Duplex incremental sheet metal forming was performed by Mier et al. with peripheral and local support using two moving tools [115, 116].

### **2.6.2 Forming Angle**

Forming angle is the angle that walls of a specimen make with the horizontal plane. Every material has its limitation to which it can be formed without rupture. Martins et al. predicted the maximum forming angle(max) using thickness and strain at the time of fracture [117]. According to the sine law

$$t_f = t_o \cdot \sin \alpha$$

Where, final thickness is  $t_f$ , initial thickness is  $t_o$  and  $\alpha$  is the wall angle. According to sine law, final thickness would be zero if the forming angle is equal to 90 degrees.

The forming thickness of the formed part can be calculated using Sine Law.  $\alpha$  is the angle of between horizontal and the sheet. According to Sine Law, it is impossible to make parts with wall angles equal to or more than 90 degrees. It is given by the equation [62] and shown in Figure 2-12.

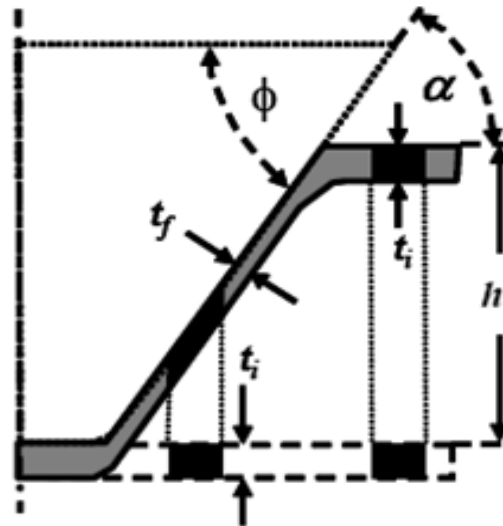


Figure 2-12 Sine law [62]

Where, final thickness is  $t_f$ , the initial thickness is  $t_i$  and  $\alpha$  is the wall angle. According to sine law, final thickness would be zero if the forming angle is equal to 90-degree. To increase wall angle, the initial thickness of the sheet can be increased but obviously, this strategy has limitations on the maximum machine load and overall part thickness specifications. Maximum forming angle is also influenced by step-down increment and tool diameter [62].

In order to achieve higher forming angles near to 90 degrees several authors have already adopted multistage strategies. To achieve higher forming angle in multiple passes, a large offset from the backing plate is preferred for the first passes since this allows for more bending, avoiding extreme strains near the top of the part and after that, the sheet is deformed in successive turns. This approach allows reducing the sheet thinning effect which leads to fracture and also to redistribute the material from the bottom of the sheet which in the case of ISF remains untouched as a result higher forming angles could be achieved with homogeneous sheet thickness [62]. Skjoedt et al. [112, 118] proposed a solution to obtain cone shape with nearly vertical walls, for ISF without support through a forming strategy.

### 2.6.3 Tool Size

Tool size affects formability and surface finish of the manufactured part. Researchers have presented different opinions on tool size effects.



As per Martin et. al. higher formability can be achieved by using smaller tool radius. Smaller tools induce higher strains in the sheet because of a concentrated zone of deformation. Furthermore, for a smaller tool the forming forces decrease due to the decrease in contact area between the tool and the metal plate hence lower stresses are attained and as a result there is a smaller probability of the sheet to fail under low-stress conditions. Due to small tool size, frictional heating is localized and high in magnitude. Both heating and strains allow material to flow easily thus increasing formability [112].

Ghulam et. al. reported that smaller tool size will increase stress concentration at the sheet metal and tool tip contact, especially when step size increases [119]. They further report in another study that pillowing effect and defects increases inversely to the tool radius and thus accuracy decreases [9].

#### **2.6.4 Step Size**

Step size directly influences formability, the duration to form the part and thus cost. Ham et al., concluded that step size has an insignificant influence on formability [120]. Ghulam et. al. reported that larger step size increase stress concentration at the sheet metal and tool tip contact [119]. Still, more evidence is required to establish this conclusion as several researchers hold that by increasing step size formability decreases. The roughness of a formed part is coupled with the step size, forming angle and size of the tool.

#### **2.6.5 Forming Speeds**

Formability increase with speed because of friction heating effects but there are several tradeoffs including higher surface roughness, increased tool wear rates, surface defects such as sheet waviness and lubricant film breakdown [121]. Forming at high rotational speeds also increases the probability of tool chatter marks on the surface[83]. Ghulam et. al. reported that the forming speed is one of the most important factors that affect the formability and that higher formability is expected at lower forming speeds [119]. Ambrogio et. al. investigated development of high speed machinery and its effects on ISF process [122].

## **2.6.6 Lubrication**

Research on lubrication in ISF is limited. Forming generally has low feed rate than milling or machining thus tool wear is not one of the major concerns but in the case of warm forming lubrication plays a key role in terms of surface roughness. Alwood et. al. reported surface damage during ISF process without the use of lubricant [17]. Ghulam et. did studies on CPTi and reported that organic lubricant is not appropriate and proposed that petroleum jelly mixed with MoS<sub>2</sub> is suitable [123].

## **2.7 Mechanics and Materials**

Researchers working in ISF have a difference of opinion over the mode of deformation where some think it is due to shearing while others think it is due to stretching [124]. There is a possibility that deformation is due to shearing, bending and stretching, but the mechanism has to be studied thoroughly to reach a conclusion.

### **2.7.1 Materials**

The experiments used to validate the fixture design reported later use both plastic and metal sheet to verify different aspects of the rigs kinematics and mechanical properties. A fundamental aspect of this approach to the design's functional validation was to understand the parameters of these materials behavior in the context of an ISF process. This was done by review of the literature.

For example, S. Le et al [125] discusses the relationship between tool, step size, feed rate, spindle speed and formability of thermoplastic sheets. Different polymers were studied to and their appropriateness for the ISF process established by considering: springback, ductility, cost and aesthetics. High formability of plastic sheet was achieved through cold forming (ISF). Yonan et.al discussed plastic flow and failure in Single Point Incremental Forming (SPIF) for conical and pyramidal shaped parts. Linear strain loading paths were applied to empirically demonstrate an analytical framework's conditions [126]. Martins et al analyzed several polymers for ISF process and established that certain polymers have particular material properties that make them suitable for ISF. For instance, polyethylene terephthalate exhibits high formability, similarly, polyamide can also attain high formability

if twisting is prevented. Polycarbonate (PC) keeps its transparency after deformation and Polyvinyl chloride displays minimum springback [127]. However, wrinkles appeared in all the parts formed from plastic sheet regardless of the composition. The literature confirmed that it was feasible to use a heated polymer sheet to test the fixture's kinematics (i.e. vertical movement) in the absence of unbalance forming loads.

A much large literature exists on the ISF of different metals. For example Meelis et. al. conducted a study to quantify the forces involved in an ISF process that used aluminum. He also concluded that there are accuracy problems in ductile materials such as steel and aluminum due to spring back [42]. Ham and Jeswiet also discussed the accuracy of the ISF process for aluminum [40]. Robert et. al. discussed the manufacturing of large components with steel using an ISF process and discussed it with respect to the kinematics of the tool. He used wide but shallow geometries with low wall angles to perform his study taking around two hours to make each part. He concluded that the parts had greatest springback at the center, similar results were reported by Muftooh et. al. [12, 128]. Researchers also performed a study on the influence of the forming strategy on the main strains [59], thickness reduction [60, 129] and strain hardening [63] during ISF process for sheet metal. He used a spiral contour and stepped tool paths to conduct his study and concluded that spiral path is the optimum one [59]. Because the creation of the ISF fixture is motivated by an ongoing investigation in the ISF of titanium sheet the literature provide the basic design parameters of loads and deflections and also provide insight into the details of the experimental validation (e.g. a spiral tool path was used to check the response to unbalanced loads). Similarly Petek et. al. performed a force analysis while using ISF to form steel sheets [110] and so this value was adopted (with an additional factor of safety) for the fixture's specification.

### **2.7.2 Forces**

The crucial parameter in the design of an ISF system (i.e. sheet fixture and tool) is the magnitude of localized force applied to the sheet. Part of this force is transferred to the structure of the equipment while rest is used to deform the sheet itself. A study of force developed during the ISF of a steel DC05 sheet by Petek et. al. reported that the maximum force was just under 2kN [110]. Blaga et. al reported that increase in force applied by the machine is directly proportional to the forming depth of the component [59]. People

working in ISF are concerned about the forces due to limitations of the CNC machines. In a study carried out by Nyahumwa, it is shown that most of the energy transmitted through the tool is used to push the sheet down i.e. axial direction of the tool. It is also concluded that if tool diameter, forming angle or step size increases the forces for the machine will also increase and step size has the minimum impact on the parameters mentioned above[83].

### **2.7.3 Deformation and strains**

#### **2.7.4 Stress**

Researchers working in ISF have a difference of opinion over the mode of deformation where some think it is due to shearing while others think it is due to stretching [124]. There is a possibility that deformation is due to shearing, bending and stretching, but the mechanism has to be studied thoroughly to reach a conclusion.

#### **2.7.5 Thickness reduction**

Thickness reduction is a key area of interest for both academia and industry. Attanasio et al. reported tool path optimisation and its effects on thickness, accuracy and surface roughness [130]. Duflou et al. analysed several output parameters including thickness, wall angle and pitch [131]. Li et al. present a multistage tool path study of ISF and tried to improve thickness distribution while forming a vertical wall [108]. In another study, he verified his numerical model with empirical results. He concluded that minimum thickness can increase if the thickness is uniformly distributed throughout the component. But springback increases due to multistage forming [132]. Young et. al. concluded that thinning is severe in steeper wall angles and could be avoided through multiple stages [60].

#### **2.7.6 Surface roughness**

The surface texture is a very important parameter in sheet metal components. In conventional processes, surface texture is dependent upon die, workpiece and forming parameters. It is very important to mention here that cost of manufacturing increases directly with the surface finish as processes such as grinding etc require time and equipment. The increased cost of the final product is justified through added value in terms of longer

lifespan, aesthetics or better function. Parts with sliding contacts with other metals or fluids for instance air have increased life span and function better if they have good surface finish. The surface finish also influences crack initiation in components under fatigue loading. Surface finish depends on surface lay, residual stress and surface roughness. Currently, the effect of residual stress is not quantified in stress analysis, thus engineers use surface roughness values to evaluate fatigue limit in mechanical engineering design problems [23]. Several researchers evaluated the influence of surface roughness on the life of component through S-N curves [24]. Researchers have divided life of component into fatigue crack initiation life and the fatigue crack growth life and they have concluded that the influence of roughness on the fatigue strength is only influencing initiation stage. It is important to mention here that fatigue crack initiation life predominantly determines the total fatigue life of a machine element [25, 26]. Hagan et. al. performed a surface roughness analysis on Al 3003 [11]. Attanasio et al. reported tool path optimisation and its effects on thickness, accuracy and surface roughness [130]. Hagan et. al. reported that spindle speed had an insignificant effect on surface roughness and minimum surface roughness was measured at 1500 r/min. He concluded that this might be due to a combined effect of surface finish of the tool and vibration of mill head [11]. Due to the importance of surface roughness because of reasons mentioned above, in current study surface roughness for formed and unformed are measured for different materials and geometrical features. Average surface roughness (Ra) is generally used to express surface roughness and is the ratio of the absolute value of the integral of surface roughness to the length of the surface. Profile of surface roughness is given in Figure 2-13 and is given by the equation. Where L is the length of the profile and Z is the measurements of a surfaces peaks and valleys and is integrated throughout the profile.

$$Ra = \left(\frac{1}{L}\right) \int |Z(y)|dy \dots\dots\dots\text{Equation 2-1}$$

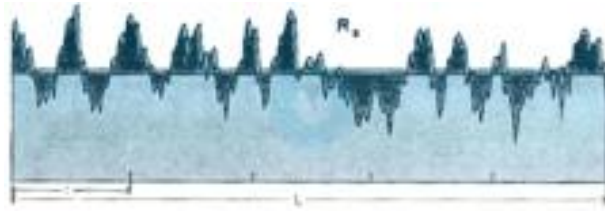


Figure 2-13 Surface roughness.

### 2.7.7 Material characterization

Material characterization is at its infant stage in ISF. Only a hand full of researchers shared microscope images, still did not discuss the change in microstructural behavior in detail. EBSD results were not found for any material type or geometry. Following are the studies reported on microstructure characterization of ISF process. Ma et. al. discussed the change of grain size and took images through a microscope at 200X [133]. Babu et. al. performed experimental studies on SS 304 and reported images of the microstructure. He reported the grains were elongated (strained) with reduced thickness, stress bands were formed and phase was changed during ISF process [134]. Babak et. al. studied microstructure, formability, and hardness at different temperatures for Magnesium alloy. He concluded that a detailed EBSD analysis is required to detect recrystallization zone [135]. Linda et. al. used laser heating during ISF process of Ti6Al4V, analysed microstructure and oxidation at different temperatures [136].

### 2.7.8 Failure

In the case of rotational symmetric ISF, there are two modes of crack propagation as shown in Figure 2-14 [137].

- Straight crack propagation
- Zigzag crack propagation

The straight circumferential crack propagation path is identical to cracks originated during conventional deep drawing or stamping processes and this type of crack propagation is generated due to the stretching mechanism. The zigzag path of crack propagation is probably caused by friction due to rotation of the tool. Crack tip at point a shown in Figure 2-15a will be at a much lower level of stress than any other point. Consequently, the propagation of the

crack stops and the rotation of the tool will drag it to point b which is similar to the initial point o restarting the crack propagation. This cyclic mechanism gives the typical “zigzag” morphology to the crack. Figure 2-14 shows different modes of deformation and failure during ISF of a conical flange with varying slope. Silva et al. discussed the mechanics behind the fracture of sheet metal between corner feature and inclined wall. They also discussed deformation and formability to enhance predictability with the help of numerical models [13].

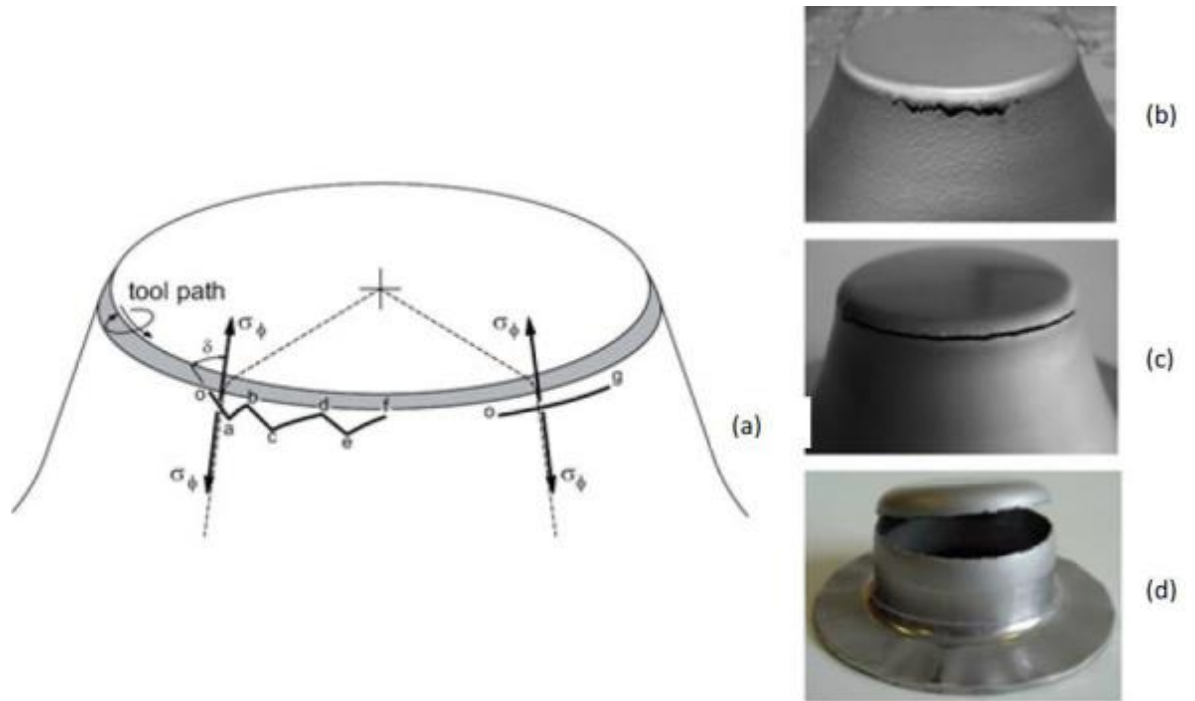


Figure 2-14 Crack propagation in ISF;(a) Scheme,(b) Zigzag,(c) Straight,(d) Straight (part obtained by conventional forming) [137].

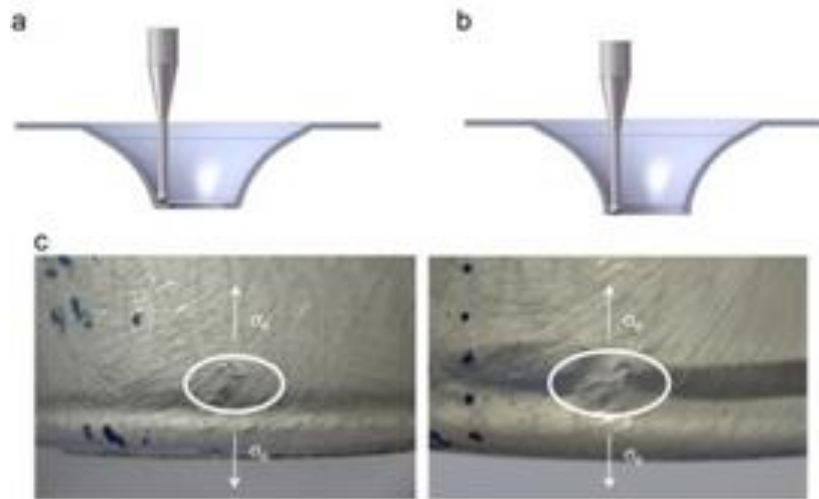


Figure 2-15 Deformation, failure and plastic deformation during ISF; (a) In-plane stretching, (b) plastic deformation, (c) Failure by cracking [13].

According to theory, fracture strains could be calculated through normalized Cockcroft-Latham [138] criterion given in

$$\int_0^{\epsilon_{eq}^{fr}} \frac{\sigma_1}{\sigma_2} d\epsilon_{eq} = C \dots\dots\dots \text{Equation 2-2}$$

Where, maximum stress is  $\sigma_1$ , and the equivalent strain and stress are given by  $\epsilon_{eq}$  and  $\sigma_{eq}$ .  $\epsilon_{fr}$  represents the fracture strain. The volume of the sheet remains constant. These results can also be explained by the empirical formula given in , where  $\epsilon_1$  and  $\epsilon_2$  are the major and minor strains [139].

$$\epsilon_1 + \epsilon_2 = \epsilon_{fr} \dots\dots\dots \text{Equation 2-3}$$

## 2.8 Process accuracy

The main shortcoming in SPF is accuracy. According to [83] most of the applications require dimensional accuracy of less than 1mm and significant number require 0.05mm as tolerance level but [140] reports 1.5mm as minimum tolerance level for SPF. Reprocessing after reversal of workpiece is suggested to correct unwanted deformation along the edge of the part. Ham et. al. also performed a study on dimensional accuracy [40]. Duflou et. al. reported improvement in accuracy through using a laser during ISF process [91]. Micari et. al. reviewed current trends about dimensional accuracy [61]. Arshad discussed accuracy and



formability of 2024, 6061 and 7475 Aluminum alloys [2]. Figure 2-16 shows the accuracy of the formed component.

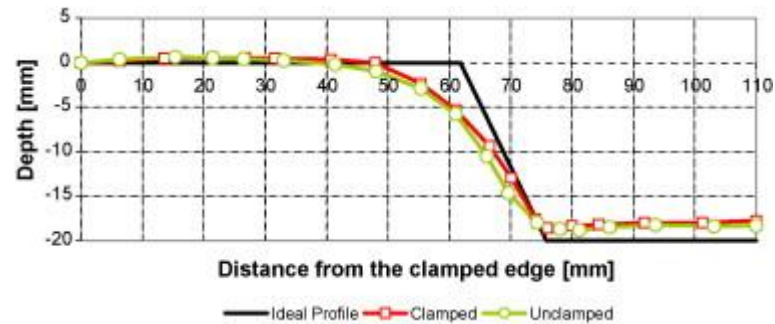


Figure 2-16 Accuracy of the formed component [61].

### 2.8.1 Springback

Besides machine tool inaccuracies spring back also plays a major role in part profile deviation from the designed one [113, 141]. There are three types of spring back

1. Local springback, continues at every displacement of the tool.
2. Global springback, that occurs after unloading and unmouting of the part .
3. Global springback after trimming the part from the sheet

### 2.8.2 Toolpath compensation

Asghar et. al. designed a toolpath to increase the accuracy of the final part [14]. Integrated accuracy improvement strategy generation of complete parts can be achieved by following a three step procedure [113, 141].

1. Identify part features and their interaction that results in accuracies.
2. Introduce compensation strategies for each individual feature and interaction based on the know-how for the specific feature or interaction.

## 2.9 Numerical Modeling

FEA modeling of ISF is important because

- It will reduce the material wasted on ISF tests.

- Save the time required to perform the tests.
- Can predict and optimize process parameters.
- Stress, strains, FLC and other properties can be predicted during manufacturing and while in use.
- Can predict service life of the manufactured part.

Explicit method is considered to be ill-suited for the prediction of springback[83]. Bambach did a benchmark analysis of the AISF process with implicit and explicit FE models for symmetric cup using Abaqus, results are shown in Figure 2-17 [142].

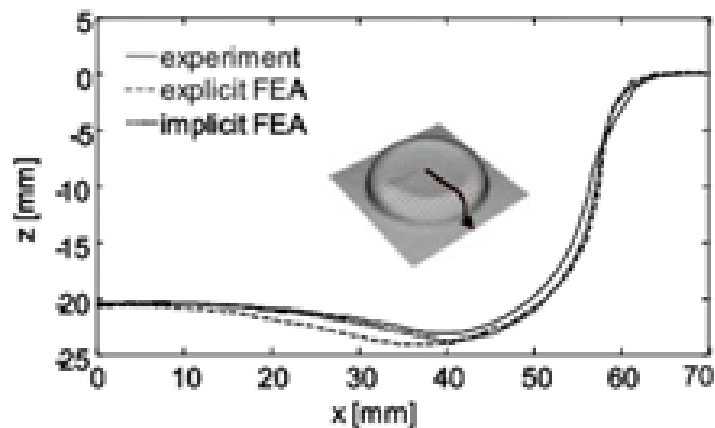


Figure 2-17 Comparison of calculated and measured part geometry[142]

Duration of calculation is the major obstacle in the models being accurate. Refinement, de-refinement approach and direct sub-structuring methods are used to reduce computing time. In RD approach grid points are added where accuracy is required and computing time is reduced by 50% [88]. According to Hirt, only deformation zone is modeled using plastic model and thus is treated by fully non-linear method which is a cheap calculation and is known as Plastic Linear Elastic (PLE) approach[106]. ISF simulation concluded that deformation is localized and is close to plane strain condition [142]. A finite element model for DC56 sheet was developed by Juncao et al. using multistage forming [143]. A simulation of pyramid forming was performed using DC04 sheet by Jun-cao et al. [144].

## 2.10 Research classification

Research in ISF can be classified into following areas [88]

### 1. Forming method

2. Sheet material
3. Tool-path strategies
4. Forming equipment
5. Forming limits
6. Process simulation

## **2.11 Economics**

Customary metal stamping processes include expenses related to the equipment's utilization and required set-up times. Punches and dies are generally fabricated to be close to the shape to be acquired and are used to enforce the preferred deformation to the sheet. Consequently, the industrial application of conventional metal stamping technology can be economically justified only for mass-production of electric and automotive appliance components, where the expenses due to die manufacturing and set-up are dispersed over a huge amount of parts [145].

### **2.11.1 Economic Analysis**

Due to high cost of the dies in sheet metal forming, conventional forming processes are suitable only for high-volume production. However, the pattern of demand for sheet metal product has undergone a change, which necessitates small-batch sizes. Single point incremental forming (SPIF) is a die-less forming process and can be employed for customizes sheet metal products made in small quantity [2]. Though the cost of the die is less, the cost of the machine tool is high in this case. Cost models for two types of parts have also been proposed. A sheet metal product is usually produced with dies and punches manufactured in accordance with shape and dimension of the components. Other than adjusting the company to a low volume production, the correct forming procedure must be selected. Following procedures should be performed for low volume efficient production during the forming process [146].

- Lead time reduction.
- Changeover time reduction between different products.
- Tool development time and cost reduction.

- Tool manufacturing time and cost reduction.
- Flexible Manufacturing System.
- Flexible tooling, e.g. incremental forming or fluid forming

### 2.11.2 Break Even Analysis

Break-even analysis is performed by classifying variable and fixed production costs. Variable costs are the expenses that vary when the production volume changes whereas fixed costs are not directly related the volume of production. Total cost which is the addition of variable and fixed costs are compared with revenue generated through sales to determine the level of sales volume or sales value. It also shows the amount of production at which the business makes neither a loss nor profit as shown in Figure 2-18.

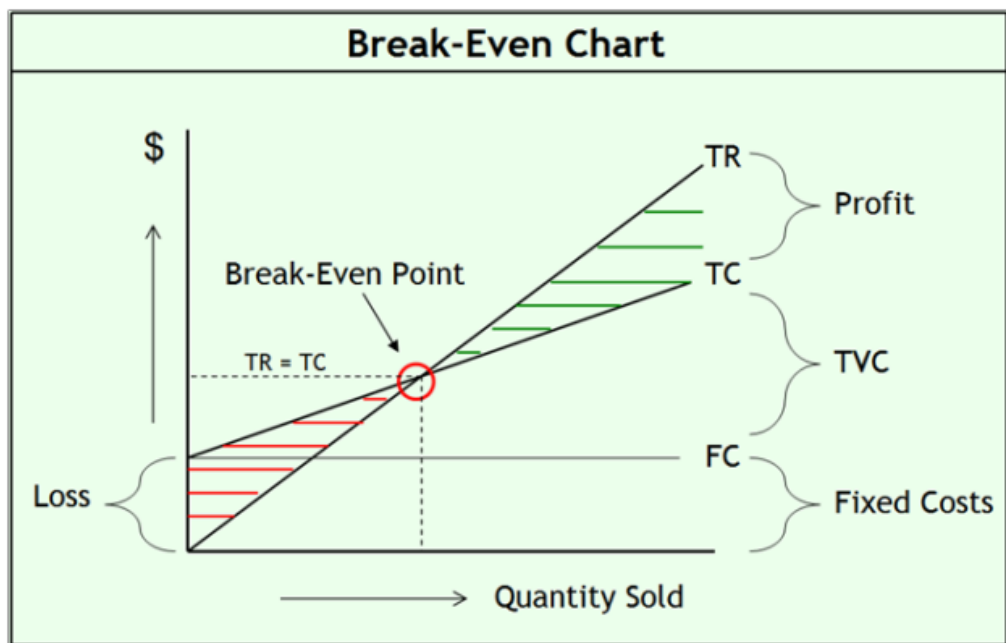


Figure 2-18 Schematic of breakeven point [146].

As shown Figure 2-18, the X-axis represents quantity sold where Y-axis represents revenue generated. FC represents the fixed cost, TVC shows total variable cost, TC is the total cost and TR is the total revenue generated. As it is evident from the picture shown that fixed cost remains the same where variable cost change with production. Loss or profit is the difference

between total cost and total revenue generated. Breakeven point is a point where the total cost is equal to total revenue generated.

### **2.11.3 Cost comparison**

The production cycle of ISF is shorter compared to the conventional production. CAD tools are used to design tool support and generate path of these forming tool. Therefore no physical tooling is required to program the path. Support tool materials are easy and fast to make and don't cost much as well. Modifications in tool path or part manufacturing can be incorporated into CAD file. New tool paths are then generated and applied on the sheet to be manufactured through forming equipment. ISF have lesser number of steps compared to conventional forming which makes it cost effective for a lower volume of part [Figure 2-19]. [146].

Comparison between ISF (Incremental Sheet Metal Forming) and Stamping is carried out for the forming of various shapes with different degrees of geometrical complexities i.e. car hood, oil tank cover, cup shape, pyramid with various radii. The Cost Model for ISF (Incremental Sheet Metal Forming) and Stamping are constructed by using estimated costs of dedicated die (fixed cost), machine (fixed cost), personnel cost (variable cost) etc. It is clear from these break-even points [Figure 2-20] that whatever the geometry of part produced incremental forming has a much lower break even. It shows that the breakeven point has slight dependence on the size of the part produced in the case of incremental forming. For relatively large parts; there is an increase in the breakeven point as compared to a smaller part in ISF [146].

### **2.12 Advantages and disadvantages of ISF**

Following advantages make ISF useful for small and medium-sized batches [88]

1. Lower cost compared to conventional forming methods.
2. ISF can be performed on a conventional CNC machine.
3. Changes in design can be carried out quickly and easily.
4. Parts are directly produced from the CAD file.
5. Forces are applied to a small region within the material.

6. The dimension of the part is restricted by the machine capacity.
7. Comparatively better surface finish.
8. Dies and molds are of low cost orr eliminated.
9. Formability is increased.

Following are the disadvantages of ISF [88].

1. More research is required to completely understand the mechanics of the process.
2. The accuracy of the process is not enough to meet strict industrial conditions.
3. No knowledge how different material types, geometries and input parameters will behave during ISF.

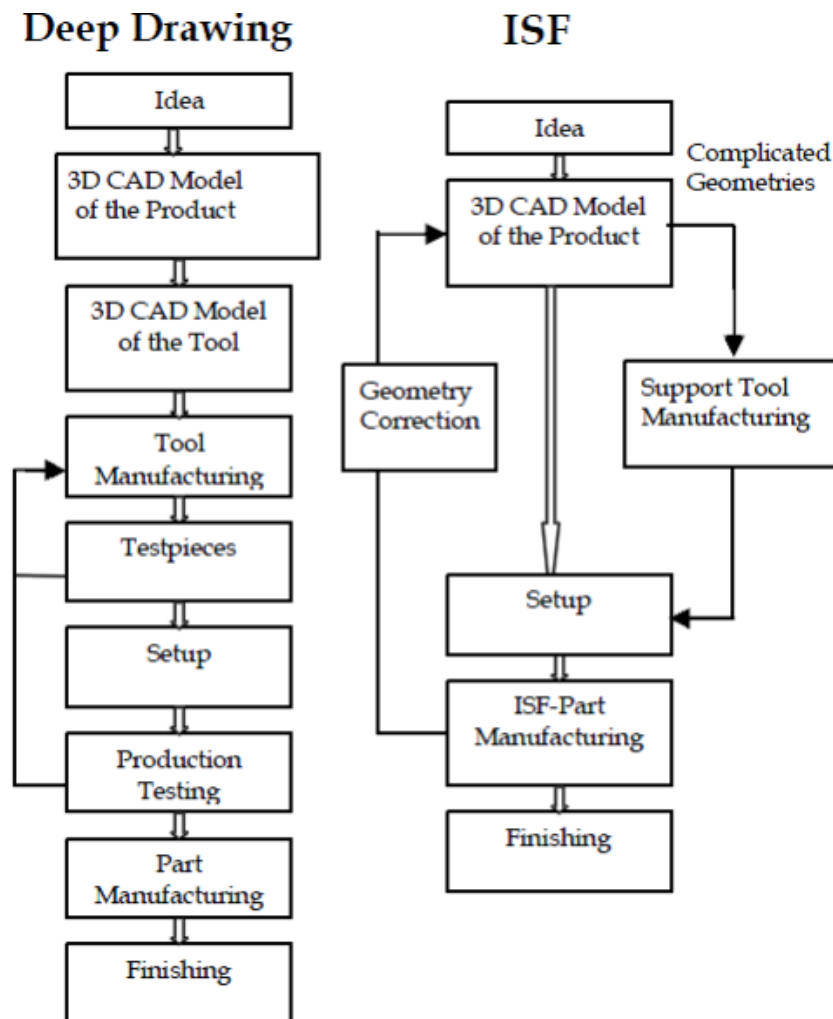


Figure 2-19 Conventional vs SPIF [146].

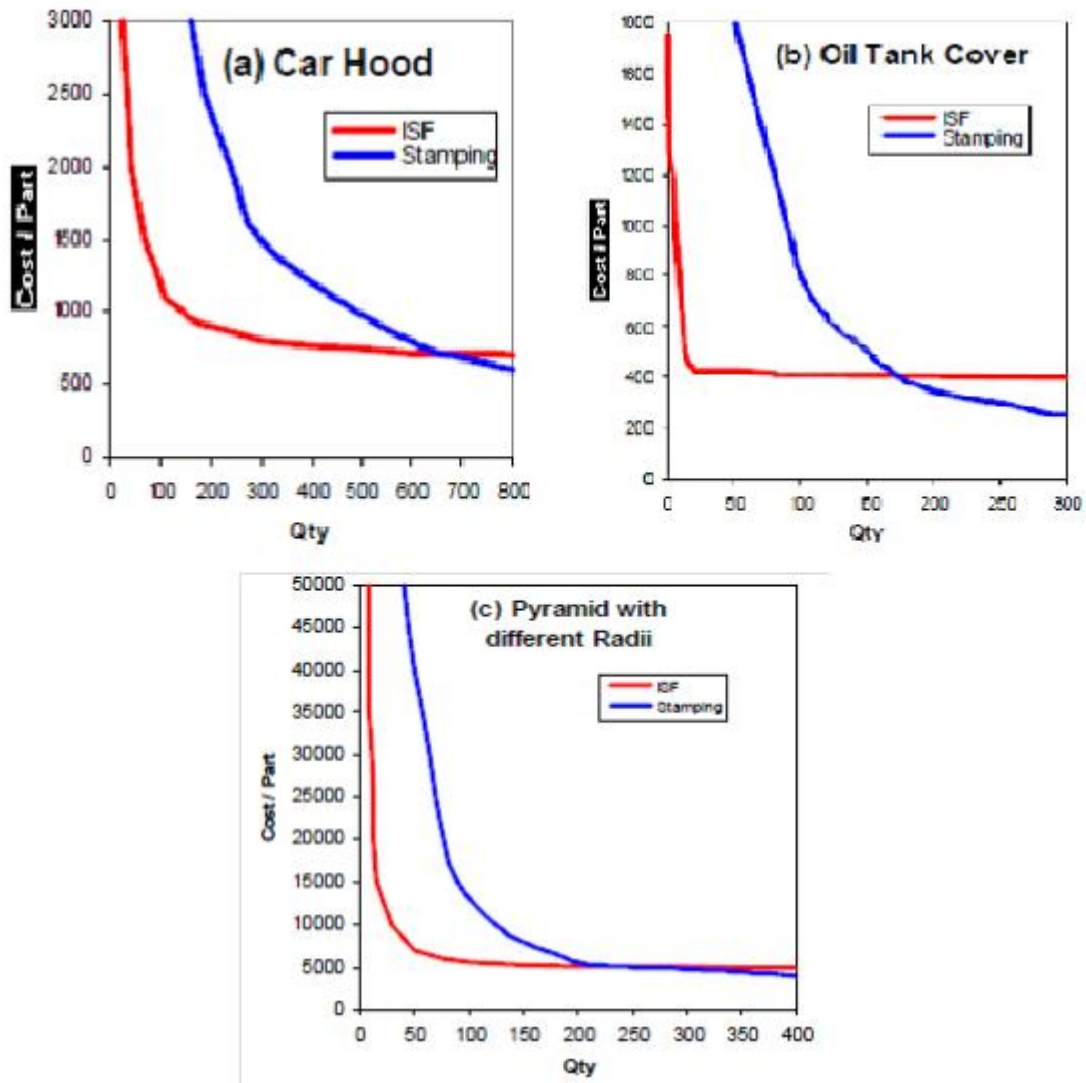


Figure 2-20 Cost comparison; (a) Car hood, (b) Oil tank cover, (c) Pyramid [146].

### 2.13 Formability

It is a well-known fact that in the case of ISF, forming limit curve is quite different than conventional one. Arshad discussed accuracy and formability of 2024, 6061 and 7475 Aluminum alloys [2]. Mode of deformation and forming limit curve in ISF are controversial subjects. Some author claims deformation is due to shearing instead of stretching and others claim the opposite. Formability as per author's point of view is a mixture of shearing, stretching and bending. The material type has the greatest effect on formability, followed by

shape. Fratini et al. elaborated the effect of common material properties on formability. According to their study, strain hardening coefficient ( $n$ ) and its interaction with the strength i.e.  $K.n$ , has the highest influence on formability. Thus material with higher hardening coefficient will have higher formability[147]. According to Bambach et. al. [142]

1. It has been agreed upon that the forming limits found in axisymmetric ISF are a straight line with a negative slope in the stretching region and the forming limits are considerably higher than those obtained by conventional Nakajima tests.
2. The forming limits depend on the forming parameters, mainly on the tool diameter and the vertical step-down value.
3. There is no agreed-upon standard for a forming test or evaluation procedure to record an FLC for AISF.
4. There is no proper definition of an FLC for AISF and it has not been differentiated between an FLC for necking and an FLC for rupture.

FLC for ISF has a negative slope with the value approximately equal to -1 as shown in Figure 2-21 and with 1 mm thickness in the principal strain space.

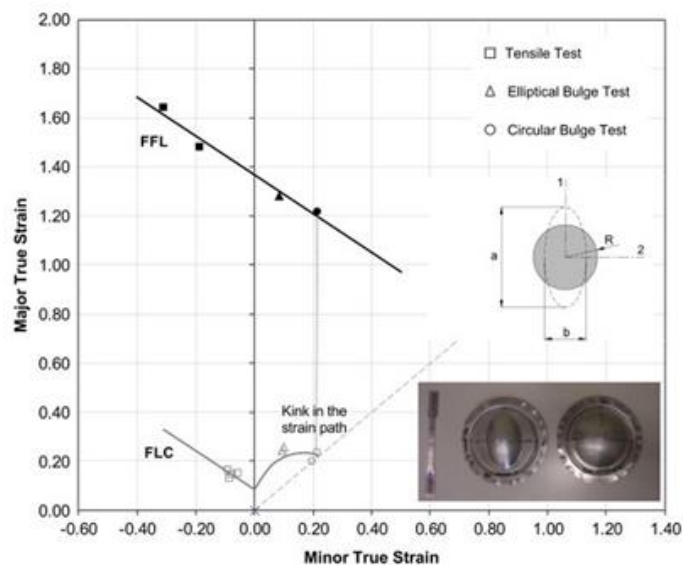


Figure 2-21 FLC and FFL for commercial sheets of Aluminum (AA1050-H111) [13]



## 2.14 Research gap summary

Given the limitation of FLC, a different method for establishing the feasibility of ISF process is proposed and shown in Figure 2-22. An easy assessment method by which design and production engineering can determine the feasibility of a given component.

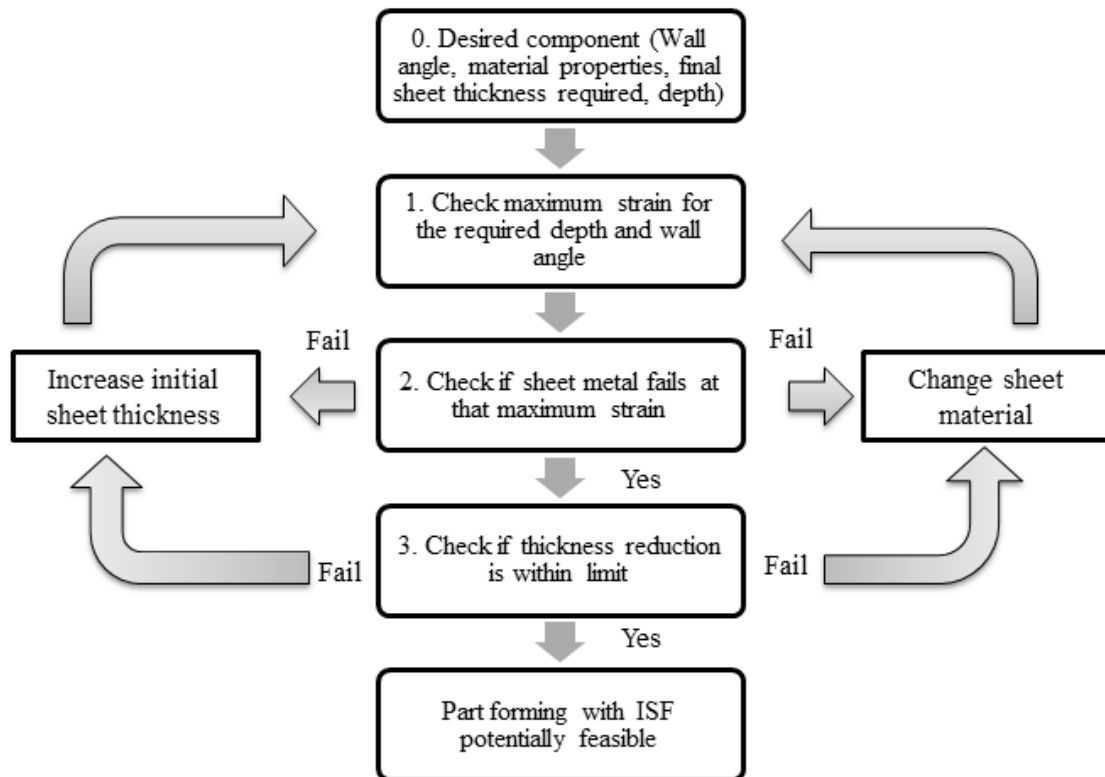


Figure 2-22 ISF-FCheck process.

Without the specific values the effectiveness of the method can only be hypothesized. Consequently, subsequent chapters establish values and investigate the relationship required to implement the method.

## 2.15 Summary

General forming processes has been used in the industry since ages such as hammering, spinning etc. Incremental Sheet Forming (ISF) is an emerging type of forming and is applicable to the automobile, aerospace and several other industries. ISF process has several advantages including but not limited to low cost, surface finish, lower lead times etc. There

are some disadvantages as well including accuracy and unknown mechanics of the process. ISF is in its infant stages and researchers are working on different aspects of ISF process.

### **3. Methodology**

This chapter details the research model, the methodology and techniques selected to deliver aims and objectives of the project. Motivation and rationale for the experiments and forming parameters are detailed.

#### **3.1 Research model selection**

While doing research, several choices have to be made by researcher through a variety of options. These options decide research methodology and structure. Reasons for selecting any particular option are dependent upon several factors. The methodology is to study if a structure of research is suitable to solve a particular problem [148]. A different set of problems needs a different type of research methodologies depending upon their nature.

Beech et. al summarized various choices at different stages a researcher has to make into a single chart . The stages a researcher has to pass through are Ontology, Epistemology, Methodology and Techniques. At each of these steps researchers have to make several choices depending upon the problem and other factors. At Ontology phase researcher decides whether their research study is either Subjective or Objective. Epistemology explains the philosophical theory of knowledge and has four choices namely Positivist, Critical Realist, Interpretivist and Action research. In Methodology procedures and principles of investigation are analysed with respect to a particular problem. Methodology can be Hypothetico-deductive, Inductive or Co-operative inquiry. Methodology is a branch of philosophy and to convert this philosophy into pragmatic tasks Techniques are required. There are several types of Techniques including Statistical testing, Experimental, Secondary data analysis, Case study, Observations, Interviews and participation. Figure 3-1 shows research paths available to researchers [149]. Current research is based on a practical manufacturing process ISF which has to be tested experimentally. Thus the path that was taken to perform this research is Objective, Critical realist, Inductive and Experimental. The path is enclosed in a blue box as shown in Figure 3-1. Experiments are generally conducted in a controlled environment such as laboratory and involve control over some factors while changing others to infer Multi-slope knowledge [150].

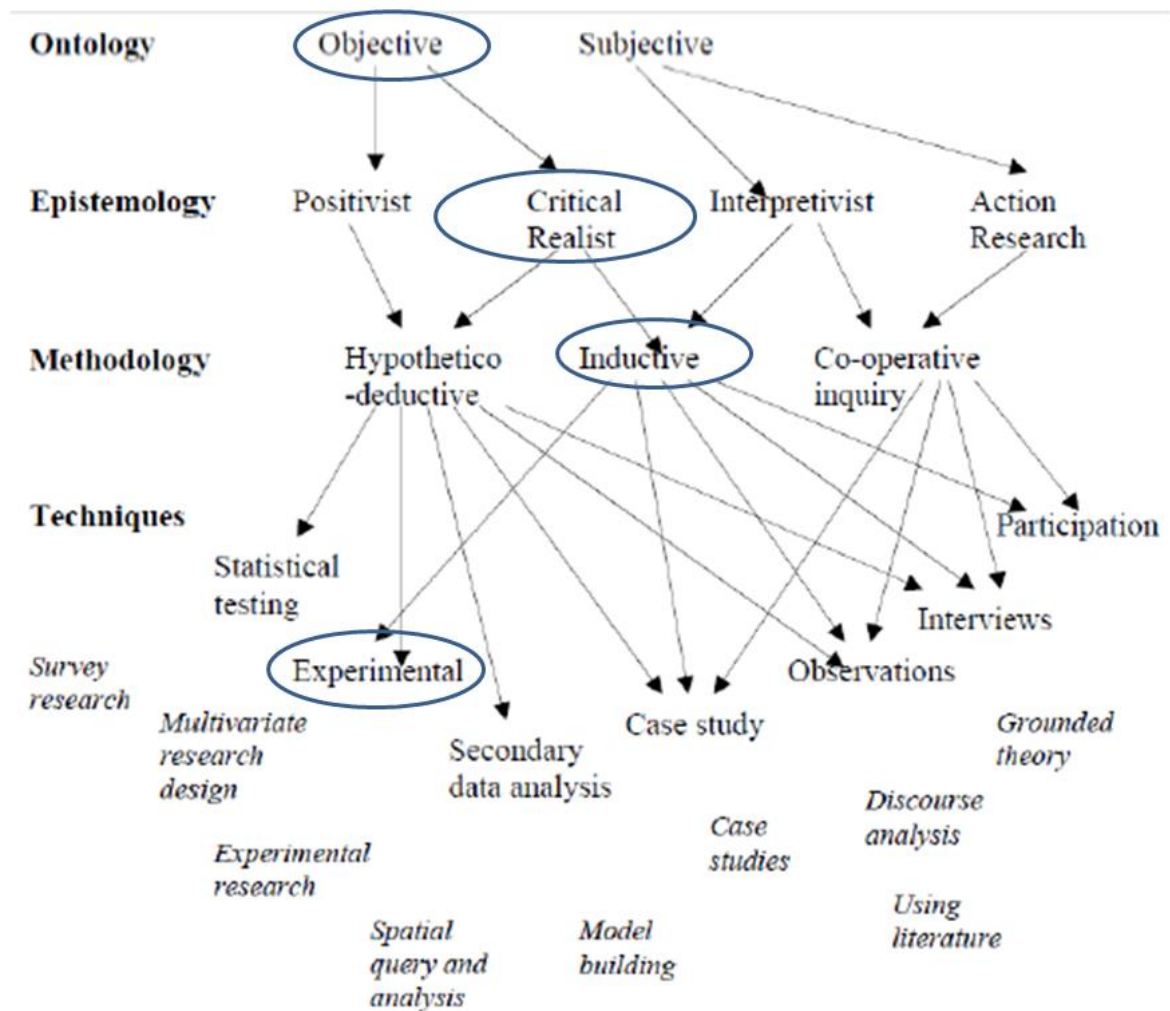


Figure 3-1 Research pathway [149].

### 3.2 Defining the experimental process

From literature review it is clear that the study of ISF is still at an early stage. The response of ISF process varies depending upon several variable including material properties, wall angle, shape, tool size etc. Although these topics have been frequently reported researched individually the whole spectrum of this process is not fully yet understood for example; surface roughness as a function of different materials, feed rates and geometric features. Hence research is limited and there are still ranges of parameters and interactions between them that are not explored yet. Thus there are no set standards or wide ranged mathematical models for the ISF process and research in several domains should be performed to fill these gaps.

Initial scoping experiments were performed on CPTi to form cup shape geometry at different heights. Based on literature review, experiments, meetings with researchers and analysis it was decided to research production rate, geometric features effects and material properties effects on accuracy, component thickness, surface roughness and resulting material properties. For wide acceptance and commercialization of this process, it is very important that this process could be used to form sheets of multiple materials into required shapes easily. ISF process is currently very slow compared to conventional forming processes. It is essential for the survival of this process to decrease overall set-up times by reducing the amount of trial and error involved during the development of the process. Figure 3-2 shows methodology of the project.

Although the objective of the project is to investigate the relationship between sheet thickness, strain and depth, it was also important to establish the sensitivity of the results to parameters such as rolling direction, tool path and materials. Furthermore, the impact of all these inputs on surface finish was quantified.

To describe this the author performed tensile tests with specimens at different rolling directions, using extensometers and acquired stress-strain graphs, strain width graphs, surface roughness analysis (before and after), fractography and other material properties. The author also performed Nakajima test for forming limit curve. Samples were prepared through water jet cutting and painted with white and black paint respectively. Tests were performed for different width of the samples using organic lubricant and analysis was run using ARAMIS® image processing software. To perform experimental tests author designed experimental procedure and equipment. The author performed a series of experimental tests with varied production rates, materials and geometries. Summary of these tests are tabulated in Table 3-1 and details are provided in chapters later.

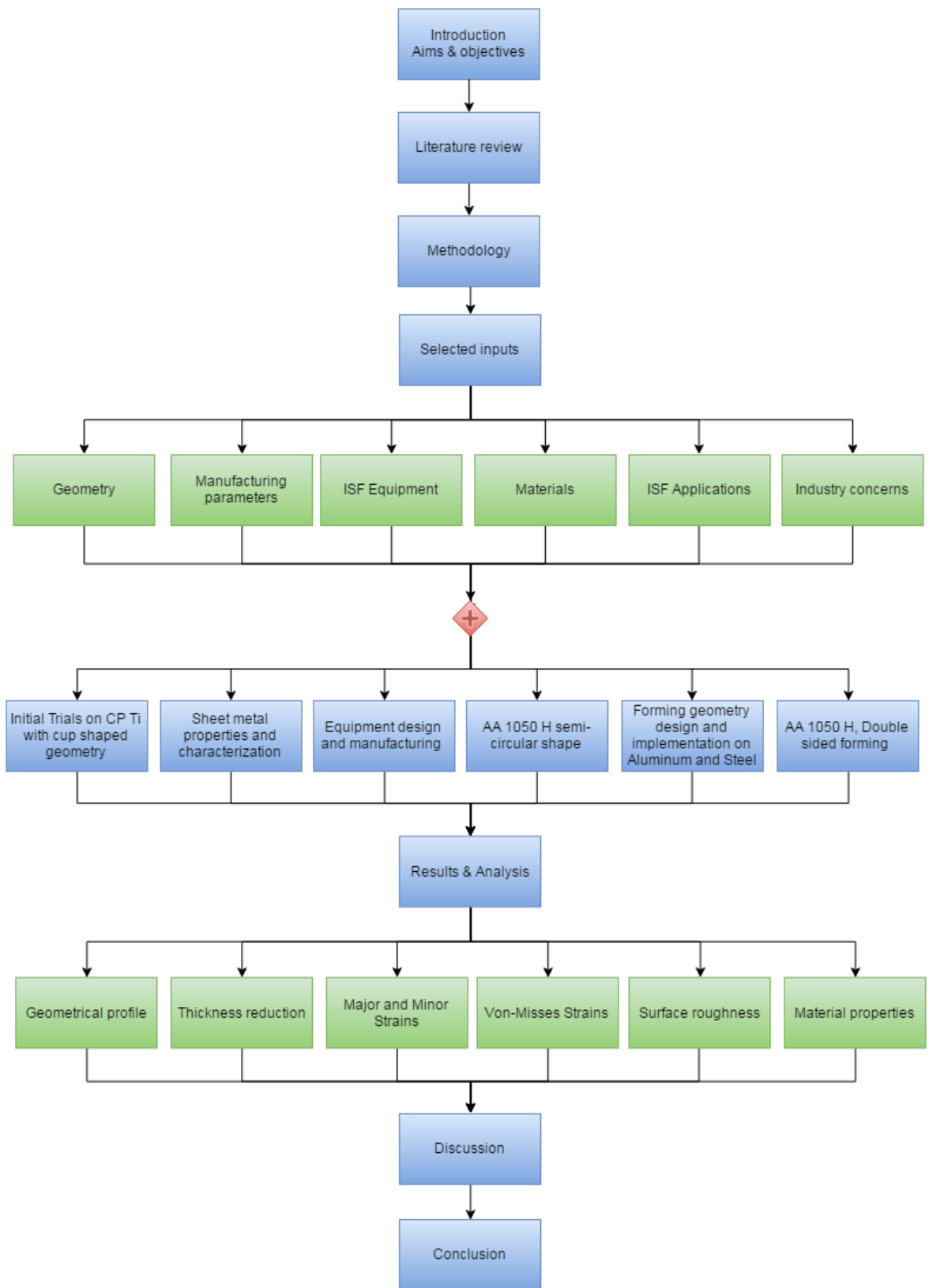


Figure 3-2 Research Mapping.

Table 3-1 Experiments performed.

<b>Geometric feature</b>	<b>Exp. ID No.</b>	<b>Material</b>	<b>Feed rate (mm/min)</b>	<b>No. of tests</b>	<b>Comments</b>
Cup	1	CpTi	700	3	3 different depths
Semi spherical	2	AA 1050 H14	1000	8	Symmetric, asymmetric, smaller size and different tools
Multi-slope	3	SS 304 L	1000	1	Till fracture, Free hanging, 0 RD
			4000	1	Till fracture, With BSP, 90 RD
				1	Till fracture, With BSP, 0RD
	4	AA 1050 H14	1000	1	Free hanging, 0 RD
			4000	1	Free hanging, 90 RD
				1	With BSP
	5	AA 2024-O	4000	1	Till fracture, With BSP
				1	5mm before fracture, With BSP
	6	AA 7075-O	4000	1	Till fracture, With BSP
1				5mm before fracture, With BSP	
Double side	7	AA 1050	5000	1	Cross before basin
		H14		1	Basin before cross

0RD = Along the rolling direction

90RD = Perpendicular to the rolling direction

BSP = Backsupporting plate

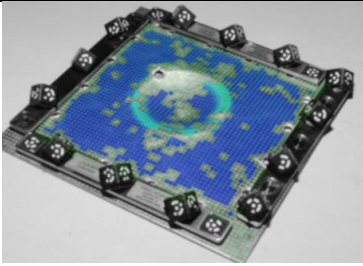
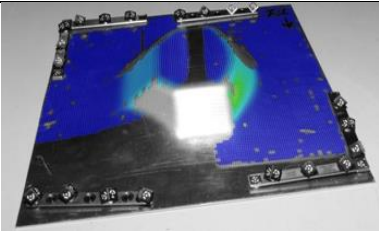
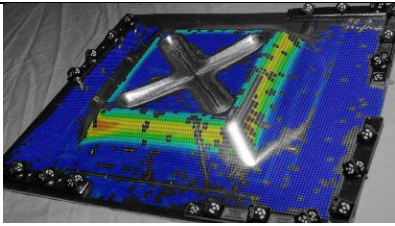
Experiments were identified by a serial number (e.g. 2-6 is Experiment 2, test 6). A list of the hardware and software used in this study are provided in Appendix E.

The number of process parameters is too large to make a design of experiment approach feasible because of the larger number of trials required. Instead, a ‘one factor at a time’ (OFAT) approach has been used to allow comparison of cases. While this does not allow every potential interaction of process parameters to be assessed, it is sufficient to allow the sensitivity of the results to changes in process setup or material.

### 3.3 Test components

ISF research based on empirical relationships between process parameters and outputs are sensitive to the geometric form of the test component used. This research adopted three test components as shown in Table 3-2.

Table 3-2 Test components.

S. No.	Name	Picture	Comment
1	Spherical		Assessment of small shapes with flexible fixture i.e. Fixture is able to move downward during the forming process
2	Multi-slope		Assessment of varying wall angles, geometric features and their interactions
3	Double sided		Assessment of interacting geometry and multiple forming directions



### **3.4 Summary**

Research design, methodology and techniques were discussed. Based on literature review and discussion with researchers, a strategy was devised to research high priority areas of ISF. Both academic and industrial concerns were targeted while selecting input and output parameters. List of experiments was provided which summarized important parameters and different studies. Limitations of the study were outlined.

#### 4. ISF parameters for spherical geometry

To investigate strain-depth and thickness-strain relationship a variety of materials and forms were investigated. This chapter reports the analysis of ISF of dome shape. Dome shapes were manufactured using AA 1050H, 1.3mm thick sheet metal. Relatively smaller working area of Aluminum sheet is 70mmx70mm while the total area is 130mmx130mm. the working area is lesser than total area because some area is used to clamp sheet in the fixture. Holes were drilled in the sheet to temporarily fix it with the help of nuts and bolts. Figure 4-1 shows the tool moves in a spiral path around the die to form the part; where tool starts from smaller diameter and moves towards bigger diameter. With the help of a positive wooden die, a convex surface was produced. The value of pitch used for the test was 0.5mm and feed rate was 1000mm/min. A milling process simulation with the tool is shown in Figure 4-1, where the material is being removed from a block. Three studies are reported in this chapter are:

- Formed dome geometry
- Influence of tool size
- Symmetric and asymmetric shape comparison

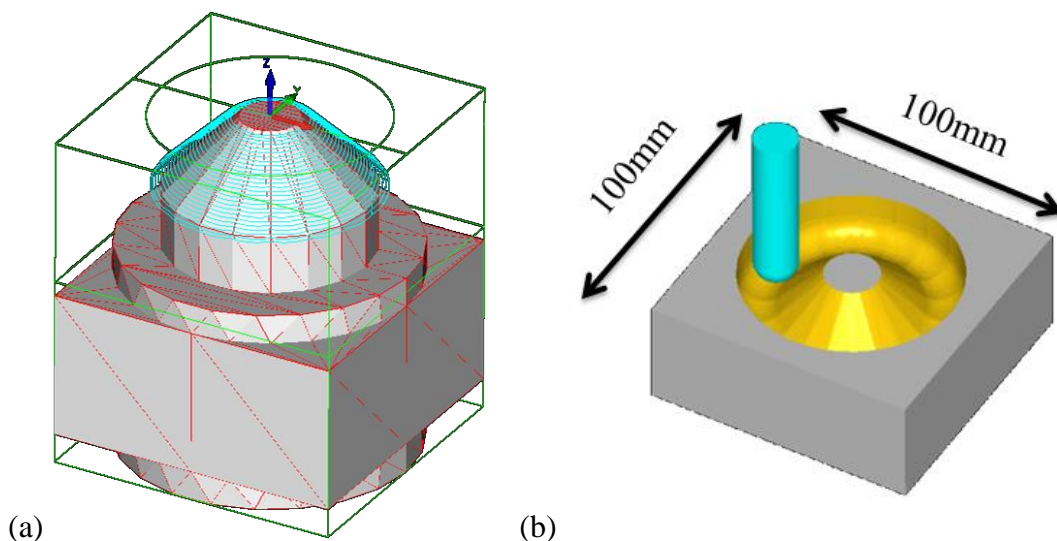


Figure 4-1 Tool path of ISF Process; (a) tool path over a die, (b) Milling process simulation.

## 4.1 Formed dome geometry

### 4.1.1 Thickness and profile

The dimensions of the ISF manufactured dome were optically measured using a GOM ATOS Triple Scan III scanner [Figure 4-2]. Because Aluminum is a highly reflective material a thin layer of paint (Ardox) was applied to create a matt surface that eliminated any specular reflection and so allowed the robust acquisition of data from the 3D scanner. The resulting point cloud was polygonized, smoothed and processed to get a final useable shape.

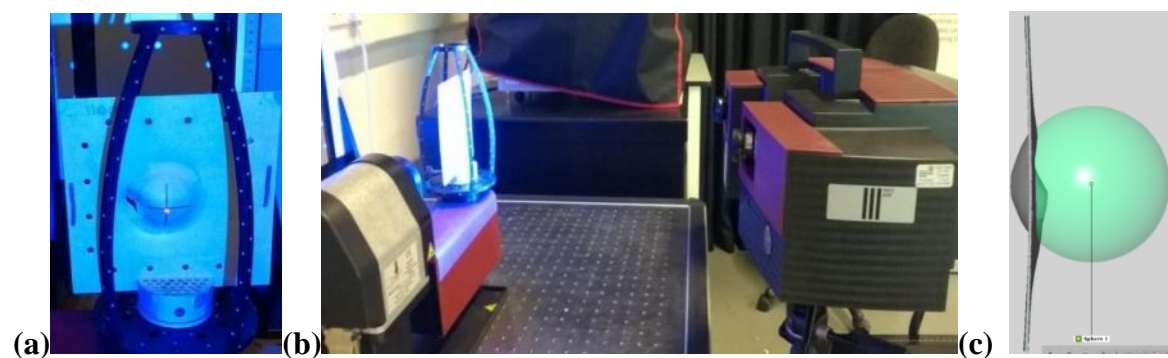


Figure 4-2 3D scanning; (a) Formed part in scanning frame, (b) Part being scanned, (c) Scanned geometry centered.

A visual assessment of the Aluminum sheet formed through ISF process suggested the part was in good condition (away from the area around the fracture) [Figure 4-3a]. The surface on both sides of the sheet is fairly smooth although a bend can be seen near the external diameter of formed shape. A grid of etched marks has disappeared from the surface where the tool was in contact with it, but are visible on the other side of the surface. It is observed through thickness profile analysis that sheet had localized thin areas shown in Figure 4-3b. These thin areas were in contact with the the tool and die.

Central green circle (A) in Figure 4-3b was in contact with die and the material was thinned over the edges of the die up to 1mm with a width of 5mm. The external circular region B was forced down through localized application of the force. The external circular region has a width of 15mm with cross-sectional area of  $7539.8\text{mm}^2$ . The internal diameter of this region was 25mm and external diameter was 50mm. This area is produced through multiple

passes of the tool over the sheet. The thickness is not uniform throughout this region and minimum thickness is observed in the middle of this region.

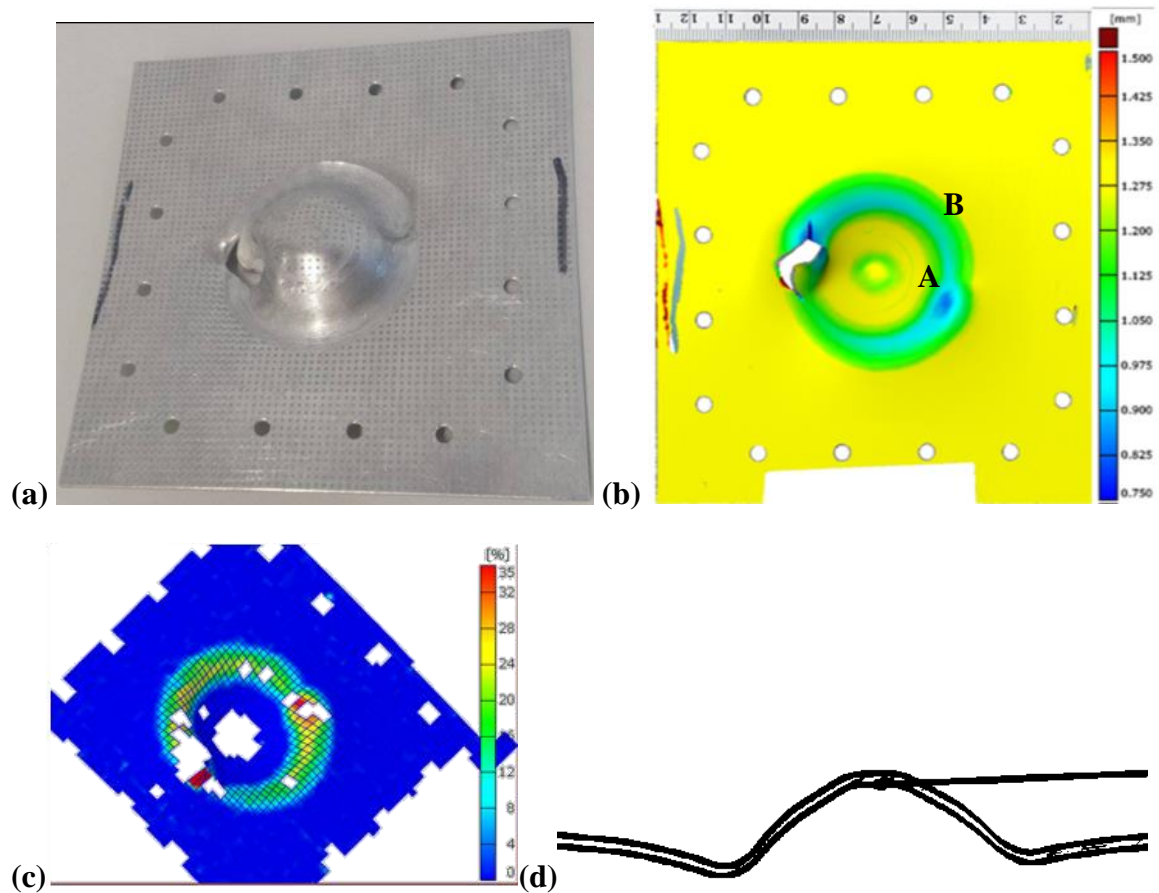


Figure 4-3 Formed part; (a) Sheet, (b) Thickness profile, (c) Percentage thickness reduction, (d) Profile.

Thickness on sides of this region is 1mm and it reduces to 0.9mm in the middle and further to 0.75mm just before the fracture. Maximum thickness reduction of 35% is observed. Thickness reduction around the corners of circular region is around 8% and increases to 20% in the middle. A thin line with 25% thinning is observed exactly in the middle of the region which increases to 35% while moving towards the fractured area as shown in Figure 4-3c. The tool should not repetitively contact sheet at same location several times to avoid this thinness effect.

The angle between the un-formed sheet and the horizontal plane is 12 degrees while the wall angle is 35 degrees and depth of the feature is 14mm. This shows that relative sizes of the forming tool and workpiece sheets have a major influence on the quality of the ISF process. It can be deduced that in the current case increasing the contact area of tool and sheet will

increase depth or flexibility of part being formed. This can be achieved through optimized tool path or part planning. Ideally formed sheet should have straight profile in the region which is not being formed, due to flexible forming fixture but it could be seen from Figure 4-3d that sheet is inclined to the horizontal plane. Surprisingly, minimum thickness and the bend location are not same.

#### 4.1.2 Strains

The aluminum sheet was electrochemically etched (before performing ISF process) with a grid of circles of 1mm diameter and 2mm apart from each other. Photographs with Nikon D300 camera were taken at various locations to digitize these circles as shown in Figure 4-4a. Two scales were used to identify the size of the part in Figure 4-4b. Major and minor strains were acquired using strain point data through Circular Grid Analysis.

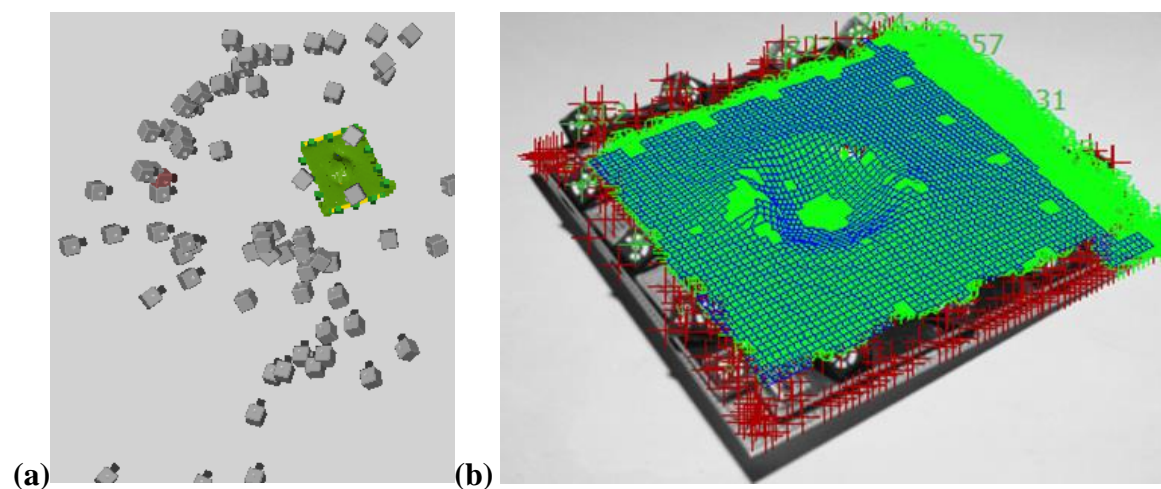


Figure 4-4 (a) Location of photos, (b) Grid over formed surface through ARGUS.

On the strain map, the blue points (under 20%) and green points (under 30%) show strain was negligible at this location [Figure 4-5a]. The yellow (under 40%) and red (under 50%) dots represent near necking and necking region respectively. The maximum major strain is 45% after which part is fractured, while the minor strain goes up to -10%. The minor strain points are distributed in 3% to -10% range as shown in Figure 4-5c. Formed area of the sheet has minor strain of -10% [Figure 4-5d]. A clear, longer and linear trend on the positive (tension) side of minor strain is shown. So it can be deduced that sheet formed with

is in the plane strain region. Different tool sizes should be researched to understand if the behavior remains similar.

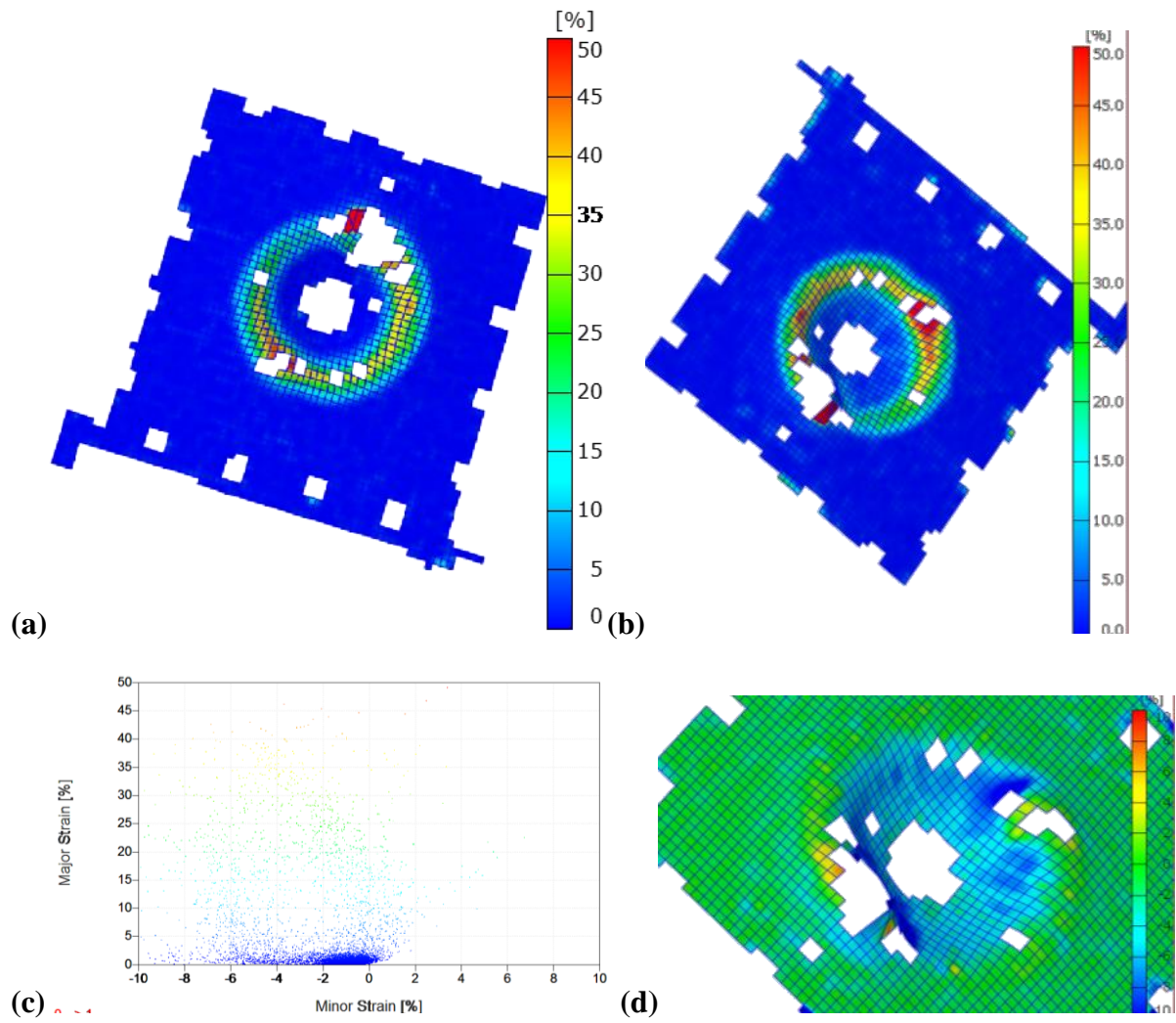


Figure 4-5 (a) Major strain, (b) Mises Strain, (c) Major and Minor strain, (d) Minor strain.

Out of two failure criteria Mises and Tresca, Mises is generally used for ductile material. Mises strain shows similar behavior but different intensity compared to Major Strain. Larger area reached 50% strain for Mises strain compared to major strain a very clear area with strains over 35% can be observed [Figure 4-5b].

## **4.2 Influence of tool size**

One aspect of ISF process knowledge that could impact on the feasibility of the ‘design feasibility assessment’ proposed is the influence the tool has on the quality of the final part and is discussed in section 2.6.3. This section reports the comparison between two different tip sizes of tool i.e. 4.5mm and 16.5mm. Both tools were used to form Aluminum sheets using a CNC machine and a flexible fixture. Comparative analyses of acquired results include thickness, profile, surface roughness, major and minor strains.

### **4.2.1 Thickness and Profile**

The overall behavior of sheet thinning is same for sheets formed by both tools as shown in Figure 4-6. Both sheets had localized thin areas although the magnitude of thinning was different. These thin areas were in contact with the tool and die. These regions are labeled A, B and C in Figure 4-6. Thinning area for tool A is 1/4th compared to tool B. This is due to a smaller contact area of tool A. Interestingly accumulation of material can also be seen in thickness profile of tool A. This might be due to chatter profile created by tool A as discussed in surface roughness. Area C shows dwell marks in the sheet. Areas with reduced thickness for both sheets are relatively lower for this region. For tool A this region also shows the thickness of 0.75mm (green) which is also visible just before the crack in area A. It can be concluded that area C has the 2nd highest probability of fracturing after area A. More thinning has occurred in area B for tool B compared to tool A. This shows that more overall force is applied on the sheet by tool B which made a mark of partial die more visible. The thinner sheet material is observed for both sheets in area A (green color, just before fracture). For tool B this area is bigger and length of material accumulation is long as well. So it can be concluded through analyzing thinning area and other parameters tool A will have less formability compared to tool B. Tool B exhibited higher sheet deformation compared to tool A in all the cases.

Formed results might vary when it comes to different feature size and shape. Tool B is better for overall shape compared to tool A. But tool A can produce finer details and features of small size. For Tool A a lower pitch is required to form a smooth part. Lower pitch means CNC has to do more work and takes more time, and thus the process becomes expensive relative to tool B. Although beyond the scope of this investigation a study is clearly required

to analyze different economic, machine life and machine utilization issues due to differences between the types of tools used for ISF process. Dwell size is also smaller for tool A compared to tool B. Ratio of Dwell size to tool tip are almost equivalent to each other for both sizes. For a set shape and fixture ratio of working area to tool-size is more for tool A compared to tool B. This means tool B cannot be used easily for smaller size objects. Ideally, both sheets should have straight profile in the region which is not being formed, due to a flexible forming fixture. Both sheets are inclined to horizontal. A sharper pointed dip could be easily seen for tool A compared to tool B.

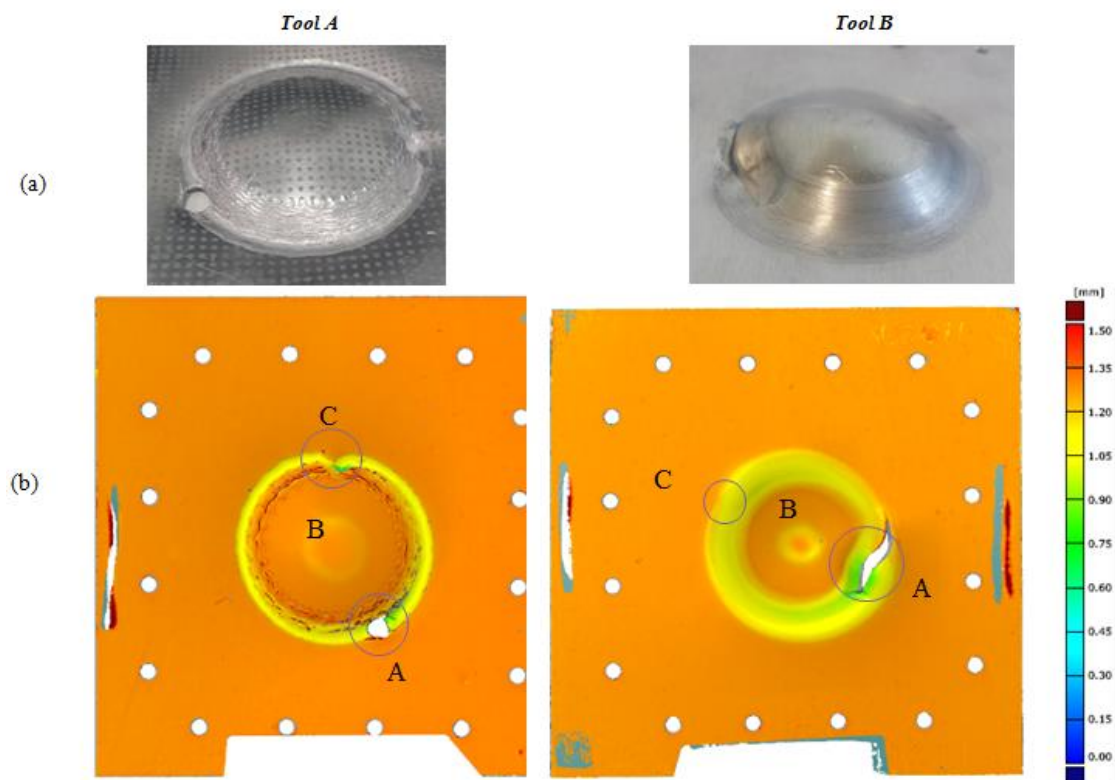


Figure 4-6 (a) Formed parts, (b) Thickness profile.

#### 4.2.2 Major and Minor Strains

The aluminum sheets were electrochemically etched before performing ISF process to mark them with circles of 1mm diameter. The distance between centers of circles is 2mm. Circles were marked on opposite side of the tool so that marks were not erased while performing the forming process. Major and minor strains shown in Figure 4-7 were acquired using strain point data through Argus by performing Circular Grid Analysis. Argus has the ability to digitize strain points and get geometric data of the complete shape of the part.



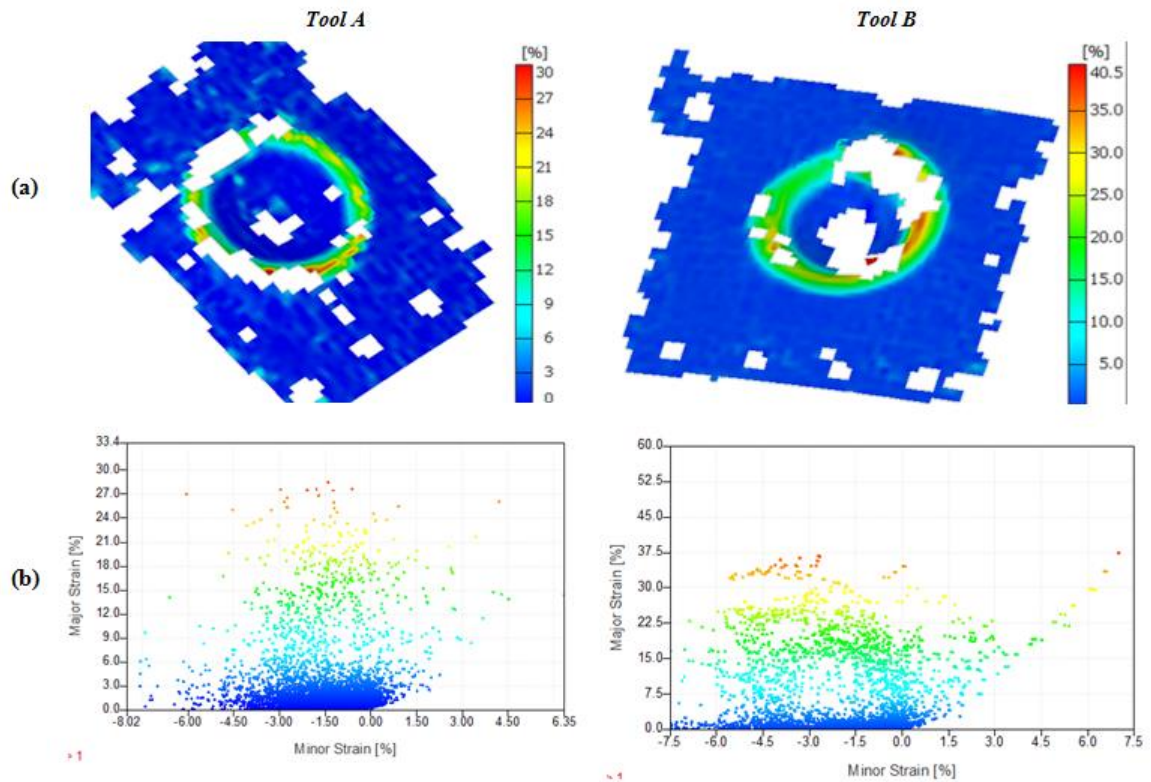


Figure 4-7 Major and Minor strain; (a) On sheet, (b)Plot.

The blue points in Figure 4-7 show strain was negligible at this location. The green and red dots represent near necking and necking region respectively. Maximum major (%) strain for tool A is dispersed under 30% while for tool B it is 37.5% with a percentage difference of 26.7% between both the values. Minor strain for tool A ranges from -7.5 to 4.5% and for tool B -7.5 to 7%. The sheet formed with tool A fractures at 27% major strain which is 10.5% lower than tool B (37.5%). Other than this trend both sheets have points in their respective necking region spreading between 0 to -6% range of minor strain. A clear, longer and linear trend on the positive (stretching) side of Minor strain is shown for tool B compared to tool A. Sheets formed with both tools are in the plane strain region. Smaller tools induce higher localized strains in the sheet because of the concentrated zone of deformation. Furthermore, for a smaller tool the localized forming forces increase due to the decrease in contact area between the tool and the metal plate while work to deform sheet remains constant. Thus more energy is transferred through a lesser area. Hence higher stresses are induced and as a result, there is a higher probability of the sheet to fail with smaller tool size under similar conditions. Due to small tool size, frictional heating will be localized and high in magnitude. Different geometries should be researched to understand if tool size behavior remains similar.

### 4.2.3 Surface roughness

In the current study surface roughness due to the tool-size was assessed by comparing values of Rz. Rz is average peak to valley height of the roughness profile. Measurement direction is perpendicular to the tool path direction. The sheet formed with tool A show very high roughness compared to tool B. Marks on the sheet for Tool A can be seen through naked eye on the formed sheet and are easily observed on the graph shown in Figure 4-8. It is observed that surface is rougher near center of sheet for tool A. Thus difference in the value of Rz are observed if different areas are taken. Average Rz for tool A is  $63.2\mu\text{m}$ . Rz for initial  $3.6\text{mm}$  is  $71.6\mu\text{m}$  and from there till  $4.8\text{mm}$  is  $5.8\mu\text{m}$  as shown in a, c. Thus a huge difference in the value of Rz is observed. Surface gets smoother in outwards direction due to repetitive contact of the tool and same area of the sheet. Thus it is recommended that smaller tool size should have a lower pitch. Average Rz for tool B was reported as  $12.1\mu\text{m}$  and remains fairly constant throughout the section of the sheet thus showing a more uniform surface roughness shown in Figure 4-9. The value of Rz is lower ( $8.3\mu\text{m}$ ) for the first  $2.9\text{mm}$  of the bigger tool, thus showing completely opposite behavior from Tool A.

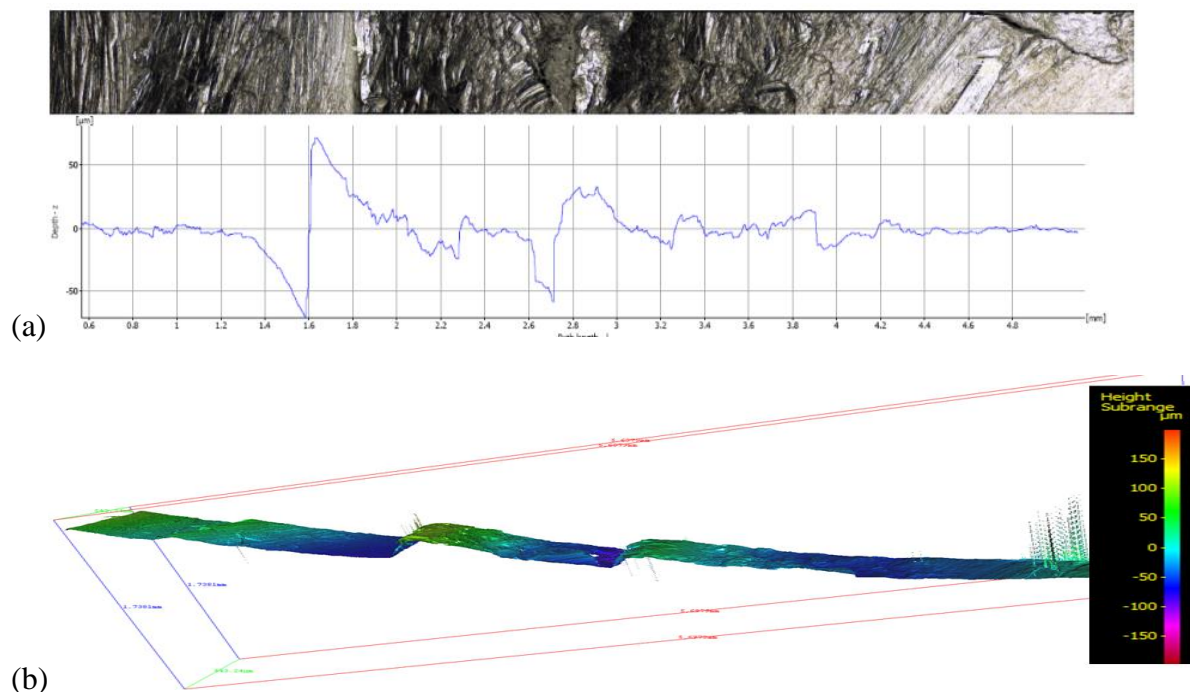


Figure 4-8 Surface roughness of tool A; (a) surface 2D profile, (b) 3D contour.

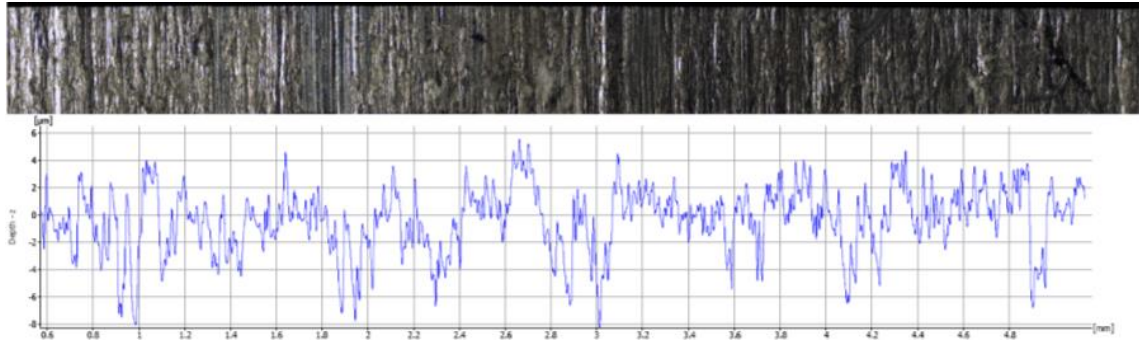


Figure 4-9 Surface roughness profile of tool B

### 4.3 Symmetric and asymmetric shape comparison

Three different tests (Case A, B and C ) were used to check the fixture's stiffness and movement under different load conditions and forming parameters (i.e. tool size and die geometry). Cases A and C are axisymmetric geometries while case B is asymmetric geometry. Most of the parameters for these three cases are the same. Varying parameters are listed below and the resulting parts are shown in Figure 4-10.

- Case A: Tool size: 4.5mm, Die at the center of Al sheet.
- Case B: Tool size: 16.5mm, Die off-center of Al sheet.
- Case C: Tool size: 16.5mm, Die at the center of Al sheet.

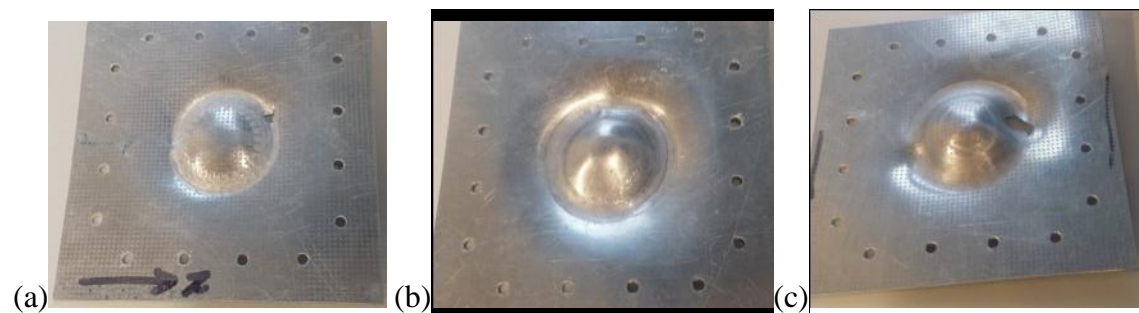


Figure 4-10: Final Aluminum sheets; (a) case A, (b) case B, (c) case C.

### 4.3.1 Part thickness and profile

Parts formed with Aluminum sheet through ISF process were observed to have a generally good condition (i.e. shape, surface finish etc) as shown in Figure 4-11. All three results show a uniform distribution of thickness in the area formed by ISF i.e. regions A and B.

Regardless of the fact that a point load is applied on the sheet at distance from center, creating a moment and a torsion, in both sheet and the flexible fixture's structure, and that the test were continued up till their failing point, a significant degree of symmetry and evenness of distribution in thickness was achieved in all the test results. This confirmed the stability and rigidity of the flexible fixture while moving vertically during ISF process. Surfaces on both sides of the sheets were fairly smooth although bends can be seen near the external diameter of the formed shape. A grid of etched marks was worn off the surface where the tool was in contact with the surface but is visible on the other side of the surface. It is observed through thickness profile analysis that all the sheets had localized thin areas [Figure 4-11]. These thin areas were in contact with the rotating tool and wooden die. Central green circle (X) was in contact with the wooden die and material was thinned over the edges of the die up to 1mm with a width of 5mm. The external circular region Y was forced down through localized dynamic application of the force. The external circular region width varies from case to case. For case A, B and C, part is formed through a rotating tool and the region Y has a width of 6mm, 8mm, 15mm with an area equal to  $6940\text{mm}^2$ ,  $9160\text{mm}^2$  and  $1021\text{mm}^2$  respectively. Case B has a non-uniform distribution of thickness reduction due to off-centered die. Region Y is deformed through multiple passes of the tool over the sheet. Thickness is not uniform throughout this region and the minimum thickness was observed in the middle of this region for all the three cases. However, magnitude of the sheet thickness varies from case to case. For case C, the thickness on sides of this region is 1.25mm and it reduces to 0.95mm in the middle and further to 0.75mm just before the fracture.

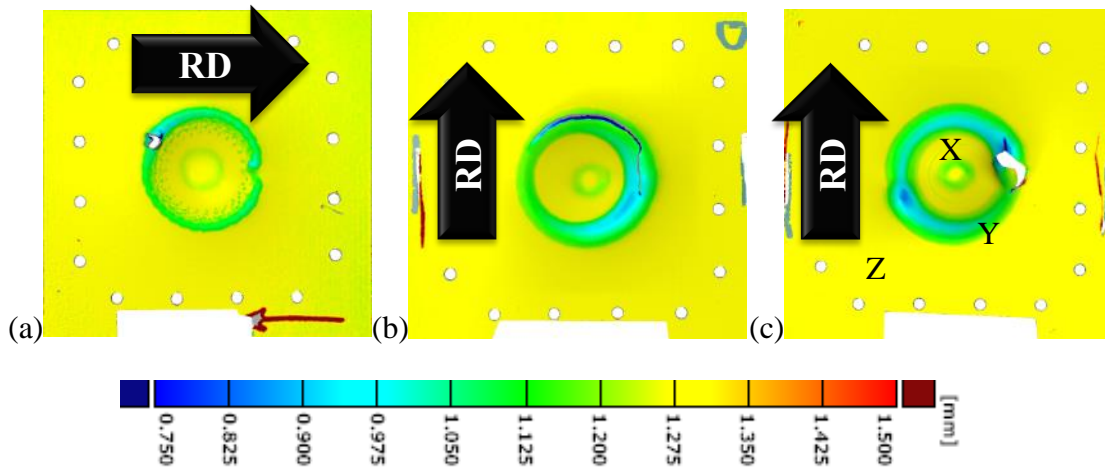


Figure 4-11: Thickness profiles of the sheet for; (a) case A, (b) case B, (c) case C.

Region Z i.e. from sides of the sheet until region Y, should have no reduction in thickness. Although region Z has no thickness reduction it does not have a straight profile as shown in Figure 4-12 and it is evident that sheet makes a small angle (less than  $10^\circ$ ) to the horizontal plane. This phenomenon occurs due to spring back and bending. Similar results have been reported previously [128]. The location of the maximum bend and minimum thickness are, surprisingly, not the same. It is observed in all three cases that crack starts along rolling direction.

It is concluded from these three cases that both the tool path and the size of forming tool compared to geometry size influence the formability and quality of the ISF process. However crucial these results confirmed that the fixture's dynamics were not impacting significantly on forming process and that the Nylon bushes had sufficient stiffness to support the process.

Thickness reduction percentage for all the three cases are observed in localized regions and shows that the flexible fixture has sufficient alignment, rigidity and freedom to move. The range of thickness reduction for all the cases is similar but the magnitude of percentage reduction in thickness varies at from case to case with respect to location as shown in Figure 4-12. For case A, region Y, the thickness reduction is between 8% to 12%. Rapid thinning is observed at the very last instant due to the tearing effect of the narrow tool (4.5mm). Case B is similar to case A but instead of thinning at a point gradual thinning in quarter of the circular region is observed. Case C shows relatively uniform distribution of thinning reduction and the sheet is thinned gradually for the whole circumference of the spiral tool

path. For case C thickness reduction around corners of the circular region is 8% and increases to 20% in the middle. A thin line with 25% thinning is observed exactly in the middle of the region which increases to 35% while moving towards the fractured area. This change of thickness across the cross-section of the sheet is due to multiple passes over the sheet. Maximum thickness reduction of 35% is observed just before cracking for all the cases. Arrows show the rolling direction of the sheet. The tool should not repetitively contact sheet at the same location to avoid this thinness effect. Tool path optimization can play the main role to avoid this to happen.

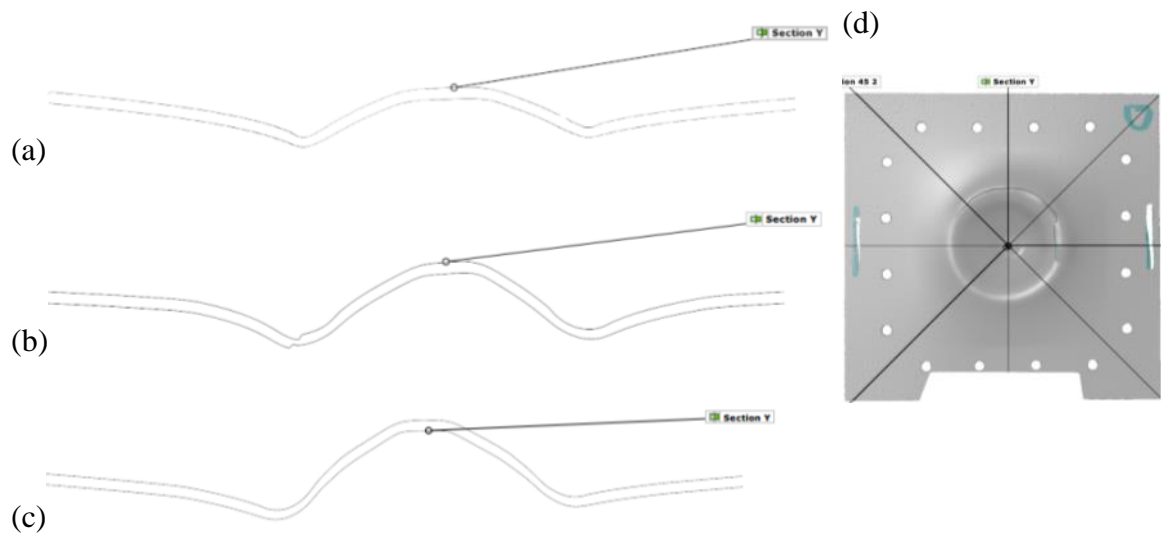


Figure 4-12 Geometric profiles of the sheet; (a) case A, (b) case B, (c) case C, (d) 3D scan of case B with section lines.

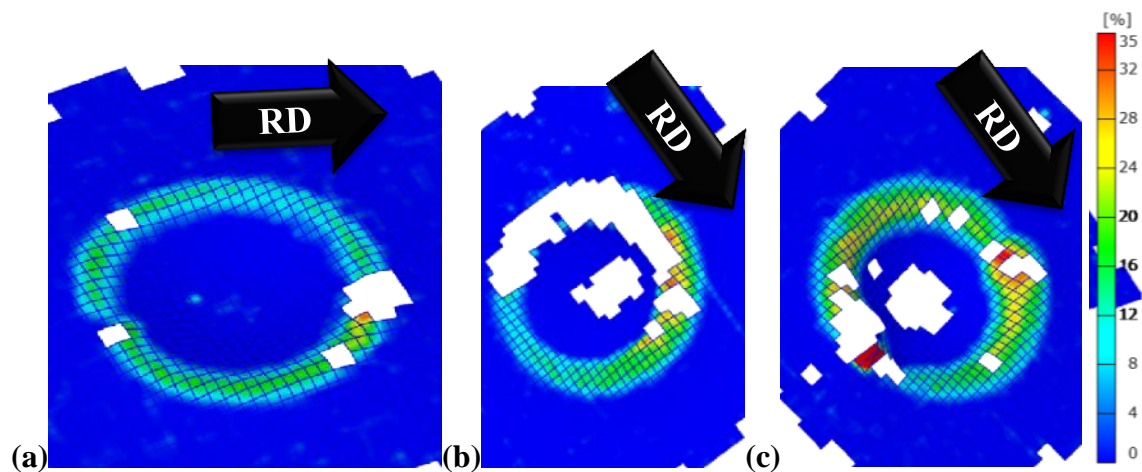


Figure 4-13: Thickness reduction % of the sheet; (a) case A, (b) case B, (c) case C.

### 4.3.2 Strain

Major and minor strains were acquired using strain point data through Circular Grid Analysis. At times some data is lost during acquisition of result which creates discontinuity or patches. This is because the circular grid is either erased or becomes very light due to forming process and thus could not be recognized by the system Figure 4-14.

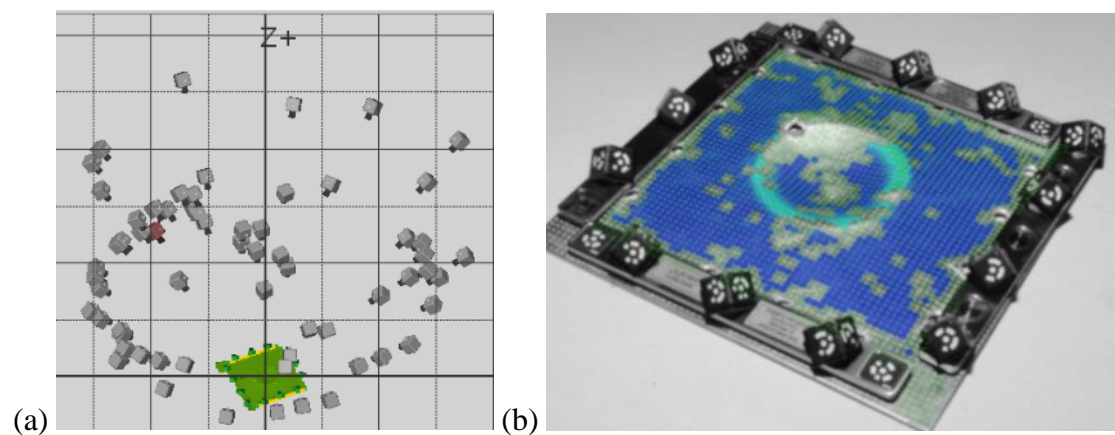


Figure 4-14 (a) Location of photos, (b) Formed surface through ARGUS.

Major strains are positive in all the three cases as shown in Figure 4-15 and confined to the localized region X and Y while rest of the area was not deformed. This demonstrates rigidity of the fixture even though it was moving vertically downward while high lateral forces were being applied on the sheet to fracture the part. For case A, major strain is zero at region Z and ranges 12% for most of the area. But as the tool is following a spiral path it increases to 35% just before it cracks. The maximum value of case B and C is 35%. Case C has the largest area under action due to higher tool size and centered die. For this case, the last pass of the rotating tool has a higher magnitude of major strain ranging from 25% to 35% distributed along the circumference.

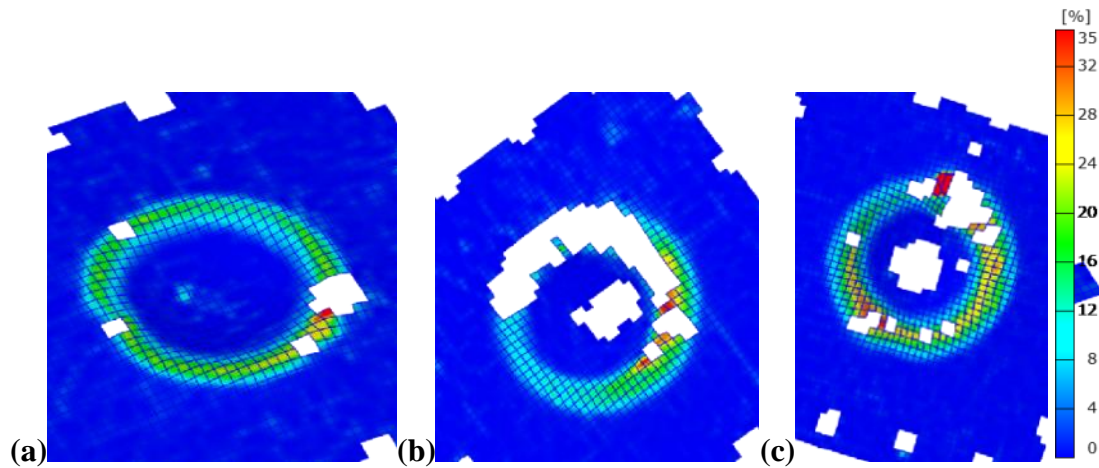


Figure 4-15: Major strain profile in the sheets; (a) case A, (b) case B, (c) case C.

The minor strain is negative for all three cases as shown in Figure 4-16. The values lie in a range of 0% to -10%. All the cases show similar behavior but case C has more clear divisions between different areas. In region X and Y strain clearly ranges from -6% to -10% while rest of area is near 0%. So it can be concluded from these three figures that the more the part is formed (higher deformation) the more area will go under compression for the positive die. It is evident from Figure 4-16 that only localized area has minor strains in negative value while it is zero across rest of the sheet, thus it can be concluded that stiffness of the fixture is sufficient to hold the sheet aligned.

Because the minor strain has negative value in all the formed regions thus it is a tension-compression case, which is known to be acting in other sheet forming processes as well. The evenness of the distribution suggests that the fixture is enabling but not distorting the ISF process.

As Von Mises strains are the equivalent strains of all six components of strains ( $\epsilon_{xx}, \epsilon_{yy}, \epsilon_{zz}, \gamma_{xy}, \gamma_{yx}, \gamma_{yz}$ ) they provide a useful metric for assessing the evenness of the sheets deformation on the fixture. Strain in other regions of the sheet would mean that fixture had moved while the sheet was being formed. For all three cases A, B and C strain was localized in regions specified by the tool path as shown in Figure 4-17. Von Mises strains in region Y vary in a range of 7% to 50% for all three tests but the distribution of strains varies from case to case. For case A, i.e. thinner tool size, most of the area remains between 10% to 20%. Strain moves from 20% to 30% across 90° of the region and suddenly ruptures the part in a comparatively small distance and goes to 50%. This is due to more localized stress because



of smaller tool size which tears sheet apart. For case B, i.e. off-center die with larger tool size, strain remain between 10% to 20% for 2/3<sup>rd</sup> of the region Y. For rest of 1/3<sup>rd</sup>. it varies uniformly and increases gradually to 50%. Case C, i.e. Centre die with bigger tool size, shows most uniformly distributed Von Mises strains range between 35% to 50%. This shows that to acquire greater formability from a part, larger tool size and centered die are the best options. Different dynamics seem to be working in all three different cases due to different input effects. It is hard to establish from current results which criteria of failure is causing rupture and what is the state of the stress in elements just before failure.

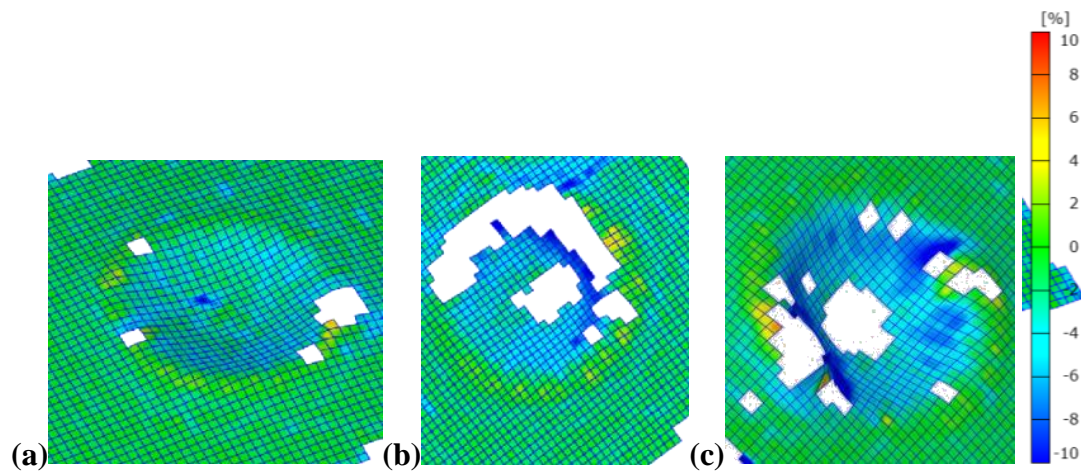


Figure 4-16: Minor strain profile in the sheets; (a) case A, (b) case B, (c) case C.

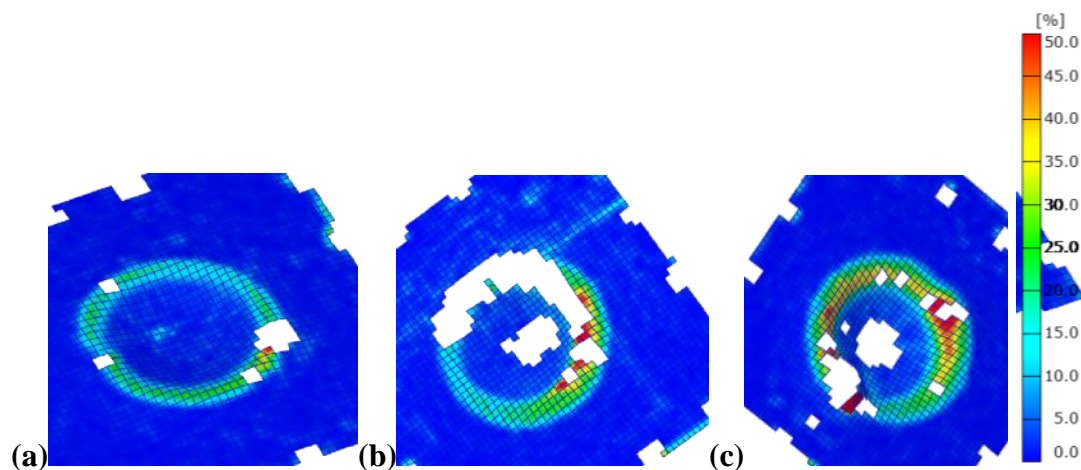


Figure 4-17: Von Mises strain profile in the sheets; (a) case A, (b) case B, (c) case C.

A graph representing all the tests performed for dome shape with the flexible fixture and the rotating tool is shown in Figure 4-18. This plot is a foundation for ISF-FCheck model and

shows similar behavior predicted in chapter 1 and 2. These tests were performed on A1050H sheet metal, different sizes of rotating tool and flexible fixture. To validate this model in further detail, Multi-slope geometry was designed and tested (Appendix C). Results of this geometry with respect to the model are discussed in chapter 5.

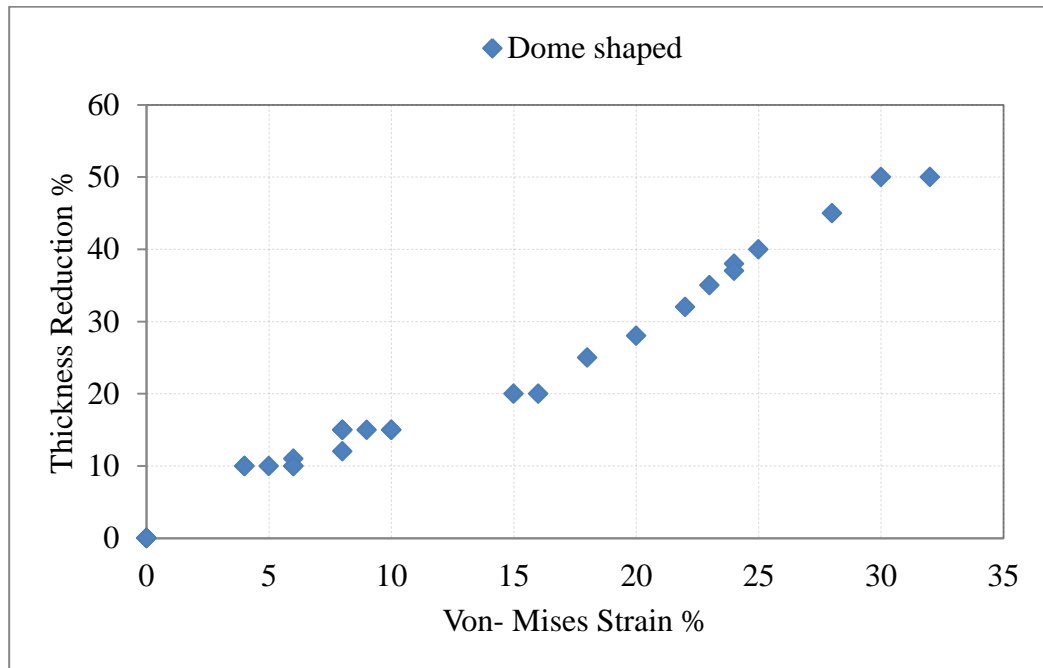


Figure 4-18: Von Mises strain % vs thickness reduction %.

#### 4.4 Summary

Several tests with varying tool sizes, flexible fixture (varying vertical depth) and different positions of the dies were performed on sheet metal. Spiral tool path was generated with CAM software for tool movement to form the geometry. After which results such as thickness reduction, profile changes, major and minor strains and Von Mises strains were acquired from these sheets using circular grid analysis, 3D scanning and other state of the art methods. It is concluded that larger tool size should be used to form the geometry. An interesting relationship, as stated in earlier chapters, was observed between Von Mises strains and thickness reduction. It is suggested that this relationship should further be explored on various wall angles and geometries.

## 5. ISF parameters for angular geometry

To investigate the relationship between strain, depth, rolling direction (RD), backsupporting plate (BSP) and thickness in asymmetric, multi-featured angular components the following investigations were done. Ten different parts were formed into Multi-slope geometry at different depths tabulated in Table 5-1. Details of the geometry and experimental procedure are given in Appendix C and geometry provided in Table 3-2,2. Four different materials i.e. SS304L, AA1050H, AA2024 and AA7075 were used to perform experiments. Complete set of results are provided in Appendix D. Strain, thickness reduction wall angle, geometric features, surface roughness and microstructure evolution were discussed for different initial sheet thickness, feedrates, rolling directions, depths and material properties. Backsupporting plate (geometry provided in Appendix C) was also used to form seven components. Backsupporting plate increased the accuracy around its edges and can be used easily to form complicated geometries. As the behavior of the formed sheets was similar, only selected results were reported in this chapter. The rest of the results are given in Appendix B.

Table 5-1 Experiments performed.

<b>Geometry</b>	<b>Material</b>	<b>Feedrate (mm/sec)</b>	<b>No. of tests (Total=10)</b>	<b>Comments</b>
Multi-slope	SS 304 L	1000	1	Part fractured, Free hanging, 0 RD
		4000	1	Part fractured, With BSP, 0 RD
			1	Part fractured, With BSP, 90RD
	AA 1050 H	1000	1	Free hanging, 0 RD
		4000	1	Free hanging, 90 RD
			1	With BSP
	AA 2024	4000	1	Part fractured, With BSP
			1	5mm before fracture, With BSP
	AA 7075	4000	1	Part fractured, With BSP
			1	5mm before fracture, With BSP

Three parts (SS1, SS2 and SS3) were formed using SS304L, 0.6mm thick sheet steel. One part (SS1) was formed hanging freely, without the use of back supporting plate. Other two components (SS2 and SS3) were formed using back supporting plate. Both these sheets were orientated in different rolling direction and were formed at different feed rates. Multi-slope geometry with different wall angles ranging from 40°-60° and their interactions were used as explained previously. A figure showing section of the geometries is given in the next section. Sheets were formed to a depth of 16mm and federate of 1000 and 4000 mm/min was used. The rest of the parameters are explained in Section 6.3.1.

## 5.1 Accuracy

The difference between the sharpness of sheet steel with and without BSP can easily be observed in Figure 5-1. The surface profile is very straight, planar and sharp for the parts formed with BSP, while the part formed without BSP is curvy with no sharp features. This shows the high utility of BSP concept and will be discussed further in this section. Section lines were defined on the scanned geometry passing through various features and areas of interest. Sections from all three parts were acquired and compared with each other. Freely hanging component (SS1) showed inward bulging and varying thickness. It is observed that various factors effect the surface profile including the distance of the feature from the clamped sheet, depth of forming and tool path. As the part was formed to a depth of 16 mm (fracture limit), no pillowing effect is visible in any of the sections in all three parts. In fact, the middle surface is absolutely straight which was rarely observed during initial experiments and literature review. Thickness reduction is observed only in the area under action.

Section X and Y of the scanned geometry for both the free hanging parts in different rolling directions are the same. Section X cuts and represents 50° and 60° wall angle shown in Figure 5-2. Although the tool follows sharp edges given in the CAD model shown but the SS1 scanned geometry has curvature. This is due to the springback of the sheet steel i.e. it gets back or tries to get back to its original position due to elastic effect. Thus at both 50° and 60° wall a curve is visible instead of a sharp edge. It is easily observed that higher wall angle has a lower radius of curvature. It is also visible evident that 60° wall angle has higher thickness reduction compared to 50° and 40°.

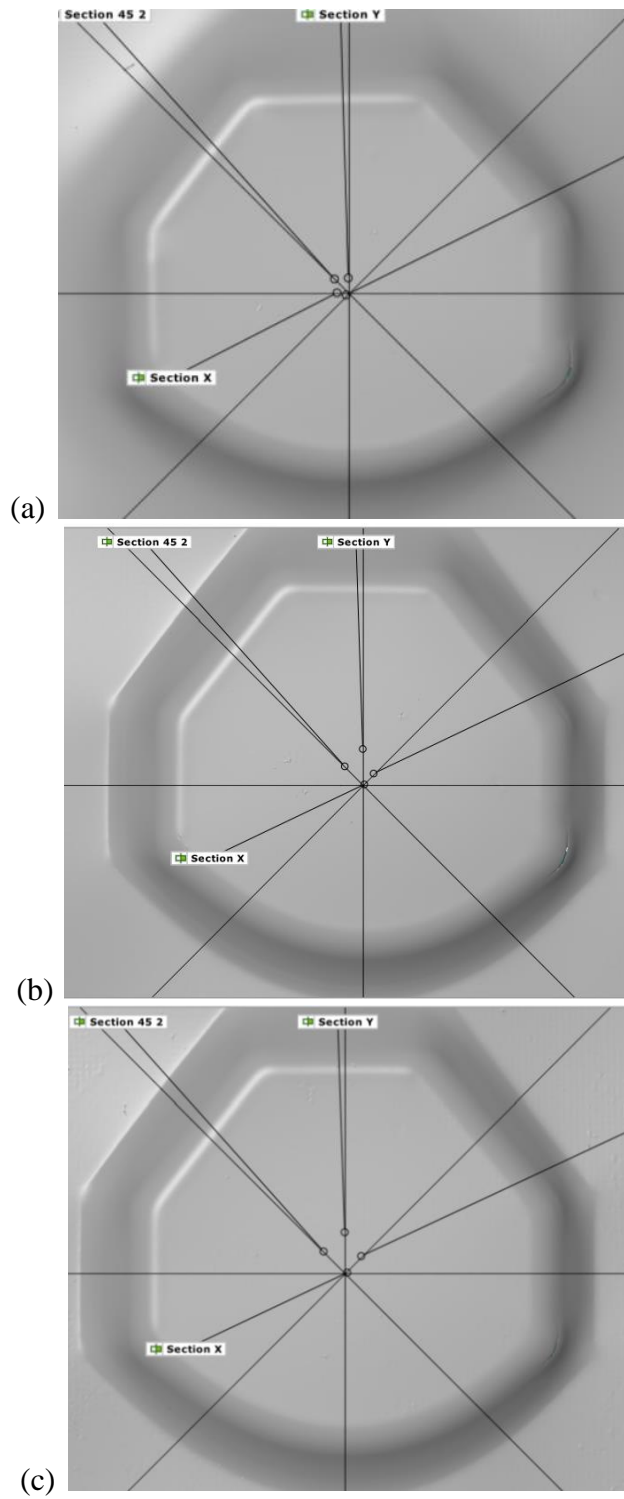


Figure 5-1 Multi-slope geometry AA1050°H; (a) without BSP SS1, (b) with BSP SS2, (c) with BSP SS3.

Wall thickness distribution uniformity decreases with increased wall angle and the area untouched by tool has no thickness reduction at all. BSP geometry SS2 and SS3 are completely different in comparison with these two sections. It has sharp edges and the sheet profile goes down very sharply compared to free hanging sheet steel. This shows that BSP concept optimized and improved acquisition of complicated axisymmetric shapes, accuracy and spring back effects. It is due to continuous stretching of the only formed area of the sheet that there is no curvature in the profile. This was not the case in the free hanging sheet as all the area of the sheet was stretched and area under action was allowed to spring back to its original position which created the undesired geometric feature. This is a big breakthrough as far as accuracy of the process is concerned. Section Y for both rolling directions of the sheet is similar and no visible difference is seen. Section Y of both the sheets show 40° wall feature and 50° curve feature [Figure 5-3]. Surprisingly 50° curve feature in section Y has the same profile as 50° wall feature in section X. 40° wall feature for both the hanging sheets follow similar behavior and has a larger radius of curvature compared to 50° and 60° respectively. BSP for this section again improves accuracy and spring back effects which further validate the results.

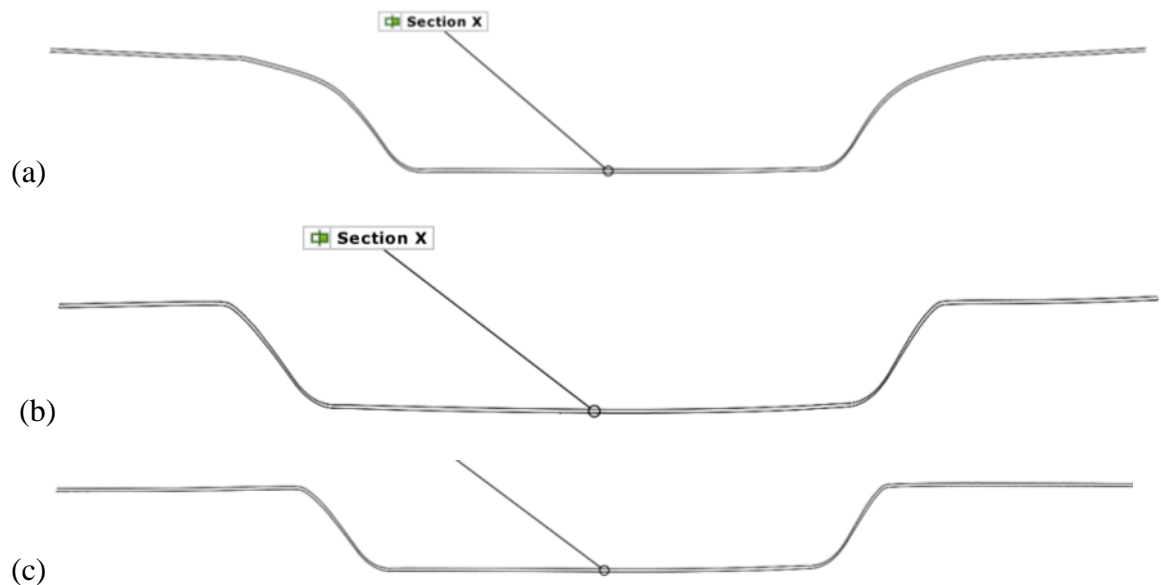


Figure 5-2 Section X; (a) SS1, (b) SS2 (with BSP), (c) SS3 (with BSP).

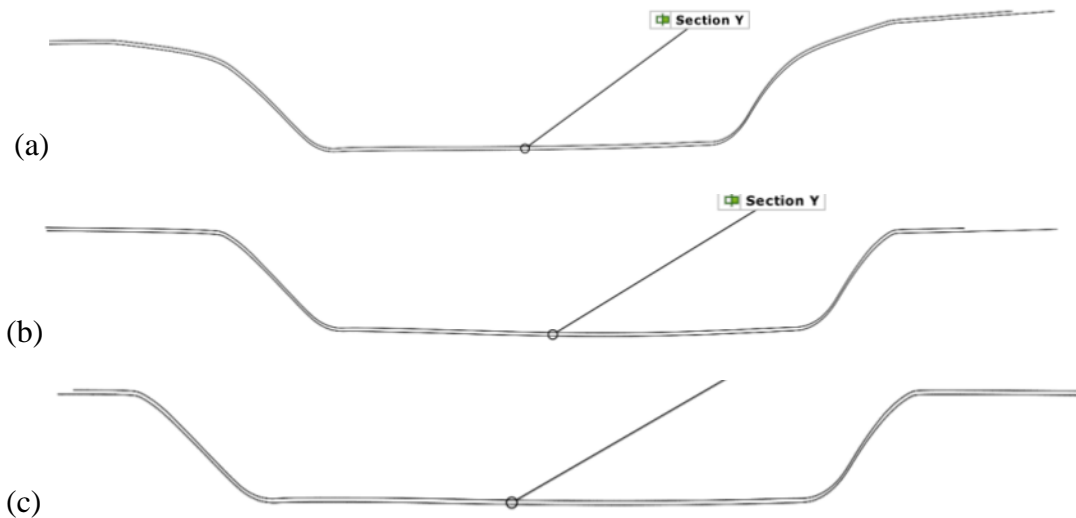


Figure 5-3 Section Y; (a) SS1, (b) SS2 (with BSP), (c) SS3 (with BSP).

The main problem in measuring part accuracy with 3D scanning is software limitations and uncontrollable human error. Scanned data of the formed parts was aligned with 3D CAD model. The software package ATOS ® was used to perform this function. As there are millions of points in 3D scanned geometry and unlike CAD model corners or edges are not specified so points were selected through visual analysis. The software package also has limited functionality in terms of aligning CAD model to 3D scanned data. It was also observed during experiments that sheet metal twisted a bit in the absence of back supporting plate. Effect of this error would be reported in the analysis of the contours.

Formed sheet steel parts show deviation from the CAD model. This deviation is important and cannot be neglected. The difference between 3D scanned results and CAD model could be observed qualitatively in Figure 5-4 and Figure 5-5. Blue color represents CAD model while grey color portrays 3D scanned geometry. Distortion is observed in the geometry as at some locations of the CAD model are visible and over the steel sheet while other locations are hidden under the sheet metal. Multiple reasons can be responsible for this deviation from the CAD model including geometry, material properties and tool path. The geometric deviation is also effected by an elastic effect of the parts (spring back). CAD model is hidden mostly on and around 60° wall angle feature which shows less spring back due to plastic deformation. Geometry shows more deviation at higher depth compared to the start of the formed part. 3D scanned geometry waves around CAD model which show the twist produced during forming of the sheet metal. It was also observed in initial experiments that

more plastic deformation led to accurate parts and lesser spring back. Higher wall angles also cause higher plastic deformation. So it can be deduced that because of higher wall angles spring back is less and accuracy has increased.

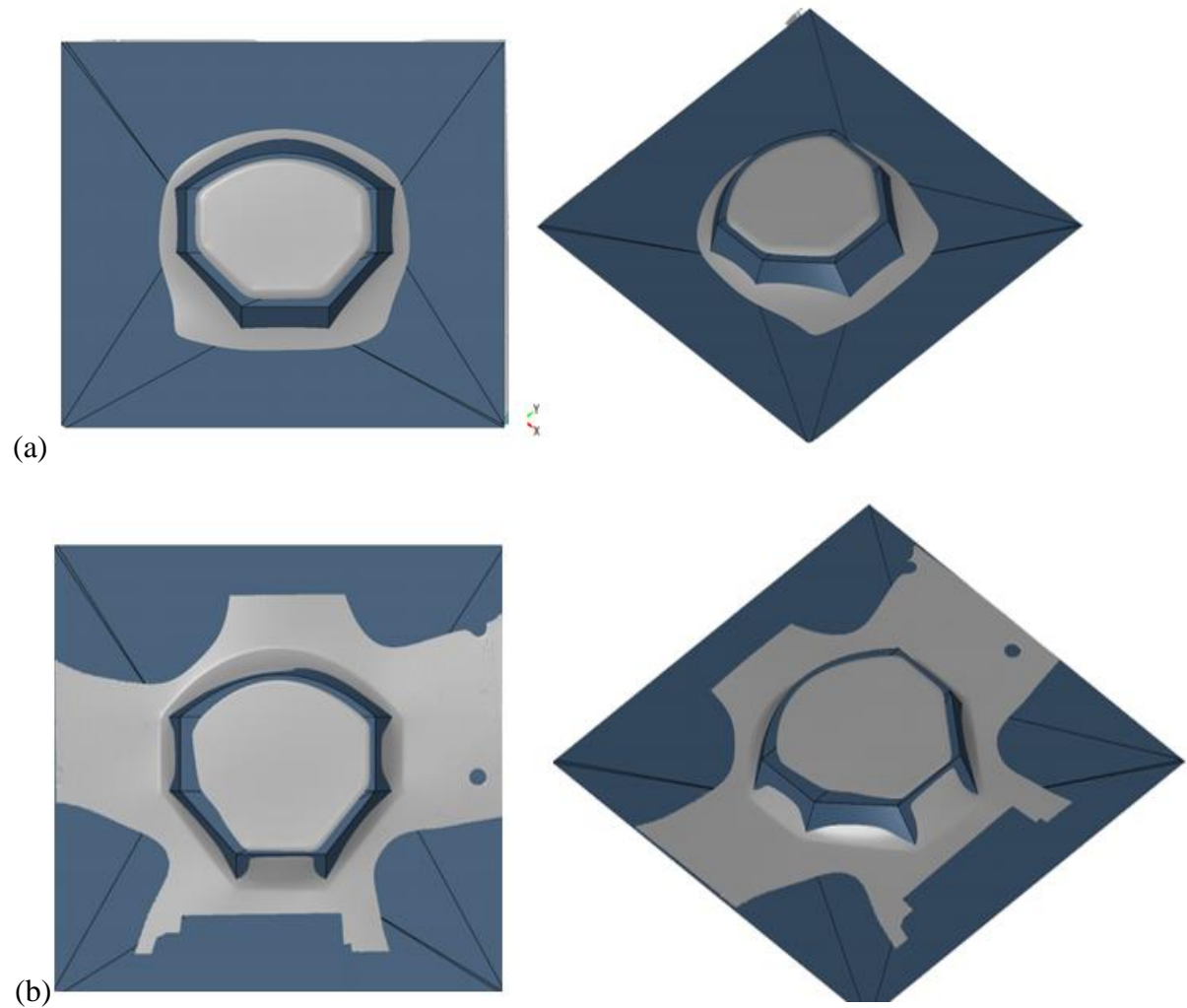


Figure 5-4 Qualitative CAD comparison; top and isometric view; (a) SS1, (b) SS3.



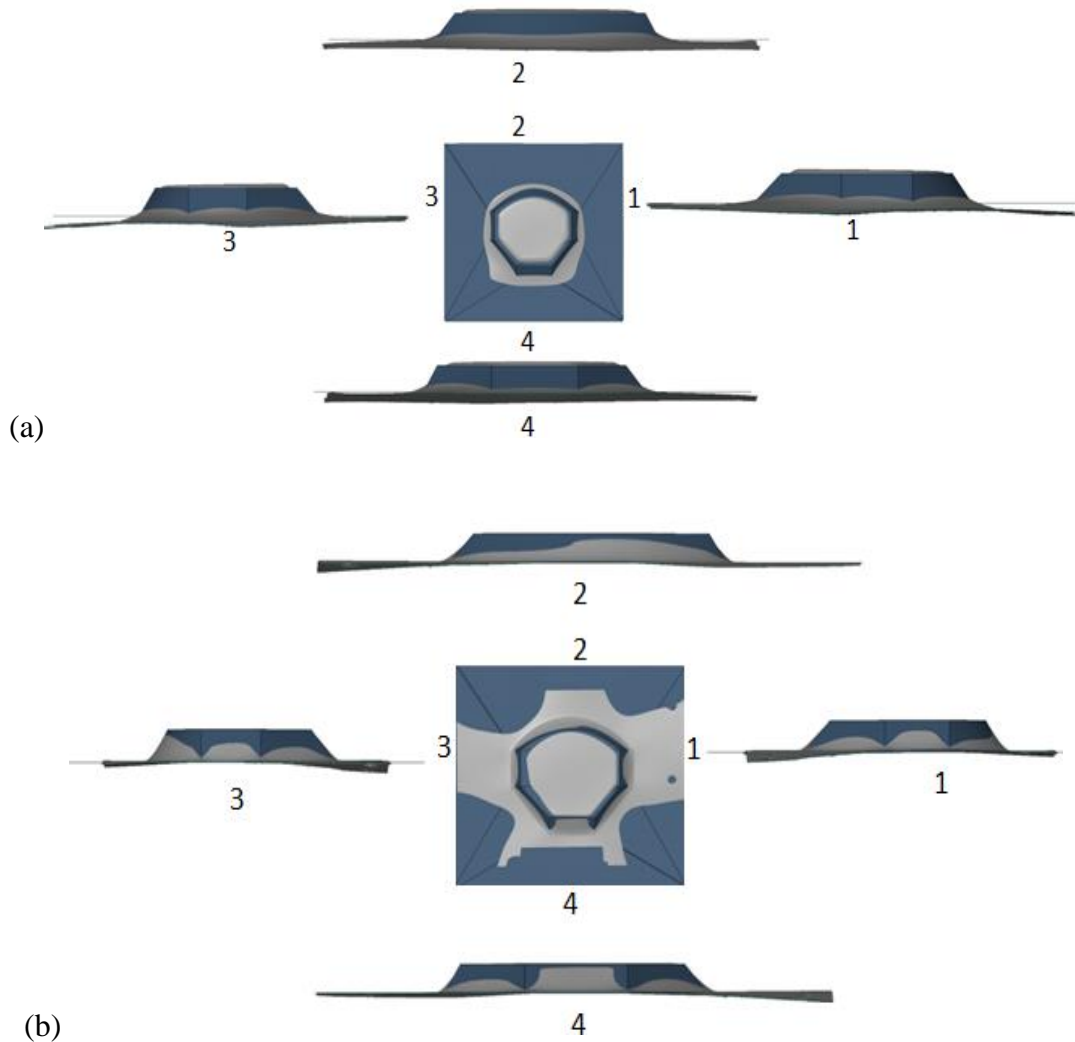


Figure 5-5 Qualitative CAD comparison; top and side views; (a) SS1, (b) SS3.

Quantitatively  $60^\circ$  wall has a maximum deviation of  $-5\text{mm}$  at the lower corner. Interestingly both corners of the  $60^\circ$  wall have maximum deviation. While the highest side of  $50^\circ$  wall angle has  $-2.5\text{mm}$  deviation and  $40^\circ$  wall feature has low or no deviation. As shown in Figure 5-6 and Figure 5-7, high deviation up to  $5\text{mm}$  is observed at the corners of the geometry. To eradicate this particular deviation concept of back supporting plate was introduced. Little or no deviation is observed in  $40^\circ$  wall, curve and rest of the features.

After performing experiments on SS304L, similar experiments were conducted on AA1050H. Three components (AA11, AA12 and AA13) with different rolling directions and forming parameters and BSP were formed. BSP was used for AA13 only while AA11, AA12 were formed in normal conditions. AA11, and AA12 were oriented at different rolling

directions. Improvement of accuracy of the final product was reconfirmed with experiments using AA2024 and AA7075 sheet metal. AA1050H and thus BSP was used for rest of four experiments on Feedrate was 1000mm/min and 4000 mm/min for these two cases respectively. Similar behavior to SS304L is observed for AA1050H, as there is no evidence of the influence of feedrate and rolling direction. Similar behaviors were observed for AA2024 and AA7075.

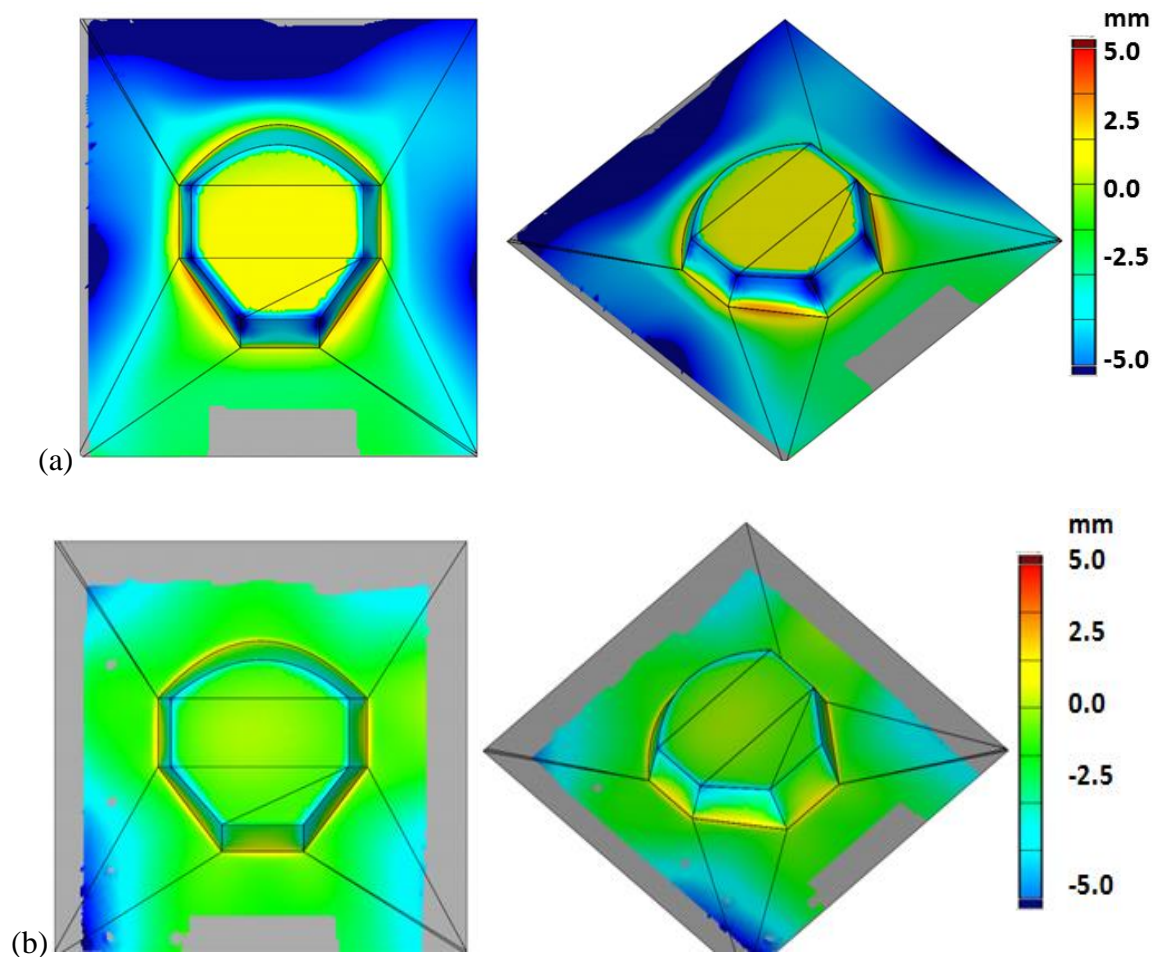


Figure 5-6 Quantitative CAD comparison; top and isometric view; (a) SS1, (b) SS2.

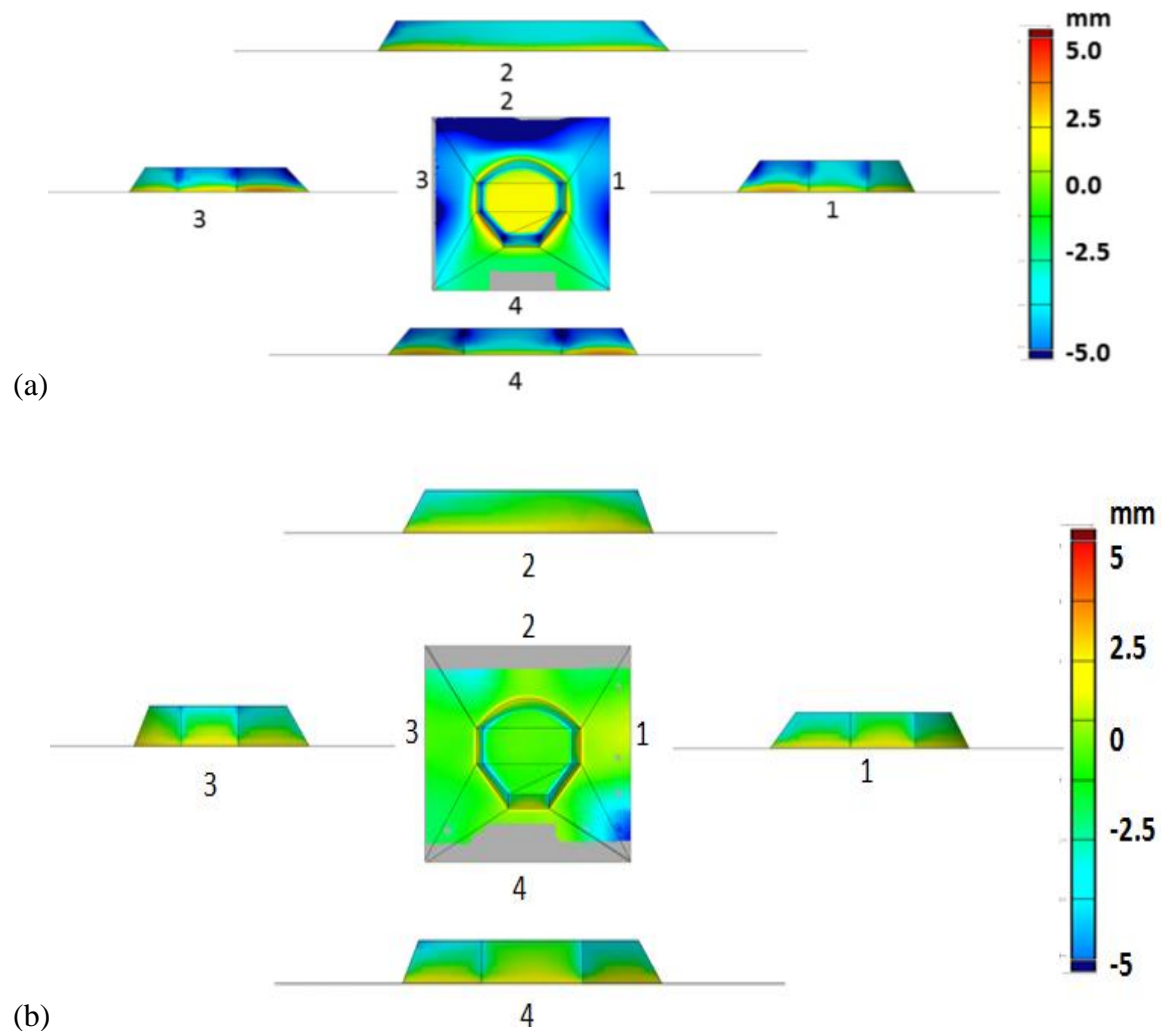


Figure 5-7 Quantitative CAD comparison; top and side views; (a) SS1, (b) SS2.

## 5.2 Thickness

The behavior of sheet steel remains similar to results of previous tests and only localized area of the sheet got affected by the ISF process. Most of the sheet other than the formed region showed no difference in thickness at all shown in Figure 5-8 and Figure 5-9. Thickness in the formed region varied from location to location. The general analysis shows thickness reduction occurred in the following hierarchy.

- a. Corners
- b. Steeper wall angles
- c. Curves
- d. Interface

The thickness reduction around the six corners varied with the wall angle of their respective geometries. Regardless of the thickness difference between themselves, all corner features had more thickness reduction than their adjacent geometries.

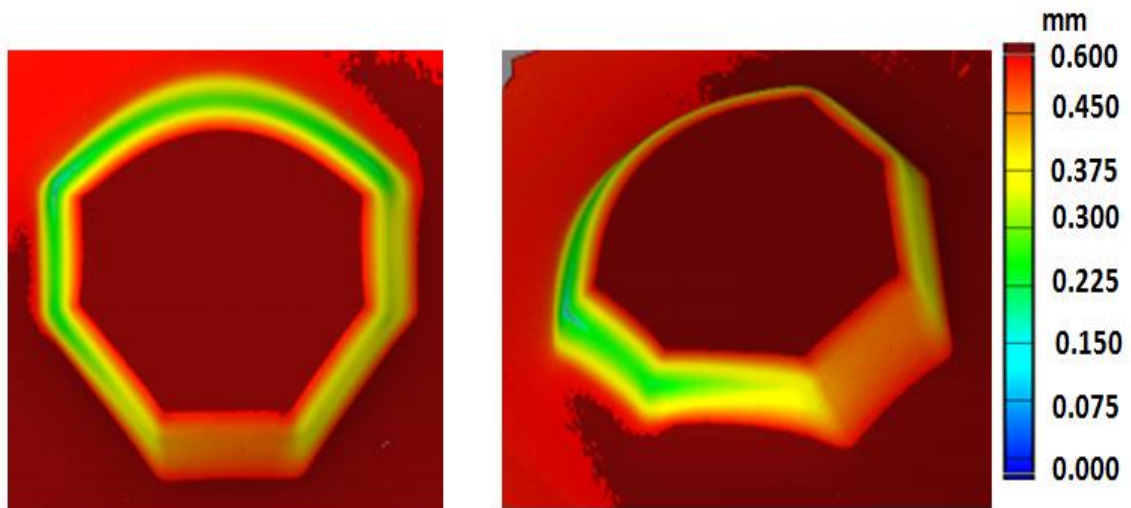


Figure 5-8 Thickness profile SS2; top and isometric view.

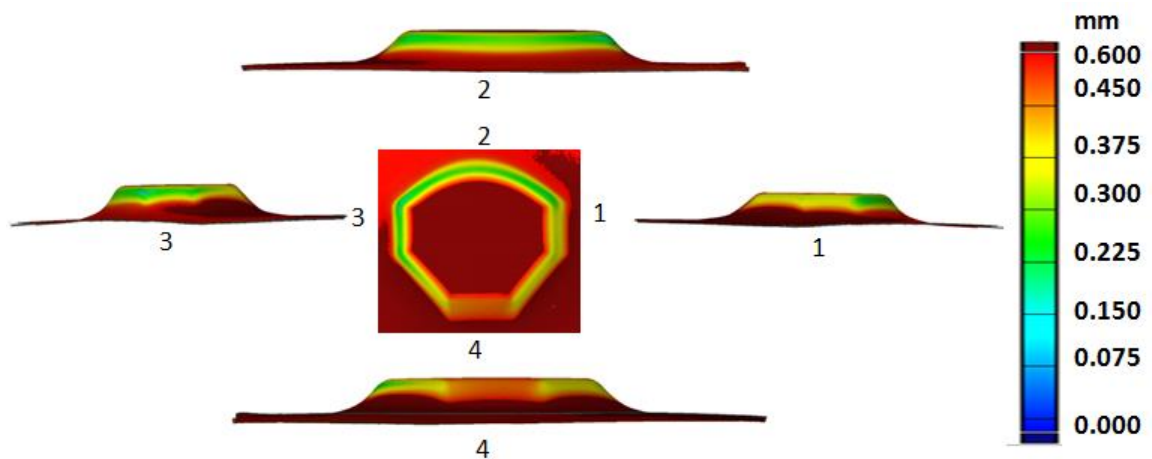


Figure 5-9 Thickness profile SS2; Top and side views.

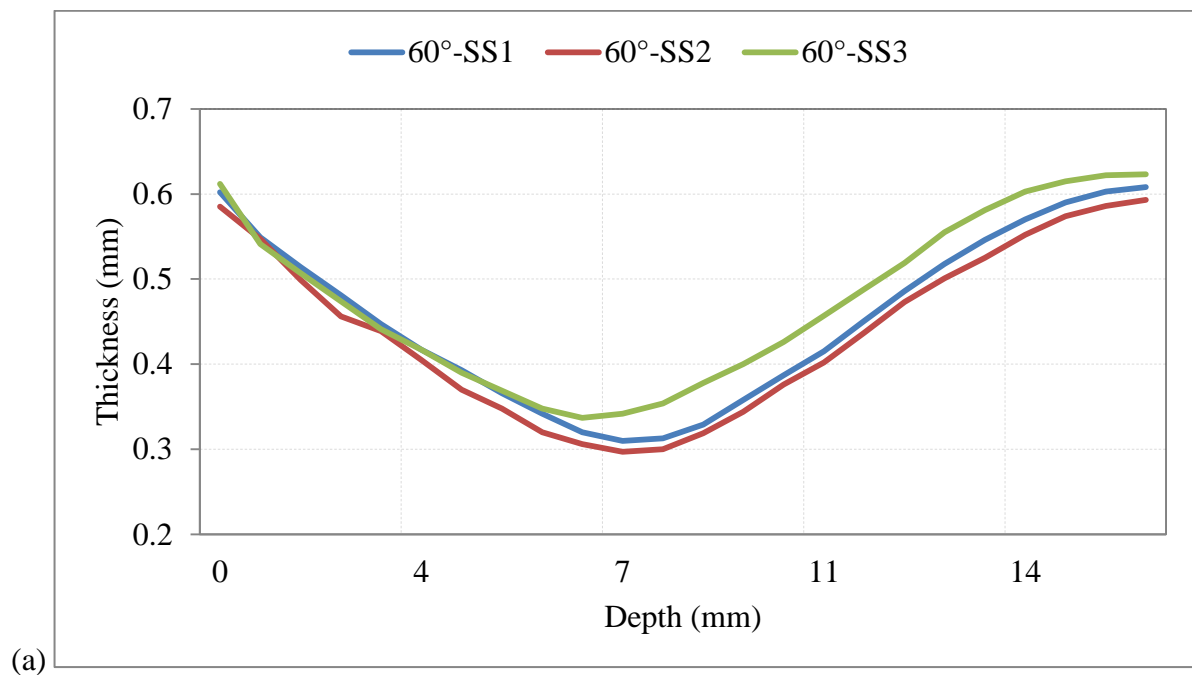
The thickness of corner feature adjacent to  $40^\circ$  wall angle is 0.45mm which is 0.15mm less than the thickness of the wall. This shows a percentage difference of 33.3% between the corner feature and the wall. For these two adjacent corners, there was no difference in thickness with respect to the height of the geometry. A different behavior was observed for corner features adjacent to higher wall angle features.

Corner feature with a wall angle of  $50^\circ$  also has lesser wall thickness compared to the wall itself. Thickness is different at both the corners. This shows that adjacent wall angles influence the thickness of the corners. The magnitude for the thickness also varies with respect to the depth of the feature. Corner towards  $40^\circ$  walls has an average thickness of 0.2mm. With respect to the depth both the top and bottom edges have a thickness of 0.25mm compared to 0.15mm thickness in the middle. More thinned location of the corner is closer to the deeper edge compared to the edge near the sheet.

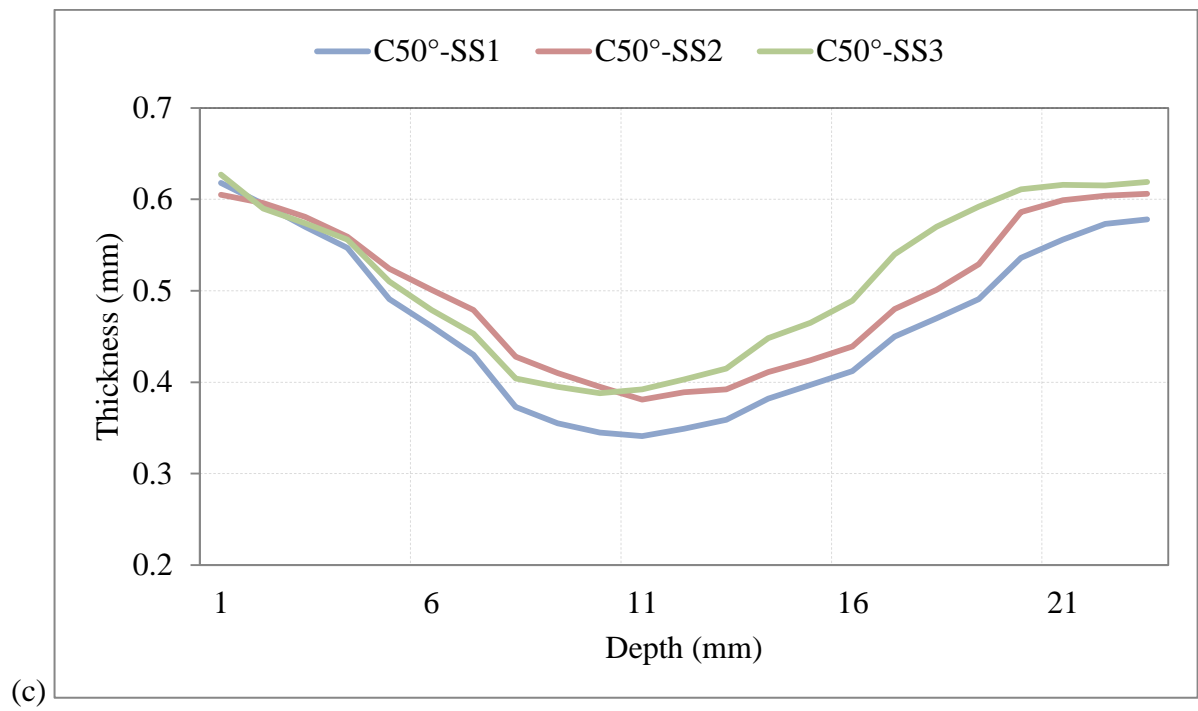
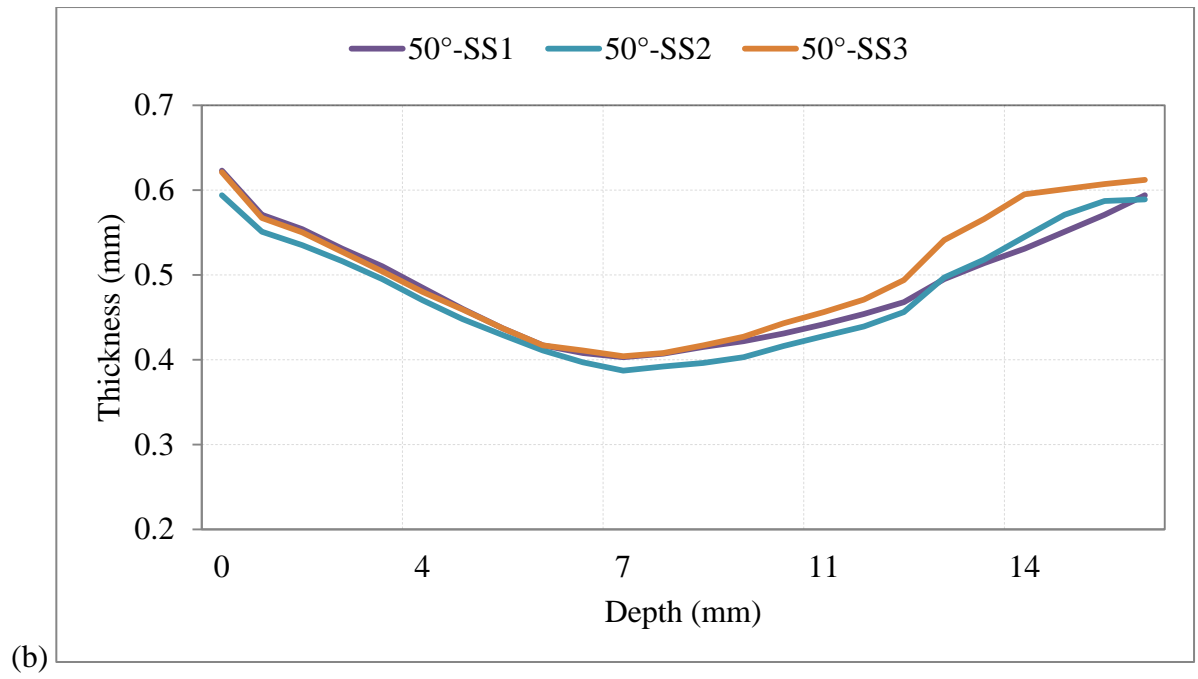
Corner features around  $60^\circ$  wall have maximum thickness reduction compared to all other corner features. It follows a similar behavior reported for  $50^\circ$  wall angle but different in magnitude. Thickness reduction is 0.35mm at top and bottom of the geometry but has a value of 0.225mm in the middle. This thickness diffuses out along both directions of the depth (z).

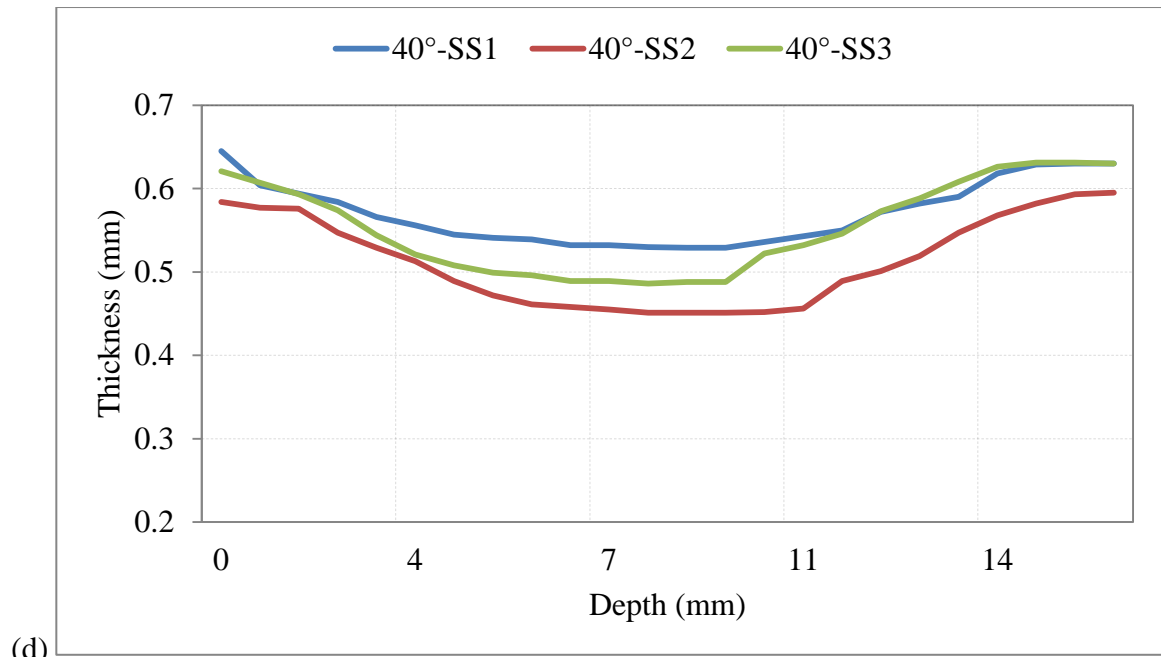
As discussed earlier wall angles have the second highest effect in the designed geometry as shown in Figure 5-10 for SS2. Straight wall feature with  $40^\circ$  wall angle has the maximum thickness of 0.4mm. There are no evident signs of changing of thickness with respect to the depth of the feature for this case. Wall feature with  $50^\circ$  angle has a thickness of 0.3mm and again there are no signs of changing of thickness with respect to the depth. Wall with  $60^\circ$  angle shows a spectrum of thickness changes ranging from 0.35mm to 0.2mm. This shows a percentage difference of 64% within the same wall. Surprisingly reduction of thickness is not directly proportional to the depth of the feature rather it is relatively the same at both the ends with a value of 0.35mm. The region with 0.2mm thickness is near the deeper end (25mm depth) and thickness reduction diffuses out at both ends. This is an interesting behavior and could happen due to a number of reasons one of which can be tool tip cover touching the surface of the sheet while it's being formed. Centre of the curve which has wall angle of  $50^\circ$  shows similar behavior to straight  $50^\circ$  degree wall. However, the corner effect is evident and easily observed on the feature. Thickness variation is similar to the previously discussed corner feature results. Maximum thickness is at the top and bottom while it's minimum near the center. Corner of the curve adjacent to  $60^\circ$  wall angle is the thinnest point in the whole geometry. The interface is termed as the buffer region between the different wall angles. Thicknesses at all the interfaces are changing within a range of 0.00mm to 0.45mm.

As noted earlier, thickness reduction does not follow the Sine law and shows a non-uniform reduction of depth for all the wall angles. The behavior is similar to all wall angles and thickness is lowest in the middle of the wall and increases on both ends. Minimum thickness for 60°, 50° and 40° is 0.3, 0.4 and 0.45mm respectively. The behavior of 50° curve region is similar to 50° wall. The difference between results of different rolling directions and feed rates is under 0.05mm. It is evident that the rolling direction and feed rate did not make significant difference in the thickness of the formed sheet. Similar behavior was observed for AA1050H, AA2024 and AA7075. No evidence of the influence of feedrate and rolling direction was found.

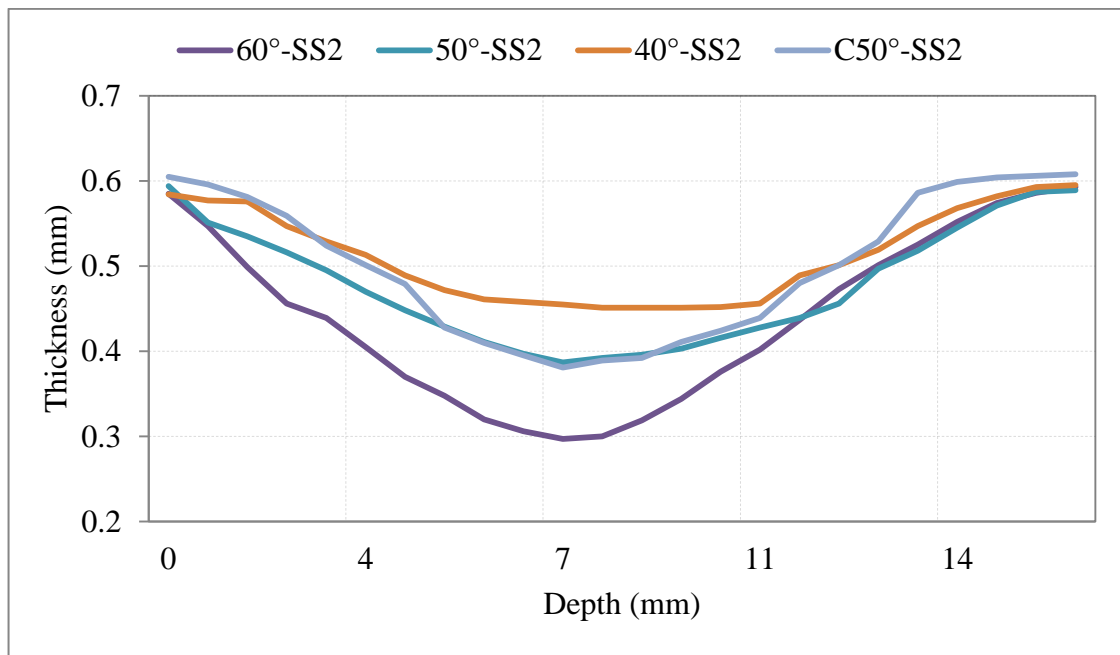


(a)





(d)



(e)

Figure 5-10 Thickness vs Depth SS2; (a) 60°, (b) 50°, (c) Curve 50°, (d) 40°, (e) Wall angle Comparison.

Series of different wall angles were chosen to find interaction between these wall angles. In general thickness reduction only occurred in the formed region and was dependent upon wall angle of the straight and curved feature. As it is evident from Figure 5-11, Figure 5-12 and Figure 5-13 thickness reduction only occurred at the area under action. Thickness reduction contours acquired from circular grid analysis are analogous to 3D scanning measurements



which reconfirm the experimental result. As expected, maximum (70%) thickness reduction is at the corners of the 60° wall angle. Thickness reduction at these corners varied with respect to the depth and values diffused out to 19% on both the edges. Thickness reduction at the corners of 50° and 40° wall angle was around 49% and 34% respectively. 40°, 50° and 60° wall has thickness reduction of 19%, 34% and 49% respectively. Thus there is 14% thickness reduction for every 10°. Thickness reduction of the curve is 34%. As shown in Figure 5-13 behavior of thickness reduction with respect to the depth or wall angle remains the same but magnitude is different. It is also observed through the plotting of the results of the wall angles in the range of 40°-60° could be acquired from this graph. Similar behavior with different magnitude was observed for AA1050H, AA2024 and AA7075. No evidence of the influence of the feedrate and the rolling direction was found.

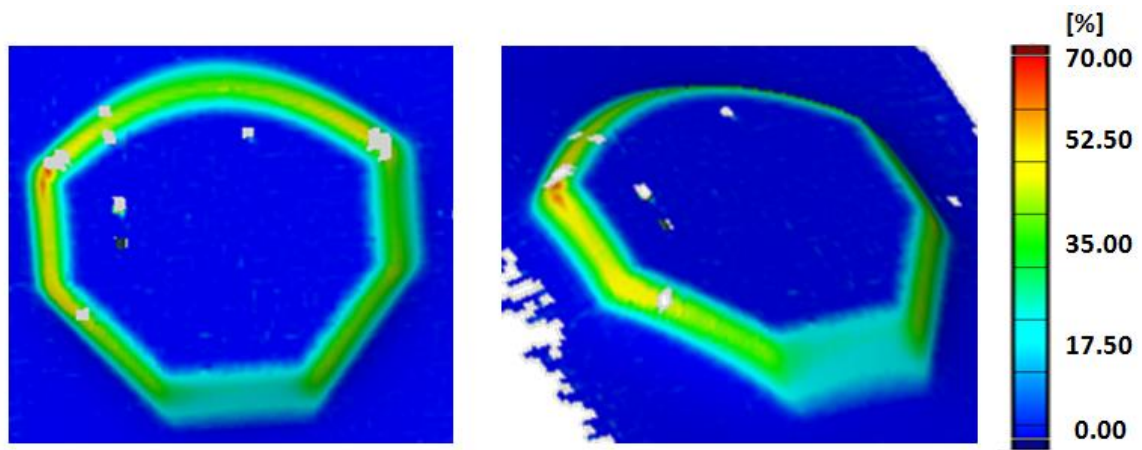


Figure 5-11 Thickness reduction of SS2 specimen; top and isometric view.

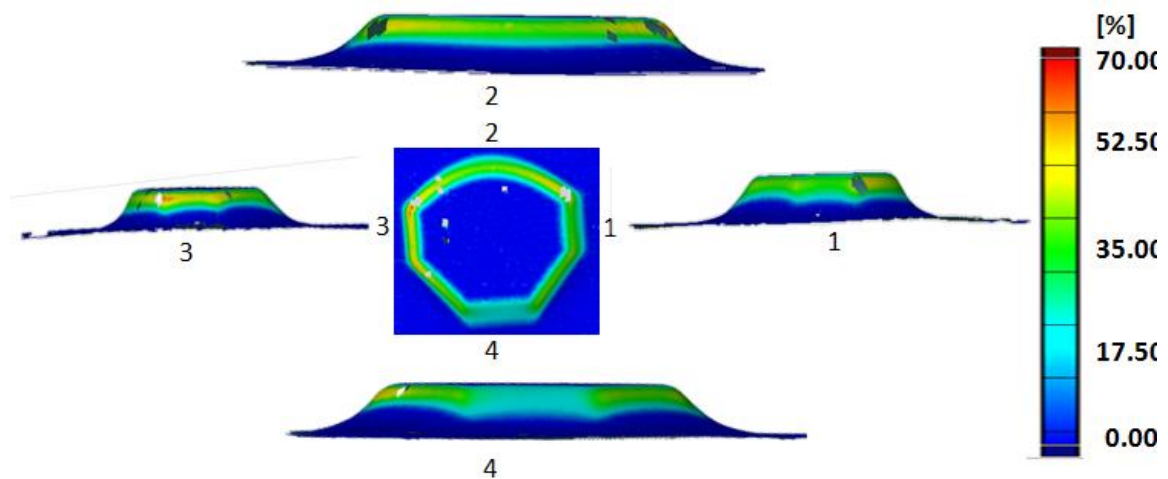
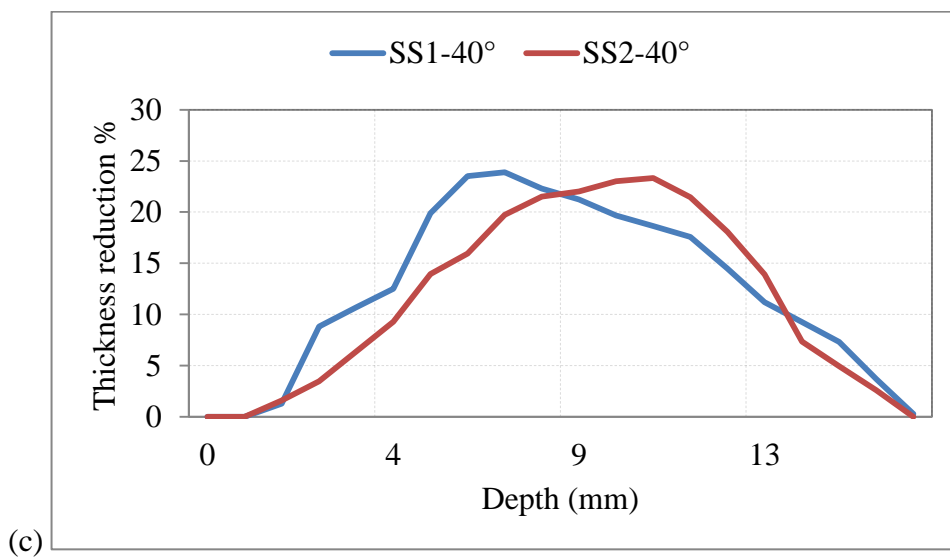
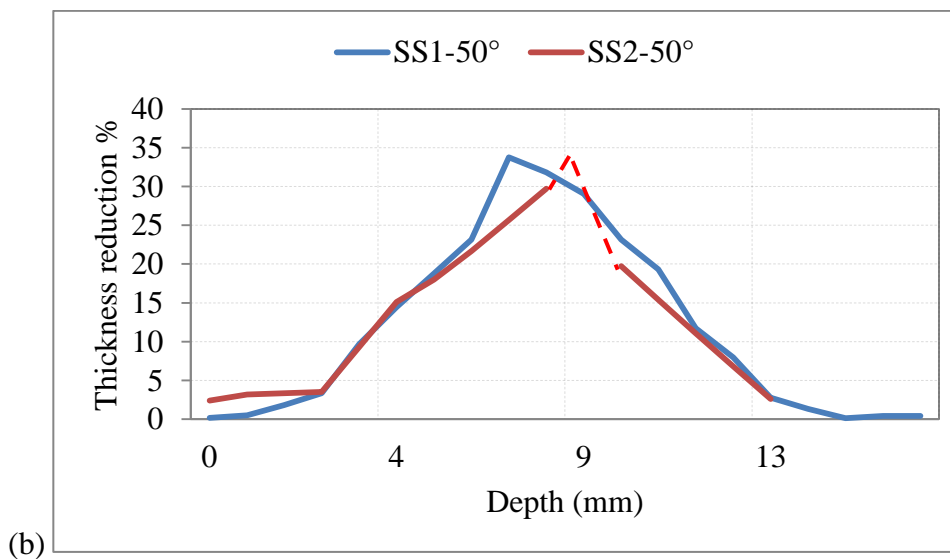
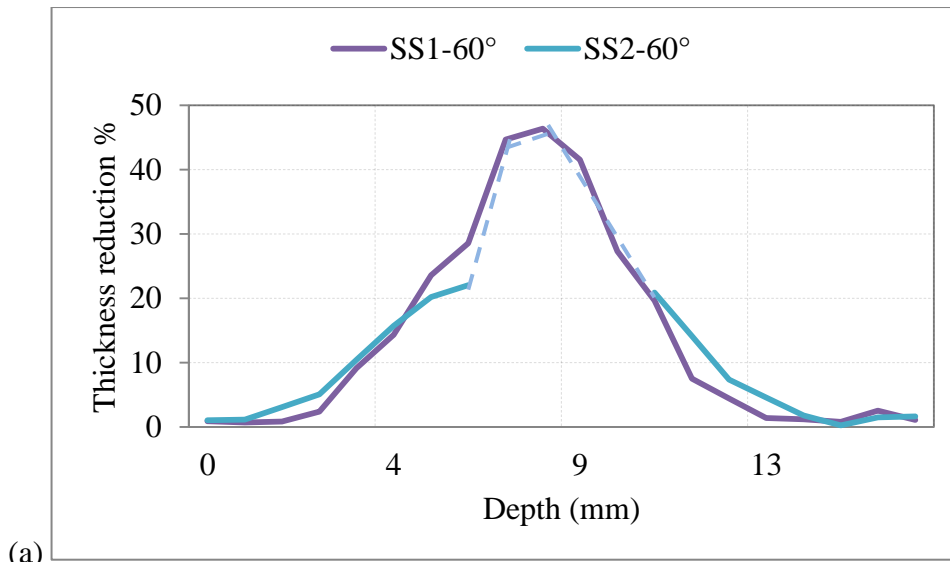


Figure 5-12 Thickness reduction of SS2 specimen; top and side views.



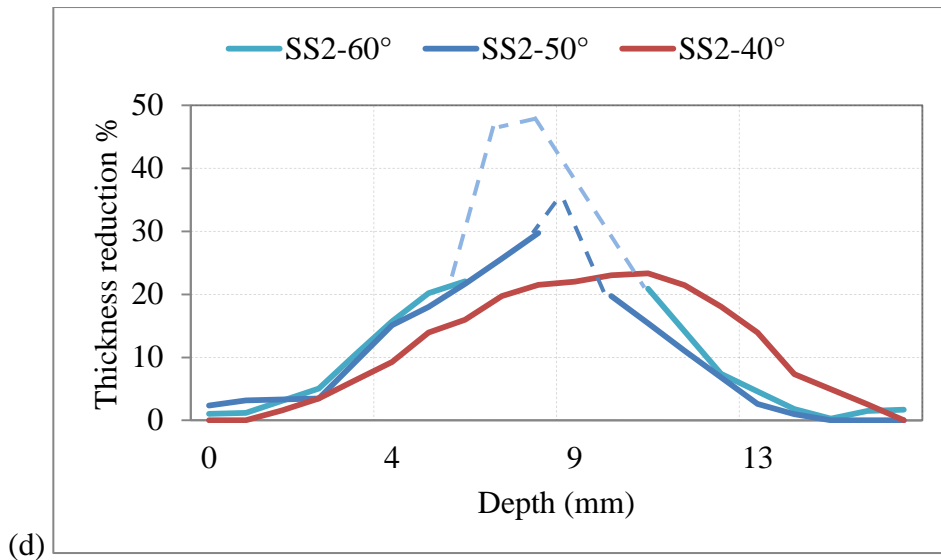


Figure 5-13 Thickness reduction% vs Depth Stainless Steel of SS specimens; (a) 60°, (b) 50°, (c) Curve 50°, (d) 40°, (e) Wall angle Comparison.

### 5.3 Major and Minor Strain

The behavior of the minor strain is similar to thickness reduction, where minor strain is highest for the corners as shown in Figure 5-14. Maximum value of 10% is observed at the corners adjacent to maximum wall angle of 60°. The value of minor strain at corners of 50° wall angle is 7%. Corners around 40° wall have more minor strain (around 5%) than rest of the formed part. This shows minor strain in the geometric features (walls and curve) is well under 5%. The curved part of the geometry showed varying minor strain ranging from -5% to 0% [Figure 5-15]. Rest of the formed and unformed shows a similar behavior of minor strain equal to or less than 0%.

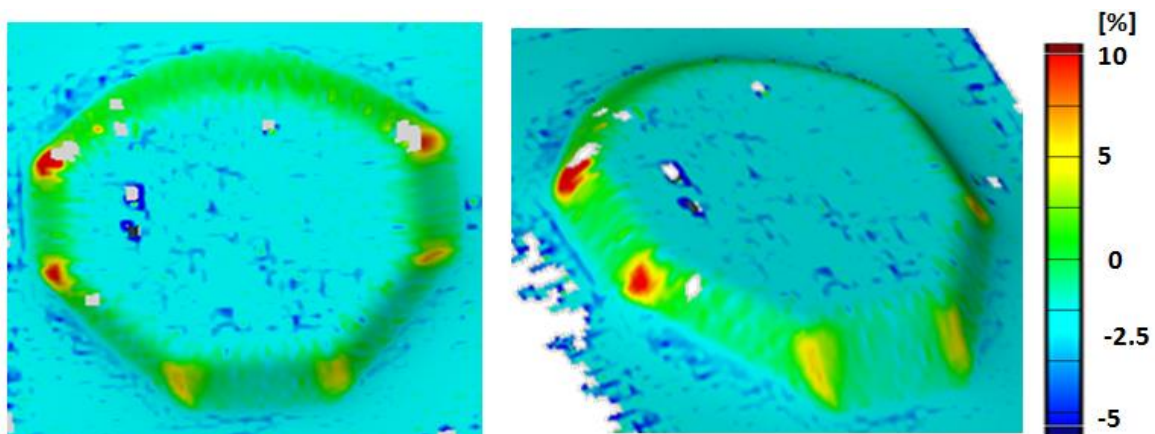


Figure 5-14 Minor strain of SS2 specimen; top and isometric view.

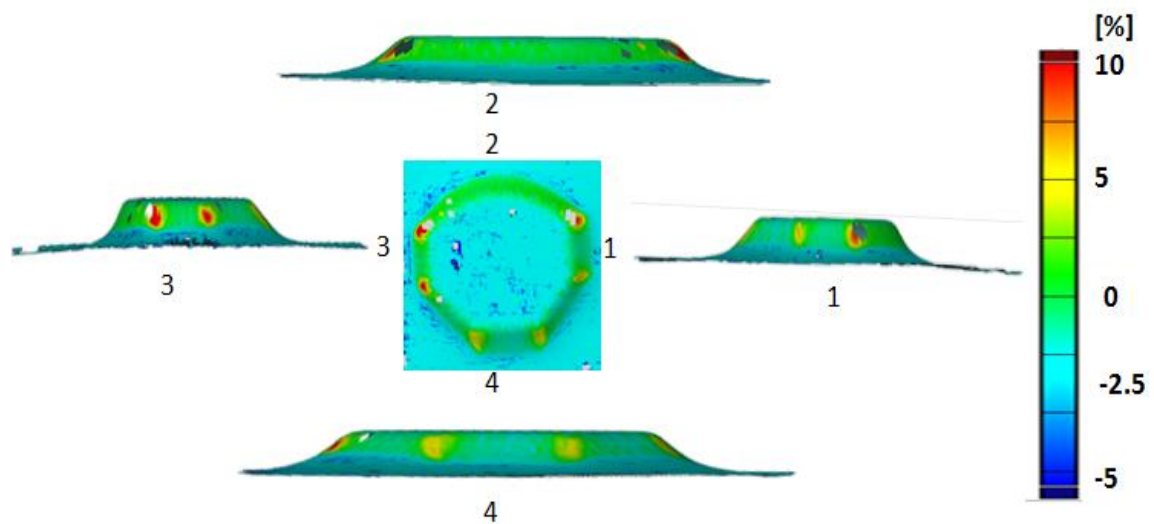


Figure 5-15 Minor strain of SS2 specimen; top and side views.

The major strain shows similar behavior to thickness reduction and minor strain and corners have maximum major strain. The maximum major strain is reported at the corners of the steepest wall angle ( $60^\circ$ ). Corners adjacent to  $60^\circ$  wall angle has a major strain of 150% while it is 75% for the edge adjacent to  $50^\circ$  wall angle. The value of corners adjacent to  $40^\circ$  wall angle has a value of 45% [Figure 11-21].

Major strain for curve starts from over 150% on both corners and is reduced gradually to 45% in the middle. This corner effect is prominent in all results of the geometry and should be understood how these properties behave for different materials.

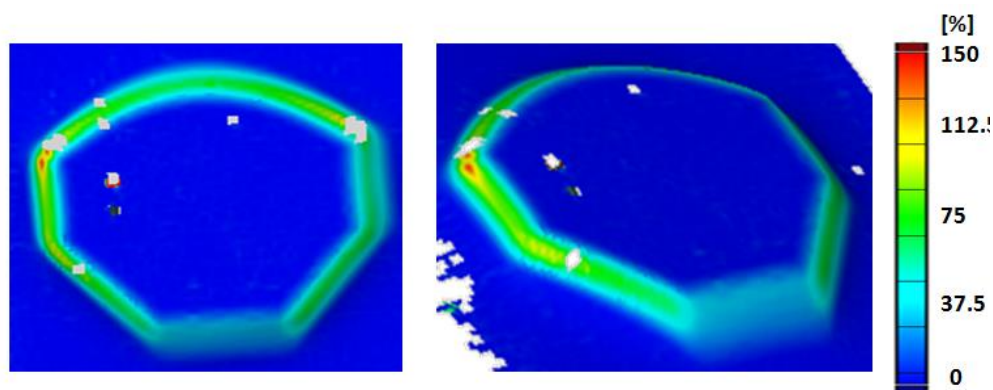


Figure 5-16 Major strain; top and isometric view.

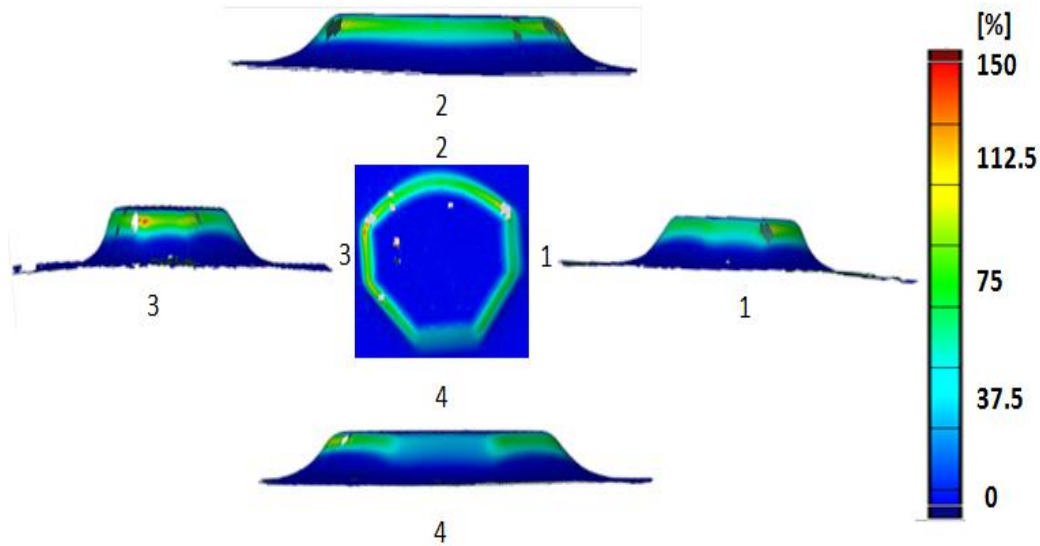


Figure 5-17 Major strain of SS2 specimen; top and side views.

Maximum major strain at 60° wall angle is 95% which diffuses out to 45% as reaching edges at the top and bottom [Figure 5-18]. Most of the area of the wall has a major strain in the range of 55% to 95%. Maximum Major strain on 50° wall angle is 45% which is in the middle similar to thickness reduction and the value diffuses out as at either end i.e.  $Z=0$  or  $Z=16\text{mm}$ . The majority of the wall area has a value of major strains in the range of 38%-45% and though its value decreases up to 30% at the corners. The interface between 40° and 50° wall has major strain over 75% and the side joining 40° and 60° wall angle has a value of over 150%. Figure 5-18 shows major strain plotted on the formed component. Major strains are also plotted on the formed part for clarity and are shown in Figure 5-18.

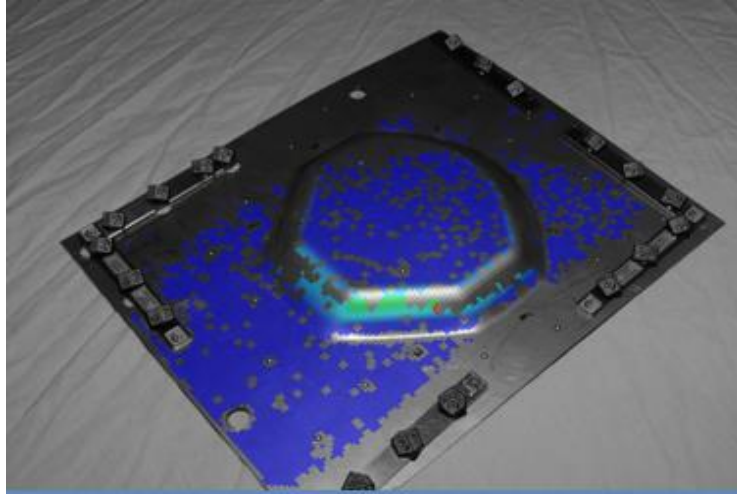


Figure 5-18 Major strains plotted on formed SS304L component.

Figure 5-19 shows major and minor strain graph. Most of the points in the graph are close to 0% minor strain which deduces that circles of the grid are mostly elongated on one side, which is a plane strain condition. Some points (on the minor strain axis) however are plotted from -20% to 20%. The points on the positive side belong to the corners of the geometry while the points on the negative side are software errors. So it is obvious to deduct that all the features of the geometry have similar internal mechanics (plane strain) other than the corners. Corners show bi-axial behavior which is due to simultaneous multiple contact points between tooltip and the sheet metal. The maximum value of the major strain is 150% at the 60° wall as discussed previously and observed through the graph. The lower major strain is reported at lower wall angles.

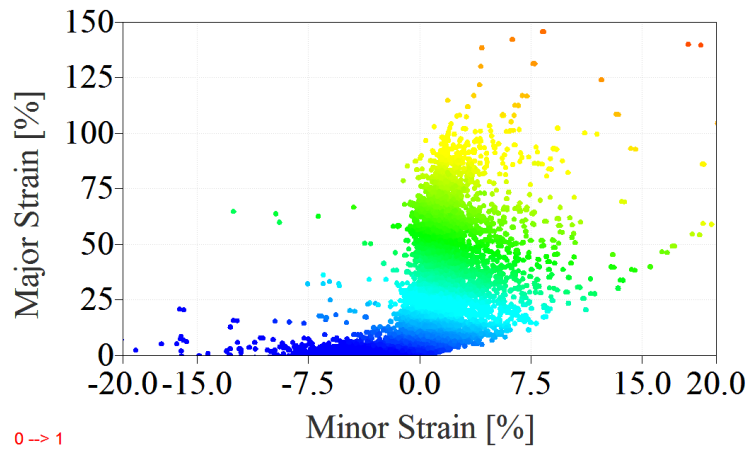


Figure 5-19 Major and minor strain graph.

#### 5.4 Von Mises strains

Von Mises strain in the formed part goes to a surprising 175% at the corners of 60° wall feature and still avoids any type of fracture as shown in Figure 5-20 and Figure 5-21.

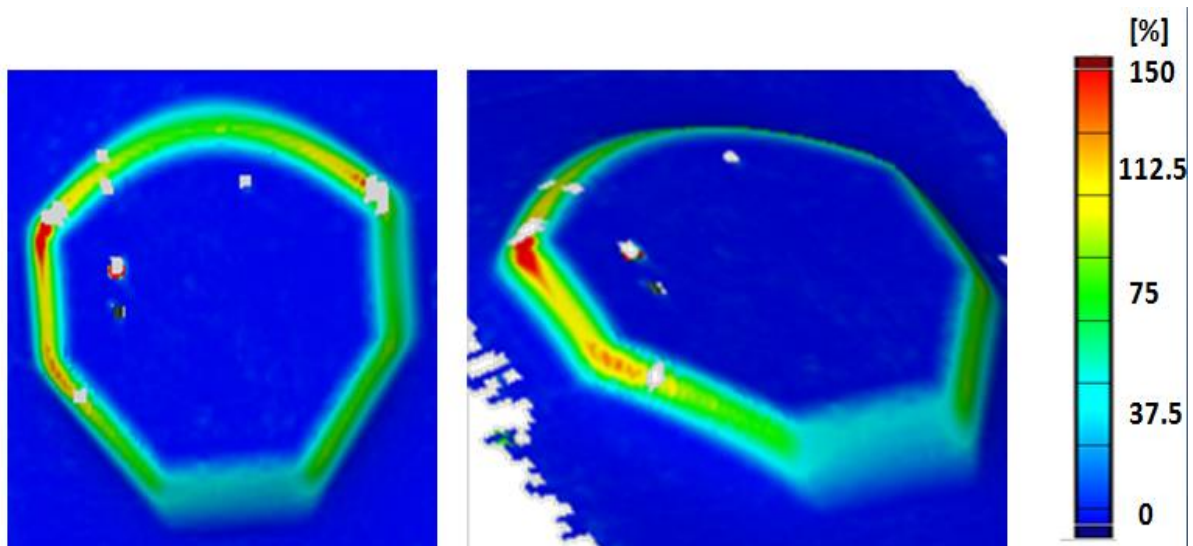


Figure 5-20 Von Mises strains, top and isometric view SS2.

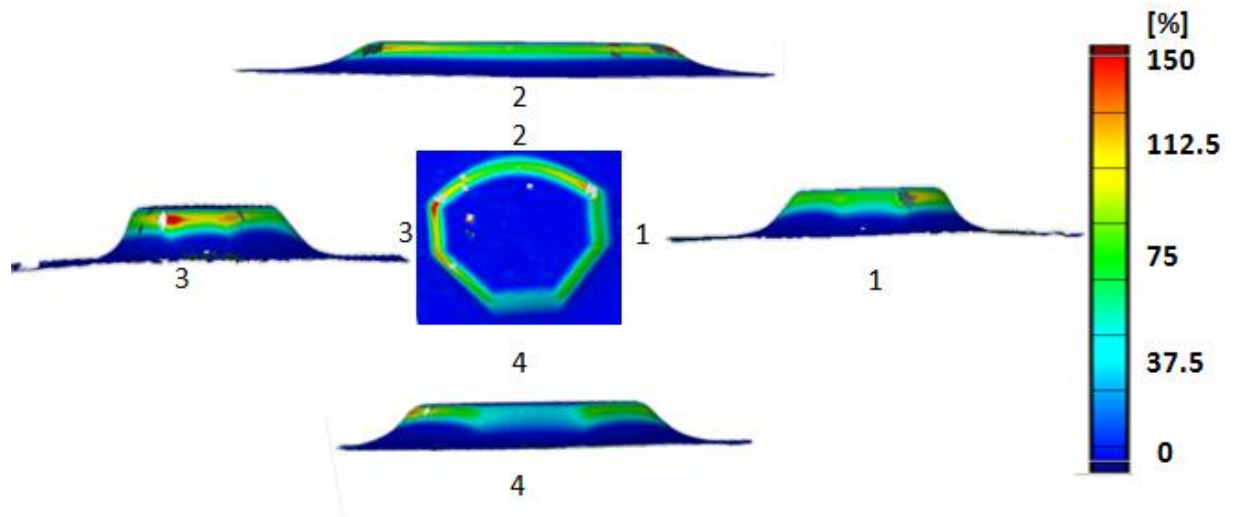


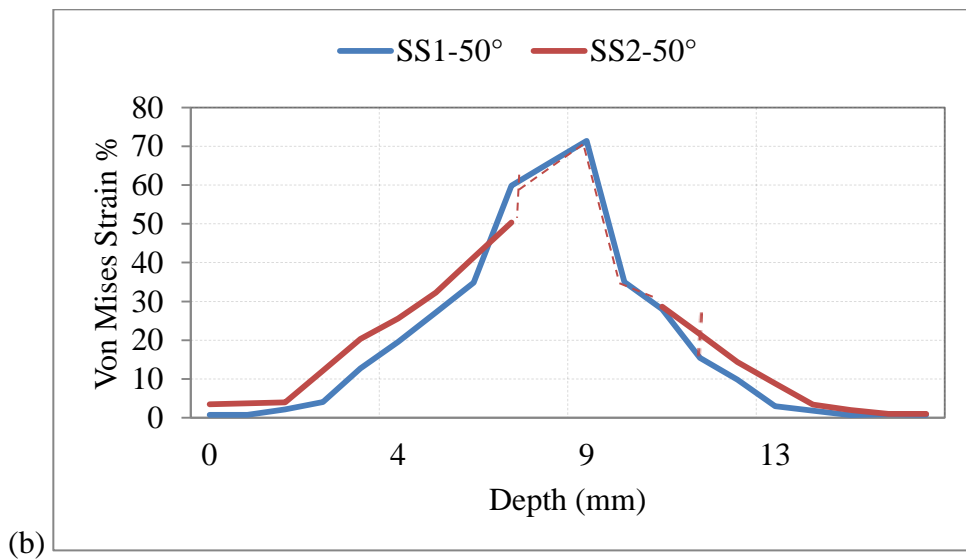
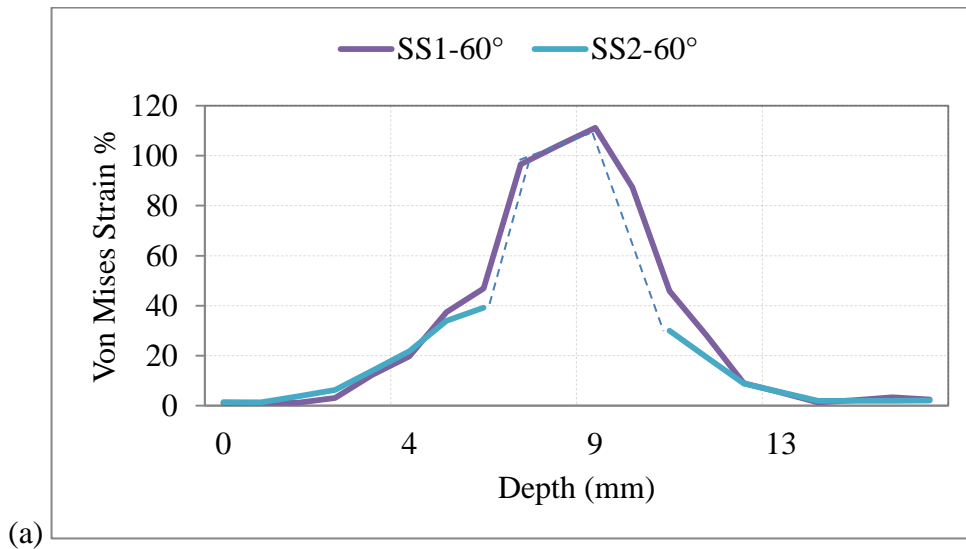
Figure 5-21 Von Mises strains, top and side view SS2.

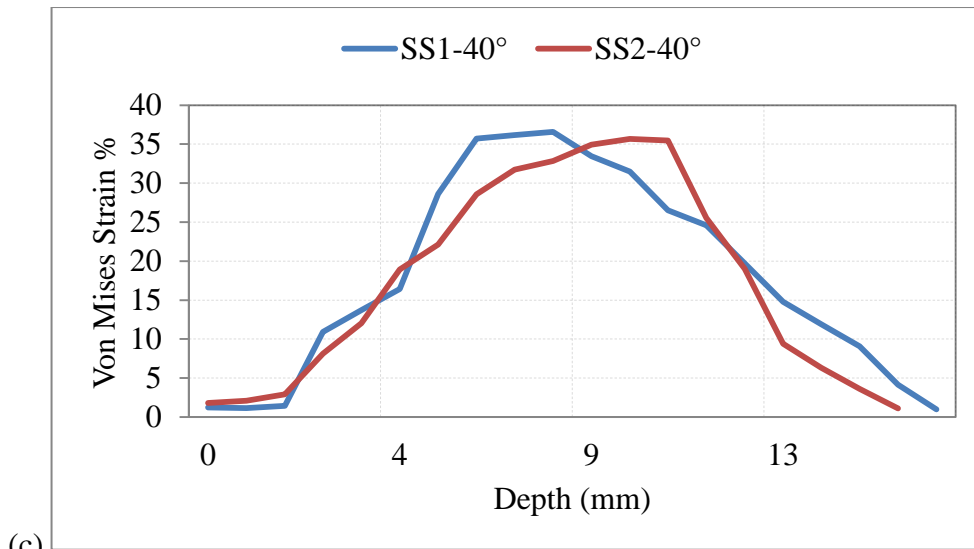
This shows that these two corners are the most prone to failure. Strain behavior remains same as thickness reduction and has a maximum value at the corners of 60° wall angle feature. Though it is highest at the center, it diffuses out to 75% along the depth of the feature. Von Mises strain around the corners, drop to 120% and then to 100% with varying depth. Maximum Von Mises strain is 75% for 50° wall angle feature. It varies with respect to the depth as discussed earlier. 40° wall angle feature has a maximum value of 45% [Figure 5-22].

Maximum Von Mises strain in 60° wall angle feature goes up to a maximum value of 95% which is placed at the centre with respect to depth of the feature. This value diffuses to 70% for most of the wall feature and 35% at the top and bottom edges. For 50° wall angle feature has a uniform value of 75% Von Mises strain and 15% at the edges. 10% Von Mises strain is observed for 40° wall angle feature and remains uniform throughout the depth. It could be deducted from this analysis that strain is more uniform at lower wall angles and the disparity due to depth increases with respect to the wall angle. Von Mises strain of curved wall feature also shows similar behavior to major strain. The maximum value of Von Mises strain for the curved wall is at the corners and it reduces at the centre of the feature. It is 150% at the right corner, 85% at the left corner and reduces to 40% in the middle. So it can be deducted that if wall angle is transitioned smoothly it is better. Varying Von Mises strain along the depth of the part is also observed in the curved feature. Strain varies in both the directions i.e. depth and varying wall angle. It is maximum for higher wall angle and lowers towards smaller wall

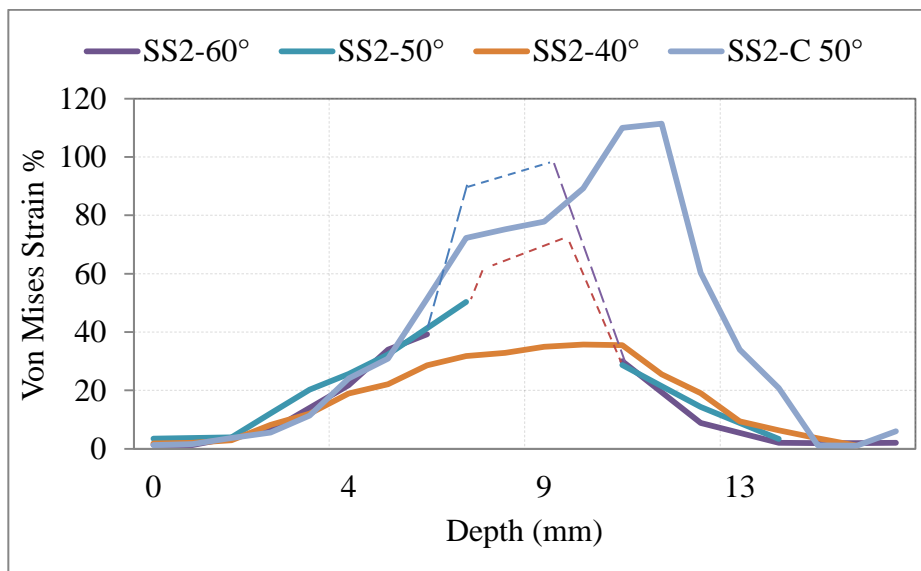


angle. It is highest near the center and diffuses out along the corners. The maximum value of strain for the feature on the right side is 150% and it diffuses out to 35% while the maximum value for the left feature is 75% and it diffuses out to 35%.





(c)



(d)

Figure 5-22 Von Mises Strain% vs Depth Stainless Steel; (a) 60°, (b) 50°, (c) 40°, (d) SS2 Wall angle Comparison.

The most interesting behavior is observed in Figure 5-23. The behavior of the curve is analogous to Stress-Strain curve. Similar behavior with different magnitude was observed for AA1050H, AA2024 and AA7075. , where two dimensionless quantities (Thickness reduction% and Von Mises Strain%) are plotted for different wall angles. Surprisingly all wall angles show similar behavior with different magnitude. The data was plotted and a mathematical model was acquired from the non-dimensional experimental data. The mathematical model for SS304L and AA1050H is a fourth-degree polynomial equation given below [Figure 5-24]. Where  $\epsilon$  is Von-Mises strain% and TR is thickness reduction %.

$$TR = -7E^{-8}\epsilon^4 + 4E^{-5}\epsilon^3 - 7E^{-3}\epsilon^2 + 9E^{-1}\epsilon - 5E^{-1} \dots\dots\dots\text{Equation 5-1}$$

$$R^2 = 0.9958$$

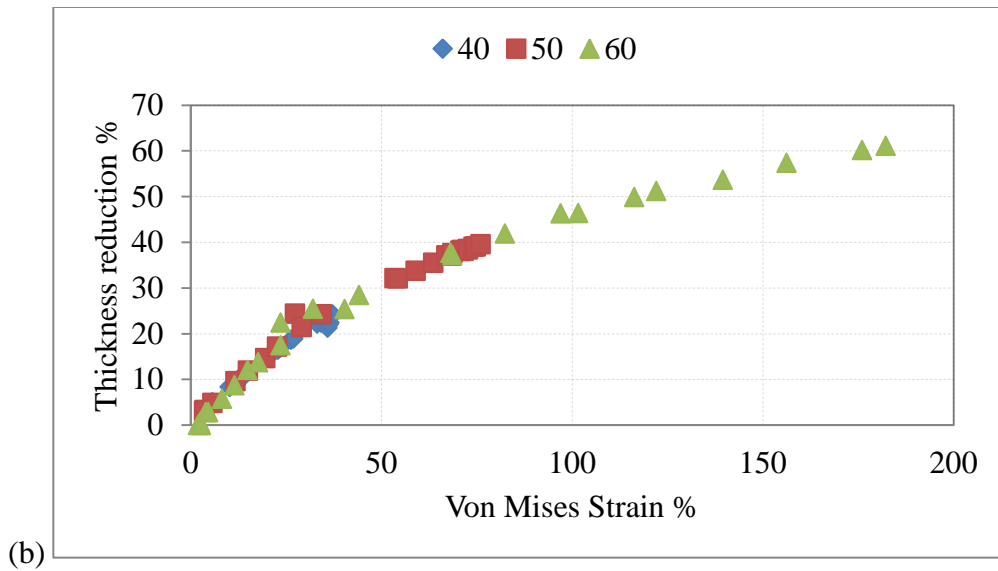
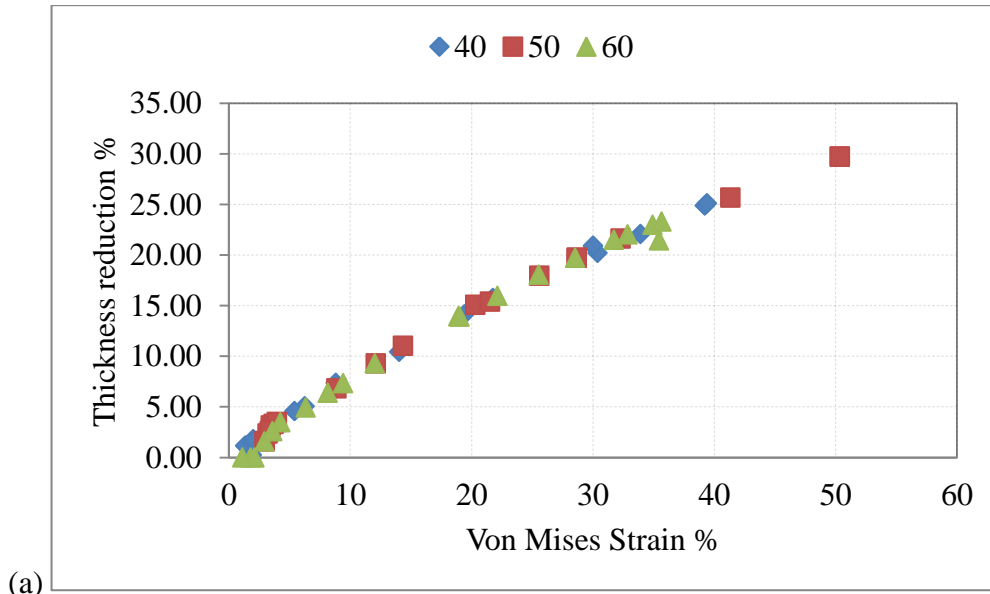


Figure 5-23 Thickness reduction% vs Von Mises Strain%; (a) SS2, (b) AA1-2.

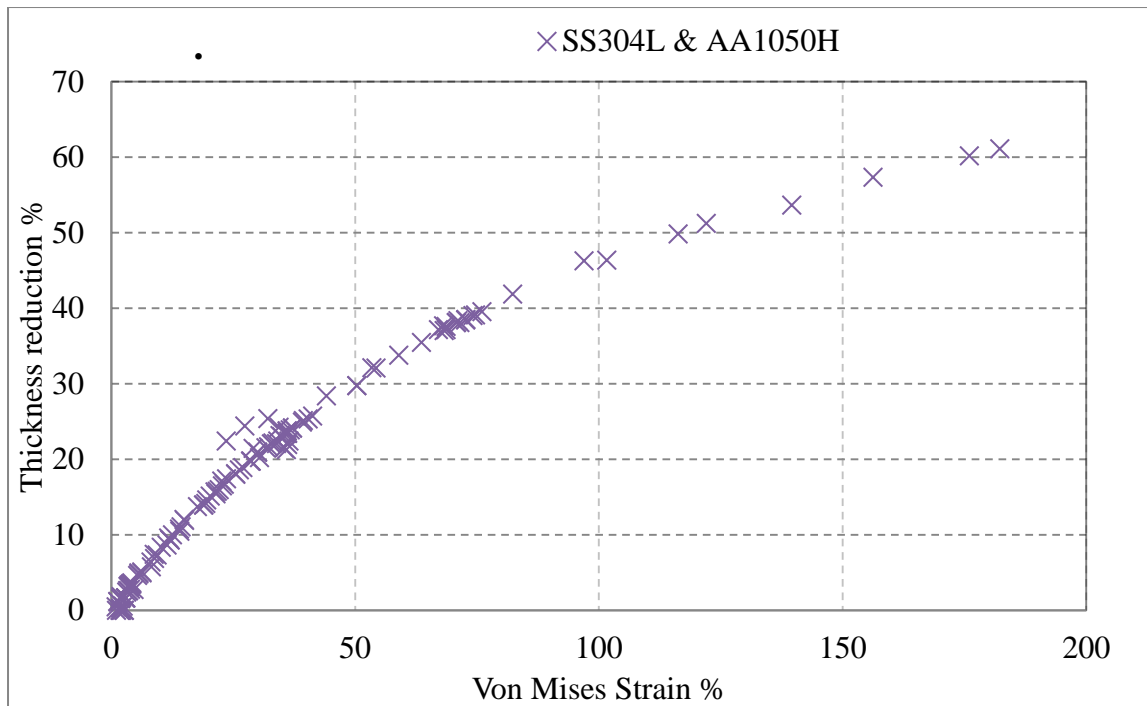


Figure 5-24 Thickness reduction% vs Von Mises Strain% for SS2 and AA1-2, combined.

Experimental data plotted for the corner feature show completely different behavior compared to the wall and curve features. Instead of convex shape, this curve has a concave shape.

Although Equation 5-1 gives an accurate estimation of the curve but still it is very important for the wider applicability of the ISF process to relate it to an analytical model and conventional forming processes. Thus an analytical relationship between strain, thickness reduction and physical aspects of the geometry such as straight wall is derived and the results of both analytical and experimental model are compared to each other. It is also very important to define the limits of the process in terms of macro-parameters such as deformation and the final sheet thickness. It is extremely important to mention that the capabilities of many sheet metal manufacturing processes are effectively characterized by forming limit curves, while this has not been possible for ISF process. In other words, there are lack of methodologies for assessing the feasibility of using ISF for particular components. Although ISF is termed completely different in comparison to conventional sheet metal forming processes, it was found that thickness reduction can be modeled in terms of an analytical model, which is similar to the models developed for conventional sheet metal forming processes.

As it is evident from the experiments that, in contrast with the tensile stress and strain phenomena, where two principal stresses are zero, ISF process goes through a plane stress deformation. This means that there is only one component of zero principal stress, thus we can develop a relatively accurate but simple theory of plastic deformation for the ISF process. Figure 5-25 shows tensile and plane stress conditions. Following equations represent the analytical model of the experimental results. Where  $\beta$  is the strain ratio and  $\alpha$  is the stress ratio.  $\varepsilon_1, \varepsilon_2, \varepsilon_3$  and  $\sigma_1, \sigma_2, \sigma_3$  are strains and stresses in the principal directions deforming under uniaxial and plane stress process [151].

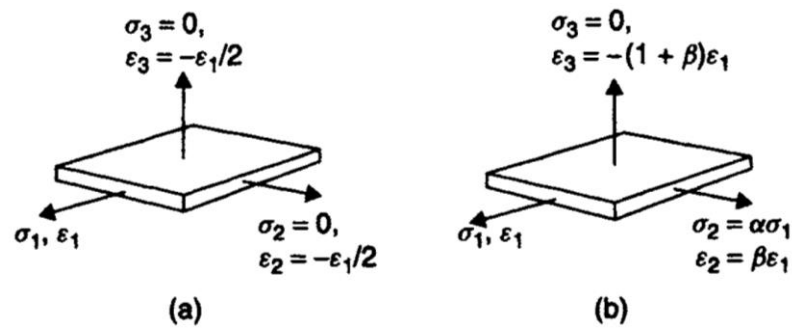


Figure 5-25 Principal strains in elements deformed during (a) Tensile test, (b) Plane strain [151].

In terms of stresses the material element under plane stress will depend upon strength or hardness of the sheet and the stress ratio ( $\alpha$ ). Generally, flow stress ( $\sigma_f$ ) is used for sheet metals strength, which depends upon deformation and changes during the process. There are several common yielding theories to explain the strain and plastic deformation in metals. Metals are polycrystalline and plastic flow occurs when shear stress reaches at a critical level on crystal lattice plane. It is thus expected that yielding will be associated to the shear stress. This has also been reported by some other researchers in the area of ISF. As per Von Mises yielding criteria the yielding will occur when the maximum shear stress reaches a critical value. At a particular instant in ISF (plane stress) process, where the flow stress is known, the stress and the strain ratio for a small deformation could be determined. Flow stress depends upon the work done on the sheet metal during the ISF process and is independent of the stress path followed. This statement is true for monotonic processes. Monotonic processes is defined as the processes where the principal strain increase smoothly in a constant direction, i.e.  $d\varepsilon_1$  increases constantly in positive direction and does not reverse. This monotonic process can be easily observed in the experimental results of the ISF process as both the non-dimensional parameters Von Mises Strain % and thickness reduction %

increases and moves constantly in positive direction and does not reverse. If this was not the case flow stress could not have been predicted through a simple theory.

With respect to work hardening hypothesis, the plastic work done per unit volume of the sheet metal is given by Figure 5-26 and represented with the Equation 5-2. This is integrated and presented in Equation 5-3 and thus the system can be represented in the form of work done per unit volume ( $\frac{W}{vol}$ ). Thus work per unit volume is a function of stress and strain for small increments of strain as shown in Equation 5-4.

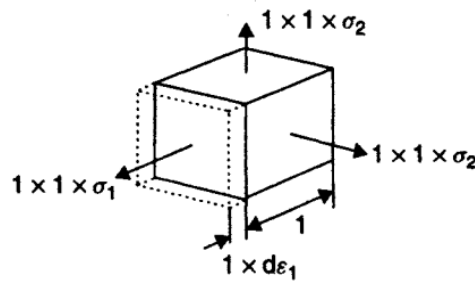


Figure 5-26 Principal element of unit side representing the force acting on a face and small deformation.

$$\frac{dW}{vol} = \sigma_1 d\epsilon_1 + \sigma_2 d\epsilon_2 + \sigma_3 d\epsilon_3 \dots \dots \text{Equation 5-2}$$

$$\frac{W}{vol} = \int_0^{\epsilon_1} \sigma_1 d\epsilon_1 + \int_0^{\epsilon_2} \sigma_2 d\epsilon_2 \dots \dots \text{Equation 5-3}$$

$$\frac{W}{vol} = f(\sigma_1, \sigma_2, \sigma_3) df_2(\epsilon_1, \epsilon_2, \epsilon_3) \dots \dots \text{Equation 5-4}$$

The equivalent stress function for plane strain stress given in Equation 5-5 becomes Equation 5-6 for a general state of stress if an isotropic material is yielding.

$$f(\sigma_1, \sigma_2, \sigma_3) = \sigma_1 \sqrt{1 - \alpha + \alpha^2} \dots \dots \text{Equation 5-5}$$

$$\sigma = \sqrt{\frac{1}{2} \{ (\sigma_1 - \sigma_2)^2 + (\sigma_2 - \sigma_3)^2 + (\sigma_3 - \sigma_1)^2 \}} \dots \dots \text{Equation 5-6}$$

Because the element is yielding while its being deformed Von-Misses stress criteria, the equivalent stress will be equal to the flow stress under a plane stress condition which is presented as Equation 5-7.

$$\sigma = \sqrt{\sigma_1^2 + \sigma_2^2 - (\sigma_2 \sigma_3)} = \sigma_1 \sqrt{1 - \alpha + \alpha^2} \dots \dots \text{Equation 5-7}$$

Required equivalent strain function is then substituted with the equivalent stress function and is given in Equation 5-8.

$$d\mathcal{E} = df_2(\varepsilon_1, \varepsilon_2, \varepsilon_3) = \sqrt{\frac{4}{3}\{1 + \beta + \beta^2\}}d\varepsilon_1 \dots \dots \text{Equation 5-8}$$

As general state of strain can be represented as Equation 5-9.

$$d\mathcal{E} = \sqrt{\frac{2}{3}(d\varepsilon_1^2 + d\varepsilon_2^2 + d\varepsilon_3^2)} \dots \dots \text{Equation 5-9}$$

During propotional and monotonic process, incremental strain  $d\mathcal{E}$  can be replaced by equivalent strain  $\mathcal{E}$  can be written as Equation 5-10 or Equation 5-11.

$$\mathcal{E} = \sqrt{\frac{2}{3}(\varepsilon_1^2 + \varepsilon_2^2 + \varepsilon_3^2)} \dots \dots \text{Equation 5-10}$$

$$\mathcal{E} = \sqrt{\frac{2}{9}\{(\varepsilon_1 - \varepsilon_2)^2 + (\varepsilon_2 - \varepsilon_3)^2 + (\varepsilon_3 - \varepsilon_1)^2\}} \dots \dots \text{Equation 5-11}$$

;

The constant volume condition dictates that sum of all three principal strains is equal to zero and is presented in Equation 5-12. By incorporating strain ratio and assuming that strain ratio remains constant i.e. process is propotional, we get the Equation 5-13 and Equation 5-14.

$$\varepsilon_1 + \varepsilon_2 + \varepsilon_3 = 0 \dots \dots \dots \text{Equation 5-12}$$

$$-(\varepsilon_1 + \varepsilon_2) = \varepsilon_3$$

$$\varepsilon_2 = \beta \varepsilon_1 \dots \dots \dots \text{Equation 5-13}$$

$$\varepsilon_3 = -(1 + \beta)\varepsilon_1 \dots \dots \dots \text{Equation 5-14}$$

As it is observed throughout the experiments that the behavior of the wall feature (curve and straight) is plane strain. We also know that the value of  $\beta = 0$  and for corner features biaxial  $\beta = 1$  [151] which is shown in Figure 5-27.

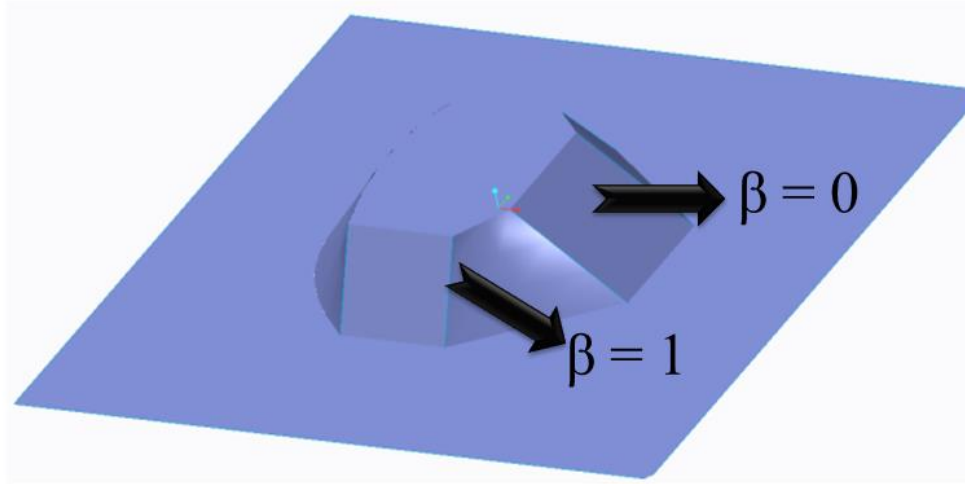


Figure 5-27 Von Mises assumption for value of  $\beta$  for wall and corner feature.

Thus for the wall feature, when  $\beta = 0$  and Von-Mises strain % and thickness reduction % are non-dimensional quantities represented by  $\varepsilon\%$  and  $\varepsilon_1\%$  respectively. Both these quantities are positive for all the elements. So,

$$\varepsilon_2\% = \beta\varepsilon_1\% = 0$$

And

$$\varepsilon_3\% = \varepsilon_1\%$$

Through substitution of the values of  $\varepsilon_1\%$ ,  $\varepsilon_2\%$  and  $\varepsilon_3\%$  and mathematical manipulation, Equation 5-15 can be written as Equation 5-16, which shows equivalent Von-Mises strain% in an element while it is deformed incrementally. Equation 5-16 which is then plotted against the experimental results.

$$\varepsilon\% = \sqrt{\frac{2}{9}\{(\varepsilon_1\% - \varepsilon_2\%)^2 + (\varepsilon_2\% - \varepsilon_3\%)^2 + (\varepsilon_3\% - \varepsilon_1\%)^2\}} \dots \dots \text{Equation 5-15}$$

$$= \sqrt{\frac{2}{9}\{(\varepsilon_1 - 0)^2 + (0 + \varepsilon_1)^2 + (0)^2\}}$$

$$= \sqrt{\frac{2}{9}\{2\varepsilon_1^2\}} = \sqrt{\frac{4}{9}\varepsilon_1^2} = \varepsilon_1\sqrt{\frac{4}{9}} \dots \dots \text{Equation 5-16}$$



Based on this analytical model, following is the comparison [Figure 5-28] of empirical and analytical results for different materials with different initial sheet thickness. The model shows close agreement with the empirical results till 100% Von-Mises strain. Further development of the strain models are required for larger strains in wall and corner features.

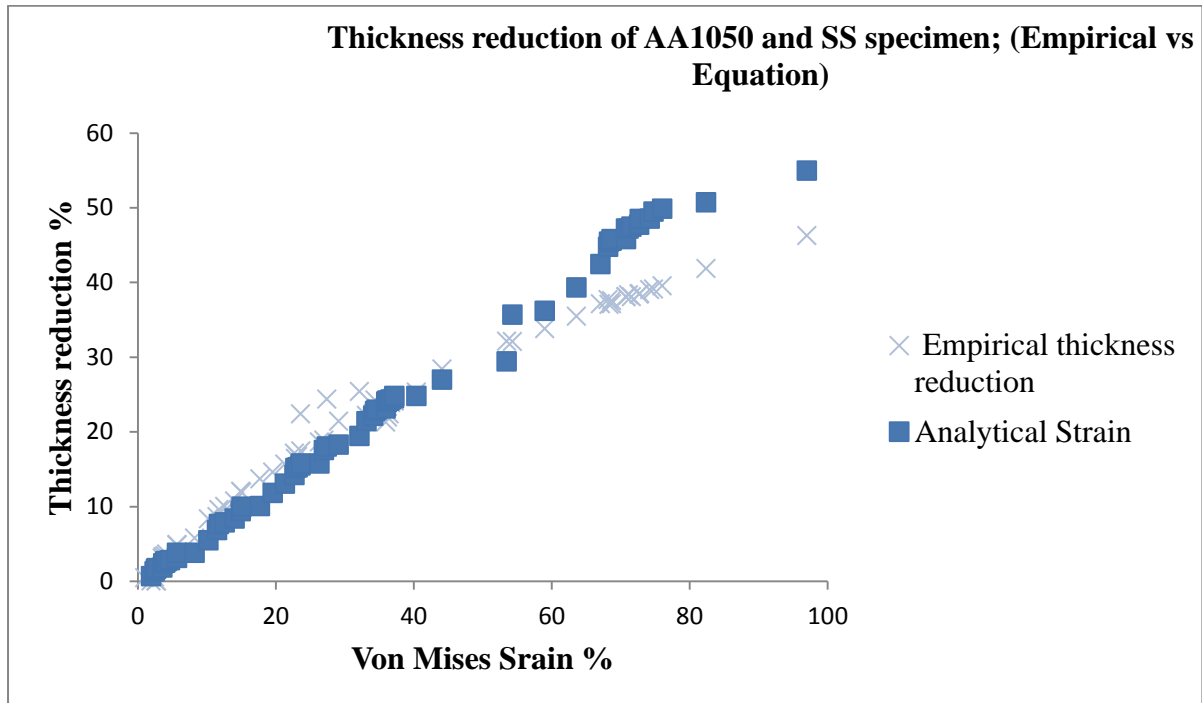


Figure 5-28 Thickness reduction% vs Von Mises Strain% for SS2 and AA1-2, combined, Empirical vs Analytical.

Depth and wall angle are the most important engineering parameters during any forming process and mostly components fail due to these two parameters. Thus it is very important to relate maximum depth and wall angle to Von Mises strains and then to the thickness reduction. To analyze this relationship maximum Von Mises strain % for each test was plotted against the maximum depth it achieved. This graph [Figure 5-29] shows results for a variety of materials at different depths. It is interesting to see that regardless of the material type and forming depth, 40° and 50° wall angle show similar behavior. This is due to the moving location of the tool tip with respect to the area of the sheet while the sheet is formed. For higher angles such as 60°, behavior is different because the same area comes in contact

with the tool repetitively. This behavior is explained intuitively with the help of a cellular model which is explained in the discussion chapter.

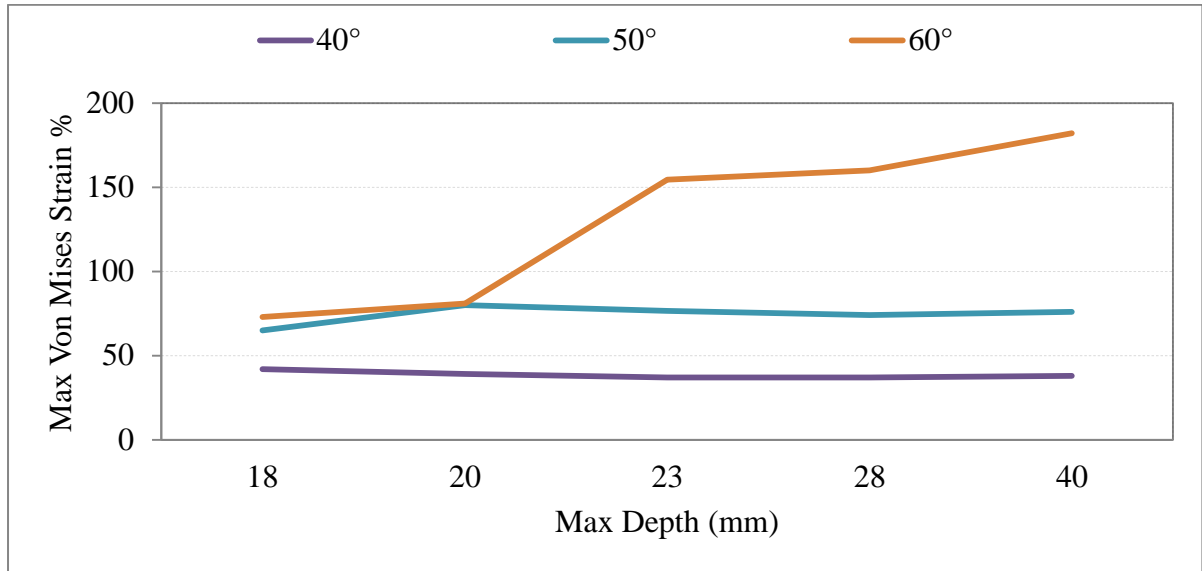


Figure 5-29 Maximum Von Mises Strain% at maximum depths for all Aluminum Alloys.

## 5.5 Surface roughness

The surface roughness of various locations was measured in the geometry. The Alicona was used to measure surface roughness [Figure 5-30]. Some of the surfaces were scanned directly while replicas were acquired for rest. The magnitude of SS304L is different while follows similar surface roughness behavior to AA1050H, AA2024 and AA7075.

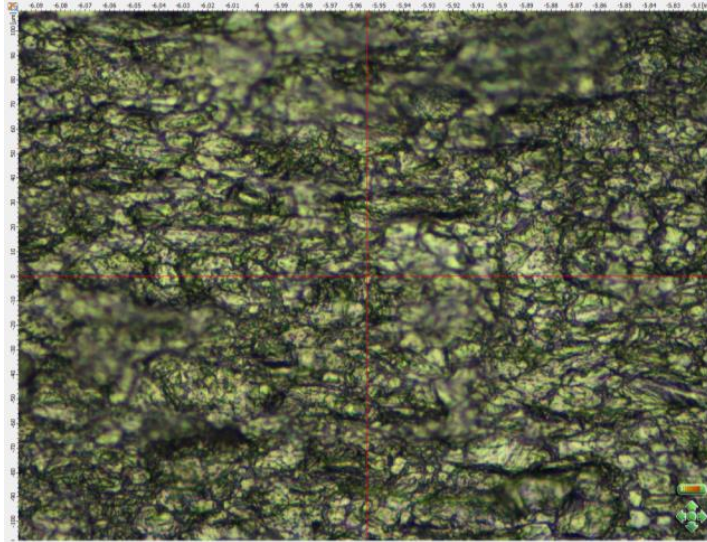
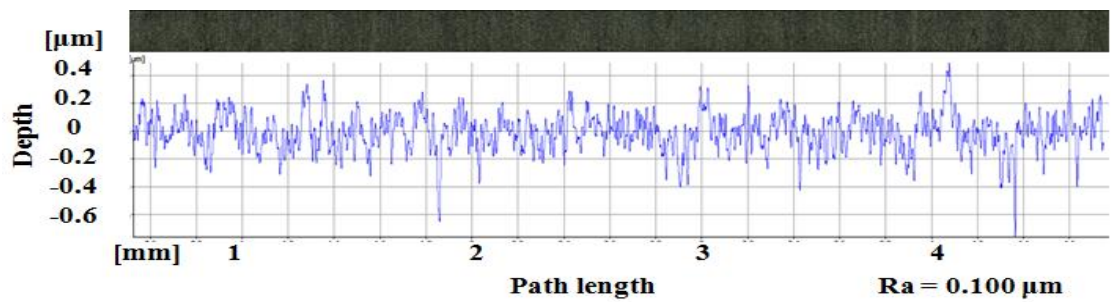


Figure 5-30 Surface view through Alicona.

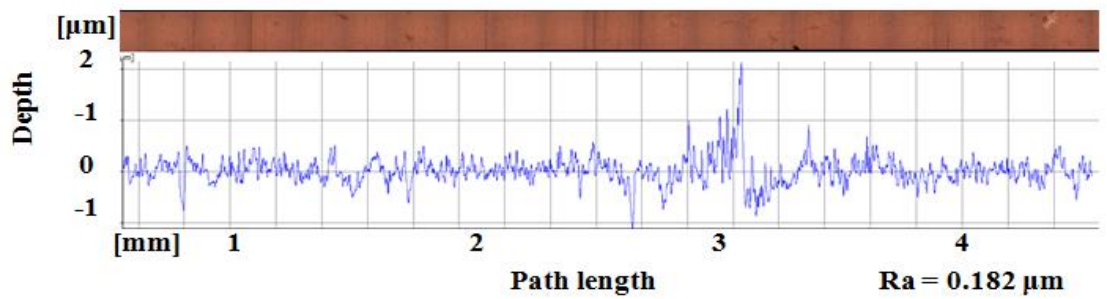
All external and internal surfaces were smooth if observed through naked eyes. Tiny semi-spherical pores with very small diameter were observed at the bent parts of the surface. The surface roughness of 40°, 50° and 60° wall feature is shown in Figure 5-31 and Figure 5-32. As expected surface roughness graph is smoothest for the un-deformed steel sheet with a value of 0.16 $\mu\text{m}$  and fluctuates between  $\pm 0.5\mu\text{m}$ . Its value for 40° wall is 0.182 $\mu\text{m}$  and the plot generally remains in -1 $\mu\text{m}$  to +2 $\mu\text{m}$  range. 50° wall has a value of 0.235 $\mu\text{m}$  and the plot mostly is slightly over -1 to +1.5 range, but fluctuation is a lot within this range, thus higher surface roughness. 60° wall has a range over  $\pm 1$  and thus a higher value of 0.34 $\mu\text{m}$ . The surface roughness of the 50° and 60° curve feature shown in Figure 5-31. The surface roughness of 50° and 60° curve behaves similar to 50° and 60° wall. The plot for 50° curve goes over -1 $\mu\text{m}$  to +1.5 $\mu\text{m}$  with a value of 0.24 $\mu\text{m}$  and the plot for 60° wall has a range over  $\pm 1$  with a value of 0.34 $\mu\text{m}$ .

Figure 5-33 shows surface roughness was plotted against wall angle. It was observed that surface roughness rises with respect to the wall angle and that curved surface has slightly lesser surface roughness compared to wall features but follows similar behavior. The graph between these two properties is not straight and curvature is observed. The relative percentage difference is calculated to know difference between two samples of wall angles. This shows the progression of surface roughness with the increase in wall angle at different steps. The first step (0° to 40°) showed a percentage difference of 44.7%, while for the next two steps (40°-50° and 50°-60°) it was reported to be 23 and 31.5 respectively. For curve

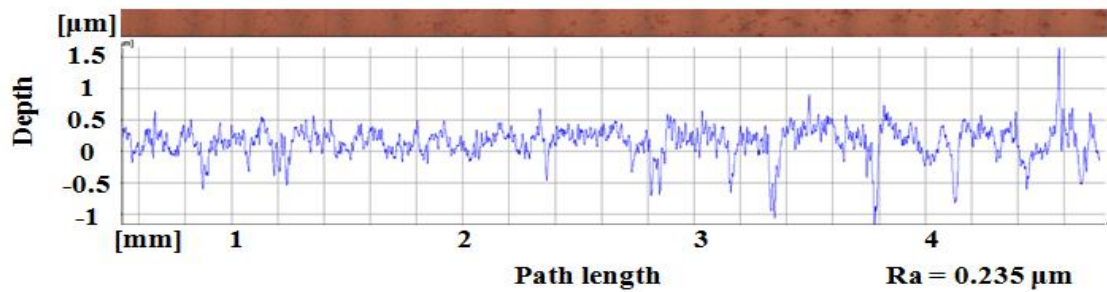
feature it was around 57.5% for 50° curve (similar to 50° wall), while it was 30.2% for 60° wall. Table 6-1 gives surface roughness values of the formed and unformed sheet metal. In general surface roughness increases with higher wall angles. Similar behavior with different magnitude was observed for AA1050H, AA2024 and AA7075. No evidence of the influence of feedrate and rolling direction was found.



(a)



(b)



(c)

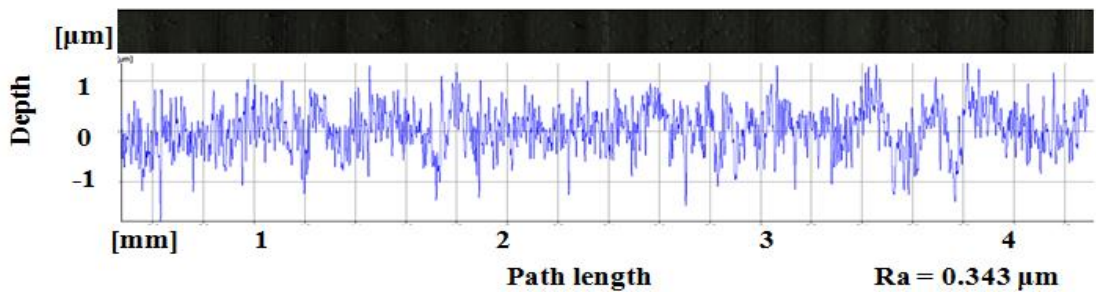


Figure 5-31 Surface roughness profiles of the straight wall feature; (a) As received, (b) 40°, (c) 50°, (d) 60°.

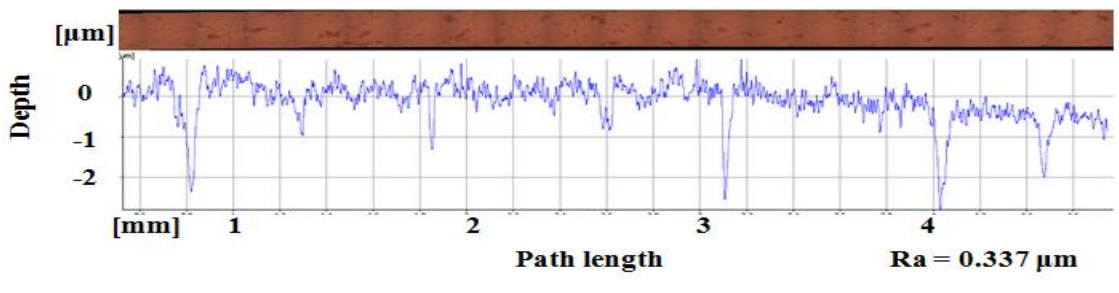
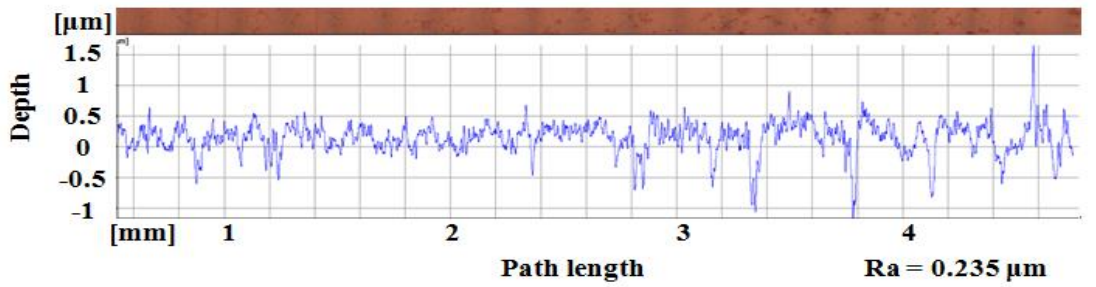


Figure 5-32 Surface roughness profiles of the curved wall feature; (a) 50°, (b) 60°.

Table 5-2 Surface roughness measurements.

Surface Wall Angle (Degrees)	Ra ( $\mu\text{m}$ )	Relative difference %
As received (0)	0.1000	0
<b>Wall feature</b>		
40	0.182	44.75138
50	0.235	22.97872
60	0.343	31.48688
<b>Curve feature</b>		
50	0.235	57.44681
60	0.337	30.26706

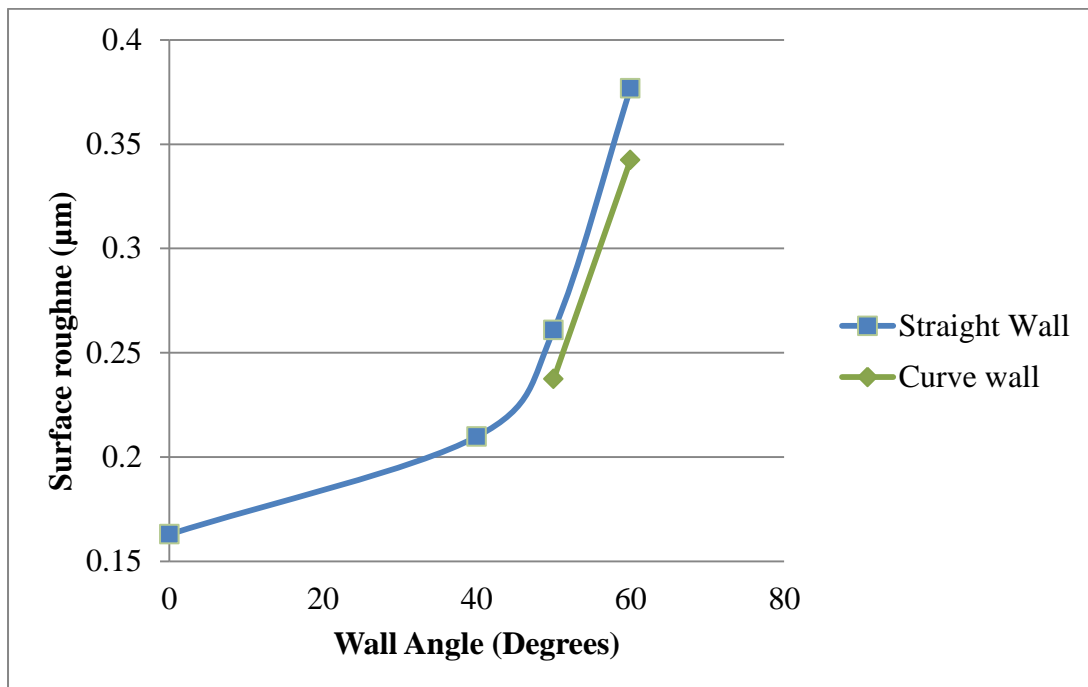


Figure 5-33 Surface roughness with respect to the wall angle.

## **5.6 Summary**

Profile of all three formed parts at different rolling directions and feedrates were discussed. Feedrate and rolling direction do not make any difference in the results. Part profiles of all three samples were discussed and compared. Parts formed with BSP showed a lot of improvement. Thickness reduction of the parts was uniform with respect to each other and the corner feature is most prone to failure. Thickness reduction varied with respect to depth in all features and had a strong correlation with strain. It was observed that strains were highest at the corners feature. Surface roughness increases with respect to wall angle.

## 6. Validation of ISF-FCheck

Having established the behavior of the ISF-FCheck parameters in previous chapters, the question arose of the generality. Would ISF-FCheck produce useful results if complex parts (i.e. with hybrid angular and spherical geometrical features) were formed using a double-sided approach?

To investigate the limits of the ISF-FCheck model, a series of “double sided ISF” tests were done. Details of the geometry and test are provided in Appendix C. As some of the real life components are formed in both positive and negative direction with respect to the sheet. Conventional forming processes can easily form parts in both directions of the initial sheet metal. As ISF is at its infant stage most of the researchers generally form parts in one direction.

The author tried an approach using ISF in both directions. Different geometries were conceptualized for this purpose and one of them was finalized due to its versatility and application in aerospace industry. Section of the geometry is given in the next section and Figure 6-1 shows the final double sided geometry. Final conceptual geometry has two features

1. Basin
2. Cross

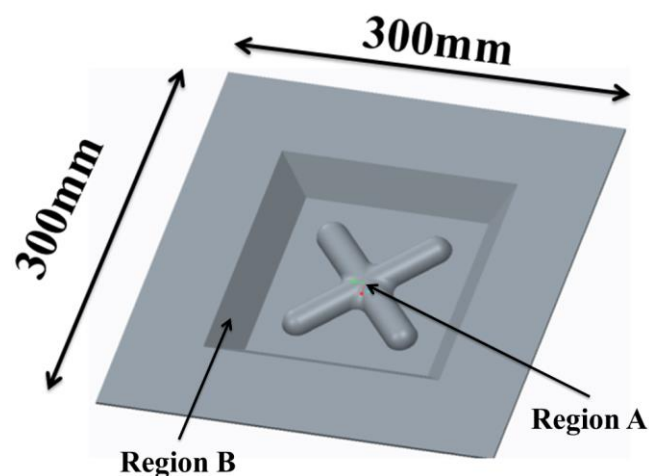


Figure 6-1 Double sided geometry.

The basin is the external feature while the cross is the internal feature of the conceptualized geometry. Both these features were formed using different sizes of tools and different



methodologies. The basin feature was created with a rotating tool tip of 25.4mm (1 inch) diameter while the cross feature was created using 12.7mm (0.5 inches) static tool. Two parts were created using following different methodologies.

1. Case A: Basin created before the cross.
2. Case B: Cross created before the basin.

AA 1050H sheet metal was used to make this part. As it is observed in previous tests that etching marks disappear when tool touches the sheet metal. So it is predicted that for capturing complete circular grid analysis data will be difficult from one side. Because of this both the sheets were etched on both sides to capture as much data as possible.

## **6.1 Manufacturing**

CNC codes for both the cross and basin feature were created using AlphaCAM ® software. Two different sizes of the tools were assigned to form geometries while writing the code. Static 12.7mm (0.5 inches) tool was used to make the cross feature in the program while the static 6.35mm (0.25 inches) tool was used to make the basin. The reason for using smaller tool for the basin feature in the program was small space between basin and the cross feature. Problems occurred during execution of the code and 6.35mm tool was replaced with 25.4mm rotating ball tip tool both in code and test. The problem is further discussed in this section. Both codes guided the tool through a spiral toolpath to form the sheet into required geometry. Feed rate to form the sheet was 5000mm/min and the pitch size was 0.2mm.

Etched AA1050H sheet metal of 2mm thickness was clamped in the fixture. The program was loaded in CNC machine and the home position of the machine was determined through methods similar to reported in previous chapters. The backsupporting plate was not used for these tests; the cross feature was placed in the centre and was small with respect to the hanging sheet. Due to this huge sprawling observed in case A as the sheet was being formed. This meant that force applied by the tool not only formed the sheet into the cross feature but also in an unwanted inclination of the sheet. This effect could be visually seen as the cross feature had more depth at the corners and less in the centre. After finishing the cross feature sheet was flipped over and code for the basin feature was executed. At the start, 6.35mm tool was used but as discussed earlier it started scratching the sheet metal instead of forming it. This was due to the inclination of the sheet because of sprawling during forming of the cross

feature. Due to this static 6.35mm tool was changed to 25.4mm rotating tip tool after recreating and loading the code in CNC machine. This tool started forming the sheet metal into required shape. Intended depth for the basin feature was 40mm but the machine was stopped earlier as it started touching the cross feature. After which sheet metal was removed and data acquisition and analysis were performed. Following are the results acquired from the part.

Case B which was not a prioritized strategy to form the part was easily applicable compared to case A. For case B, the basin feature was formed before the cross feature. Pillowing effect was not observed at the central region and the area was straight. Sheet metal was then rotated and the tool was calibrated with respect to the formed geometry. Cross feature was then formed on this raised (formed) geometrical feature and the corners of the basin feature served as supports for the hanging sheet.

## 6.2 Profile and accuracy

Each of the ISF manufactured “cups” was optically measured using a GOM ATOS Tripple Scan III scanner for accurate scans with detailed resolution. Aluminum is a highly reflective material and initially 3D scanner was not able to acquire data properly because of the specular reflection. Thus a thin layer of paint (Ardox) was applied to create a matt surface. After acquiring data from the 3D scanner the point cloud was polygonized, smoothed and processed to get the final useable shape as shown in Figure 6-2.

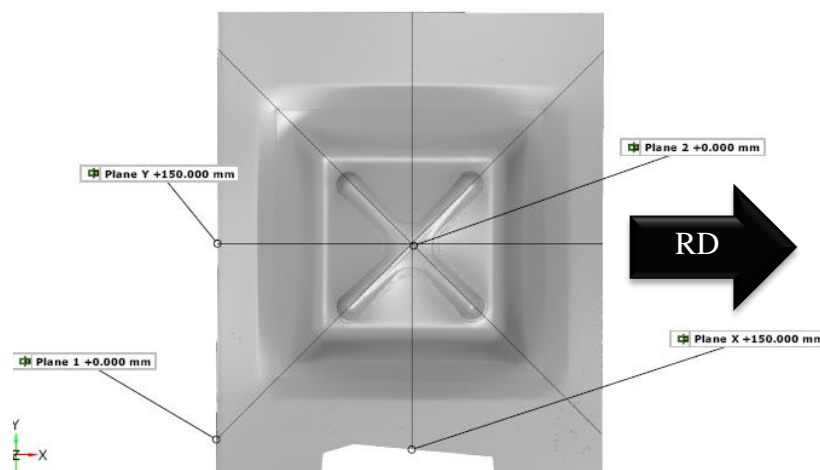


Figure 6-2 Scanned CAD model with sections.

Four sections were created in the scanned geometry. Because of symmetry, only two sections will be discussed i.e. X and 45-degree plane [Figure 6-3]. Although Cross feature is in the middle of the plane X yet it is not visible in this section due to sprawling effect discussed earlier. The sheet profile does bend in a curvature due to cross feature. Thickness is highest at the ends for the basin feature and reduces as it moves towards cross feature. Similar behavior was observed and reported in previous chapters as well. The plane at 45° shows a section of both cross and the basin feature. Basin feature has a similar profile as discussed in the X plane. In the middle region, the sheet goes down because of start region using a circular profile. The middle area of this profile is at the same level and straight. This shows that this part of the sheet bent as per code but the adjacent material deformed unwantedly. Due to which depth of the feature seems to be lesser than the required value.

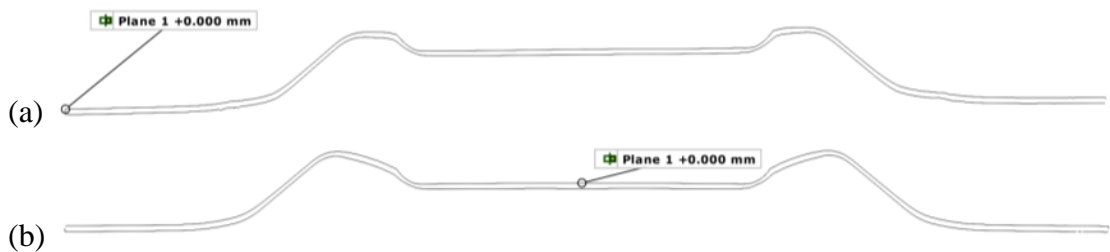


Figure 6-3 Section profile (45); (a) Case A, (b) Case B.

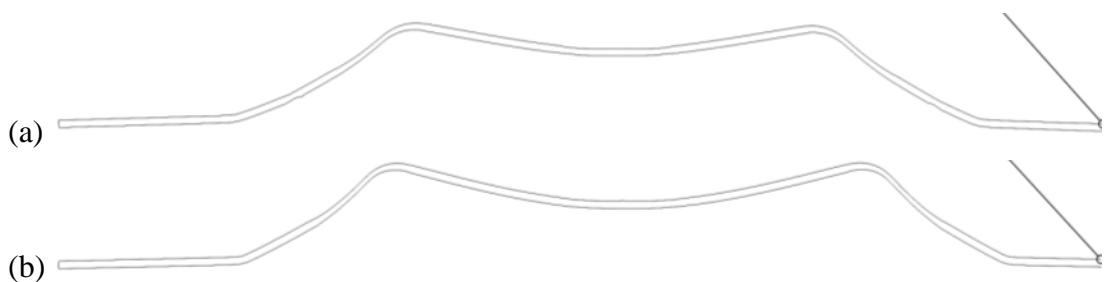


Figure 6-4 Section profile (45); (a) Case A, (b) Case B.

In short, the required profile is successfully achieved at this section line but further research is required to get exact shape around this section. Backsupporting plate would be excellent for this purpose. The combination of double sided ISF and backsupporting plate would be an interesting area to explore.

As discussed previously blue geometry is the CAD and grey is the scanned geometry [Figure 6-5]. It is observed through all of the experiments that accuracy of the geometry depends on several features such as tool size, tool path, geometry required, and material properties. Furthermore software accuracy, smartness and capabilities also affect final CAD comparison. Basin feature for both the cases A and B show similar results, while differences could be observed in the cross feature. For double sided forming, it is visible that sheet has sprawled and covered the CAD model in region B i.e. outermost region. It is also interesting to observe that scanned model covering CAD model changes with respect to length. It is minimum at the edges and maximum in the centre. Formed part edges are also not sharp at the ends in region A. The CAD model covers scanned part in region B. This is partly due to change in tool compensation and partly due to springback of the sheet metal. The scanned model is over the CAD model in central region C. This is due to several reasons, one of which is that sheet was not properly deformed for the central region due to sprawling effect. Another reason is springback of the sheet to come back to its original shape. The sprawling effect is easily visible in this region as formed part goes below CAD model as was observed in sections as well.

These geometrical issues could be easily solved using backsupporting plate concept. It is interesting how CAD and formed part cover each other at different locations. This behavior is similar to all four legs of cross feature and adjacent sides which show repeatability of the results. For case B cross region have relatively better results compared to case A. Scanned region is not seen over the CAD model and lesser sprawling is observed. This is due to the manufacturing strategy applied to form the sheet metal. The four walls of the basin feature serve partially as a BSP and thus reducing sprawling. More accurate results could easily be achieved using a BSP.

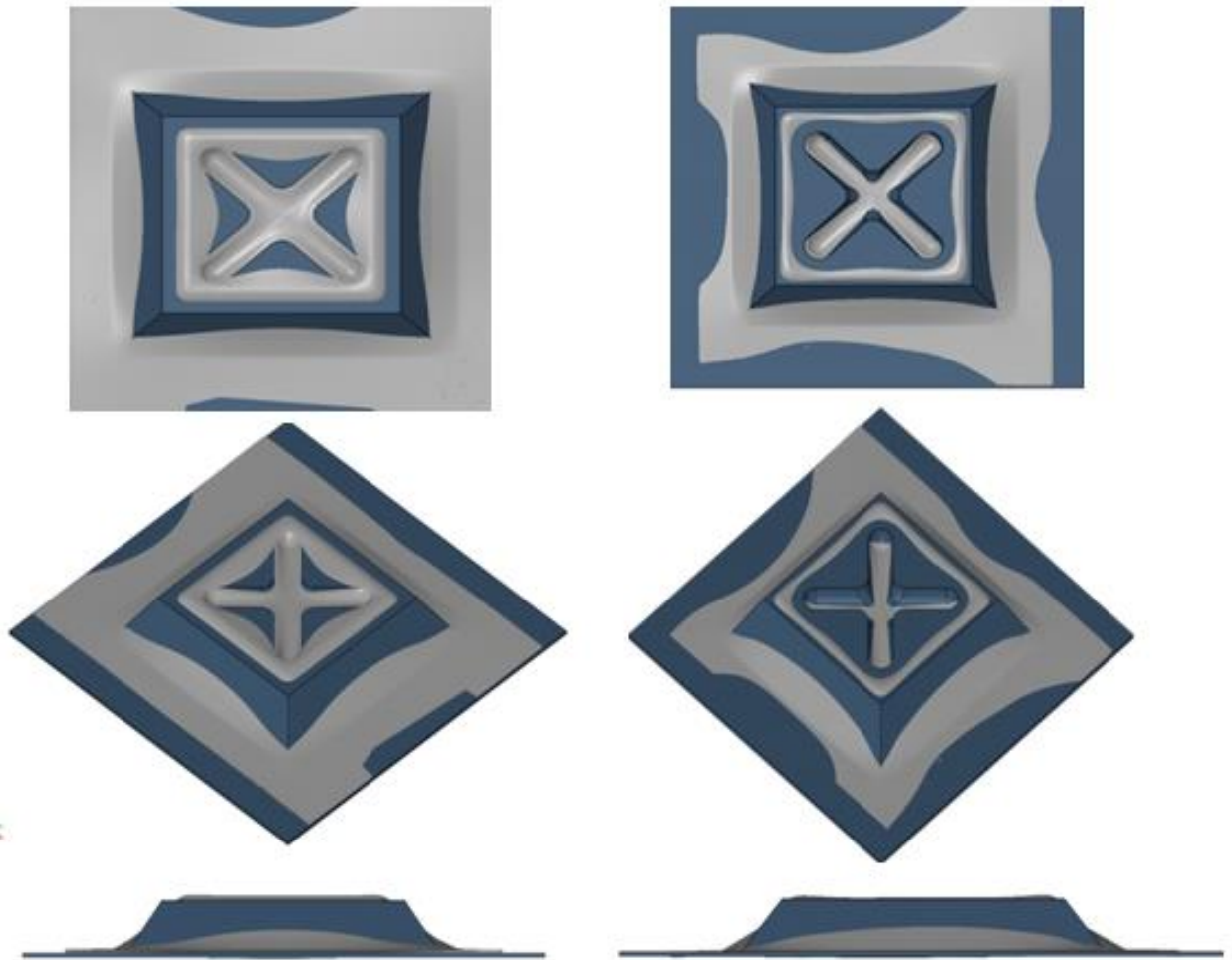


Figure 6-5 CAD comparison; (a) Case A, (b) Case B.

As the cross feature was formed before the basin feature the sheet metal sprawled inwards and the feature was not formed as required. This is why a big difference of 5mm is observed for case A at the cross feature. Other reasons for this deviation from CAD model is springback. Similar behavior was observed during manufacturing the part and it was suggested that a square backsupporting plate should have been used to form this geometry. The second test suggested otherwise which will be discussed in the coming section. Interestingly, both negative and positive values can be observed in the buffer region between the cross and the basin feature. This shows the waviness of sheet metal between double side formed region. Deviation from the CAD model is -3mm at the central part where the legs of the cross feature meet and goes to 0mm and then 3mm while going outward as shown in Figure 6-6.

The accuracy of Case B is much higher if compared to case A, although both the cases show that formed sheet metal parts deviated from the original CAD geometry. The outer side of the basin feature shows around 4mm for both the case studies. Basin feature itself has higher accuracy and deviation of 0mm compared to CAD model. This could be because of the closeness of the formed area to the fixture, straight sheet and no deformed feature in the middle to create complexity. The corners of the basin wall also show better results (less than -2mm) compared to case A (-6mm). Cross feature and buffer zone between the basin and the cross feature show 0mm deviation. The sprawling effect is observed in an area adjacent to the cross feature because of which deviation up to -5mm is reported within a very small region. The cross feature is considerably accurate and has almost 0mm deviation at the edges of the leg from the CAD model.

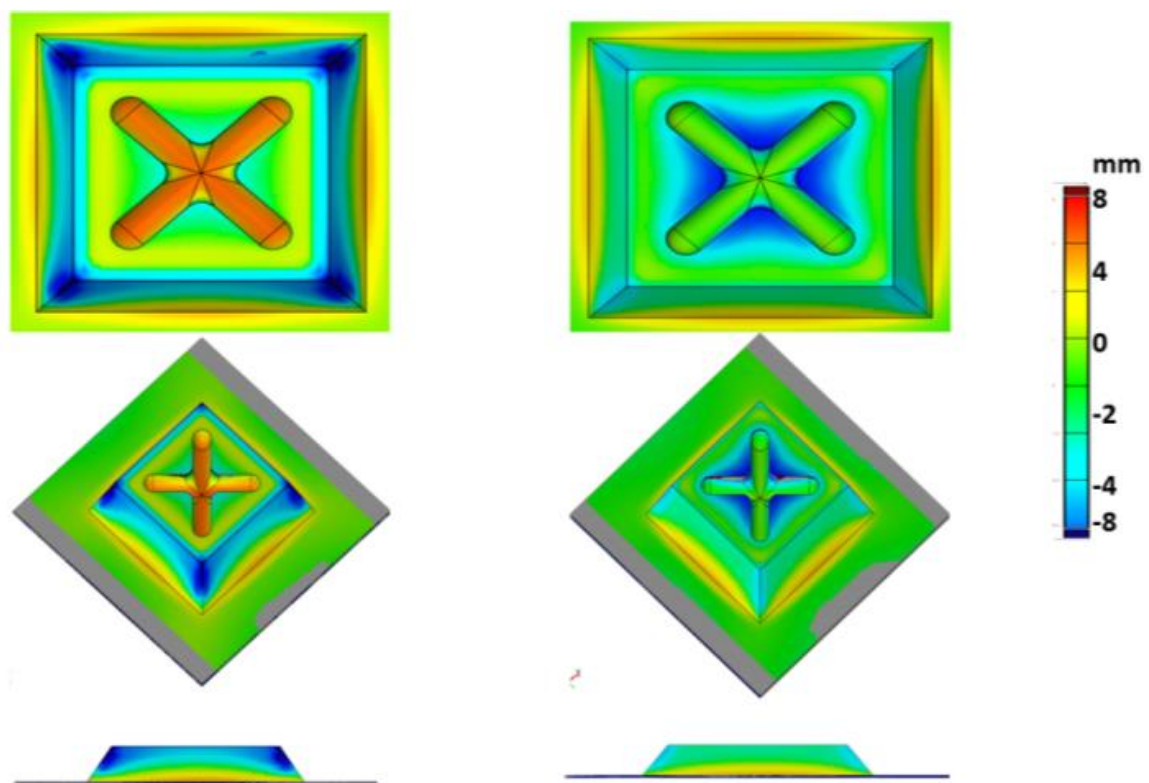


Figure 6-6 Quantitative CAD comparison; (a) Case A, (b) Case B.

### 6.3 Thickness reduction

Similar behavior of thickness reduction was observed as seen in previous tests. Only the locations formed by the tool showed thickness reduction. Outermost sharp thickness reduction in a line is due to scratching of the sheet metal with 6.35mm tool due to sprawling effect as discussed earlier. After which a wider a basin area could be seen in Figure 6-7. Behavior of thickness reduction for this geometry is same as mentioned in previous chapters for 40-degree wall angle for AA 1050H which reconfirms the repeatability of results in different geometries and parameters. For Case A (Cross created before the basin) Thickness is 1.7mm at top and bottom corners of the basin geometry and is around 1.3mm in most of the deformed area. Thickness further reduces to 1.1mm around the corners of the basin geometry. Thickness across cross feature varies throughout but overall behavior is the same for all the four legs of the geometry which further reconfirms the results. Thickness at the start of the leg goes down to 1mm and increases to 1.5mm adjacent to that region. As we move towards centre of the cross feature thickness increases to 1.7mm and becomes 1.9mm in the centre. This shows that sheet metal in the central region is not deformed at all but through the section, we noticed that geometry is straight as originally formed.

For Case B (Basin created before cross), the basin feature has similar depth variation compared to case A. Thickness variation of the cross feature for Case B is different in the central region compared to Case A. Thickness at the start of the leg is around 1mm and then to 1.8mm nearer to the middle of the cross feature. Higher thickness reduction is observed near the corner in the direction of the tool movement.

Thickness reduction data acquired through image processing of circular grid also shows similar results to 3D scanning and is relatable to previous AA1050H tests discussed in previous chapters. Thickness is lowest at the centre and increases at both the edges of the basin feature. It is reduced to 15% at both the edges and 35% in the middle regions while it reduces to 38% at the corners of adjacent surfaces of the basin. Cross feature shows thickness reduction up to 50% at the start of the leg which goes down sharply to 25% around it. Thickness reduction is 15% in most of the region and is not reduced at all (0%) in the central region of the legs.

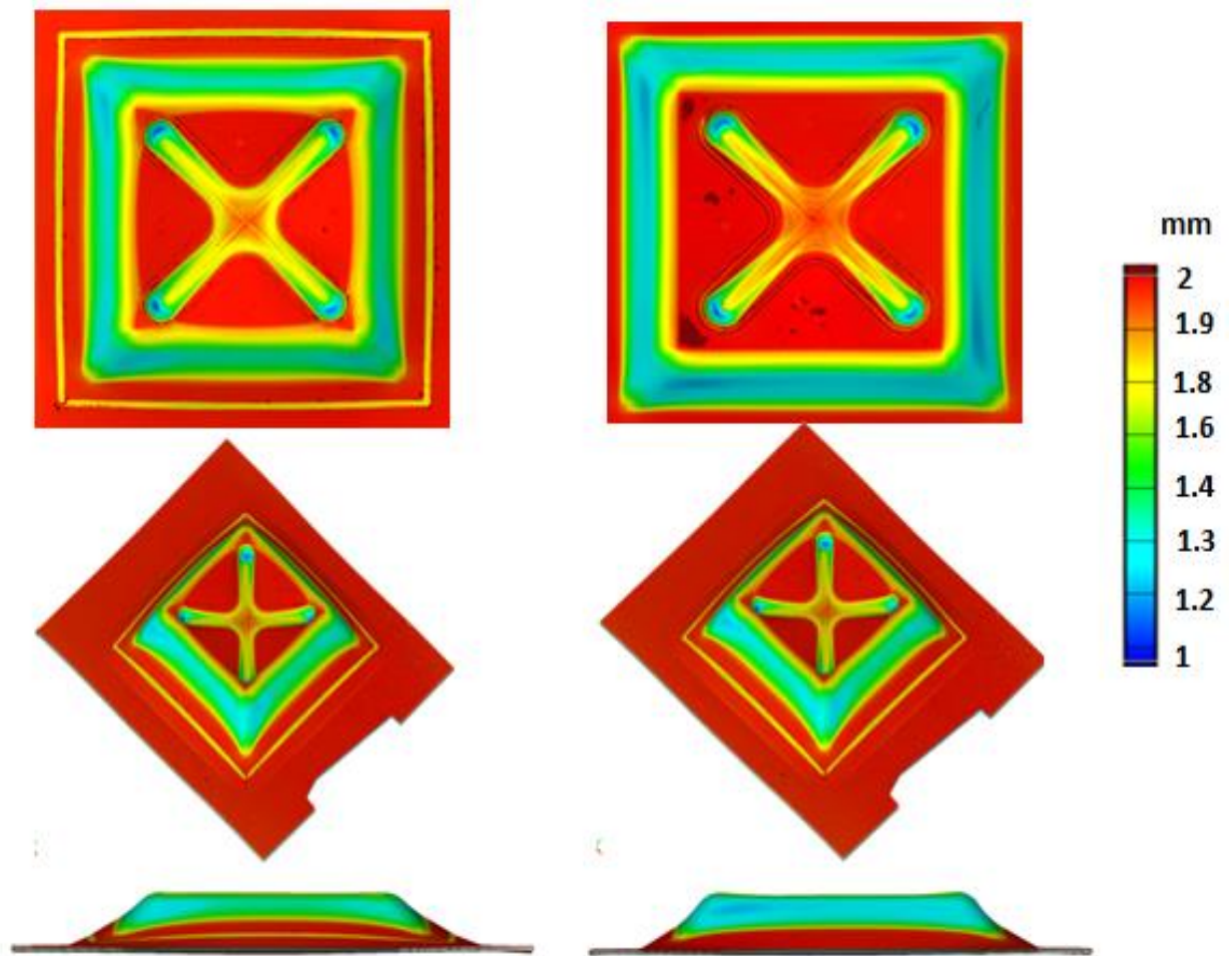


Figure 6-7 Thickness comparison; (a) Case A, (b) Case B.

Similar thickness reduction behavior is observed for the basin feature in case B. For the cross feature, comparatively lower value of both strain and thickness reduction is observed because of a lower depth of the feature. Thus each feature or area of the sheet has strain and thickness reduction phenomena, which is highly localized and independent from the rest of the geometry.



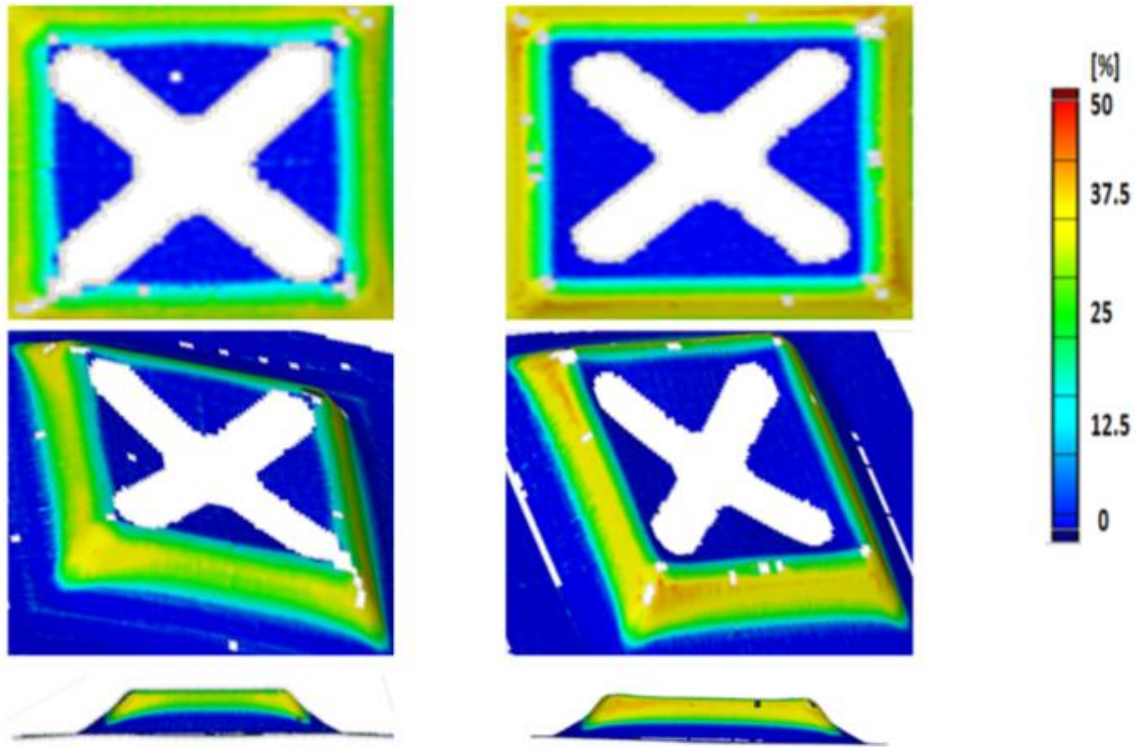


Figure 6-8 Thickness reduction comparison; (a) Case A, (b) Case B.

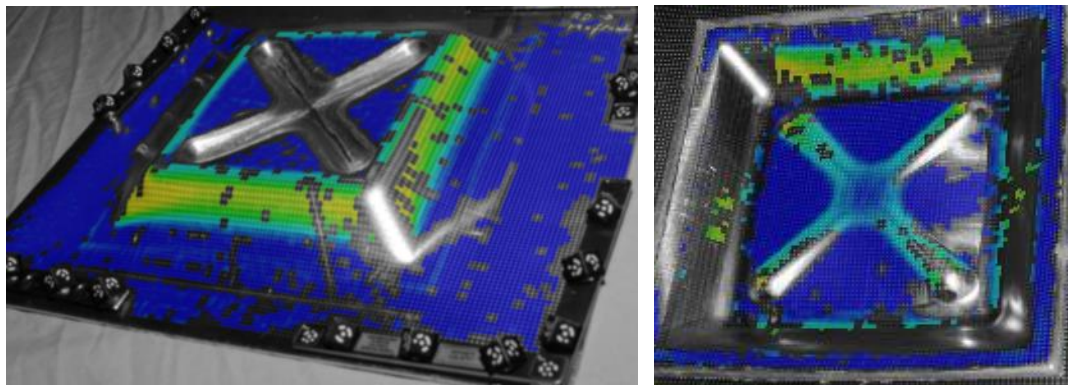


Figure 6-9 Thickness reduction % plotted on the component.

#### 6.4 Major and Minor Strain

The major strain shows different behavior compared to previous parts. Maximum major strain in the basin is not at the corners but adjacent to it with a value of 60% [Figure 6-10]. Surprisingly major strain at the corners is the lowest most with a value of 30%. Major strain in rest of the basin feature varies with respect to the depth. It is 15% at the top and bottom edges, 45% in most of the middle region with a sharp 60% line in the middle. Maximum

major strain in cross feature is observed at the start of the leg (40%) which sharply drops down to a value of 15% for rest of the feature. As expected it is 0% in the middle region and rest of the area between cross feature and the basin feature. Similar behavior is observed for both the case A and case B. Figure 6-11 show major strain plotted on the double sided component.

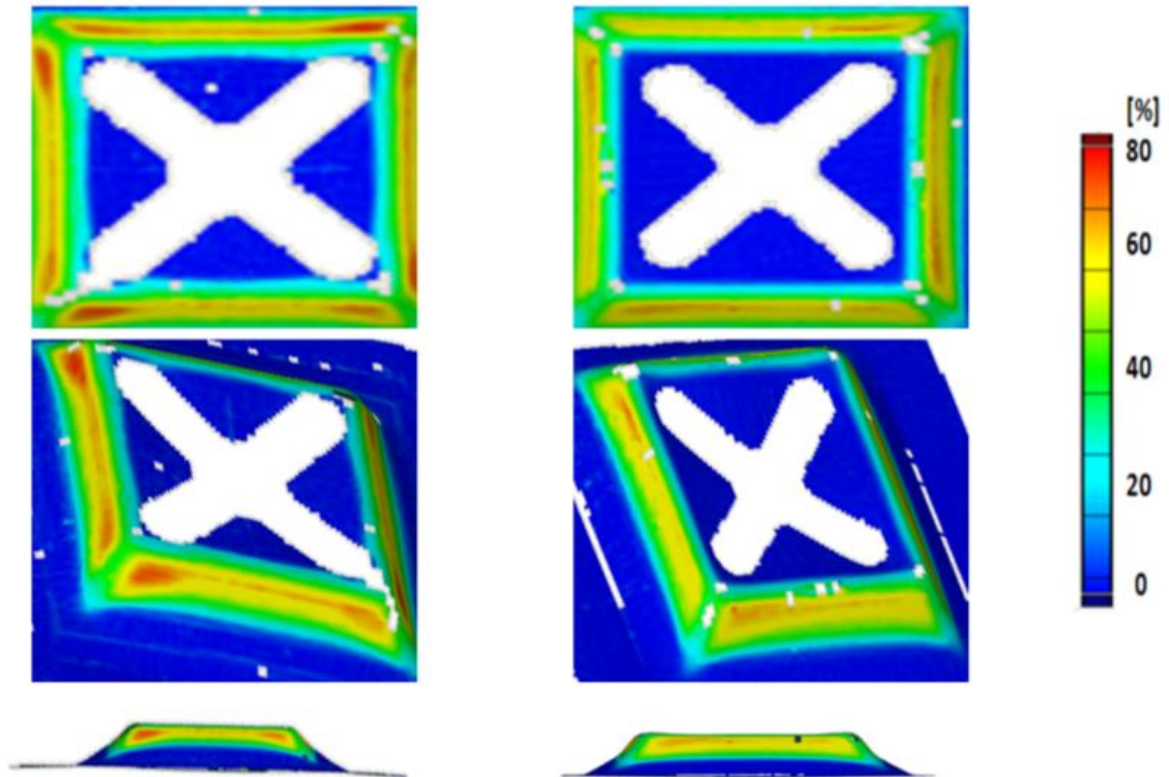


Figure 6-10 Major strain comparison; (a) Case A, (b) Case B.

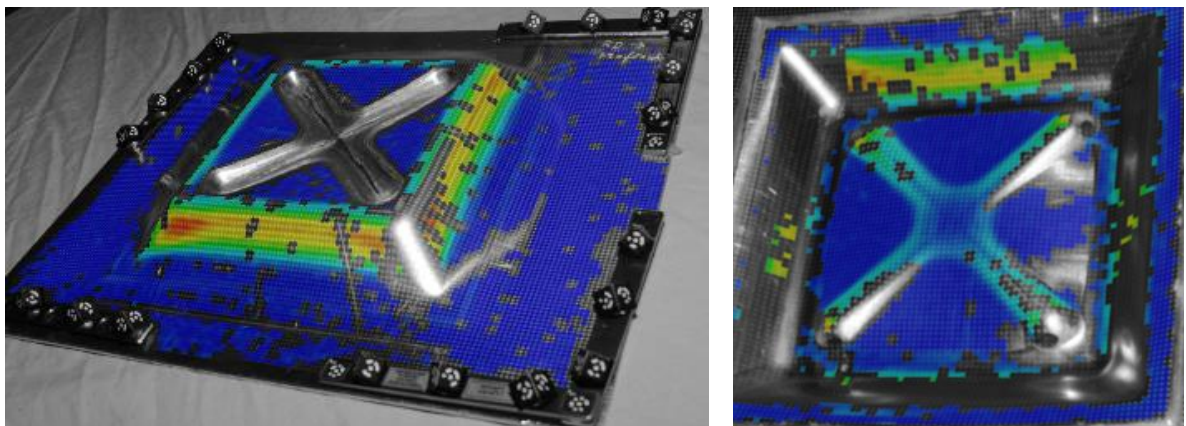


Figure 6-11 Major strain plotted on the component.

For the basin feature the value of minor strain is maximum (25%) at the corners and drops sharply to 15%. Major strain is in the range of 0 to 5% for rest of the geometry [Figure 6-12]. The maximum value of minor strain is at the start of the leg feature and is 30%. It sharply goes down to 15% and then 5% for rest of the geometry. The major strain in central region of the cross feature is 0% as it is not deformed.

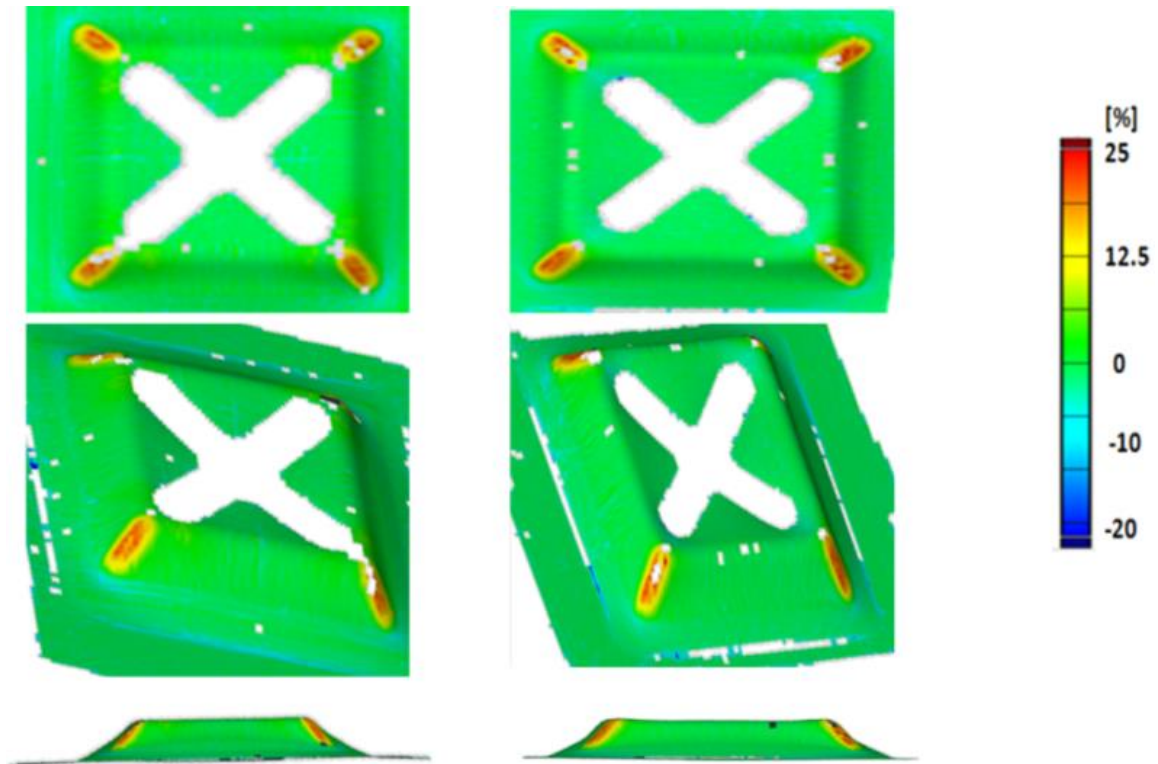


Figure 6-12 Minor strain comparison; (a) Case A, (b) Case B.

Most of the points on the major and minor strain graph for both the basin and cross feature are on the plane strain region. So it could be concluded that plane strain test is relatable to the results. Corners of the basin feature and the start of the leg region in cross feature show a different behavior (Bi-axial). The reason is how the tool interacts with the sheet metal. For the leg corners tool is in multiple contact with the sheet metal and thus different mechanics are observed. Values from this location go up to 30% on minor strain axis which is shown Figure 6-13.

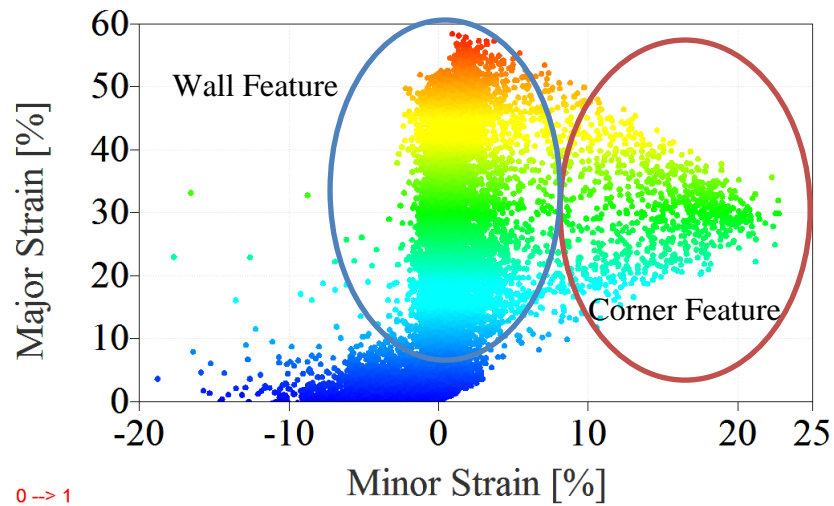


Figure 6-13 Major and minor strain.

### 6.5 Von Mises strain

Both case A and case B show similar results for all geometric features as shown in Figure 6-14. Von Mises strain for the basin feature follow similar behavior to previous parts. Maximum Von Mises strain is observed at the corners with a value of 80% [Figure 6-15]. It decreases along the length of the geometry. With respect to depth in the plane region, minimum Von Mises strain is at the edges (20%) and the maximum is 60% a bit off centred from the middle. As expected cross feature has the maximum strain of 70% at the circular geometry. This strain drops sharply to 40% in a small region. Most of the cross feature has 20% strain while the centre region has 0% strain. Interestingly, more Von Mises strain is observed around the corner in the direction of tool movement. Strain% to the depth and thickness reduction% behavior is similar to the cases detailed during previous chapters as shown in Figure 6-16 and thus validates the model.

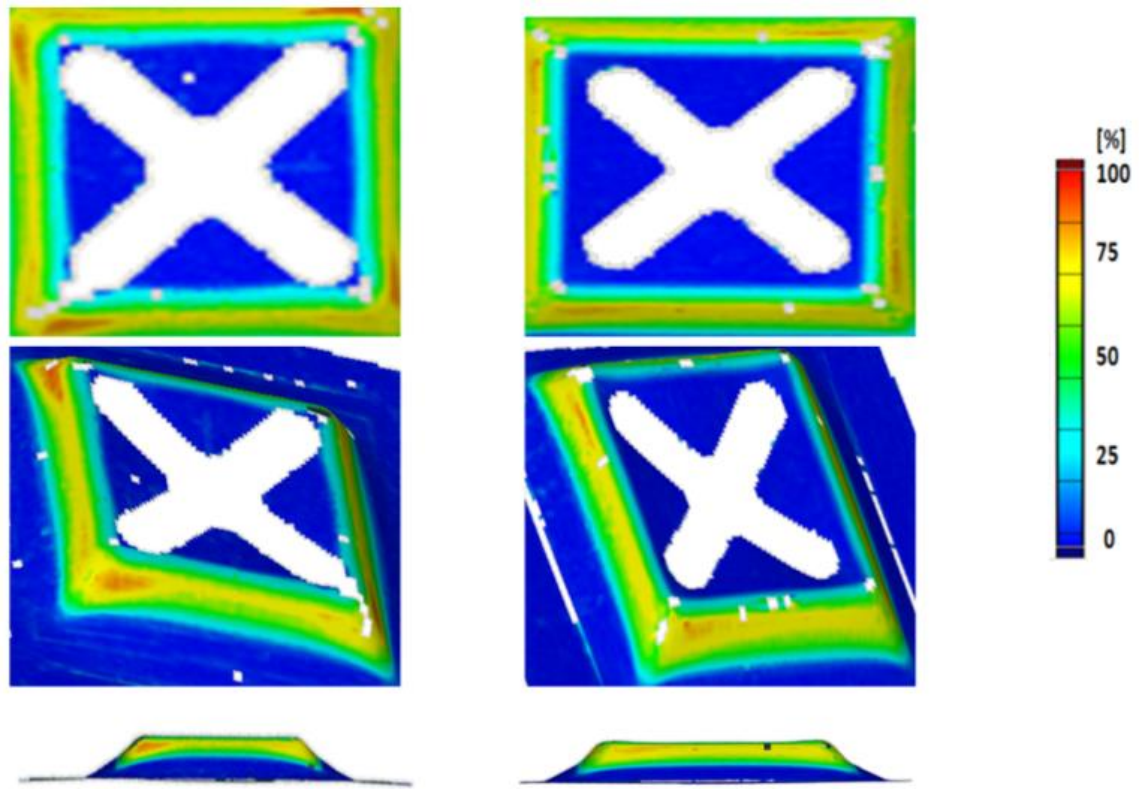


Figure 6-14 Von Mises strain comparison; (a) Case A, (b) Case B.

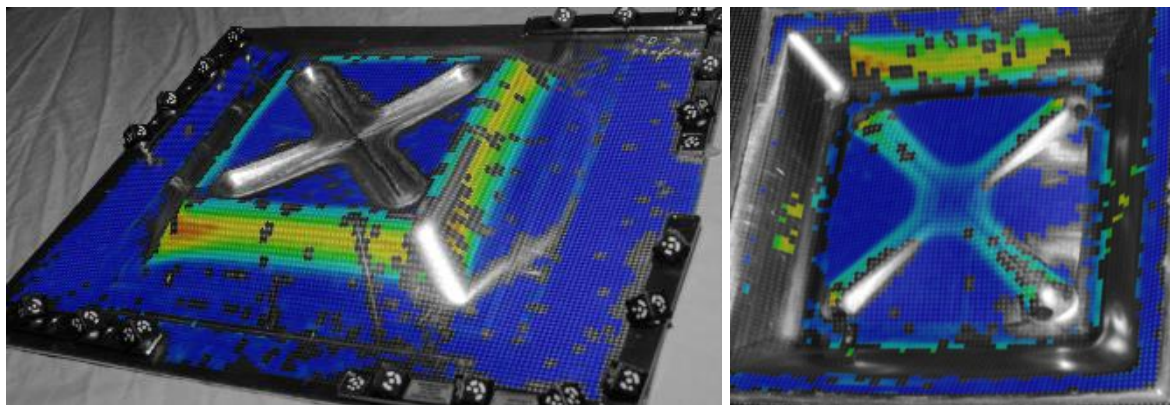


Figure 6-15 Von Mises strain plotted on component.

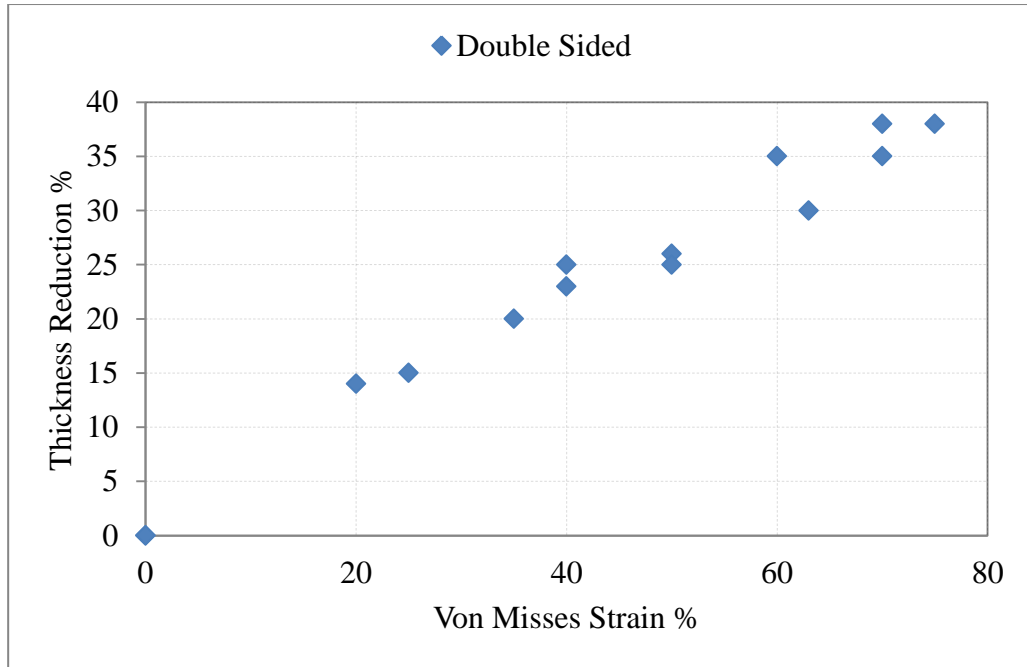


Figure 6-16 Thickness reduction% vs Von Mises Strain% for Basin and Cross features.

## 6.6 Surface roughness

The surface roughness of various locations was measured in the geometry. Alicona was used to measure surface roughness [Figure 6-17]. Some of the surfaces were scanned directly while replicas were acquired for the rest. Double sided formed sheet (AA1050H) follows similar surface roughness behavior to previous studies performed on SS304L, AA1050H, AA2024 and AA7075.

External surfaces were smooth but internal surfaces were rough when observed through naked eyes. The surface roughness of the cross and the basin feature is shown in Figure 6-18. As expected surface roughness graph is smoothest for the un-deformed sheet metal. 50° wall has a value of 0.242 $\mu\text{m}$  and the plot mostly is slightly over the  $\pm 1.5$  range, but there is a lot of fluctuation within this range, thus higher surface roughness. Value for the cross feature is 8 $\mu\text{m}$  and the plot generally remains in  $\pm 20\mu\text{m}$  range. The surface roughness of 50° wall feature behaves similarly to other 50° wall features previously discussed. Table 6-1 gives surface roughness values of the formed and unformed sheet metal. In general surface roughness increases with higher wall angles.



Figure 6-17 Surface view through Alicona.

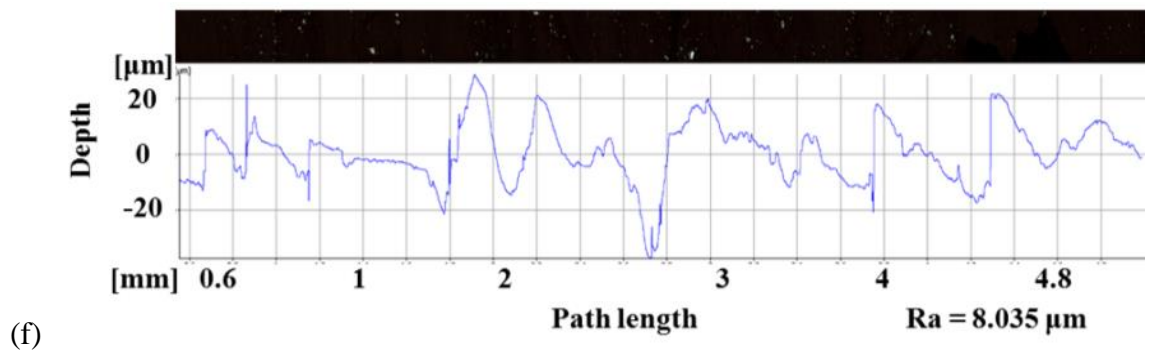
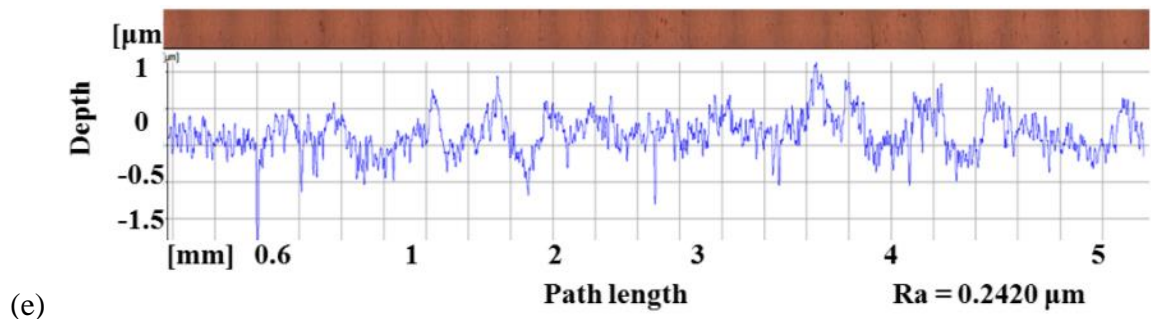


Figure 6-18 Surface roughness profiles; (a) 50° wall, (b) Cross feature.

Table 6-1 Surface roughness measurements.

<b>Surface</b>	<b>Ra (<math>\mu\text{m}</math>)</b>
<b>As received</b>	0.1629
<b>Basin feature</b>	0.2420
<b>Cross feature</b>	8.035

## 6.7 Summary

Some complex components are formed by ISF process in both positive and negative direction with respect to the sheet. Conventional forming processes can easily form parts in both directions of the initial sheet metal. ISF is at its infant stage most of the researchers generally form parts in one direction. In this chapter, the author tried an approach to using ISF in both directions. Different geometries were conceptualized for this purpose and one of them was finalized due to its versatility and application in aerospace industry. Final conceptual geometry has two features (basin, cross) in both directions. Both these features were formed using different sizes of tools and different methodologies. AA 1050H sheet metal was used to make this part. Results such as thickness reduction, major and minor strains, Von Mises strains and surface roughness were discussed. The results re-verified the ISF-FCheck procedure and the basin wall (which was more prone to failure), followed similar behavior as seen in previous cases.



## **7. Discussion and conclusion**

In this chapter, the work is summarized and the significance of the results discussed with respect to initial aims and objectives. Aims and objectives, the limitations of the work and future work are reviewed. Qualitative and quantitative models are proposed. Conclusions are drawn by discussing the results.

### **7.1 Aims and Objectives**

The aims of this research were stated in chapter 1 as:

- Understanding the interaction of geometric, material and manufacturing ISF process parameters with resulting properties such as quality, production, mechanics and materials.
- Creation of easy and quick assessment method by which design and production engineering can determine the feasibility of ISF for a given component.

The objectives of this research were stated in chapter 1 as:

- Through literature review, identify a possible methodology for feasibility assessment.
- Identify and perform experiments to determine the parameter for a feasibility methodology (e.g. different materials, geometries, feedrates, production rate, accuracy, the effect of rolling direction, thickness, surface roughness, strains and material properties).
- Analysis of results and detail the feasibility assessment methodology's strengths and limitations.

### **7.2 The deformation process**

Incremental Sheet Forming (ISF) is a family of processes where the movement of a spherical tool causes highly localized deformation of material in the surrounding area [3]. Schematics of the process are shown in Figure 7-1. Initially, the metal sheet is straight (un-deformed) and is clamped between the top and the bottom plate. The spherical tool is controlled through a program and is fixed in a numerically controlled machine. It moves along a spiral (helical, discrete incremental depth pitch) toolpath with a defined pitch, feedrate and

rotation. When the tool comes in contact with the sheet metal, a pointed load is applied by the tool on a small area of the sheet metal. Sheet metal, thus deforms when the tool forces the material in the downward direction. As the tool follows a contour path it deforms a small area of the sheet metal continuously and thus a large deformation is seen in the final part. The thickness of the metal sheet reduces as it is being formed (intermediate stage), till the tool reaches the final stage.

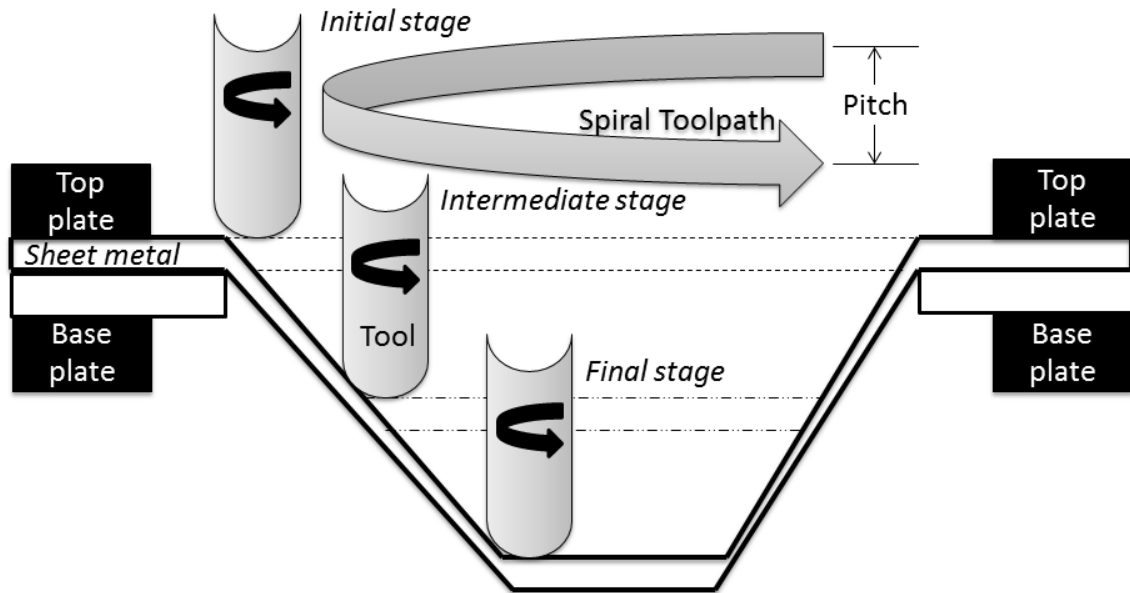


Figure 7-1 ISF process schematics.

### 7.2.1 Cellular model

The mechanics of the process can be envisaged qualitatively by visualizing the deforming geometry as being composed as a series of cells (where each block represents a discrete volume of material). This cellular model is illustrated in Figure 7-2 where one side of a formed part shown with wall angle  $\gamma$ . Length is divided into the formed and unformed region. The circumferential length (C.L.) changes as the part is being formed. Initial length of the part is C.L.1, which increases and becomes C.L.2 at intermediate and C.L.3 at the final stage. To explain this model, it is assumed that the number of layers blocks within this sheet metal is 5 (representing, say, a 2mm AA7075 sheet). As the tool moves downward and contacts the surface of the sheet metal, it applies a pointed load on the sheet metal (blocks in this case), because of which these blocks rearrange (i.e. deformed). Because of this rearrangement, the circumferential length of the sheet metal increases from the initial to the

final stage. Thus the number of blocks in the thickness direction decreases from 5 (initial stage), to 4 (intermediate stage), to 2 (final stage). This thickness reduction is dependent upon the wall angle and the depth of the feature. The increase in the wall angle or depth, will increase the circumferential length but decrease the thickness. Fracture in the sheet is observed when the tool applies a force to last layer of cells and the number of blocks available to carry the load (i.e. stress) is insufficient, so the Ultimate Tensile Strength of the material is exceeded and thus a fracture occurs in the geometry. This model also provides intuitive understanding of why a greater tool size means larger numbers of blocks rearrange themselves, thus a smooth transition could be arranged, while a smaller tool size will apply the same force to a smaller number of blocks (i.e. high stress). Thus the sheet metal is more prone to failure. Figure 7-2 shows cellular model concept, via rearrangement of square blocks at the initial, the intermediate, the final and the fracture stage. Where,  $D_0 < D_1 < D_2 < D_3 < D_4$ , and  $C.L.1 < C.L.2 < C.L.3 < C.L.4$ . Numbers of blocks in the thickness direction are reduced from  $D_0$  to  $D_4$ . Previously, several researchers have reported experimental results which are analogous to cellular model [59, 133].

This model also helps understand the interaction of depth, wall angle and the volume under action of the tool. Greater depth and higher wall angle will result in higher circumferential length and thus higher rearrangement of the blocks compared to lower depth or lower wall angle.

Although a cellular model allows a qualitative understanding of the sheet thinning to be developed, it says nothing about springback. So the disadvantage of the model is that it does not support springback phenomena.

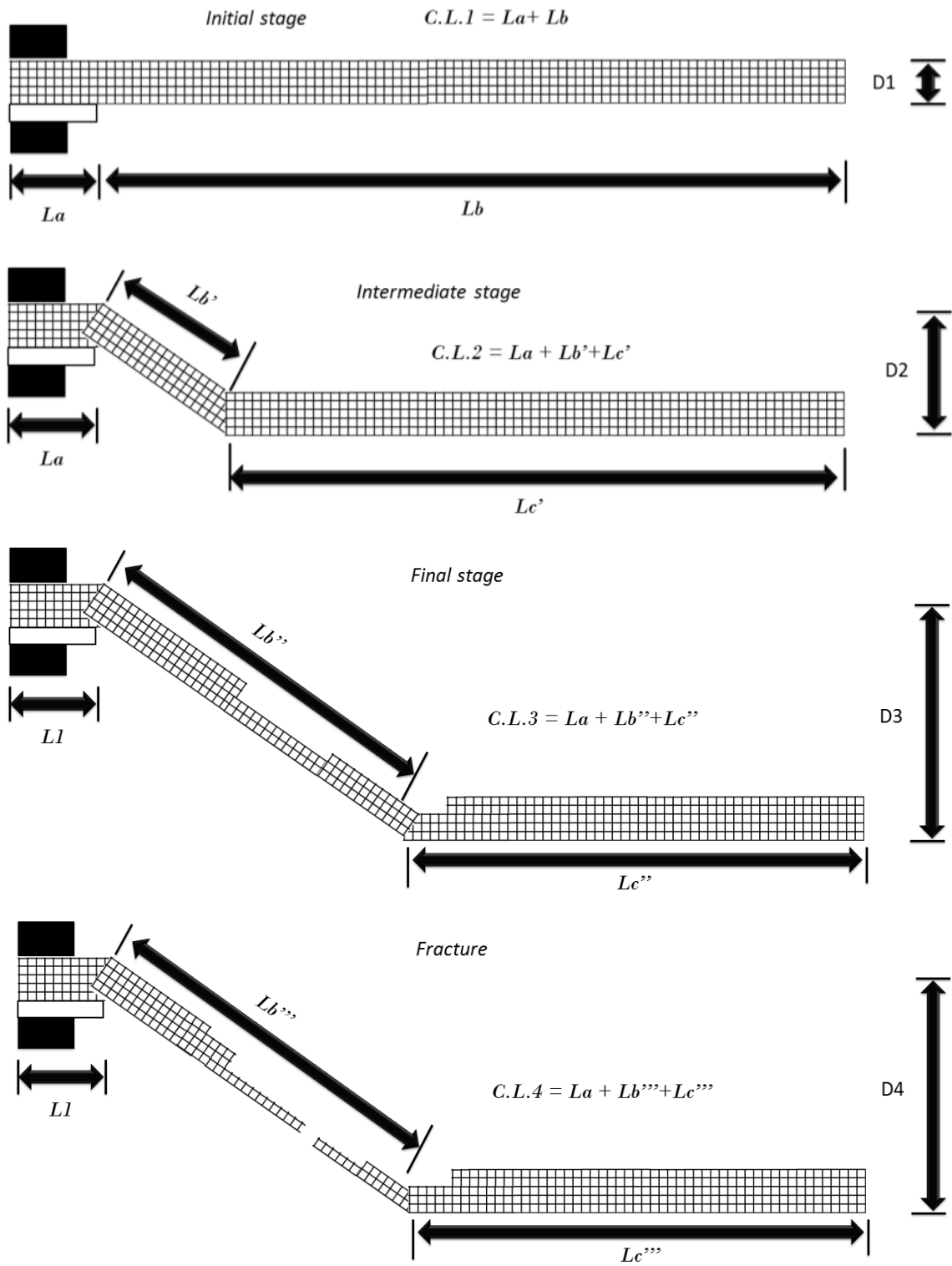


Figure 7-2 Cellular visualisation of deformation process.

## 7.2.2 Internal mechanics of the deformation process

Although the ISF process is easily described in qualitative terms, the exact nature of the internal mechanics of the deformation process are still debated. The major and minor strain plots recorded in this research suggest that the **wall** and **curve** features of the experiments are in a plane strain condition. Plane strain condition means these geometric features, walls or curves, at different forming angles, depth and rolling directions are formed by the forces analogous to the plane strain loading condition. In other words, the sheet material is stretched like a specimen under direct loading as it moves on both sides of the pointed load applied by the tool. Figure 7-3 shows movement (i.e. displacement) of this material in both directions thus imitating direct loading condition. Hence the condition is plane strain condition and the limit of the process can be evaluated through tensile testing or plane strain failure criteria. As it is clear that all such type of loadings has Crack Mode I, which is the opening mode [152]. Ductile fracture is observed through fractography after the crack is initiated. In contrast, for **corner features**, the tool pushes the material out (rearranges), in all the directions (unlike direct loading condition), thus corners show a biaxial condition as shown in Figure 7-3. For this condition major strain has a higher positive value.

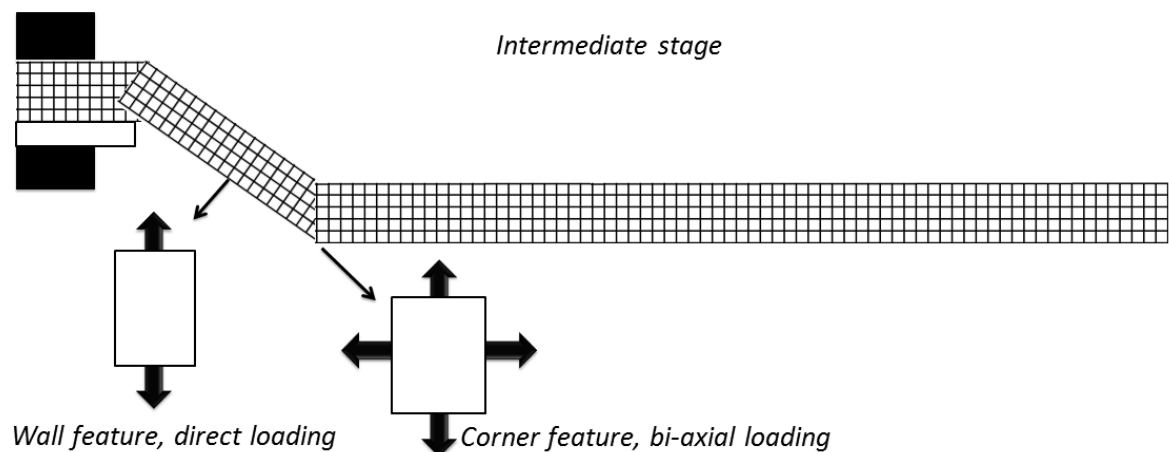


Figure 7-3 Internal loading on material.

It has been observed throughout this experimental study that ISF is a highly localized process and limit of the formed component depends upon strain%, material properties and sheet thickness at that particular location and have an insignificant effect upon rest of the component. In locally deformed areas, however, the strain% can be converted to the stress, or used directly, to compare with the failure criteria. The maximum strain that could be

induced in a sheet during ISF process is analogous to the maximum strain found through the plane strain material testing. The final thickness of the sheet metal is another very important parameter that determines the local levels of stress and the volume of material that can be displaced, so sheet metal with higher thickness is more formable. The volume under action is dependent upon the tool size and the sheet thickness. Thus the part will be safe till it is under the fracture limit of strain% or material properties. Thus at a particular location, strain, volume under action (sheet thickness and tool contact area) and material properties define the formability of the sheet metal [Figure 7-4]. Thus gives a conclusion of the state of a point under loading during ISF process.

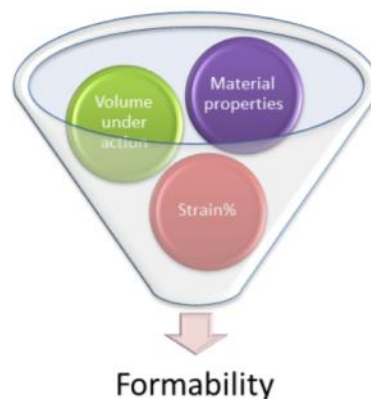


Figure 7-4 ISF formability.

### 7.3 Qualitative model

The experimental data generated by the project and literature has allowed, the qualitative relationship between the input and the output parameters to be established. Table 7-1 shows dependency of input and output parameters.

The qualitative model, illustrated in a generic form for a geometric feature applicable to any material type, depth, forming angle, feed rate etc. **Figure 7-5 illustrates a generic process variable A (which can be thickness, equivalent strain, grain elongation and surface roughness at different depths and forming angles of the formed part).** A tool with diameter  $D$  moves downward in a spiral tool path with a pitch while sheet metal is deformed to intermediate and final stage of the formed part. Top and bottom plate clamps the sheet metal while backsupporting plate helps increase the accuracy of the formed shape. The sheet has an initial variable value ( $A_1$ ), which varies with the location as  $A_x$  ( $x = 2, 3, 4$ ) (where

$A_1$ ,  $A_2$  and  $A_3$  refers to the location on the formed depression ). If we consider two wall angles  $\emptyset$ ,  $\Upsilon$ ; where  $\emptyset > \Upsilon$ , then the qualitative model predicts that at any given stage (intermediate or final),  $A_x$  for the greater wall angle will be lower i.e.  $A_2 > A_3$  and  $A_4 > A_5$ . The value of  $A_x$  for any wall angle for the intermediate stage would be higher than the final stage i.e.  $A_2 > A_4$  and  $A_3 > A_5$ . This diagram has been evaluated for the thickness and equivalent strains for different materials such as SS304L, AA1050H, AA2024, AA7075.

Through further research, this qualitative model can be applied to other output parameters such as residual stress, hardness etc. **Development of such a qualitative model could potentially assist manufacturing engineers apply ISF process, as the only parameter they have to measure is final value  $A_5$ .** If  $A_5$  is within design limits, the rest of the parameters could be inferred to also be within design limits. This diagram is sensitive to ratio of the tool size and pitch to the feature depth.

To further explain the application of this qualitative model, output parameter thickness ( $t$ ) is considered. The qualitative model will change as shown in Figure 7-6 and could be applied in the following scenario. The tool moves downward following a spiral toolpath. The tool starts from a depth of 0mm and goes up to a final depth of 40mm at the final stage passing through the intermediate stage of 20mm. If one wall angle is  $\emptyset = 60^\circ$  and the other is  $\Upsilon = 40^\circ$ ; where  $\emptyset > \Upsilon$  and the initial thickness ( $t_1$ ) of the sheet metal is 2mm. Then the diagram suggests that the initial thickness and the thickness of the area not being formed will always have the same value regardless of its location. It also suggests that initial thickness would be greater than all other areas. At any given stage, intermediate or final, the thickness for the greater wall angle will be lower i.e.  $t_2 > t_3$  and  $t_4 > t_5$ . Thickness for any wall angle for the intermediate stage would be higher than the thickness at the final stage i.e.  $t_2 > t_4$  and  $t_3 > t_5$ . **If  $t_5$  is within design limits, rest of the parameters ( $t_1$ ,  $t_2$ ,  $t_3$ ,  $t_4$ ) will be within design limits.** This logic and the qualitative model are applicable to other parameters such as equivalent strain, grain elongation and surface roughness at different depths and forming angles of the formed part.

Table 7-1 Dependent Inputs and outputs of ISF process.

Inputs	Geometric feature	Wall angle	Angle between features	Depth	Material properties	Sheet thickness	Rolling direction	Microstructure	Toolpath strategy	Pitch	Feedrate	Tool size	Dies	Clamping & Fixture
<b>Outputs</b>														
Production rate				X					X	X	X	X	X	X
Accuracy	X			X	X				X			X	X	
Formability	X	X	X	X	X	X		X	X			X		
Cost	X			X					X	X	X	X	X	X
Final thickness	X	X	X	X		X			X			X		
Major&Minor Strains	X	X	X	X					X			X		
Von Mises Strains	X	X	X	X					X			X		
Surface roughness		X	X							X		X		
Material properties	X	X	X	X	X	X	X	X	X			X		
Internal Mechanics	X											X		
Microstructure	X	X	X	X	X	X	X	X	X			X		
Fracture					X			X						

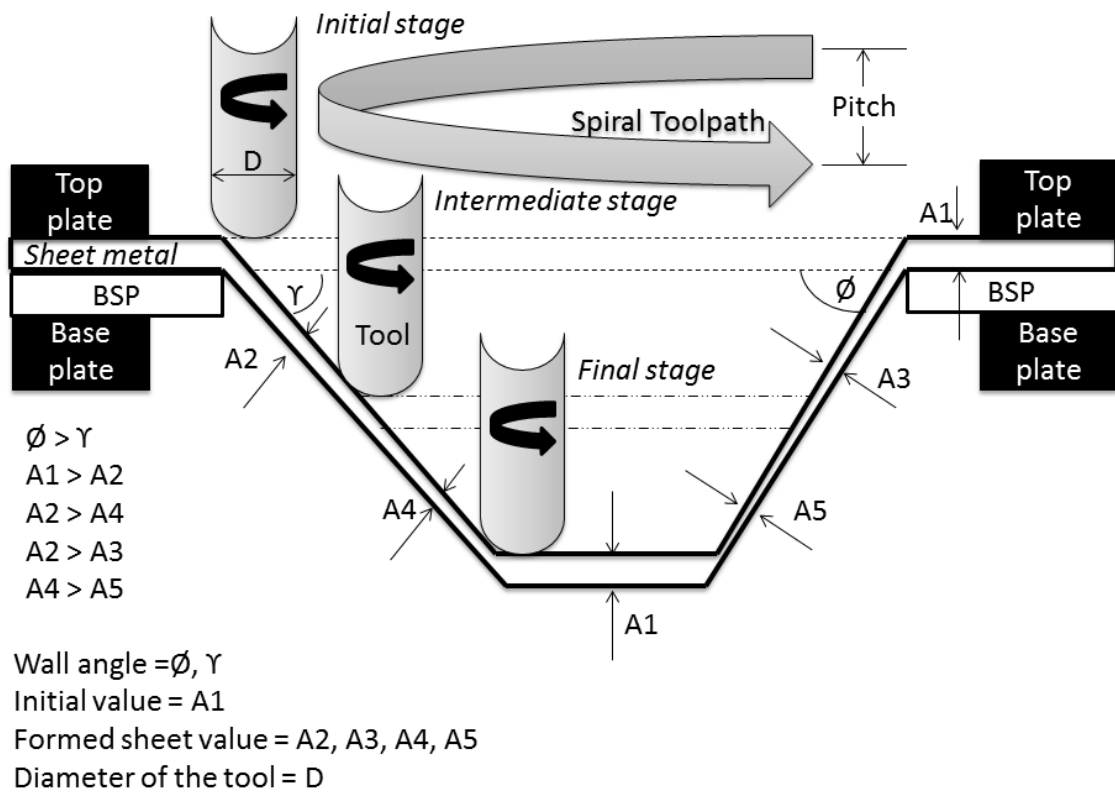


Figure 7-5 Qualitative ISF parameter relationships.



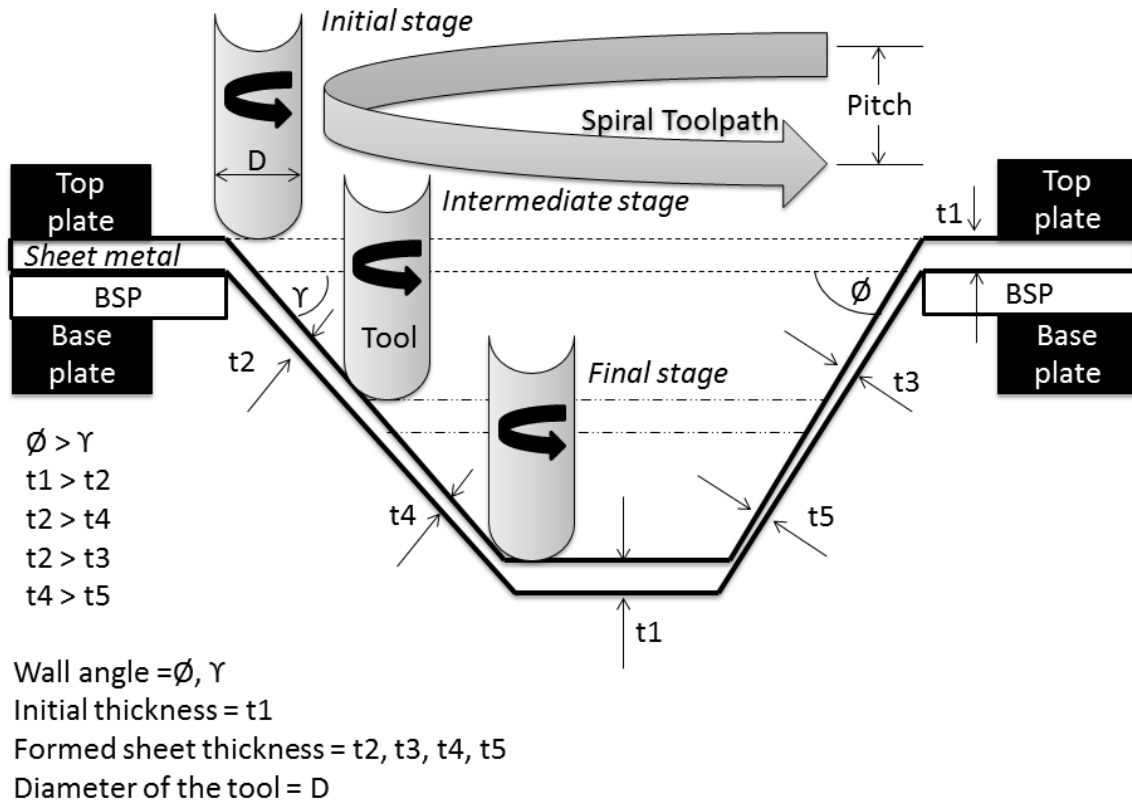
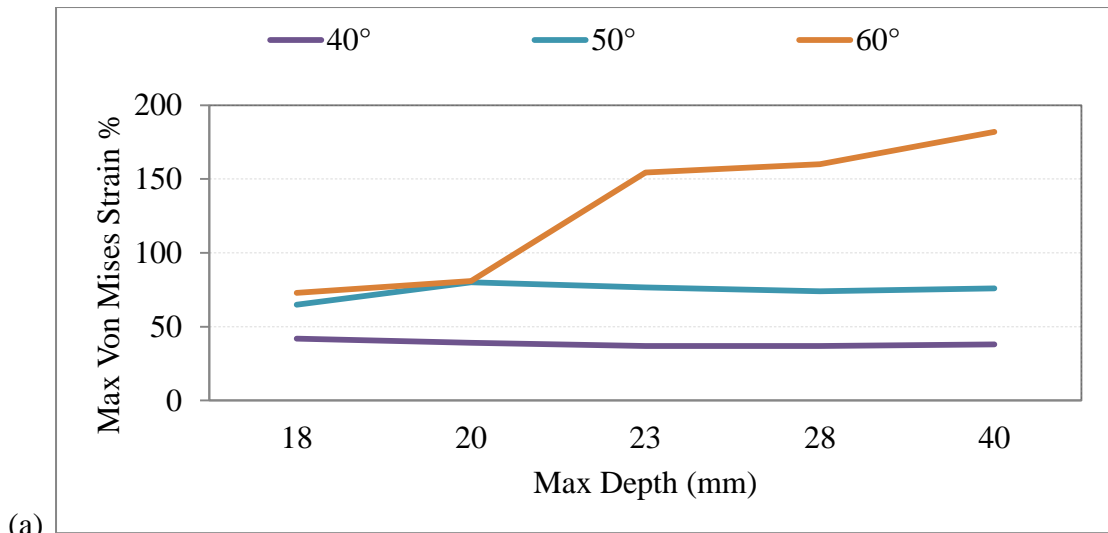


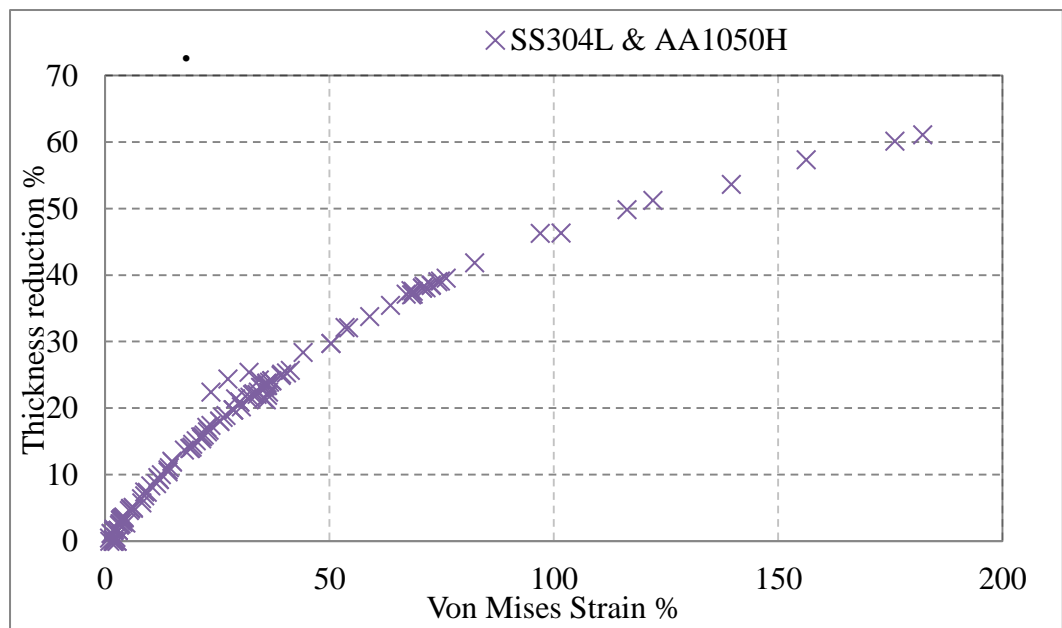
Figure 7-6 Qualitative model for thickness.

#### 7.4 Quantitative results

Quantitative results from the experiments are the basis of qualitative model and quantitative design check procedure. Key to this is the general relationship between strain and sheet thickness that is shown in Figure 7-7 and Figure 7-8. Figure 7-7a shows results for a variety of depths for a variety of materials. It is interesting to see that regardless of the material type and depth of forming  $40^\circ$  and  $50^\circ$  wall angle show similar behavior. This is due to the moving location of the tool tip with respect to the area of the sheet while the sheet is formed. For higher angles such as  $60^\circ$ , behavior is different because the same area comes in contact with the tool repetitively. This behavior can be understood intuitively with the help of cellular model. Figure 7-7b shows a graph plotted between Von Mises strain and thickness reduction between two different materials (SS304L and AA1050H), with different initial sheet thickness (0.6mm and 2mm) with multiple wall angles ( $40^\circ$ - $60^\circ$ ), geometric features (straight wall and curve), different rolling directions and feedrates (1000mm/sec and 4000mm/sec), yet showing similar results. Maximum Von Mises strain % for each test was plotted against the maximum depth it achieved.



(a)



(b)

Figure 7-7 (a) Maximum Von Mises Strain% at maximum depths for all Aluminum (b)Thickness reduction% vs Von Mises Strain% for SS2 and AA1-2, combined.

Figure 7-8 confirms the strain to the depth and thickness reduction behavior for double sided complex geometries. It is similar to the cases mentioned previously, and thus confirms the relationship established by the single side ISF process. This is because of the constant volume as discussed in Chapter 5.

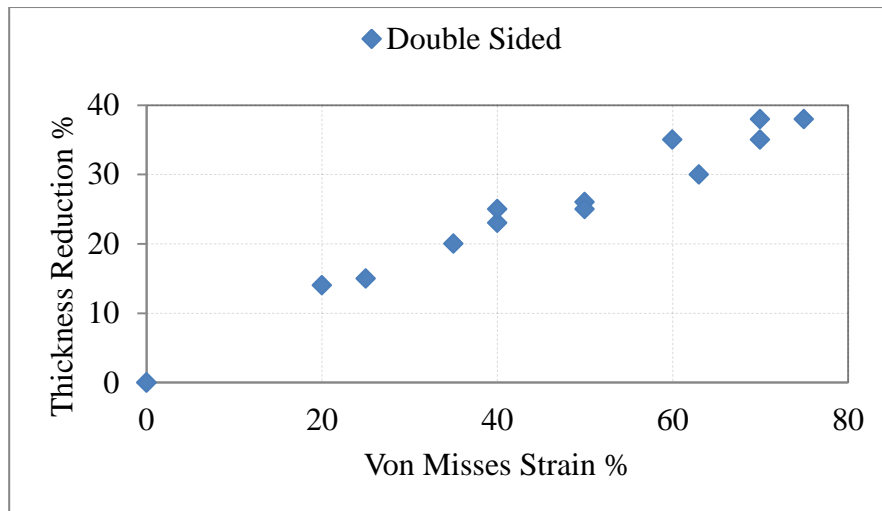


Figure 7-8 Thickness reduction% vs Von Mises Strain% for Basin and Cross features for double sided sheet forming.

### 7.5 Quantitative design check

A very simple example is provided here, to explain how the results, assessment method logic [Figure 7-9] and the qualitative model can be used to support the application of the ISF process. Consider, an engineer who wants to form a sheet metal using incremental sheet forming. From experimental results, it is evident that rolling direction and feedrate does not significantly influence the final component. Although anisotropy does effect the micro-properties but no such differences is observed at macro level. So sheet could be oriented in any direction and feedrate is only limited by machine capability. Results have also established the fact that only sheet under tool action will be affected by ISF process (so areas which are not in contact with the tool will not change). The area under tool action will be deformed and the circumferential length of this part will increase from  $L_b$  to  $L_b''$  and strain will follow the curved profile, which is discussed in previous case studies and is shown in Figure 7-10. General properties and influences on the formed part are checked through Table 7-1.

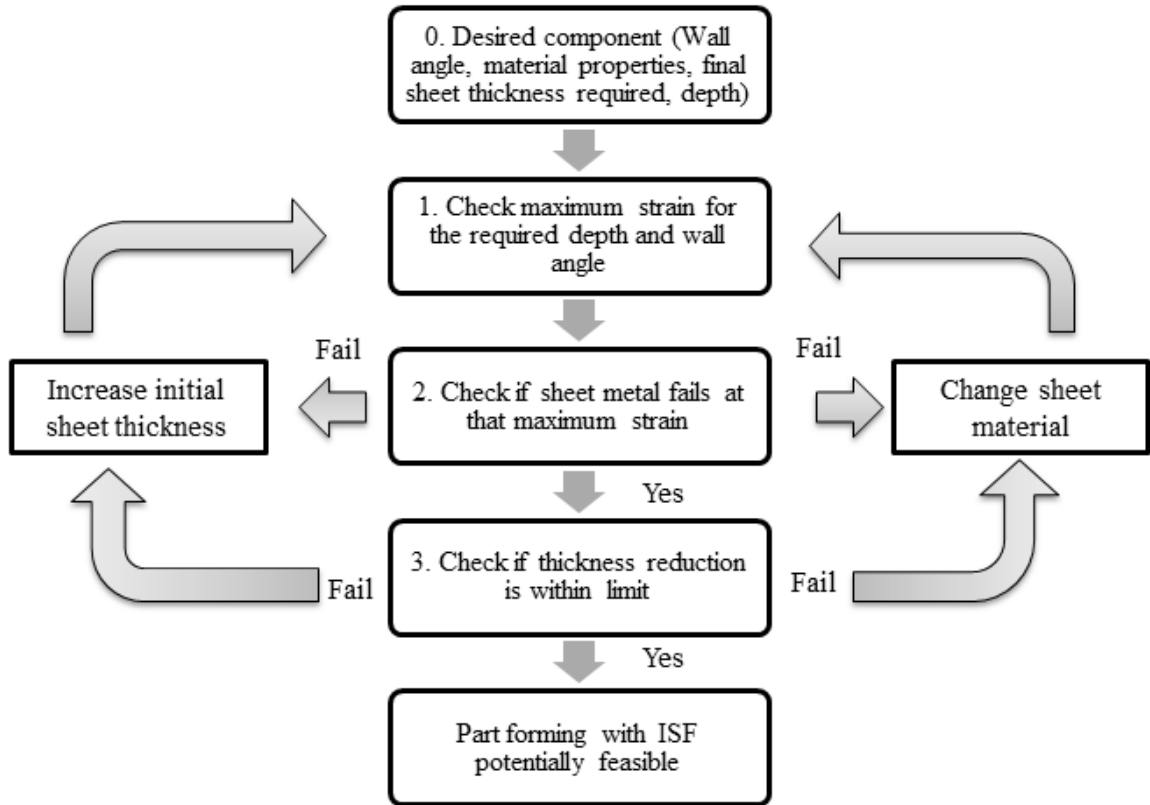


Figure 7-9 ISF-FCheck process.

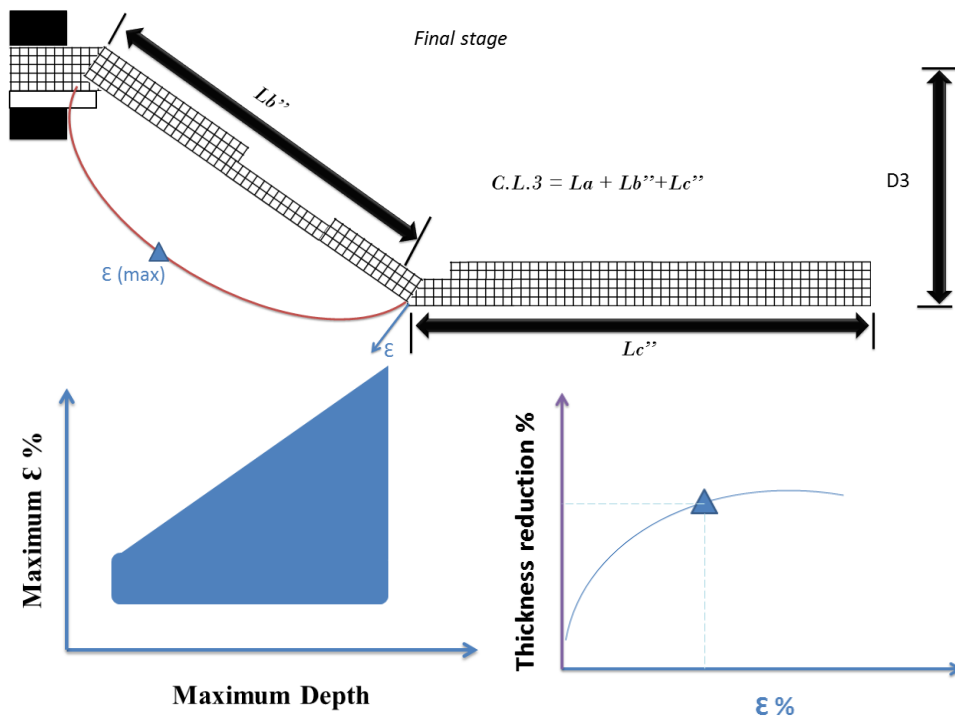


Figure 7-10 Application of cellular model for quantitative design check.

The engineer will use Figure 7-7 to calculate Maximum strain (Max  $\epsilon$ ) from the given depth and wall angle for a material specified. If the value of the maximum strain does not cross the limiting value of the plane strain, it will not fracture. The thickness of the final formed sheet can then be calculated from strain% vs thickness reduction % graph [Figure 7-7]. Forming will fail due to high strain. Through these results and the model; the initial required thickness of the sheet can be calculated if a minimum final thickness of the sheet is provided by the customer. For instance, if the initial selected sheet thickness of the sheet metal is 1 mm and the desired component which has a maximum wall angle of  $40^\circ$  (range between  $20^\circ$  to  $40^\circ$ ) should be at least 0.85mm thick with a depth of 20mm (Step 0) [Figure 7-11]. The maximum value for the strain is 45% for wall angle of  $40^\circ$  at position  $A_5$ . As discussed earlier,  $A_5$  is the point at maximum wall angle and depth compared to other features in the geometry and thus will have the maximum strain in the geometry (Step 1). The rest of the features in the formed part will have lower values of strain compared to  $A_5$  and thus calculation of properties of those regions are not required. If the material is not failing under value of maximum strain at  $A_5$  region, then move on to step 3 (Step 2). This strain of 45% produces a thickness reduction of 27%, and thus the final sheet thickness will be  $0.73\text{mm} < 0.85\text{mm}$ , so this formed component will fail due to sheet thickness (Step 3). Manufacturing engineer will thus select an increased sheet thickness (1.5mm) and only final sheet thickness will be calculated for location  $A_5$  i.e.  $1.095\text{mm} > 0.85\text{mm}$  (Increase initial sheet thickness). As region  $A_5$  has thickness greater than required, thus as per all other regions will have more thickness and less strain than the limiting value. General properties and influences on the formed part are checked through Table 7-1.

## 7.6 Limitations

ISF-F Check model only checks for failure but does not account surface finish, material properties and accuracy. Data presented or model developed is for the given set of manufacturing parameters and ductile materials. Further research is required to implement and check these models on a variety of input parameters. The current research was focused on wall features; model should be implemented on corner features to check its feasibility.

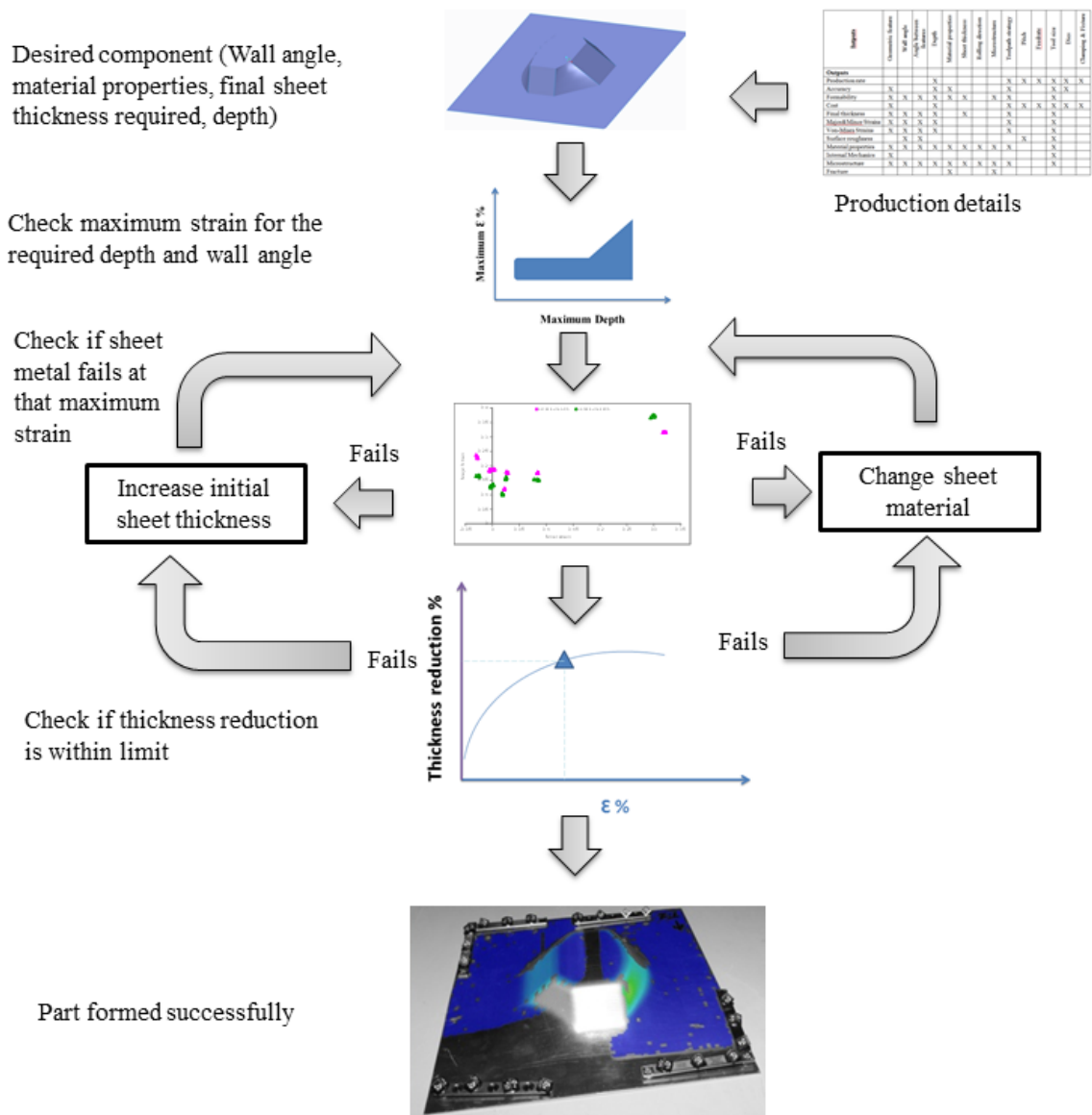


Figure 7-11 Assessment methodology.

## 7.7 Future work

- The size of the features can be changed to see size sensitivity of the study.
- Cellular model can be coded and evaluated for different materials and geometric features.
- Cellular model and assessment model can be applied to industrial products.

- Double sided ISF process should be improved using backsupporting plate through further research.

## 7.8 Conclusion

- It is validated through experiments that a simple ISF-FCheck model can successfully predict if a given component is feasible to form through ISF process.
- Regardless of the material type and depth of forming 40° and 50° wall angle show similar behavior when Maximum Von Mises strain % was plotted against the maximum depth. This is due to the moving location of the tool tip with respect to the area of the sheet while the sheet is formed. For higher angles such as 60°, behavior is different but failure can be predicted from the range provided in the method. This behavior is explained intuitively with the help of cellular model.
- Thickness reduction can be calculated through strain and checked whether the formed part will be within the required limits. A material, sheet thickness, rolling direction, feedrate independent graph was plotted and similar behavior was observed for thickness reduction % and Von Mises strain % for various materials and geometries.

Relationships between different input and output parameters were observed. With the help of this knowledge a conclusive table, qualitative model and Cellular model was introduced. The qualitative model, conclusive table and model can be easily used by the industry to solve ISF problems. Increasing production rate, accuracy, evaluating formability, microstructural evolution, internal mechanics and dependency of the process parameters upon each other were successfully achieved. Cellular model is put forward to graphically conceptualize the forming process. It represents formability not only in terms of the material properties and the geometry (wall angle and depth) but also the thickness of the sheet metal.

## 7.9 Summary

This chapter discusses the results of all the experiments in terms of aims and objectives of the research. A model for the ISF process is also developed through careful analysis of the relationship between the input and output parameters. Based on the discussion of the results

and the model, internal mechanics of the ISF process were explained. Limitations of the current work and future directions of research are explained. Conclusions were given at the end.



## References

1. Forum, M., *Vision 2030 - The UK Metals Industry New Strategic Approach*, in *The UK Metals Industry's New Strategic Approach*. 2015.
2. Arshad, S., *SINGLE POINT INCREMENTAL FORMING, A study of Forming Parameters, Forming limits and Part accuracy of Aluminium 2024, 6061 and 7475 alloys*. 2012, KTH Royal Institute of technology: Stockholm, Sweden.
3. Hagan, E. and J. Jeswiet, *A review of conventional and modern single-point sheet metal forming methods*. Proceedings of the Institution of Mechanical Engineers, Part B: Journal of Engineering Manufacture, 2003. **217**(2): p. 213-225.
4. Amino, H., et al. *Dieless NC forming, prototype of automotive service parts*. in *Proceedings of the 2nd International Conference on Rapid Prototyping and Manufacturing (ICRPM), Beijing*. 2002.
5. Tekkaya, A.E., et al., *Surface reconstruction for incremental forming*. Production Engineering, 2007. **1**(1): p. 71-78.
6. Malhotra, R., et al., *Accumulative-DSIF strategy for enhancing process capabilities in incremental forming*. CIRP Annals-Manufacturing Technology, 2012. **61**(1): p. 251-254.
7. Jeswiet, J., et al., *Asymmetric single point incremental forming of sheet metal*. CIRP Annals-Manufacturing Technology, 2005. **54**(2): p. 88-114.
8. Gardezi, S.A.R., et al., *SMALL BATCH SIZE SHEET METAL PRODUCTS MANUFACTURED BY SINGLE POINT INCREMENTAL FORMING PROCESS: ECONOMIC ANALYSIS*.
9. Hussain, G., *Experimental investigations on the role of tool size in causing and controlling defects in single point incremental forming process*. Proceedings of the Institution of Mechanical Engineers, Part B: Journal of Engineering Manufacture, 2013: p. 0954405413498864.
10. Adams, D. and J. Jeswiet, *A new model for contact geometry in single-point incremental forming*. Proceedings of the Institution of Mechanical Engineers, Part B: Journal of Engineering Manufacture, 2015. **229**(6): p. 982-989.
11. Hagan, E. and J. Jeswiet, *Analysis of surface roughness for parts formed by computer numerical controlled incremental forming*. Proceedings of the Institution of Mechanical Engineers, Part B: Journal of Engineering Manufacture, 2004. **218**(10): p. 1307-1312.
12. Lendel, R., et al., *SINGLE POINT INCREMENTAL FORMING OF LARGE-SIZE COMPONENTS*. Journal for Technology of Plasticity, 2014. **39**(1).
13. G. Centeno, M.B.S., V.A.M. Cristino, C. Vallellano, P.A.F. Martins, *Hole-flanging by incremental sheet forming*. International Journal of Machine Tools and Manufacture, 2012. **59**: p. 46-54.
14. Asghar, J., et al., *Tool path design for enhancement of accuracy in single-point incremental forming*. Proceedings of the Institution of Mechanical Engineers, Part B: Journal of Engineering Manufacture, 2013: p. 0954405413512812.
15. Adams, D. and J. Jeswiet, *Design rules and applications of single-point incremental forming*. Proceedings of the Institution of Mechanical Engineers, Part B: Journal of Engineering Manufacture, 2014: p. 0954405414531426.
16. Aoyama, S., et al., *Apparatus for dieless forming plate materials*. Europäisches Brevet EP0970764, 2000.
17. Allwood, J., N. Houghton, and K. Jackson. *The design of an incremental sheet forming machine*. in *Advanced Materials Research*. 2005. Trans Tech Publ.
18. Meier, H., O. Dewald, and J. Zhang. *A new robot-based sheet metal forming process*. in *Advanced Materials Research*. 2005. Trans Tech Publ.

19. Leach, D., A. Green, and A. Bramley. *A new incremental sheet forming process for small batch and prototype parts*. in *9th International Conference on Sheet Metal, Leuven*. 2001.
20. Callegari, M., et al., *Incremental forming of sheet metal by means of parallel kinematics machines*. *Journal of manufacturing science and engineering*, 2008. **130**(5): p. 054501.
21. Rauch, M., et al., *Tool path programming optimization for incremental sheet forming applications*. *Computer-Aided Design*, 2009. **41**(12): p. 877-885.
22. Gatea, S., H. Ou, and G. McCartney, *Review on the influence of process parameters in incremental sheet forming*. *The International Journal of Advanced Manufacturing Technology*, 2016: p. 1-21.
23. Deng, G., et al. *Evaluation of the effect of surface roughness on crack initiation life*. in *ICF12, Ottawa 2009*. 2013.
24. Ås, S.K., B. Skallerud, and B.W. Tveiten, *Surface roughness characterization for fatigue life predictions using finite element analysis*. *International Journal of Fatigue*, 2008. **30**(12): p. 2200-2209.
25. Newman, J., et al., *Fatigue mechanics: an assessment of a unified approach to life prediction*, in *Advances in fatigue lifetime predictive techniques*. 1992, ASTM International.
26. Jelaska, D.T., S. Glodez, and S. Podrug. *Numerical modelling of the crack propagation path at gear tooth root*. in *ASME 2003 International Design Engineering Technical Conferences and Computers and Information in Engineering Conference*. 2003. American Society of Mechanical Engineers.
27. Fang, Y., et al., *Analytical and experimental investigations on deformation mechanism and fracture behavior in single point incremental forming*. *Journal of Materials Processing Technology*, 2014. **214**(8): p. 1503-1515.
28. Decultot, N., et al. *Single point incremental sheet forming investigated by in-process 3D digital image correlation*. in *EPJ Web of Conferences*. 2010. EDP Sciences.
29. Hamilton, K. and J. Jeswiet, *Single point incremental forming at high feed rates and rotational speeds: Surface and structural consequences*. *CIRP Annals-Manufacturing Technology*, 2010. **59**(1): p. 311-314.
30. Durante, M., et al., *The influence of tool rotation on an incremental forming process*. *Journal of Materials Processing Technology*, 2009. **209**(9): p. 4621-4626.
31. Malhotra, R., et al. *Identification of Deformation Mechanisms Responsible for Failure in Incremental Forming using a Damage Based Fracture Model*. in *AIP Conference Proceedings*. 2011. AIP.
32. Centeno, G., et al., *Experimental study on the evaluation of necking and fracture strains in sheet metal forming processes*. *Procedia Engineering*, 2013. **63**: p. 650-658.
33. Oleksik, V., et al. *The influence of geometrical parameters on the incremental forming process for knee implants analyzed by numerical simulation*. in *AIP Conference Proceedings*. 2010. AIP.
34. Bhattacharya, A., et al., *Formability and surface finish studies in single point incremental forming*. *Journal of manufacturing science and engineering*, 2011. **133**(6): p. 061020.
35. Jackson, K. and J. Allwood, *The mechanics of incremental sheet forming*. *Journal of materials processing technology*, 2009. **209**(3): p. 1158-1174.
36. Lasunon, O. and W. Knight, *Comparative investigation of single-point and double-point incremental sheet metal forming processes*. *Proceedings of the Institution of Mechanical Engineers, Part B: Journal of Engineering Manufacture*, 2007. **221**(12): p. 1725-1732.
37. Ambrogio, G., L. Filice, and F. Gagliardi, *Formability of lightweight alloys by hot incremental sheet forming*. *Materials & Design*, 2012. **34**: p. 501-508.

38. Benedetti, M., et al., *Single-point incremental forming of sheet metals: Experimental study and numerical simulation*. Proceedings of the Institution of Mechanical Engineers, Part B: Journal of Engineering Manufacture, 2015: p. 0954405415612351.
39. Kurra, S., et al., *Parametric study and multi-objective optimization in single-point incremental forming of extra deep drawing steel sheets*. Proceedings of the Institution of Mechanical Engineers, Part B: Journal of Engineering Manufacture, 2015: p. 0954405414564408.
40. Ham, M. and J. Jeswiet, *Dimensional accuracy of single point incremental forming*. International Journal of Material Forming, 2008. **1**(1): p. 1171-1174.
41. Bosetti, P. and S. Bruschi. *Springback Evaluation of Parts Made by Single-Point Incremental Sheet Forming*. in *ASME 2011 International Mechanical Engineering Congress and Exposition*. 2011. American Society of Mechanical Engineers.
42. Pohlak, M., J. Majak, and R. Küttner. *Manufacturability and limitations in incremental sheet forming*. in *Proc Est Acad Sci Eng*. 2007.
43. Allwood, J.M., D. Braun, and O. Music, *The effect of partially cut-out blanks on geometric accuracy in incremental sheet forming*. Journal of Materials Processing Technology, 2010. **210**(11): p. 1501-1510.
44. Allwood, J.M., et al., *Closed-loop feedback control of product properties in flexible metal forming processes with mobile tools*. CIRP Annals-Manufacturing Technology, 2009. **58**(1): p. 287-290.
45. JESWIET, J., *Rapid proto-typing with incremental single point forming*. Revue internationale de CFAO et d'informatique graphique, 2000. **15**(2-4): p. 177-183.
46. Singh, D. and P.V. Rao, *A surface roughness prediction model for hard turning process*. The International Journal of Advanced Manufacturing Technology, 2007. **32**(11-12): p. 1115-1124.
47. Chauhan, S. and K. Dass, *Optimization of machining parameters in turning of titanium (grade-5) alloy using response surface methodology*. Materials and manufacturing processes, 2012. **27**(5): p. 531-537.
48. Bhardwaj, B., R. Kumar, and P.K. Singh, *Surface roughness (Ra) prediction model for turning of AISI 1019 steel using response surface methodology and Box-Cox transformation*. Proceedings of the Institution of Mechanical Engineers, Part B: Journal of Engineering Manufacture, 2014. **228**(2): p. 223-232.
49. Kuram, E. and B. Ozcelik, *Multi-objective optimization using Taguchi based grey relational analysis for micro-milling of Al 7075 material with ball nose end mill*. Measurement, 2013. **46**(6): p. 1849-1864.
50. Jeswiet, J., D.J. Young, and M. Ham. *Non-traditional forming limit diagrams for incremental forming*. in *Advanced Materials Research*. 2005. Trans Tech Publ.
51. Park, J.-J. and Y.-H. Kim, *Fundamental studies on the incremental sheet metal forming technique*. Journal of Materials Processing Technology, 2003. **140**(1): p. 447-453.
52. Kim, Y. and J. Park, *Effect of process parameters on formability in incremental forming of sheet metal*. Journal of materials processing technology, 2002. **130**: p. 42-46.
53. Filice, L., L. Fratini, and F. Micari, *Analysis of material formability in incremental forming*. CIRP annals-Manufacturing technology, 2002. **51**(1): p. 199-202.
54. Shim, M.-S. and J.-J. Park, *The formability of aluminum sheet in incremental forming*. Journal of Materials Processing Technology, 2001. **113**(1): p. 654-658.
55. Malhotra, R., et al., *Mechanics of fracture in single point incremental forming*. Journal of Materials Processing Technology, 2012. **212**(7): p. 1573-1590.
56. Allwood, J., D. Shouler, and A.E. Tekkaya. *The increased forming limits of incremental sheet forming processes*. in *Key Engineering Materials*. 2007. Trans Tech Publ.

57. Jackson, K.P.a.A., J.M., *The mechanics of incremental sheet forming*. Journal of Materials Processing Technology, 2008. **209**: p. 1158-1174.
58. Iseki., H., *An approximate deformation analysis and FEM analysis for the incremental bulging of sheet metal using a spherical roller*. Journal of Materials Processing Technology, 2001. **111(1-3)**: p. 150- 154.
59. Blaga, A. and V. Oleksik, *A Study on the Influence of the Forming Strategy on the Main Strains, Thickness Reduction, and Forces in a Single Point Incremental Forming Process*. Advances in Materials Science and Engineering, 2013. **2013**.
60. Young, D. and J. Jeswiet, *Wall thickness variations in single-point incremental forming*. Proceedings of the Institution of Mechanical Engineers, Part B: Journal of Engineering Manufacture, 2004. **218(11)**: p. 1453-1459.
61. Micari, F., G. Ambrogio, and L. Filice, *Shape and dimensional accuracy in single point incremental forming: state of the art and future trends*. Journal of Materials Processing Technology, 2007. **191(1)**: p. 390-395.
62. J.R. Duflou, J.V., B. Belkassam , J. Gub, H. Sol, C. Henrard, A.M. Habraken, *Process window enhancement for single point incremental forming through multi-step tool paths*. CIRP Annals - Manufacturing Technology, 2008. **57**: p. 253-256.
63. Hagan, E. and J. Jeswiet, *Effect of wall angle on Al 3003 strain hardening for parts formed by computer numerical control incremental forming*. Proceedings of the Institution of Mechanical Engineers, Part B: Journal of Engineering Manufacture, 2003. **217(11)**: p. 1571-1579.
64. Nam, N.T., *Hot incremental forming of magnesium and aluminum alloy sheets by using direct heating system*. Proceedings of the Institution of Mechanical Engineers, Part B: Journal of Engineering Manufacture, 2013. **227(8)**: p. 1099-1110.
65. Emmens, W.C., G. Sebastiani, and A.H.v.d. Boogaard, *The technology of Incremental Sheet Forming - a brief review of the history*. Journal of Materials Processing Technology, 2010. **210(8)**: p. 981-997.
66. G, B.W. and M.J.G. F, *Method of dielessly forming surfaces of revolution*. 1967, Google Patents.
67. Leszak, E., *Apparatus and process for incremental dieless forming*. 1967, Google Patents.
68. Mason, B., *Sheet metal forming for small batches*. Bachelor thesis, Univ. of Nottingham, 1978.
69. Iseki, H., K. Kato, and S. Sakamoto, *Flexible and incremental sheet metal forming using a spherical roller*. Proc. 40th JJCTP, 1989. **41**: p. 44.
70. Matsubara, S., *Incremental backward bulge forming of a sheet metal with a hemispherical head tool-a study of a numerical control forming system II*. Journal-Japan Society for Technology of Plasticity, 1994. **35**: p. 1311-1311.
71. Jeswiet, J., E. Hagan, and A. Szekeres, *Forming parameters for incremental forming of aluminium alloy sheet metal*. Proceedings of the Institution of Mechanical Engineers, Part B: Journal of Engineering Manufacture, 2002. **216(10)**: p. 1367-1371.
72. Yamashita, M., M. Gotoh, and S.-Y. Atsumi, *Numerical simulation of incremental forming of sheet metal*. Journal of materials processing technology, 2008. **199(1)**: p. 163-172.
73. Al-Ghamdi, K. and G. Hussain, *The pillowing tendency of materials in single-point incremental forming: experimental and finite element analyses*. Proceedings of the Institution of Mechanical Engineers, Part B: Journal of Engineering Manufacture, 2014: p. 0954405414530906.
74. Allwood, J., et al., *A novel method for the rapid production of inexpensive dies and moulds with surfaces made by incremental sheet forming*. Proceedings of the Institution of Mechanical Engineers, Part B: Journal of Engineering Manufacture, 2006. **220(2)**: p. 323-327.

75. Allwood, J., G. King, and J. Duflou, *A structured search for applications of the incremental sheet-forming process by product segmentation*. Proceedings of the Institution of Mechanical Engineers, Part B: Journal of Engineering Manufacture, 2005. **219**(2): p. 239-244.
76. Yoon, S. and D. Yang, *Investigation into a new incremental forming process using an adjustable punch set for the manufacture of a doubly curved sheet metal*. Proceedings of the Institution of Mechanical Engineers, Part B: Journal of Engineering Manufacture, 2001. **215**(7): p. 991-1004.
77. Adams, D. and J. Jeswiet, *Single-point incremental forming of 6061-T6 using electrically assisted forming methods*. Proceedings of the Institution of Mechanical Engineers, Part B: Journal of Engineering Manufacture, 2014. **228**(7): p. 757-764.
78. Tandon, P. and O.N. Sharma, *Experimental investigation into a new hybrid-forming process: Incremental stretch drawing*. Proceedings of the Institution of Mechanical Engineers, Part B: Journal of Engineering Manufacture, 2016: p. 0954405416645983.
79. Asgari, A., M. Sedighi, and M. Riahi, *Design and development of an incremental sheet metal hammering system using mass damper*. Proceedings of the Institution of Mechanical Engineers, Part B: Journal of Engineering Manufacture, 2015: p. 0954405415599929.
80. Zhang, Q., et al., *The high-pressure liquid jet incremental forming for the aluminum sheet*. Proceedings of the Institution of Mechanical Engineers, Part B: Journal of Engineering Manufacture, 2014: p. 0954405414539930.
81. J., H.E.a.J., *A review of conventional and modern single point sheet metal forming*. Journal of Engineering Manufacture, 2003: p. 213-225.
82. Nam Ho Kim, K.K.C., Jiun Shyan Chen, *Die shape design optimization of sheet metal stamping process using mesh free method*. International Journal for Numerical Methods in Engineering, 2001. **51**: p. 1385-1405.
83. J. Jeswiet, F.M., G. Hirt, A. Bramley, J. Duflou, J. Allwood, *Asymmetric Single Point Incremental Forming of Sheet Metal*. CIRP Annals - Manufacturing Technology, 2005: p. 623-650.
84. Lu, B., et al., *A study of incremental sheet forming by using water jet*. The International Journal of Advanced Manufacturing Technology, 2016: p. 1-11.
85. Kovács, G.L. and I. Paniti, *Re-make of Sheet Metal Parts of End of Life Vehicles- Research on Product Life-Cycle Management, in Digital Product and Process Development Systems*. 2013, Springer. p. 239-253.
86. Jeswiet J., H.E., *Rapid proto-typing of a headlight with sheet metal*. 2001.
87. J., J. *Recent results for SPIF*. in *Seminar on Incremental Forming*, Cambridge University. 2004.
88. S. B. M. Echrif, M.H., *Research and Progress in Incremental Sheet Forming Processes*. Materials and Manufacturing Processes, 2011: p. 1404-1414.
89. Centre, A.F.R., *Use of incremental sheet forming for the manufacture of cranial plates*. 2014.
90. Isekia, H.N., *Vertical wall surface forming of rectangular shell using multistage incremental forming with spherical and cylindrical rollers*. Journal of Materials Processing Technology, 2002 **130**: p. 675-679.
91. Duflou, J.R.C., B. Verbert, J. De Baerdemaeker, H., *Laser Assisted Incremental Forming: Formability and Accuracy Improvement*. CIRP Annals, 2007. **56**: p. 273-276.
92. Centeno, G., et al., *Hole-flanging by incremental sheet forming*. International Journal of Machine Tools and Manufacture, 2012. **59**: p. 46-54.
93. Powell, N. and C. Andrew, *Incremental forming of flanged sheet metal components without dedicated dies*. Proceedings of the Institution of Mechanical Engineers, Part B: Journal of Engineering Manufacture, 1992. **206**(1): p. 41-47.

94. Kitazawa, K. *Incremental sheet metal stretch-expanding with CNC machine tools*. in *Proceedings of 4th ICTP*. 1993.
95. Bambach, M., G. Hirt, and S. Junk. *Modelling and experimental evaluation of the incremental CNC sheet metal forming process*. in *7th International Conference on Computational Plasticity*. 2003.
96. Hirt, G. *Tools and Equipment used in Incremental Forming*. in *1st Incremental Forming Workshop, University of Saarbrücken*. 2004.
97. Dufloy, J.R., A. Szekeres, and P. Vanherck. *Force measurements for single point incremental forming: an experimental study*. in *Advanced Materials Research*. 2005. Trans Tech Publ.
98. Ambrogio, G., L. Filice, and G. Manco, *Warm incremental forming of magnesium alloy AZ31*. *CIRP Annals-Manufacturing Technology*, 2008. **57**(1): p. 257-260.
99. Jeswiet, J., *Incremental single point forming*. *TRANSACTIONS-NORTH AMERICAN MANUFACTURING RESEARCH INSTITUTION OF SME*, 2001: p. 75-80.
100. Zhu, H., W.W. Lin, and J.L. Bai. *An Overview of the Sheet Metal CNC Incremental Forming Toolpath Generation*. in *Advanced Materials Research*. 2012. Trans Tech Publ.
101. Thibaud, S., et al., *A fully parametric toolbox for the simulation of single point incremental sheet forming process: Numerical feasibility and experimental validation*. *Simulation Modelling Practice and Theory*, 2012. **29**: p. 32-43.
102. Ambrogio, G., L. Filice, and F. Micari, *A force measuring based strategy for failure prevention in incremental forming*. *Journal of Materials Processing Technology*, 2006. **177**(1): p. 413-416.
103. Dufloy, J., et al., *Experimental study on force measurements for single point incremental forming*. *Journal of Materials Processing Technology*, 2007. **189**(1): p. 65-72.
104. Basics, D.S.M.F.a., *Incremental Sheet Forming*, I.F.I.o.M.T.a.F. Technology, Editor. 2015: Germany.
105. Paniti, I., *Adaptation of Incremental Sheet Forming into cloud manufacturing*. *CIRP Journal of Manufacturing Science and Technology*, 2014. **7**(3): p. 185-190.
106. Hirt, G. *Tools and Equipment used in Incremental Forming*. in *1st Incremental Forming Workshop*. 2004. University of Saarbrücken.
107. Junchao, L., S. Junjian, and W. Bin, *A multipass incremental sheet forming strategy of a car taillight bracket*. *The International Journal of Advanced Manufacturing Technology*, 2013. **69**(9-12): p. 2229-2236.
108. Liu, Z., Y. Li, and P.A. Meehan, *Vertical wall formation and material flow control for incremental sheet forming by revisiting multistage deformation path strategies*. *Materials and manufacturing processes*, 2013. **28**(5): p. 562-571.
109. Ham, M. and J. Jeswiet, *Single point incremental forming and the forming criteria for AA3003*. *CIRP Annals-Manufacturing Technology*, 2006. **55**(1): p. 241-244.
110. Petek, A., K. Kuzman, and B. Suhač, *Autonomous on-line system for fracture identification at incremental sheet forming*. *CIRP Annals-Manufacturing Technology*, 2009. **58**(1): p. 283-286.
111. Li, Y.L., et al. *Experimental study and efficient prediction on forming forces in incremental sheet forming*. in *Advanced Materials Research*. 2014. Trans Tech Publ.
112. Mecnica, E., *Dissertation Master Thesis*. 2009, University of Lisbon.
113. Amar Kumar Behera, J.V., Bert Lauwers, Joost R. Dufloy, *Tool path compensation strategies for single point incremental sheet forming using multivariate adaptive regression splines*. *Computer-Aided Design*, 2013: p. 575.
114. Paniti, I. and J. Somló, *Novel Incremental Sheet Forming System with Tool-Path Calculation Approach*. *Acta Polytechnica Hungarica*, 2014. **11**(7): p. 43-60.

115. Meier, H., B. Buff, and V. Smukala. *Robot-Based Incremental Sheet Metal Forming—Increasing the Part Accuracy in an Automated, Industrial Forming Cell*. in *Key Engineering Materials*. 2009. Trans Tech Publ.
116. Meier, H., C. Magnus, and V. Smukala, *Impact of superimposed pressure on dieless incremental sheet metal forming with two moving tools*. *CIRP Annals-Manufacturing Technology*, 2011. **60**(1): p. 327-330.
117. Martins, P.A.F.B., N. Skjoedt, M. Silva, M.B., *Theory of single point incremental forming*. *Journal of Strain Analysis*, 2008. **43**: p. 15-35.
118. Skjoedt M., B.N., Endelt B. and Ingarrao G. *Multi-stage strategies for single point incremental forming of a cup*. in *11th ESAFORM conference on metal forming*. 2008.
119. Hussain, G., L. Gao, and N. Hayat, *Empirical modelling of the influence of operating parameters on the spifability of a titanium sheet using response surface methodology*. *Proceedings of the Institution of Mechanical Engineers, Part B: Journal of Engineering Manufacture*, 2009. **223**(1): p. 73-81.
120. Ham M, J.J., *Single point incremental forming and the forming criteria for AA3003*. *CIRP Annals- Manufacturing technology*, 2006. **55**: p. 241-244.
121. Hagan, E., Jeswiet, J, *Analysis of surface roughness for parts formed by computer numerical controlled incremental forming*. *Proc. IMechE. J. Engineering Manufacture*, 2004. **218**: p. 1307-1312.
122. Ambrogio, G., et al., *On the high-speed Single Point Incremental Forming of titanium alloys*. *CIRP Annals-Manufacturing Technology*, 2013. **62**(1): p. 243-246.
123. Hussain, G., et al., *Tool and lubrication for negative incremental forming of a commercially pure titanium sheet*. *Journal of Materials Processing Technology*, 2008. **203**(1): p. 193-201.
124. Silva MB, S.M., Atkins AG, Bay N, Martins PAF, *Single Point Incremental Forming & Formabilit /Failure Diagrams*. *Journal of Strain Analysis for Engineering Design*, 2008. **43**: p. 15-36.
125. Le, V., A. Ghiotti, and G. Lucchetta, *Preliminary studies on single point incremental forming for thermoplastic materials*. *International Journal of Material Forming*, 2008. **1**(1): p. 1179-1182.
126. Yonan, S.A., et al., *Plastic flow and failure in single point incremental forming of PVC sheets*. *Express Polymer Letters*, 2014. **8**(5): p. 301-311.
127. Martins, P., et al., *Single point incremental forming of polymers*. *CIRP Annals-Manufacturing Technology*, 2009. **58**(1): p. 229-232.
128. Siddiqi, M.U.R., et al., *Mechanics and Material Behavior of CpTi during Incremental Sheet Forming Process.*, in *Ti-2015: The 13th World Conference on Titanium*, M.M.S. The Minerals, Editor. 2015: Sandiego, California, USA.
129. Filice, L., *A phenomenology-based approach for modelling material thinning and formability in incremental forming of cylindrical parts*. *Proceedings of the Institution of Mechanical Engineers, Part B: Journal of Engineering Manufacture*, 2006. **220**(9): p. 1449-1455.
130. Attanasio, A., E. Ceretti, and C. Giardini, *Optimization of tool path in two points incremental forming*. *Journal of Materials Processing Technology*, 2006. **177**(1): p. 409-412.
131. Dufflou, J., et al., *Improved SPIF performance through dynamic local heating*. *International Journal of Machine Tools and Manufacture*, 2008. **48**(5): p. 543-549.
132. Li, J., P. Geng, and J. Shen, *Numerical simulation and experimental investigation of multistage incremental sheet forming*. *The International Journal of Advanced Manufacturing Technology*, 2013. **68**(9-12): p. 2637-2644.
133. Ma, L. and J. Mo, *Three-dimensional finite element method simulation of sheet metal single-point incremental forming and the deformation pattern analysis*. *Proceedings of the Institution of Mechanical Engineers, Part B: Journal of Engineering Manufacture*, 2008. **222**(3): p. 373-380.

134. Subramanian, C. and V. Senthil Kumar, *Experimental Studies on Incremental Forming of Stainless Steel AISI 304 Sheets [J]*. J. Eng. Manufact, 2012. **226**(7): p. 1224-1229.
135. Taleb Araghi, B., et al. *Investigation on incremental sheet forming combined with laser heating and stretch forming for the production of lightweight structures*. in *Key Engineering Materials*. 2011. Trans Tech Publ.
136. Mosecker, L., et al. *Deformation mechanisms of Ti6Al4V sheet material during the incremental sheet forming with laser heating*. in *Key Engineering Materials*. 2013. Trans Tech Publ.
137. Silva MB, S.M., Atkins AG, Bay N, Martins PAF, *Revisiting the fundamentals of single point incremental forming by means of membrane analysis*. International Journal of Machine Tools & Manufacture, 2008. **48**: p. 73-83.
138. Oh, S., C. Chen, and S. Kobayashi, *Ductile fracture in axisymmetric extrusion and drawing—part 2: workability in extrusion and drawing*. Journal of Engineering for Industry, 1979. **101**(1): p. 36-44.
139. Iseki, H., *An approximate deformation analysis and FEM analysis for the incremental bulging of sheet metal using a spherical roller*. Journal of Materials Processing Technology, 2001. **111**(1): p. 150-154.
140. Bramley, A.N., *Incremental Sheet Forming Process for Small Batch and Prototype Parts*, ed. F.V.a.M. Kleiner. 2001.
141. Amar Kumar Beheraa, B.L., Joost R. Duflou, *An Integrated Approach to Accurate Part Manufacture in Single Point Incremental Forming using Feature Based Graph Topology Key*. Engineering Materials, 2012. **504**: p. 869-876.
142. M. Bambach, M.T.a.G.H., *Experimental and numerical analysis of forming limits in CNC incremental sheet forming*. Key Engineering Materials, 2007. **344**: p. 511-518.
143. Li, J., et al., *Thickness distribution and design of a multi-stage process for sheet metal incremental forming*. The International Journal of Advanced Manufacturing Technology, 2012. **62**(9-12): p. 981-988.
144. Jun-chao, L., L. Chong, and Z. Tong-gui, *Thickness distribution and mechanical property of sheet metal incremental forming based on numerical simulation-TNMSC*. The Chinese Journal of Nonferrous Metals. **22**(1).
145. L Filice, L.F., F Micari, *Formability in Incremental Forming*. CIRP annals-Manufacturing technology, 2002.
146. Gardezi, S.A.R., *Economic Analysis of low volume sheet metal products manufactured by single point incremental forming process*. 2008, UET Lahore: Pakistan.
147. Flores, P.D., L. Bouffioux, C. Lelotte, T. Henrard, C. Pernin, N. Van Bael, A. He, S. Duflou, J. Habraken, A.M., *Model identification and FE simulations: Effect of different yield loci and hardening laws in sheet forming*. International Journal of Plasticity, 2007. **23**: p. 420-449.
148. Creswell, J.W., *Research design: Qualitative, quantitative, and mixed methods approaches*. 2013: Sage publications.
149. Beech, N., *Research Methodology Course Notes: Strathclyde Business School*. 2005.
150. Gray, P.S., et al., *The research imagination: An introduction to qualitative and quantitative methods*. 2007: Cambridge University Press.
151. Hu, J., Z. Marciniak, and J. Duncan, *Mechanics of sheet metal forming*. 2002: Butterworth-Heinemann.
152. Anderson, T.L. and T. Anderson, *Fracture mechanics: fundamentals and applications*. 2005: CRC press.
153. AFRC, *AFRC Core research ISF report*. 2012-2013.
154. Y.N. Wang, H., *Review, Texture analysis in hexagonal materials*. Materials Chemistry and Physics, 2003. **81**: p. 11-26.



155. Committee, A.I.H., *ASM handbook: Materials selection and design*. Vol. 20. 1997: CRC Press.
156. Shigley, J.E., *Shigley's mechanical engineering design*. 2011: Tata McGraw-Hill Education.
157. Min, J., J. Lin, and J. Li, *Forming limits of Mg alloy ZEK100 sheet in preform annealing process*. *Materials & Design*, 2014. **53**: p. 947-953.
158. Hussaini, S.M., et al., *Development of experimental and theoretical forming limit diagrams for warm forming of austenitic stainless steel 316*. *Journal of Manufacturing Processes*, 2015. **18**: p. 151-158.
159. Ma, B., et al., *Prediction of forming limit in DP590 steel sheet forming: An extended fracture criterion*. *Materials & Design*, 2016. **96**: p. 401-408.
160. Standard, I., *Metallic Materials—Sheet And Strip—Determination of Forming Limit Curves—Part 2: Determination of Forming Limit Curves in the Laboratory*. International Organization for Standardization, 2008. **20087**: p. 12004-2.
161. Siddiqi, M.U.R., et al., *Incremental Sheet Forming fixture design and implementation.*, in *Computer-Aided Production Engineering: Manufacturing Research and its Applications in the 21st Century*, T.U.o. Edinburgh., Editor. 2015, Proceedings of Institution of Mechanical Engineers and Institution of Engineering and Technology.: Edinburgh, United Kingdom.
162. Pugh, S., *Total design: integrated methods for successful product engineering*. 1991: Addison-Wesley.
163. Ferracane, J.L., *Hygroscopic and hydrolytic effects in dental polymer networks*. *Dental Materials*, 2006. **22**(3): p. 211-222.
164. Sepe, M., *Dimensional Stability After Molding*. *Plastics Technology*, 2013.
165. Richardson, E., *Investigating the characterisation and stability of polyamide 6, 6 in heritage artefacts*. 2009, University of Southampton.
166. Kim, J., H. Jang, and J.W. Kim, *Friction and wear of monolithic and glass-fiber reinforced PA66 in humid conditions*. *Wear*, 2014. **309**(1): p. 82-88.
167. Moghbelli, E., R. Banyay, and H.-J. Sue, *Effect of moisture exposure on scratch resistance of PMMA*. *Tribology International*, 2014. **69**: p. 46-51.
168. Carlson, E., D. Automotive, and K. Nelson, *Nylon Under the Hood*. *Automotive engineering*, 1996. **104**(12): p. 84-89.
169. Nash, A., *Support for a seat*. 1997, Google Patents.
170. Downs, J.B., et al., *Intermittent mandatory ventilation: a new approach to weaning patients from mechanical ventilators*. *CHEST Journal*, 1973. **64**(3): p. 331-335.
171. Stubbersfield, E.M., *Brake shaft bearings*. 1987, Google Patents.
172. Henry, S.L., *Radiator shutter mechanisms*. 1966, Google Patents.

## **8. Appendix A -Initial scoping experiments**

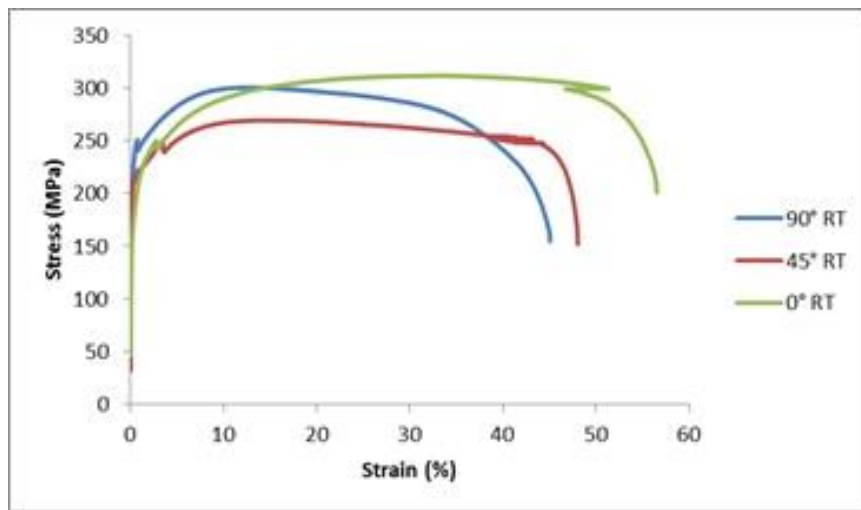
To build up experimental experience and familiarity with the ISF process a number of scoping investigations were performed focused on questions reported in the literature. The literature review, suggested that variation in basic material properties of CpTi such as stress and strain occur under different rolling conditions. To investigate this phenomena sheets of various materials were etched and clamped on fixtures. Hemispherical tool was used to manufacture cup shaped parts using a CNC machine. Sheet was clamped through nuts and bolts in fixture. Area of each sheet was 300mmX300mm. Consequently, the study results with the investigation and measurement of material and physical properties. The cup shape parts were produced with three different depths (i.e. 12mm, 17mm and 27mm). Results such as profile variation, thickness, major and minor strain and material behavior were reported. These experiments will lead to design of further experiments and eventually a multi-scale model of ISF process.

Empirical and modeling results of tensile testing of Titanium are discussed with respect to different rolling directions. Etching and manufacturing process parameters are reported. Results acquired i.e. strains, springback, thickness and profile with 3D scanning are discussed. Sample preparation technique and microstructure observed with SEM is also part of this section. Results are analyzed and conclusions and methodology is derived from it.

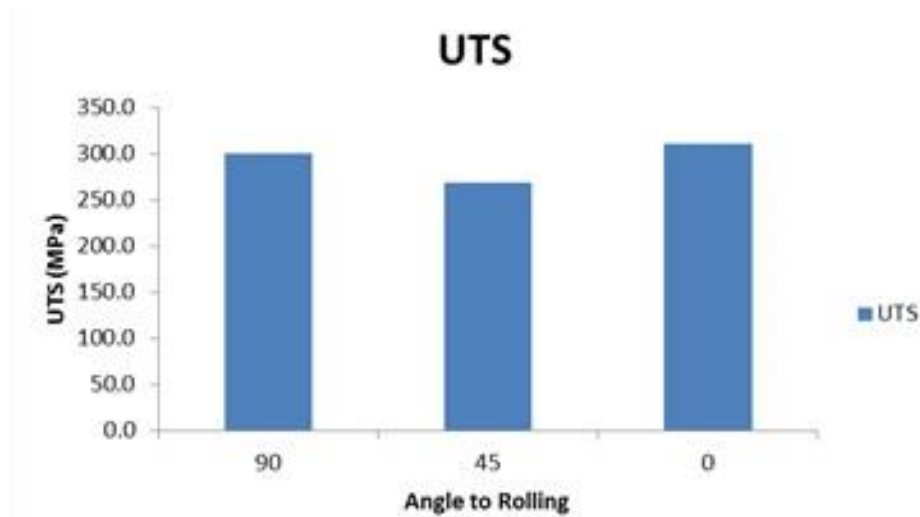
### **8.1 Tensile testing and modeling**

Tensile test of the specimen show that rolling direction influences some of the material properties [Figure 8-1]. Maximum strain is recorded when loading is applied parallel to the rolling direction and minimum strain is recorded when it is applied perpendicular to the rolling direction. Strain is in between the two extreme values for 45 degrees. It is clear from the figure all tests showed that titanium experiences ductile behavior regardless of the rolling direction. Surprisingly, 0 and 90 degrees show more strength (load bearing capacity) i.e. 300 MPa than 45 degrees (250 MPa). Figure 8-2 shows the thinning profile of the three specimens. 0 degree specimen has a localized thinning effect i.e. cracked area is effected and thinned; specimen thickness in rest of the area is not or very minutely reduced. Compared to 0°, 45° more area of specimen is influenced by the tensile test and thus it shows more

ductility than 0° specimens. 90° shows most distributed effect of stress, strain and thickness and thus is the most ductile direction compared to 0° and 45°. This concludes that the properties are not the same in all directions. This conclusion is used during manufacturing to check different ISF parameters.



(a)



(b)

Figure 8-1 Tensile tests CPTi; (a)Stress-Strain curve, (b)Rolling angle to strength.

Table 8-1 Tensile tests CPTi.

Orientation (°)	UTS (MPa)	Elongation (%)
0	312	45
45	269	48
90	300	56

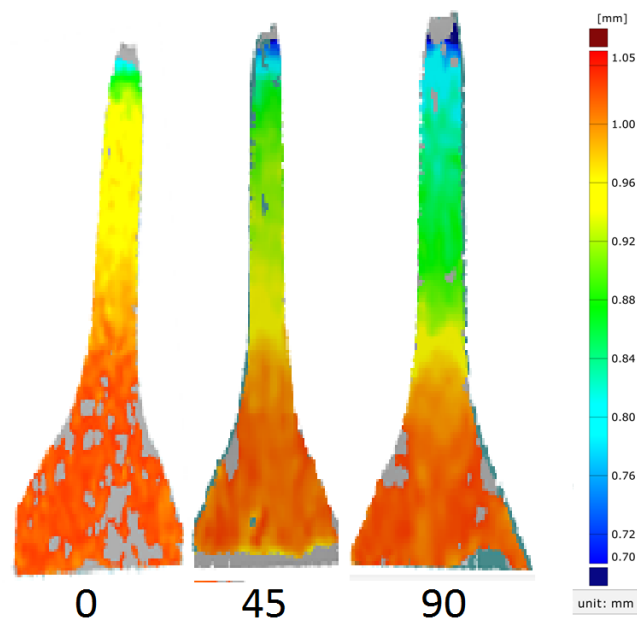


Figure 8-2 3D scan results of tensile testing.

Tensile test was modeled numerically using Finite Element Analysis. Model of the specimen was prepared in Solid Works. Model was then meshed, material properties were assigned and loads were applied. Problem was solved using ABAQUS. Stress-Strain graph [Figure 8-3] shows good agreement between actual and numerical results. The model can be further enhanced to incorporate the yielding curve. The methodology can then be used to model ISF process.

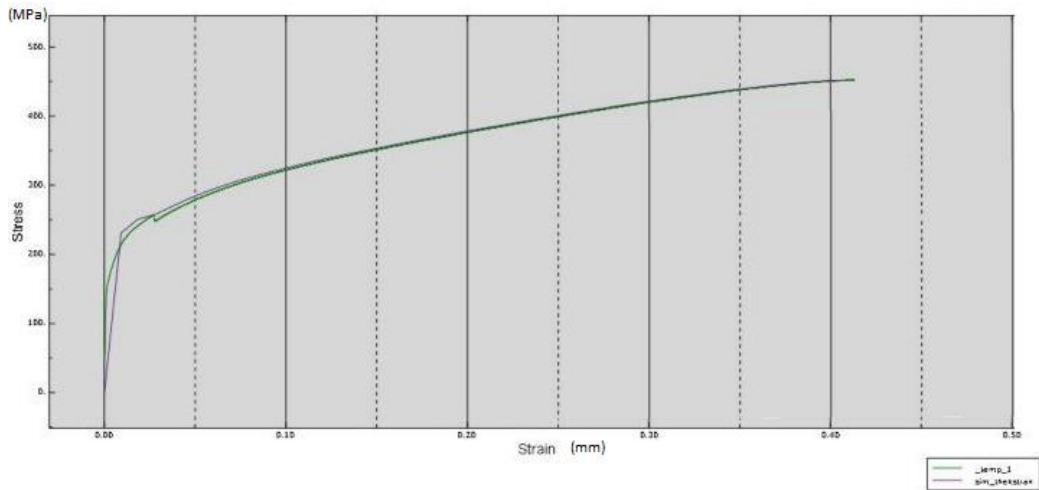


Figure 8-3 Validation of Numerical Model of UTM specimen

## 8.2 Manufacturing

### 8.2.1 Etching

Etching is permanent chemical marking of metal sheets used for various purposes. Titanium sheets were etched using acid and etching equipment. Etching equipment consists of a roller, regulator and wires. The roller was positively charged where the sheet was attached with the negative terminal of the equipment. Specific voltage was applied across the circuit. Fine point sheet was used between the roller and Ti sheet for marking purposes. Sheet and roller was wet with water and acid. Etching was performed by rolling the roller over the sheet. Etching is done to calculate major and minor strains using strain points. Figure 8-4 shows etched part after manufacturing.

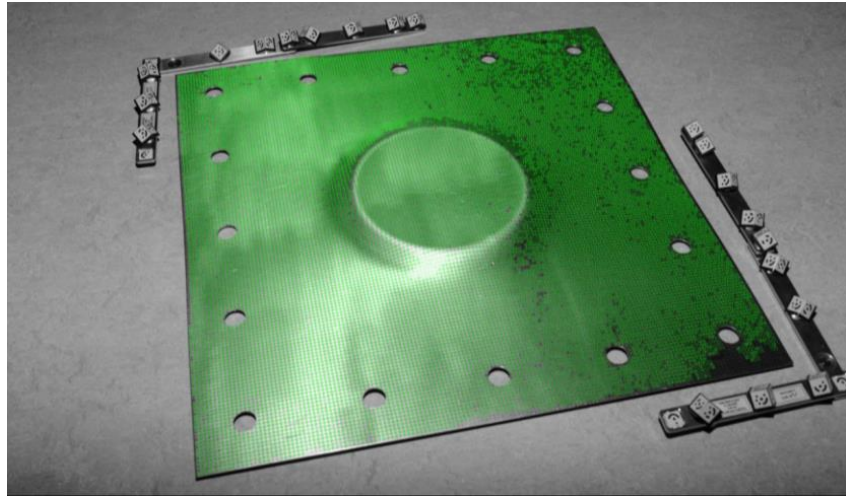


Figure 8-4 Etched part with markers

### 8.2.2 Parameters

Research on rig size parameters were done by Amir and Rahul at AFRC [13, 153]. Figure 8-5 shows rig, forming tool, sheet and blank holder. Initially, cup shaped parts were produced and analyzed to understand the process completely. Five parts were manufactured using two different tool paths.

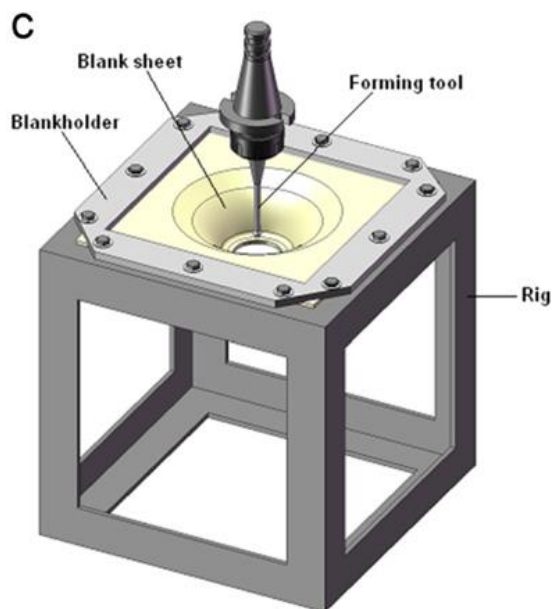


Figure 8-5 ISF rig, hole flanging [13]

5 axis CNC machine and custom developed round shaped tool of ½” diameter was used to manufacture the parts. Ti sheet was clamped in the rig using nut and bolts. Localized force was applied using round shaped tool which deformed the sheet step by step. Following are the parameters used to manufacture the parts

Drawing Depth = 12mm, 17mm and 27 mm

Feed rate = 700 mm/min

Pitch size = 0.5 mm

Time to ISF/sample = 40 min

Two methodologies were used to manufacture the part. In Methodology 1 the tool circulated in constant radius around a virtual axis and went down in z direction with a constant step size. The final shape of the tool path resembles a vertical spring. In Methodology 2 tool circulated in a varying diameter and step size. The tool completed two cycles in order to reduce spring back effect. End shape of the tool path resembles a swirl in fluid. Part was removed from the rig after manufacturing. Final part is shown in the Figure 8-6.

### **8.3 3D Scanning**

Manufactured cup shaped parts were scanned using 3D scanner. Ti is a highly reflective material and initially 3D scanner was not able to acquire data properly. Thin layer of paint was applied to solve this problem and acquire data effectively. After acquiring data from 3D scanner the profile was polygonized, smoothed and processed to get final useable shape. Thickness profile and shape of part was acquired through 3D scanning and will be explained later on in the results section. Figure 8-6 shows scanned profile of a manufactured part. Crack produced due to ISF process can also be seen quite easily.

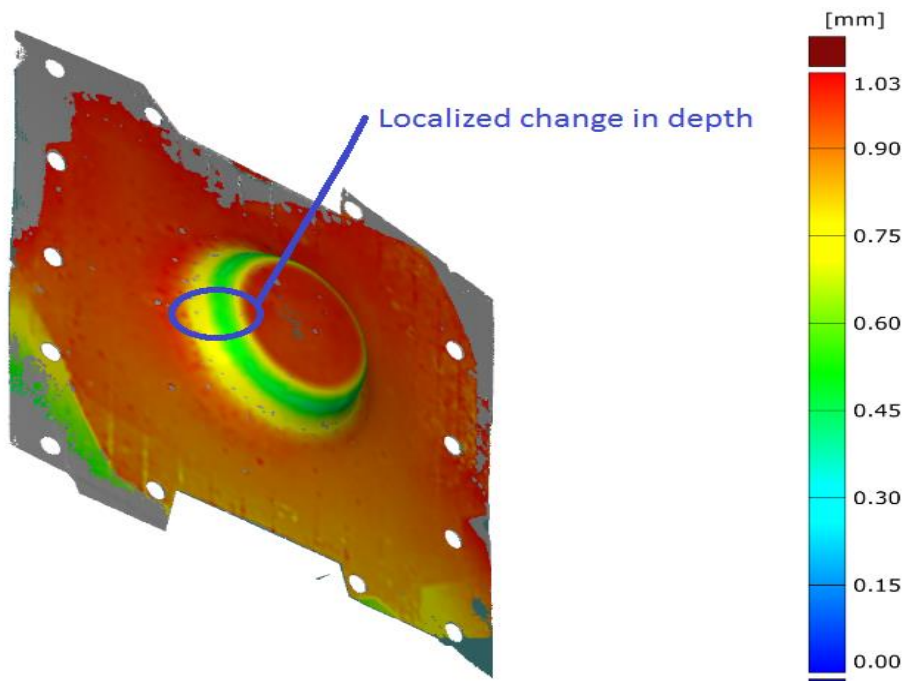


Figure 8-6 3D scan of manufactured part

### 8.3.1 Major and Minor strain

Major and minor strains shown in Figure 8-7 were acquired using strain point data through ATOS. The blue markings are representing that these points did not come under any strain or strain was negligible here. The encircled green dots show that sheet is nearing the necking conditions and the red dots represents that necking has started. The region identified is close to plane strain region and if the major strain exceeds 25% necking will start.

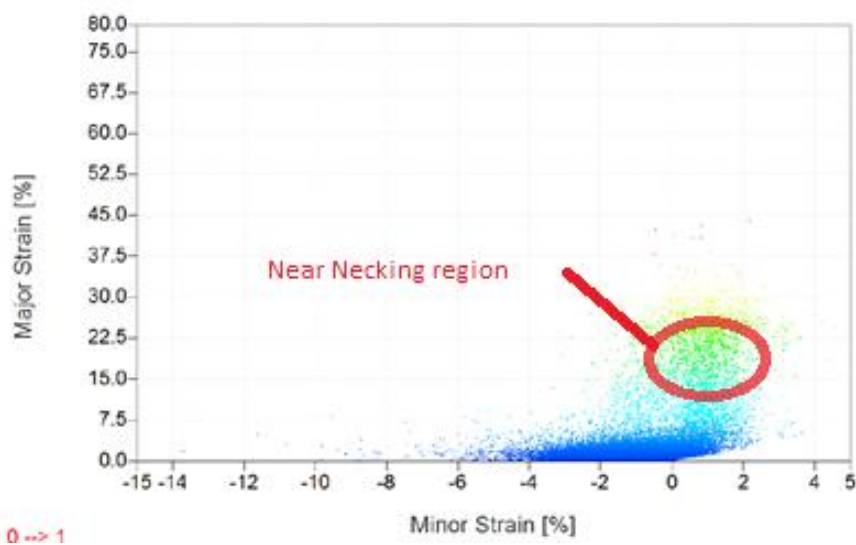




Figure 8-7 Major and Minor strain.

### 8.3.2 Springback

Springback is reported frequently in forming processes and described in detail during literature review. Springback is shown in Figure 8-8 and it is a linear function with depth and strain. Intended depth is depth of the programmed tool and measured depth is depth at the corners. It is concluded that dimensional accuracy of Ti alloy for ISF process would be around -2mm i.e. if forming depth of a tool is 25mm the sheet depth will be around 23mm.

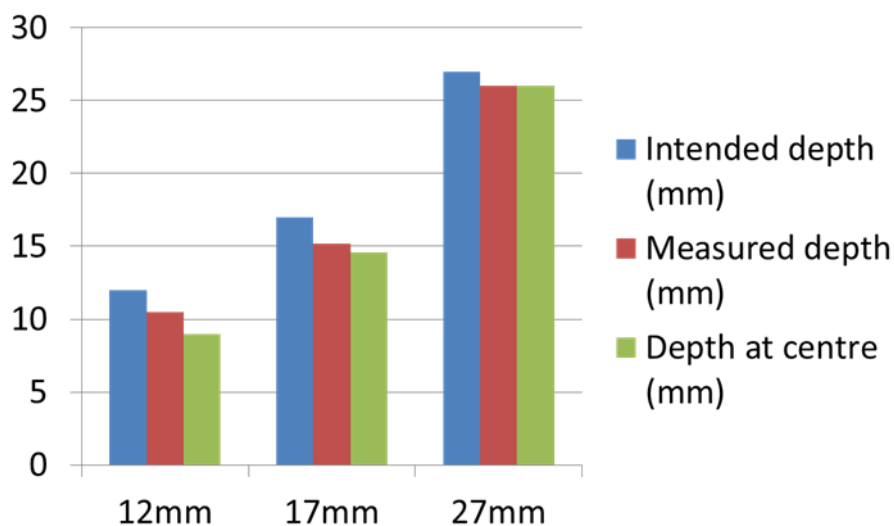


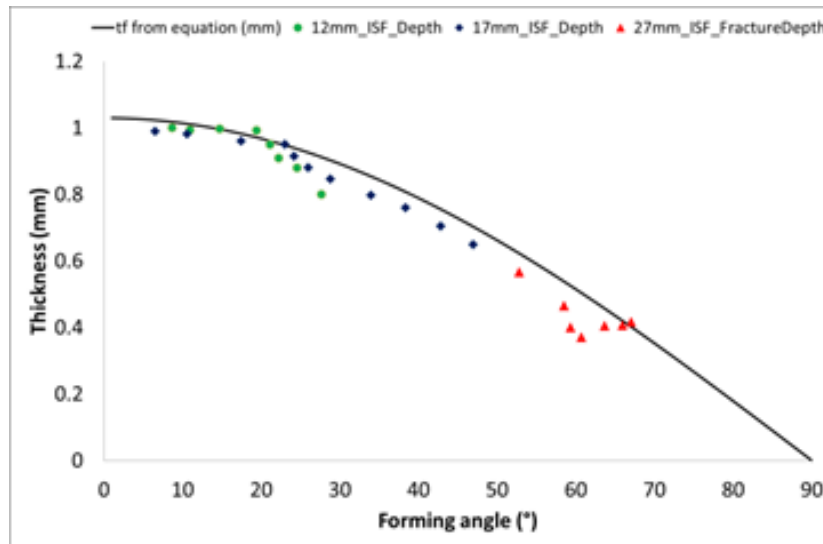
Figure 8-8 Springback.

### 8.3.3 Thickness and profile

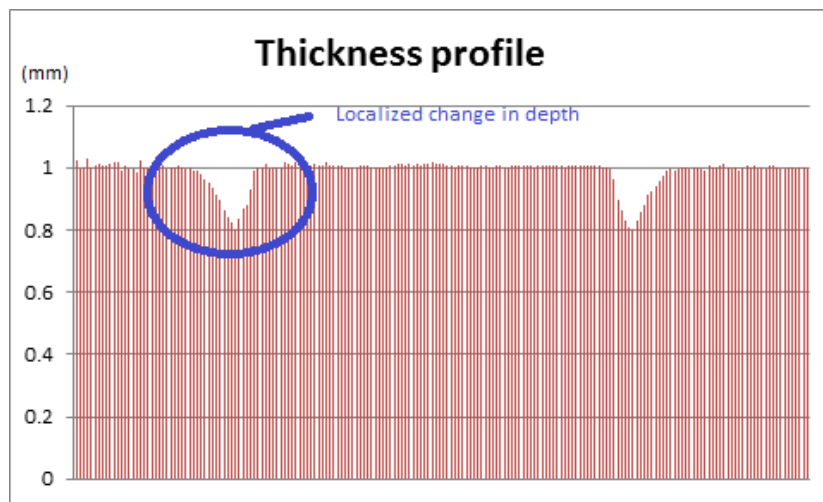
Thickness profiles were acquired experimentally through 3D scanning and ARGUS programming [Figure 8-9]. Sections were marked at the middle of the part to get data at specific location as shown in the figure. After that lines on that section were selected to calculate thickness of the part. A specifically written program was executed to acquire thickness data from 3D scanned images.

Thickness profiles show major differences between the two methodologies applied to manufacture the parts. As expected Methodology 1 shows a constant thickness throughout the profile and thinning is observed at a localized area. Cracks propagated in the same region and this location had high strain levels. Moving from center to side in this localized area the

cross section area of the sheet decreases and reduces approximately to zero for some tests and then increases to its original value. Author's point of view is that material of very localized area is used to acquire the shape of the part and if better optimized tool paths are used results can be improved. Figure 8-9b shows that thickness of the sheet decreases as the forming angle and forming depth increases.



(a)



(b)

Figure 8-9 (a) Wall angle[153], (b) Thickness profile.

A major difference in profile of different parts is observed. Figure 8-10 shows deformation profile of two geometries deformed till a limit of 10 mm and 17 mm respectively using ISF. Base of the part deformed till 10 mm is curved and depth is also varying in radial direction while 17 mm has a flat base with uniform depth. So it is concluded that better geometries can be attained by deforming the sheet to maximum.

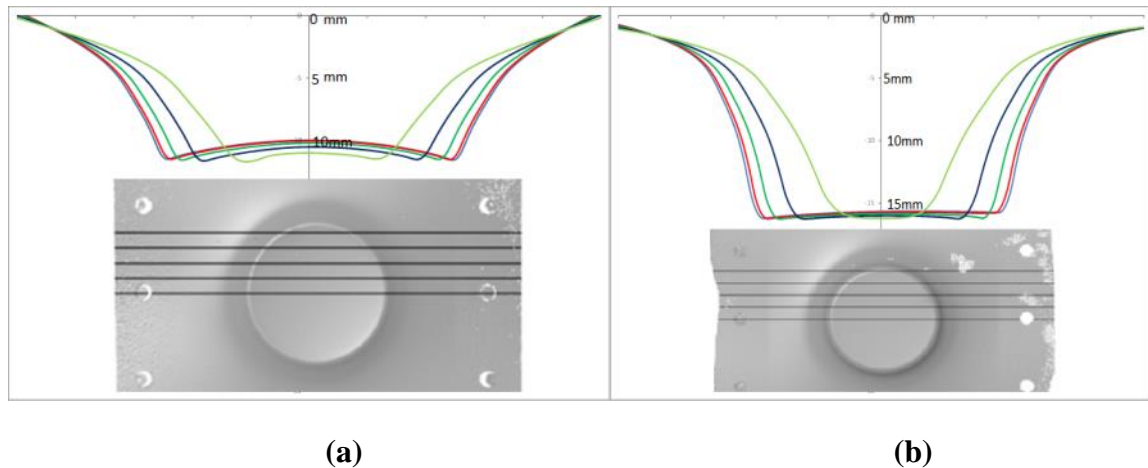


Figure 8-10 Deformation profile; (a) 10mm, (b) 17mm.

## 8.4 Material Characterization

Following are the steps performed for material characterization.

### 8.4.1 Sample preparation

Sample preparation used to determine microstructure through SEM and EBSD is more of an art than a science. Continuous visual inspection and experience is required throughout sample preparation. Sample preparation process has following steps

1. Sample removal/ cutting
2. Determining the rolling direction
3. Mounting sample with copper powder
4. Grinding stages
5. Polishing stages
6. Vibrator

## 7. Microscopy throughout

Sample was removed from the sheets using wire cut as per requirement. Initially three locations were selected to find the microstructure and were named as A,B and C respectively as show in Figure 8-11. Rolling direction was known and was marked on the samples. Rolling directions are important while performing SEM or EBSD analysis on the samples. Copper powder was used for mounting due to better conductivity and clear imaging of the samples. Mounting was done at room temperature. Three grinding steps were performed to prepare sample with 200P, 600P and 1200P grinding papers respectively. Details of the parameters used are provided in Table. Grinding uses parallel rotation while polishing uses contra direction of rotation.

Polishing is done using fine liquid diamond solution, spread on the 9 um polishing cloth. Volume of diamond liquid is spread as per requirement on the polishing cloth and is used for minutes. Grinding paper is thrown away while polishing cloth is washed and kept for further use. Sample is kept in vibrator for 10-12 hours with 0.5  $\mu\text{m}$  polishing diamond liquid. Sample is kept in vibrator with water for half an hour to clear the particles on the sample. Polishing cloth is the washed and fixed above the vibrator. Sample is checked by naked eye and optical microscope throughout the preparation process. It is important to mention here that this procedure, its steps r parameters are not constant. One or many steps may be repeated or changed as per requirement for sample preparation.

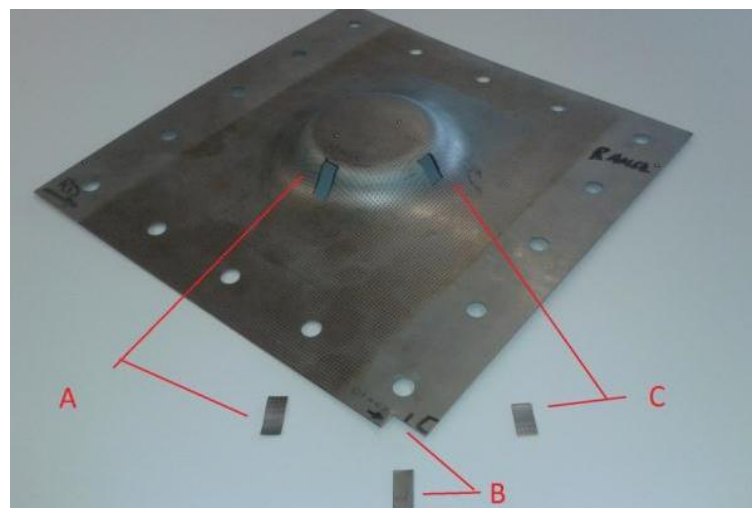


Figure 8-11 Samples taken out from ISF sheet.

## 8.4.2 Microstructure

After sample preparation images were taken using microscope to check surface profile and waviness. After checking suitability for Scanning Electron Microscope (SEM) and Electron backscatter diffraction (EBSD), samples were used to take images. SEM images [Figure 8-12] show that original undeformed sheets have proper hexagonal grain structure. Grain size measured through SEM images is in the range of 15-30  $\mu\text{m}$  before applying any external force on the sheet. Grains elongate in one direction and hexagonal structure is changed after ISF process was performed as shown in Figure 8-13. Microstructure of the deformed sheet does not have uniform grain morphology. Change in microstructure is due to the external force applied during the process. Elongation of the grains is directly proportional to the thickness of the sheet i.e. the more thinner the sheet the more elongated the grains.

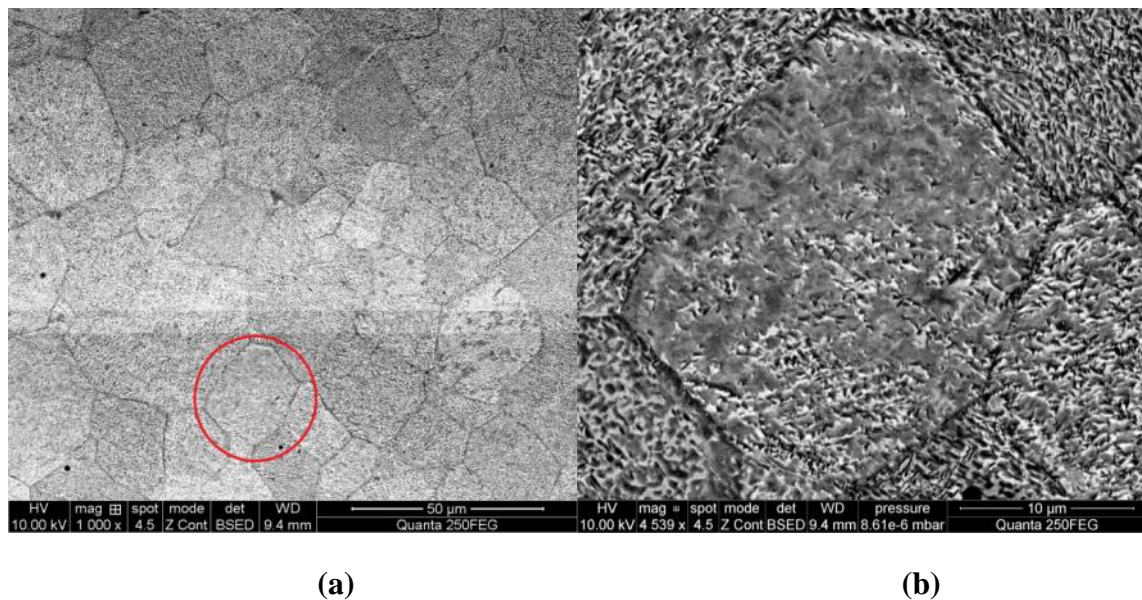


Figure 8-12 Microstructure of undeformed sheet at different magnifications; (a) 1000X, (b) 3000X.

Mechanical properties of crystals depend on the material crystal structure and orientation. Elastic modulus, strength, toughness, Poisson's ratio are some of the examples, same is verified by Wang et.al.[154]. It is difficult for the grain boundaries to slide in transverse direction than longitudinal direction. Texture toughening and strengthening have been reported in hexagonal materials. Due to this reason we can see different mechanical properties, for instance tensile strength discussed earlier, in different orientations. So by

relating physical properties to the microstructure we can safely say that slip will require more force when load is applied in transverse angle i.e. compared to the longitudinal one. Microstructure morphology in hexagonal materials is quiet interesting and has different deformation from cubic materials. This is because HCP has limited slip systems deformation mode is frequently due to twinning[154]. Twins are observed in Figure 8-14.

All these results helped author in better understanding the ISF process and effects of varying different parameters.

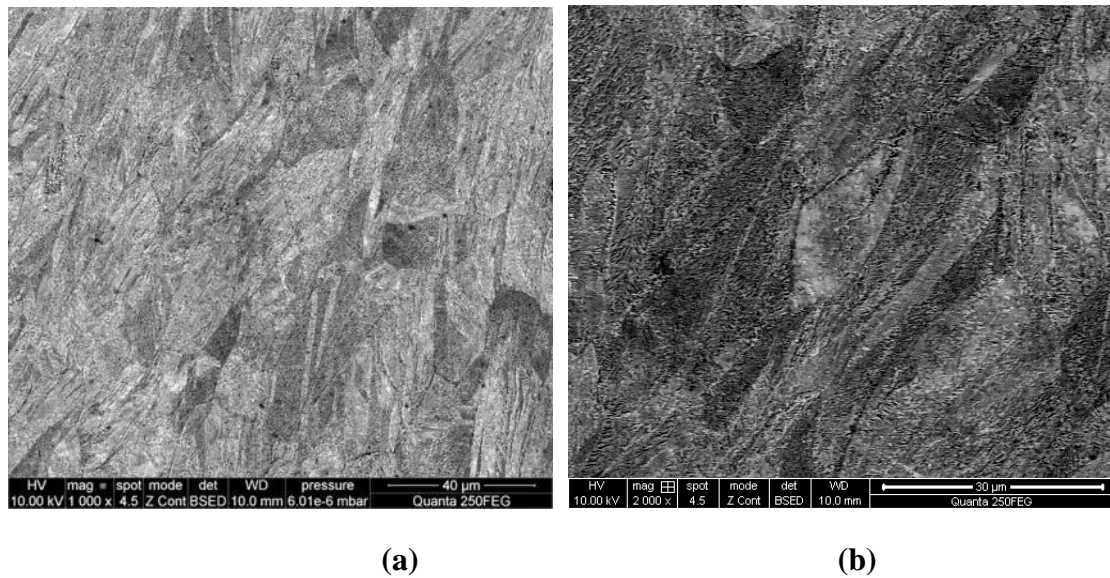


Figure 8-13 Microstructure of deformed sheet; (a) 1000 x, (b)2000x

Study of fracture surface of CpTi enables us to analyze failure behavior in detail. Fractography images [Figure 8-14] show that fracture during ISF process is mostly ductile. Pores can easily be seen in A identifying ductile fracture and brittle fracture can be seen in B. Images were taken through SEM.

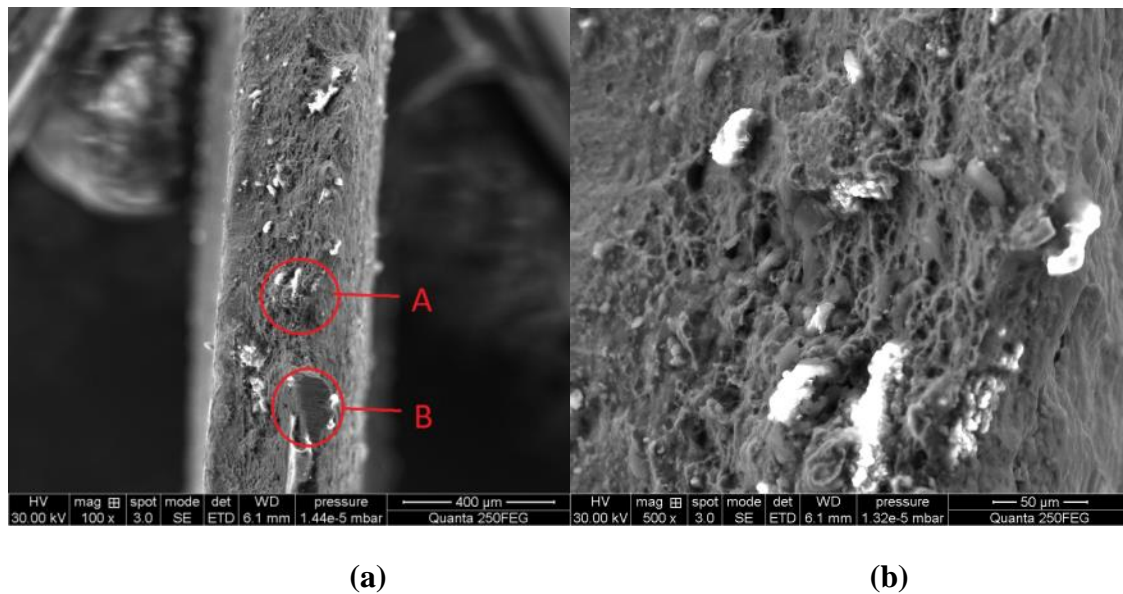


Figure 8-14 Fractography (a) 100X, (b) 500X.

## 8.5 Summary

Present work focuses on the single point incremental sheet forming studies performed to understand the effect of forming tool design on material flow behavior at room temperature. Specially designed forming tool as well as flexible fixture setup for clamping the sheet blank to be formed is adopted. Sheets of commercial purity Titanium alloy (Grade 4) is used for performing ISF trials at room temperature. Circular grid analysis (CGA) technique using GOM Argus® software is used to analyze of surface strain distribution at different locations of the finished parts. The percentage reduction in thickness of sheets and degree of spring back after ISF process was analyzed using a 3D scanner and GOM ATOS®. Parameters derived from room temperature tensile tests and data from forming limit curves (FLC) are used as input parameters to perform finite element analysis (FEA) for understanding the material flow behavior as well as the evolution of strain during ISF process. ABAQUS® Explicit software (Version 6.13) will be used to perform the FEA. Scanning electron microscopy is characterization tool used to study aspects of microstructure as well as mode of fractured surfaces.

Mechanical properties are not same in all rolling directions. 90 degree shows most distributed effect of stress, strain and thickness and thus is the most ductile direction compared to 0 and 45. This effect should be considered during ISF process. Numerical

model show good agreement with empirical results and could be used in modeling ISF process. Major and minor strain does not follow normal Forming Limit Curve (FLC) and have higher forming limit compared to conventional forming processes. Dimensional accuracy of Ti alloy for ISF process would be around -2mm i.e. if forming depth of a tool is 25mm. Tool path should be optimized to increase formability of the sheet. This will also help in uniform thickness distribution required for commercial purposes.

Mechanical properties together with microstructure of a Cp-Ti were investigated for ISF. It was observed that rolling directions influences mechanical properties which affect manufacturing parameters and microstructure. Microstructure of Cp-Ti is changed from regular hexagonal to irregular elongated shapes after ISF process is performed. Slip and twinning are highly dependent on crystal morphology and orientation. This is the reason why mechanical properties also depend upon them.



## **9. Appendix B - Material testing and data acquisition**

This chapter discusses the material properties of the materials used and their selection. These properties are acquired through tests, literature review or provided by the supplier. Tensile tests of specimens for different rolling directions were reported. Forming limit curve for different width of specimen width was discussed. Fractography and microstructure of the sheet metal was also discussed.

### **9.1 Material selection**

Several components used in aerospace, automotive and biomedical are made with Titanium, Aluminum or Steel sheet metal using conventional forming processes [15]. Materials are tested and analyzed to optimize manufacturing parameters to reduce cost and increase production rate of the process [21]. In this study we have experimented with all these shapes and their interaction between each other for SS304L, AA1050H, AA2024, AA7075 and CpTi. Real life components will have several geometrical features interacting with each other; some examples of the geometry are given in the following text. These geometric features influence internal mechanics and thus the type of test required to check the material.

Aerospace parts for internal and external use can be easily made using ISF process. For instance external parts are fuselage, wing covers and aileron cover while internal parts are air ducts, doors, wash basins and storage compartments. Fuselage, wash basin and storage compartments have wall feature only while door, wing and aileron cover have curved features. These components are made of CpTi, AA7075, AA2024 or composite materials.

During automotive manufacturing different sheets of metal are joined together through rivets, welding, nuts and bolts. These components are generally made of SS304L, AA1050H and AA2024.

Cranial, facial and ankle surgeries are very common with biomedical practitioners. Currently it is very costly and time consuming to make these components and patients have to go through a waiting list to receive components These components are mostly made from CpTi and could easily be formed using ISF within minutes.

Knowledge of material properties and microstructural behavior of the post and pre formed sheet metal are very important, as they will be used in practical applications in different industries. In current study FLC tests and tensile tests were performed on the steel sheet material. FLC results were plotted with major and minor strain results of the formed component. Microstructural behavior of pre and post formed sheet metal was acquired and difference in microstructure was reported. Microstructure and material properties change due to dislocation movement in the crystal structure because of the applied strain on the sheet metal. Thickness reduction is directly proportional to the strain applied at a particular wall angle. As failure criteria in industry are based on strain and components formed through ISF generally fail due to thinning of sheet metal; failure prediction and component stability is discussed with respect to these two parameters

## 9.2 Material composition

Stress-strains graphs and relations are among the most significant and important materials properties which describe formability, work hardening and strength. Tensile tests were used to evaluate these fundamental properties in this work. The objective of the work was to relate these properties and specimen's microstructure to formed components and their microstructures. This will help establish knowledge regarding basic mechanics of the ISF process. As per literature review, the material composition and properties for SS304L are tabulated in Figure 9-1 and Figure 9-2 [155, 156].

Table 9-1 Material Composition.

<b>Component</b>	<b>Wt. %</b>
C	Max 0.08
Cr	18 - 20
Fe	66.345 - 74
Mn	Max 2
Ni	8 - 10.5
P	Max 0.045
S	Max 0.03
Si	Max 1

Table 9-2 Physical and mechanical properties.

<b>Properties</b>	<b>Metric</b>
Density	8 g/cc
Ultimate Tensile Strength,	505 MPa
Yield Tensile Strength	215 MPa
Elongation at Break	70 %
Modulus of Elasticity	193 - 200 GPa
Poisson's Ratio	0.29
Shear Modulus	86 GPa

### 9.3 Tensile tests

Tensile tests on SS304L will be reported in this section. Dimensions of these standards were detailed from ASTM and are given in Table 9-3. Specimens for tensile tests were manufactured from the 0.6mm SS304L sheet using water jet cutter as shown in Figure 9-1. Six specimens were tested at two different strain rates mm/min. Specimens were cut at 0°, 45° and 90° from the direction of sheet metal rolling (RD), shown in Figure 9-2.

Table 9-3 Tensile specimen details.

Material	SS304L
Specimen type	Flat Specimen
Test standard	ASTM-E8/E8M
Strain rate A	$10^{-2} \text{ s}^{-1}$
Strain rate A	$10^{-3} \text{ s}^{-1}$

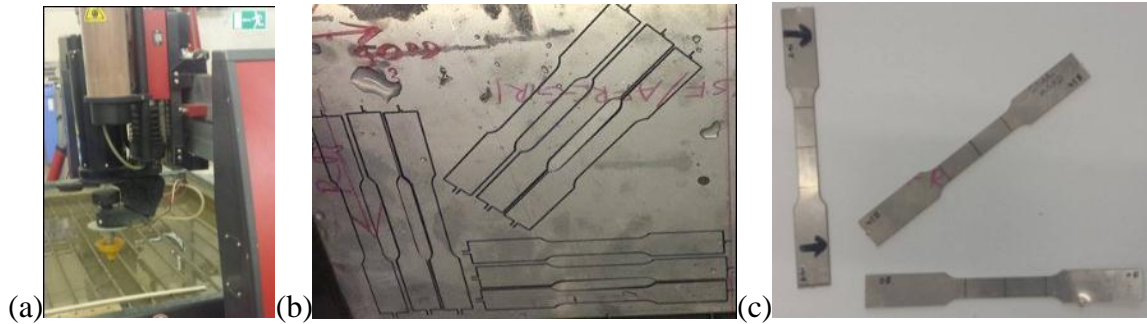


Figure 9-1 Specimen preparation; (a) Waterjet cutting, (b) Samples on the sheet metal, (c) Samples at 0°, 45° and 90° RD.

ASTM tensile test standard “ASTM-E8/E8M” was used. Experimental data such as Yield strength, Young’s Modulus, stress strain graphs and strain hardening were acquired by performing tests at room temperature. Zwick/Roell Z150 Material Testing Machine and Extensometer were used along with software to perform these tests shown in Figure 9-2. Limit of the extensometer for recording strain is 0.4, after which it is not capable to record data. Pointed micrometer, vernier caliper and scale were used to gather thickness reduction data from the crack tip. Stress strain and thickness reduction was plotted. All these results were then analyzed comparatively for different rolling directions and strain rates. Following are the steps to perform the test:

- Machine and software was turned ON and specimen was held in the grippers.
- Extensometer was applied on the specimen.
- The specimen was loaded at given strain rates until the fracture occurred.
- Data was recorded, calculated and plotted.

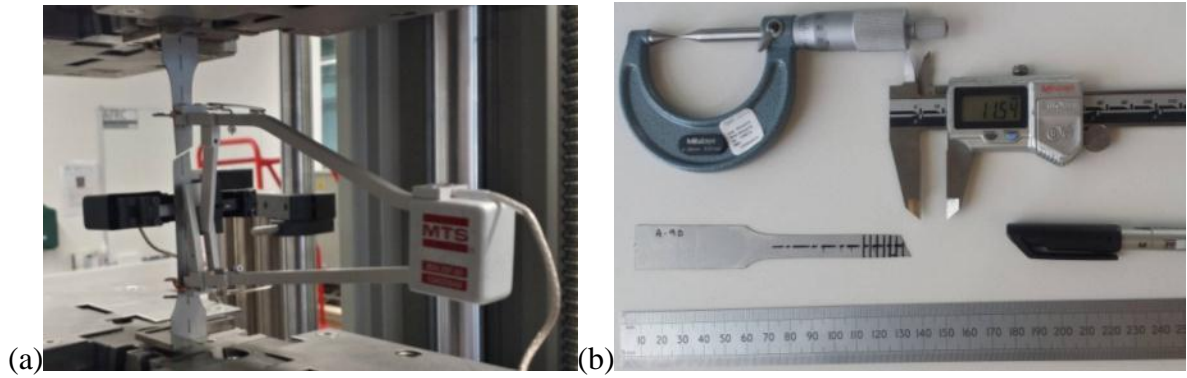


Figure 9-2 Equipment used for Tensile tests and data acquisition; (a) UTM, (b) micrometer, vernier-calipers and scale.

As it was mentioned earlier that six tests were performed for two different strains (A and B) and three different rolling directions ( $0^\circ$ ,  $45^\circ$  and  $90^\circ$ ). All curves show a typical elastic and elastic-plastic behavior. The transition between both the behaviors was smooth and Luders band did not occur. Yield strength for all the cases is around 300MPa and the ultimate tensile strength is under 1000MPa. The results of these tests are presented as AvsB and analysis of different rolling directions Figure 9-3 shows true stress and strain graph for  $0^\circ$ ,  $45^\circ$  and  $90^\circ$  respectively. For all the three cases A shows slightly higher values compared to B. We can conclude that although strain rate does influence stress-strain curve, the effect is generally negligible. For both cases A and B, stress and strain show very small difference between different rolling directions Figure 9-4.

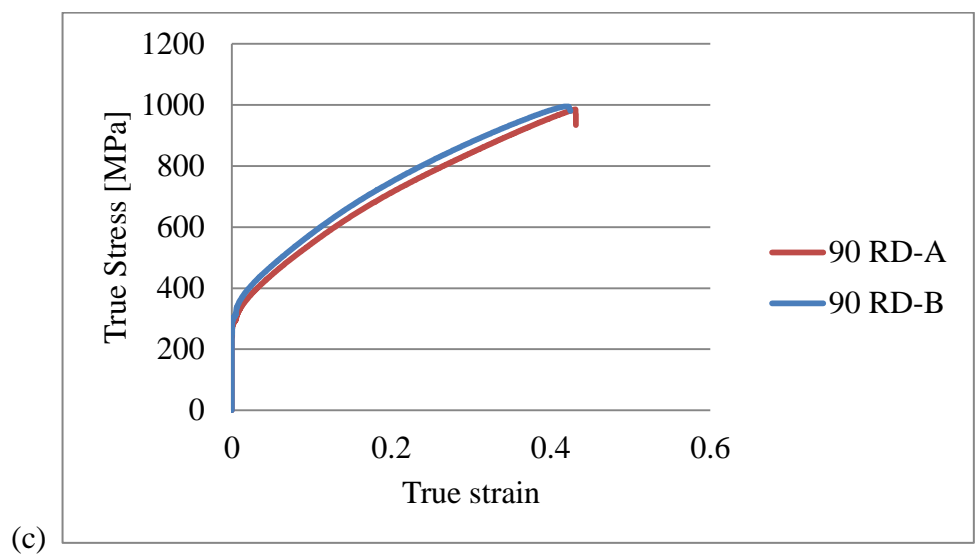
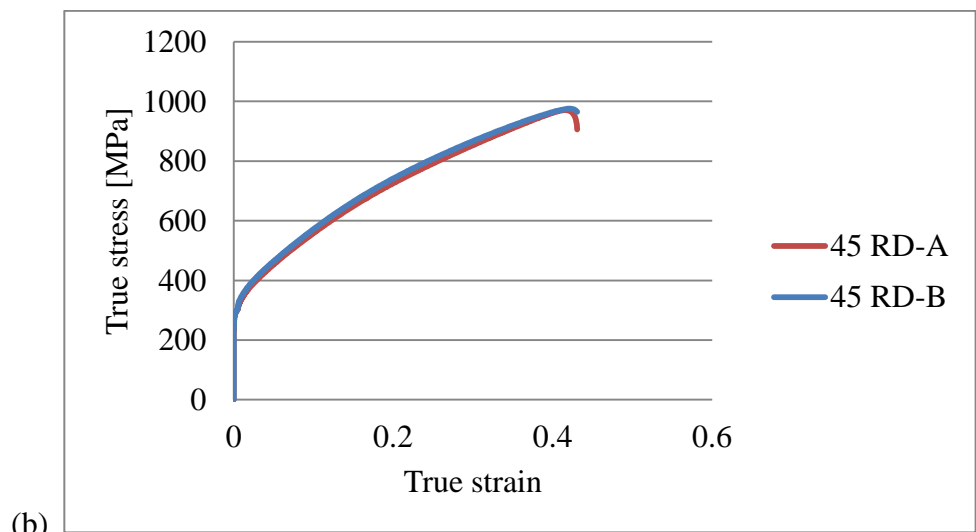
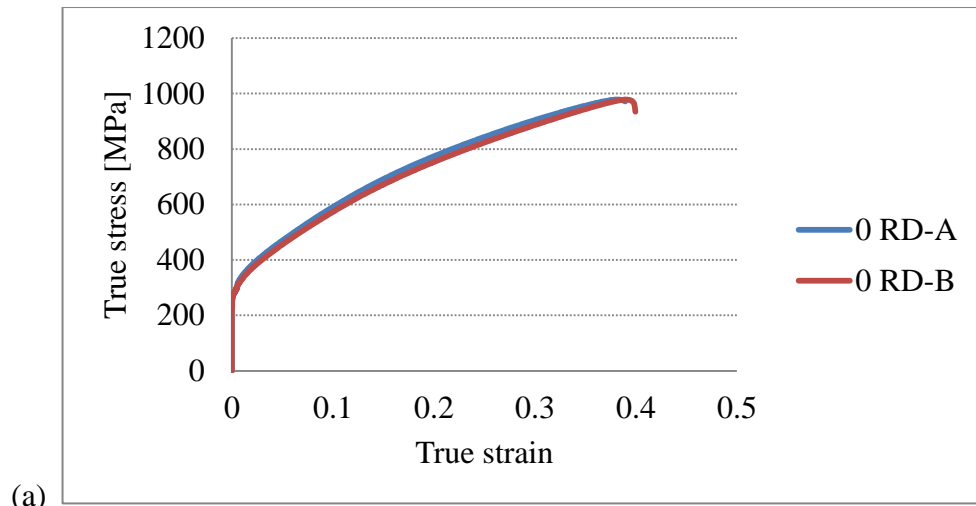


Figure 9-3 Stress-strain graphs, AvsB; (a) 0RD, (b) 45RD, (c) 90RD.

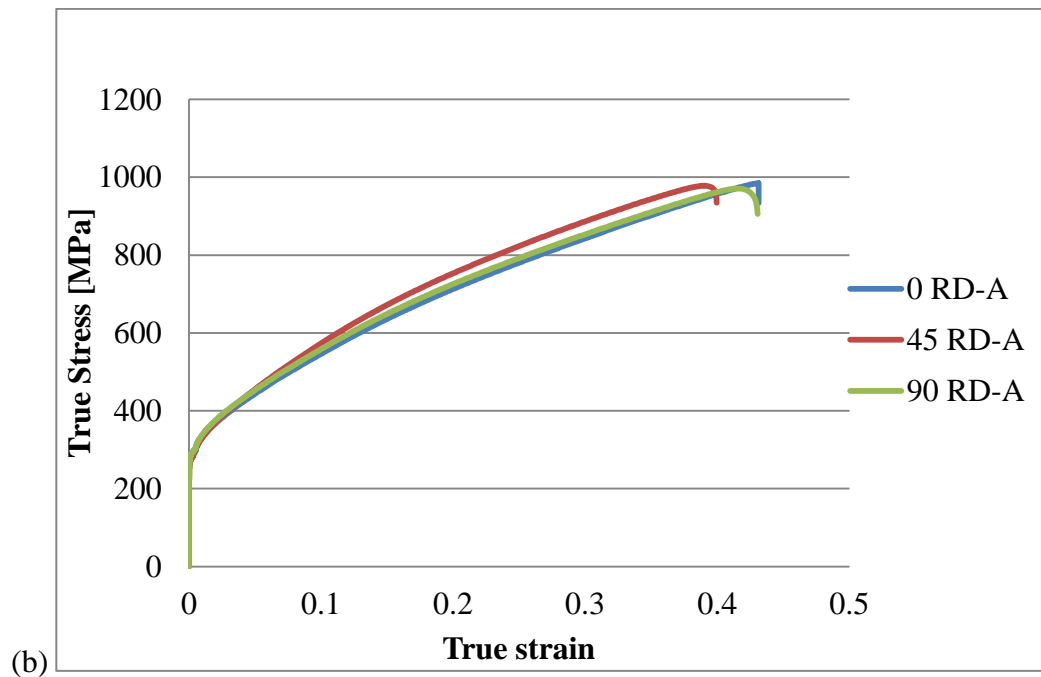
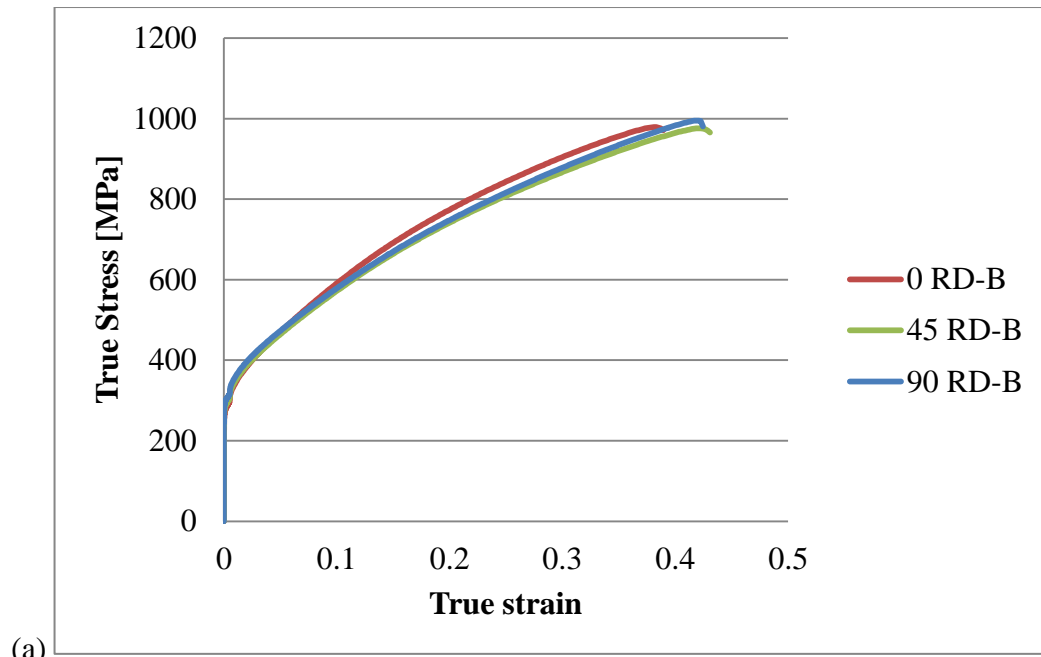


Figure 9-4 Stress-strain graphs at different rolling directions; (a) strain rate A, (b) strain rate B.

### 9.3.1 Critical material properties

The material properties are tabulated in Table 9-4, where R represents average Lankford coefficient and shows plastic anisotropy of rolled sheet metal. It is a scalar quantity and is used as an indicator of the formability of sheet metal. The value of this coefficient is close to 1 for all the cases and thus it can be predicted that anisotropy might not have any effect on the ISF tests. This statement is yet to be checked by performing ISF tests in different rolling directions. The value of R is the highest for 45RD, intermediate for 90RD and lowest for 0RD for all the cases.

n is strain hardening coefficient which is a material constant and is used in calculation of strain during work hardening. It plays a critical role during sheet metal forming and because of the larger value of n, the flow stress increases with strain. Thus distribution of strain is uniform throughout the formed sheet and formability increases. The value of n for the specimens ranges from 0.28 to 0.32, which is typical for metallic elements. n is comparatively higher for both strain rate A than B for all the rolling directions. It is maximum for 0RD, intermediate for 45RD and lowest for 90RD for all the cases.

K is the strength coefficient of steel and is calculated from stress-strain graph. The value of K is highest for 0RD, intermediate for 45RD and lowest for 90RD for all the cases. The value of K is higher for strain rate B compared to A for all the cases. The value of K for all the specimens range from 1103MPa to 1234MPa. The flow rule is given by

$$\sigma = K \varepsilon^n \dots\dots\dots\text{Equation 9-1}$$

where  $\sigma$  is the stress and  $\varepsilon$  is the strain.

$\sigma_y$  is the yield strength of the material and has a maximum value for strain rate B for all the cases. The value of yield strength is the highest for 0RD, intermediate for 45RD and lowest for 90RD for strain rate B.  $\nu$  is the Poisson's ratio, which is ratio of lateral to axial strain and is highest for 45RD for both A and B strain rates. The value of Poisson's ratio ( $\nu$ ) for all the specimens ranges from 0.45 to 0.56.



Table 9-4 Material properties.

	R	n	K(MPa)	$\sigma_y$ (MPa)	$\nu$
0 RD-A	0.852492	0.3233	1224.731	618.5294	0.448688
0 RD-B	0.946391	0.315095	1234.488	652.5975	0.479804
45 RD-A	1.279746	0.296104	1122.937	582.8385	0.562917
45 RD-B	1.342474	0.289558	1129.104	623.0624	0.548677
90 RD-A	0.842626	0.297442	1103.297	599.6611	0.46404
90 RD-B	0.80618	0.281574	1122.415	615.5336	0.453402

#### 9.4 Nakajima Test

Deformation in stainless steel is generally ductile. Ductility allows materials to distribute stresses along the area of the cross section and in case of forming, sheet being formed into the required shape. Forming Limit Curve (FLC) is used to evaluate ductility of material in sheet metal forming [157, 158]. The FLC (also known as forming limit diagram) introduced by Keeler and Goodwin during 1960's, has been used to predict failure in forming processes. Bolin et. a. presented an extended fracture criteria for FLD in DP590 steel sheet [159]. Because of importance FLC test, Nakajima tests [160], which are widely used, were performed on SS304L using Zwick/Roell machine coupled with GOM ARAMIS to acquire FLC. Up till now FLC was determined through calculation of strains via stretched patterns of lines or circles. Different means such as microscopes, measuring strips and magnifying glasses were used to measure these strains. These techniques have several limitations including user dependency, pattern sharpness, time consumption and pattern resolution. Results produced with ARAMIS system are repeatable. According to ISO 12004 recommendations, a stochastic pattern are applied using a color spray on the specimens. The specimens were first painted white and then with small dots of black so the Optical 3D deformation system can acquire data from it. Number of measurement points increase considerably due to this approach. ARAMIS divides areas into smaller pieces and optimizes the calculations based on sub pixel range. Various photographs are taken by three cameras at several stages. Image processing algorithm is used to measure locations of the dots in a 3D

co-ordinate system. Thus entire surface of the sheet metal and its deformation could be traced in a 3D system and a complete deformation behavior up till fracture is captured. Through this information of surface strain, major and minor strains are plotted along with strain paths. Thickness reduction is also calculated through this system and exported to other file formats. Silicon lubricant was cut from the sheet and was placed between the punch and the blank for all the specimens. During the tests a force was applied, the punch traveled upwards and drew the sheet blank into the die cavity. Drawing depth of the tests is increased till the specimen fractures. Load and drawing depth is recorded for each test.

Limitations of the sheet metal forming process can be predicted through forming limit curve and diagram. The Nakajima test is a well-known method to determine sheet metal properties through FLC. It is based on ‘deformation until fracture’ via hemispherical tool. Sheets were cut into arc-shaped, using water jet cutter into specimens with waist widths ranging from 40mm to 120mm.

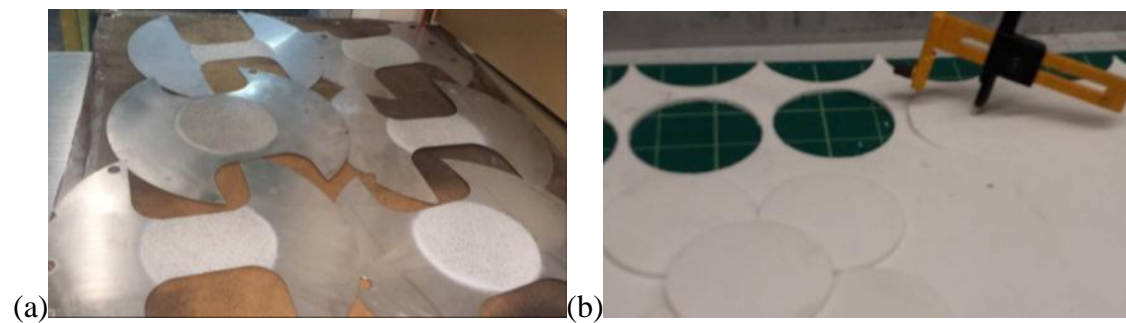


Figure 9-5 FLC test preparation; (a) Specimen, (b) Lubricant.

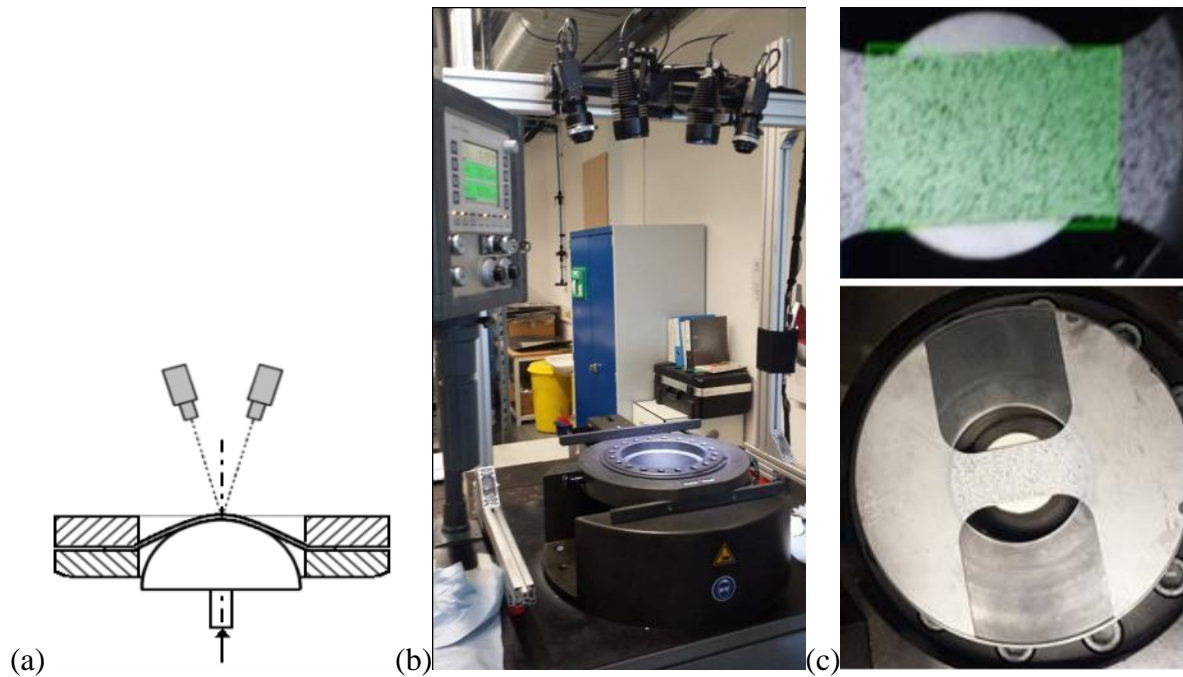


Figure 9-6 FLC; (a) Test arrangement, (b) Measurement setup, (c) Durig the process.

Limitations of the sheet metal forming process can be predicted through forming limit curve and diagram. The Nakajima test is a well-known method to determine sheet metal properties through FLC. It is based on ‘deformation until fracture’ via hemispherical tool. In the current study, FLC of 0.6mm thick SS304L sheet is evaluated. Table 9-5 shows results of six different geometries and punch velocity, force and stroke readings directly from the testing machine. Figure 9-7 shows the forming limit curve test results. Rest of the results are shown in Appendix A.

Table 9-5 FLC specimen data.

<b>Specimen width (mm)</b>	<b>Punch velocity (mm/s)</b>	<b>Punch force (KN)</b>	<b>Max. Stroke (mm)</b>
40	1.70	29.58	67.34
50	1.15	36.97	66.71
60	1.13	44.90	68.92
80	1.16	58.65	68.23
100	1.15	71.61	67.15
120	1.15	86.08	69.57

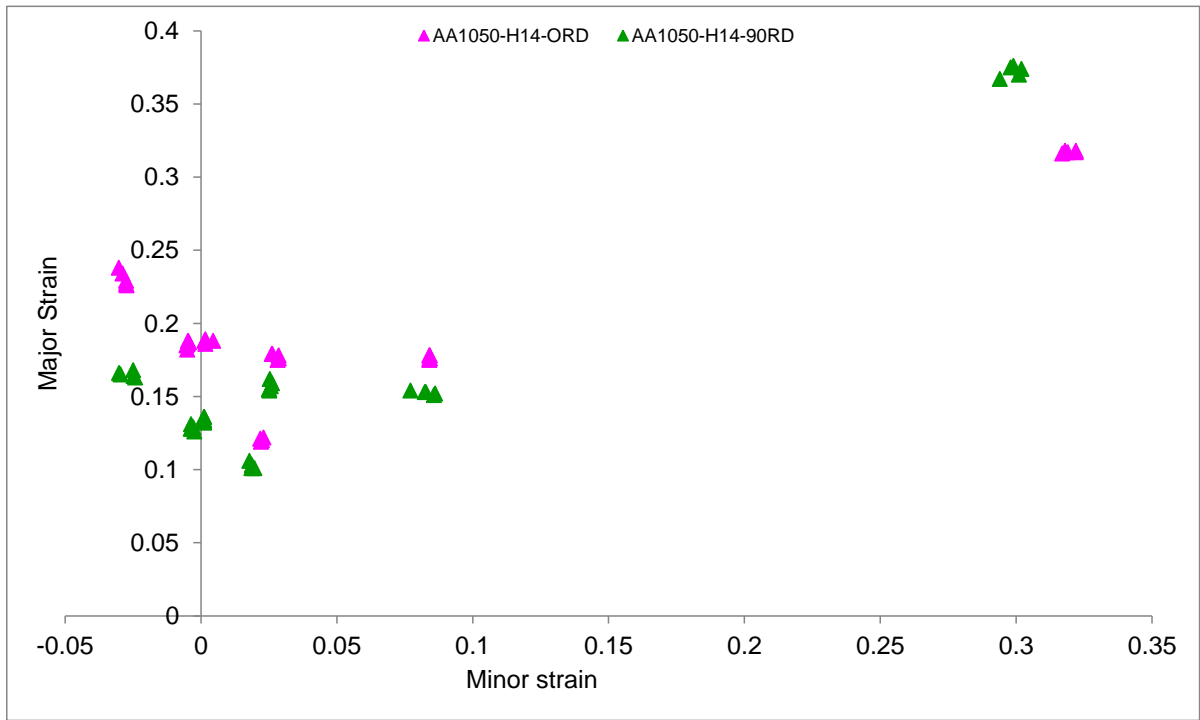


Figure 9-7 Forming Limit Curve AA1050H.

### 9.5 Surface roughness

Surface roughness of the specimens were measured to investigate a pattern between different rolling directions and strain rates. Figure 9-8 shows surface roughness results for all the specimens while Table 9-6 reports all the results. It was observed that surface roughness increased from 0RD to 90RD for strain rate A but this pattern was not observed for strain rate B. It was concluded after analysis of all the samples that there is no identifiable pattern in the surface roughness results, thus strain rates do not affect surface roughness.

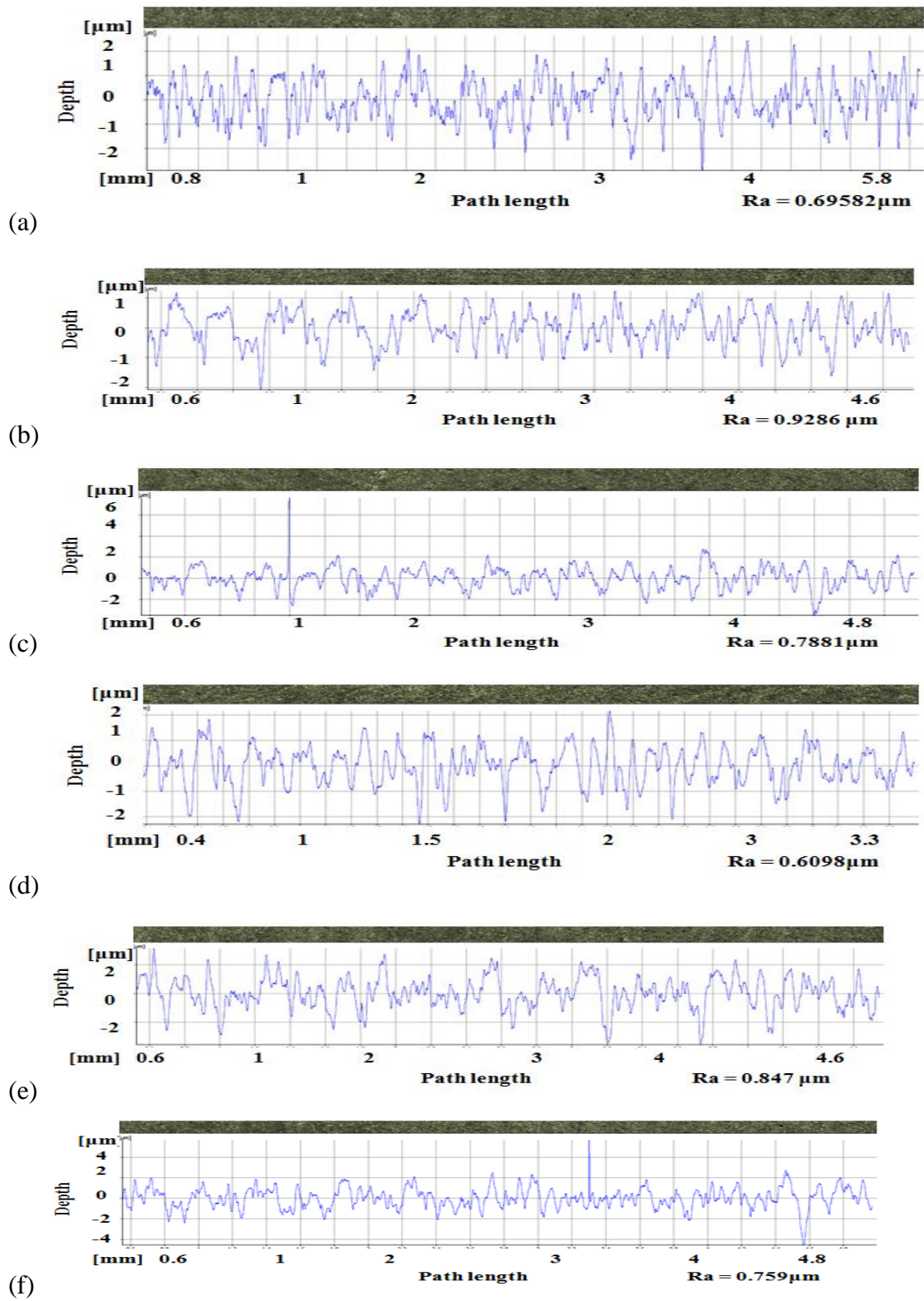


Figure 9-8 Surface roughness of tensile specimens; (a) 0A, (b) 0B, (c) 45A, (d) 45B, (e) 90A, (f) 90B.

Table 9-6 Surface roughness of tensile specimens.

Specimen	Surface roughness( $\mu\text{m}$ )
0A	0.6958
0B	0.9286
45A	0.7881
45B	0.6098
90A	0.847
90B	0.759

## 9.6 Microstructural characterization and Fractography

Microstructure analysis and fractography was performed using SEM and EBSD. EBSD is a surface sensitive technique thus it is very important that sample surface is prepared properly and is free from any contamination or oxidation. Sample preparation of SS304L for microstructural analysis had several steps and is very critical because electrons escape from within tens of nanometers of the specimen surface. As the surface is tilted at an angle to acquire EBSD data, it is very important that surface topography should be kept to a minimum value. One undeformed and three deformed samples (one each for 40°, 50° and 60°) were selected and numbered using a scribe. Selected samples were cut from the formed part using Buehler Abrasimatic 300. These samples were then mounted on a conductive holder using superglue. These samples were polished initially using Buehler EcoMet 300 and grinding paper of several sizes. As samples were taken from deformed walls, it took a lot of time and effort to make samples flat. Grinding papers of 600P, 800P, 1200P, 2500P and 4000P were used on each sample after which electropolishing was used. Electropolishing not only removes material from the surface but also removes surface deformation layer and surface irregularities. It is ideal for sample preparation and works on electrolytic action. Struers Lectro-pol-5 electrolytic polisher with Electrolyte A2 was used to polish steel samples. Flowrate of 14 mm<sup>3</sup>/sec and 40 volts was used for 20 seconds. Sample was carefully placed on the machine as both the sample and the hole of the machine were very small. Curve on the machine showing flatness of the samples turned straight for all the samples, showing good quality of the samples. After this process was finished, samples were placed in a methanol beaker and then transferred to an ultrasonic kettle.

Specimens were left in the beaker for 15 minutes and were dried as soon as they were removed from methanol. Specimens were then joined to a holder using double-tape and placed in Oxford Instruments Quanta 250 FEG SEM using an L-key. Samples were kept straight for SEM and fractography while they were tilted at 70° for EBSD.

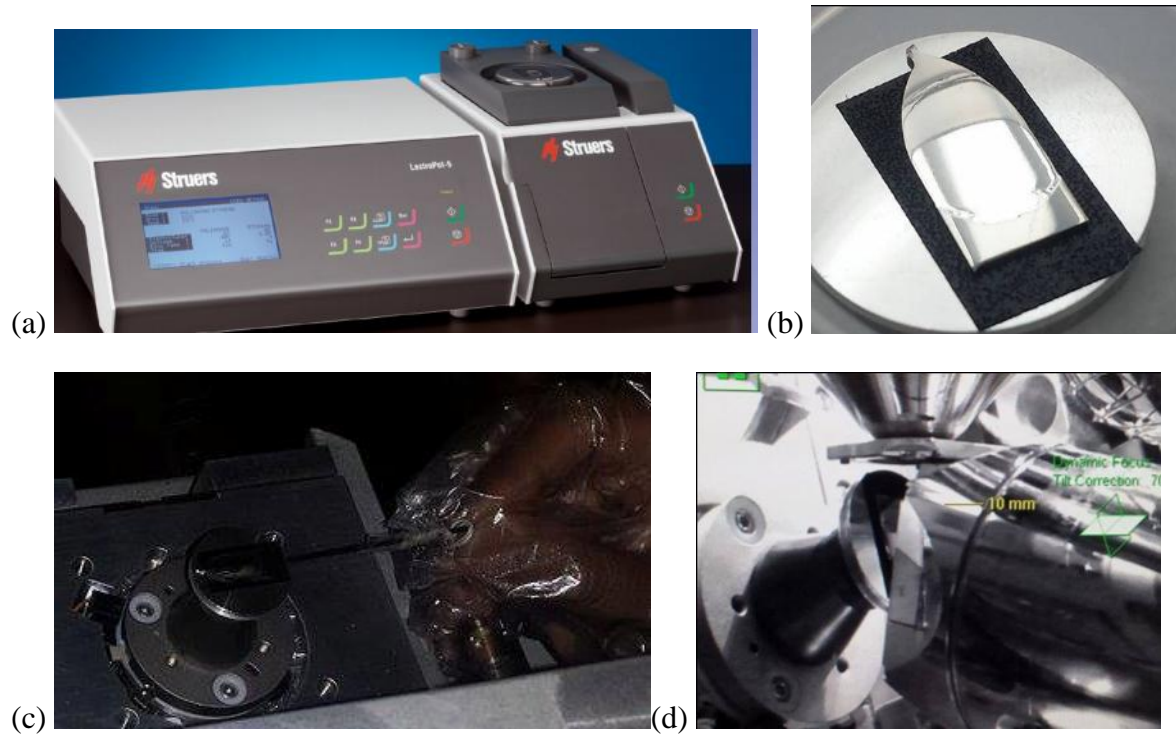


Figure 9-9 Sample preparation and mounting; (a) Electropolishing machine, (b) Sample mounted after polishing, (c) Sample mounted on SEM/EBSD, (d) Sample tilted for EBSD.

Figure 9-10 shows the fracture morphology of the Stainless Steel 304L at 0°, 45° and 90° after tensile testing. A ductile dimpled fracture is observed through SEM image at high magnification with a range of sizes distributed like honeycomb. Due to tensile loading microvoids are formed after necking, which then propagate into cracks with rough surfaces. The crack is due to static stress overload, thus the fracture involved plastic deformation, was less catastrophic and high energy fracture mode. Shear lips and large neck shrink were also observed. It is observed through stress strain diagrams that the crack then rapidly propagated through at 45° along the shear direction. As detailed in previous study of CpTi, this study also shows that the specimen failed under tension and thus the crack mode I will be acting on specimen. Precipitates are also observed in the SEM images. It can be concluded from the

results that SS304L is ductile in nature and exhibits features of a dimple fracture. Fractography images of rest of the samples are provided in Appendix A.

## **9.7 Summary**

This chapter discusses the material properties of the materials used and their selection. These properties are acquired through tests, literature review or provided by the supplier. Tensile tests of specimens for different rolling directions were reported. Forming limit curve for different width of specimen width was discussed. Fractography and microstructure of the sheet metal was also discussed.



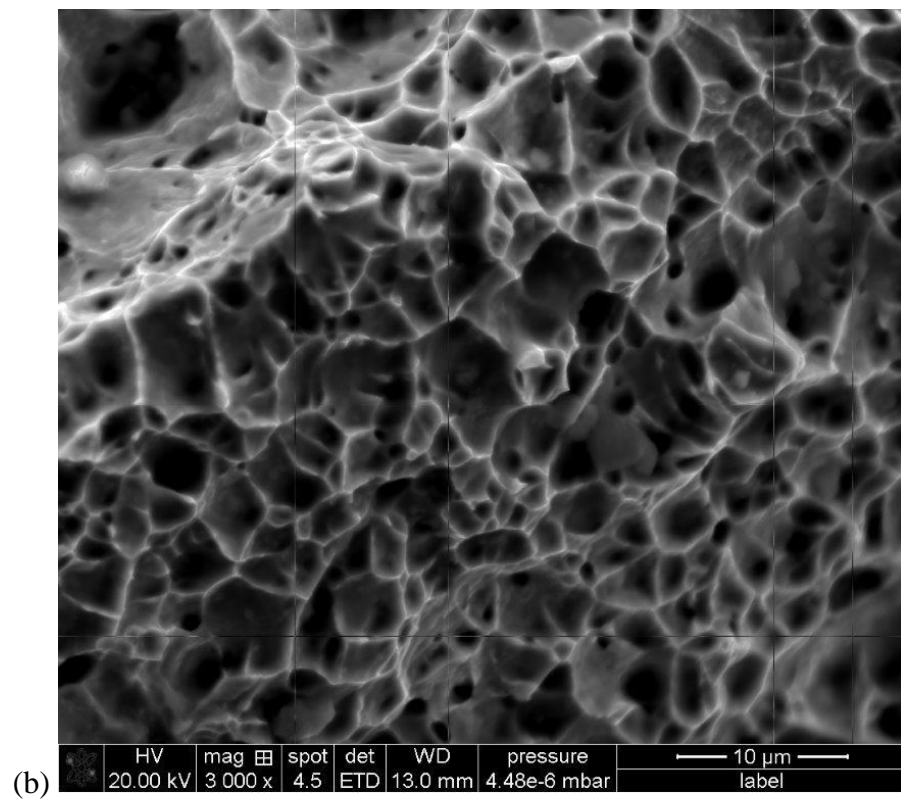
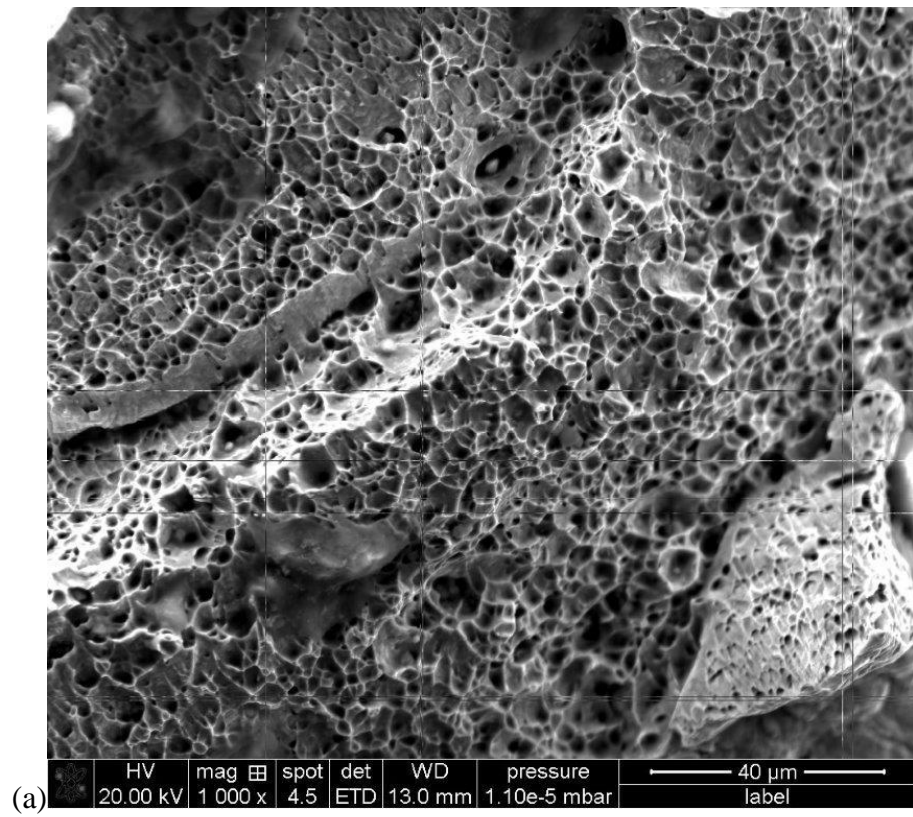


Figure 9-10 Ductile fracture SS304L, ORD-A; (a) 1000X, (b) 3000X.

## **10. Appendix C - Design and implementation of equipment and geometries**

To answer questions about mechanics about ISF process it is important to have a proper experimental setup and geometries to carry out ISF process. Geometry, Die, tool and fixture design for process can minimize number of uncontrolled parameters and help understand the process efficiently and effectively. By this we can acquire measureable and reproducible results. List of hardware and software is provided.

### **10.1 Design and manufacturing of the tool**

Incremental sheet forming (ISF) is an emerging manufacturing technique in which sheet metal is formed through application of localized force using a moving tool. One gap in ISF process knowledge is the impact of different types of tools on the quality of the final component. The following sections describe a contribution to filling this gap. As part of an ongoing program to understand this aspect of the process, this paper reports the evaluation of five different conceptual designs of rotating tool and the experimental assessment of the most promising one. The selected concept attempts to decrease friction during the ISF process by incorporating a rolling element bearing to allow rotation between tool and workpiece. Prototype tool was used to form Aluminum sheets using a CNC machine and a flexible fixture. The thickness, shape, surface roughness and strain of the formed components were then measured.

To investigate mechanics of the ISF process an experimental test rig was designed, manufactured and commissioned. The forming equipment consists of flexible fixture and rotating tool. The flexible fixture slides in vertical direction as the sheet is being formed [161]. The tool was designed to support load and forming depth required to deform the material. Five different conceptual designs of tool were evaluated and the one which was judged to have the best ability to freely rotate around its axis while a part is being formed was selected for detailed design. The design concepts were modeled using 3D software and several critical components were analyzed using Finite Element Analysis.

During the design process the worse-case (i.e. maximum) forming force was estimated to be 5KN [7, 110]. It was observed during initial experiments (Chapter 3), and confirmed by the literature review, that the maximum forming depth attained for geometries was around 27mm for cold forming of a 300mm X 300mm square of titanium during a single point ISF process [128]. However the forming depth obviously varies depending upon material, input parameters and conditions of forming (e.g. lubrication and temperature). So consequently the system was designed to accommodate a maximum deformation of 100mm (in a vertical direction) of 130mm x 130mm square sheets whose deformable area (i.e. away from the nuts securing the edges) would be 70mm x 70mm square.

### **10.1.1 Design of the tool**

The literature review identified two fundamental type of tools used for ISF process

- Static type
- Rolling type

While most of the reported research has used statics tools the few researchers to investigate rolling tools claim they reduced friction between sheet and tool and thus increase formability of the material. To investigate the interactions between tool size (i.e. diameter) and the reduced friction of a rolling tool an experimental tool was required. To create this a brain storming process was used to generate different conceptual designs of ISF tool and an expert panel employed to review them.

The authors' previous experience of ISF with static (i.e. non-rotating) tools [128] provided an understanding of the nature of the ISF process and allowed a number of modular concepts for rolling tools to be quickly generated. The modularity is motivated by the desire to easily replace worn out or damaged parts.

Conceptual design 1 and 2 show roller ball enclosed between two cylindrical geometries [Figure 10-1. The concept consists of

1. Base ( to be fixed in chuck)
2. Ball (tool tip)
3. Cover (to hinder ball from escaping)

Main difference between concept 1 and 2 is method of restraining the ball in the tool. In concept 1 the ball is restrained with a solid metal clasp as shown in Figure 10-2. A hole is drilled through the tool to connect hollow volume to ball. This volume will store lubricant to reduce friction during ISF process. To constrain the ball in the tool a covering cylindrical geometry is used. This would be screwed upon the base geometry. Problem with this setup was that the geometry used to restrain the ball was covering more than 50% of the ball. This would impose difficult, or impossible, constraints on the forming process (e.g. when the tool had to be inclined to make contact with the sheet). In concept 2 solid metal behind the ball was replaced with a metallic strip to reduce the friction and thus would result in an increase in tool life. Two different sub-concepts are shown in Figure 10-1 b and c. Different metallic strip designs are used in both concepts and concept 2 has integrated cover and base. Problem with this design are related to manufacturing and material characteristics for instance strength and deflection of metallic strip. In this design, the load is applied at a localized location in the tool i.e. metal strip supporting the roller ball and it might get damaged due to this load. This setup also covers more than 50% of the roller ball which will hinder forming process.

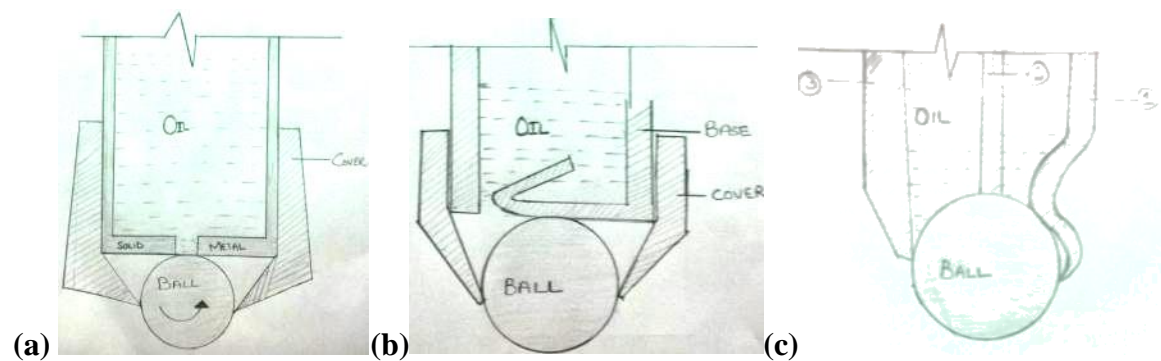


Figure 10-1 Tool conceptual designs; (a) Concept 1, (b) Concept 2A, (c) Concept 2B.

It is known from the literature review and initial experiments that the tool moves largely in horizontal plane and consequently the resultant forces are also greater in that direction as well [110, 128, 161]. Similarly it can also be deduced that most of the frictional forces are in radial direction. More brainstorming resulted in what is termed the bearing concept [Figure 10-2]. This concept has the following components:

1. Base ( to be located and held in CNC chuck)

2. Rolling Element Bearing ( to reduce radial friction)
3. Tool rod (to support and locate the hemispherical tool tip)

Essential the base is fitted in chuck and tool is free to rotate around an axis to reduce friction while a part is being formed. Relative to the horizontal direction; motion, force and friction in vertical direction is negligible Figure 10-2.

Concept 4 and 5 considers both horizontal and vertical motion of the tool Figure 10-2b,c. The difference between concepts 4 and 5 was that concept 3 had a roller (bearing) at center and concept 4 had an off-center roller. Both rollers were connected to the end of the tool via a shaft. This shaft is the most critical part in both concepts and has highest probability of failure. Table 10-1 shows the design selection matrix employed to ranks the designs. Each concept is scored for particular parameters (durability, stability, ease of use etc) as better (+1) or worse (-1) with respect to their functionality.

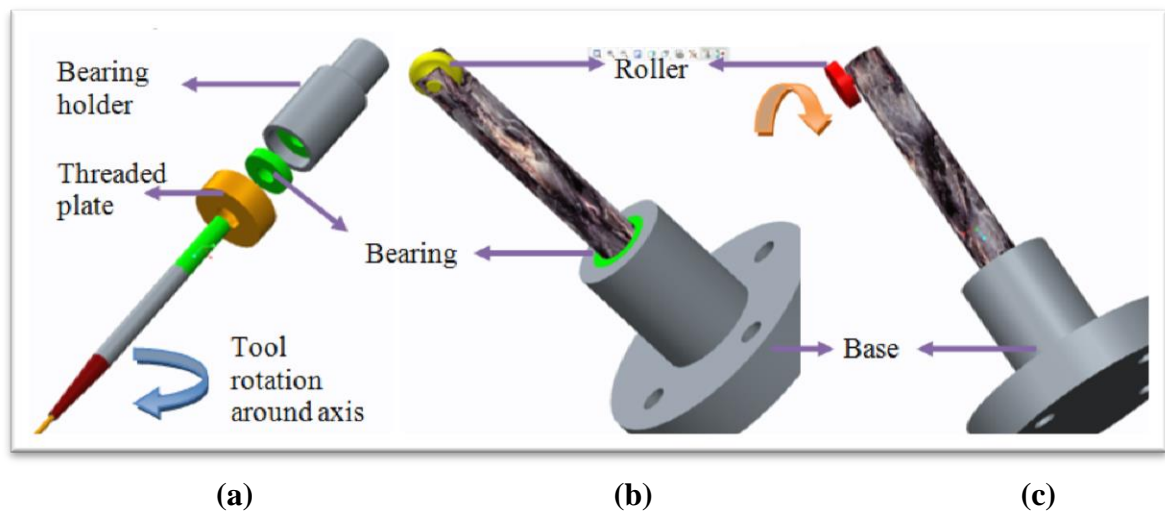


Figure 10-2 3D models; (a) Exploded assembly view of concept 3, (b) Concept 4, (c) Concept 5.

Table 10-1 Design selection matrix.

<b>Concept</b>	<b>1-Ball solid back</b>	<b>2- Ball point</b>	<b>3- Bearing- axis</b>	<b>4- Roller center</b>	<b>5-Ball bearing off-center</b>
Ease of Manufacturing	1	-1	1	-1	1
Ease of use	-1	-1	1	1	0
Efficiency	0	0	1	-1	-1
Durability	0	-1	1	1	-1
Stability	1	-1	0	0	-1
Accuracy	1	1	1	1	-1
Stuck	1	1	1	0	1
Resistance to forces	1	1	1	1	1
Modular design	1	1	1	1	1
<b>Total</b>	<b>5</b>	<b>0</b>	<b>8</b>	<b>3</b>	<b>0</b>

After assessing the concepts idea No 3 was selected for further detailed design and prototyping.

### 10.1.2 Manufacturing of Tool

The selected tool design was expanded to consist of the following components:

1. Base
  - a. Chuck Base (to be held in chuck of CNC) [Figure 10-3a]
  - b. Bearing holder (which is holding two bearings) [Figure 10-3b]
  - c. Threaded plate (to cover the bearings and align tool stick)
2. Two thrust bearings (to align and hold tool stick) [Figure 10-3b]
3. End tool
  - a. Tool stick (it goes through both the bearings)
  - b. Tool tip (placed in tool stick, in a hole and gas welded, made up of hard steel) [Figure 10-3b, c, d]

The chuck base was manufactured from a solid cylindrical steel billet. The bearing holder was made from a hollow steel billet and external threads were made on bearing holder to fit a cover (a threaded plate with a hole) on the forming tool side. The bearing holder locates two thrust bearings and has a hole which allows the end of the tool to rotate freely. The base is welded to bearing holder because:

- A. Higher load will be applied at joining location.
- B. There is no future need to separate base from bearing holder.



Figure 10-3 Manufacturing and commissioning of tool; (a) Block, (b) Thrust bearings in the tool, (c) Hemispherical tool, (d) Tool while performing ISf process, (e) Wooden die.

Furthermore bearings can be changed from tooltip side by opening a threaded plate. Hex cap screw was added to threaded plate perpendicular to tool stick. Purpose of adding it was to get better alignment of tool stick and avoid deflection of tool stick. This will be particularly useful while forming high strength materials such as Titanium. Two thrust bearings were then push fitted in bearing holder. Thrust bearings will support vertical load and align tool during ISF process. Steel was used to manufacture tool rod and a push fit used to fix a tool rod through two thrust bearings. Two tool sizes were manufactured initially i.e. 4.5mm and 16.5mm diameter. For thin tool i.e. 4.5 mm shown in Figure 10-3d, steel rod used to manufacture tool stick was tapered at tool tip end for uniform stress distribution and to avoid interference of tool and other equipment. Hole was drilled at tool tip side to seat tool tip. Tool tip manufactured with hard steel was inserted in the hole drilled in tool stick and gas welding was used to join it permanently to tool stick. For thick tool i.e. 16.5mm shown in Figure 10-3c, end was rounded to make a semi-spherical shape at the end. Commissioned setup including tool, fixture, wooden die and sheet is shown in Figure 10-3d,e.

## **10.2 Design and manufacturing of fixture**

ISF system can be classified as positive, or negative, depending on whether the sheet material is progressively deformed onto a protrusion or a cavity. In negative systems the workpiece is held on a static fixture, whereas in positive ISF the fixture must be incrementally lowered onto a protruding die. Although the vertical movement of positive ISF fixtures is easily illustrated schematically, its implementation is challenging; if the descent is actuated the motion has to be carefully coordinated with those of the forming tool; if free sliding on vertical columns the rig must move without jamming or rocking. This paper reports the development and testing of a positive ISF fixture design that uses nylon sleeve bushes rather than the traditional linear rolling element bearings. After reviewing the functional requirement and various approaches to ISF fixtures the paper details the design process from concept generation to experimental assessment.

To assess if the fixture's nylon's bushes moving on steel columns provide sufficient torsional stiffness a number of symmetric and asymmetric trial components were formed using modular wooden dies and a rotating tool with multiple diameters. The results were assessed for signs of misalignment or stick-slip vertical movements. Measurement of formed



comments properties such as major, minor strains, thickness reduction and geometric profile are discussed. The results suggest that a fixture mounted on nylon bushes moving on steel column has sufficient lateral rigidity combined with vertical compliance to support ISF processes.

### 10.2.1 Methodology

Frequently ISF capability is determined by the size of the fixture that can be mounted on the worktable of the CNC milling machine (the most common arrangement) [12]. The fixture is usually composed of a base plate and a top plate, which holds the sheet clamped round the edges by a series of threaded fasteners [13]. Forming is caused by the pressure created by the forming tool as it follows a path generated by CAM software [14] that generates localized stresses that cause the material to yield and deform [7]. ISF process evolution and validation are discussed in greater detail in next section of the paper.

In positive ISF processes the sheet is progressively deflected onto a protrusion whereas in negative ISF processes the sheet moves into a cavity [Figure 10-4]. In both cases the design of the fixture is important in determining the success of the process. However the fixture used for positive ISF must combine vertical movement with sufficient stiffness to ensure the twisting moments caused by forming operations do not cause significant deflections.

This paper details the process of designing and assessing a fixture for positive ISF that uses nylon bushes to create a sheet mounting frame that is free to move vertically while resisting horizontal twisting. A series of component parts, produced on the prototype fixture, are used to assess if the structure's deflections impact on the geometry of the formed components.

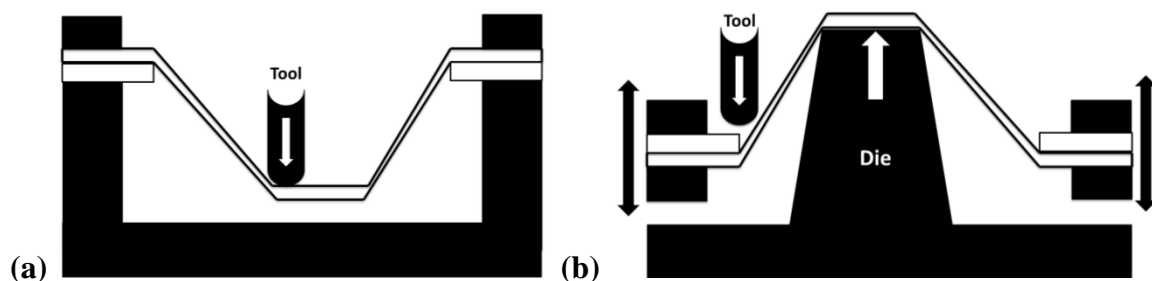


Figure 10-4 Types of Incremental Sheet Forming Fixtures; (a) Positive, (b) Negative.

### **10.2.2 Fixture Design Methodology**

The authors adopted Pugh's methodology for engineering design [162] that describes a systematic process which progresses through stages of requirements generations, specification, concept generation, concept selections, prototyping, testing, detail design and assessment. Subsequent sections briefly describe each of these stages.

The requirement for an ISF fixture arose from an ongoing project to develop ISF processes for titanium sheet on CNC machines. The breadth of the investigation meant that the fixture had to be capable of supporting both positive and negative ISF operations while being sufficiently ridged to ensure the deflecting forces remained vertical.

### **10.2.3 Fixture Requirements: Deformation forces and forming depth**

The crucial parameter in the design of an ISF system (i.e. sheet fixture and tool) is the magnitude of localized force applied to the sheet. Part of this force is transferred to the structure of the equipment while rest is used to deform the sheet itself. A study of force developed during the ISF of a steel DC05 sheet by Petek et. al. reported that the maximum force was just under 2KN [110]. Because the objectives is a fixture to support the investigation of ISF processes for titanium and aluminum sheets the design must support load and forming depth typically needed to deform the material. These are estimated as a force of 5kN which if applied through a 16.5mm diameter tool, will create a pressure of 333 MPa. Pressure on tool and sheet will increase if the tool tip has a smaller diameter.

Forming depth is also an important design parameter for an ISF fixture. It was observed by the authors through initial experiments and the literature review that maximum forming depth attained for geometries (of this particular sheet size) are around 27mm for cold forming titanium sheet using SPIF [128]. This forming depth (27mm) could vary depending upon temperature, sheet thickness, surface finish, tool pitch and sheet size.

Given the above it was concluded that the design specification for an ISF fixture was that it had to accommodate maximum deformation of 100mm in vertical direction, enable the forming of sheets with a 110mm x 110mm cross-sectional area and have a useable area of around 70mm x 70mm. Ideally this area should be able to increase to 300mm x 300mm with

useable area up to 250mm x 250mm by scaling up size of the fixture. On the bases of these parameters five conceptual designs were generated and analyzed.

#### **10.2.4 Fixture Design Concepts**

The following concepts for a fixture to support ISF were generated and numbered:

1. Springs: Four thin pillars with tension springs pulling sheet holder down.
2. Servo: Servo motor controlling vertical movement on ball screws.
3. 4 pillars: Four pillars serving as guide rails and fixture free to move vertically.
4. Scissors: Scissors design takes sheet holder down with pin in the middle.
5. 3 pillars: Three pillars serving as guide rails for vertical movement.

Different conceptual designs were created by author during brainstorming. Designs were discussed with supervisors in the perspective of current equipment's being used for ISF process. Conceptual design 1 shows four parts as shown in Figure 10-5.

1. Static upper plate
2. Sheet holder
3. Die and base
4. Load cell

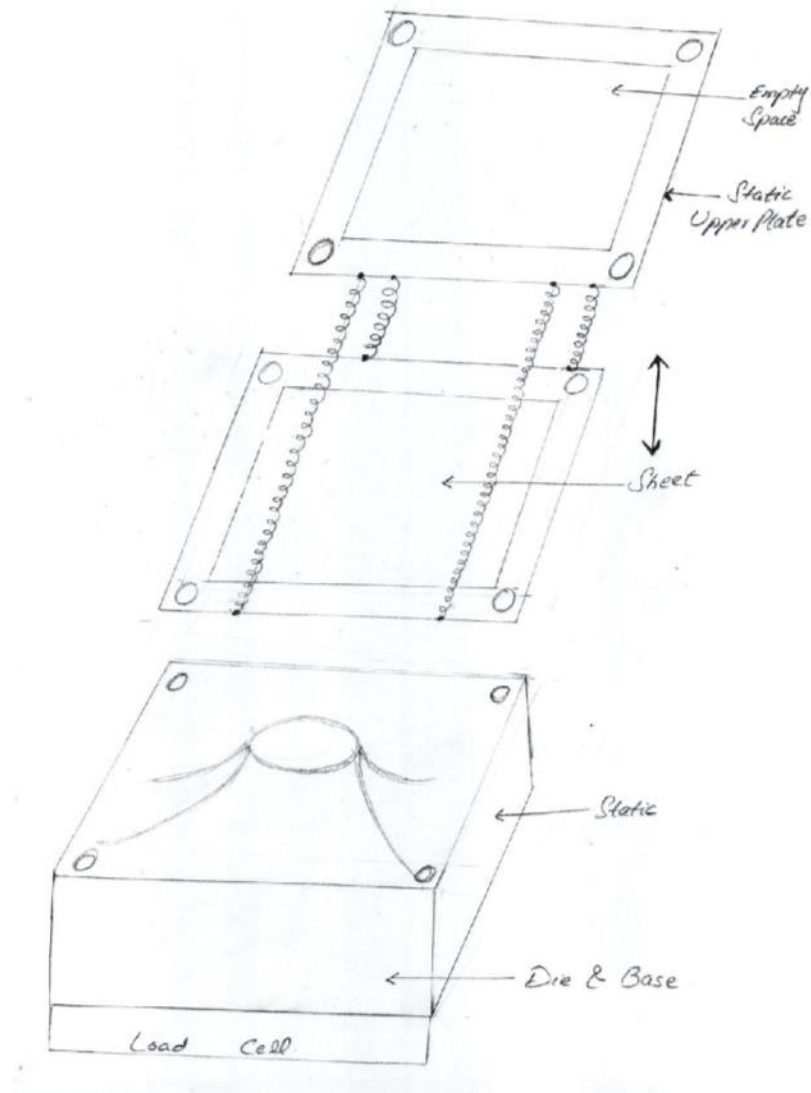


Figure 10-5: Conceptual design 1

First three parts are connected to each other through columns passing through given holes. Sheet holder is able to move in vertical direction where all other parts are stationary. There are four compression springs pushing the sheet holder down while the sheet is being formed. Movement of sheet could allow better material flow compared to static sheet option. Upper static sheet has empty space so that tool can work through that space. Base and die are the same which reduces manufacturing cost and movement of objects with respect to each other. Figure 10-6 shows conceptual design 2 with motorized movement of sheet holder frame. Basic concept of the machine is same as conceptual design 1. There are three noticeable differences.

1. Motorized movement instead of springs
2. Upper static frame is not required
3. Lead screw is used to convert rotary motion in to linear

Motion of sheet holder should be synchronized with the tool.

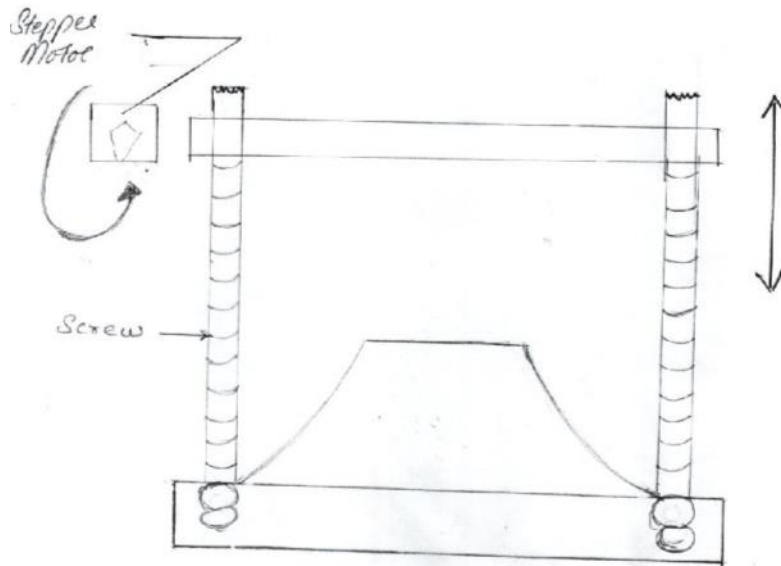


Figure 10-6: Conceptual design 2.

Conceptual design 1 and 2 had some inherent complications due to which conceptual design 3 was generated and selected.

Conceptual design is an improvement of conceptual design 1. Upper static plate is removed in this design and compression springs are replaced with tension springs. Die can be replaced for different experiments so the design is modular compared to its previous version. Motorized motion is not selected to avoid complications as the conceptual design 3 can perform same function as 2.

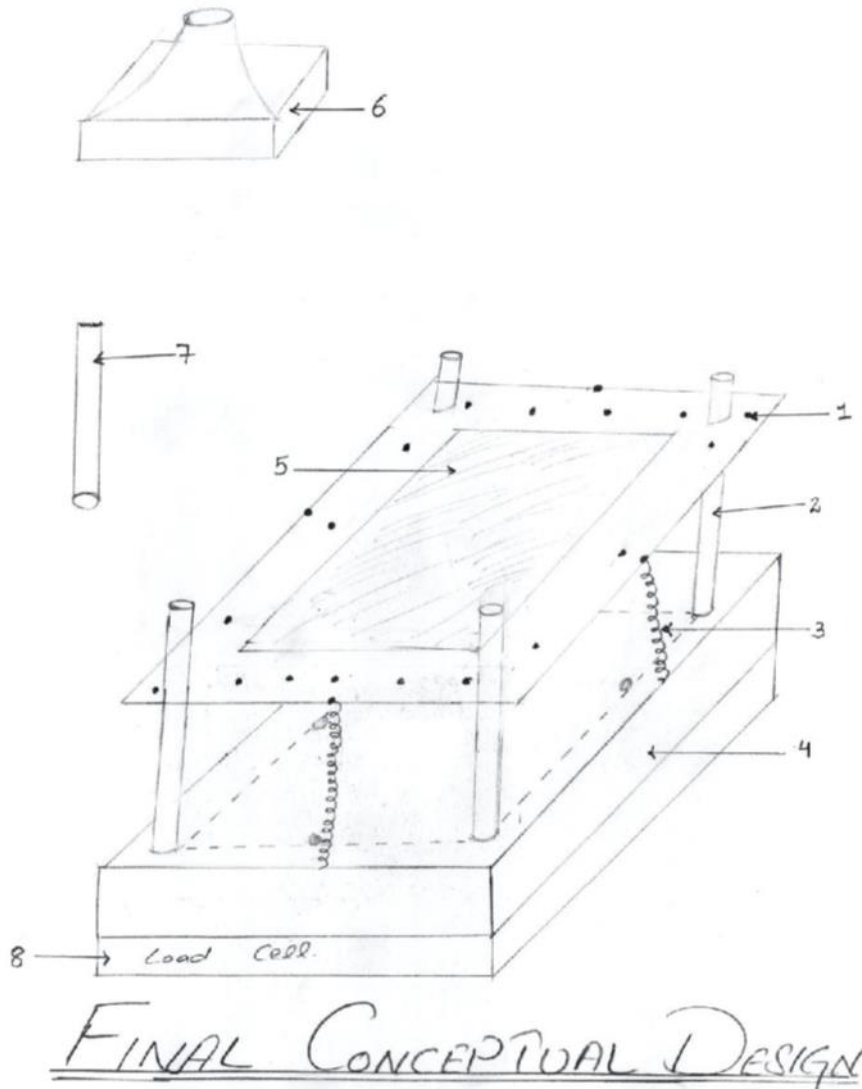


Figure 10-7: Conceptual design 3.

Following are the parts given in Table 10-2.

1. Sheet holder
2. Support column
3. Spring
4. Base
5. Sheet
6. Die
7. Tool
8. Load cell

Conceptual design 4 gives a totally new perspective of movement of sheet. Moving mechanism is different compared to concept 3 where holder plate slides across vertical columns. Concept contains links, which are attached to upper and lower portion of mechanism in pairs through pins. Each link has 3 rotational joints. Relative motion of link with respect to other components of mechanism describes final motion and constraints of joint and mechanism. Joint 1 of mechanism can only move in vertical direction, joint 2 moves in XY plane while joint three only moves in horizontal direction. Images of concept 4 are not provided due to data protection issues. Figure 10-7 shows design selection matrix for all the designs. Concepts considered and criteria used to assess their relative strength are reported.

Table 10-2 Concept selection matrix.

<b>Concepts</b>	<b>1 Spring</b>	<b>2 Servo</b>	<b>3 4 pillars</b>	<b>4 Scissors</b>	<b>5 3 pillars</b>
<b>Assessment Criteria</b>					
Ease of Manufacturing	1	-1	1	1	1
Ease of use	0	-1	0	1	1
Efficiency	1	0	1	1	1
Durability	1	-1	1	0	1
Stability	-1	1	1	-1	1
Accuracy	0	0	0	1	1
Stuck	-1	1	-1	1	1
Modular design	-1	-1	1	1	1
<b>Total</b>	0	-2	4	5	8

As a result of qualitative ranking in the design matrix three concepts were chosen for quantitative analysis i.e. concept 3, concept 4 and concept 5 were selected for modeling. 3D CAD models were created for three concepts. After part modeling, all the parts were assembled using dynamic features, for instance, pin joints and sliders, of software package Creo. This enabled authors to visualize strengths and weaknesses of various concepts while analyzing their movement. Several changes to the original concept were made during modeling due to realization of the fact that there would be manufacturing or assembly problems. Two concepts are modeled using 3D software and several critical components such as pin and links were analyzed using Finite Element Analysis software package ANSYS. Models are shown in Figure 10-8.

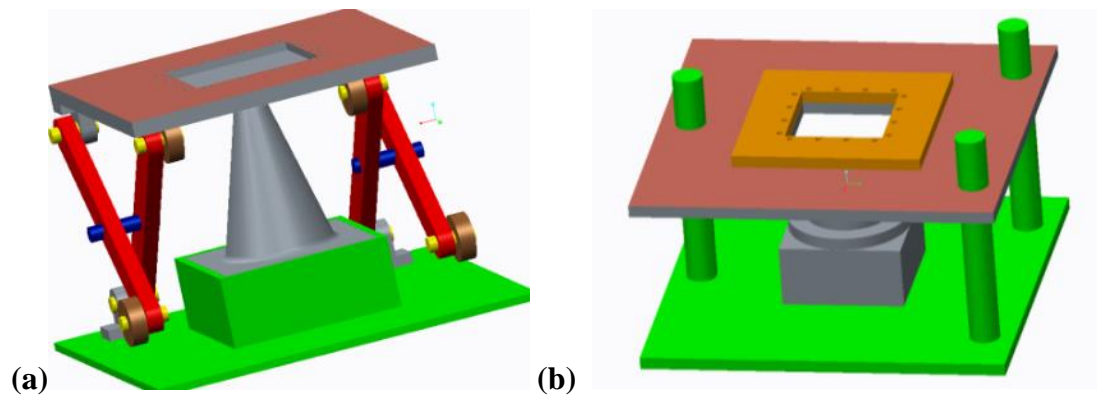


Figure 10-8 3D CAD of fixture concepts; (a) Concept 4: scissors, (b) Concept 5: 3 pillars.

### 10.2.5 Prototype assessment

Concept 4 was prototyped to check the stability of the design for ISF process. Mojo® 3D printers were used to make joints between base/holder and links. Prototype was made at full scale as shown in Figure 10-9. Four rollers move along a straight path and let the sheet holder change its vertical position while keeping its horizontal position constant.

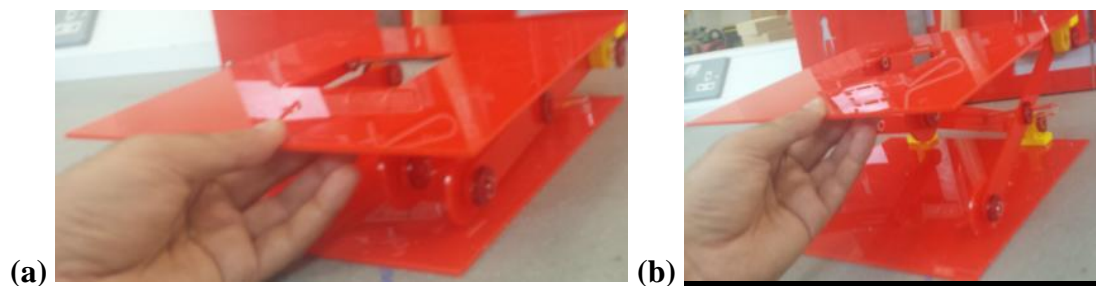


Figure 10-9 Scissor concept prototype at different levels (a) lowest, (b) highest.



Inspection of the concept 4 prototype suggested that there were issues with its lateral stiffness. Although several modifications to the initial design were made these changes only reduced, rather than eliminated, the lateral movement, or play, in the fixture. These trials concluded that concept 4 had inherently lower stiffness in the lateral direction, thus it was decided that concept 5 would be developed further.

### **10.2.6 Detailed design and validation**

After detailed design a functional prototype of the ISF fixture based on Concept 5 was created. Steel and wooden dies with different forms were manufactured to check the kinematic and mechanical behavior of the concept 5 prototype. These dies [Figure 10-10c] are modular and can be replaced easily for forming symmetric and asymmetric shapes. [65]. Indeed 3D printed polymer dies could also be used with the fixture. Nylon bushes (rather than linear rolling element bearing) were used to enable free movement of fixture on the three columns. These bushes were selected because they have high stiffness coupled with low friction rate.

There are different types of materials used to manufacture polymer bushes including teflon, nylon, phenolics and delrin. Due to current load and environmental conditions nylon was selected for bush material. Nylon is self-lubricating, resist to abrasion and has a low wear rate. Several polymers absorb water from atmosphere and thus are hygroscopic [163]. With relative humidity of 40-65%, i.e. at normal environmental conditions, moisture content in nylon will hover around 1.5-2% by weight, consequently the possibility of expansion has to be considered [164]. Typically the increase in size can equal 0.5-0.6% in an unfilled nylon 6/6 at room temperature [164-167]. However many processors will purposely condition their nylon parts as they are being molded to shortens the time frame required for the part to reach equilibrium from weeks, or even months, to a couple of days. Because of which polymers have very low capacity to absorb further moisture at room temperatures [165].

Given the compliment nature of nylon 6/6 [168], the environment of the machine shop and the fact similar bushes have been employed successfully in analogous machine designs [169-172] any effects of moisture on the nylon bush bearings were judged to be negligible.

### 10.2.7 Kinematic assessment

The fixture was initially tested on a hard polymer sheet to check its vertical kinematics. The polymer sheet was placed between the upper and lower holders and secured with nuts and bolts as shown in the Figure 10-10a. A hand held heater was used to simulate the vertical movement associated with the ISF process in the absence of an unbalanced force. The heater was revolved around the cone of the die to simulate ISF tool path. Heated air flow directed at a localized area increased the temperature of the polymer sheet. This increase in temperature and the fixture weight forced sheet to deform into shape of die. Figure 10-10a shows the initial position of the sheet when sheet started deforming and Figure 10-10b shows final deformed part. This test validated the ability of fixture to move vertically and was considered successful since no jamming or rocking effects were observed. Although this experiment was successful but it did not include any lateral forces and did not check for stiffness and torsional resistance of the structure subjected to the loads required for an ISF process. To check fixture for these conditions further tests were performed on aluminum sheet using rotary tool.

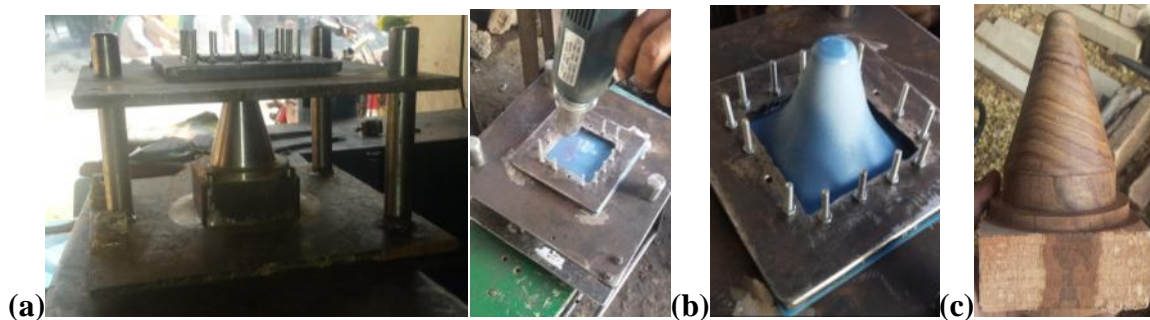


Figure 10-10 Testing on polymer sheet; (a) Start, (b) Finish, (c) Wooden die.

### 10.2.8 Mechanical Assessment

Several tests using metallic sheets were performed using the flexible fixture to check its stability, alignment, stiffness, torsional resistance and freedom of movement. The rotating tool and a wooden die were used to perform these experiments. The rotational speed of the tool depends upon the relative velocity between the tool and the metal sheet. Thrust bearings are used to align and hold the tool stick while it's rotating Figure 10-11a. Rotation is helpful

in reducing friction between the metal sheet and the tool. Sheets were formed until the point of fracture (maximum depth) to check the behavior of fixture under extreme operating conditions. This was done because all three components of force increase in magnitude with the forming depth and the force applied to the sheet and the fixture reaches a maximum just before fracture. Three of these tests are reported in current study. The fixture and tool were mounted on a 3-axis CNC milling machine as shown in Figure 10-11 and an ISF process was carried out on an Aluminum sheet (AA1050).

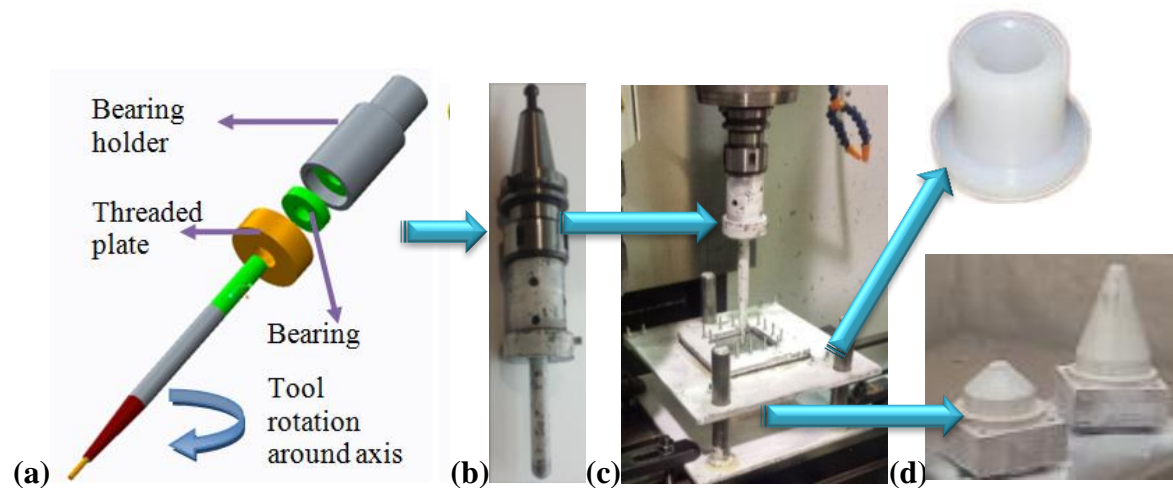


Figure 10-11 ISF equipment; (a) CAD model of rotating tool (4.5mm Dia), (b) Rotating tool (16.5mm Dia), (c) Equipment mounted on CNC, (d) Nylon bushes and wooden Dies.

### 10.3 Design and implementation of experimental geometry

Previously author worked on conventional conical and spherical shapes. After analysis of previous results and literature review it was decided that a new shape pertaining several wall angles should be designed. Several shapes of geometries produced through ISF were studied. Normally cones, spheres and rectangular geometries with similar wall angles were reported as shown in Figure 10-12. Part geometry's complex effects manufacturing time and forming force. At time multistage forming toolpath is required which further takes up machine time and human resources. Due to these issues generally researchers work on truncated pyramid and cone might not present the whole picture. Although some researchers have worked on other shapes given in the Figure 10-13. Mostly geometries were basic but some researchers tried new geometries and formed commercial components [Figure 10-14].

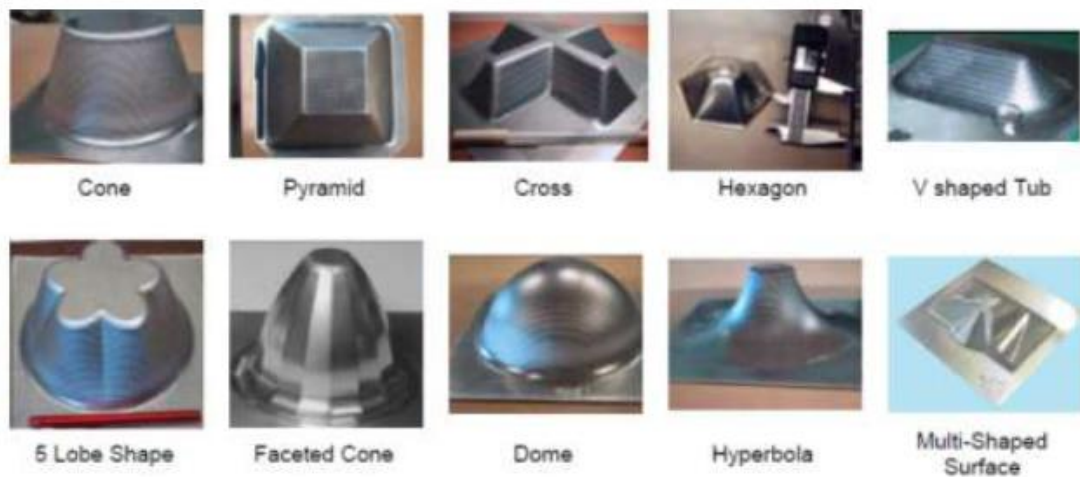


Figure 10-12 Complex geometries formed through ISF.



Figure 10-13 Reflexive surface for headlights [49].



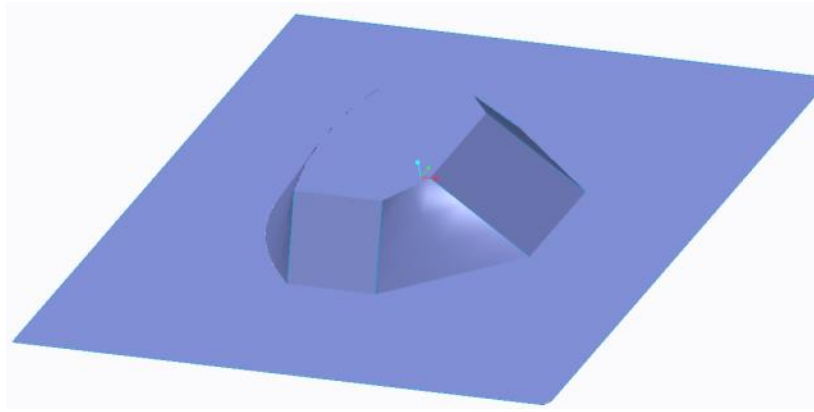
Figure 10-14 Automotive heat/vibration shield [87].

### 10.3.1 Multi-slope

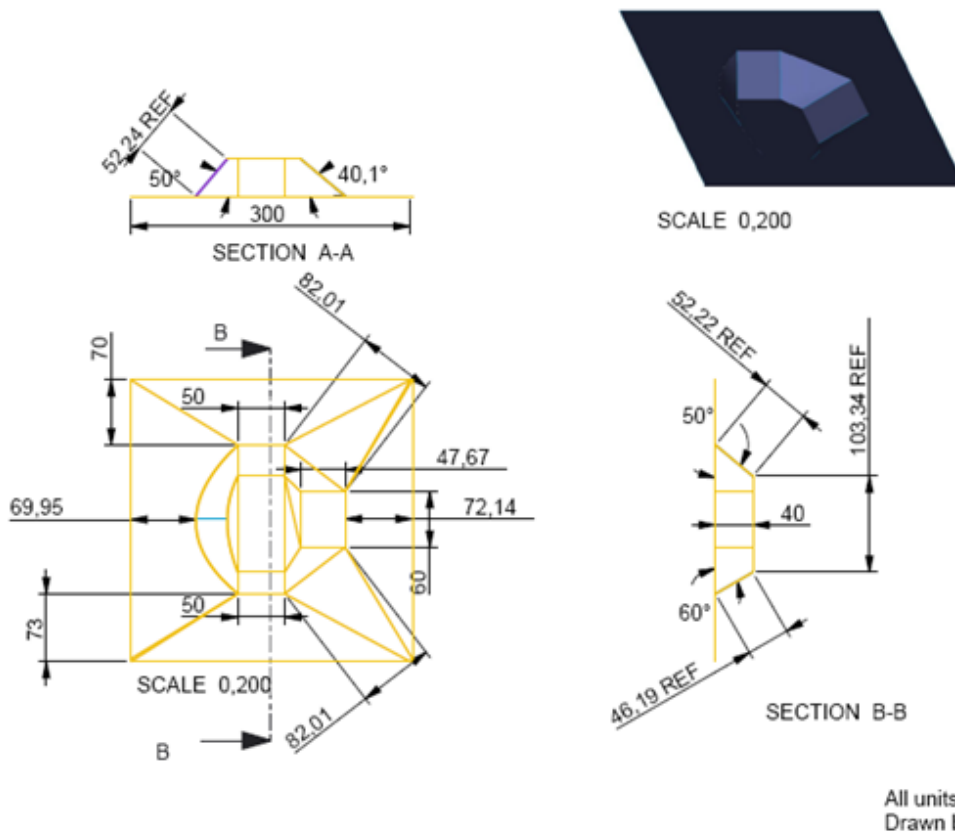
However, these geometries were mostly to acquire a required commercial shape and were not meant for research purposes. After analysis of previous research several new ideas of geometries were put forward by the author. These geometries were assessed qualitatively and a final geometry was selected. Selected geometry will be referred as “Multi-slope” in the text [Figure 10-15]. The geometry had the following features

- a. Three Rectangular walls with  $40^\circ$ ,  $50^\circ$  and  $60^\circ$  angles.
- b. A curve with wall angle  $50^\circ$ .
- c. A curve with transitional wall angle from  $50^\circ$  to  $60^\circ$ .
- d. Transitional regions between different wall angles ( $40^\circ$  to  $50^\circ$  and  $40^\circ$  to  $60^\circ$ ) with varying width along depth.

After conceptual sketches, a CAD geometry was then modeled using software package Creo. SS 304 L, AA 1050 H, AA 2024 and AA 7075 was used to form this geometry. Depth of the geometry varied with material type.



(a)



(b)

Figure 10-15 CAD model of the designed shape (a) Isometric view, (b) Drawing details.

As listed in Table 3-1 several tests were performed using “Multi-slope” geometry. Larger size (300mmX300mm) sheets with static fixture were used for these set of experiments. Some sheets were completely free formed and an area of 250mmX250mm was left simply hanging while others used back supporting plate.

A Multi-slope concept of back supporting plate was used to form the sheet metal to improve accuracy of the acquired geometry. Backsupporting plate is a thick steel plate (8mm in this case) with a pattern cut in the middle to support area of the sheet not being formed. Pattern was designed in Creo and imported to water jet cutter which cut the sheet as shown in Figure 10-16a. This plate was placed in the middle of the tool and lower part of the fixture. This reduced the area left hanging to zero. Fillets were introduced at the edges of backsupporting plate to avoid shearing at these points [Figure 10-16b]. This backsupporting plate was introduced to increase accuracy of the formed part. A gauge of 10mm height was used to relate vertical height (Z) to the CNC machine as shown in . After placing backsupporting plate on the fixture, position of internal edges was recorded through gauge so that coordinate system and home position of the CNC code could be aligned with the physical system [Figure 10-18].

Sheet metal was clamped in the fixture instead of using nuts and bolts shown in Figure 10-18a. Clamping instead of bolting sheet in the fixture saved time and cost to drill holes and screw and unscrew bolts in the fixture. This particular step can dramatically improve production rate in commercial setups using ISF process and it is recommended that a study should be performed to determine magnitude of savings through eliminating drilling and bolting. CAD model shown in the figure was used to create toolpath using software package AphaCam shown in Figure 10-19b.

Pitch of the toolpath was 0.2mm and a rotating tool with 1inch (2.54cm) diameter was used to form the sheet. A compensation space of 3mm was provided between the back supporting plate and the tool which was absent in free hanging geometry toolpath. Figure 10-19c shows tool on the sheet and about to start ISF process.

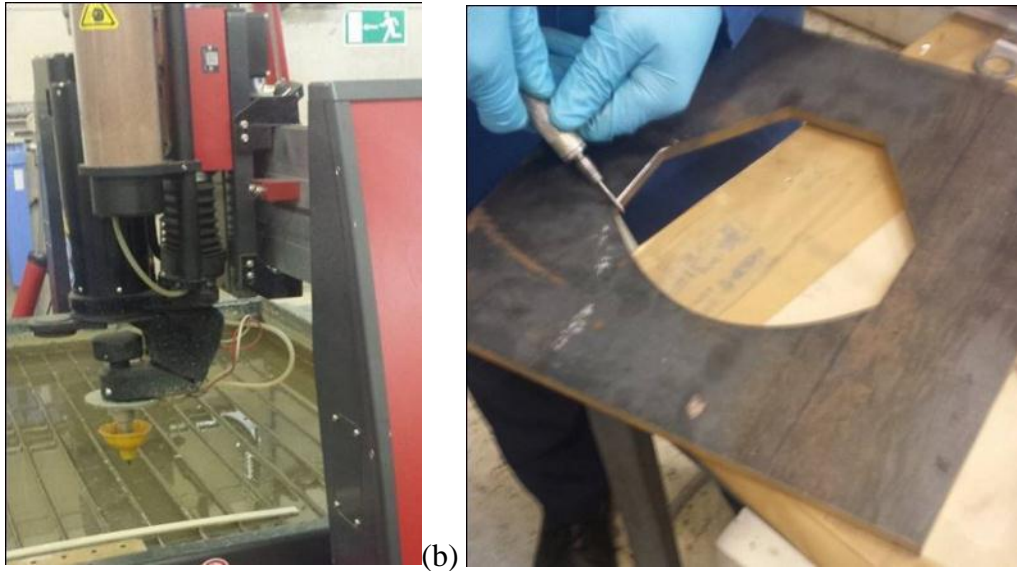


Figure 10-16 Manufacturing of backsupporting plate; (a) Water jet cutting, (b) Smoothing.

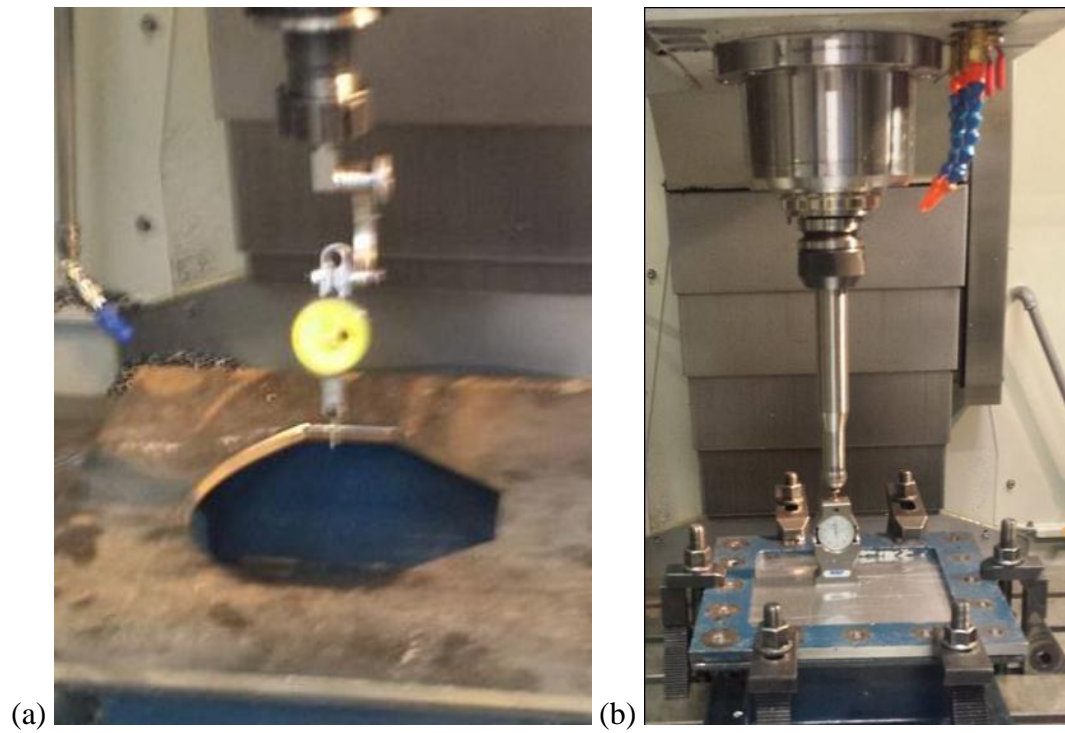


Figure 10-17 Setup of system with guages; (a) X and Y (lateral), (b) Z (depth).



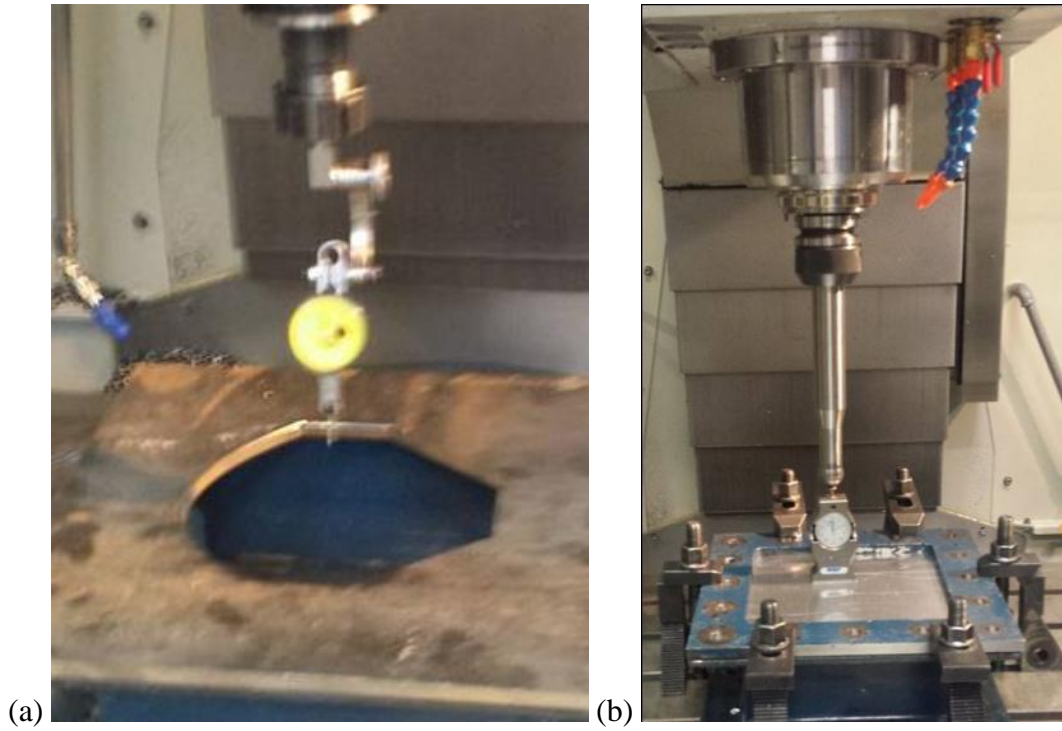


Figure 10-18 Setup of system with gauges; (a) X and Y (lateral), (b) Z (depth).

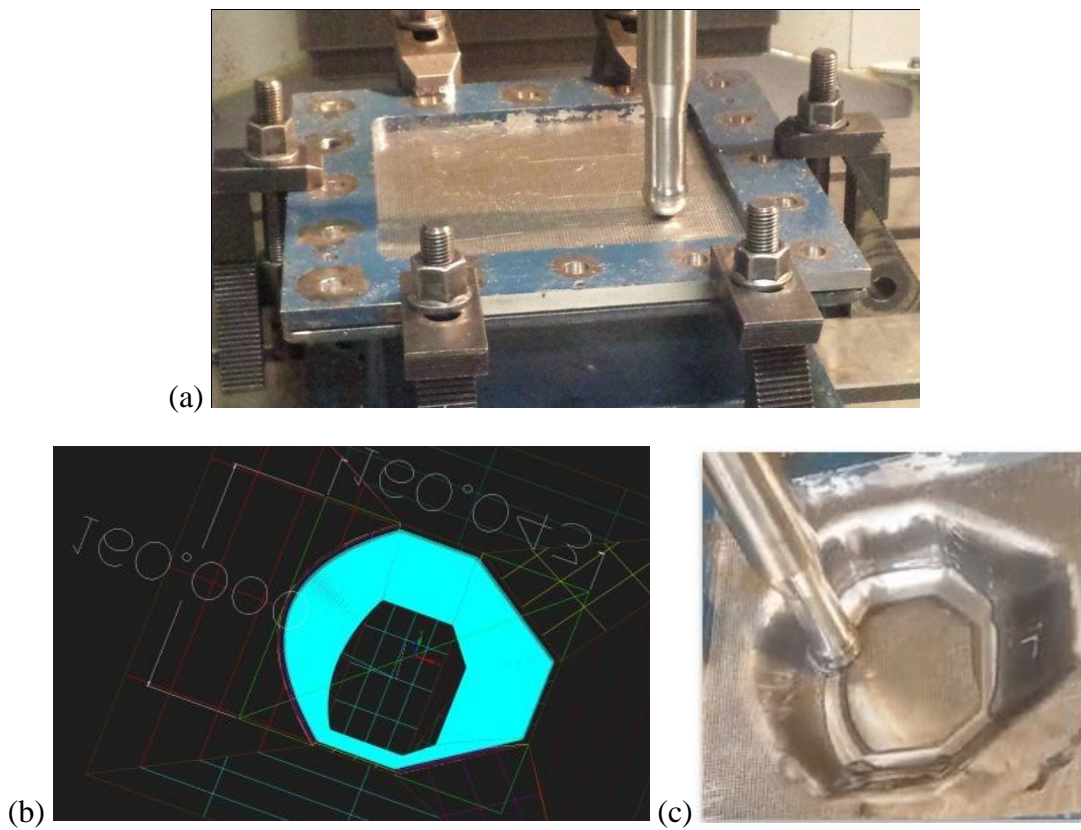


Figure 10-19 ISF process for Multi-slope geometry; (a) Start, (b) Tool path generated in Alphacam, (c) Tool forming the sheet metal.

### 10.3.2 Double sided

After checking Multi-slope geometry for several materials and parameters author came up with idea of double side forming for further complicated shape shown in Figure 10-20. Initial experiments to check this idea were performed on AA 1050 H. A geometry inspired by aerospace parts was finalized. In contrast to previous geometries discussed, this one has features on both sides of the sheet metal. The features in this geometry will be referred as “Cross” and “Basin” in the text. Cross feature is in the middle of the geometry while the basin feature is at the sides. The design was modeled in Creo.As explained for “Multi-slope”, a similar setup technique with gauges was used for double sided geometry.

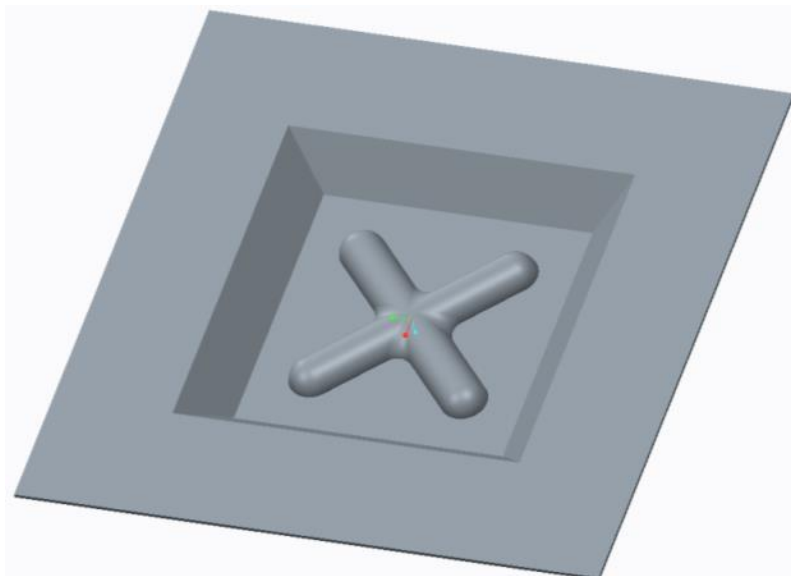


Figure 10-20 Double sided geometry.

## 10.4 Data acquisition equipment

Although a list of equipment is provided in still equipment to perform 3D scanning and etching is discussed in detail.

### 10.4.1 3D Scanning

The dimensions of the ISF manufactured shapes were optically measured using a GOM ATOS Triple Scan III scanner [Figure 10-21b]. This is a 3D scanner which uses blue light technology and digitizes geometries to take precise measurements. Because sheet metals

used for these studies are highly reflective material a thin layer of paint (Ardox) was applied to create a matt surface that eliminated any specular reflection and so allowed the robust acquisition of data from the 3D scanner. Reference markers were applied on both sides and tritop scale bars and reference markers were placed as shown in Figure 10-21a. Tritop camera was used to capture reference points. Parts were scanned using Atos with focus at center of part, as shown in Figure 10-21b. Twelve scans were acquired, six on each side of the part using default scan settings. Scanning was performed at approximately 30 degrees, which ensured part was not scanned perpendicular. As perpendicular part's reflections will cause overexposure. Vice was cut out manually from the scanned data. The resulting point cloud was polygonized, smoothed and processed to get final useable shape. 3 point alignment using obvious features was created as shown in Figure 10-21d. These results were compared to CAD model. Part thickness, CAD comparison, and part profile were extracted from the data.

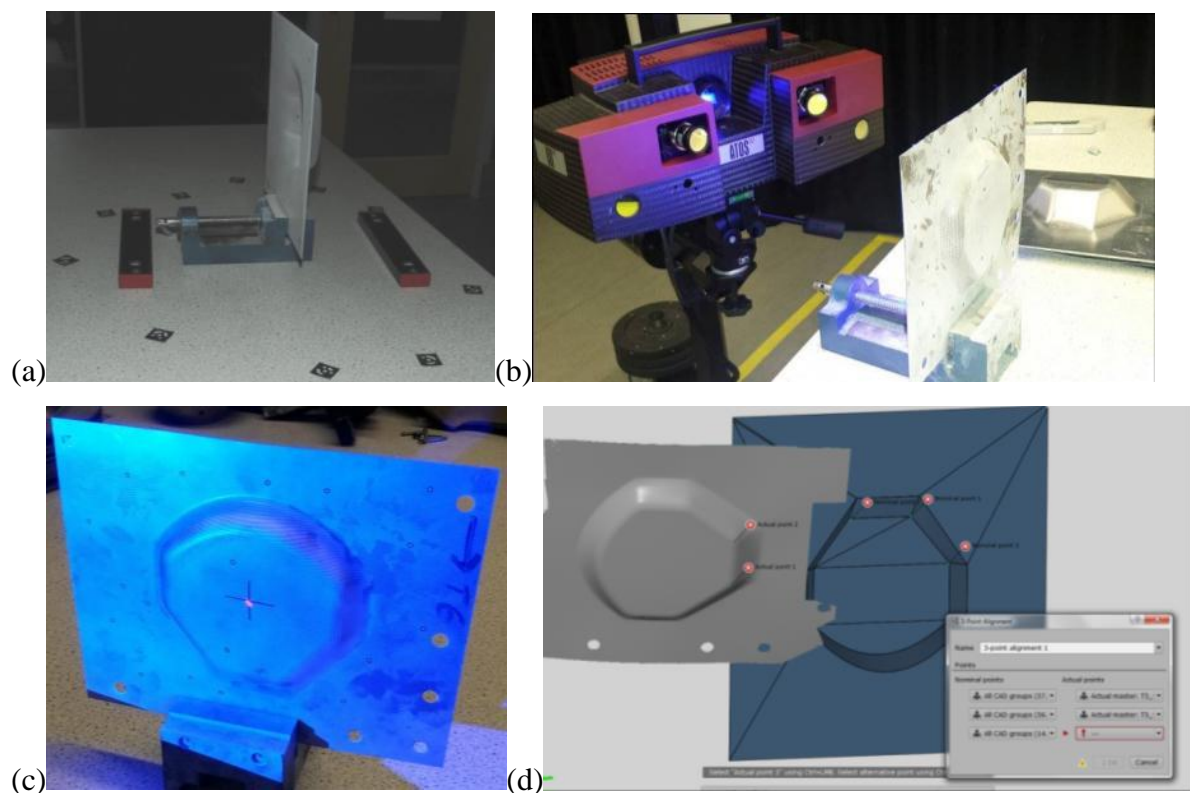


Figure 10-21 ATOS 3D scanner; (a) Tritop scale bars and reference markers, (b) While scanning, (c) Focus at the center (d) CAD comparison.

### 10.4.2 Surface Strains

Permanent sheet marking on the metal sheets were performed through etching process. Metal sheets were etched using Electrolyte No. SC82 and Neutralyte No. 2. EU classic electrolyte system [Figure 10-22a] with 12volts DC current was used. It is used to create high quality electrolytic marks (grids) on metal surfaces through marking process using electrolyte and stencil [Figure 10-22b] to perform circular grid analysis. Marking sheet of 1mm point mark with 2mm distance between them was used shown in Figure 10-22c. Roller [Figure 10-22c] and sheet were wet with acid and etching was performed by rolling the roller over metal sheet. Etching helps in acquiring data related to circular grid analysis which includes thickness reduction, Von Mises strains, major and minor strains. Etched sheet can be seen in and images were acquired through Nikon 300 camera. Image processing analysis was run using ARGUS software and results were recorded.

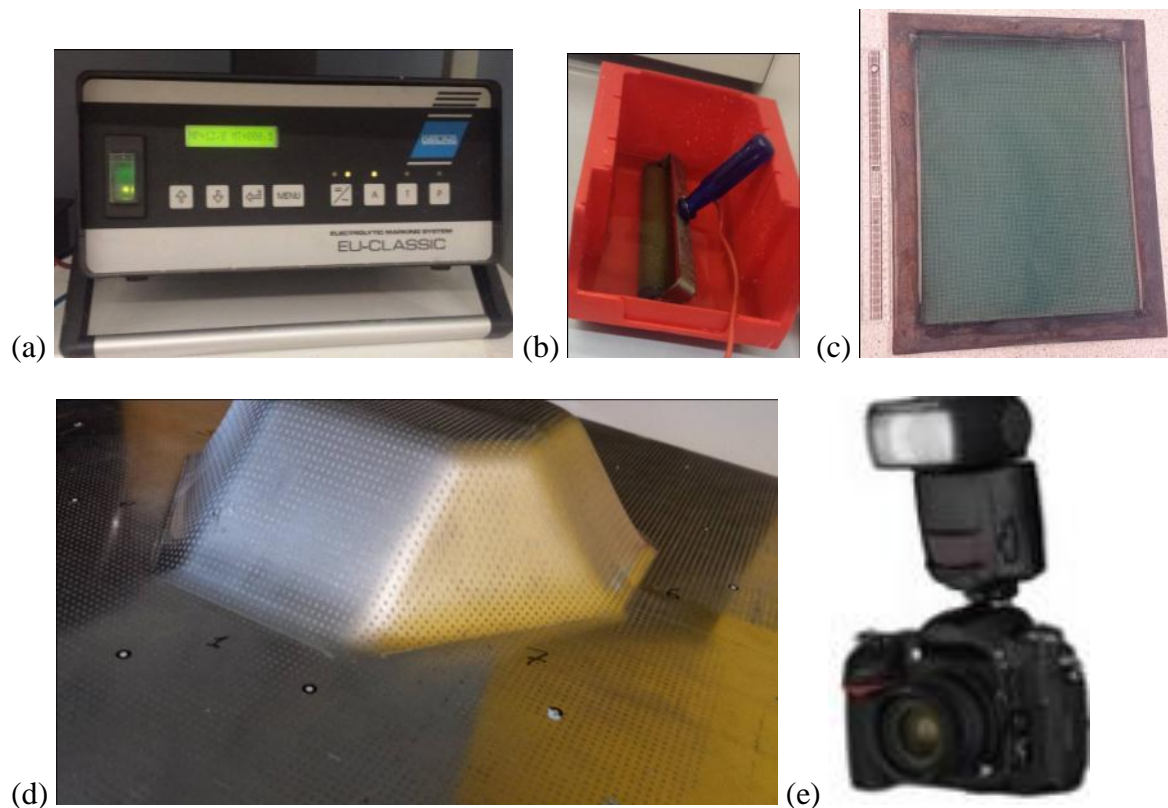


Figure 10-22 Surface strain equipment; (a) EU classic electrolyte system, (b) Roller submerged in Electrolyte, (c) Marking sheet, (c) Marked Sheet, (d) Nikon Camera.

### 10.4.3 Surface roughness

Surface roughness data was acquired through Alicona Infinite Focus IFM G4 shown in Figure 10-23a. This machine is used for surface profile form and roughness measurement through digitisation of surface based on focus variation through non-contact optical 3D surface profiling. Gel gun was used to get replicas of some surfaces to get scanned [Figure 10-23b]. These samples were then placed under Alicona with 50X zoom and the geometry was scanned as per ISO standards. After scanning the geometry it was aligned with the coordinate system of the software as shown in Figure 10-24. After which analysis was performed and surface profile and roughness were calculated.

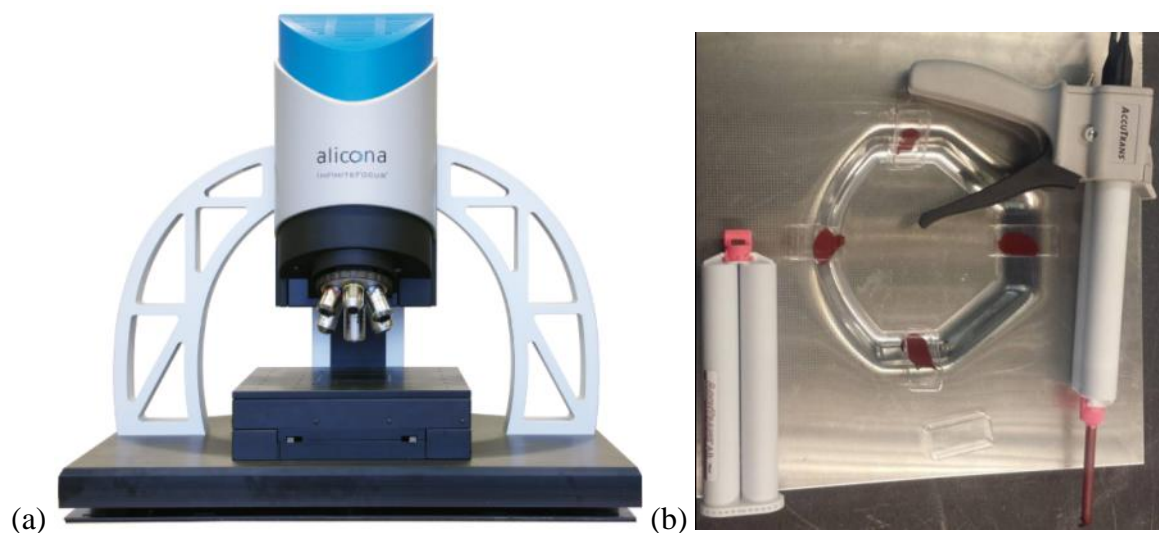


Figure 10-23 Surface roughness; (a) Gel gun, (b) Alicona infinite focus.

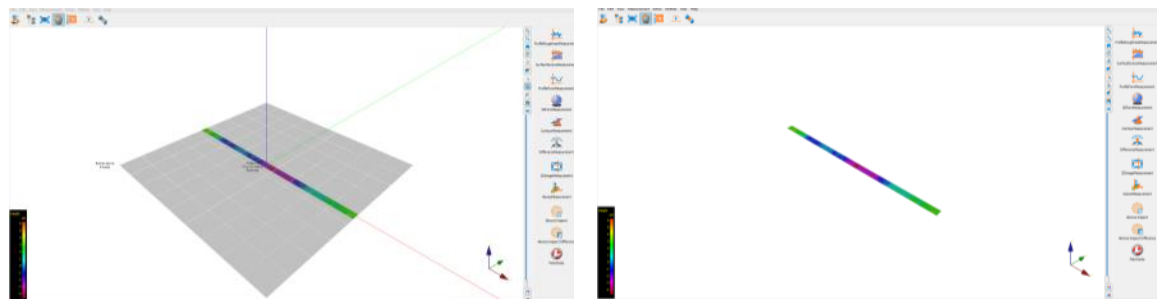


Figure 10-24 Aligning geometries with software co-ordinates

## 10.5 Summary

A Multi-slope tool for ISF process was successfully designed, manufactured and commissioned. The tool is able to rotate relative to surface and thus friction is reduced between tool and sheet surface. Author created several concepts and evaluated against the design specifications of Incremental Sheet Forming Process. 3D modeling, visualization and finite element analysis and functional prototypes were assessed before manufacturing the flexible fixture with nylon bushes. The results suggested that the Scissors design did not have sufficient lateral (i.e. horizontal) stiffness so consequently a 3 pillars concept with nylon bushes was selected as the final design. Polymer sheet with industrial heater was used to check the functionality and the large vertical movement of the fixture during ISF process. Two new geometries “Multi-slope” and “Double sided” were designed and modeled after analyzing several geometric features. Data acquisition equipment for 3D scanning, surface roughness and surface strains were reported.

## 11. Appendix D – Multi-slope geometry results

### SS304L Results

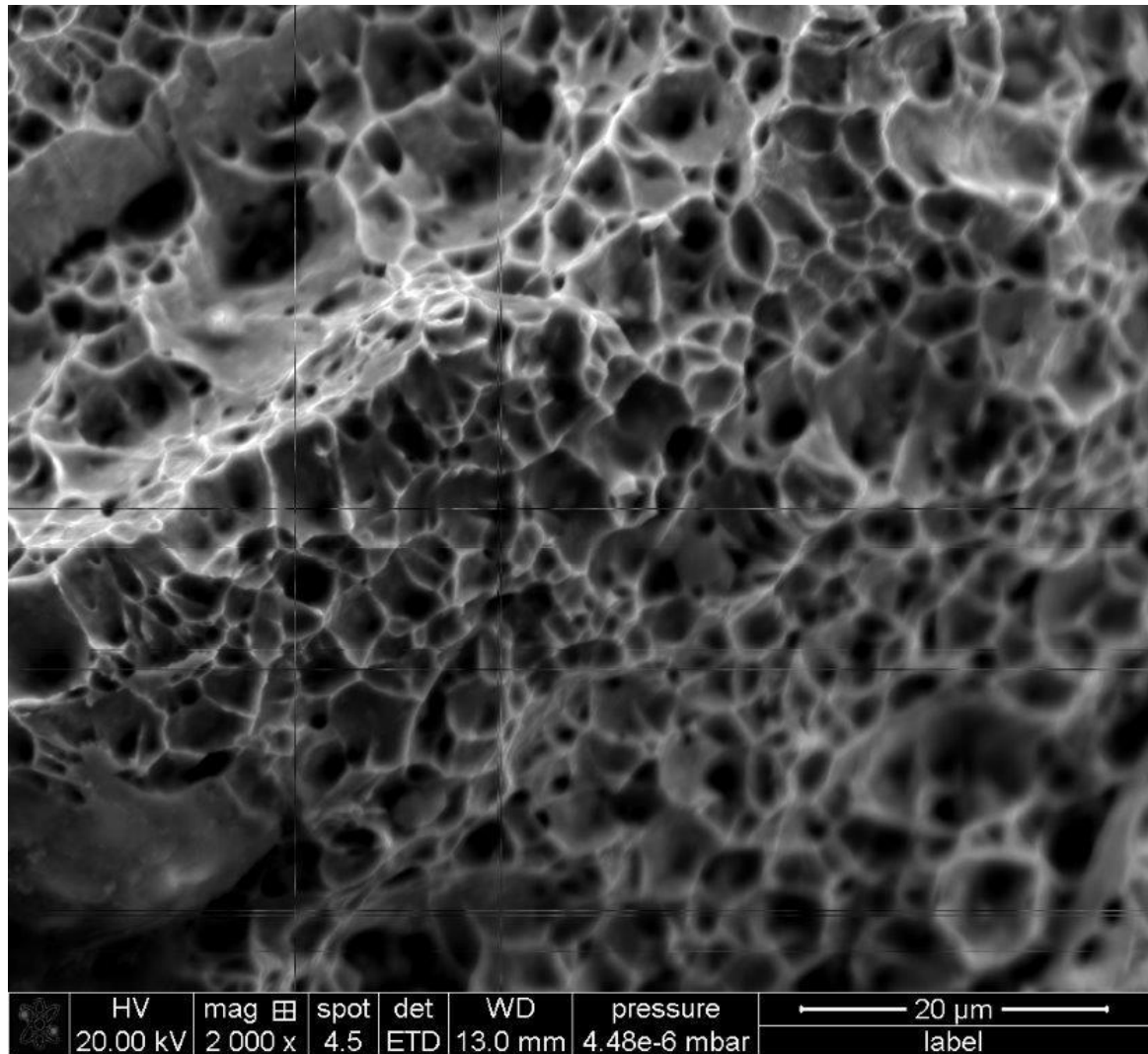
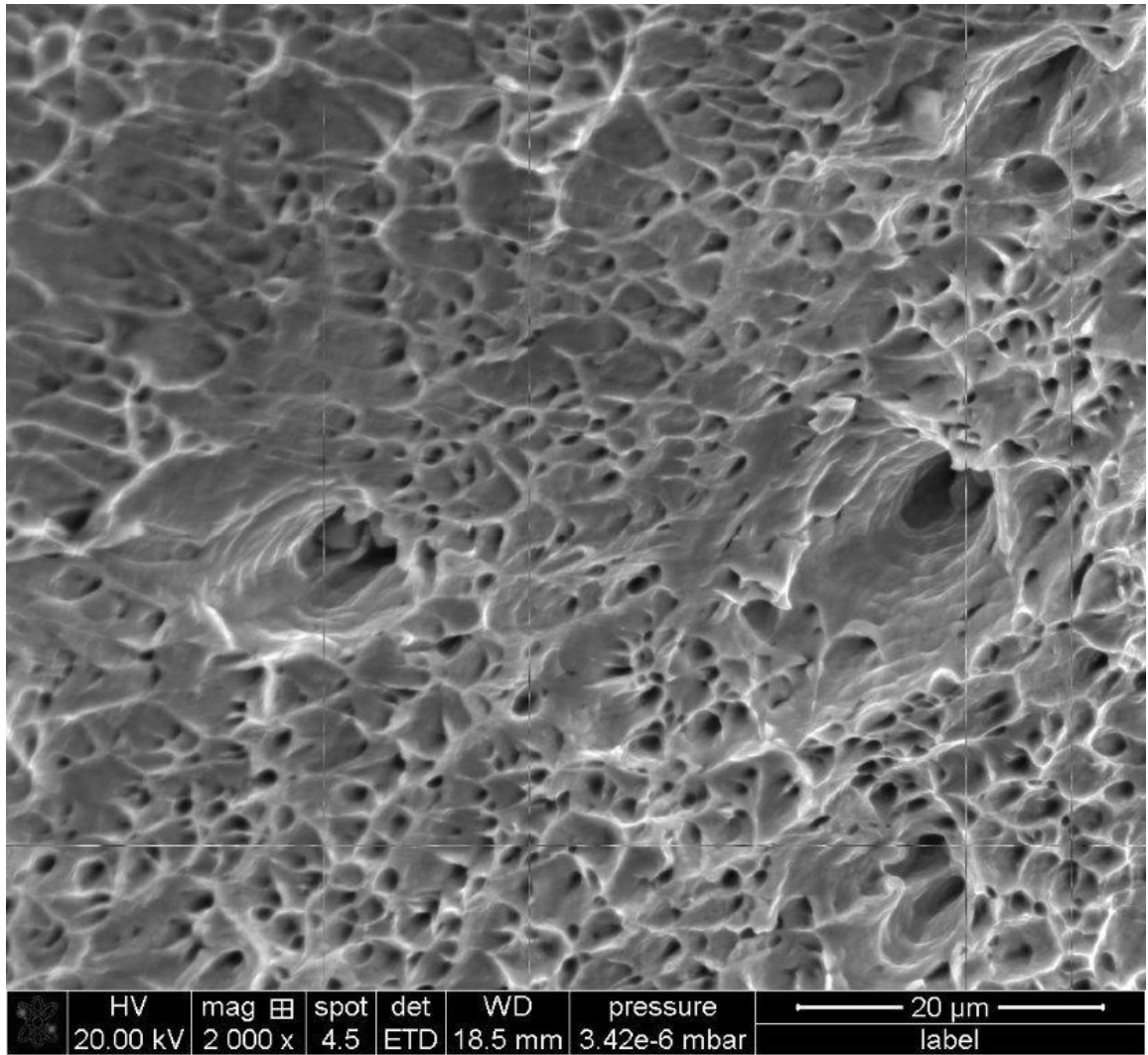
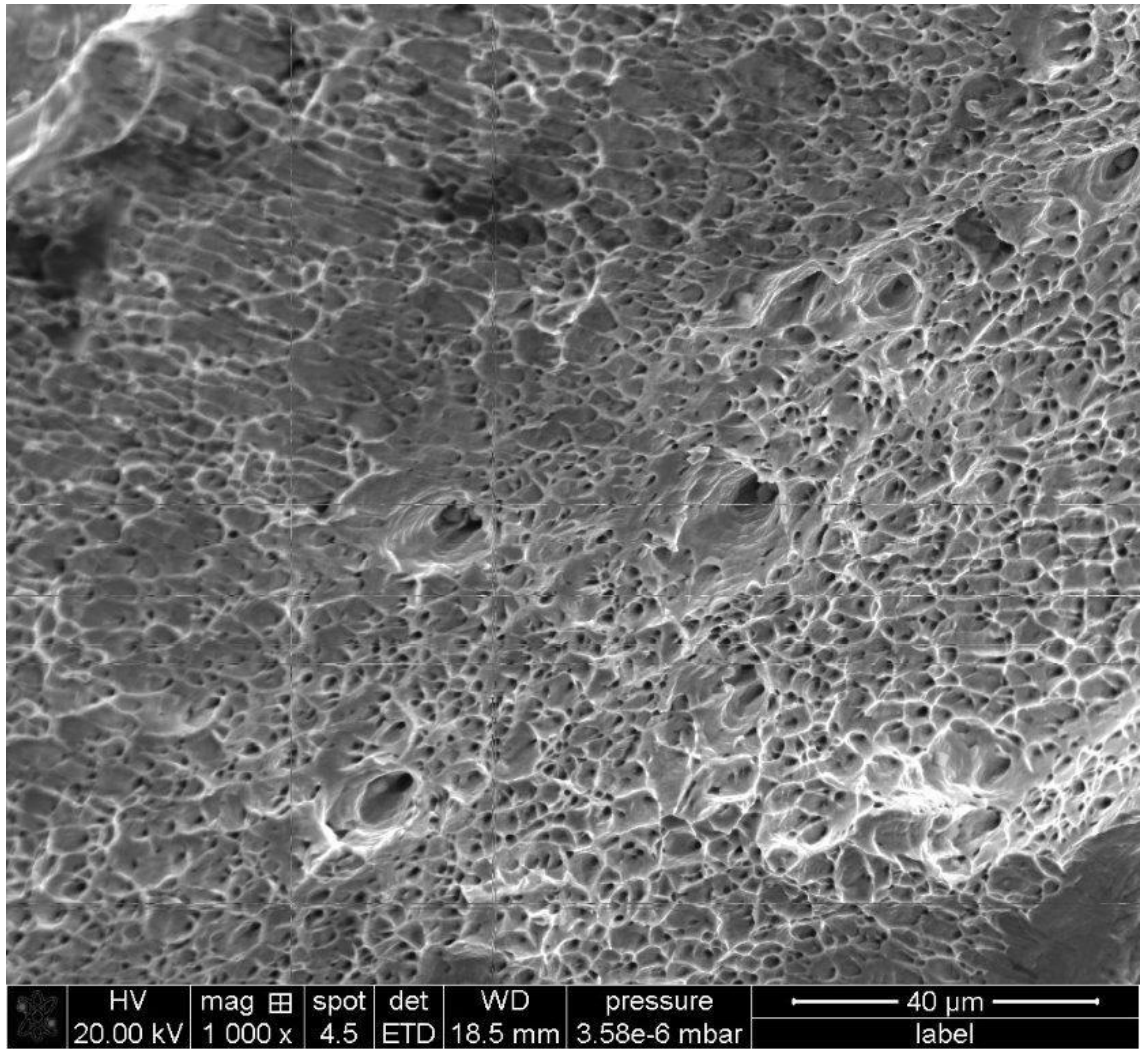


Figure 11-1 Ductile fracture SS304L, ORD-A at 2000X.

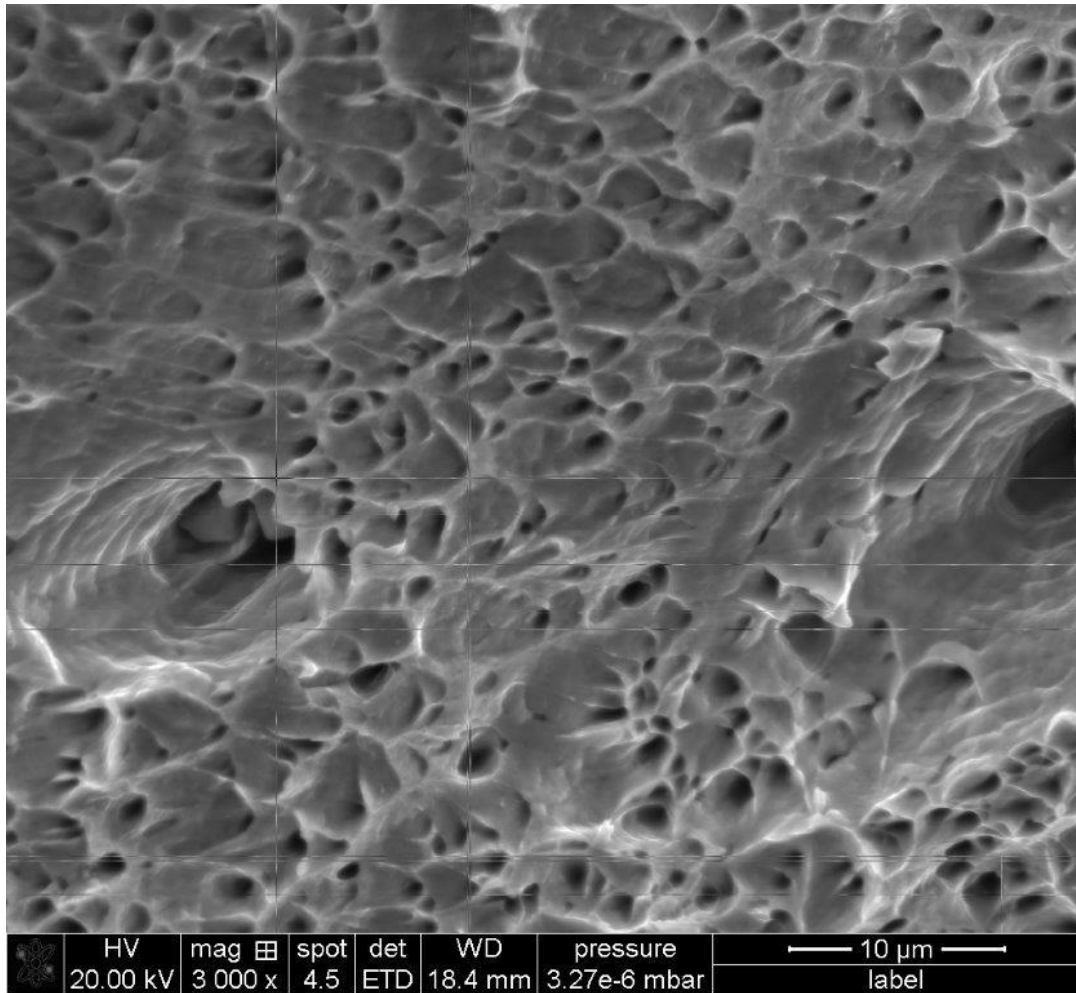


(a)



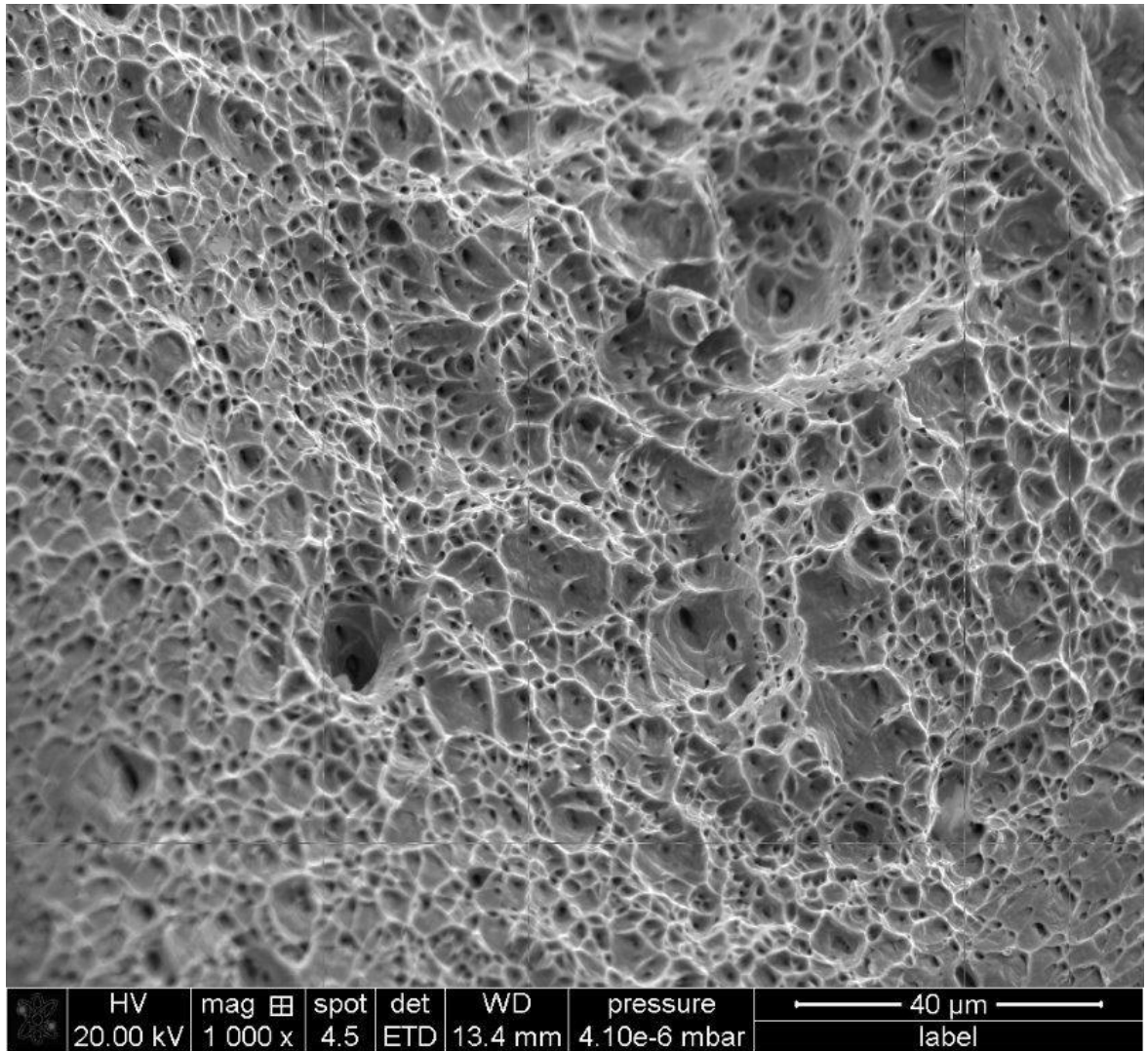


(b)

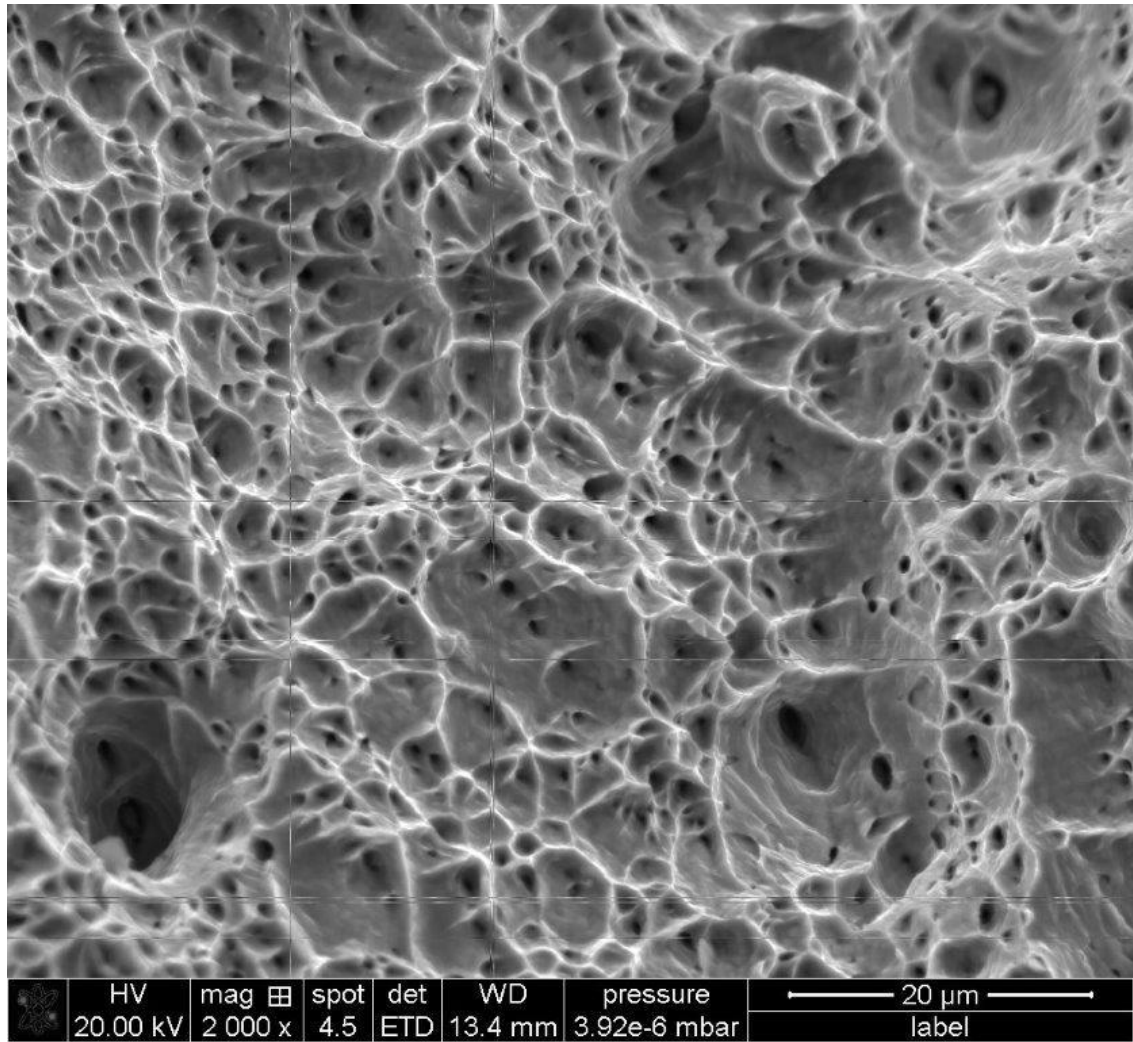


(c)

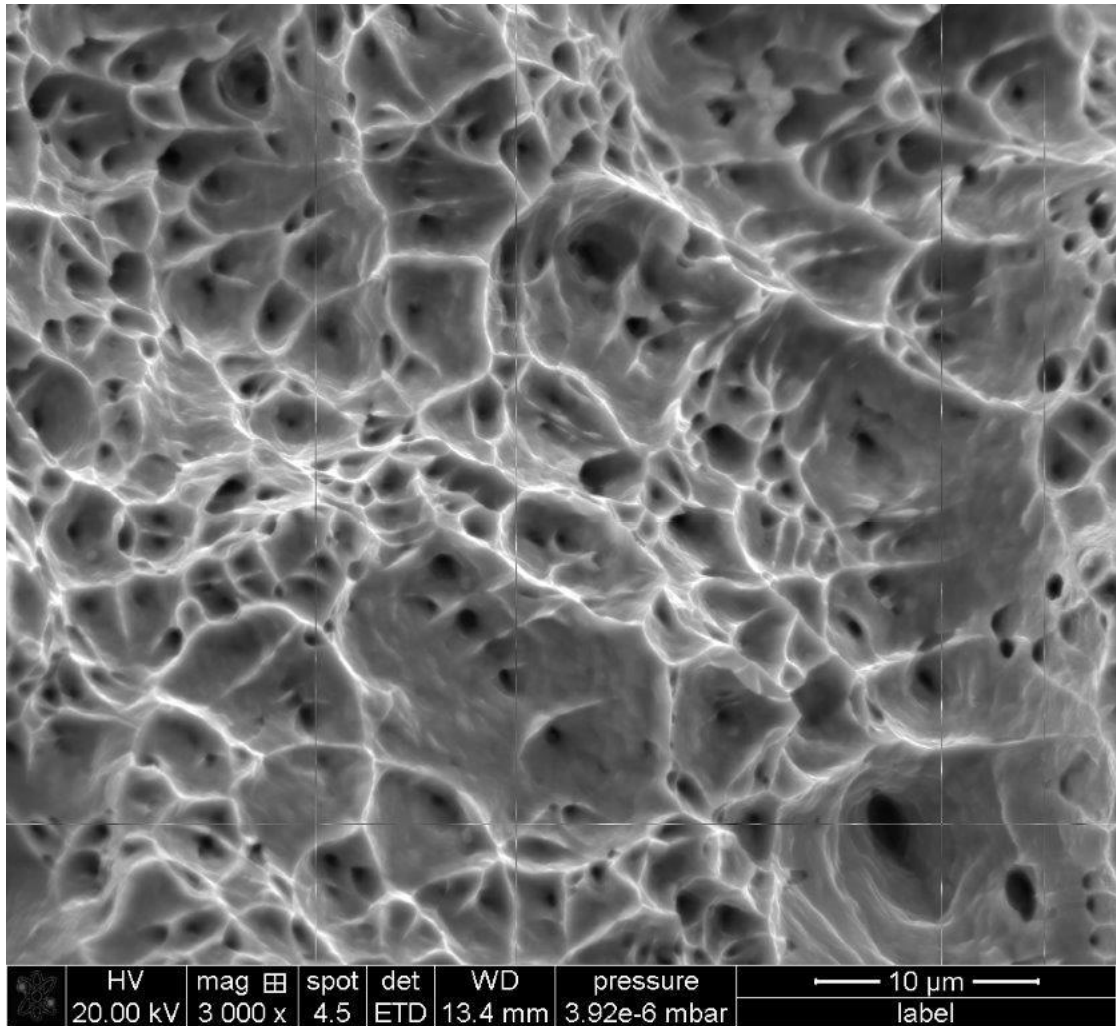
Figure 11-2 Ductile fracture SS304L, 45RD-A; (a) 1000X, (b) 2000X , (c) 3000X.



(a)



(b)



(c)

Figure 11-3 Ductile fracture SS304L, 9ORD-A; (a) 1000X, (b) 2000X , (c) 3000X.

## AA1050H Results

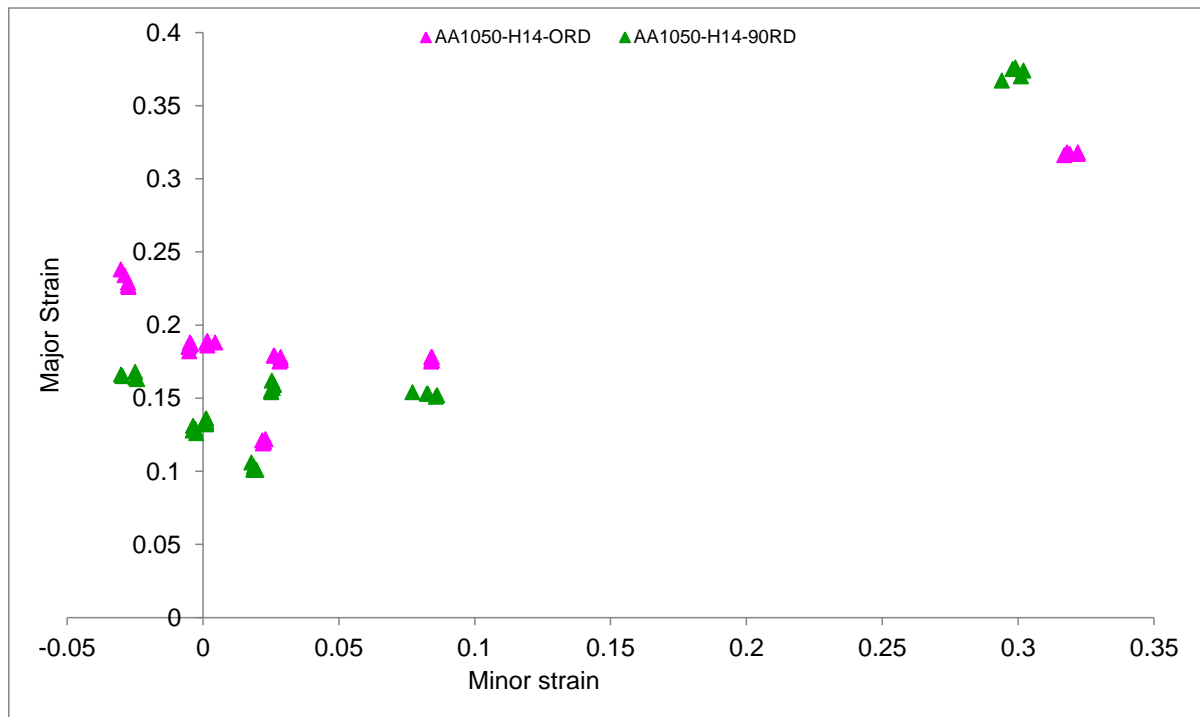


Figure 11-4 Forming Limit Curve AA1050

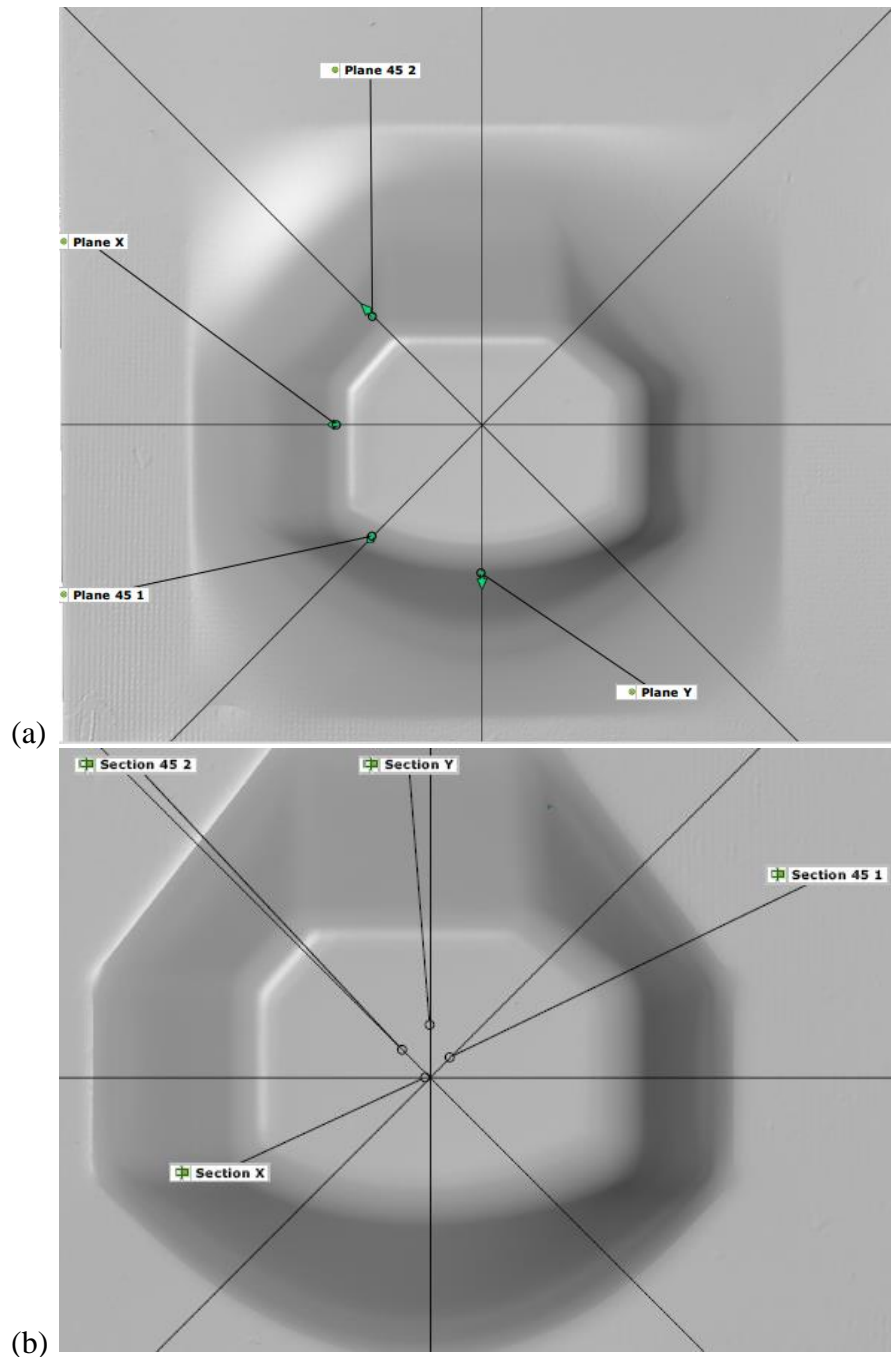


Figure 11-5 Multi-slope geometry AA1050°H; (a) without BSP, (b) with BSP.

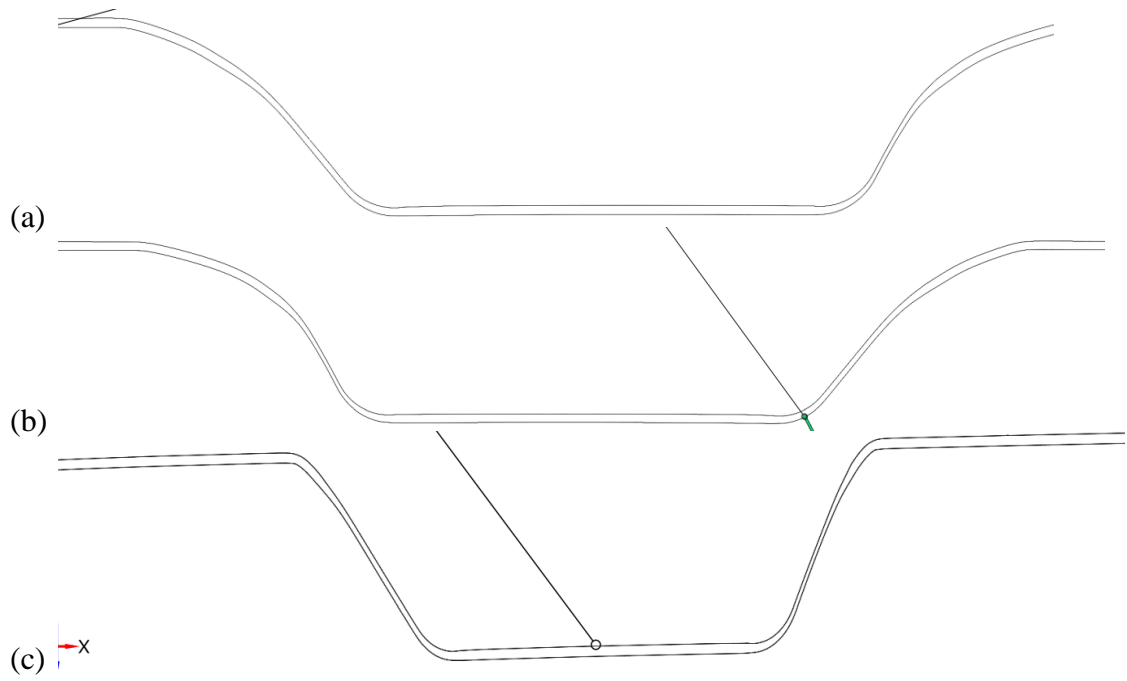


Figure 11-6 Section X; (a) AA1-1050H, (b) AA2-1050H (c) AA3-1050H.

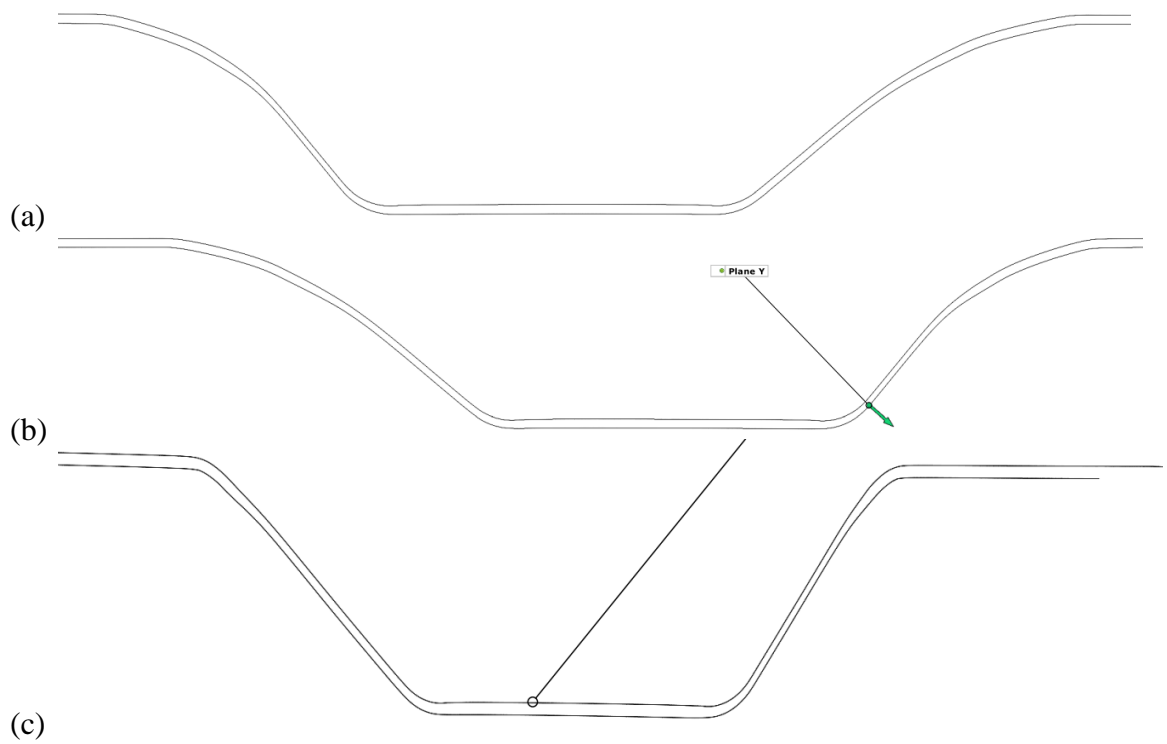


Figure 11-7 Section Y; (a) AA1-1050H, (b) AA2-1050H (c) AA3-1050H.



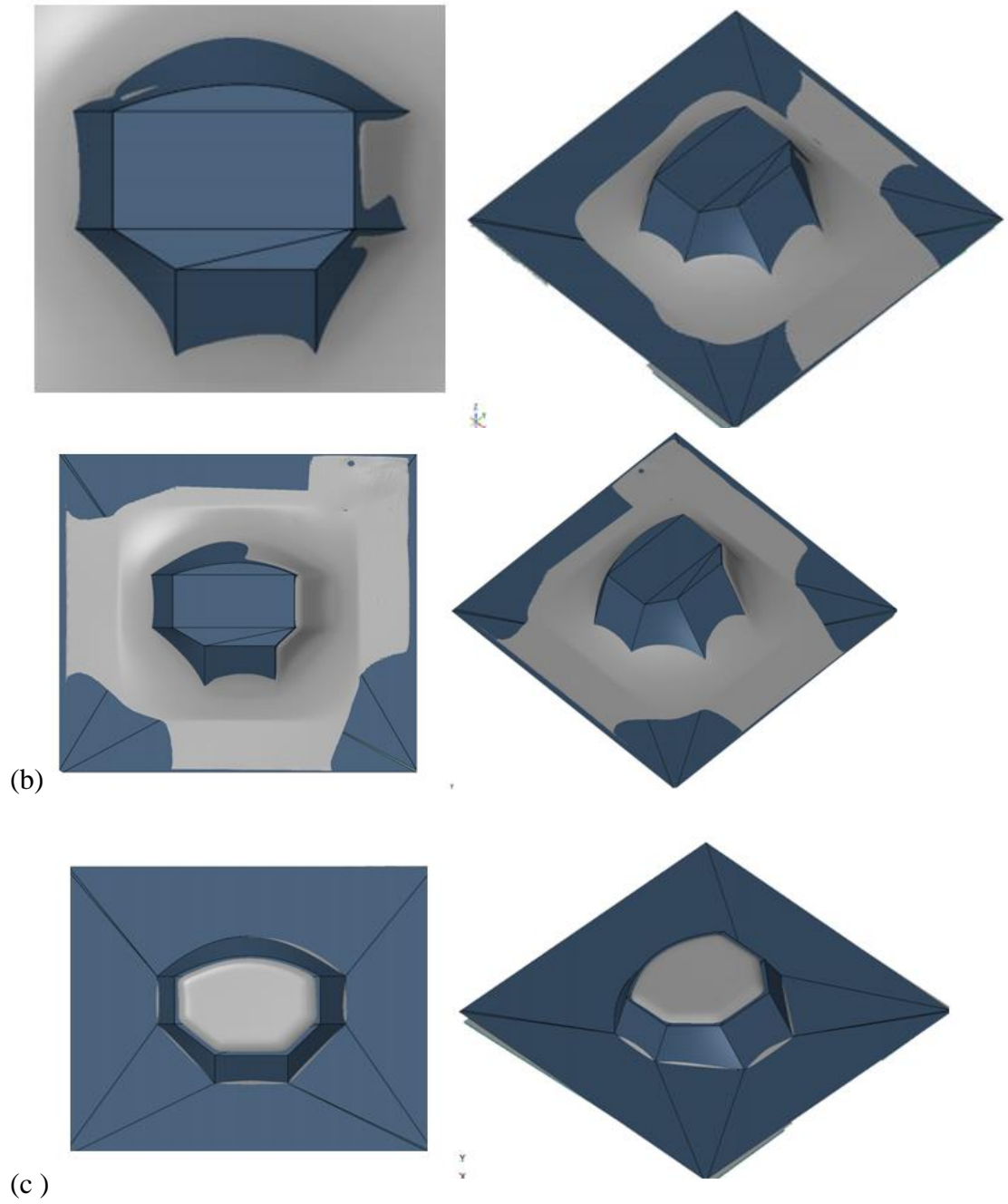


Figure 11-8 Qualitative CAD comparison; top and isometric view; (a) AA1-1050H, (b) AA2-1050H (c) AA3-1050H.

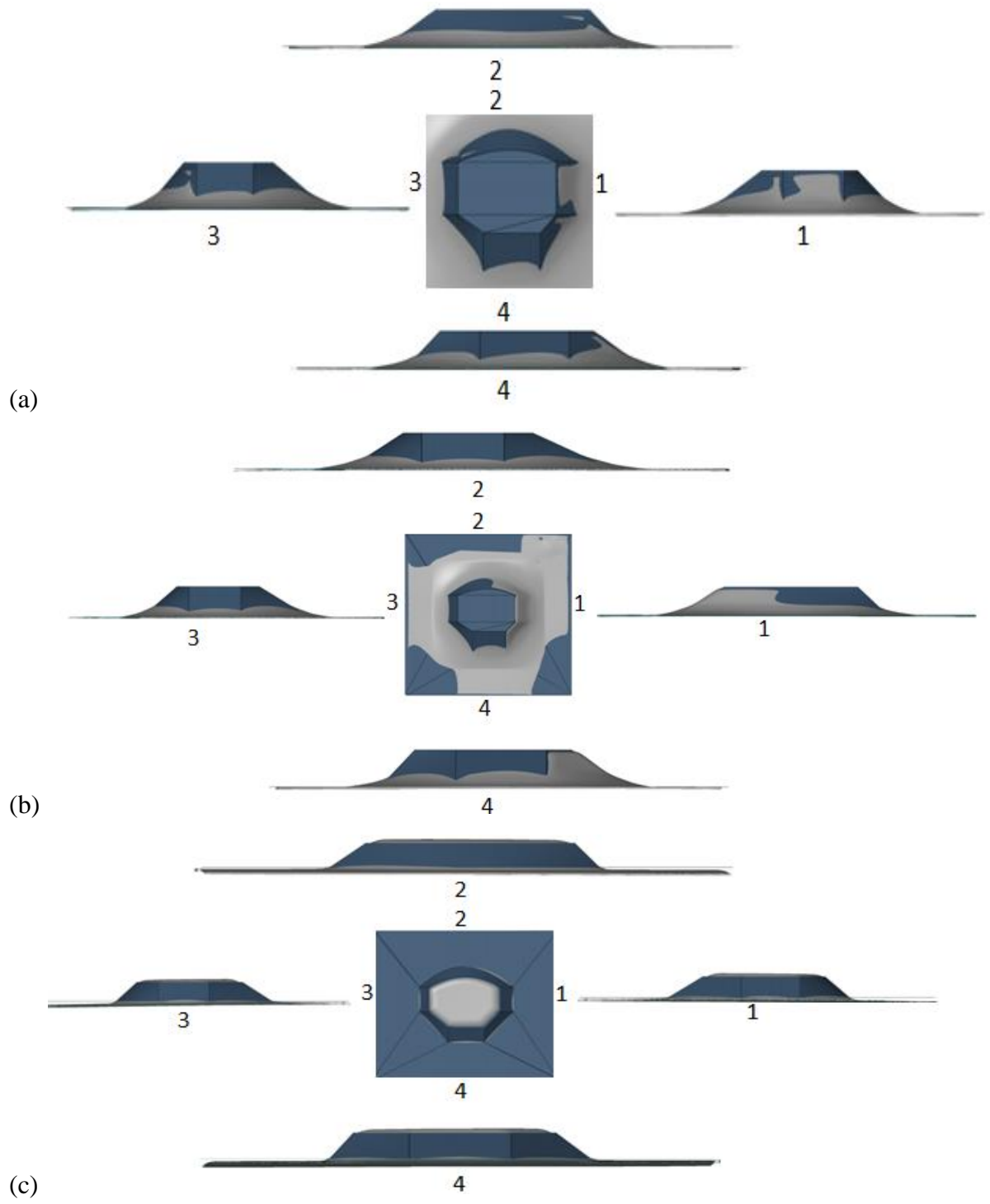


Figure 11-9 Qualitative CAD comparison; top and side views; (a) AA1-1050H, (b) AA2-1050H (c) AA3-1050H.

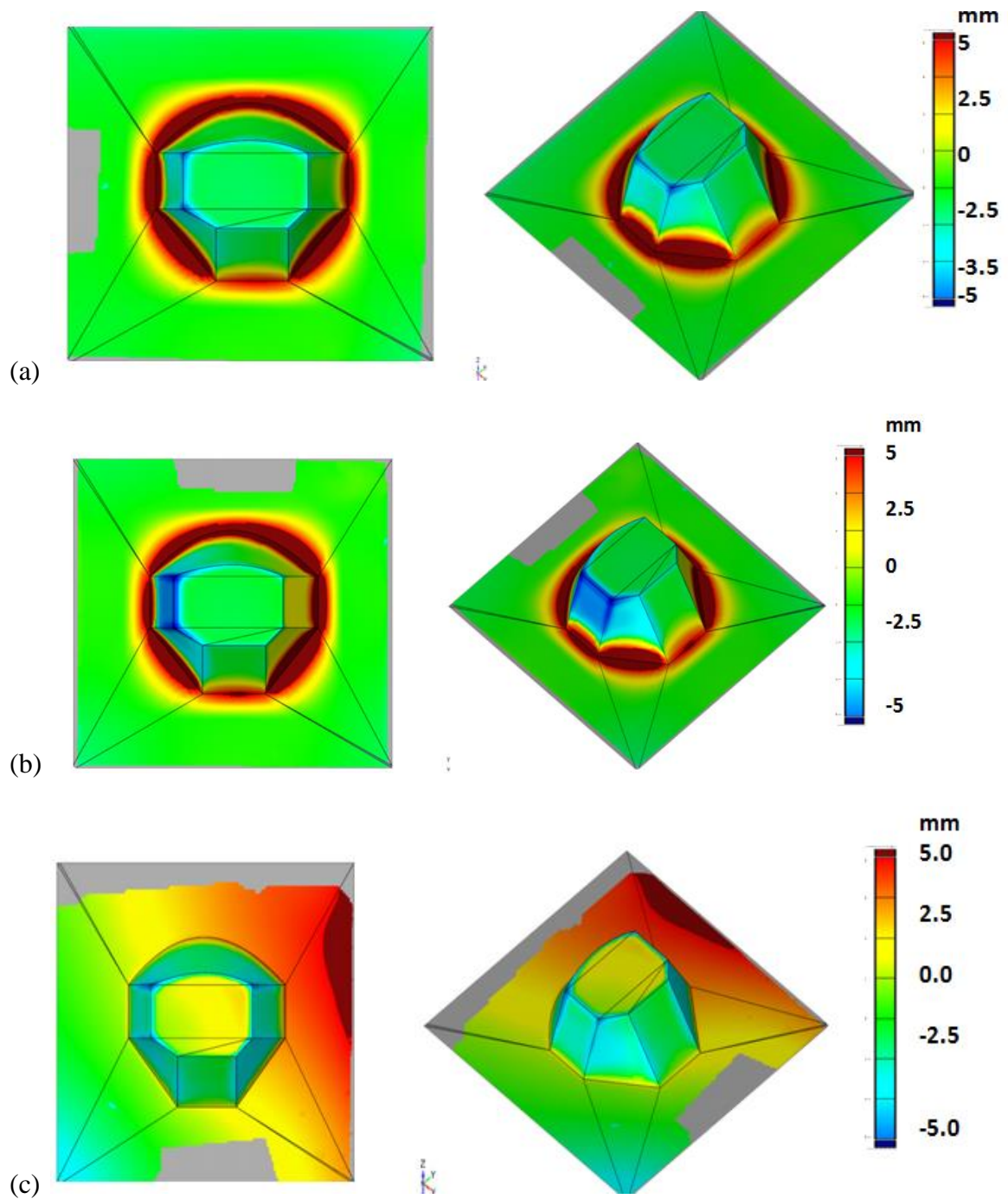


Figure 11-10 Quantitative CAD comparison; top and isometric view; (a) AA1-1050H, (b) AA2-1050H (c) AA3-1050H.

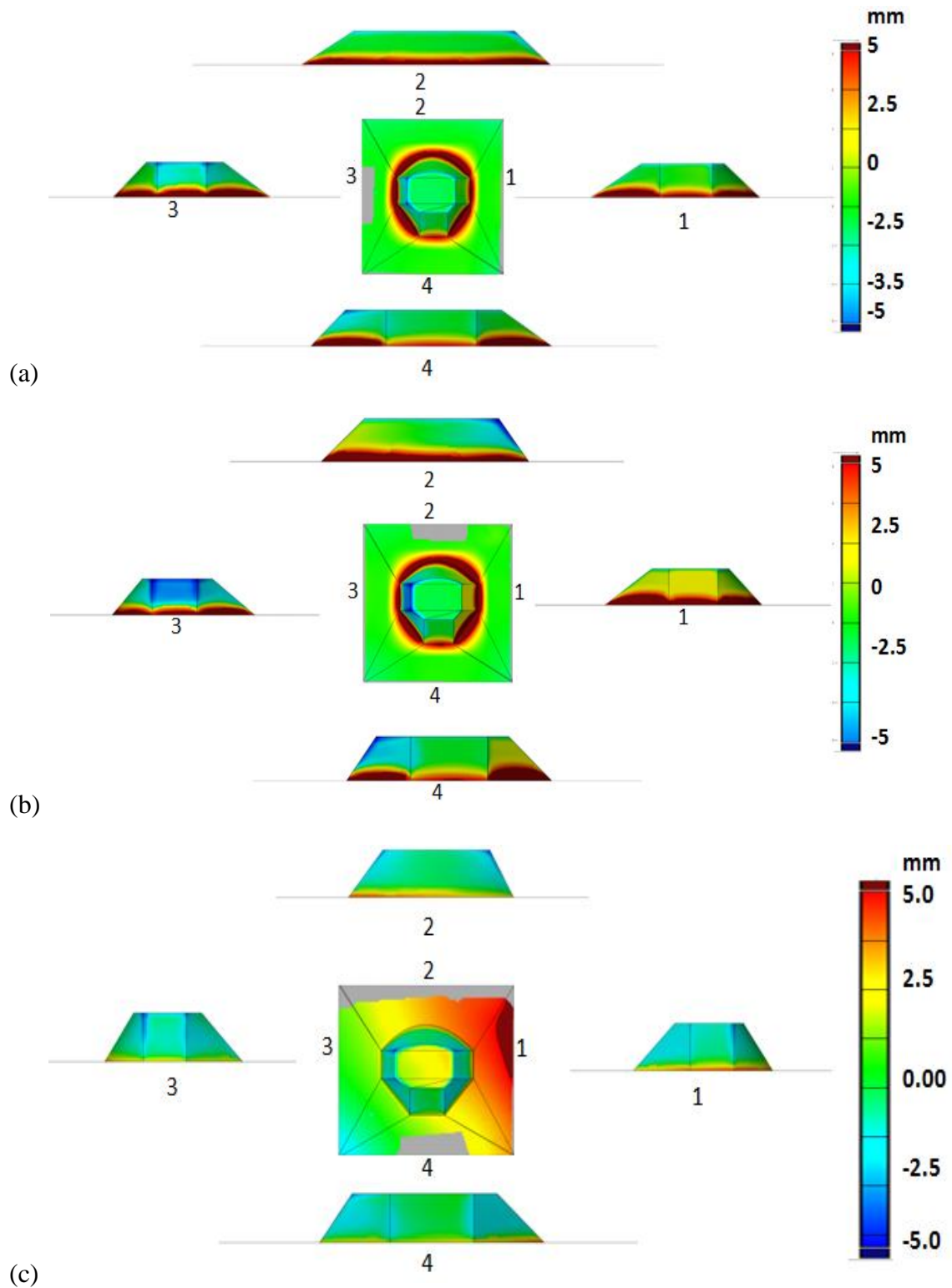


Figure 11-11 Quantitative CAD comparison; top and side views; (a) AA1-1050H, (b) AA2-1050H (c) AA3-1050H.

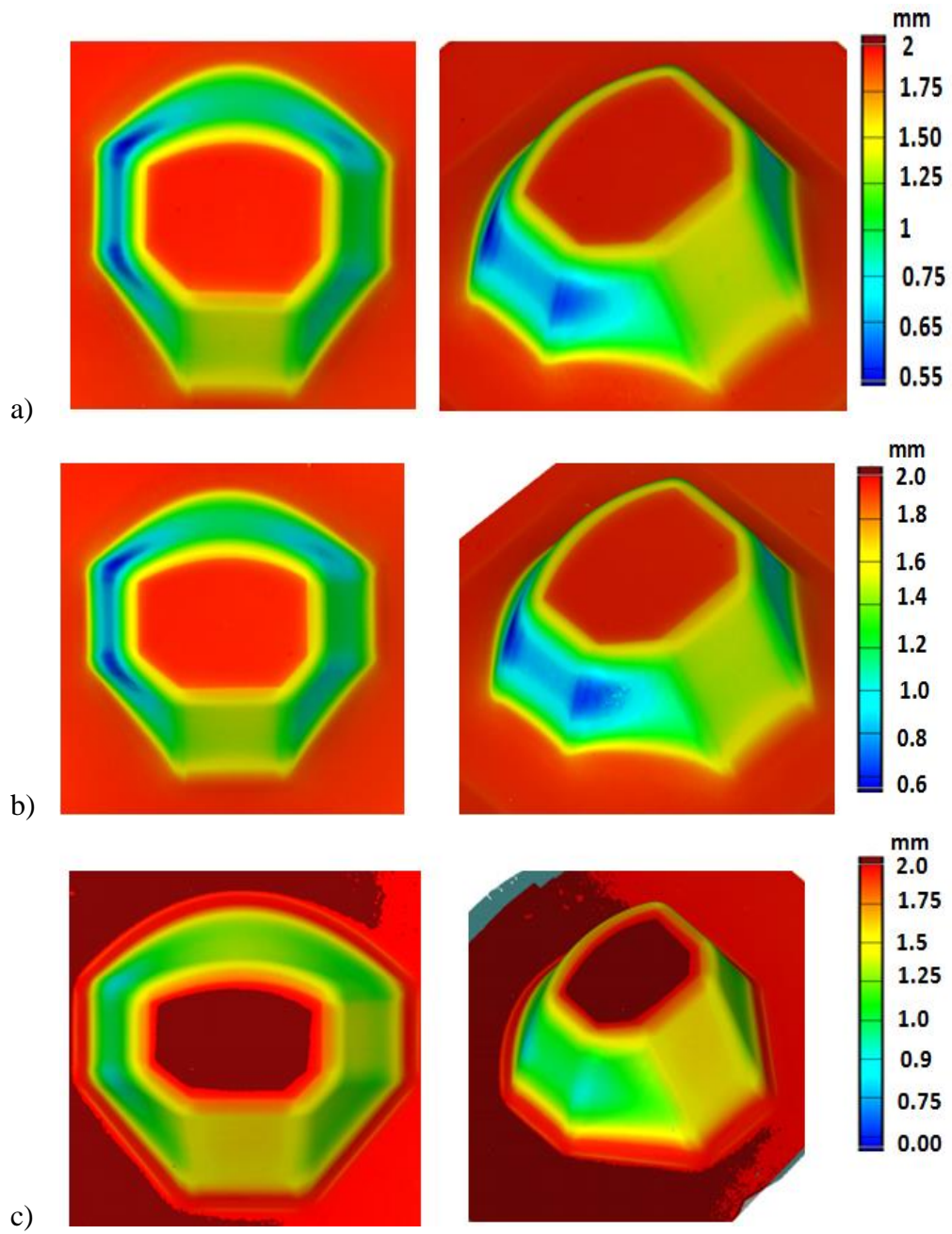


Figure 11-12 Thickness profile, top and isometric view; (a) AA1-1050H, (b) AA2-1050H (c) AA3-1050H.

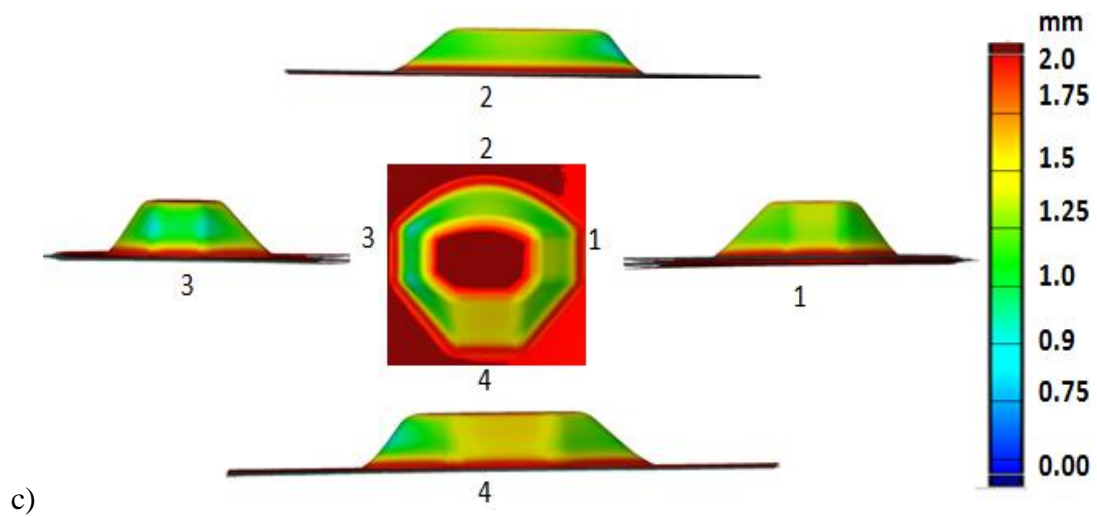
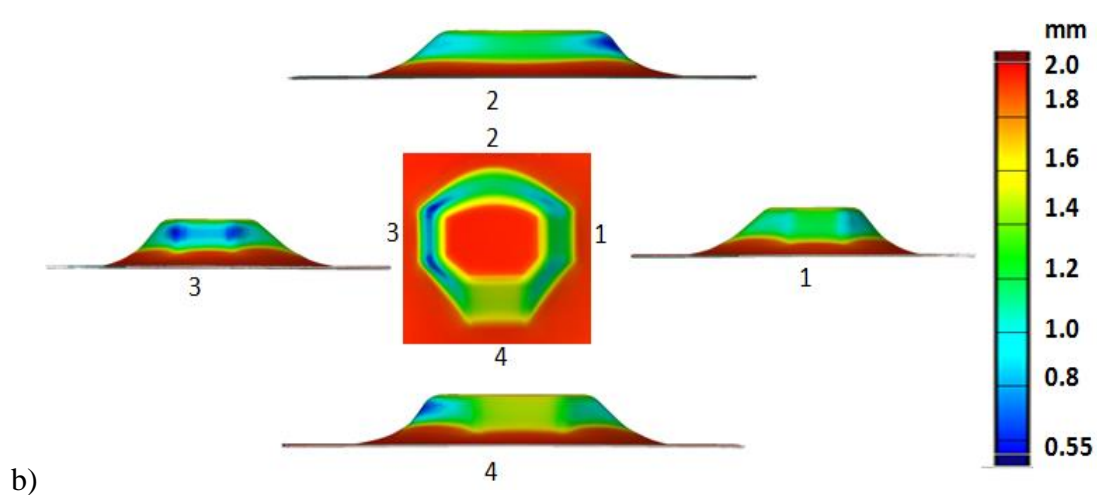
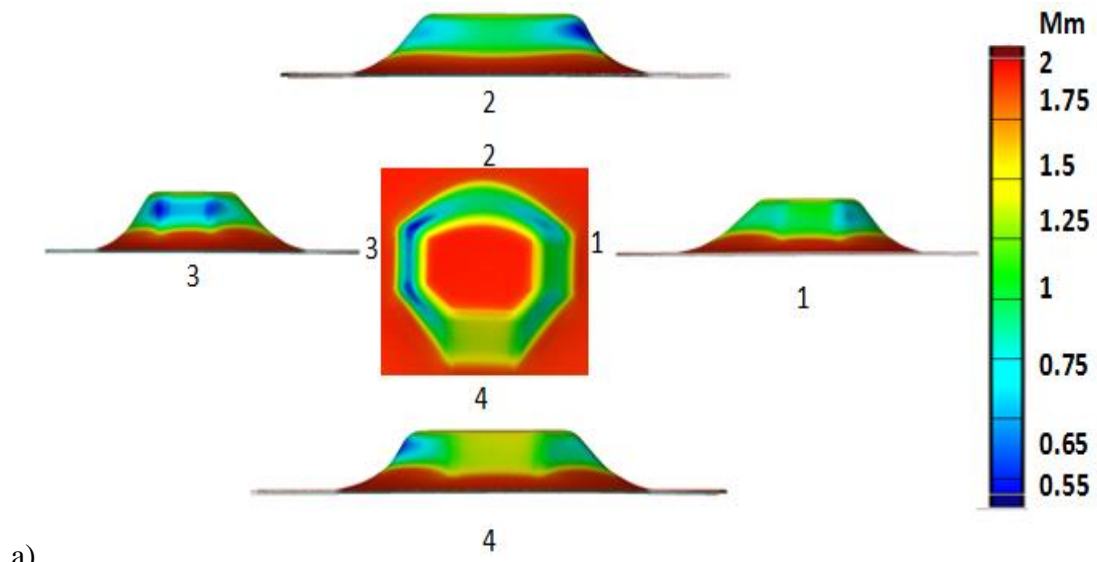
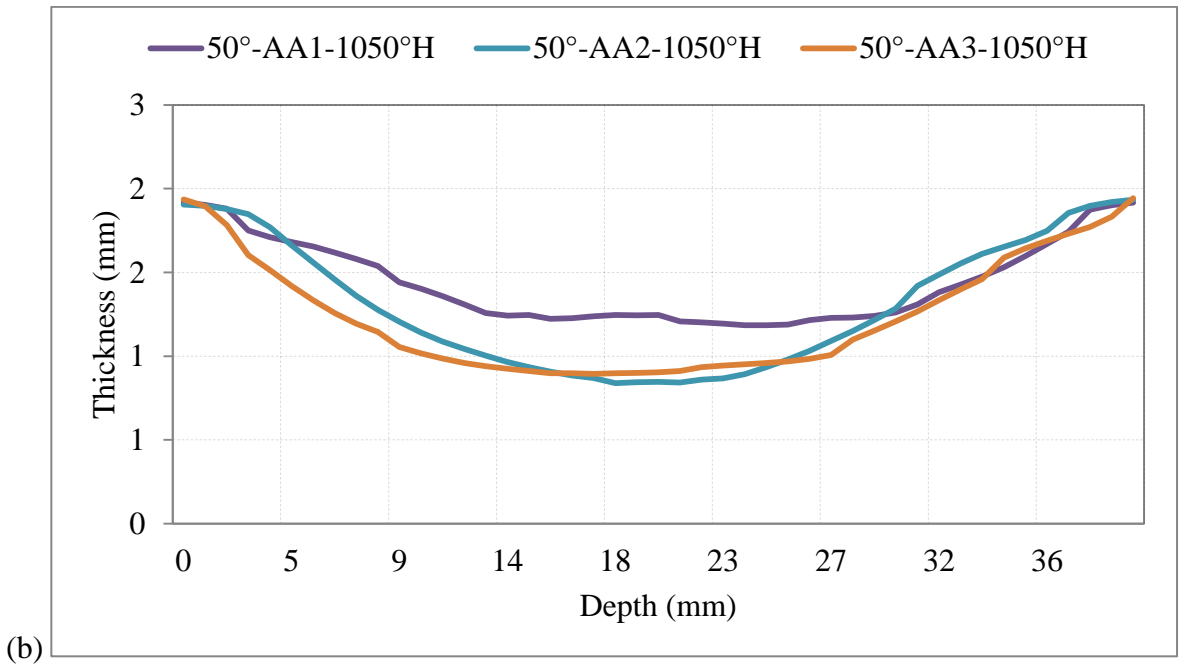
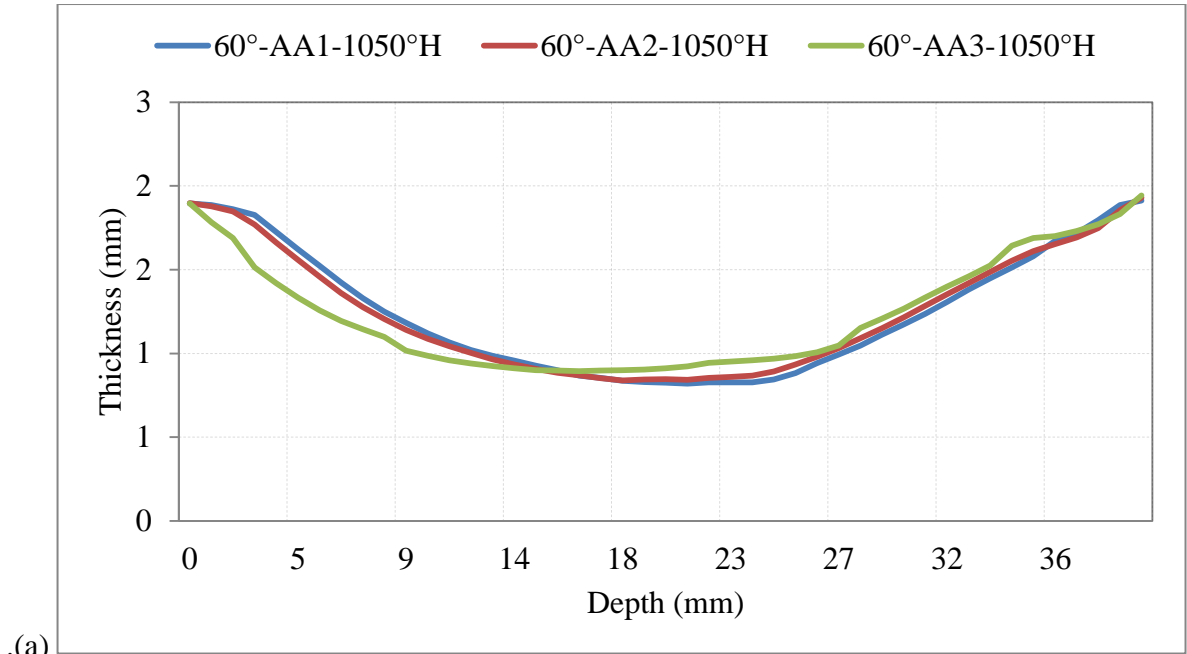
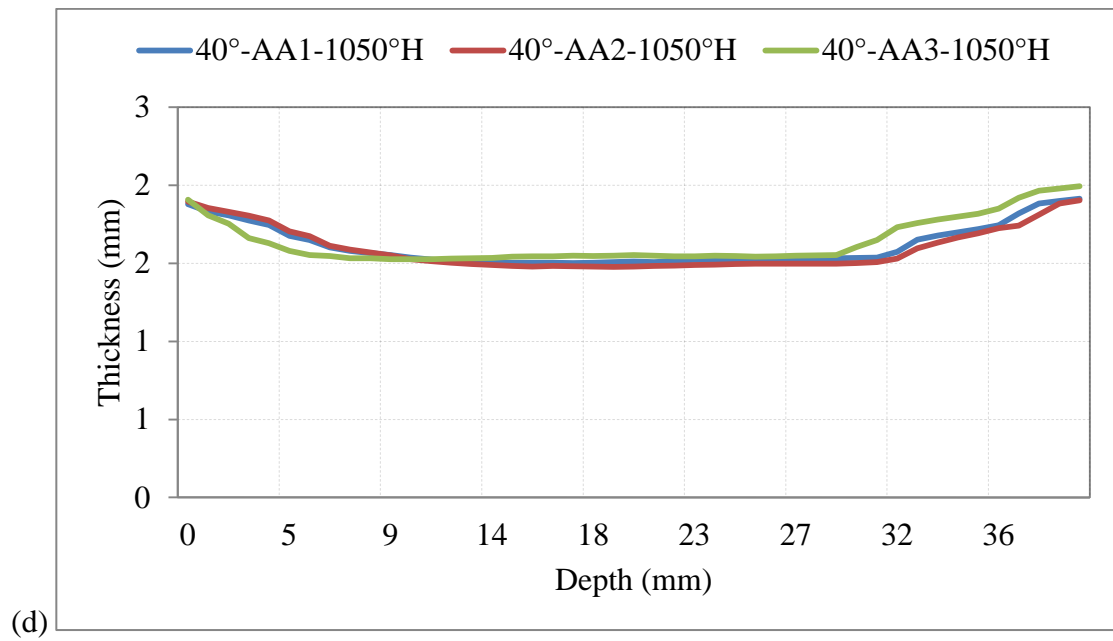
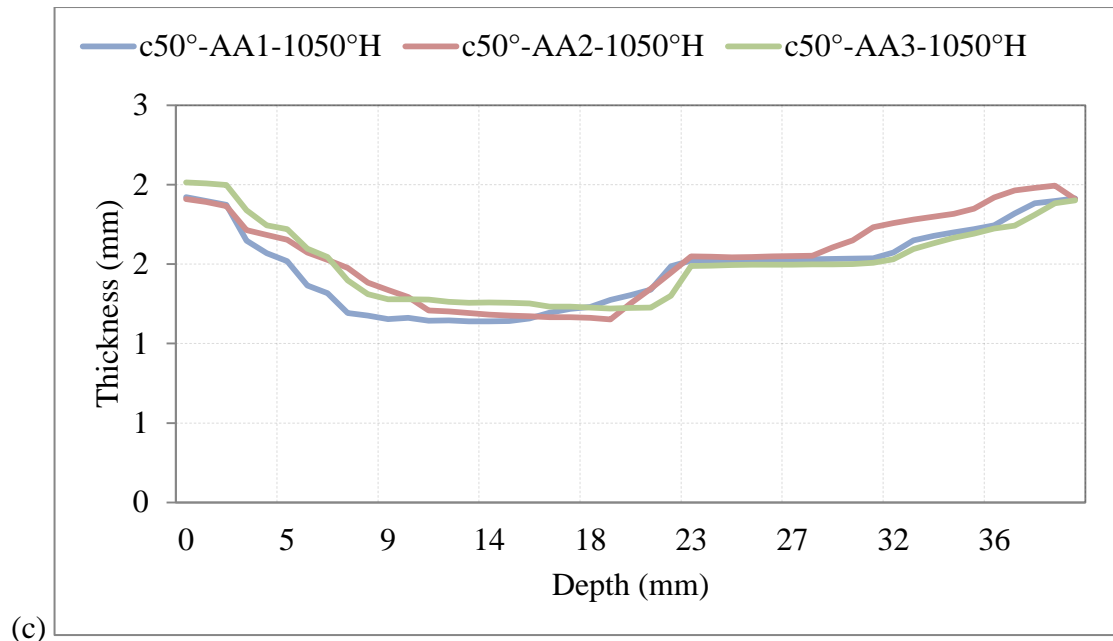
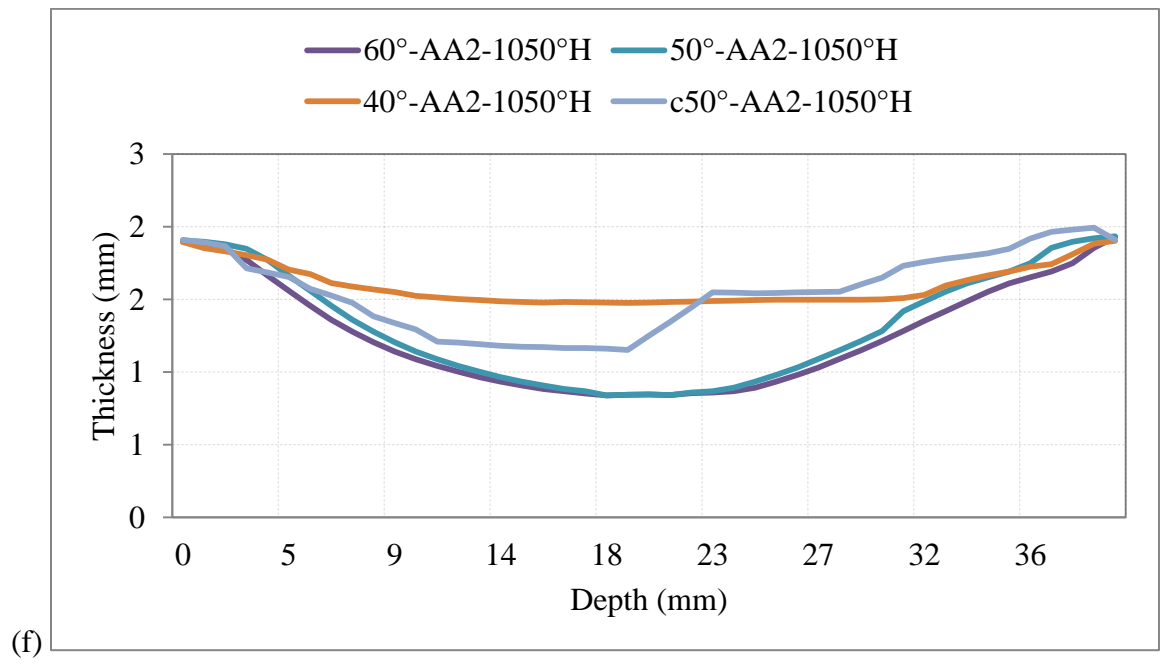
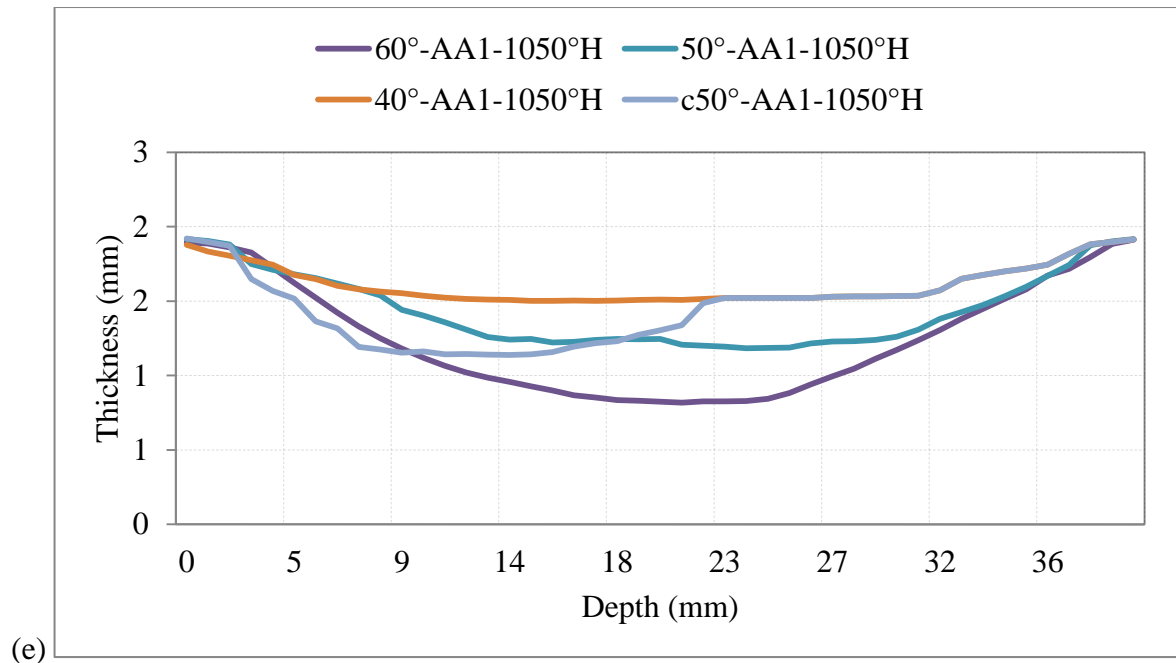


Figure 11-13 Thickness profile top and side views; (a) AA1-1050H, (b) AA2-1050H, (c) AA3-1050H.









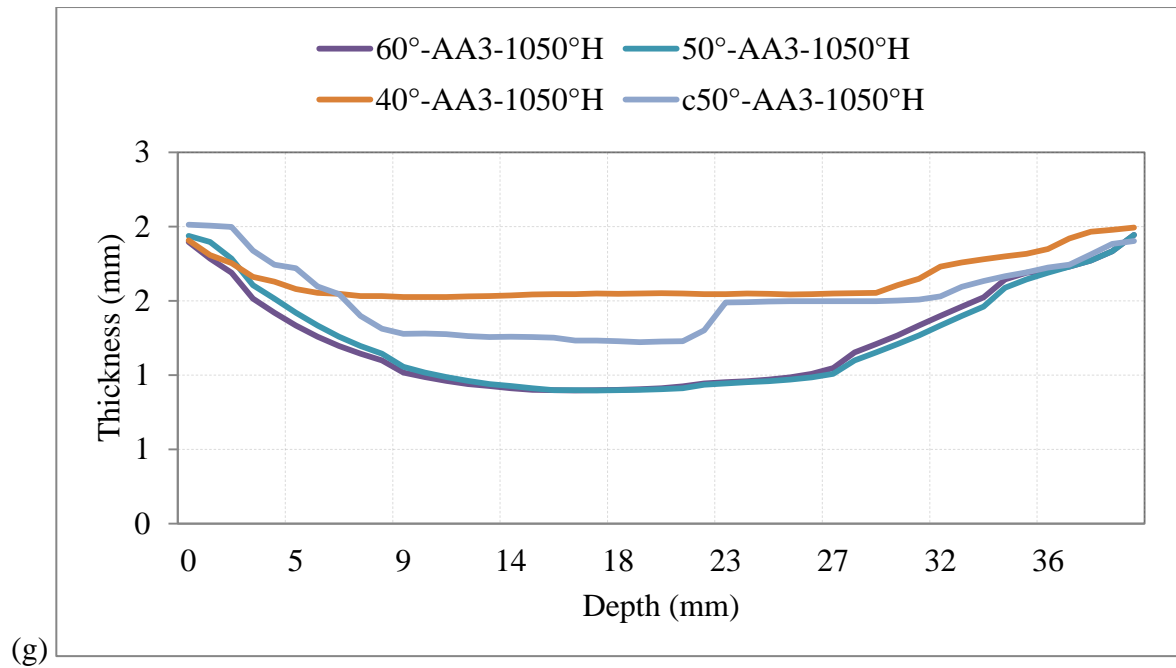


Figure 11-14 Thickness vs Depth AA1-7075 AA2-7075 & AA3-1050H; (a) 60°, (b) 50°, (c) Curve 50°, (d) 40°, (e) Wall angle Comparison AA1-1050H, (f) Wall angle Comparison AA2-1050H, (g) Wall angle Comparison AA3-1050H.

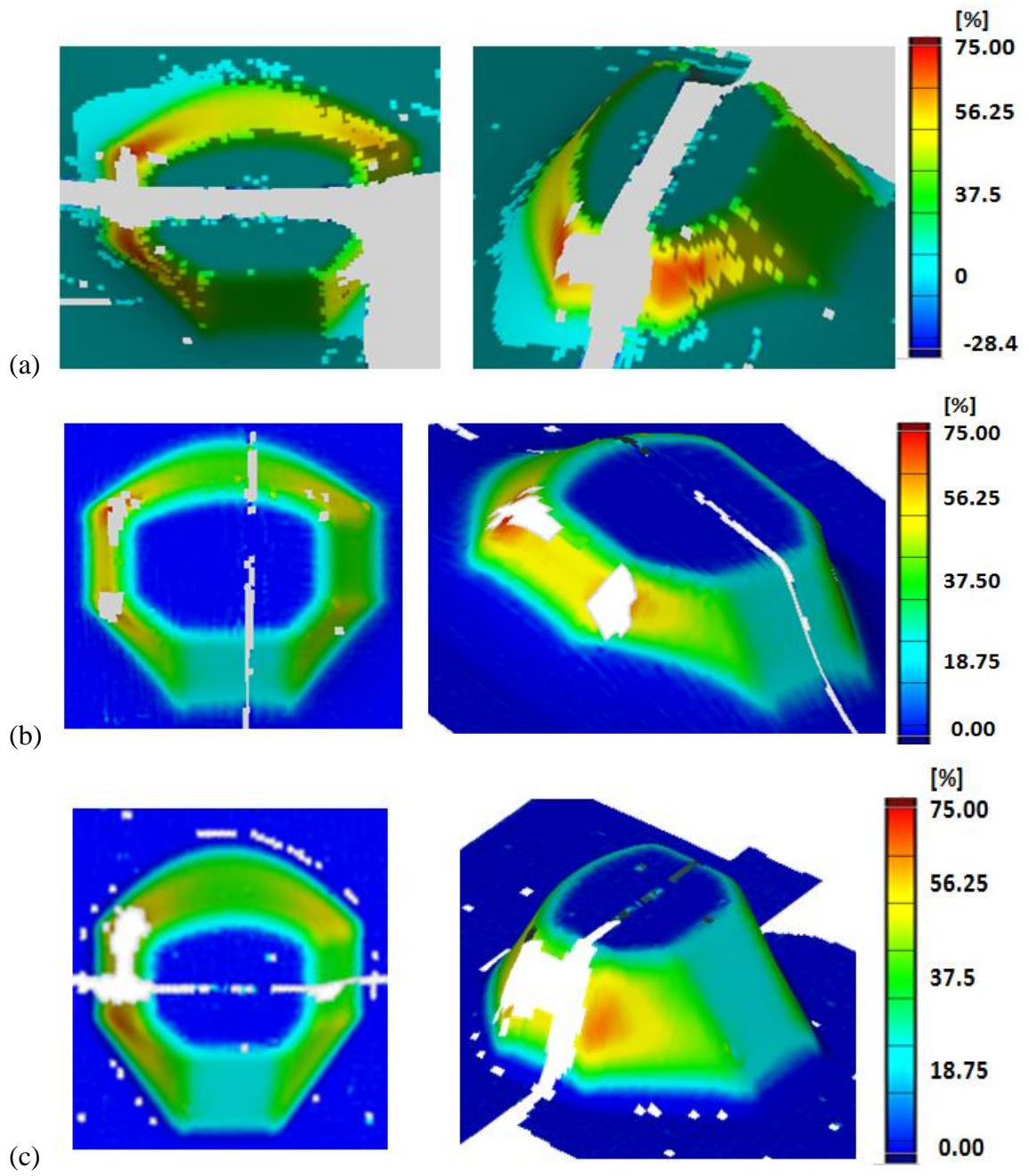


Figure 11-15 Thickness reduction; top and isometric view , (a) AA1-1050H, (b) AA2-1050H (c) AA3-1050H.

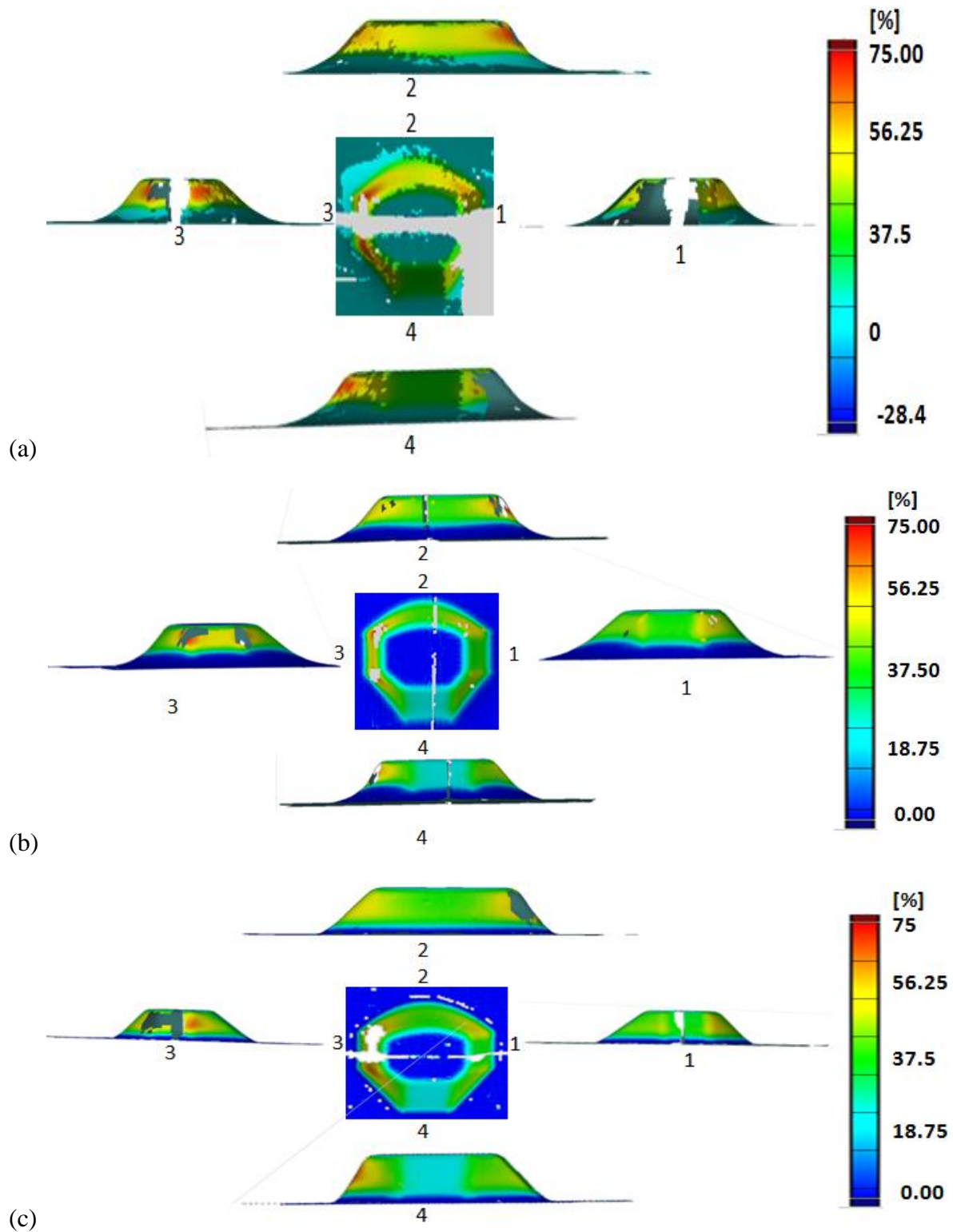
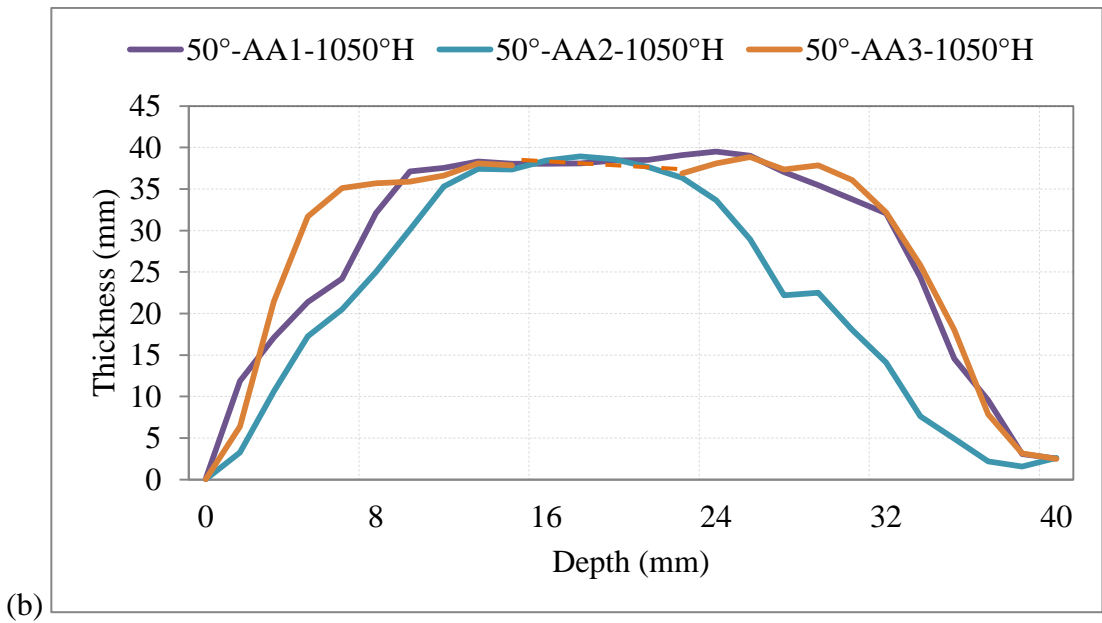
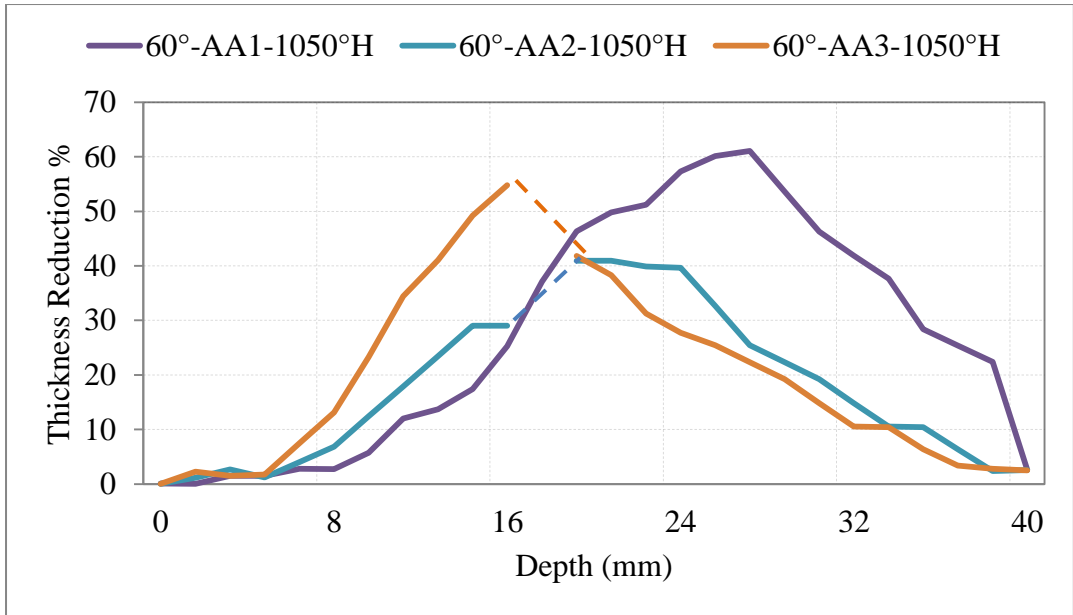
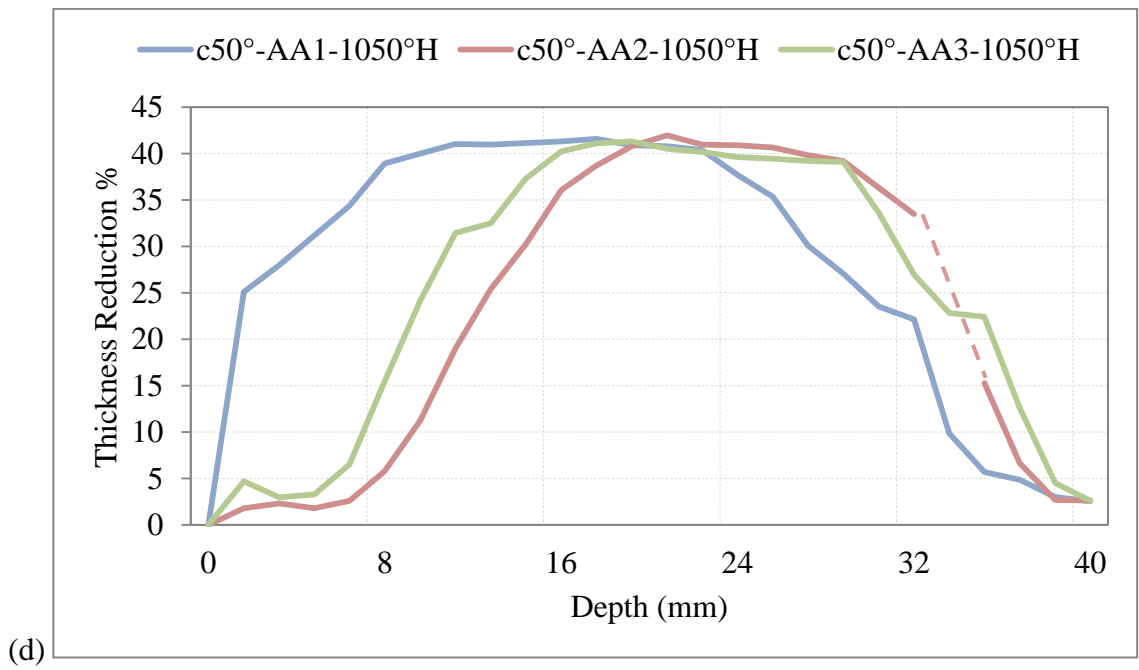
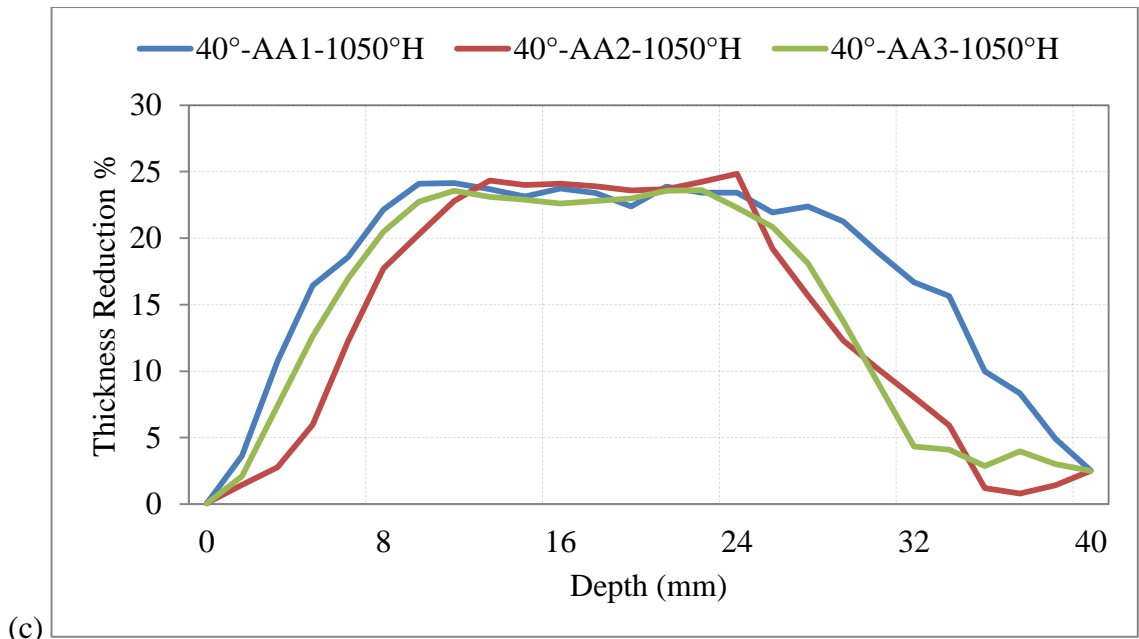
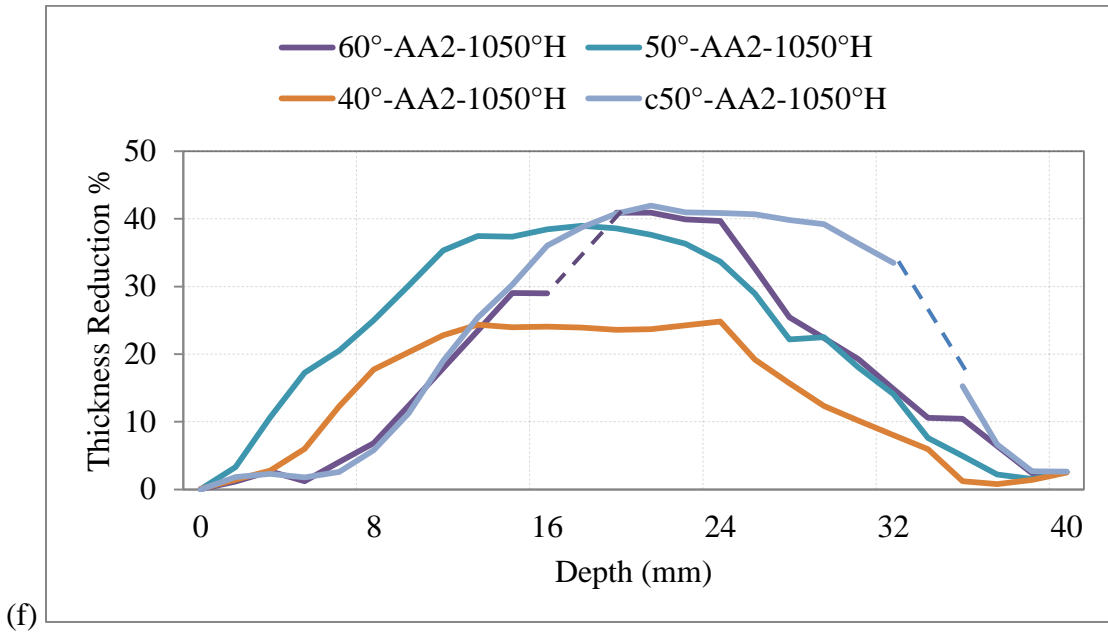
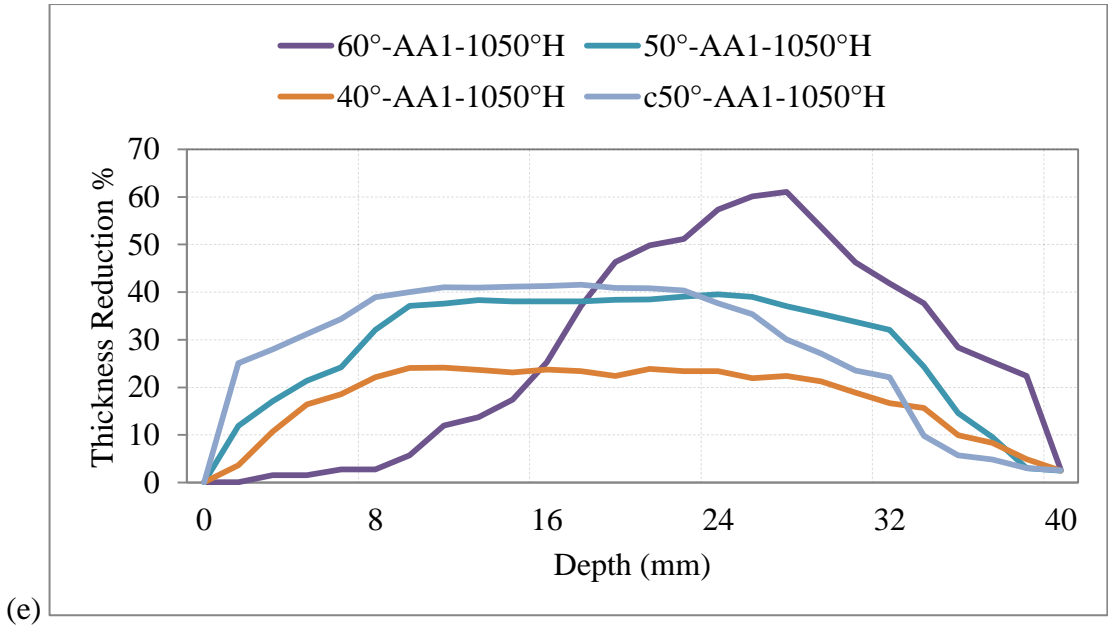


Figure 11-16 Thickness reduction; top and side views, (a) AA1-1050H, (b) AA2-1050H (c) AA3-1050H.



(b)





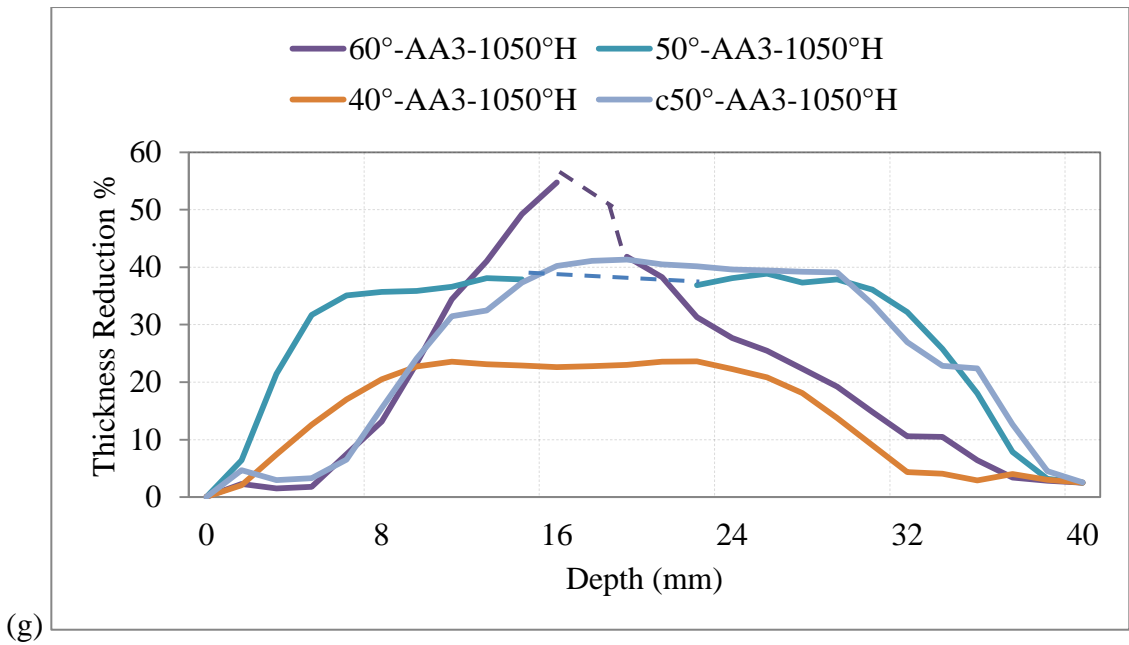


Figure 11-17 Thickness reduction% vs Depth AA1-1050H AA2-1050H & AA3-1050H; (a) 60°, (b) 50°, (c) 40°, (d) Curve 50°, (e) Wall angle Comparison AA1-1050H, (f) Wall angle Comparison AA2-1050H, (g) Wall angle Comparison AA3-1050H



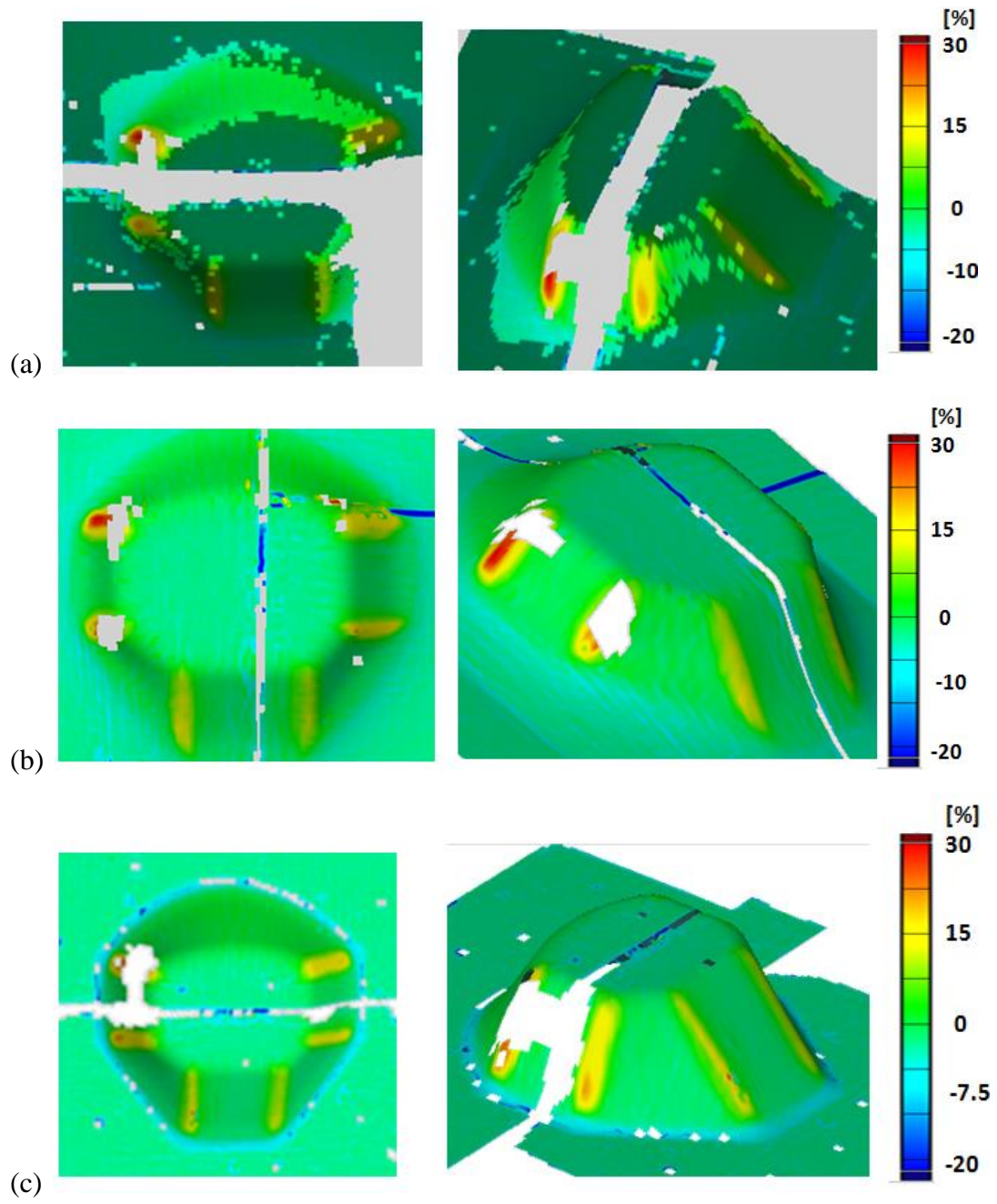


Figure 11-18 Minor strain; top and isometric view (a) AA1-1050H, (b) AA2-1050H (c) AA3-1050H.

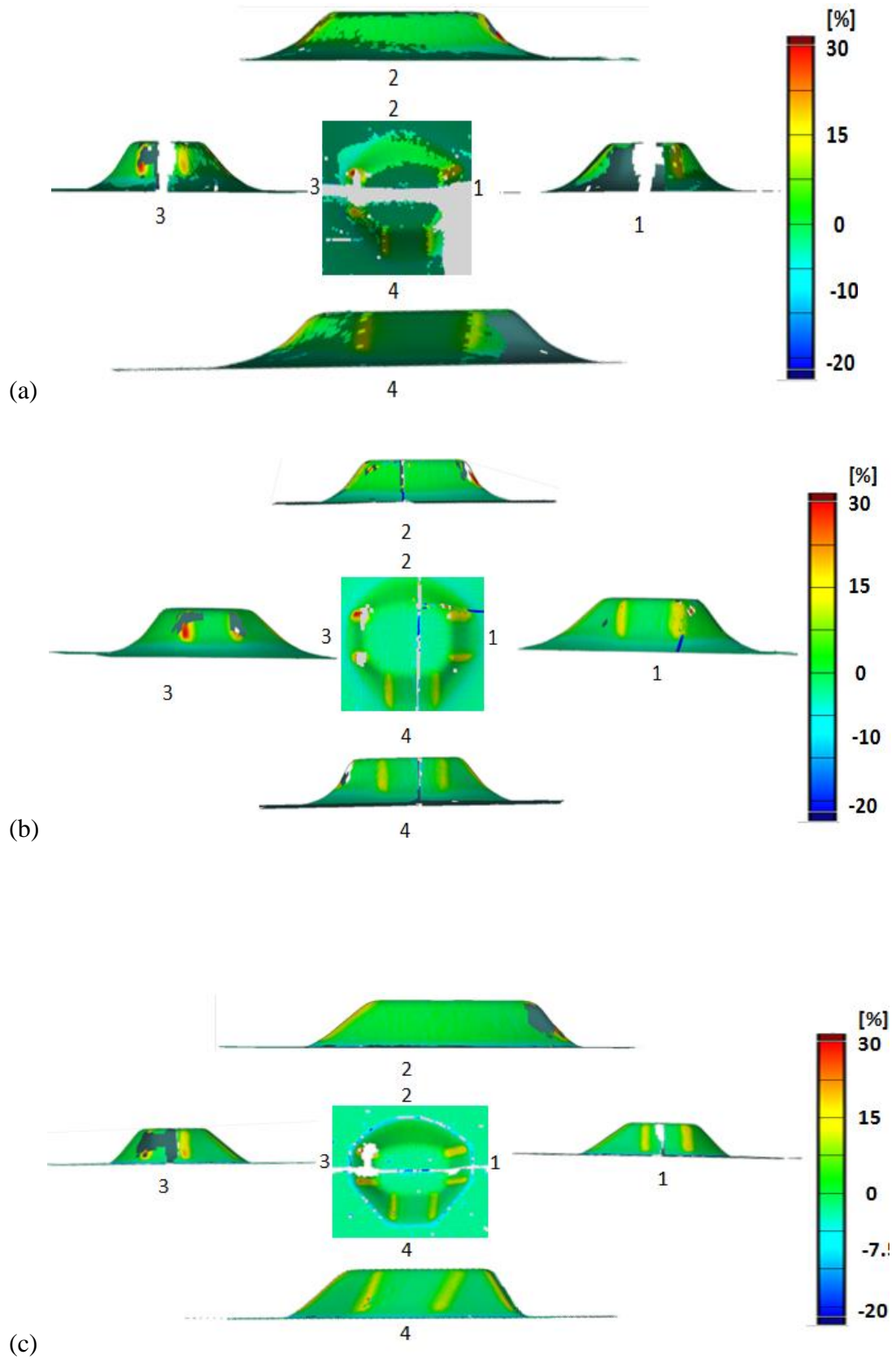


Figure 11-19 Minor strain; top and side views (a) AA1-1050H (b) AA2-1050H (c) AA3-1050H.

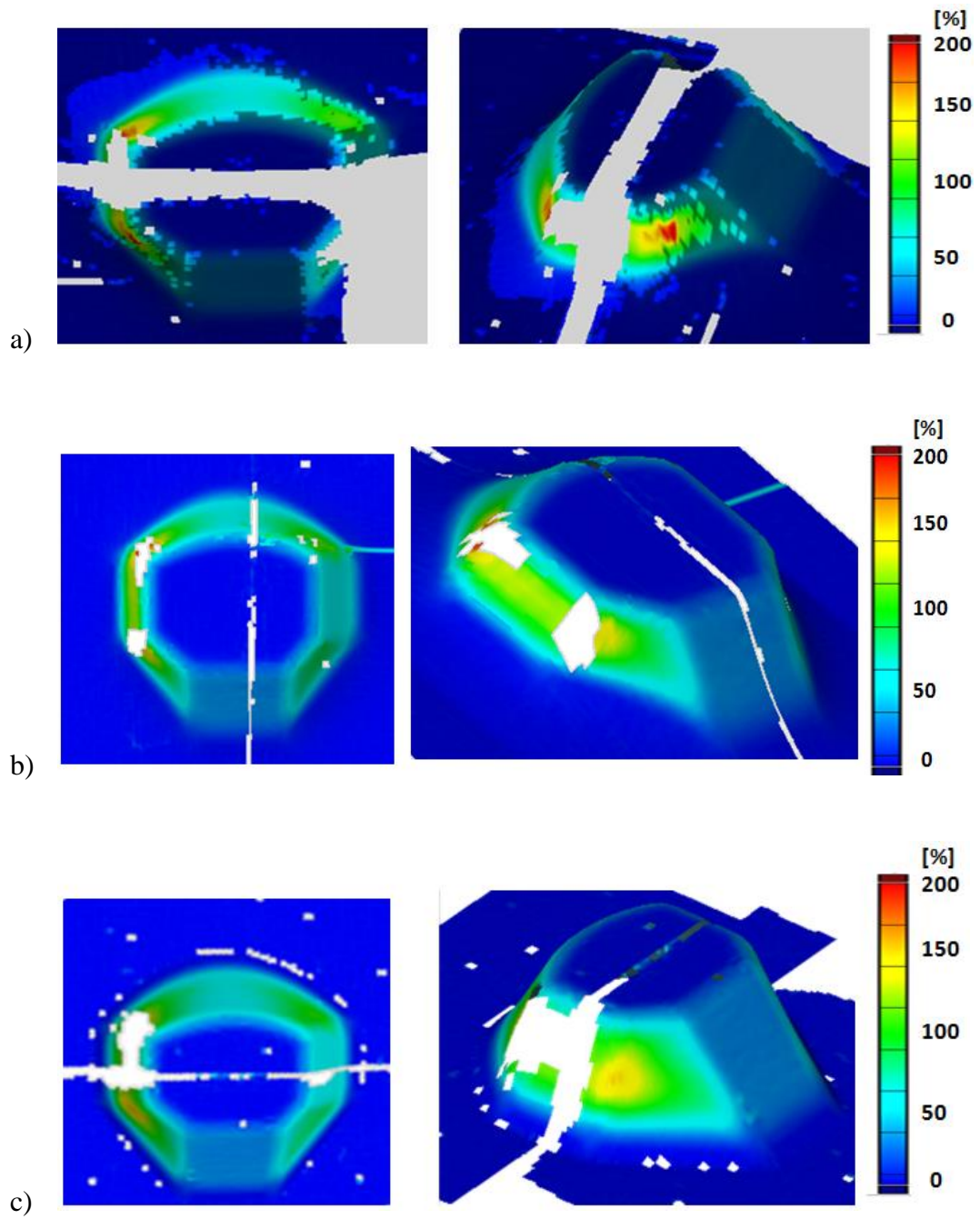


Figure 11-20 Major strain; top and isometric view (a) AA1-1050H, (b) AA2-1050H (c) AA3-1050H.

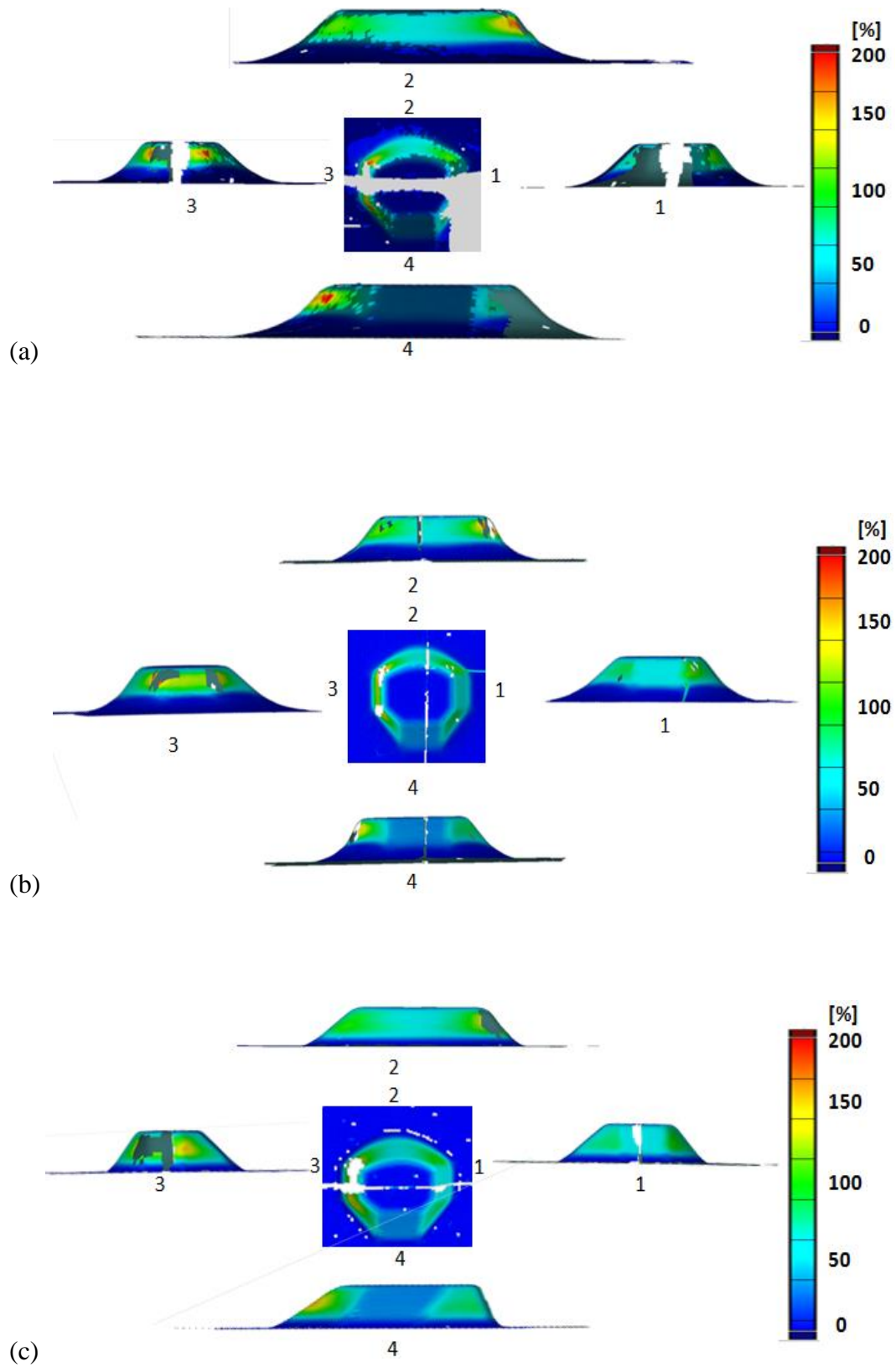
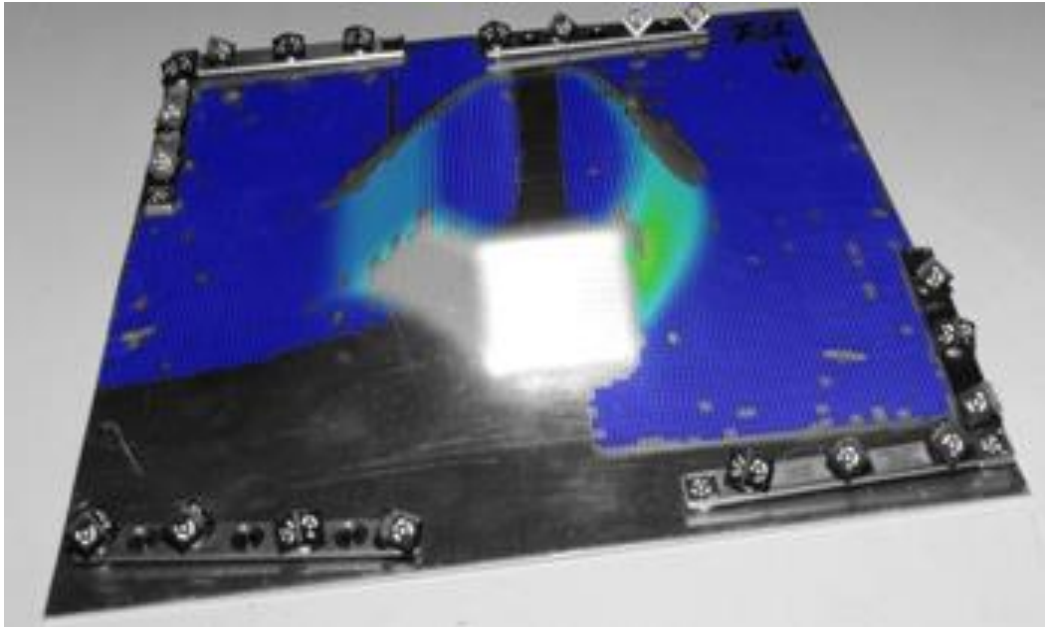
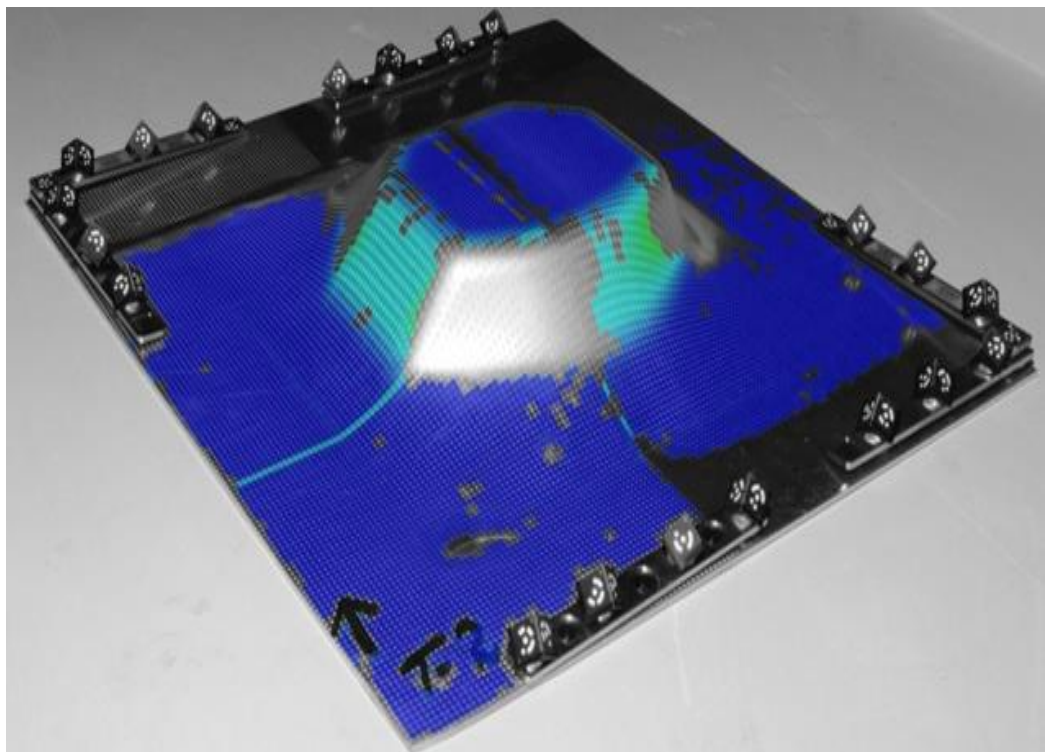


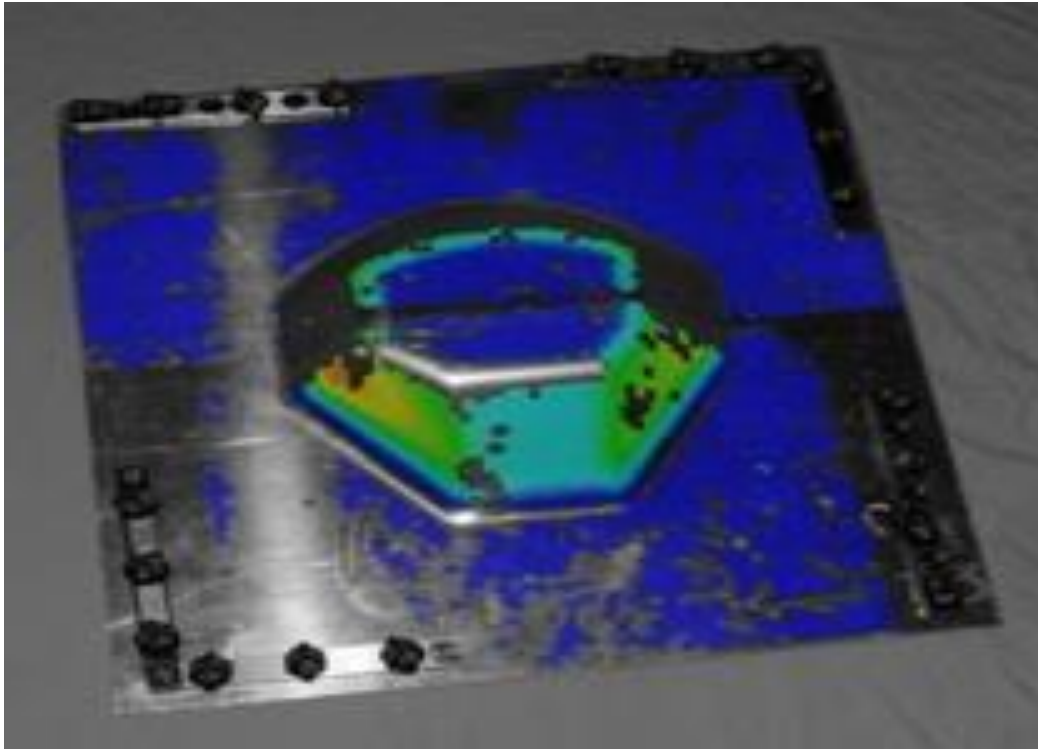
Figure 11-21 Major strain; top and side views (a) AA1-1050H, (b) AA2-1050H, (c) AA3-1050H.



a)



b)



c)

Figure 11-22 a) Major strains plotted on formed AA1-1050H, (b) Major strains plotted on formed AA2-1050H component (c) Major strains plotted on formed AA3-1050H component.

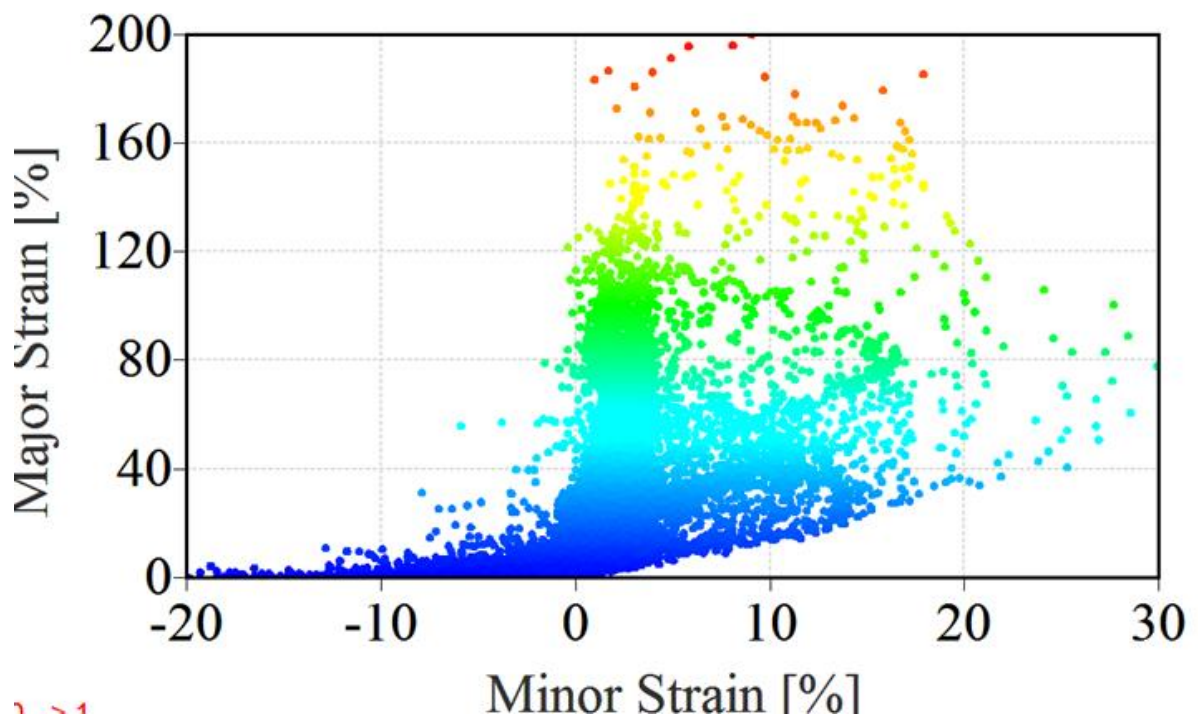


Figure 11-23 Major and minor strain graph AA1-1050H.

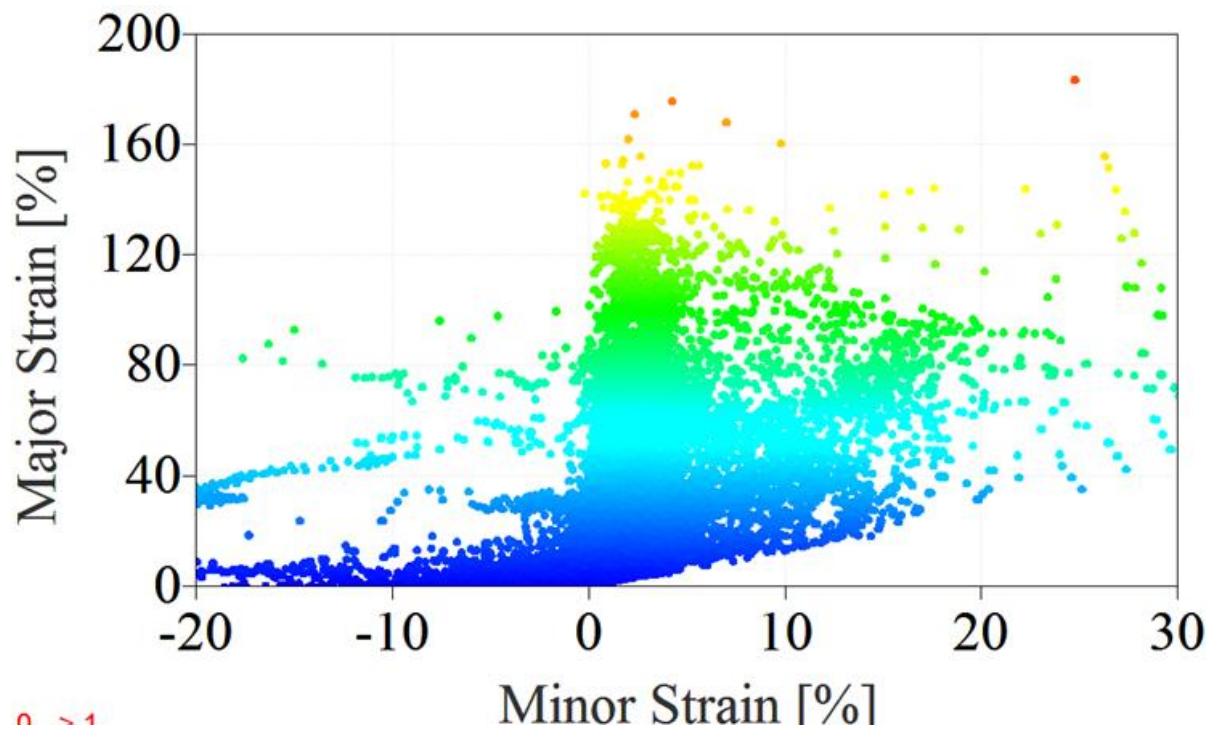


Figure 11-24 Major and minor strain graph AA2-1050H.

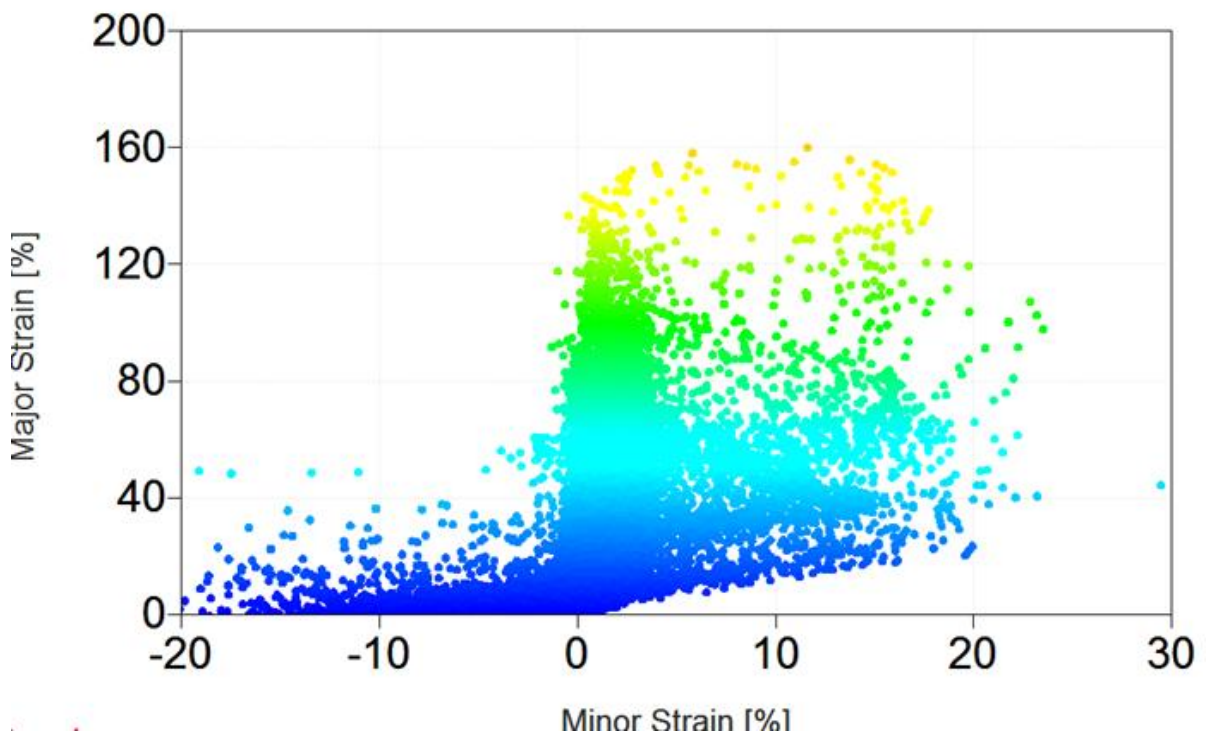


Figure 11-25 Major and minor strain graph AA3-1050H.

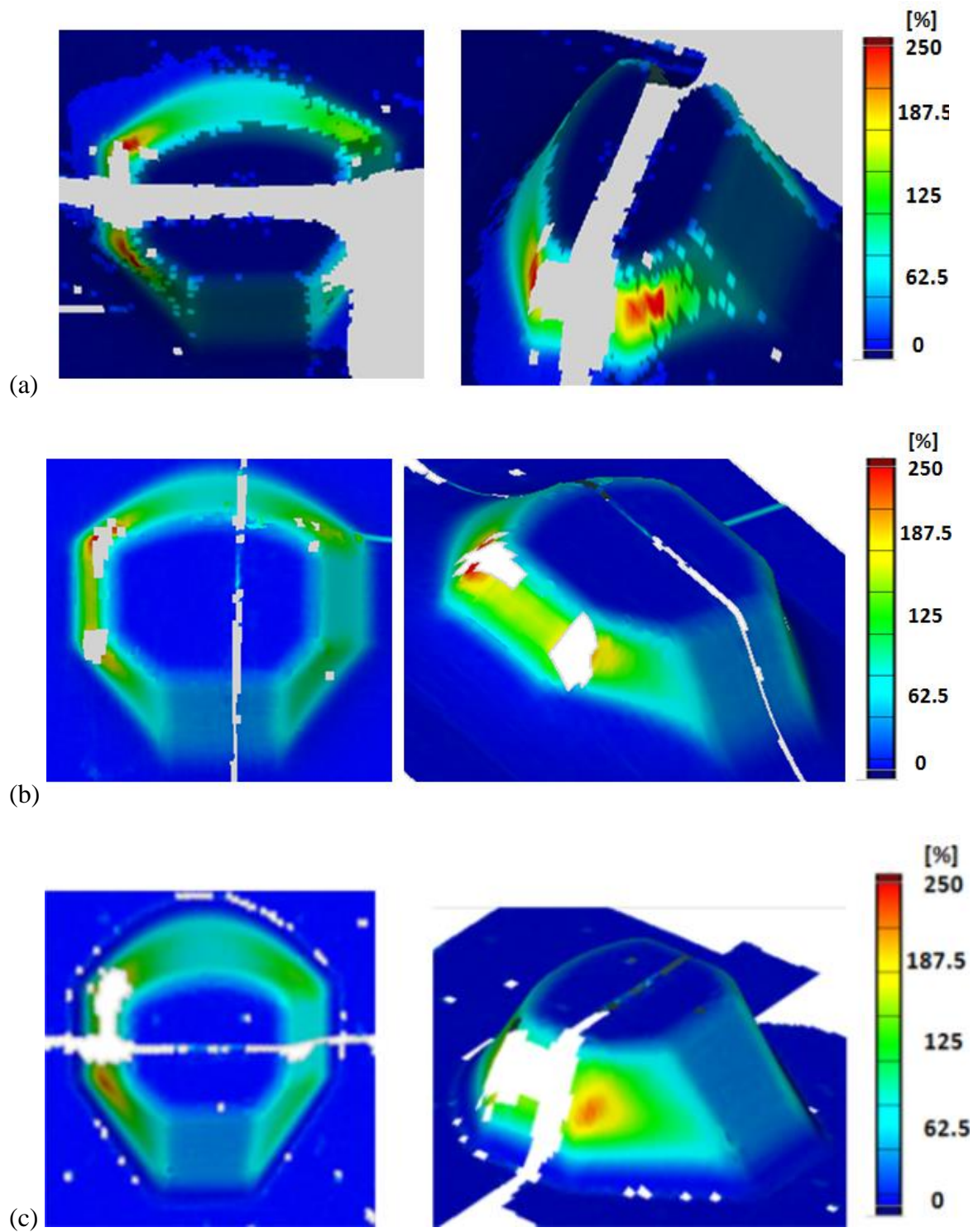


Figure 11-26 Von Mises strains, top and isometric view; (a) AA1-1050, (b) AA2-1050, (c) AA3-1050.



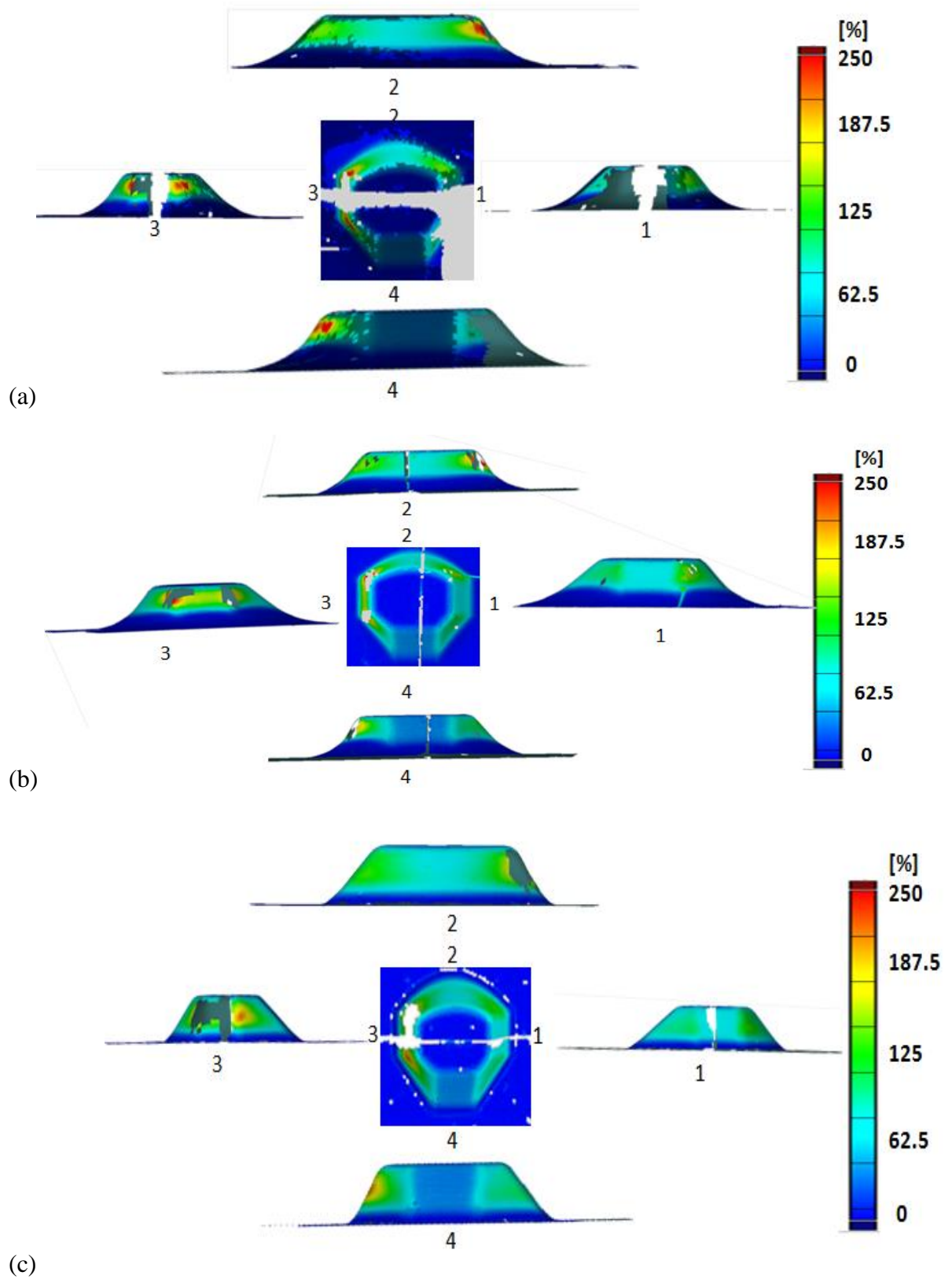
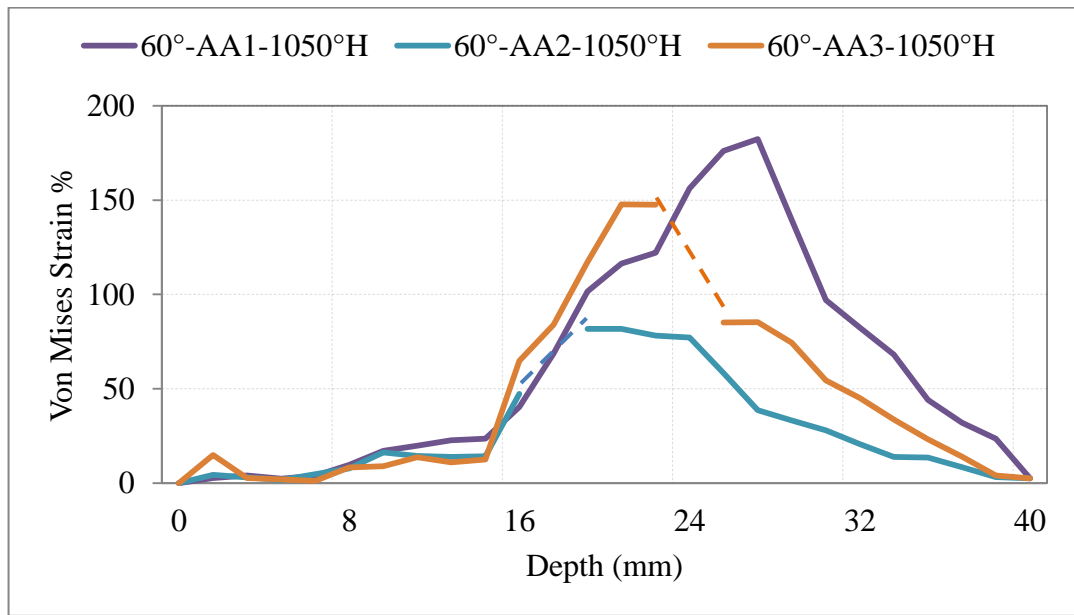
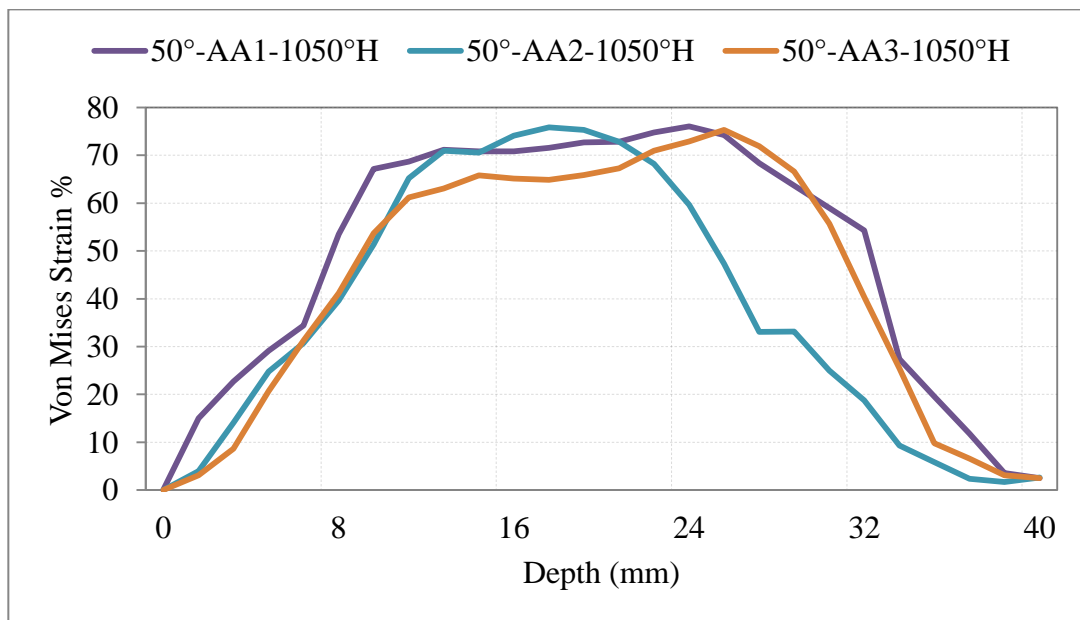


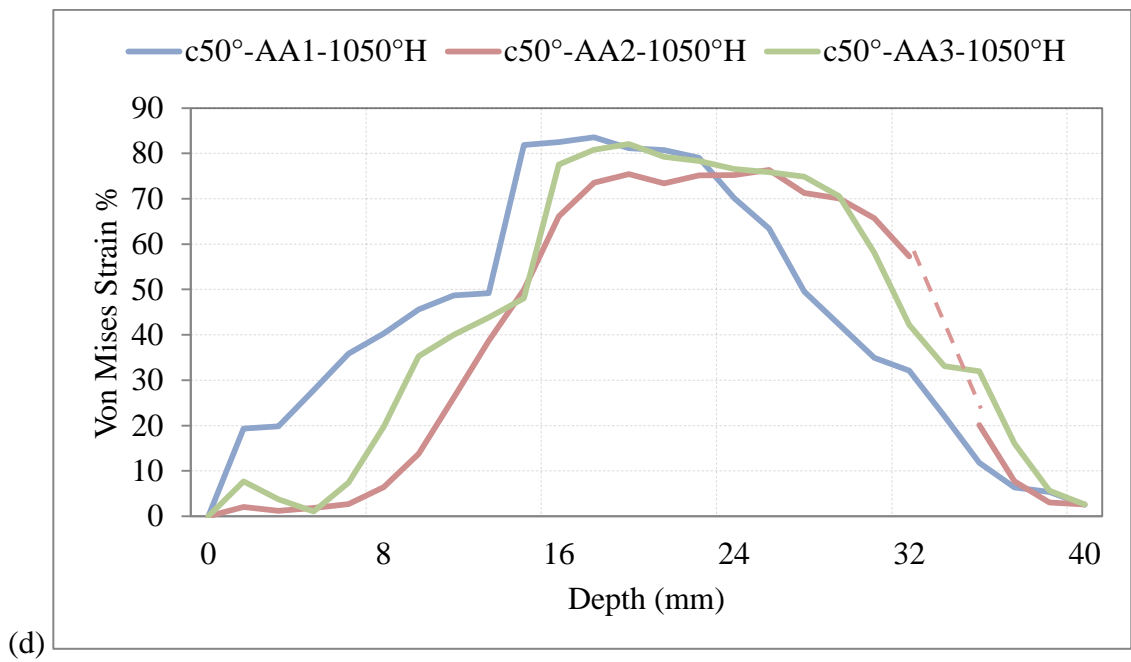
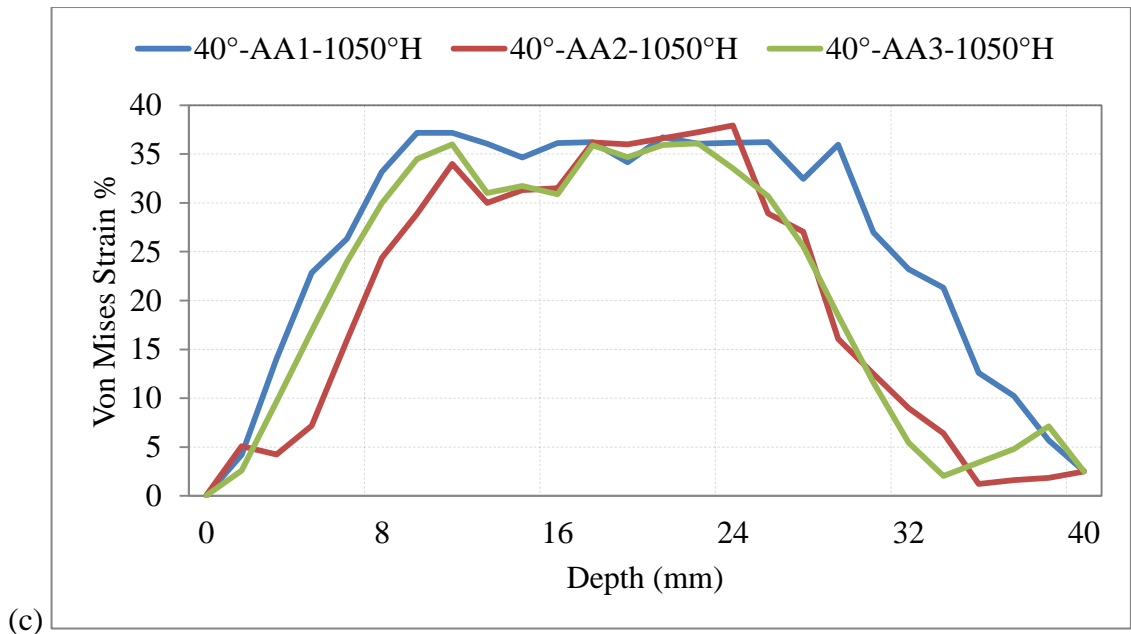
Figure 11-27 Von Mises strains, top and side view; (a) AA1-1050, (b) AA2-1050, (c) AA3-1050.

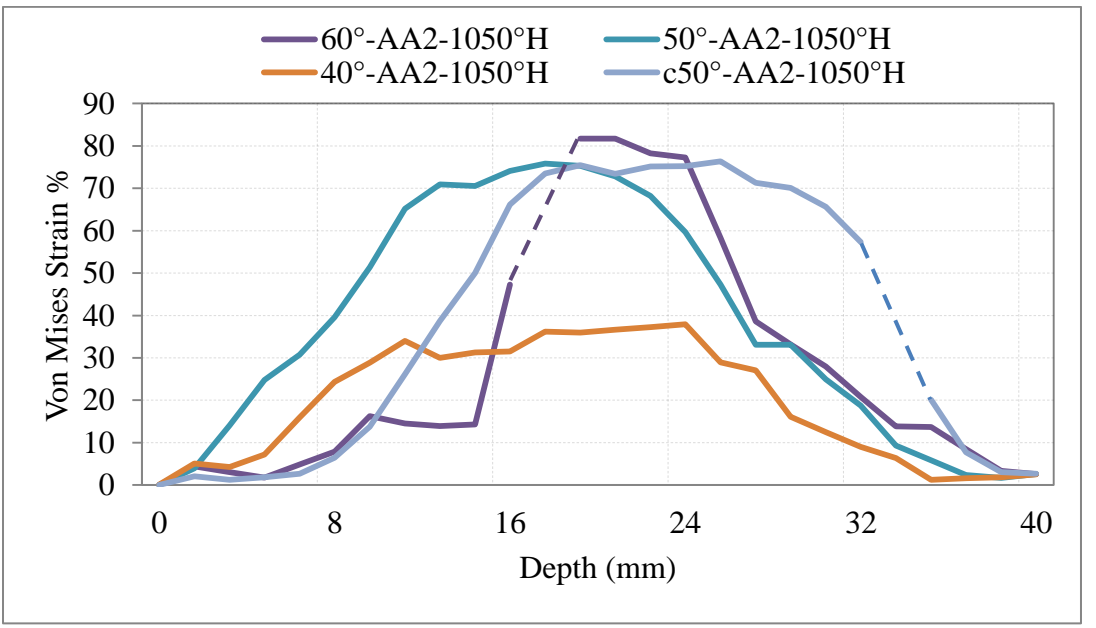
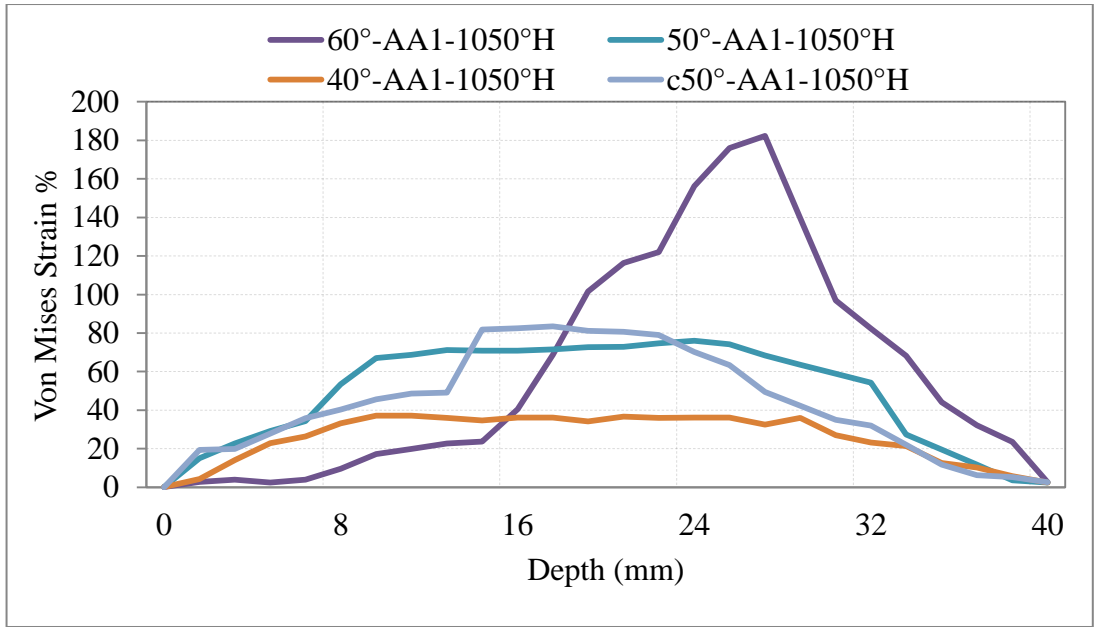


(a)



(b)





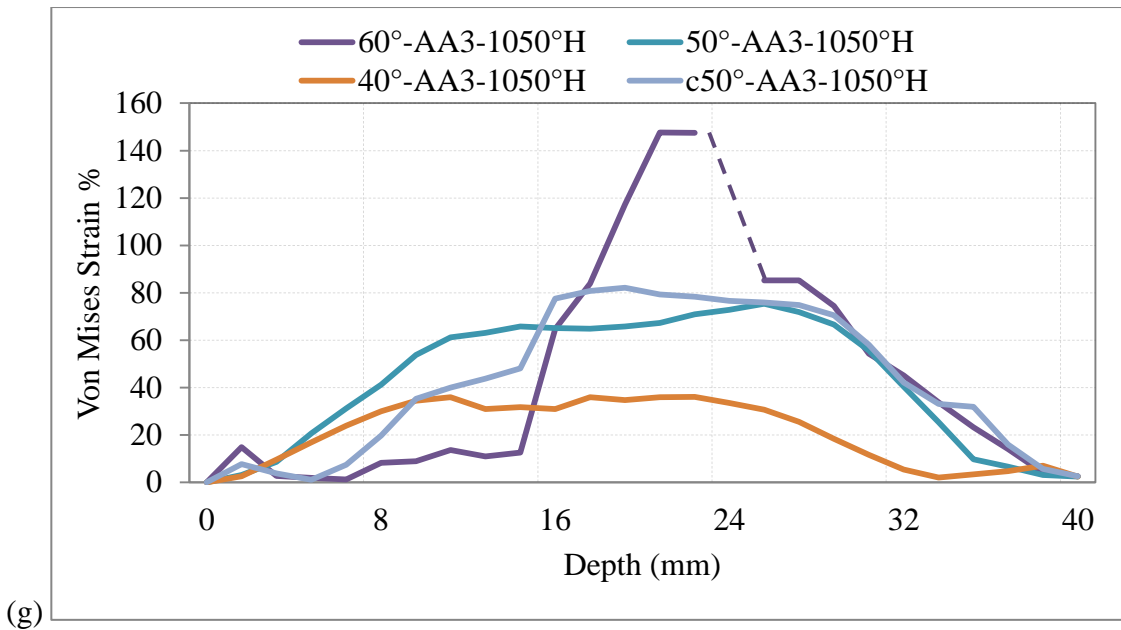
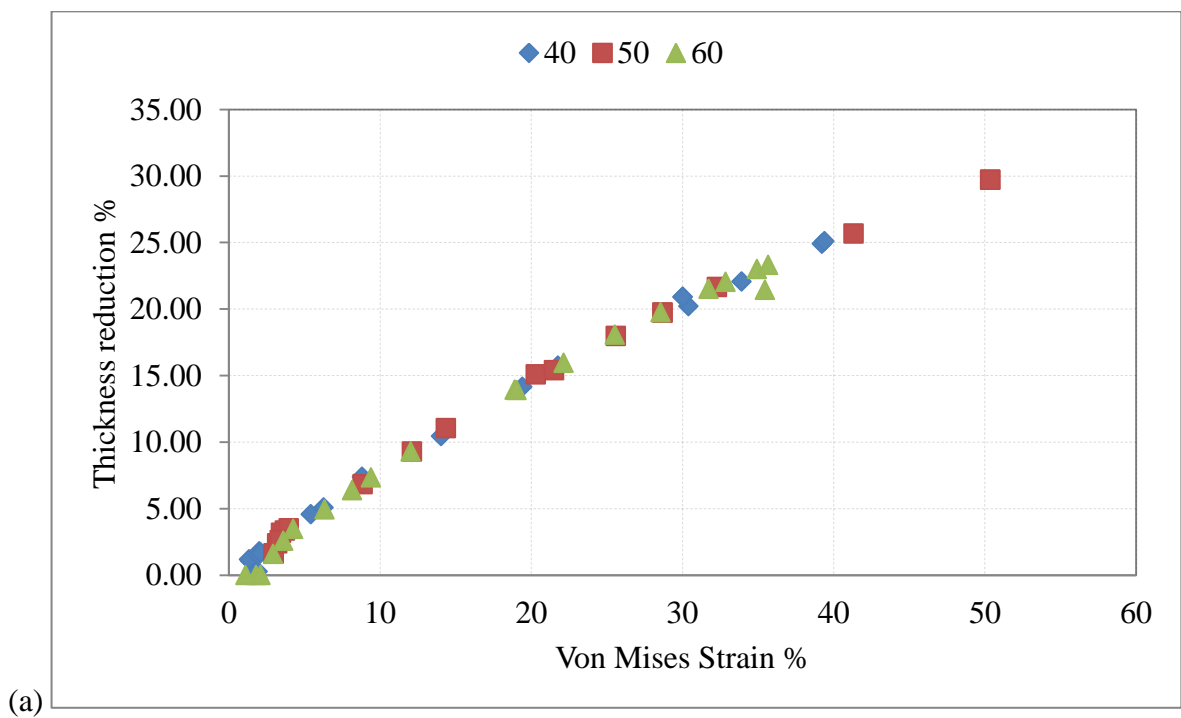


Figure 11-28 Von Mises Strain% vs Depth AA1-1050 AA2-1050H & AA3-1050H; (a) 60°, (b) 50°, (c) 40°, (d) c50° (e) Wall angle Comparison AA1-1050H, (f) Wall angle Comparison AA2-1050H (g) Wall angle Comparison AA3-1050H.



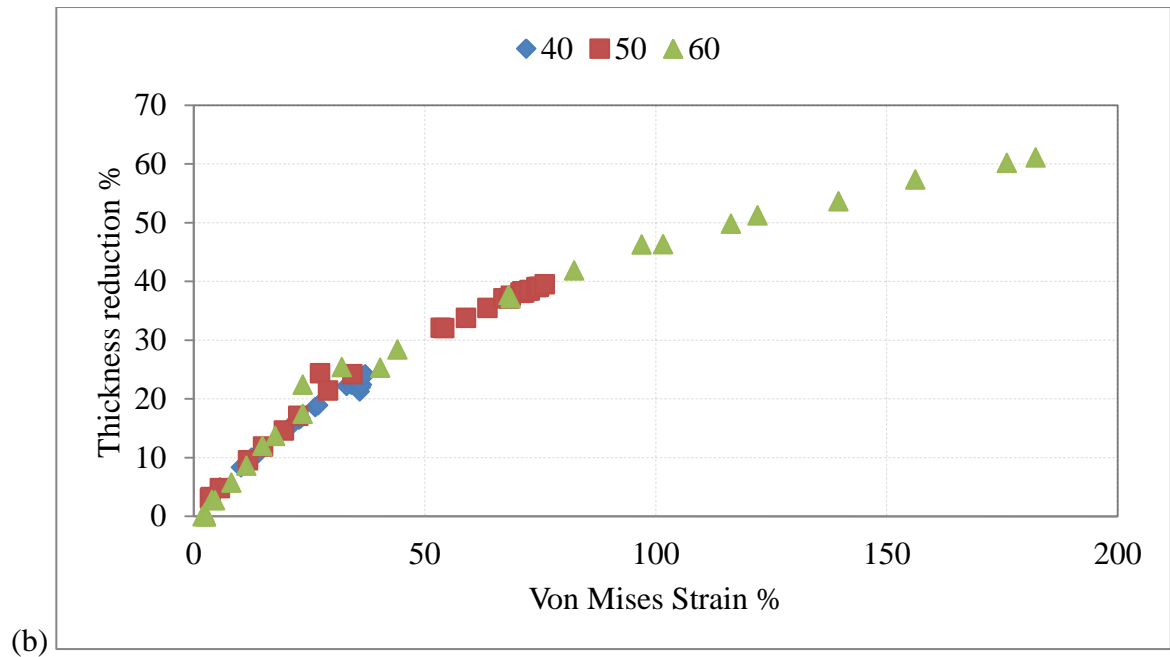


Figure 11-29 Thickness reduction% vs Von Mises Strain%; (a) AA1-1050H, (b) AA2-1050H.

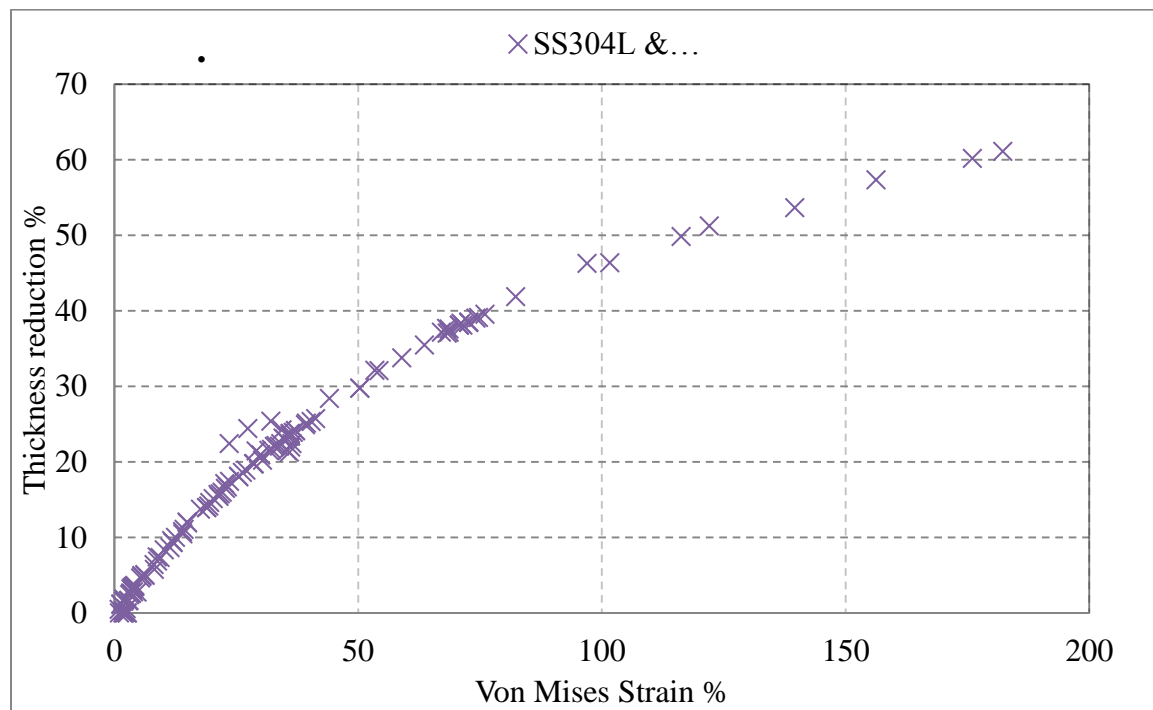


Figure 11-30 Thickness reduction% vs Von Mises Strain% for AA1-1050H and AA2-1050H, combined.

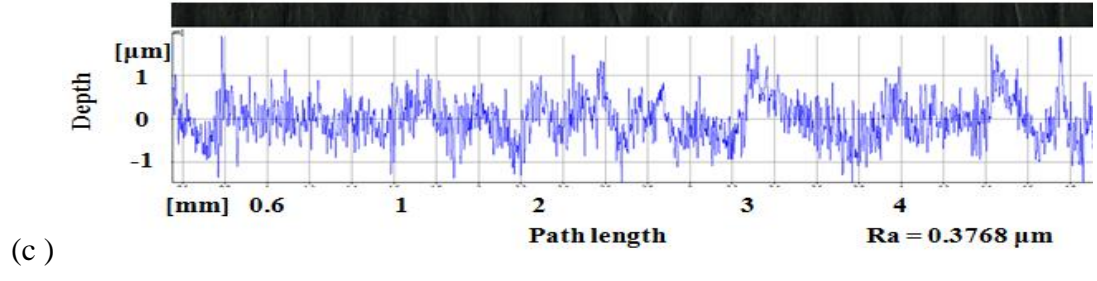
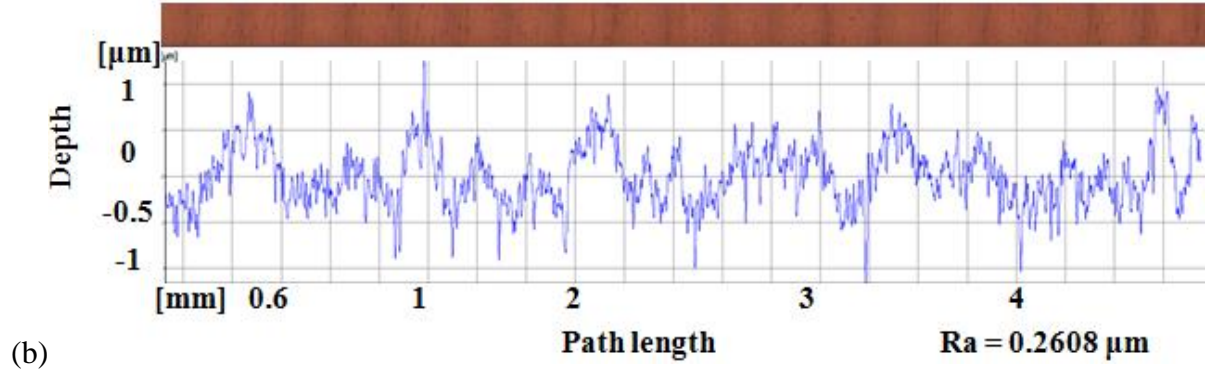
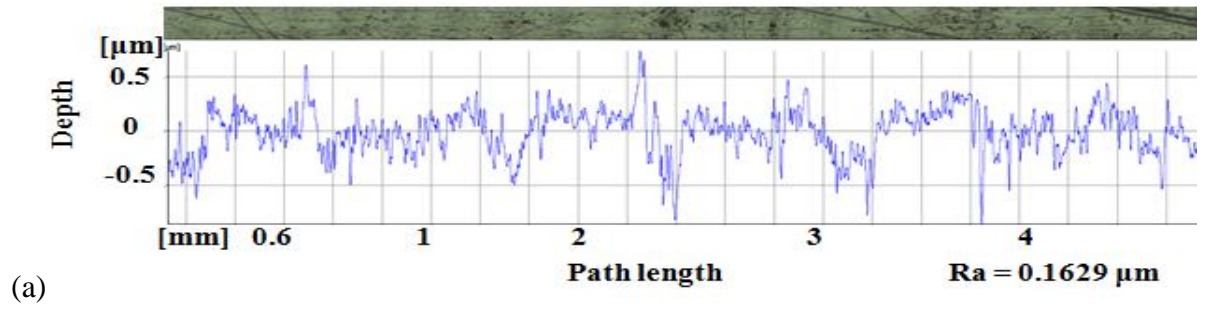
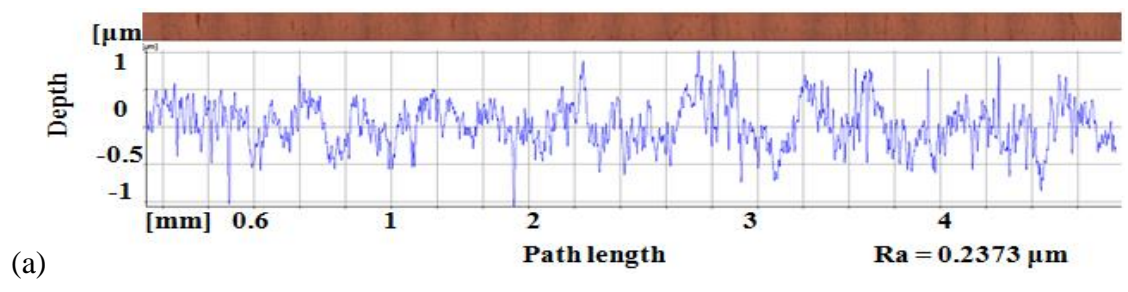
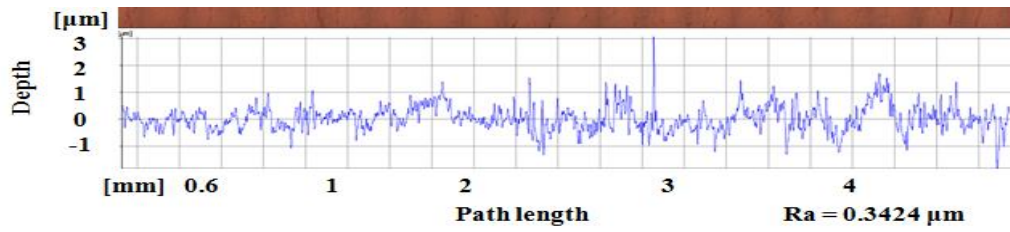


Figure 11-31 Surface roughness profiles of the straight wall feature; (a) As received, (b) 50°, (c) 60°,





(b)

Figure 11-32 Surface roughness profiles of the curved wall feature; (a) 50°, (b) 60°,

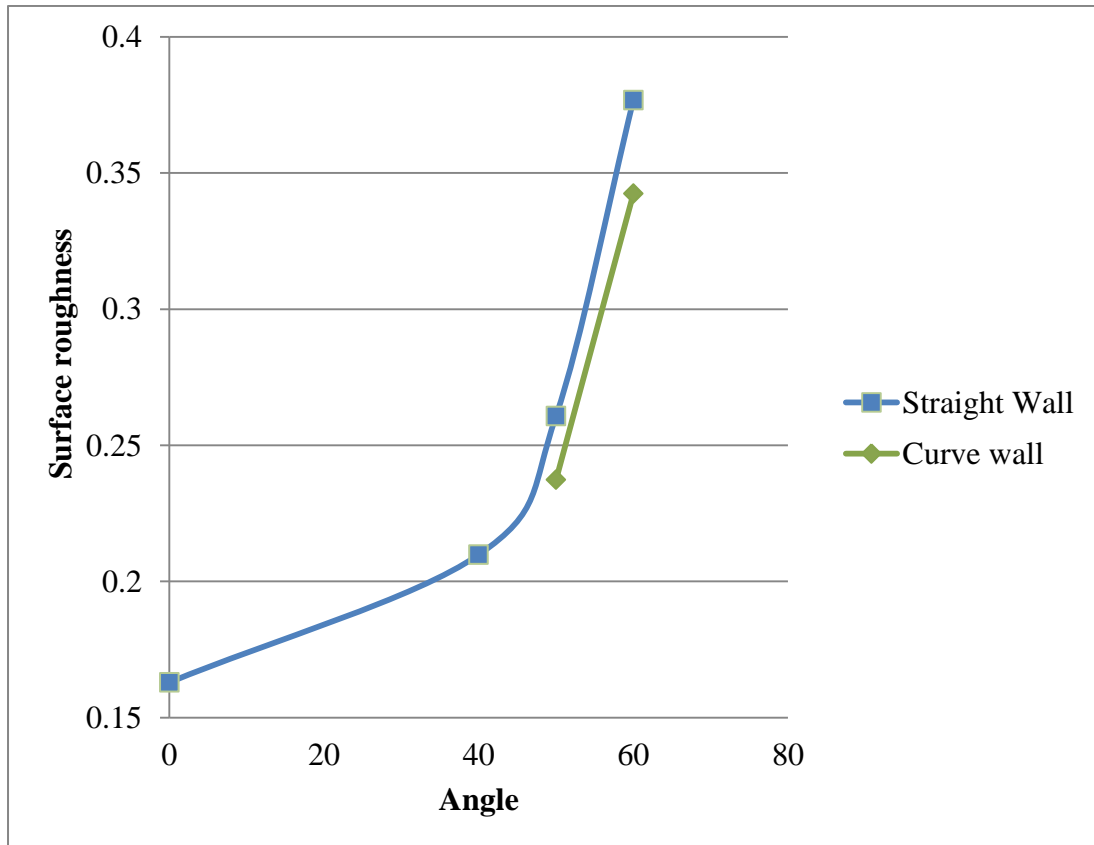


Figure 11-33 Surface roughness with respect to the wall angle.



Table 11-1 Surface roughness measurements.

<b>Surface</b>	<b>Ra (<math>\mu\text{m}</math>)</b>	<b>Relative difference %</b>
As received	0.1629	0.00
<b>Wall feature</b>		
40°	0.2098	22.35
50°	0.2608	19.56
60°	0.3768	30.79
<b>Curve feature</b>		
50°	0.2373	31.35
60°	0.3424	30.70

## AA2024 Results

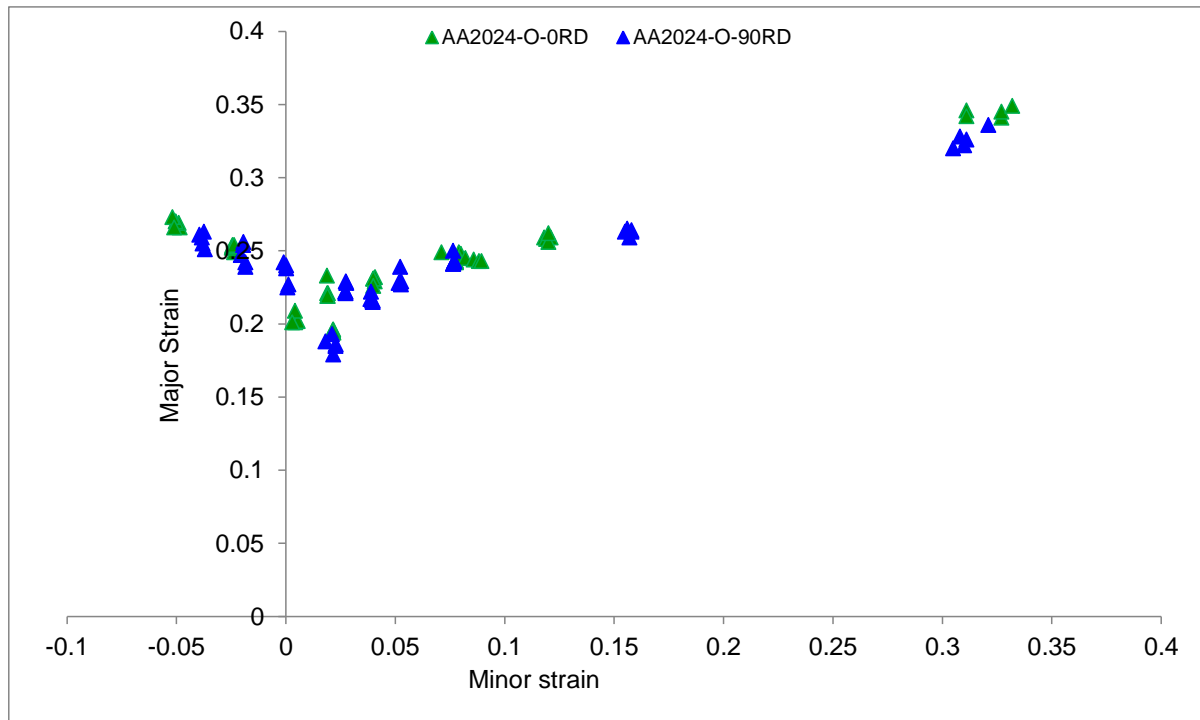
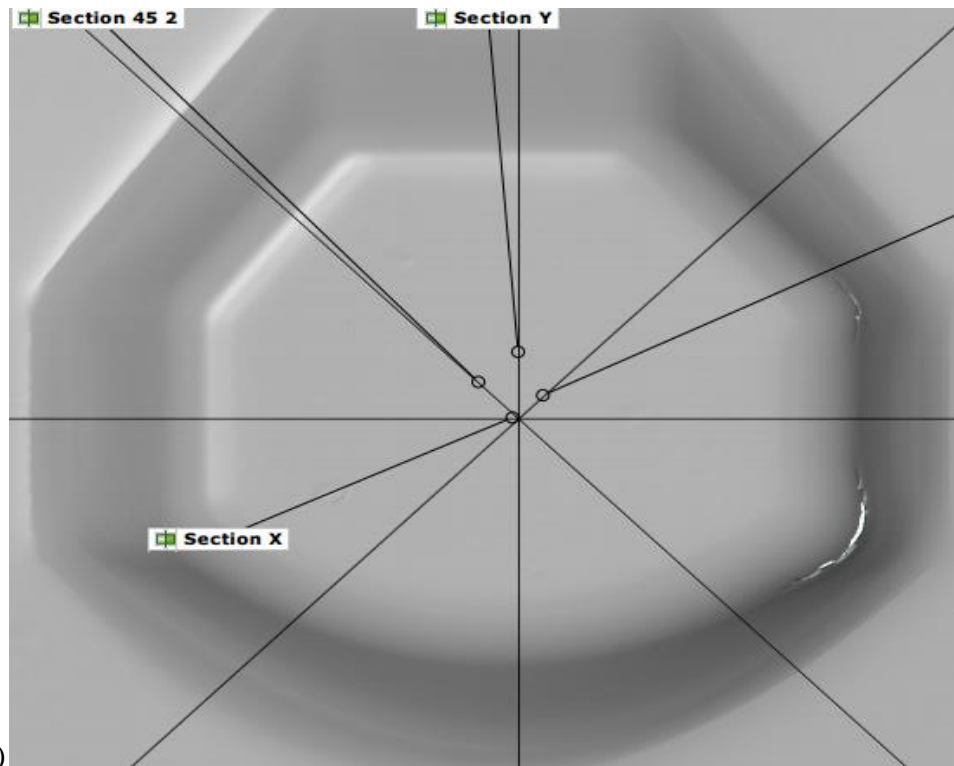
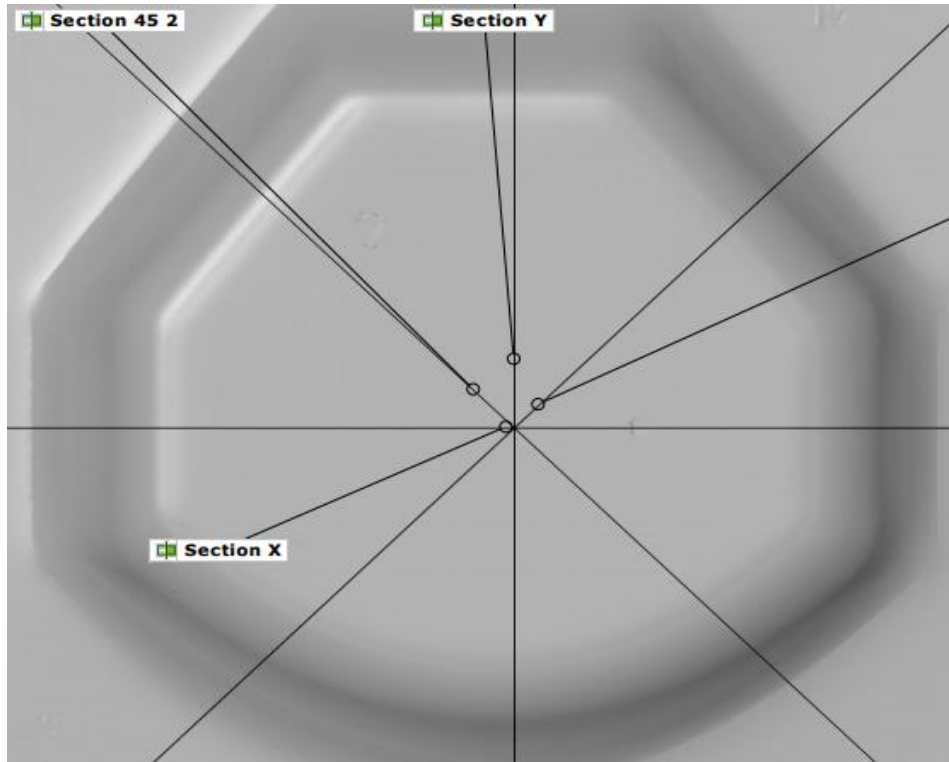


Figure 11-34 Forming Limit Curve AA2024.



(b)

Figure 11-35 Multi-slope geometry; (a) AA1-2024, (b) AA2-2024.

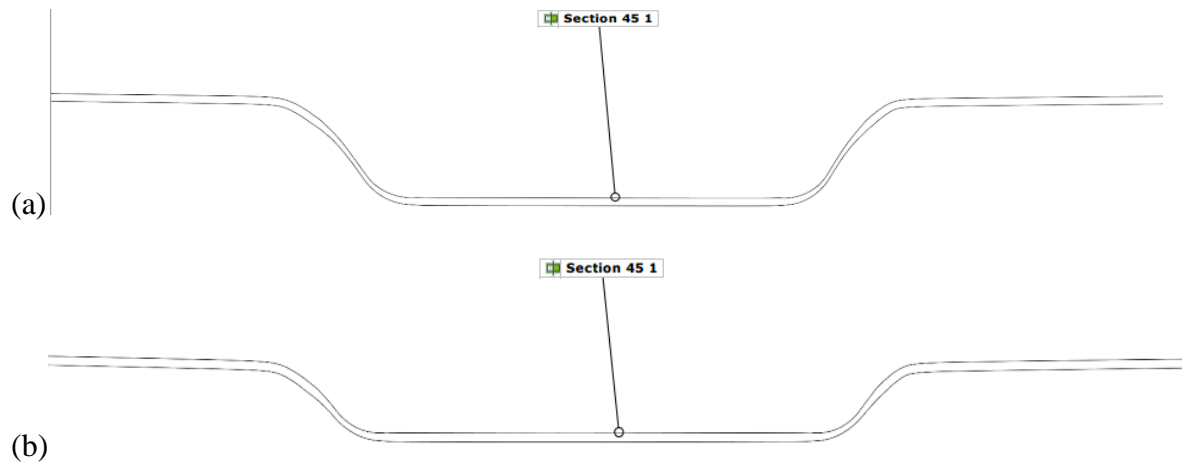


Figure 11-36 Section X; (a) AA1-2024, (b) AA2-2024.

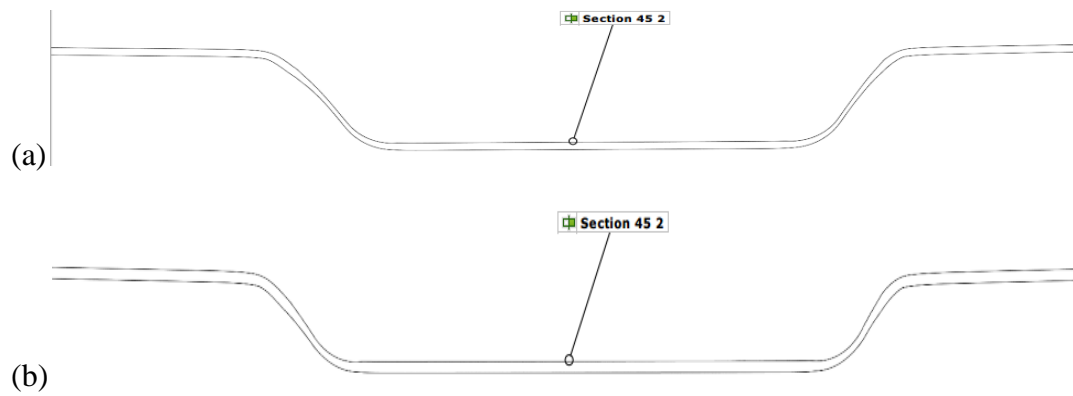


Figure 11-37 Section Y; (a) AA1-2024, (b) AA2-2024.

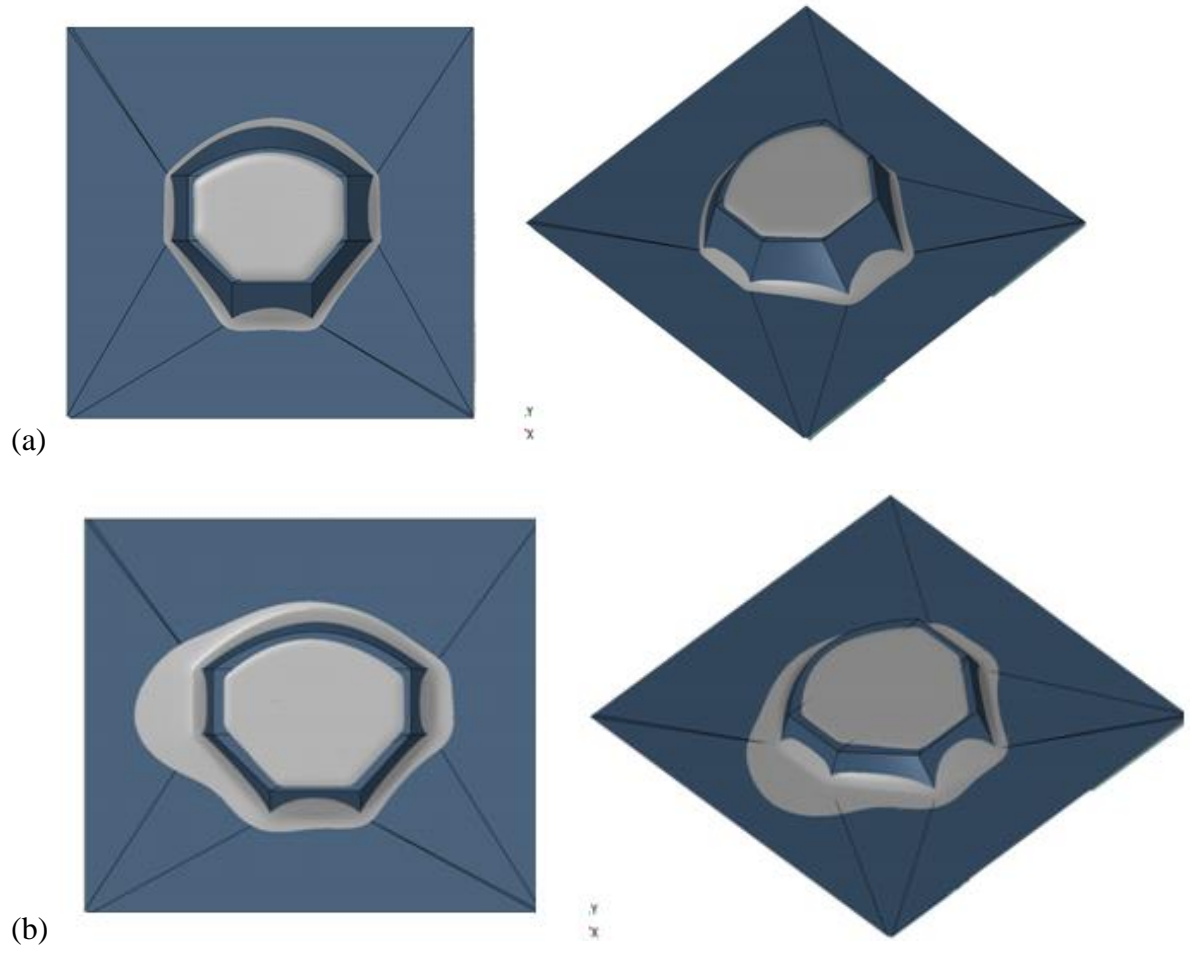


Figure 11-38 Qualitative CAD comparison; top and isometric view; (a) AA1-2024, (b) AA2-2024.

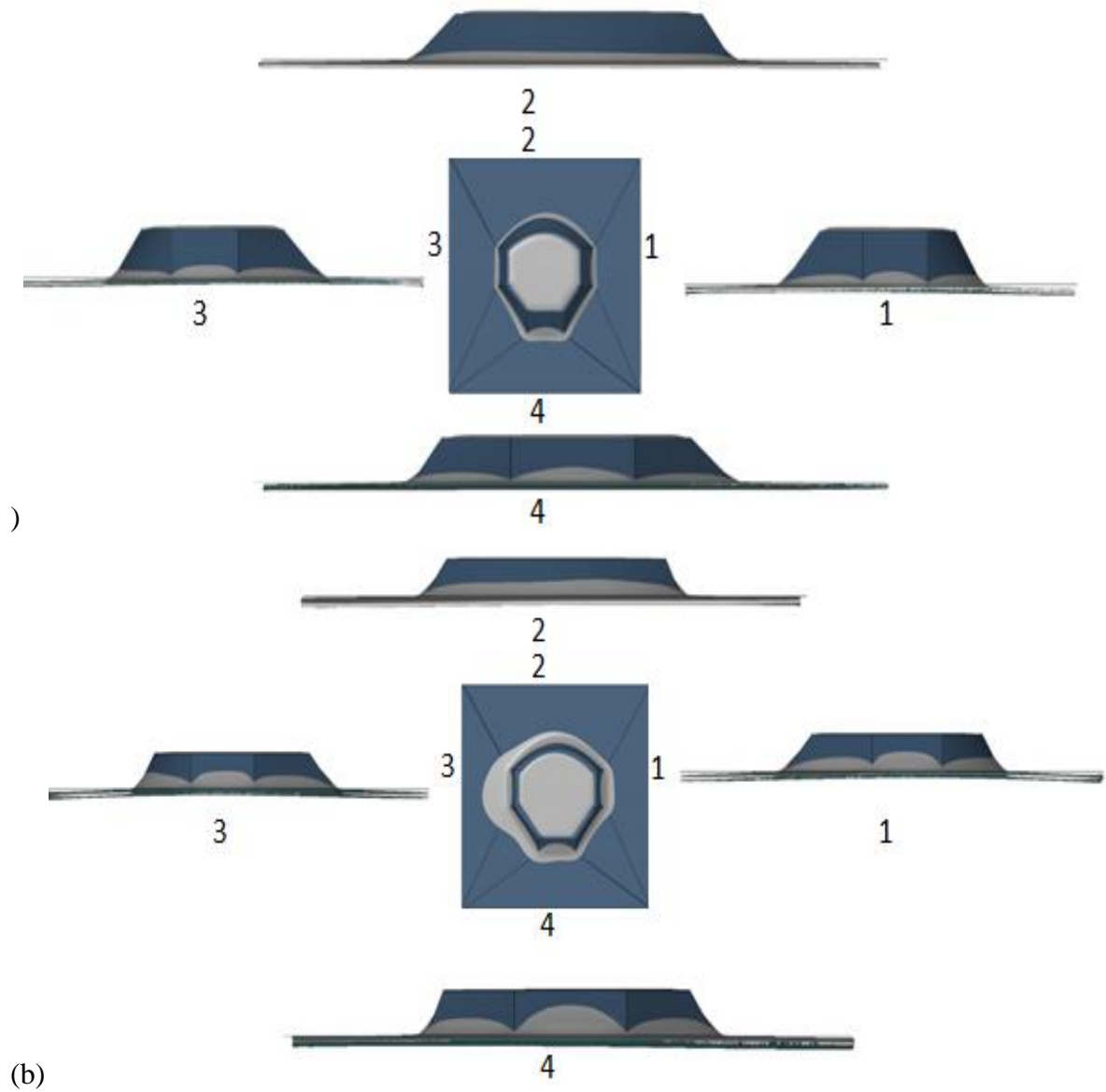


Figure 11-39 Qualitative CAD comparison; top and side views; (a) AA1-2024, (b) AA2-2024.

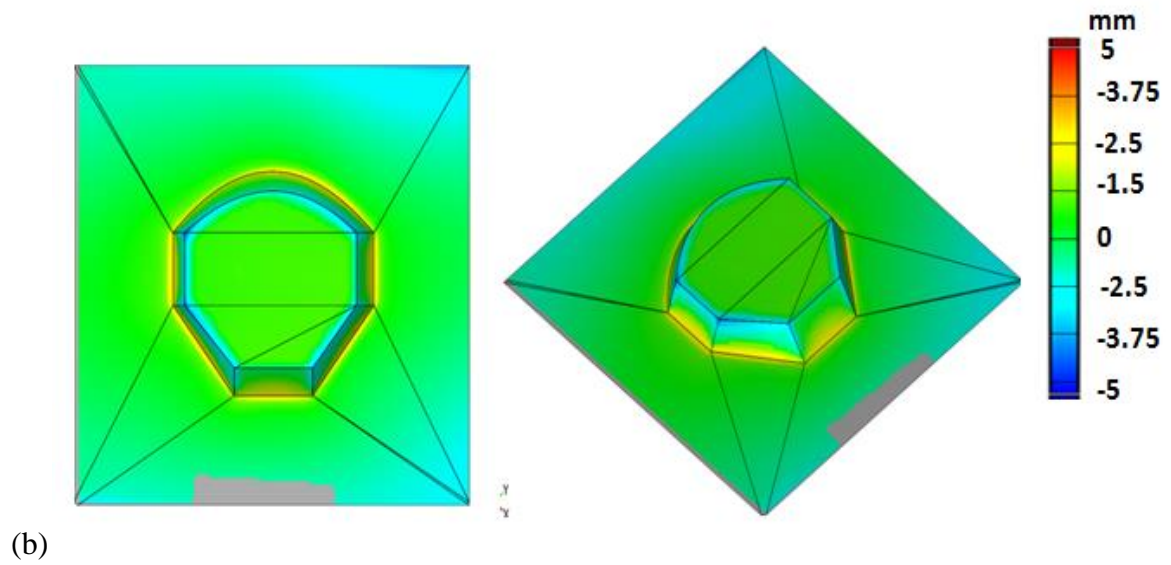
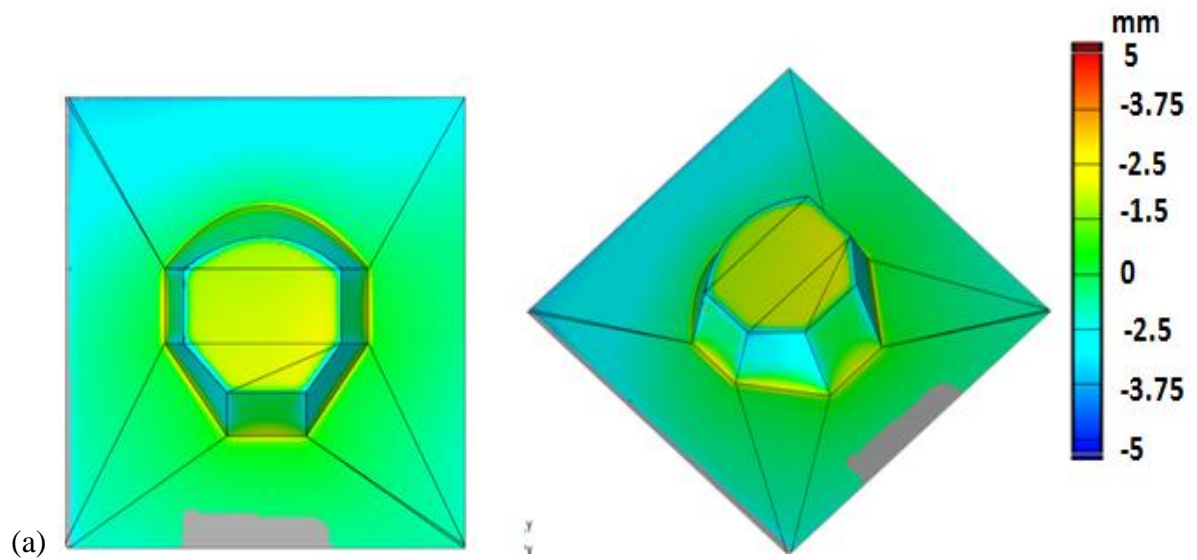


Figure 11-40 Quantitative CAD comparison; top and isometric view; (a) AA1-2024, (b) AA2-2024.

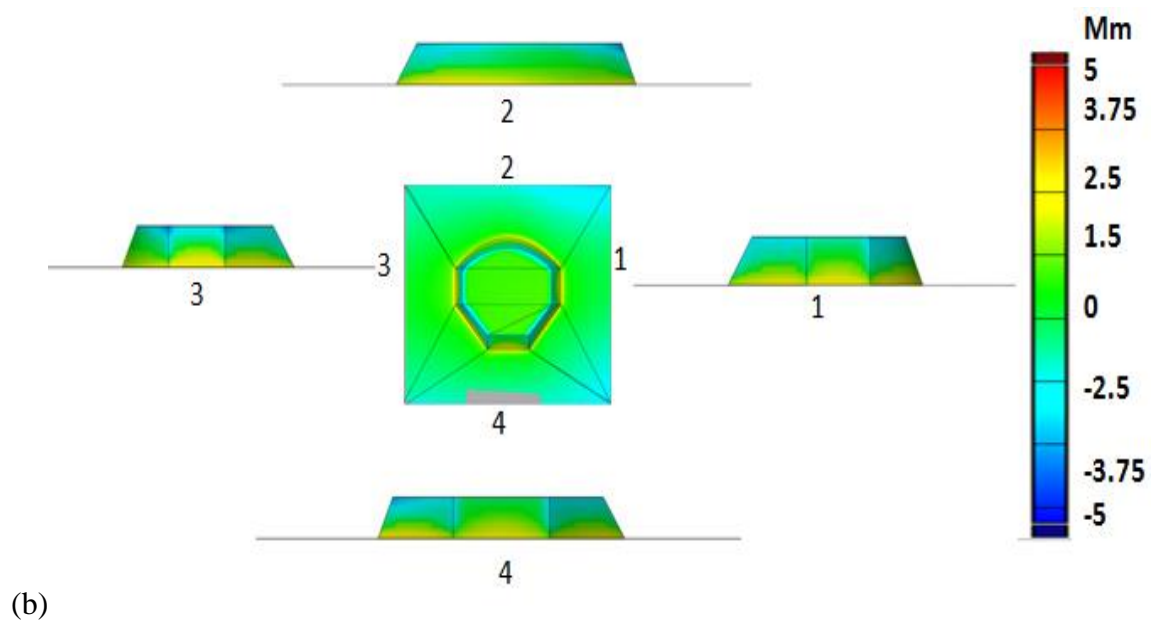
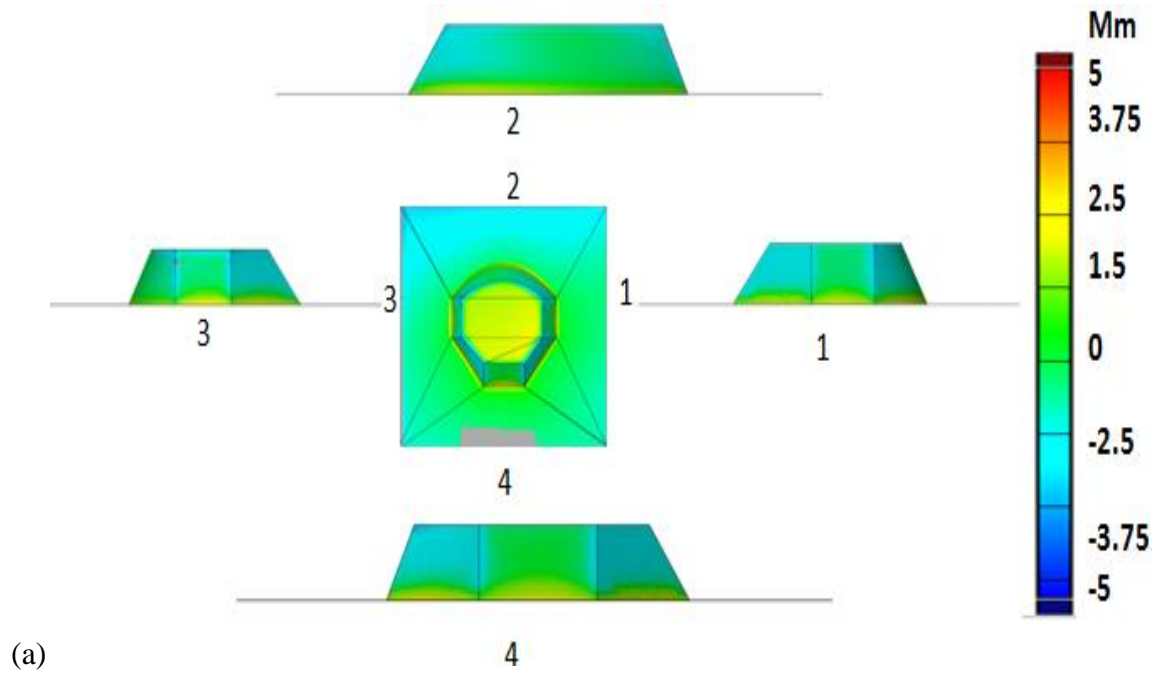


Figure 11-41 Quantitative CAD comparison; top and side views; (a) AA1-2024, (b) AA2-2024.



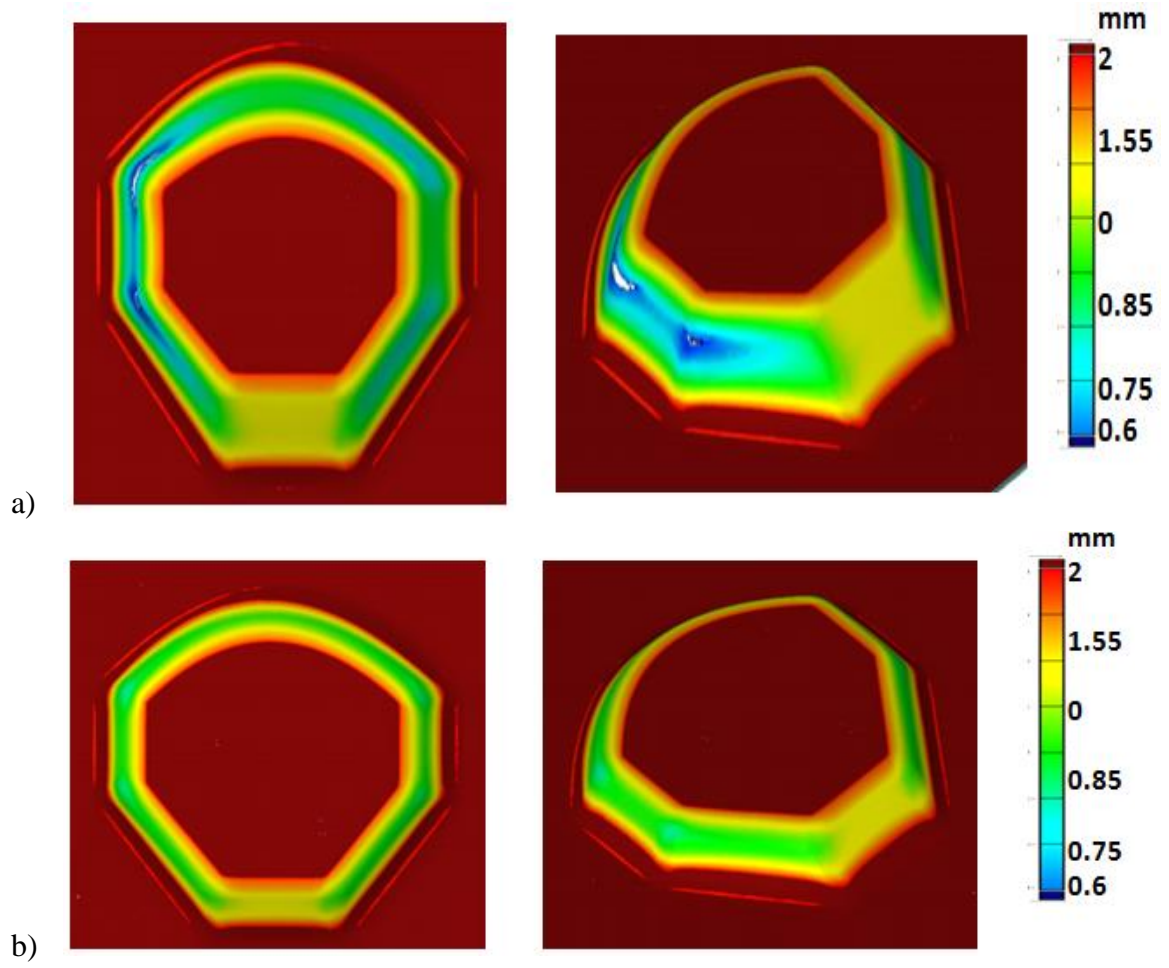


Figure 11-42 Thickness profile, top and isometric view; (a) AA1-2024, (b) AA2-2024.

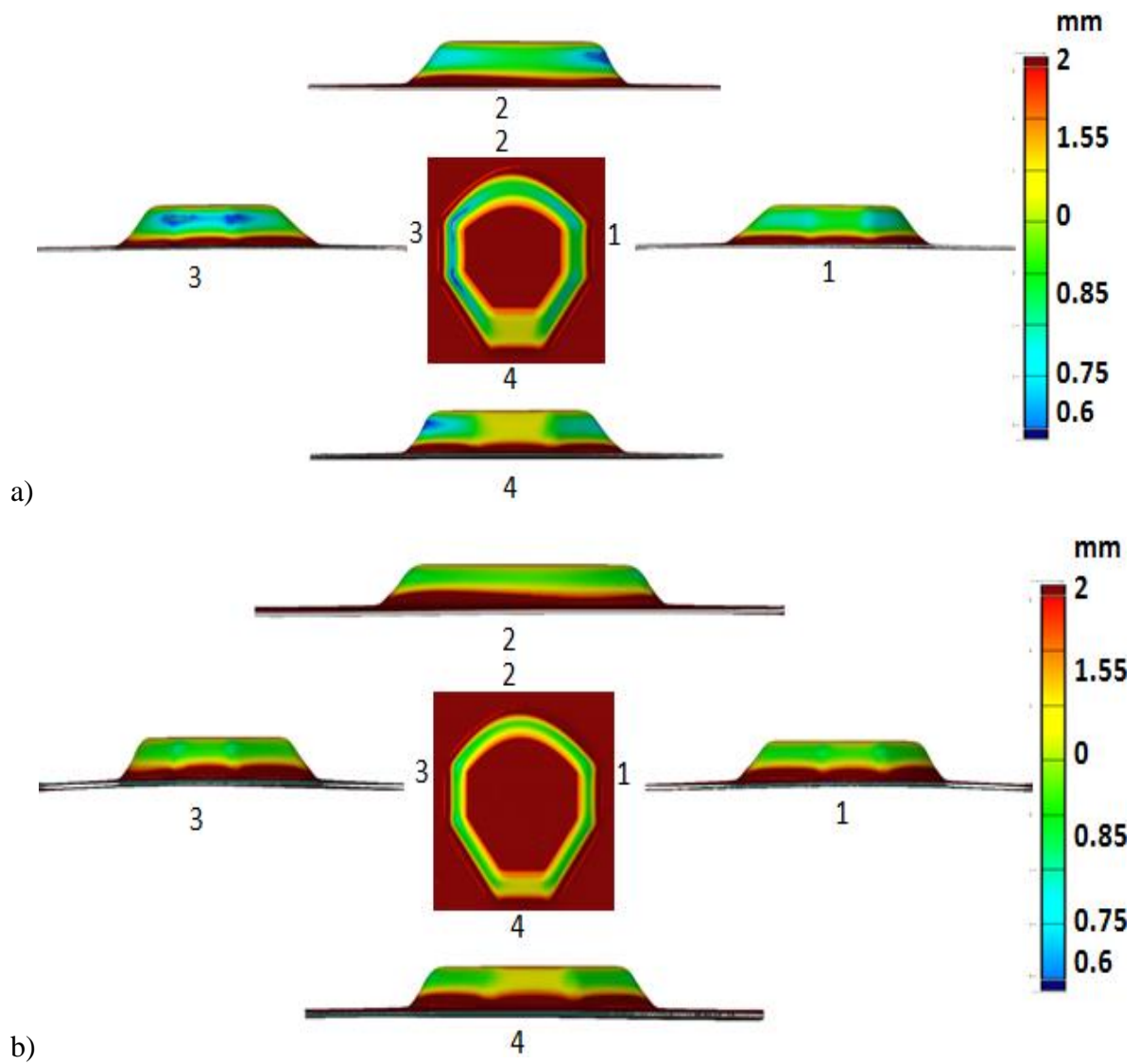
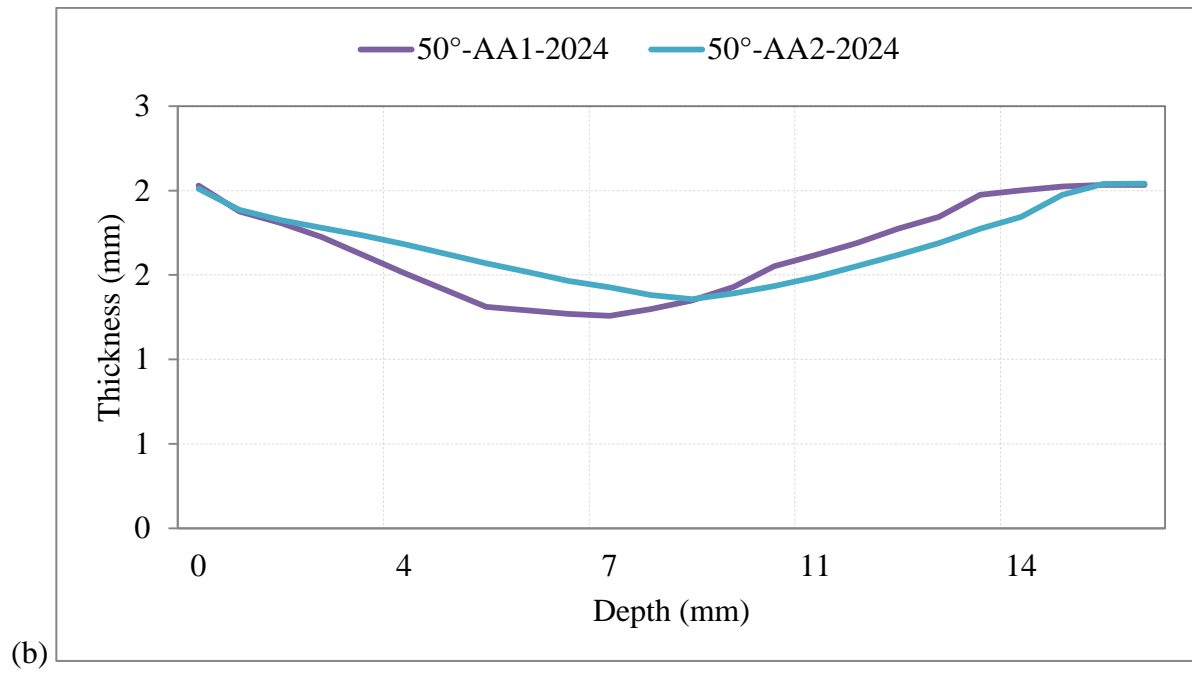
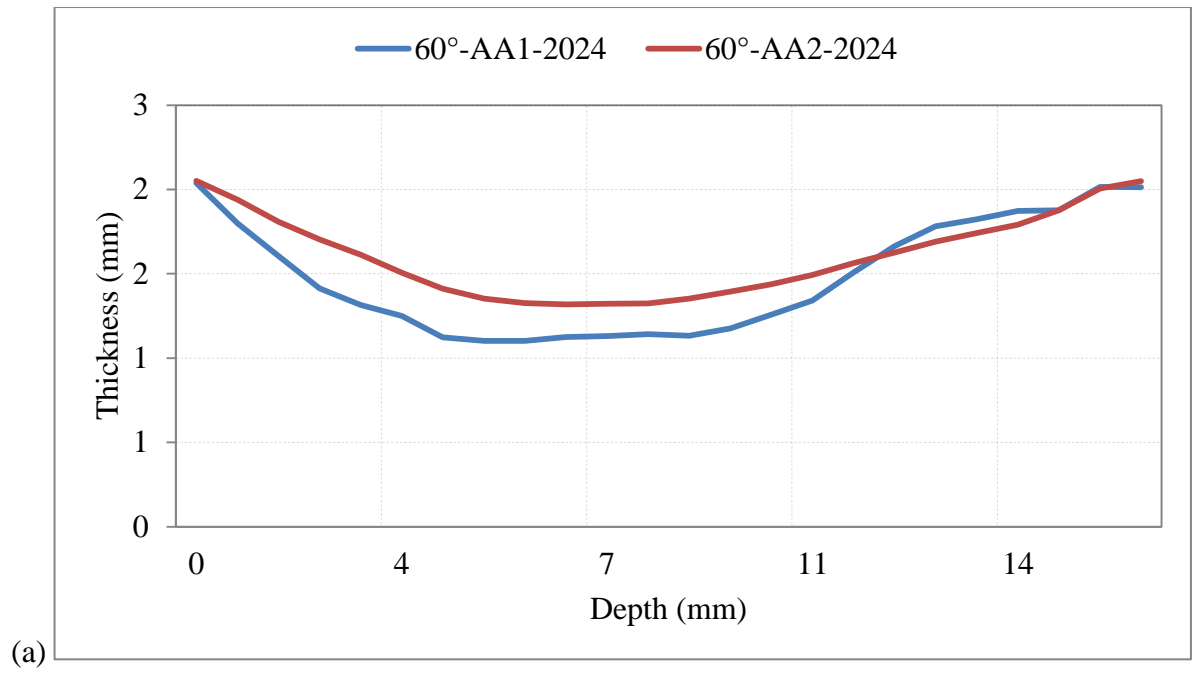
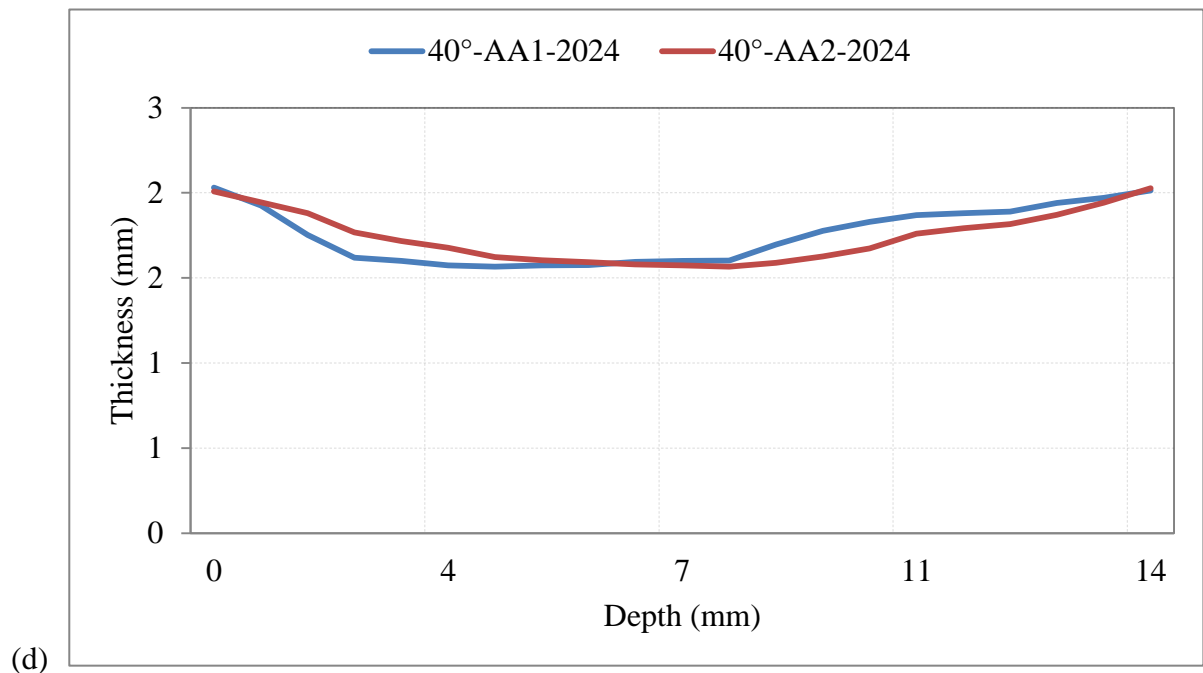
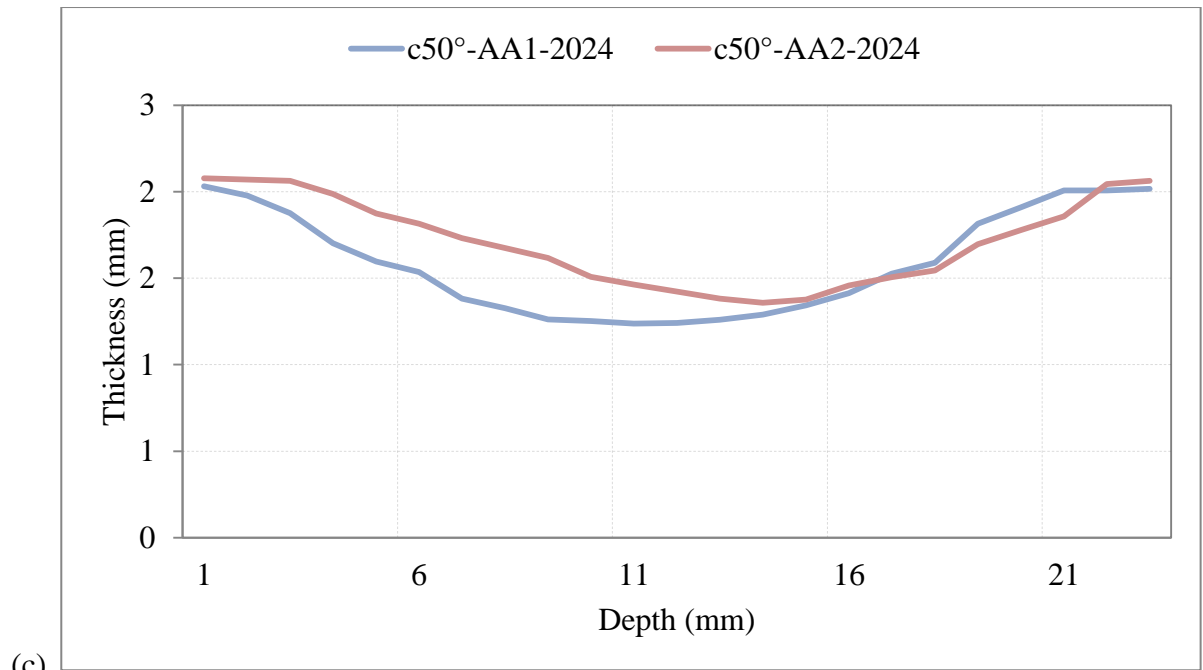


Figure 11-43 Thickness profile top and side views; (a) AA1-2024, (b) AA2-2024.





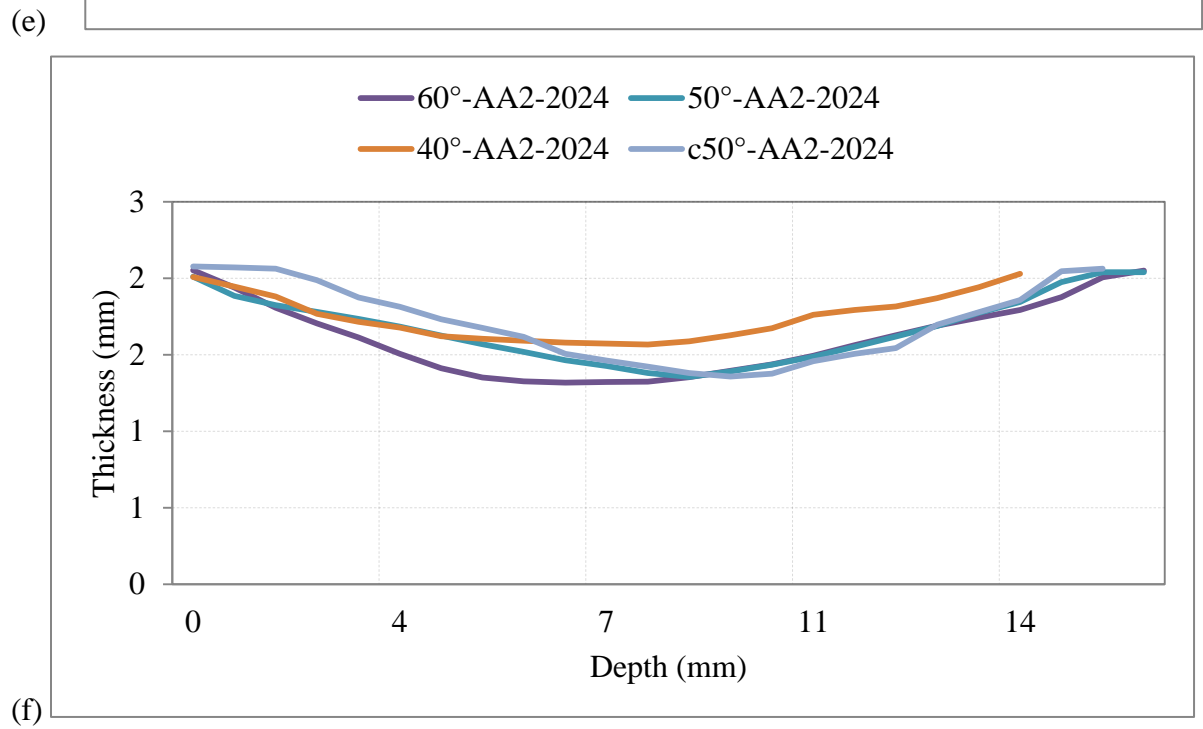
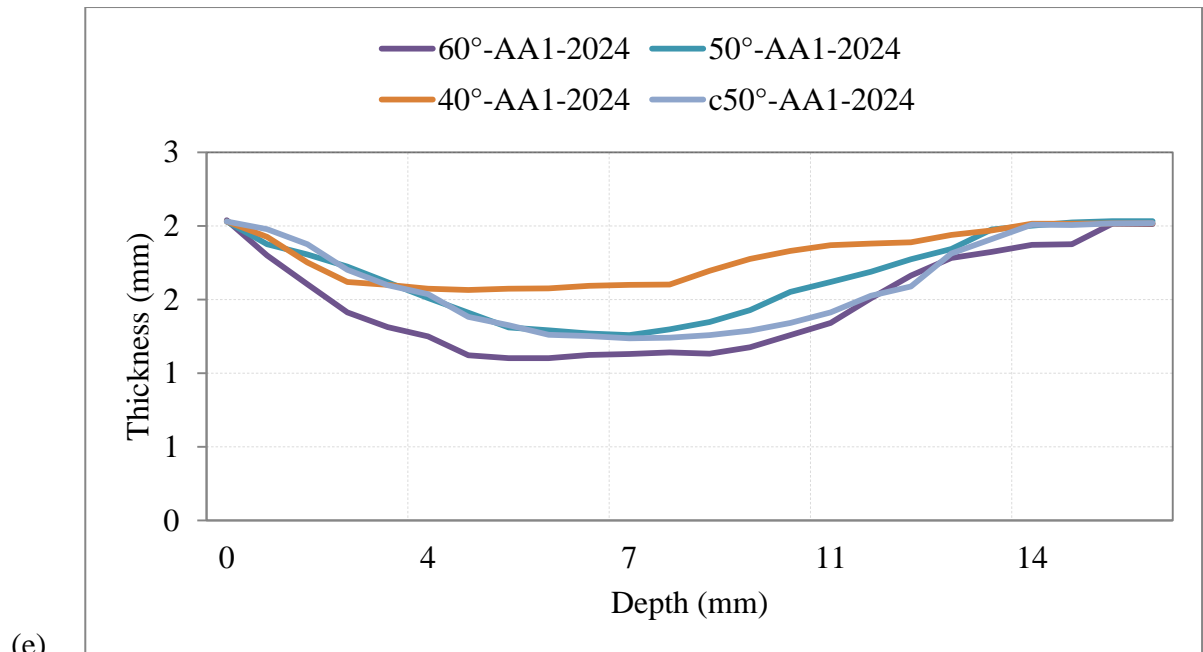
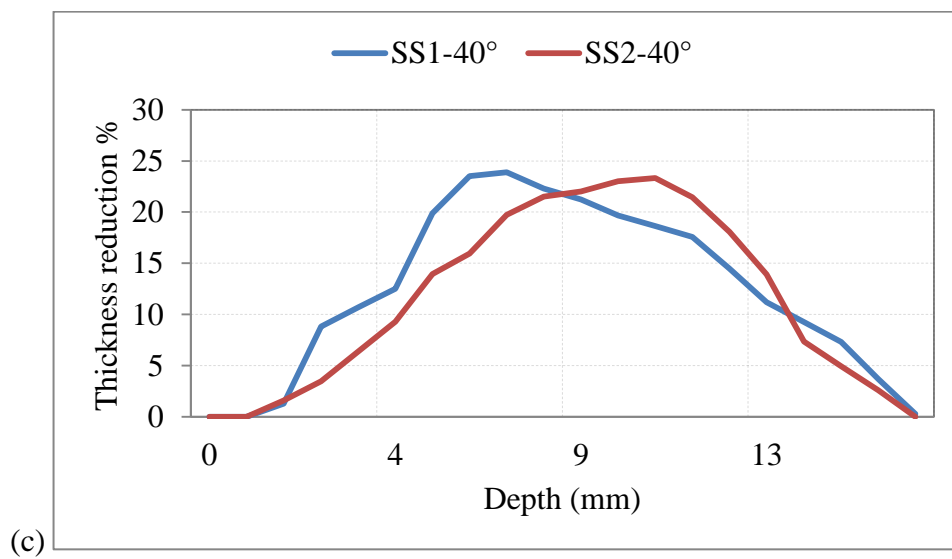
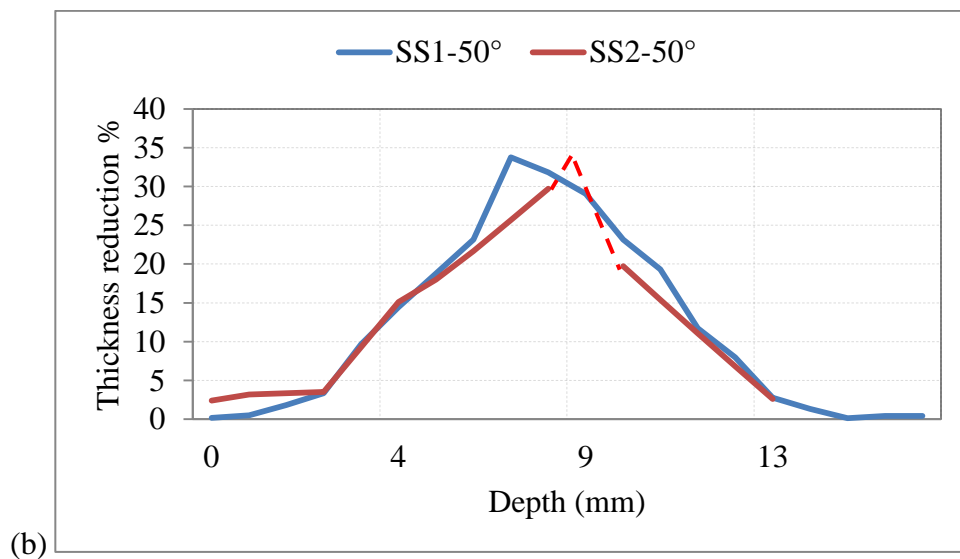
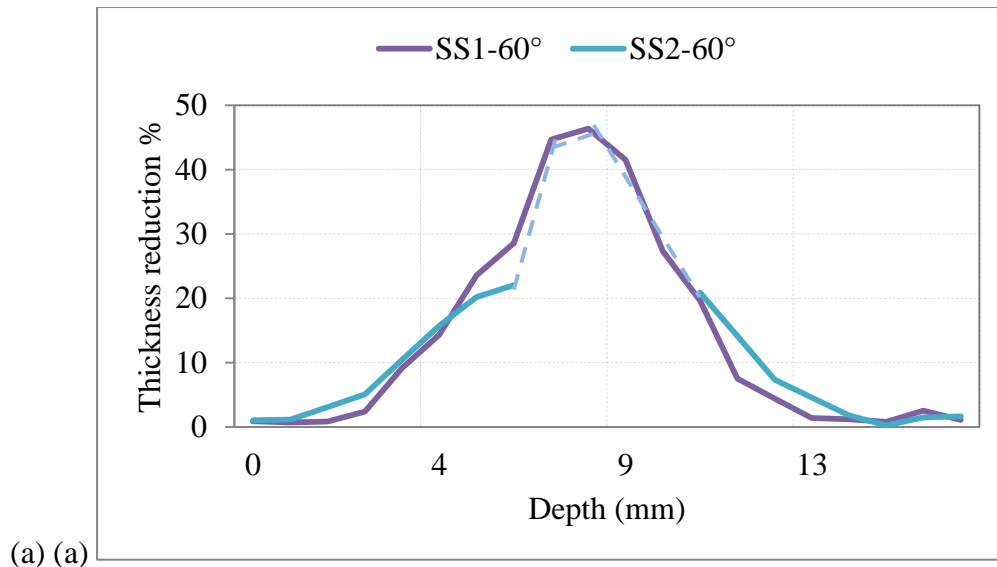


Figure 11-44 Thickness vs Depth AA1-2024 & AA2-2024; (a) 60°, (b) 50°, (c) Curve 50°, (d) 40°, (e) Wall angle Comparison AA1-2024, (f) Wall angle Comparison AA2-2024 .



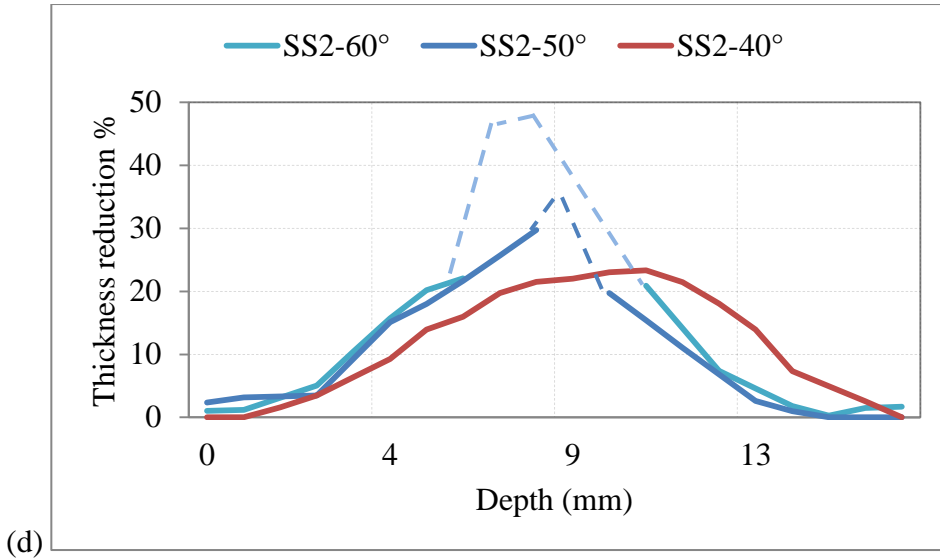


Figure 5-13

Figure 11-45 Thickness reduction% vs Depth AA1-2024 & AA2-2024; (a) 60°, (b) 50°, (c) Curve 50°, (d) 40°, (e) Wall angle Comparison AA1-2024, (f) Wall angle Comparison AA2-2024 .

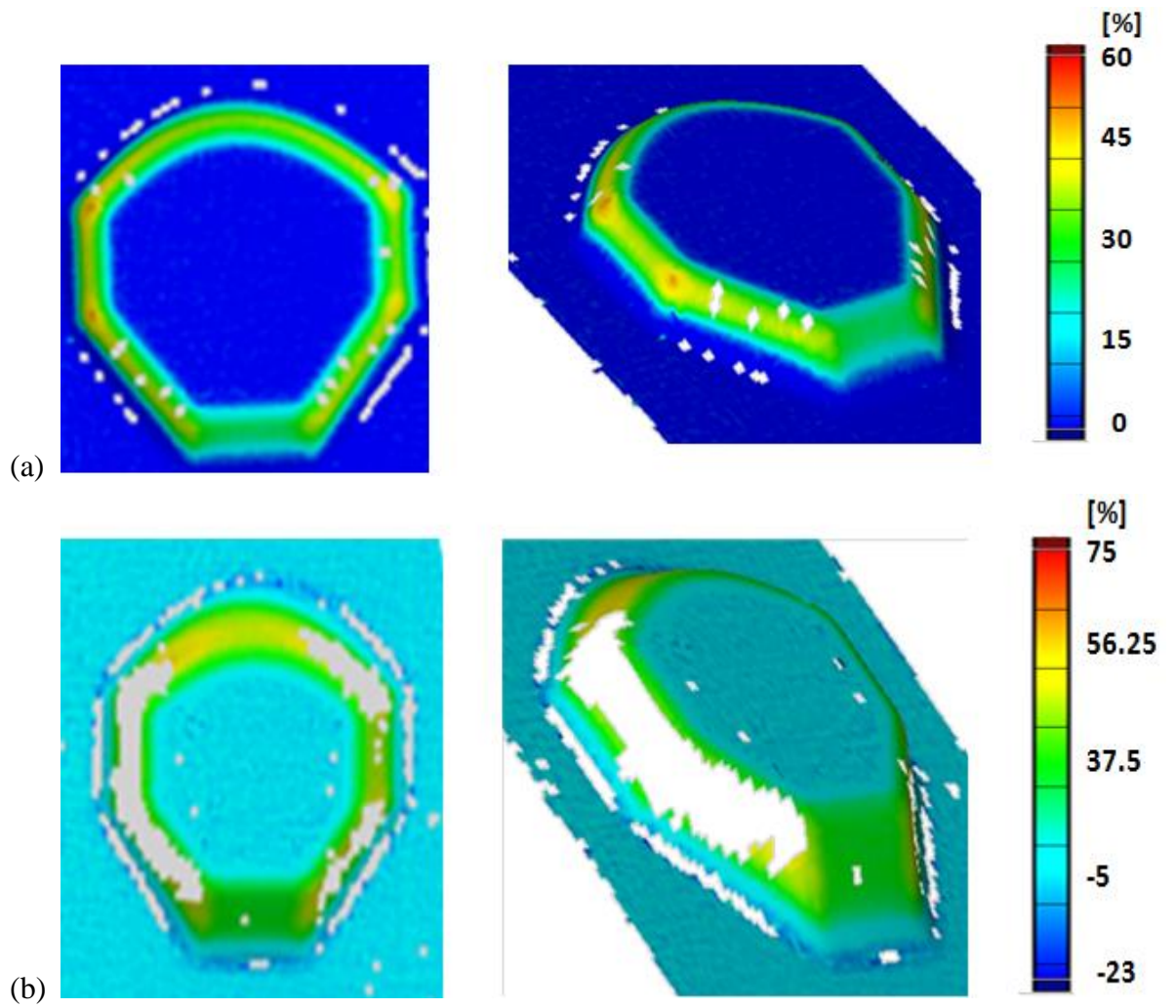


Figure 11-46 Thickness reduction; top and isometric view , (a) AA1-2024, (b) AA2-2024



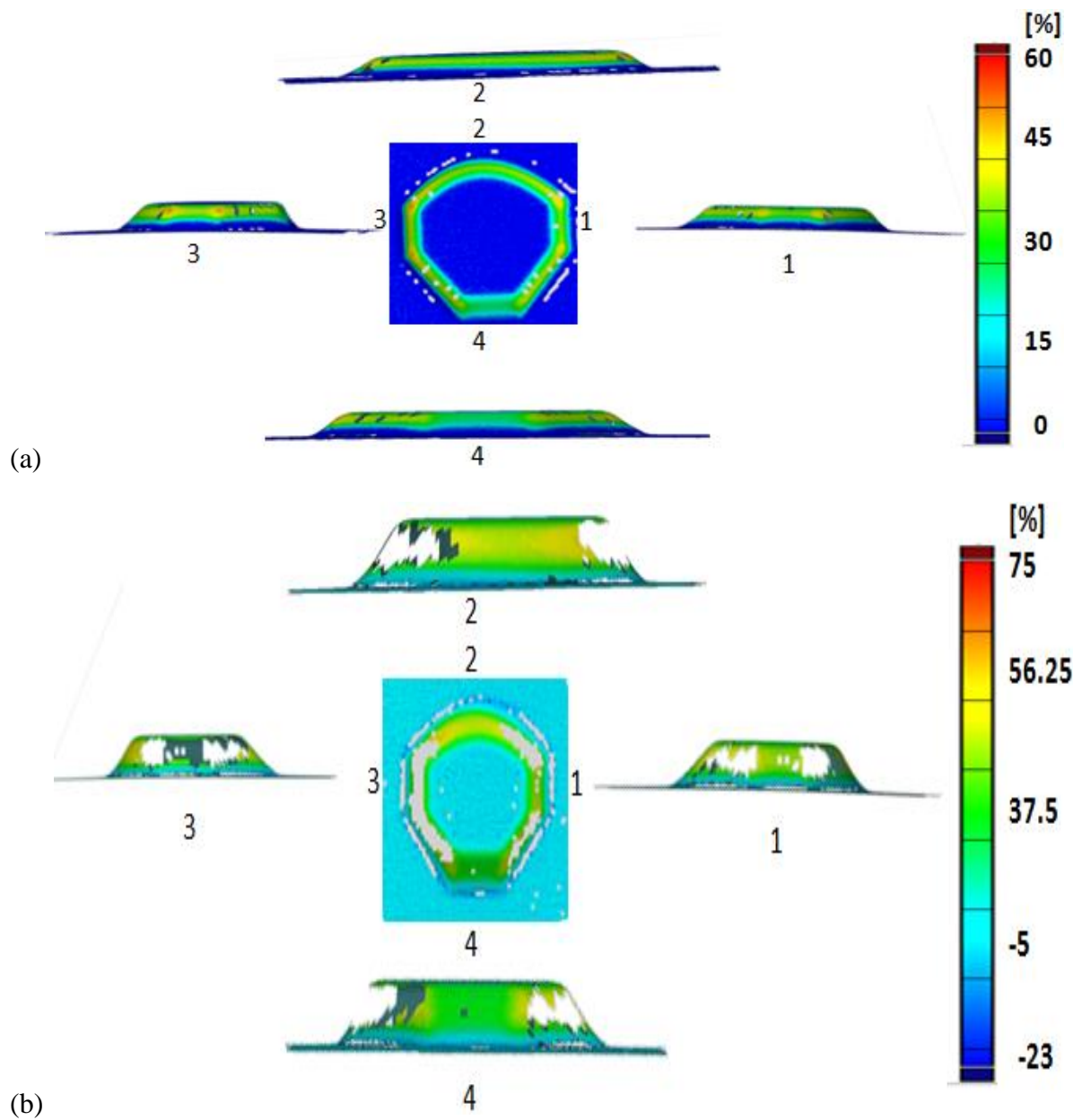
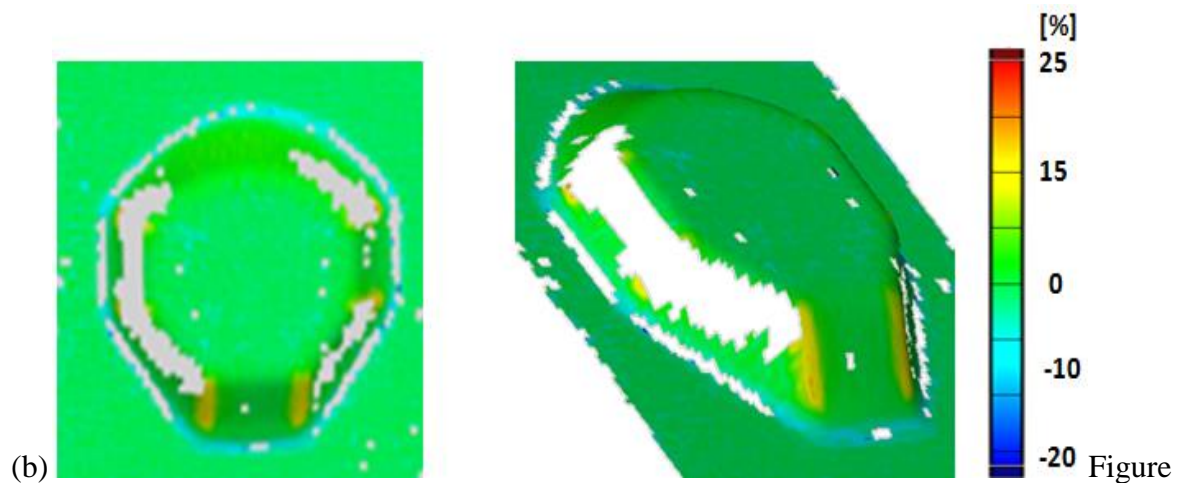
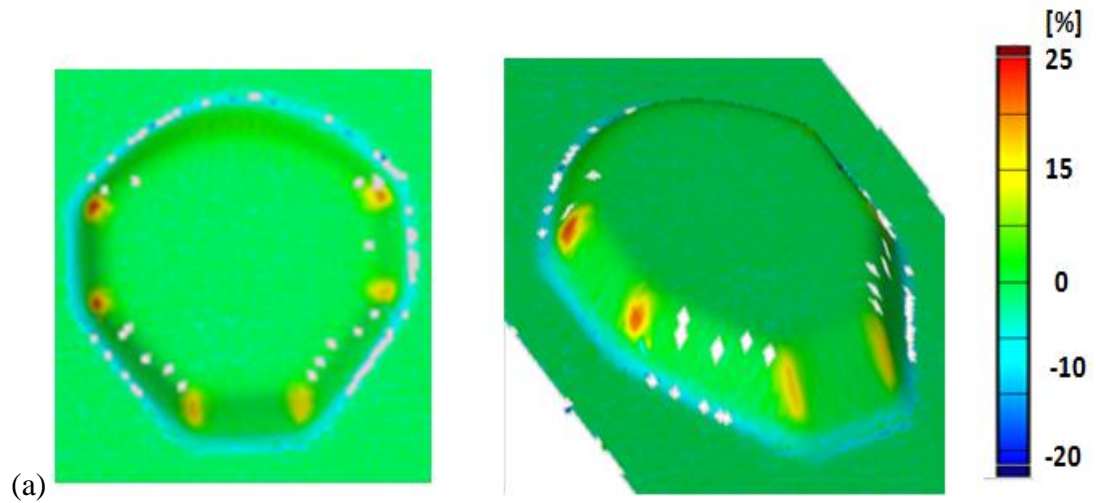


Figure 11-47 Thickness reduction; top and side views, (a) AA1-2024, (b) AA2-2024.



11-48 Minor strain; top and isometric view (a) AA1-2024, (b) AA2-2024.

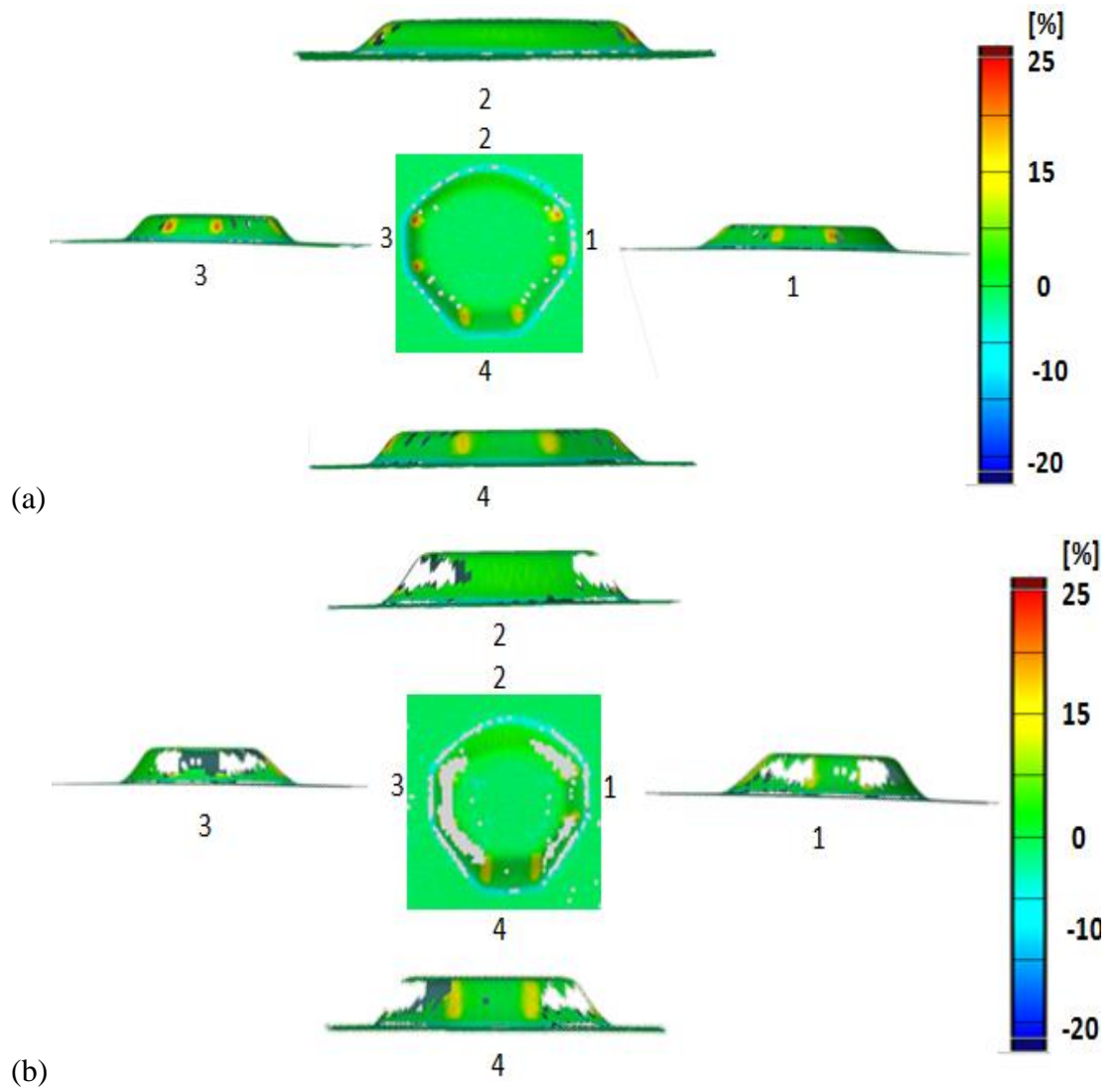


Figure 11-49 Minor strain; top and side views (a) AA1-2024 (b) AA2-2024.

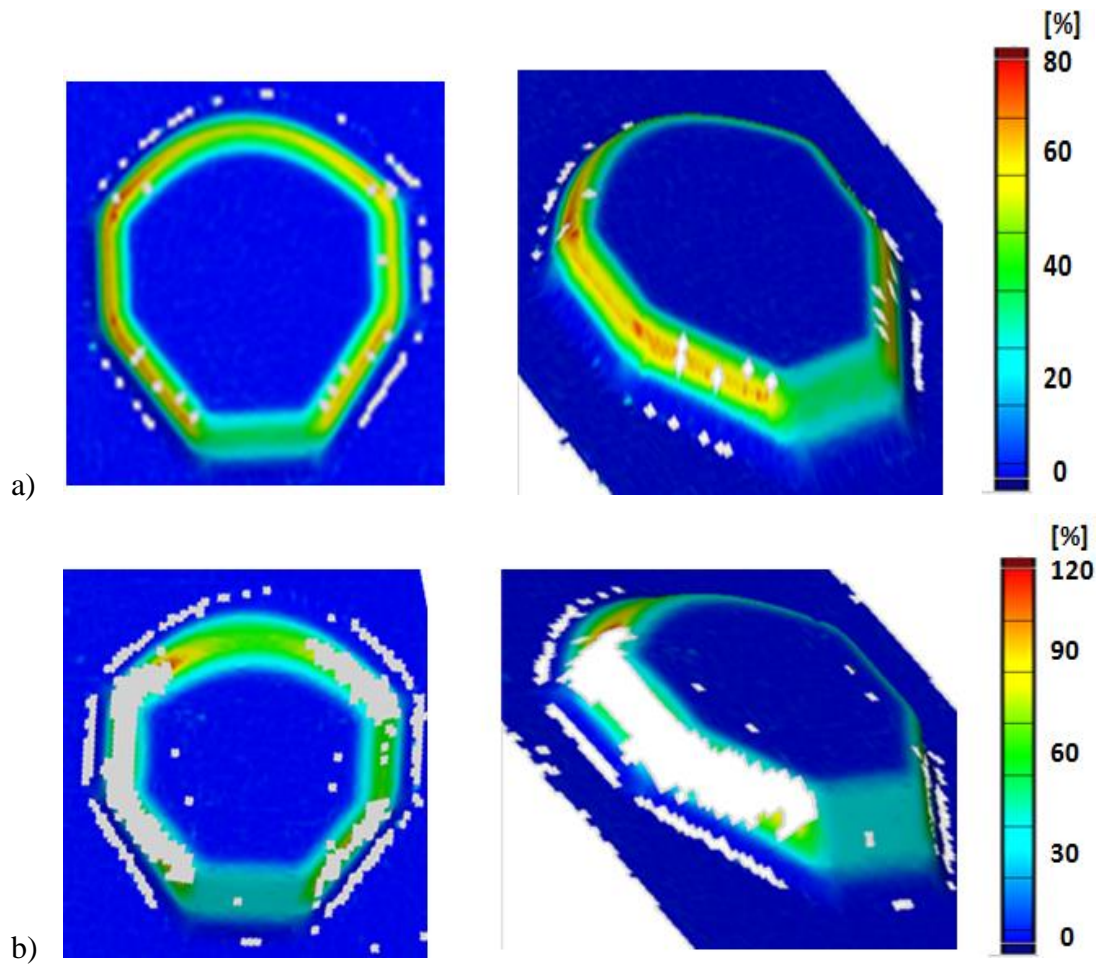
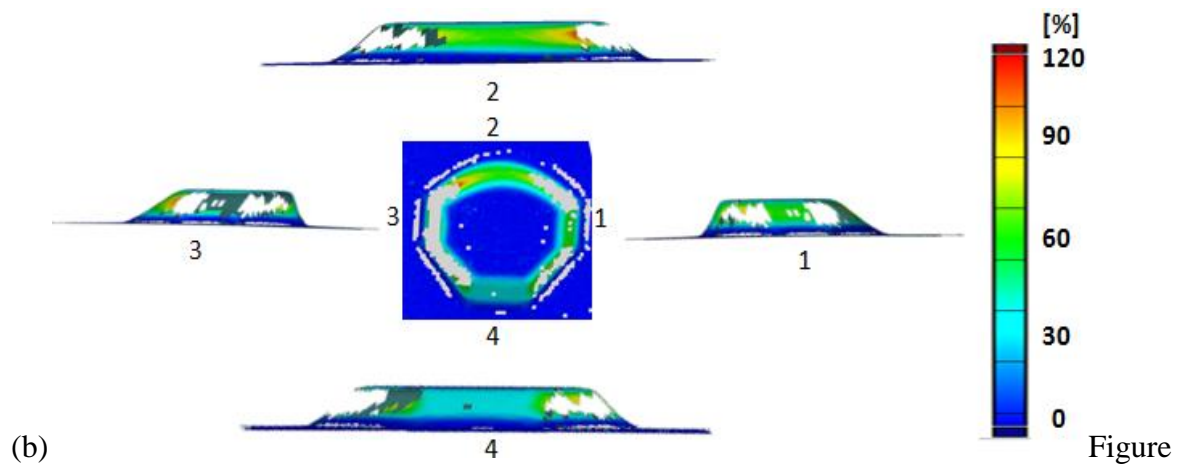
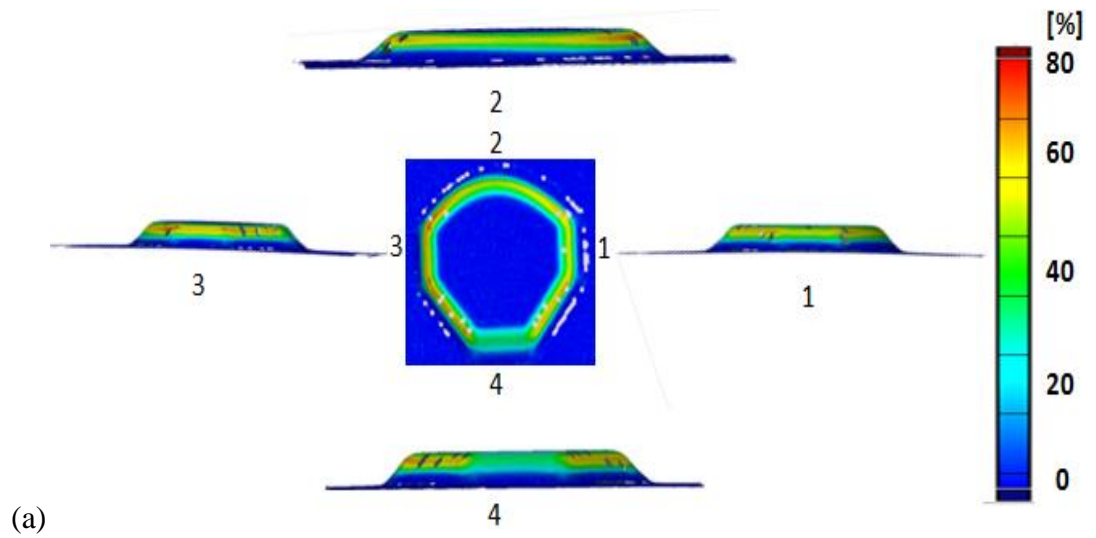


Figure 11-50 Major strain; top and isometric view (a) AA1-2024, (b) AA2-2024.



11-51 Major strain; top and side views; (a) AA1-2024, (b) AA2-2024.

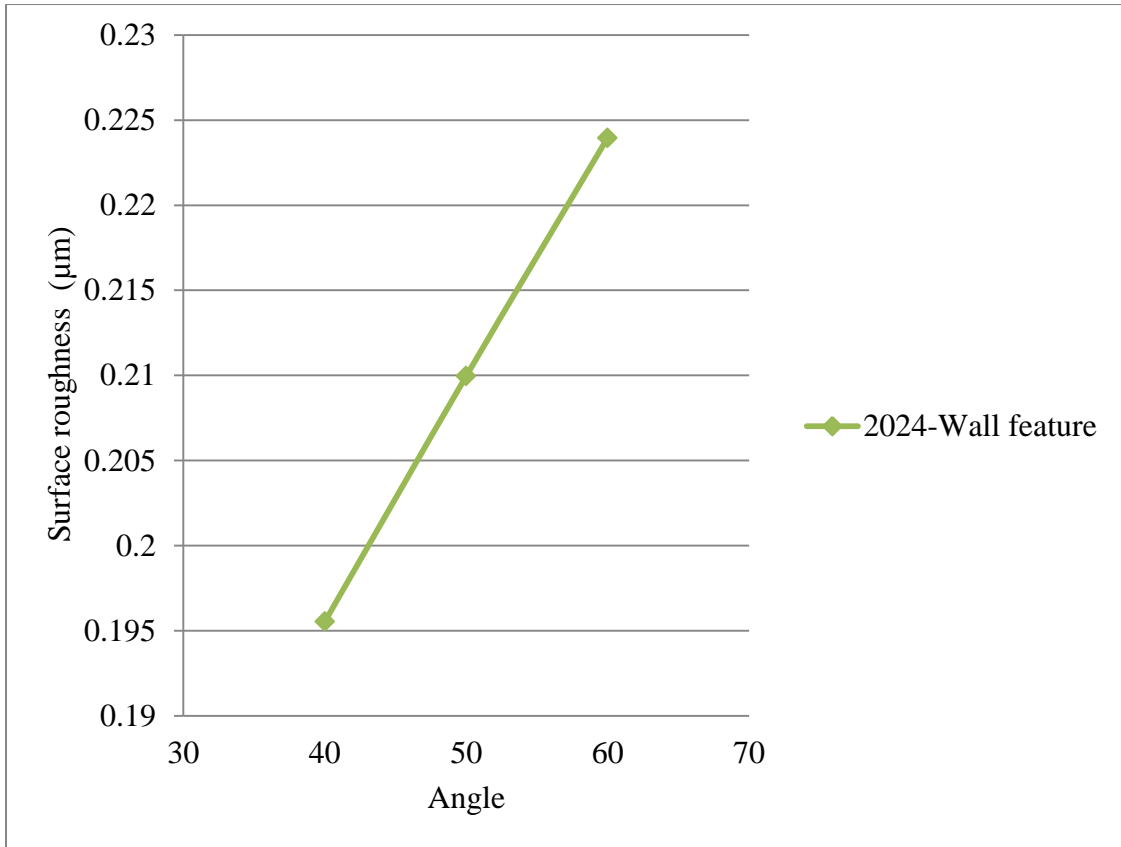


Figure 11-52 Surface roughness- 2024

Table 11-2 Surface roughness- 2024

<b>Wall feature</b>	
<b>Wall Angle</b>	<b>Ra (µm)</b>
40	0.19553
50	0.20996
60	0.22396
<b>Curve feature</b>	
0.16348	
<b>Corner feature</b>	
0.55172	

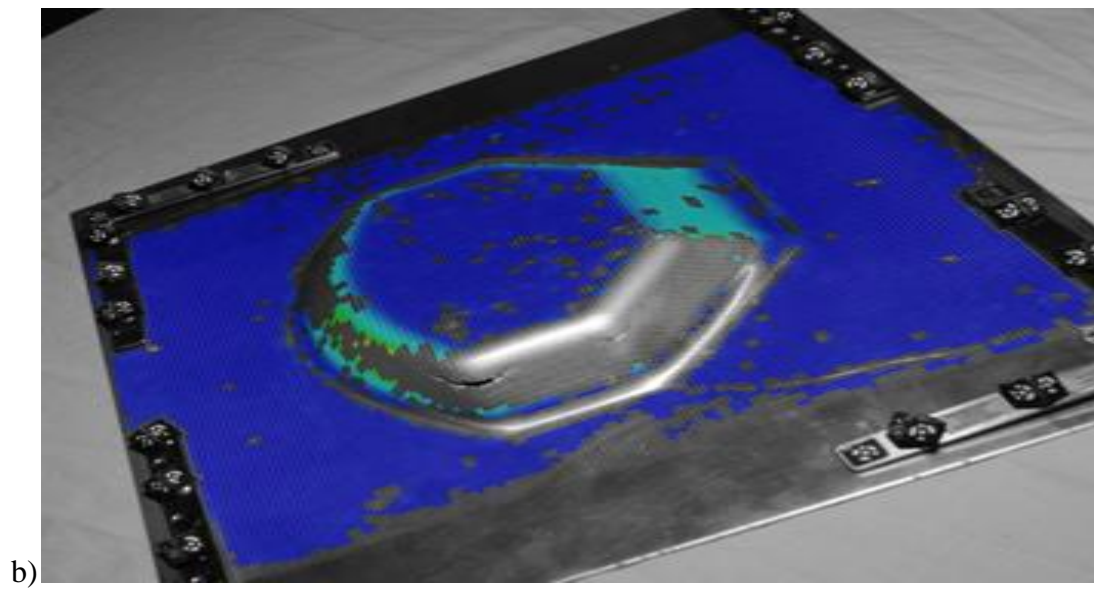
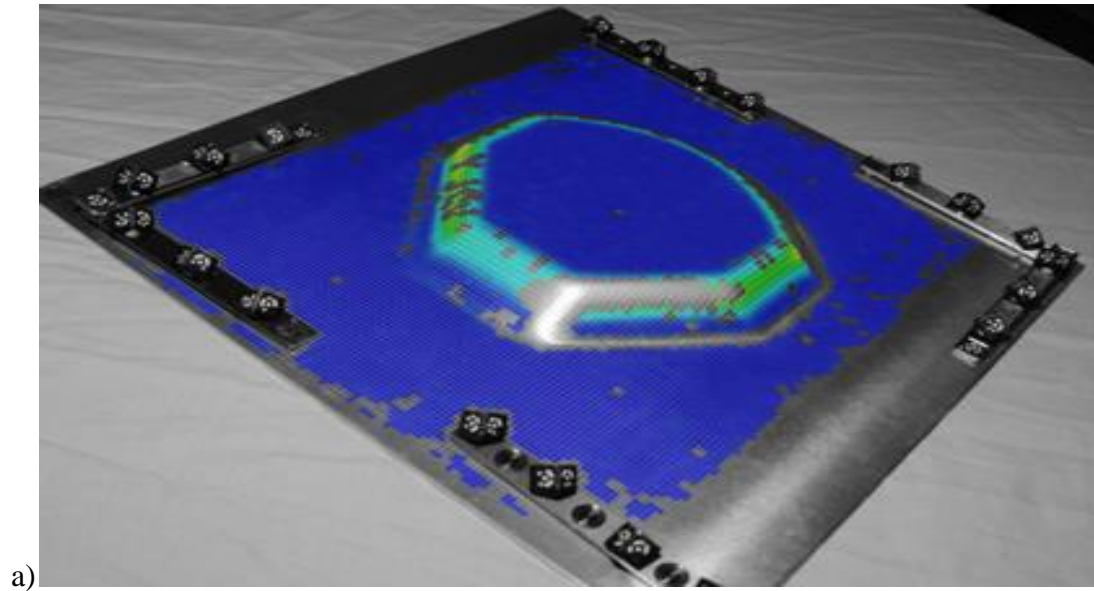


Figure 11-53 a) Major strains plotted on formed component; (a) AA1-2024, (b) AA2-2024.

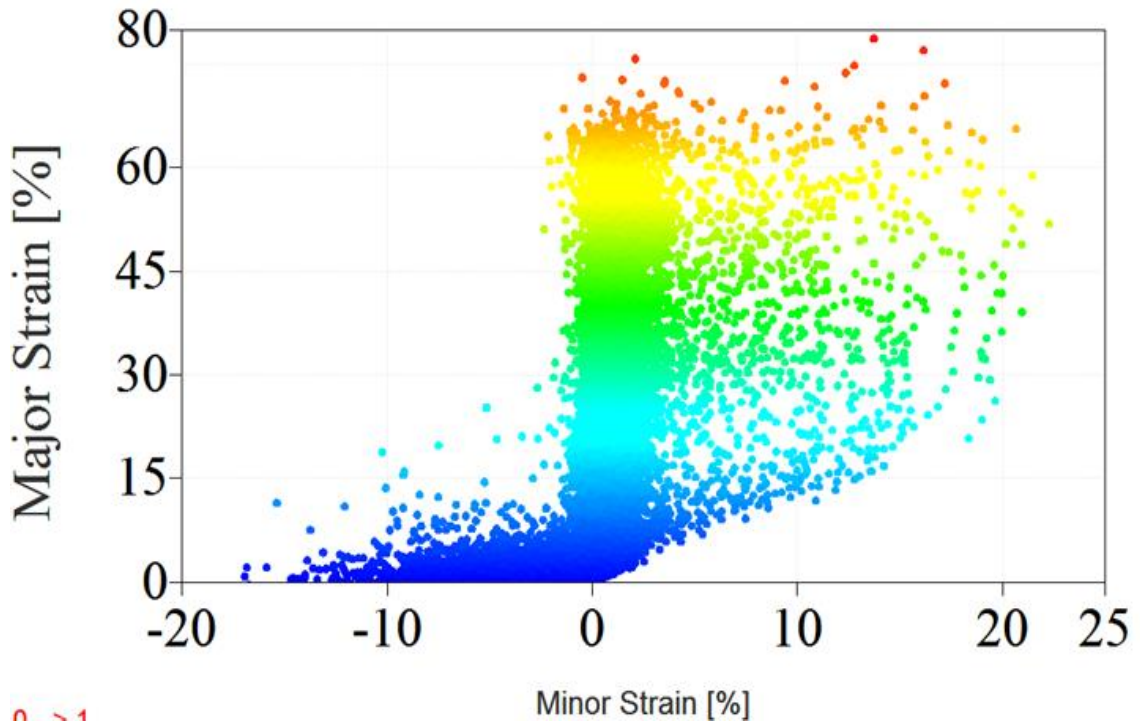


Figure 11-54 Major and minor strain graph AA1-2024.

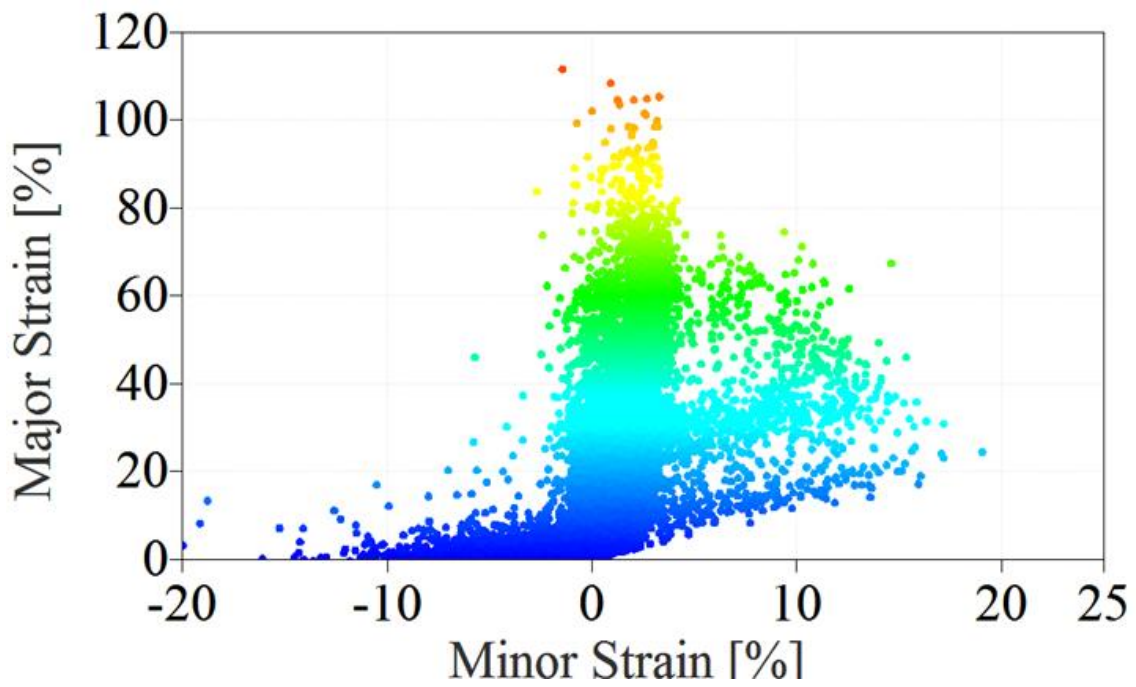
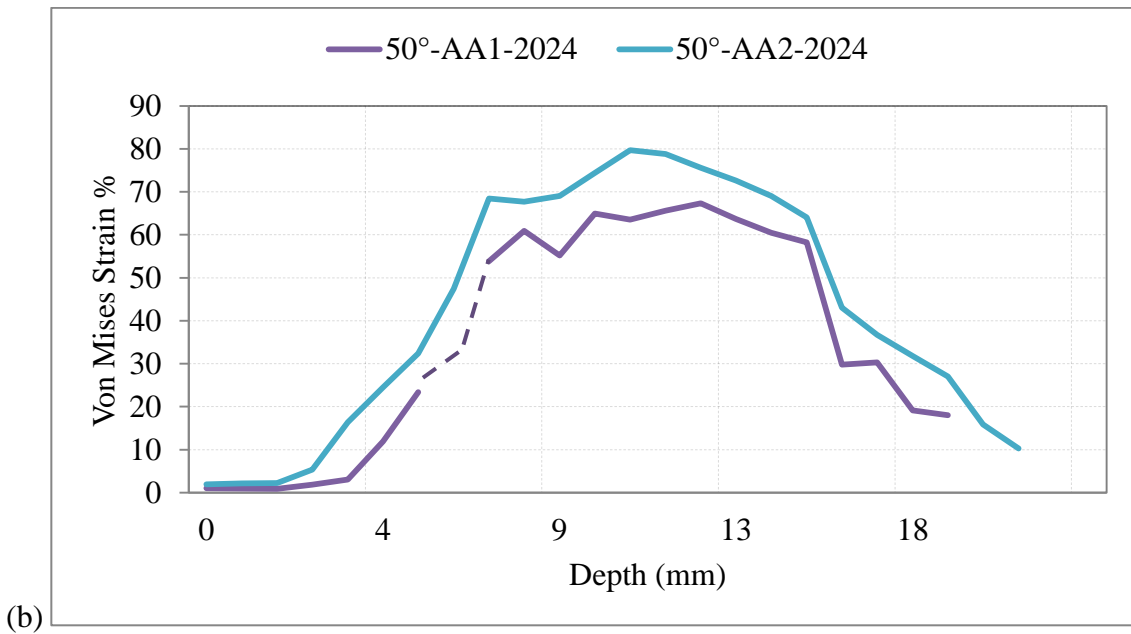
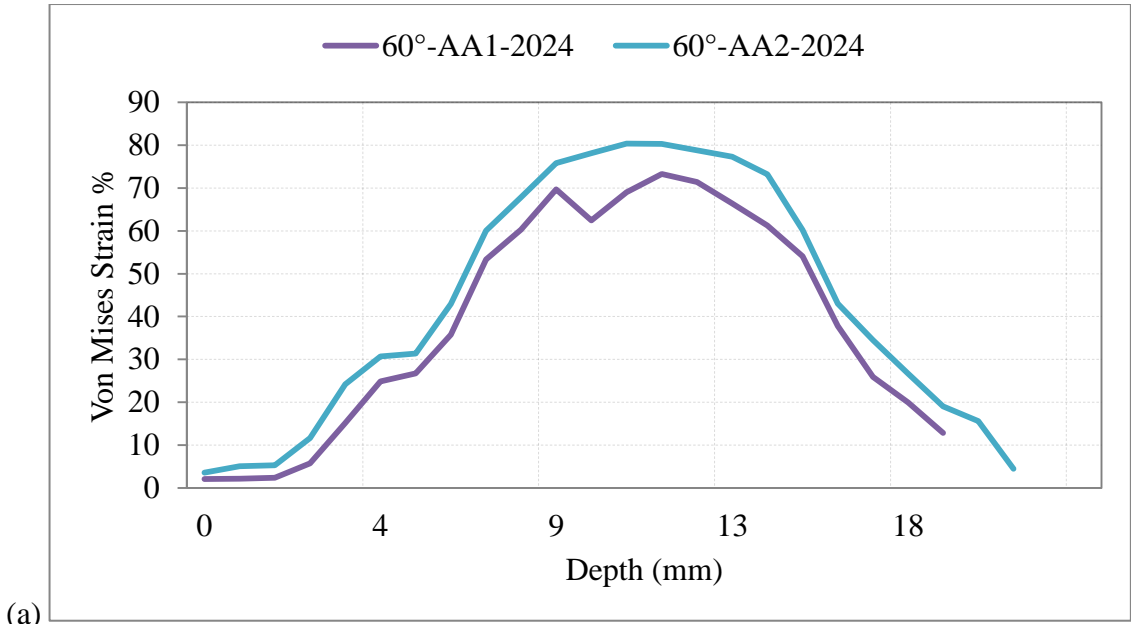
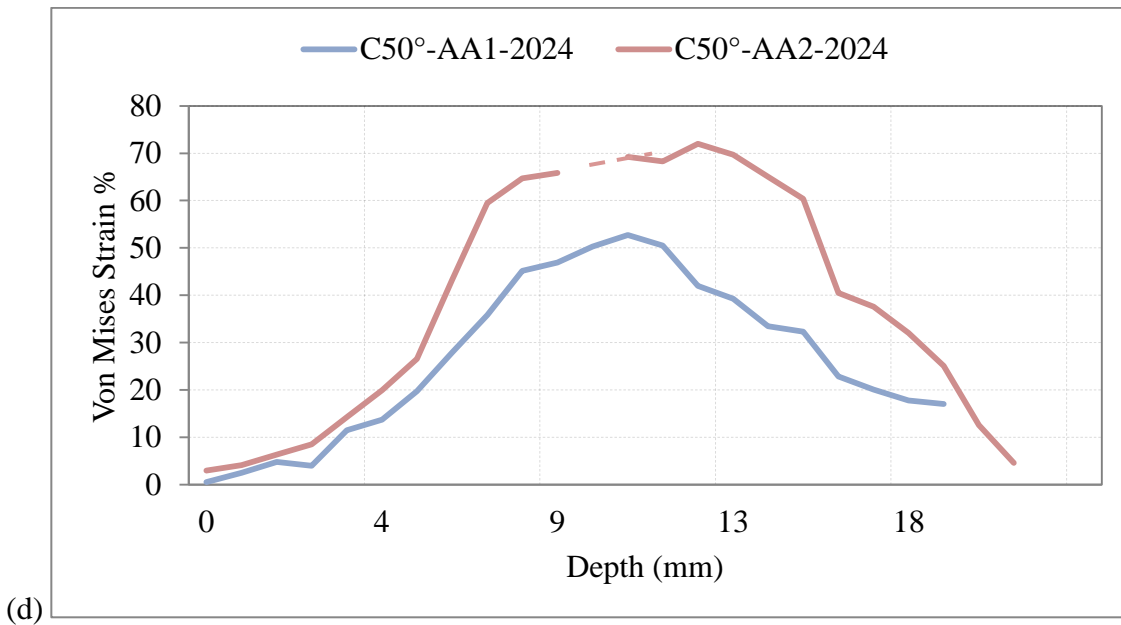
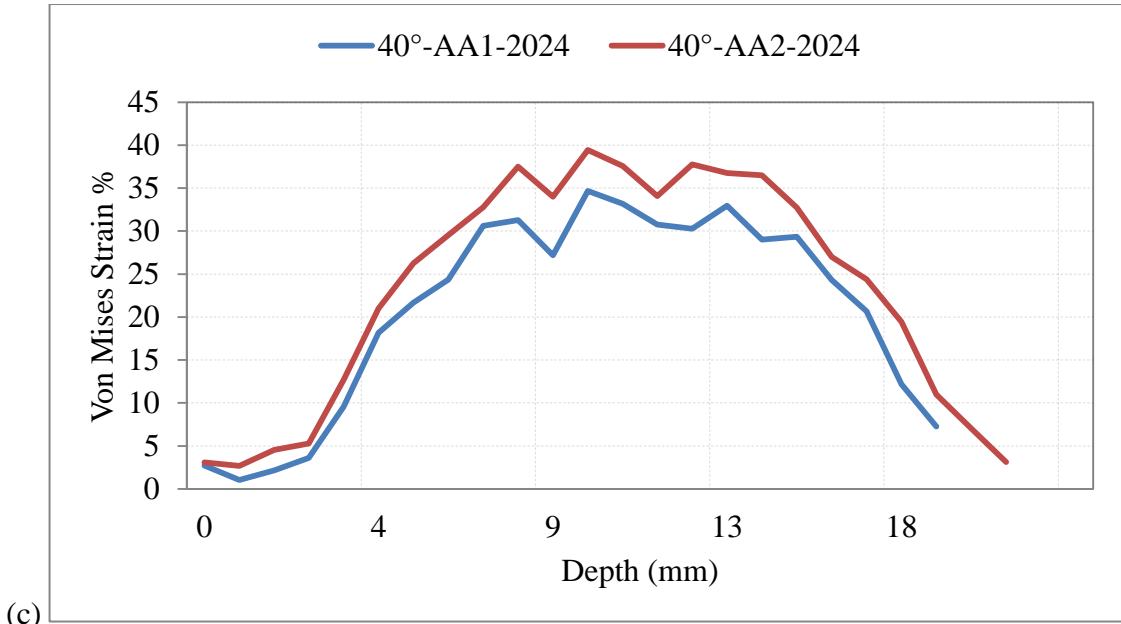
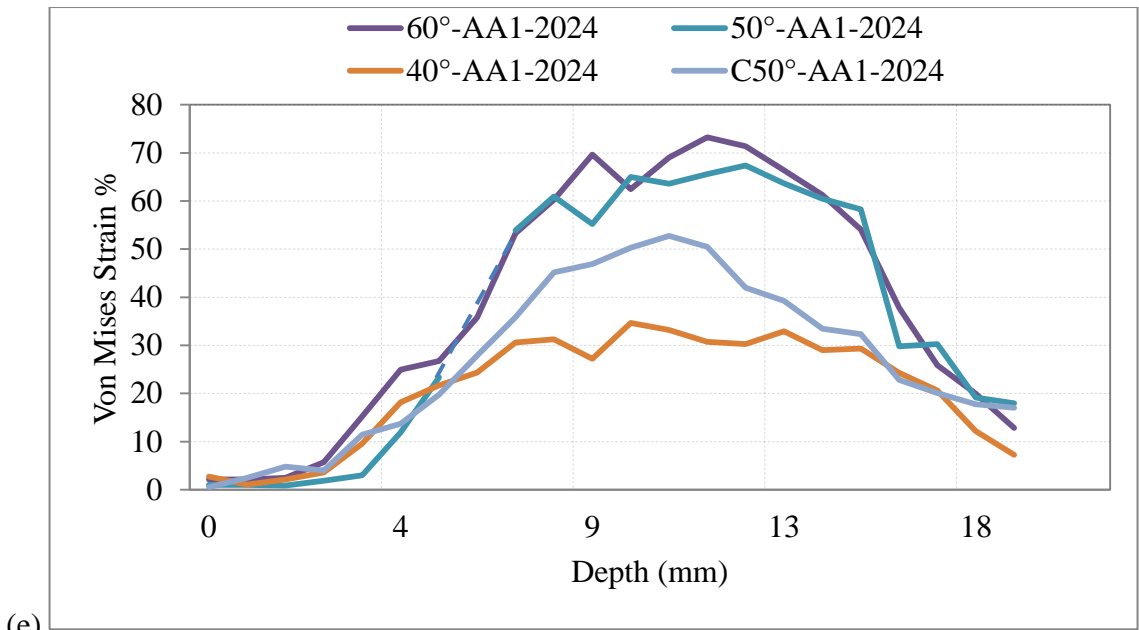


Figure 11-55 Major and minor strain graph AA2-2024.

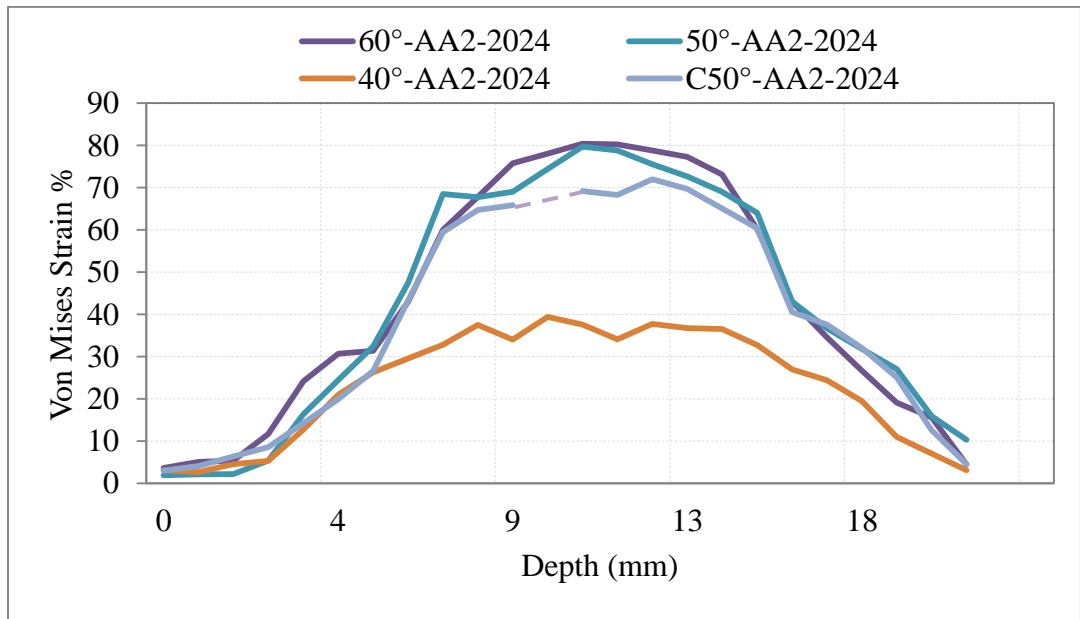






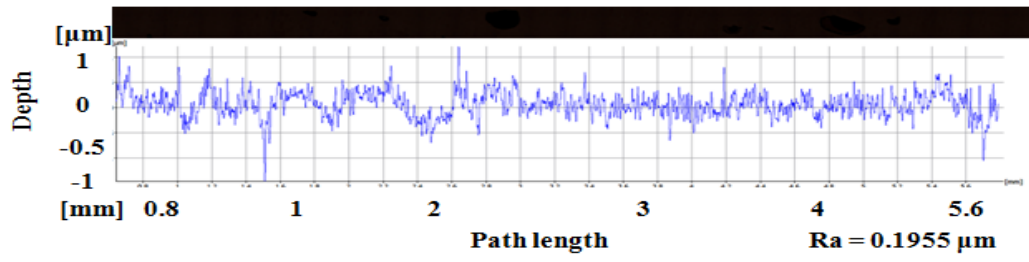


(e)

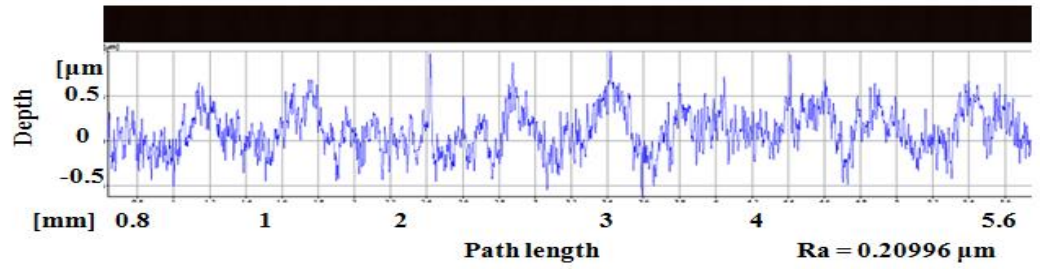


(f)

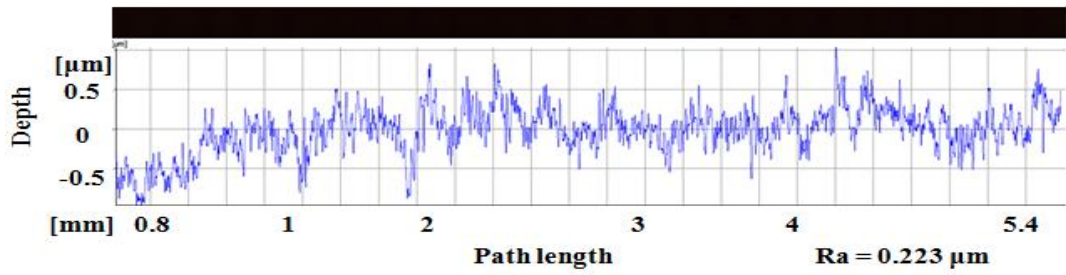
Figure 11-56 Von Mises Strain% vs Depth AA1-2024 & AA2-2024; (a) 60°, (b) 50°, (c) 40°, (d) c50° (e) Wall angle Comparison AA1-2024, (f) Wall angle Comparison AA2-2024.



(a)



(b)



(c)

Figure 11-57 Surface roughness profiles of the straight wall feature 2024; (a) 40°, (b) 50°, (c) 60°.

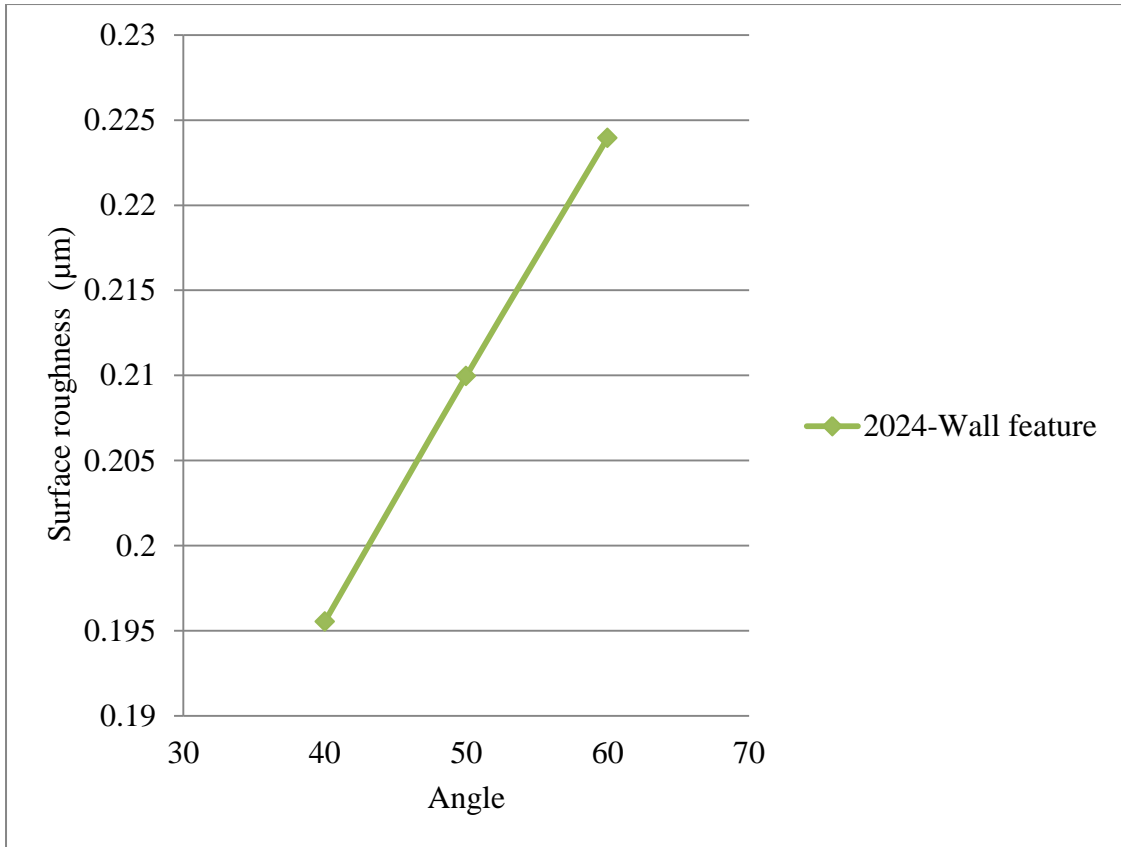


Figure 11-58 Surface roughness- 2024

Table 11-3 Surface roughness- 2024

Surface	Ra (µm)
Wall feature	
40	0.19553
50	0.20996
60	0.22396
Curve feature	
	0.16348
Curve feature	
	0.55172

## AA7075 Results

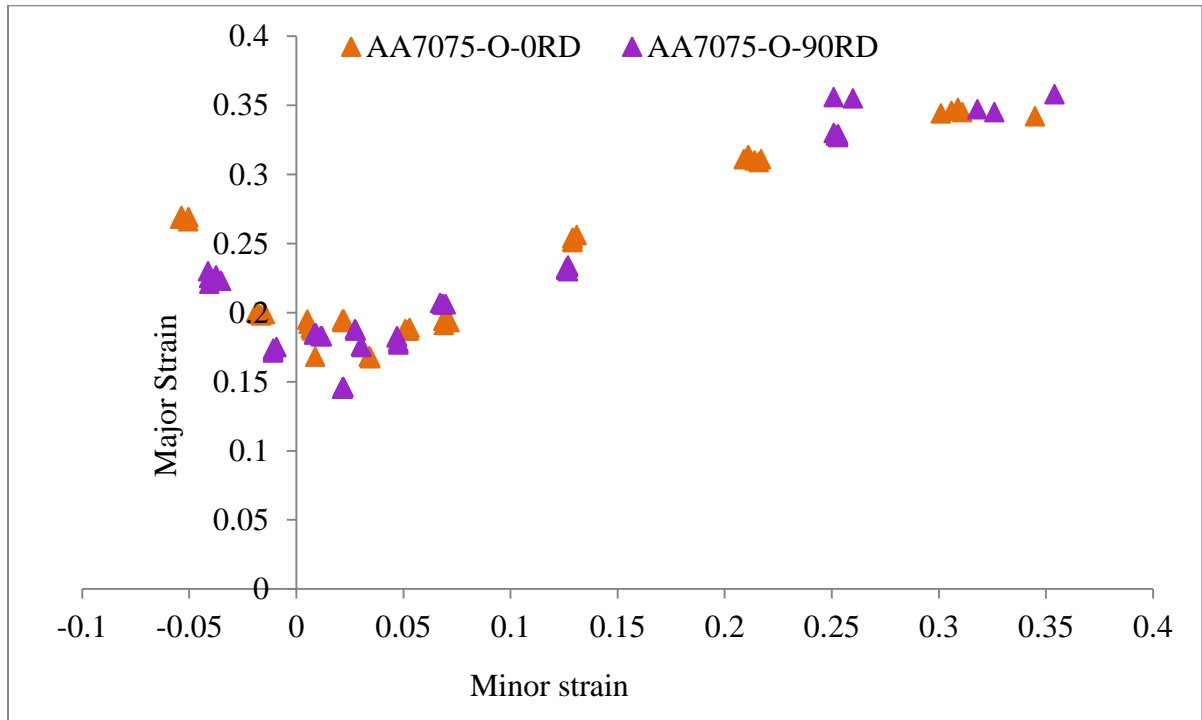


Figure 11-59 Forming Limit Curve AA7075

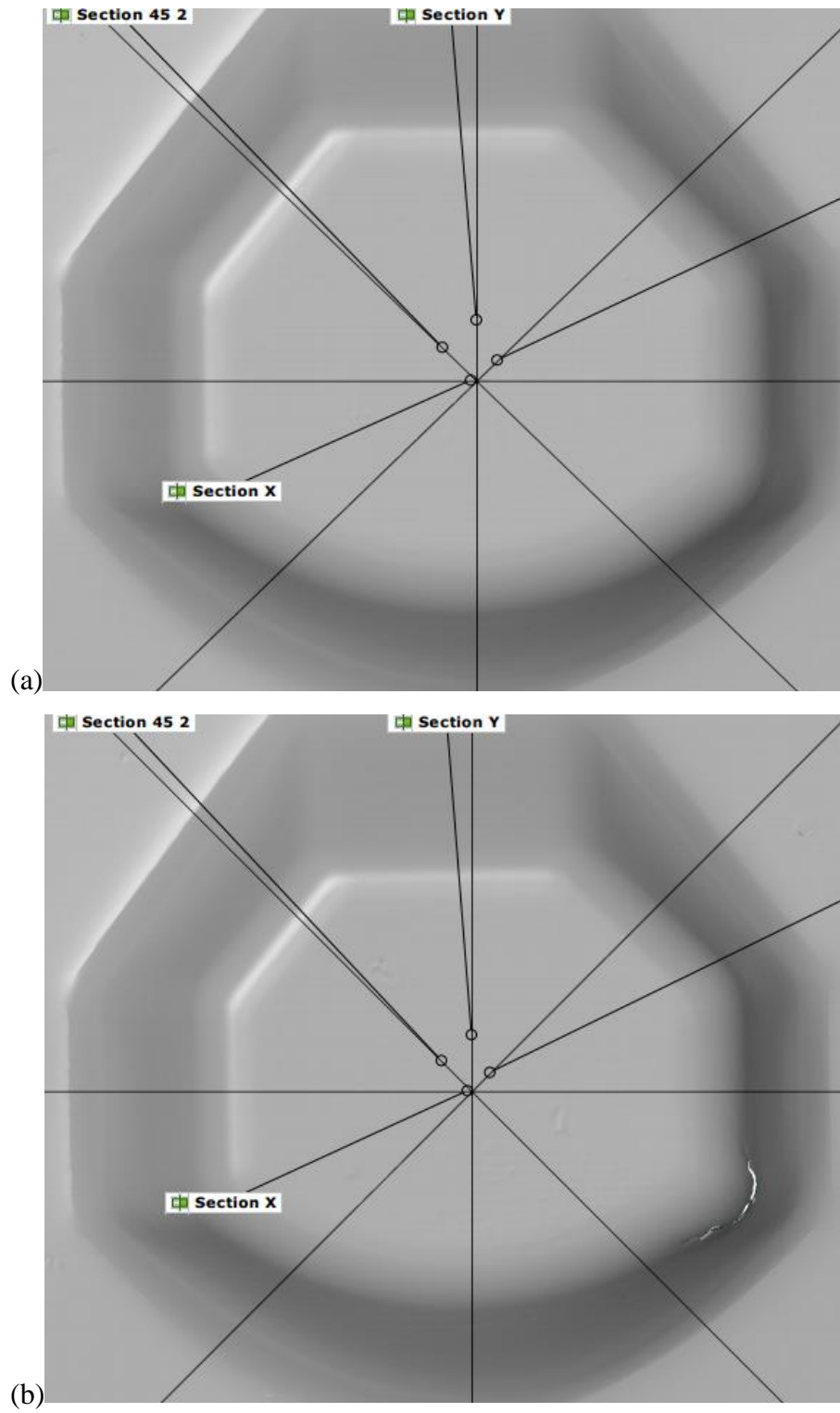


Figure 11-60 Multi-slope geometry; (a) AA1-7075, (b) AA2-7075.

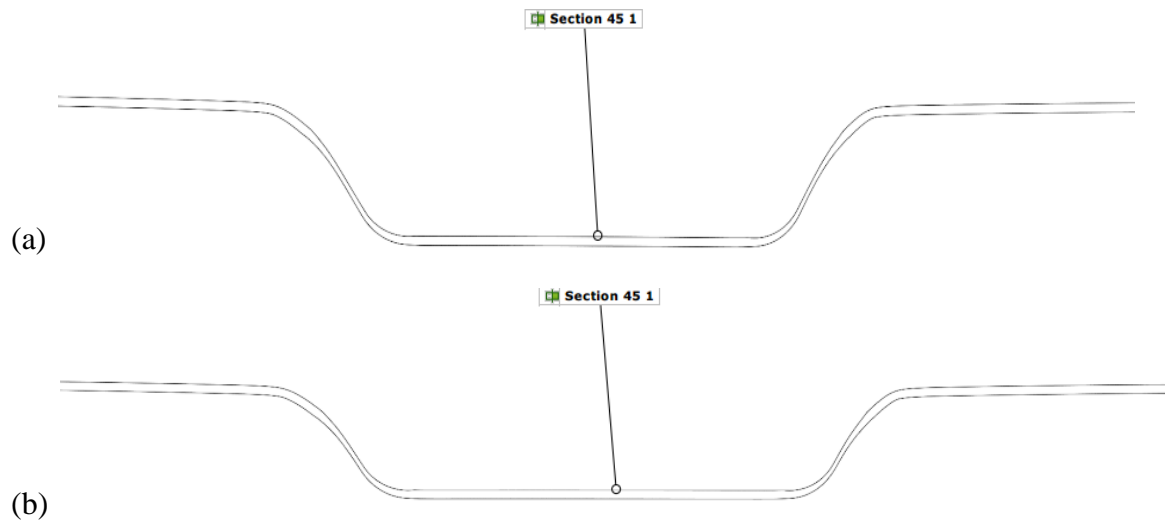


Figure 11-61 Section X; (a) AA1-7075, (b) AA2-7075.

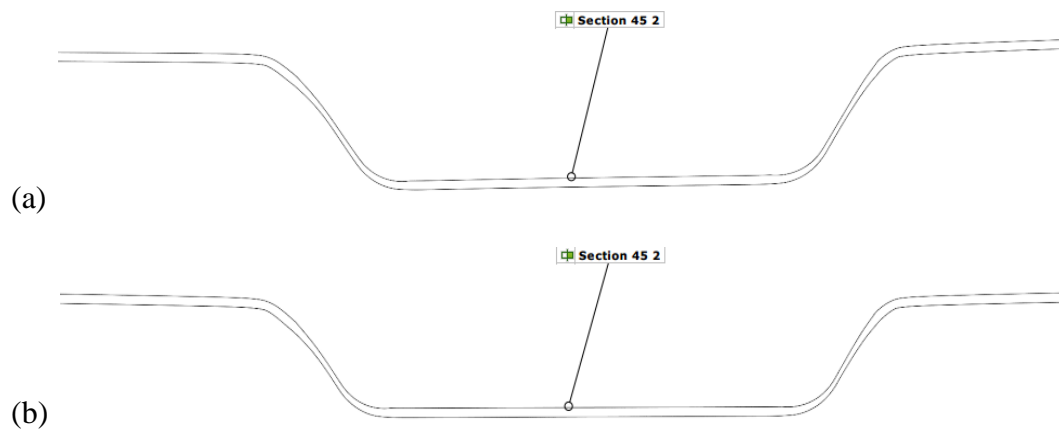


Figure 11-62 Section Y; (a) AA1-7075, (b) AA2-7075.



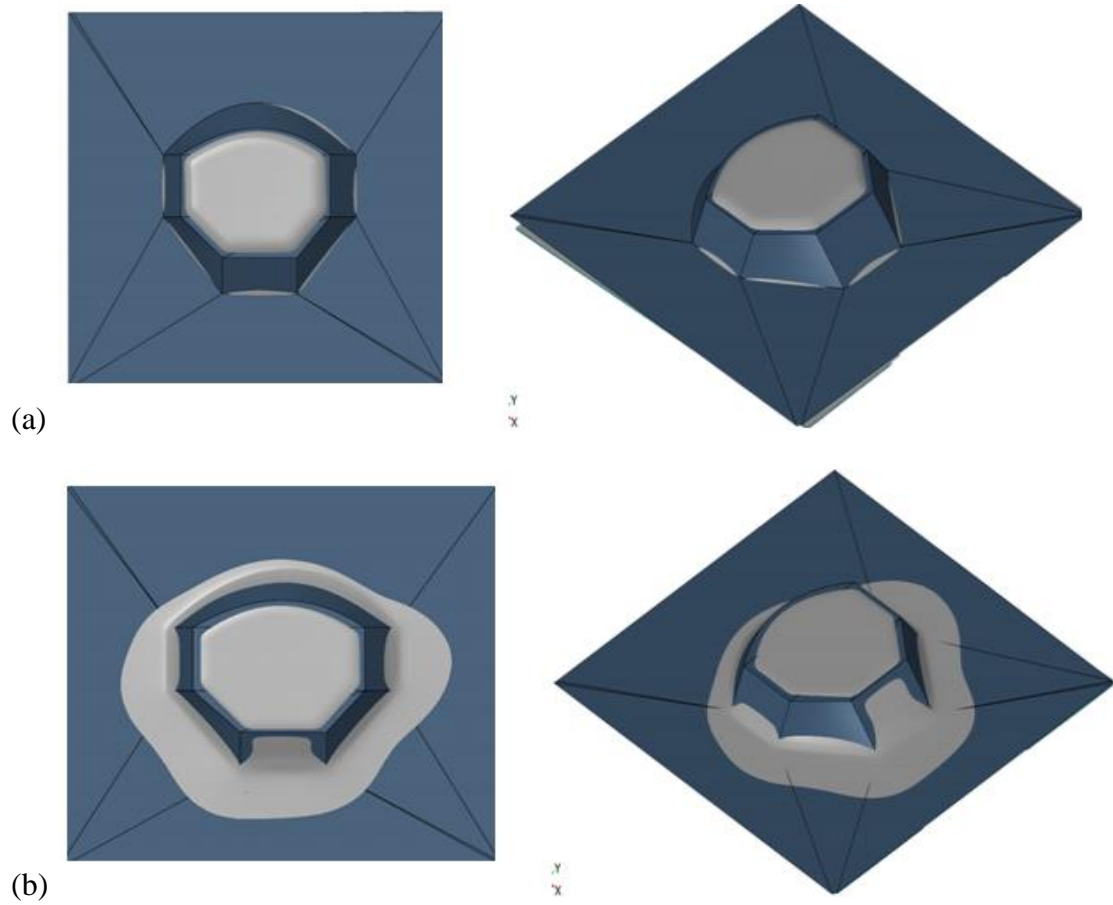


Figure 11-63 Qualitative CAD comparison; top and isometric view; (a) AA1-7075, (b) AA2-7075.

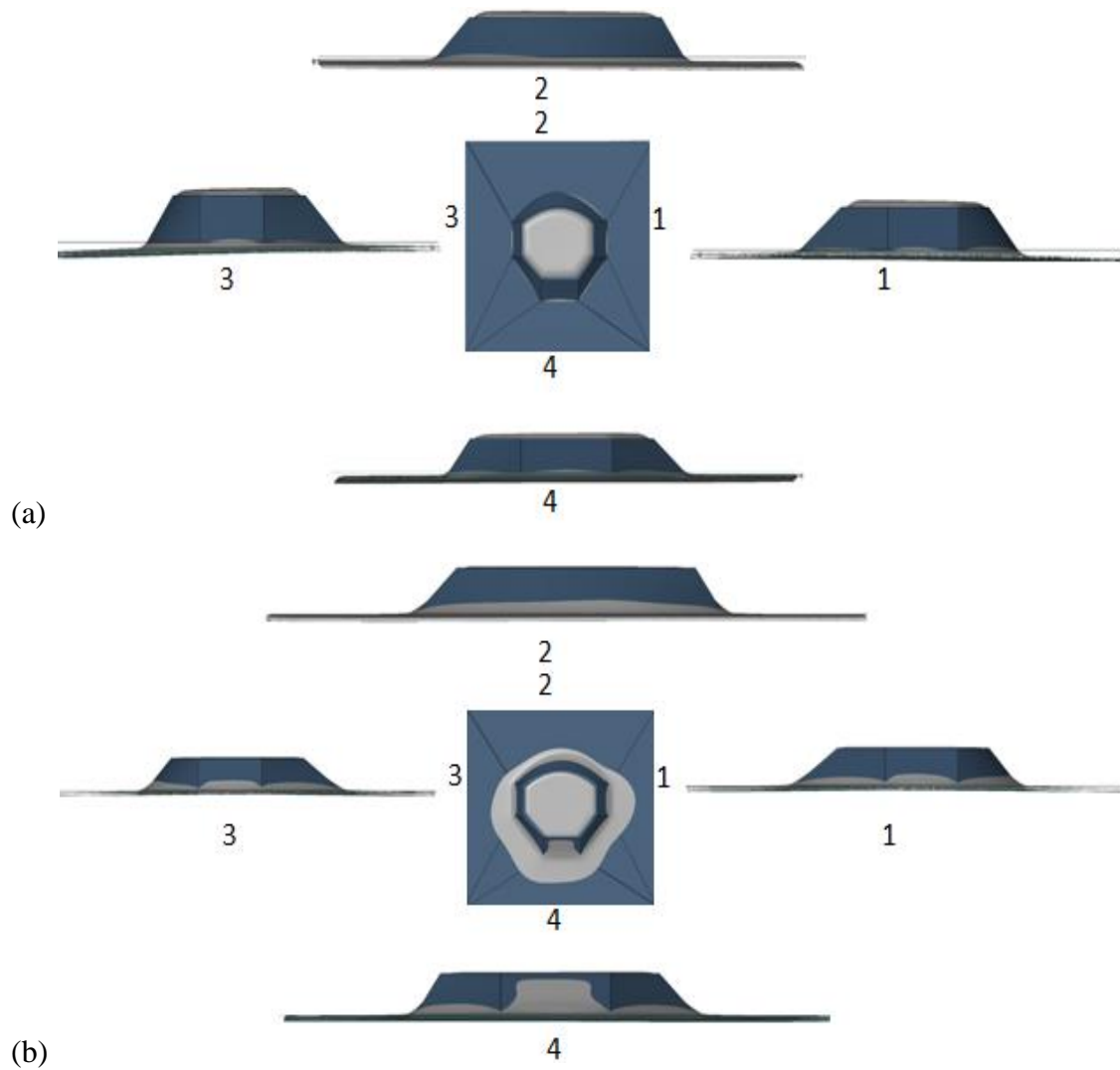


Figure 11-64 Qualitative CAD comparison; top and side views; (a) AA1-7075, (b) AA2-7075.

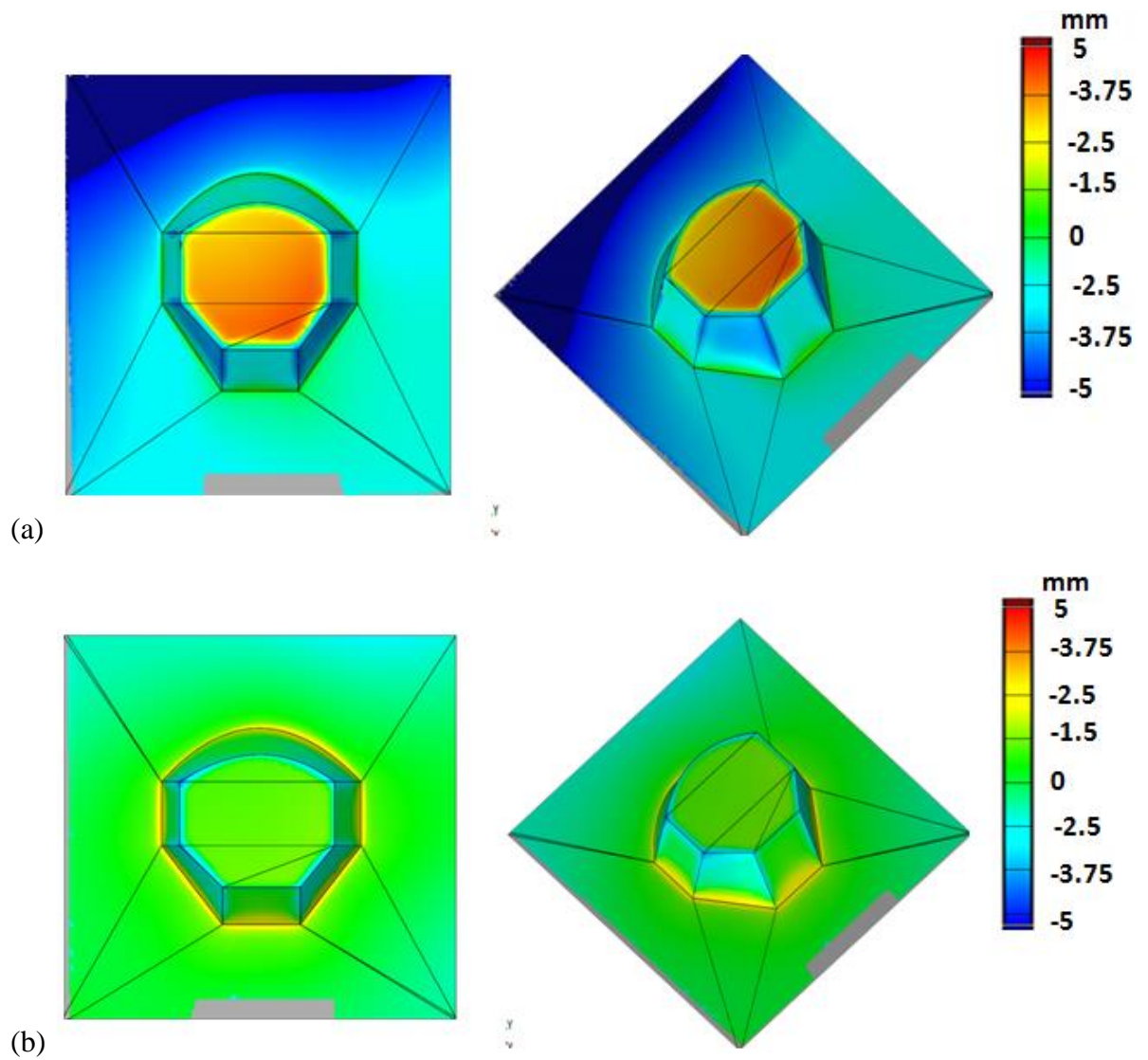


Figure 11-65 Quantitative CAD comparison; top and isometric view; (a) AA1-7075, (b) AA2-7075.

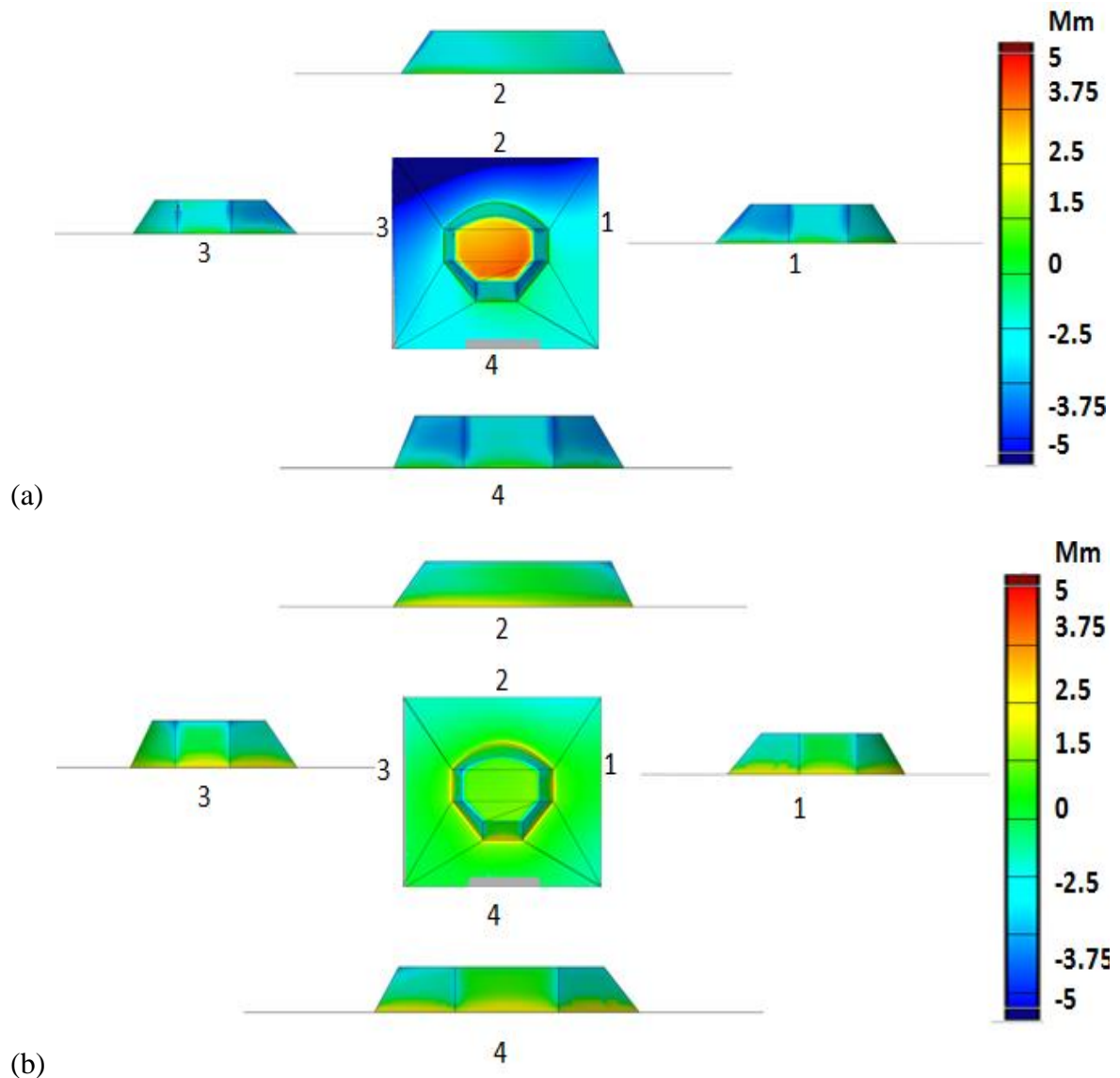


Figure 11-66 Quantitative CAD comparison; top and side views; (a) AA1-7075, (b) AA2-7075.

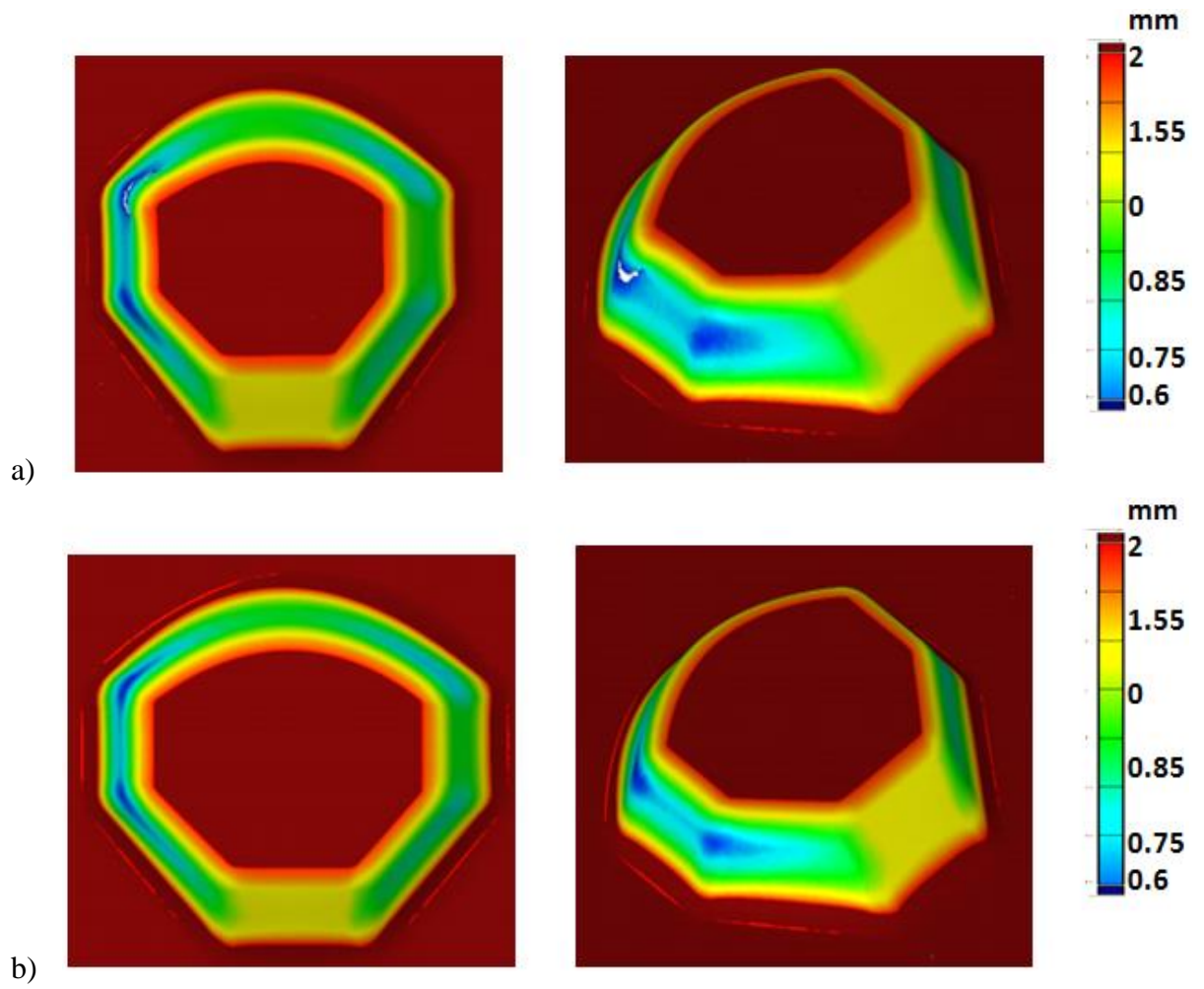


Figure 11-67 Thickness profile, top and isometric view; (a) AA1-7075, (b) AA2-7075.

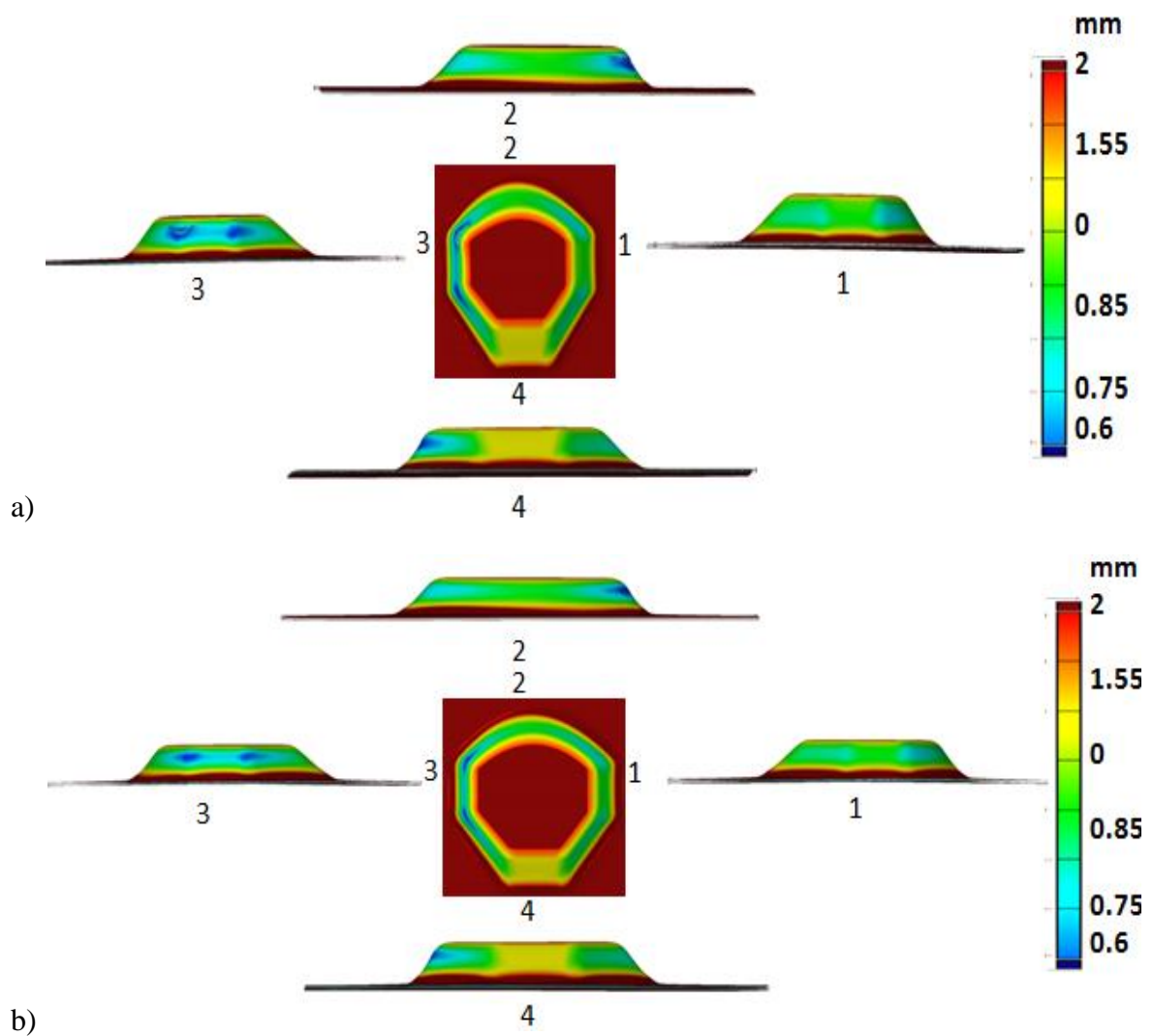
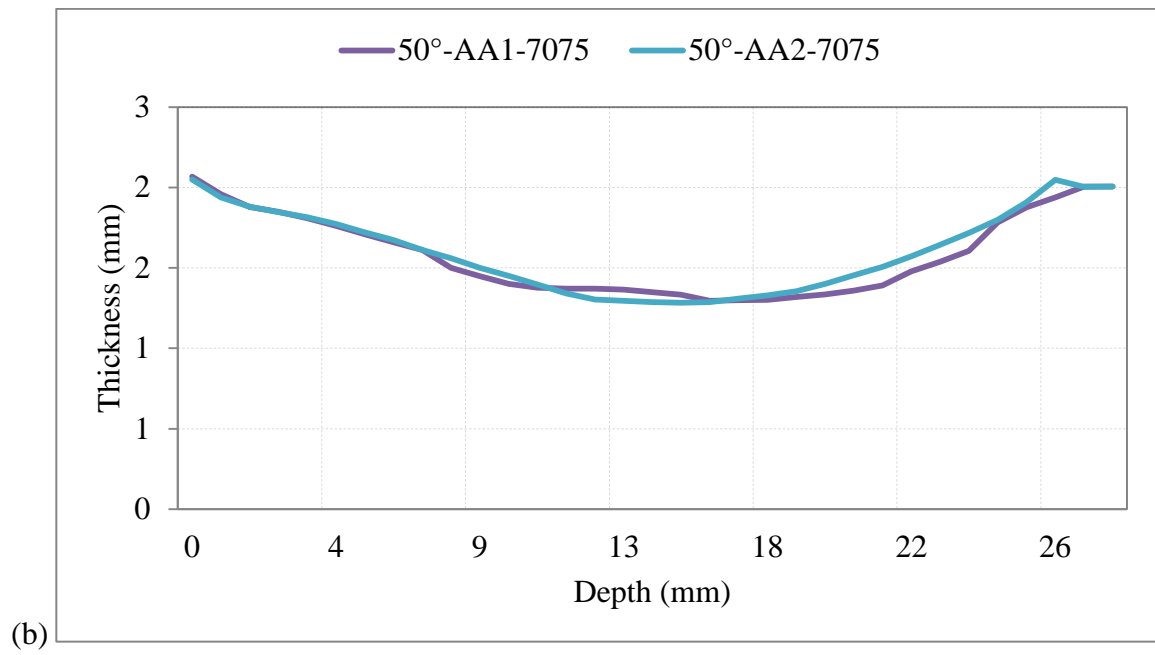
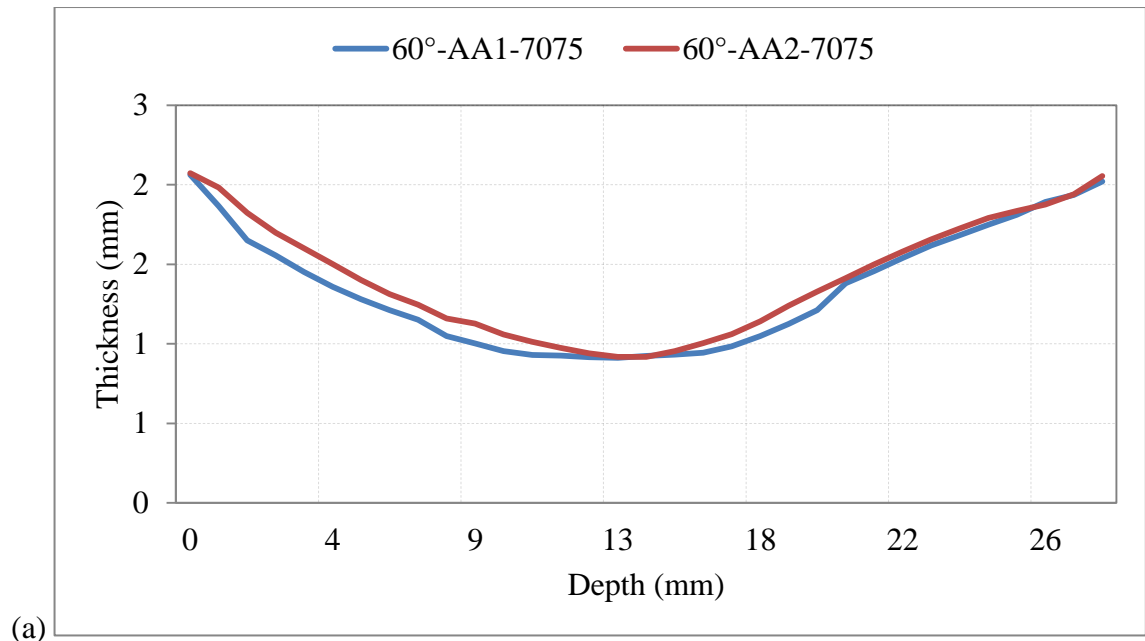
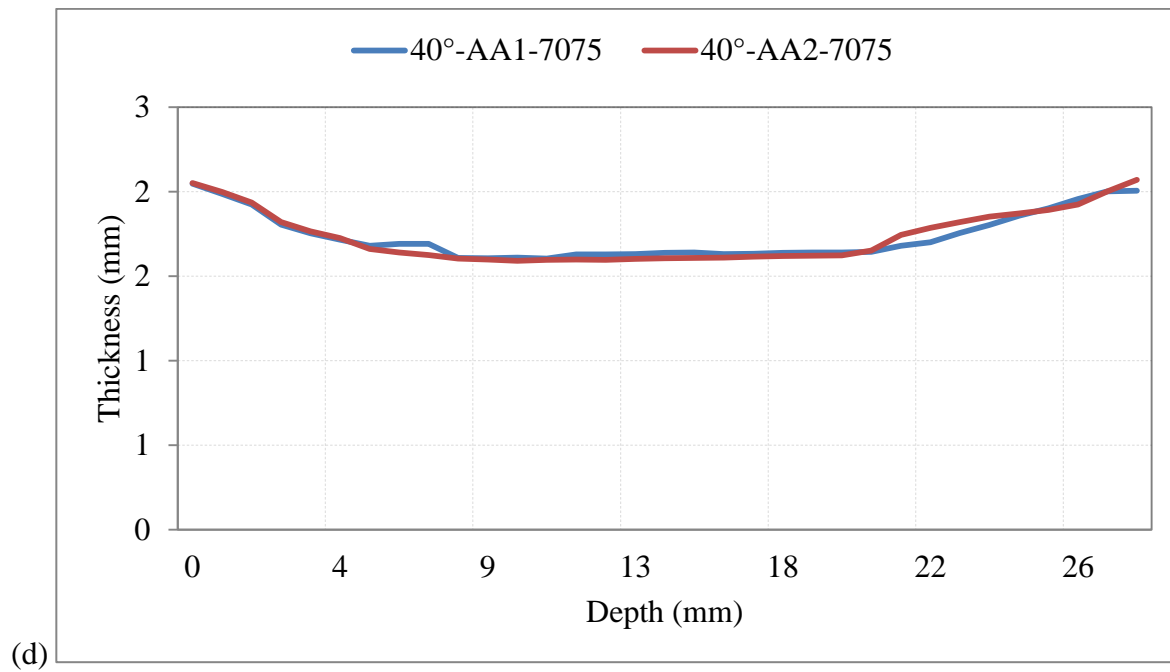
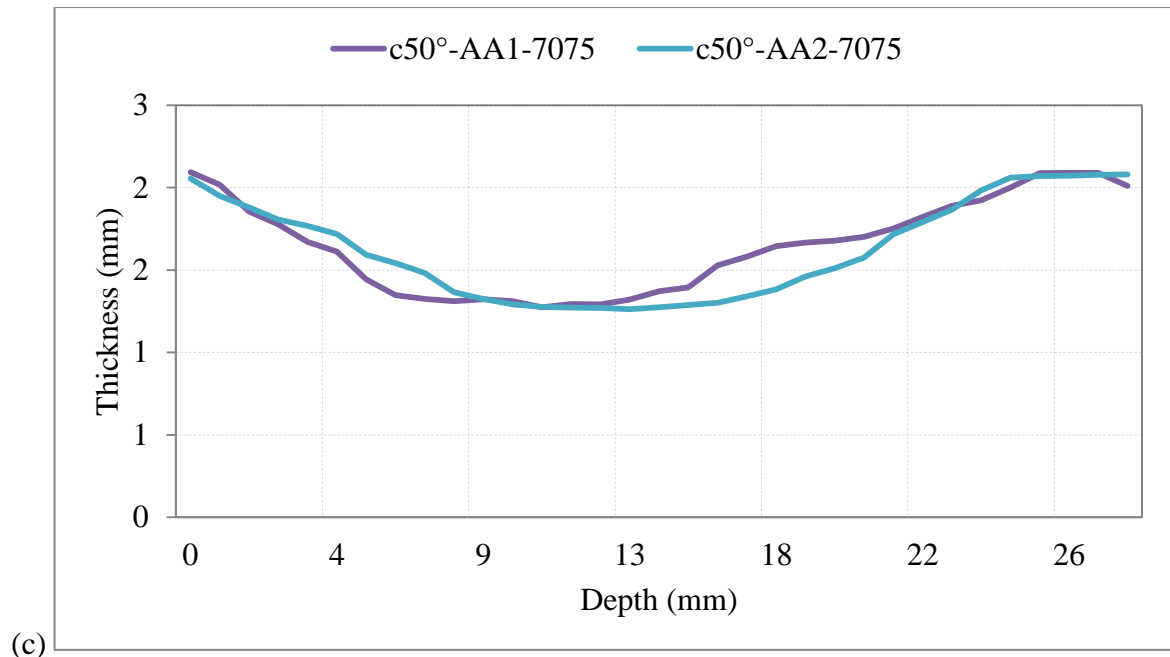


Figure 11-68 Thickness profile top and side views; (a) AA1-7075, (b) AA2-7075.







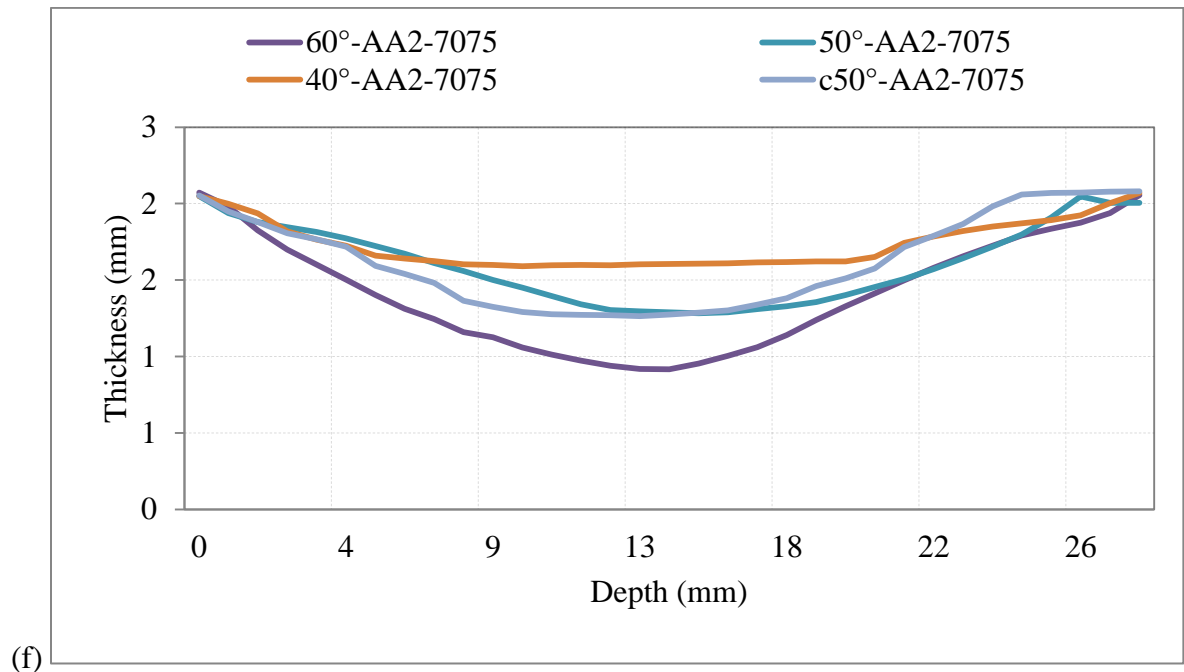
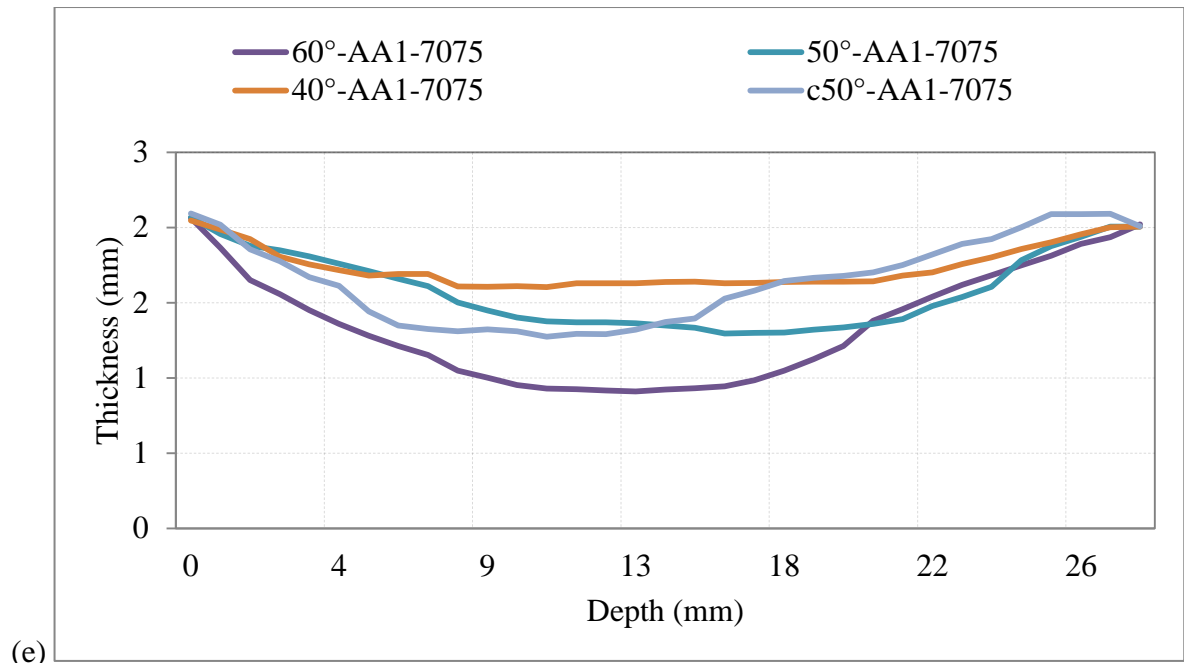


Figure 11-69 Thickness vs Depth AA1-7075 & AA2-7075; (a) 60°, (b) 50°, (c) Curve 50°, (d) 40°, (e) Wall angle Comparison AA1-7075, (f) Wall angle Comparison AA2-7075.

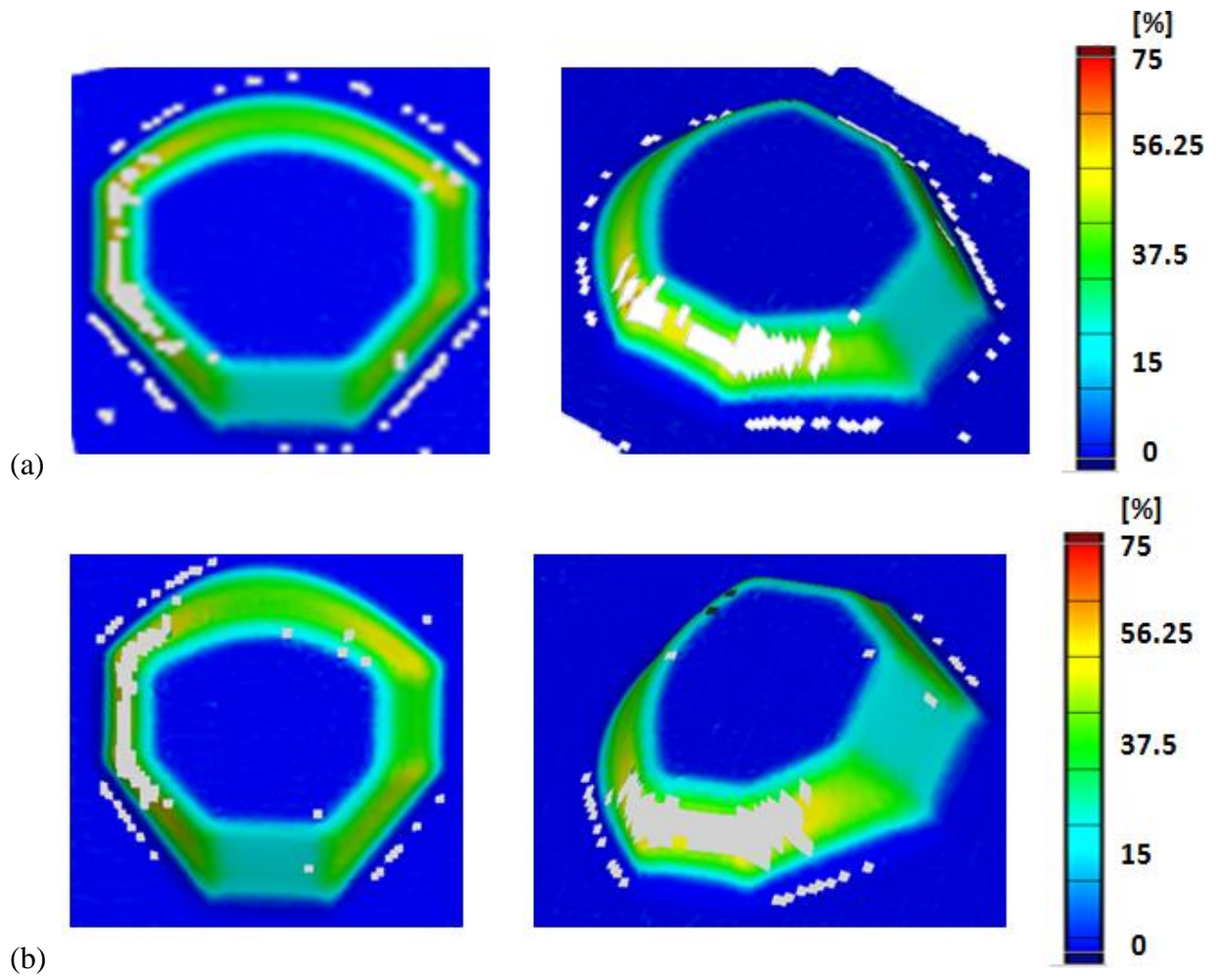


Figure 11-70 Thickness reduction; top and isometric view , (a) AA1-7075, (b) AA2-7075.

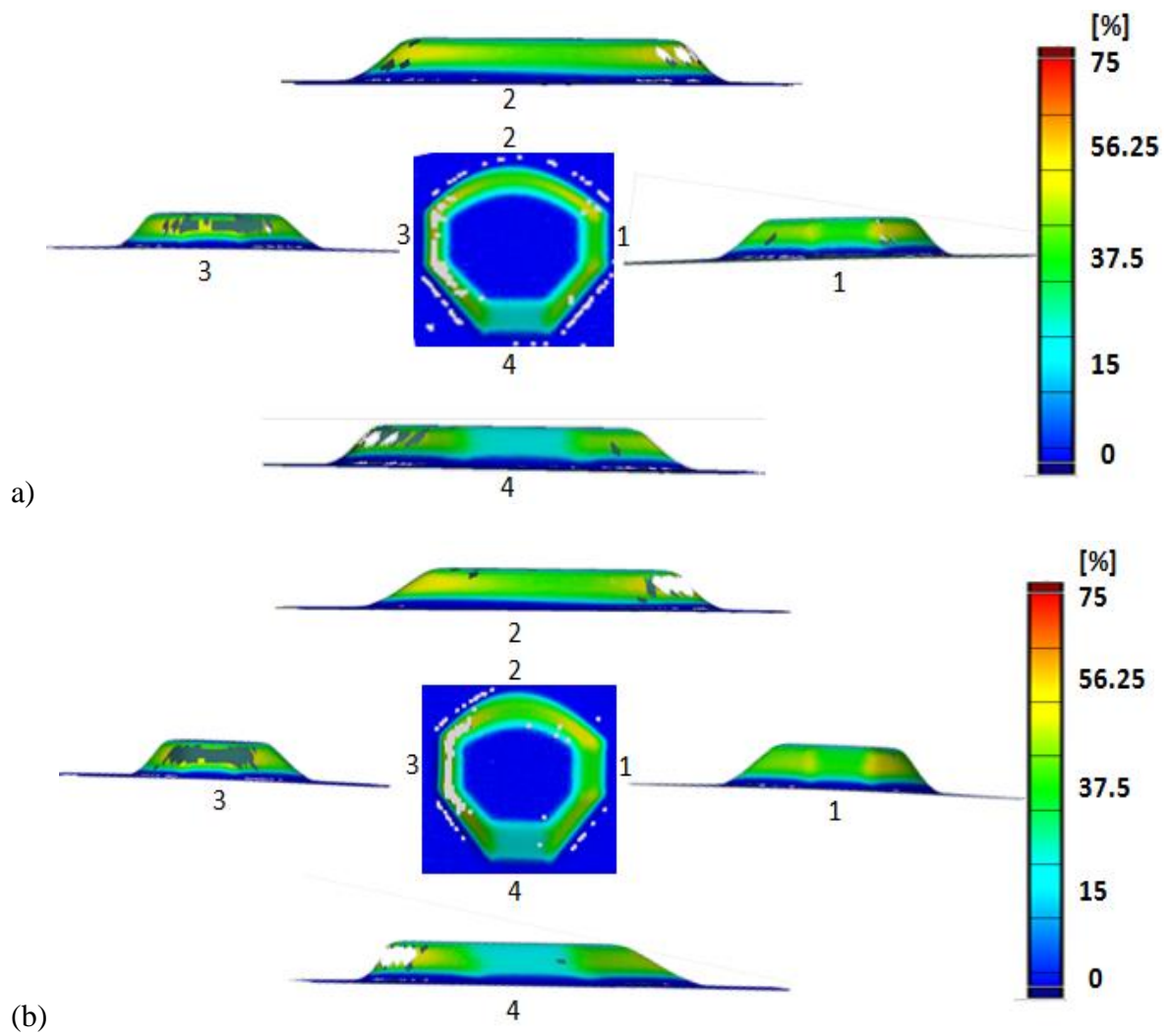
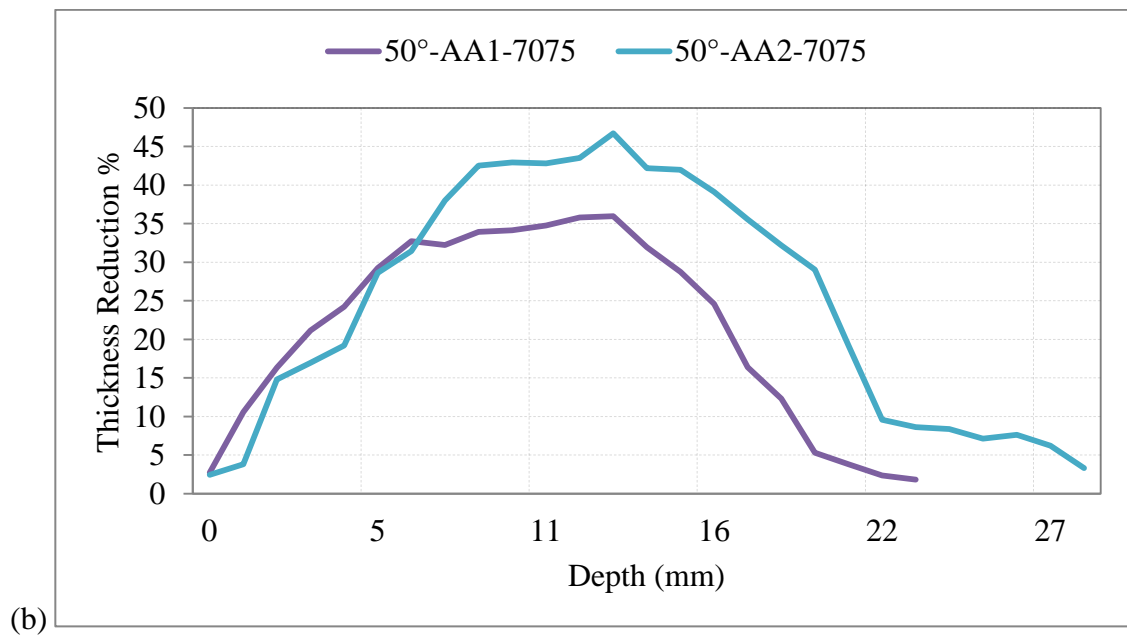
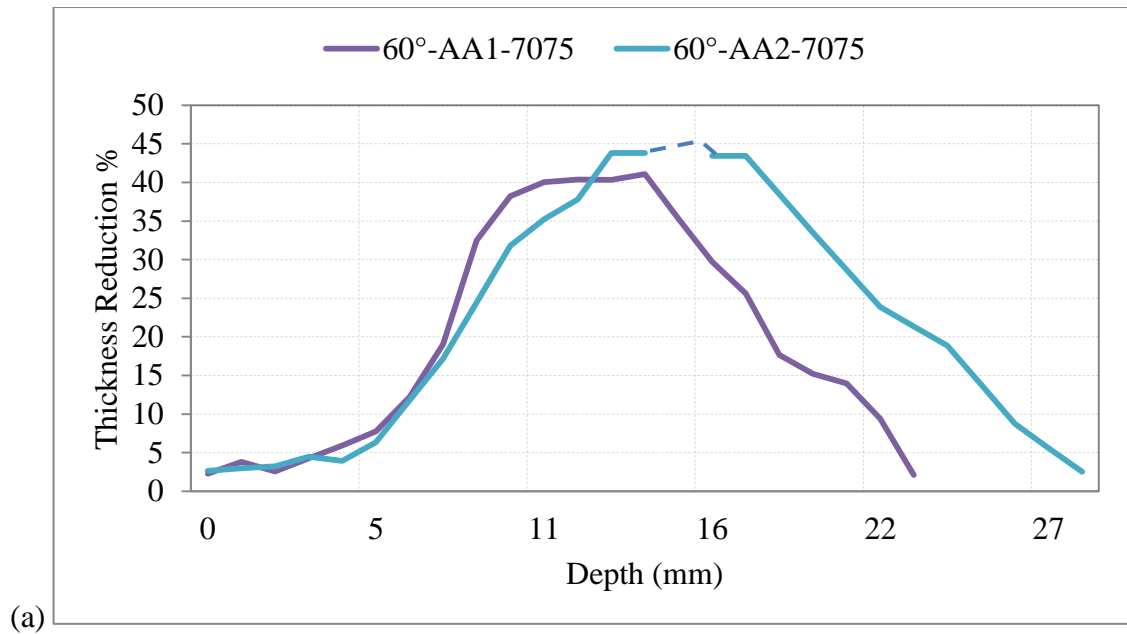
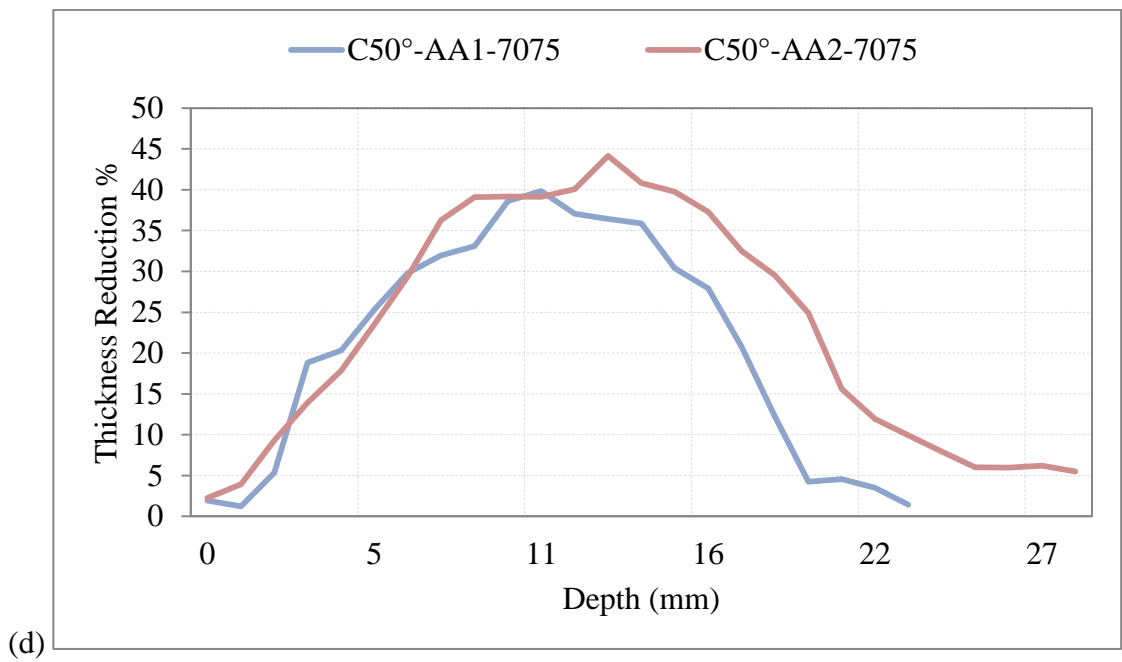
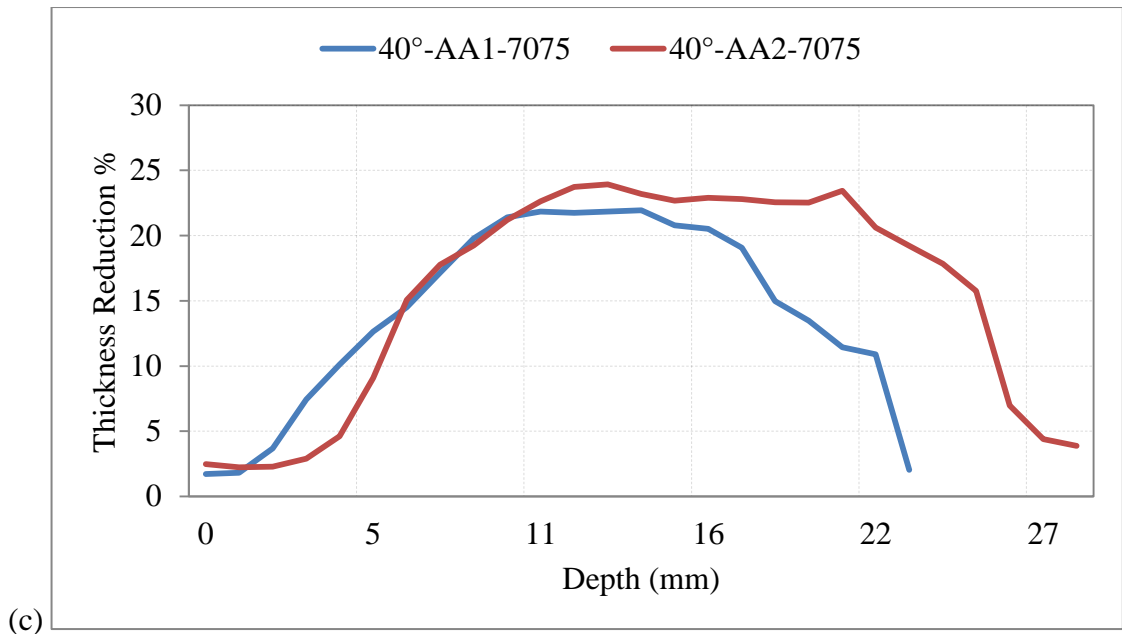


Figure 11-71 Thickness reduction; top and side views, (a) AA1-7075, (b) AA2-7075.





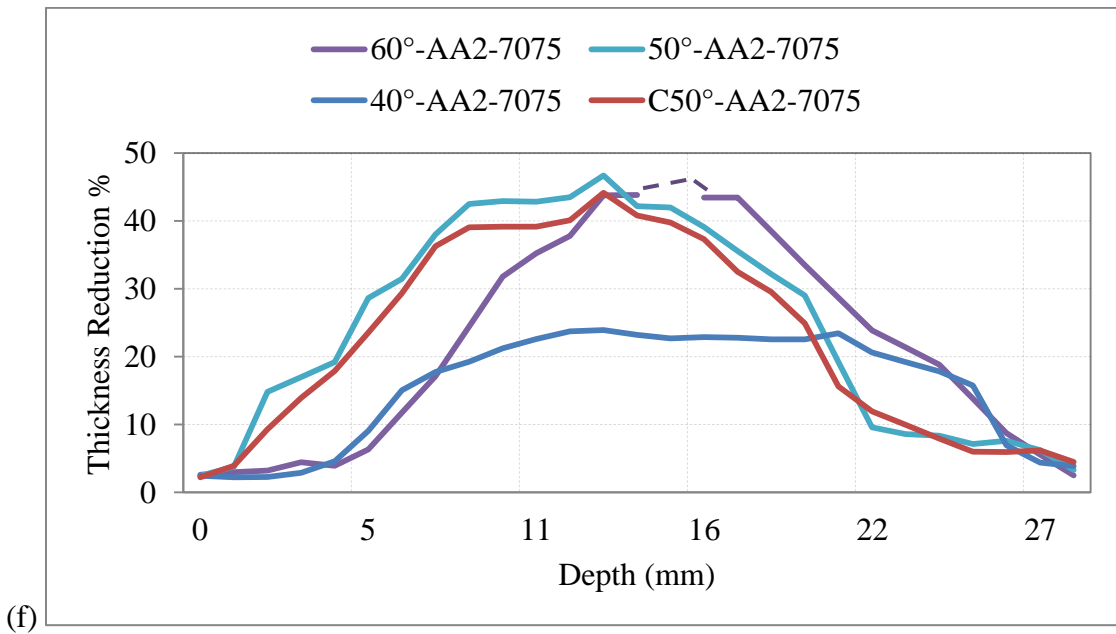
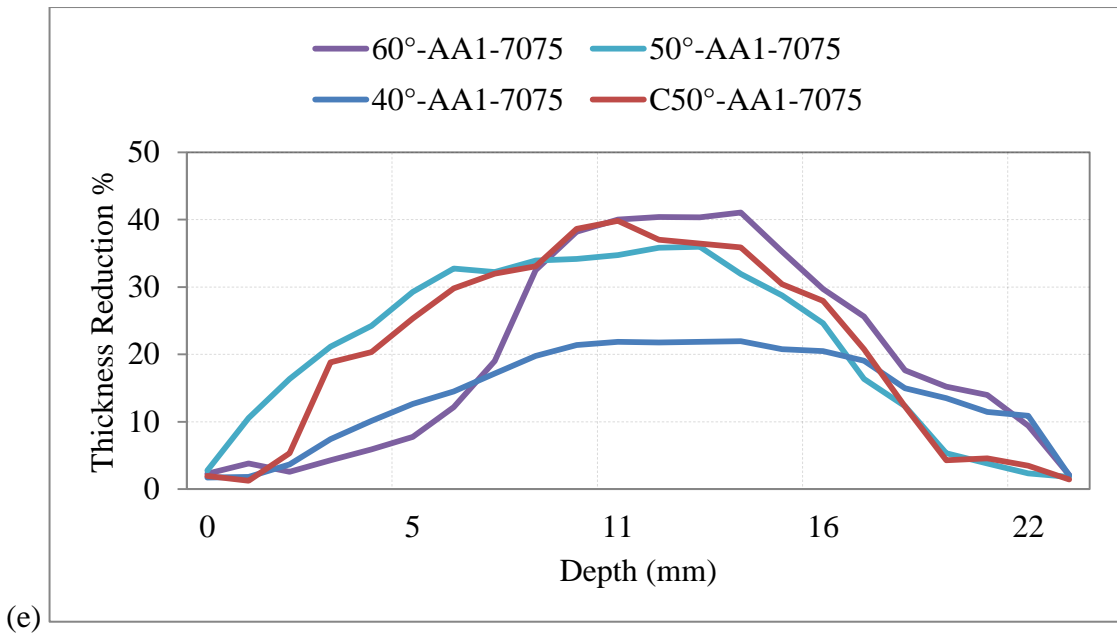


Figure 11-72 Thickness reduction% vs Depth AA1-7075 & AA2-7075; (a) 60°, (b) 50°, (c) 40°, (d) Curve 50°, (e) Wall angle Comparison AA1-7075, (f) Wall angle Comparison AA2-7075.

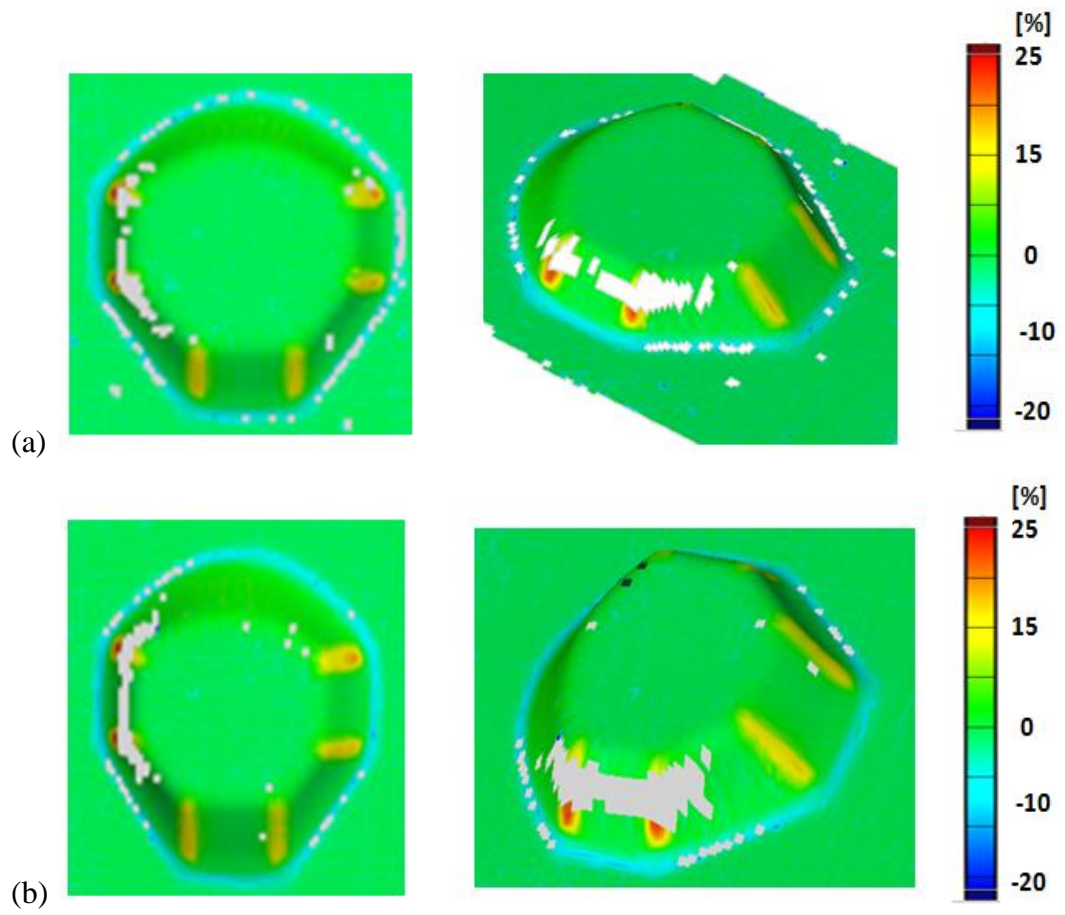


Figure 11-73 Minor strain; top and isometric view (a) AA1-7075, (b) AA2-7075.

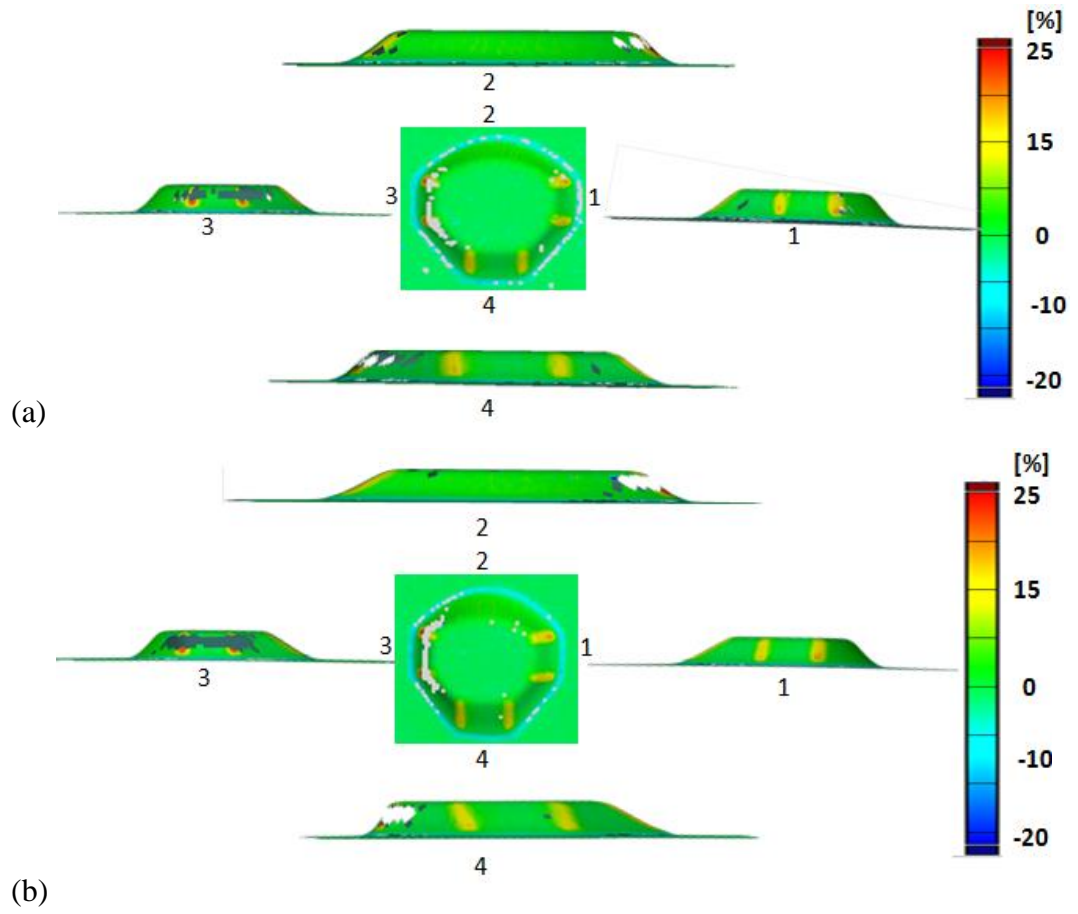


Figure 11-74 Minor strain; top and side views (a) AA1-7075 (b) AA2-7075.



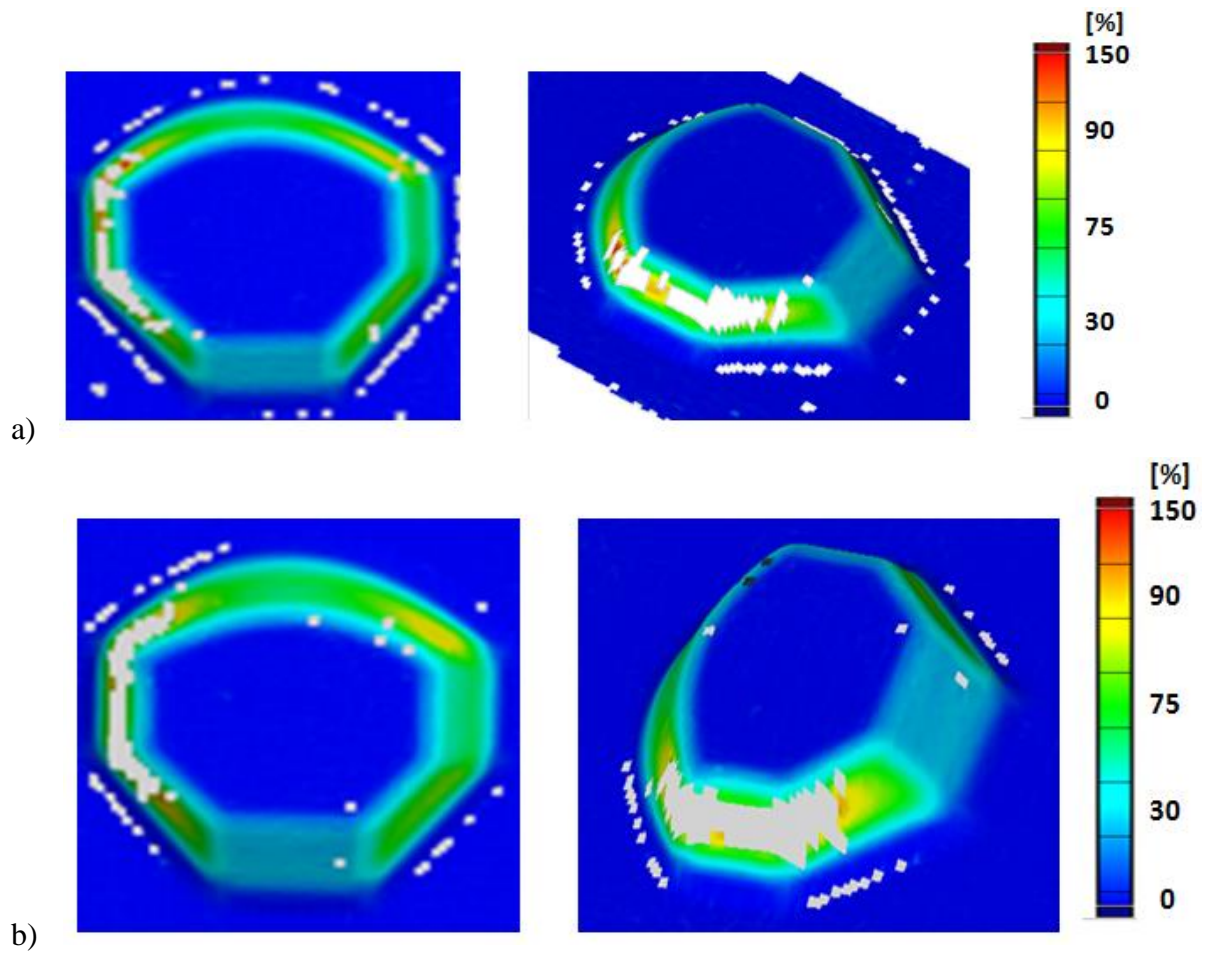


Figure 11-75 Major strain; top and isometric view (a) AA1-7075, (b) AA2-7075.

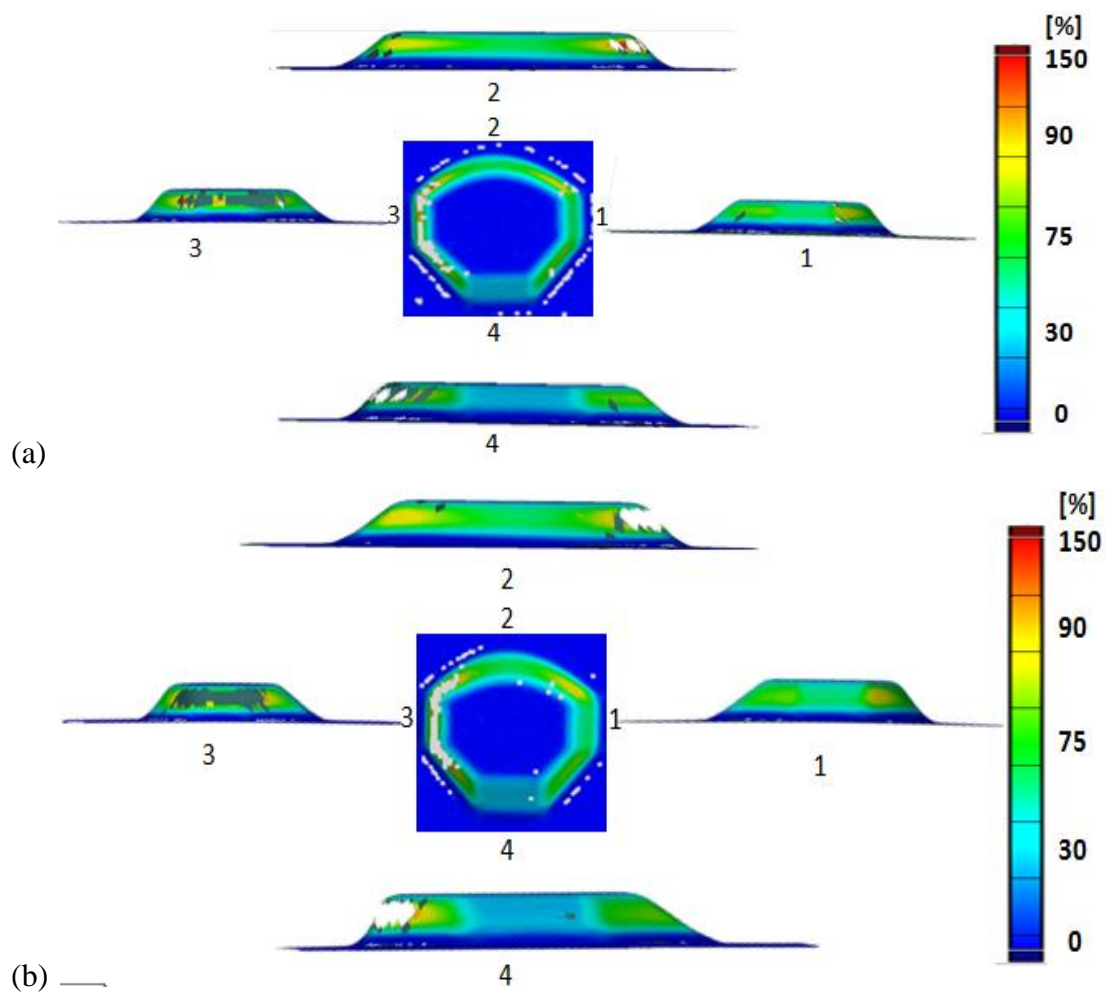
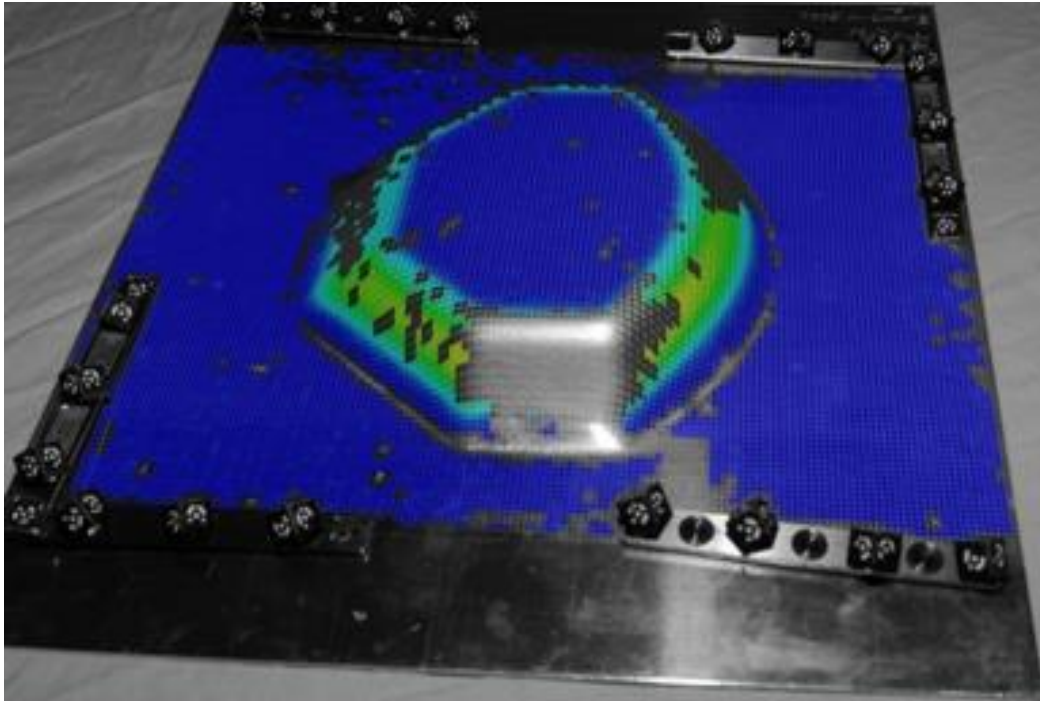
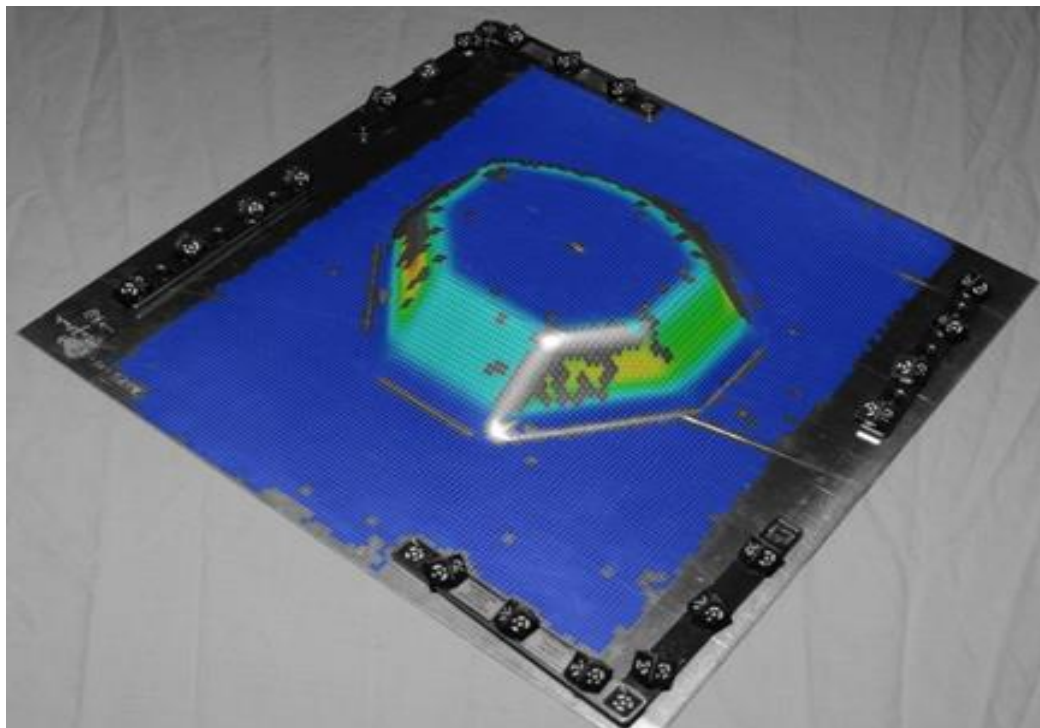


Figure 11-76 Major strain; top and side views (a) AA1-7075, (b) AA2-7075.



a)



b)

Figure 11-77 a) Major strains plotted on formed AA1-7075, (b) Major strains plotted on formed AA2-7075 component.

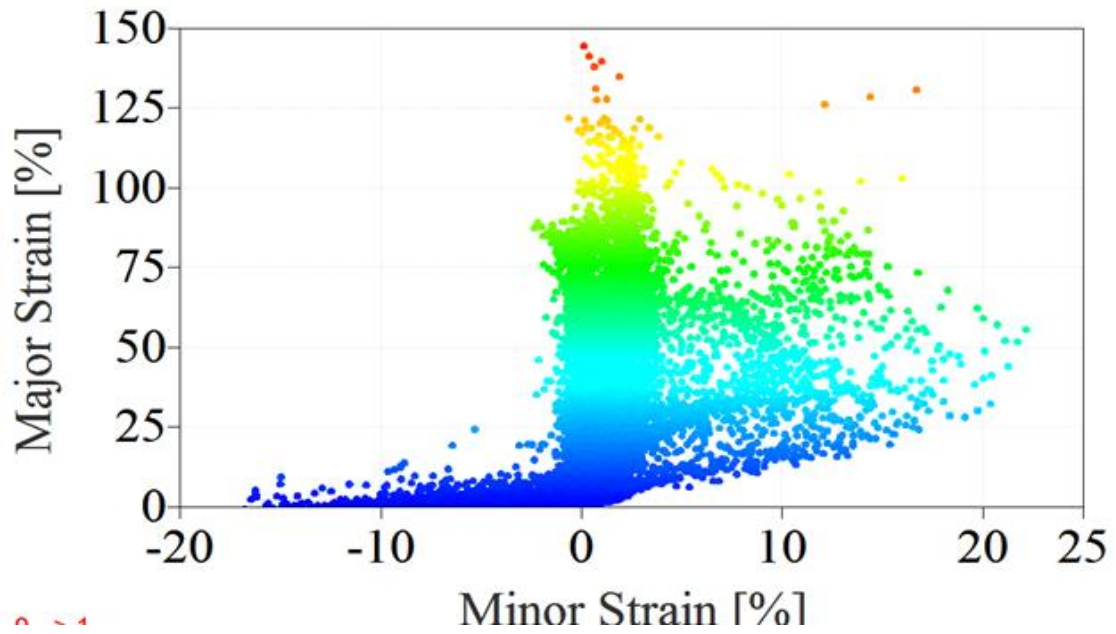


Figure 11-78 Major and minor strain graph AA1-2024.

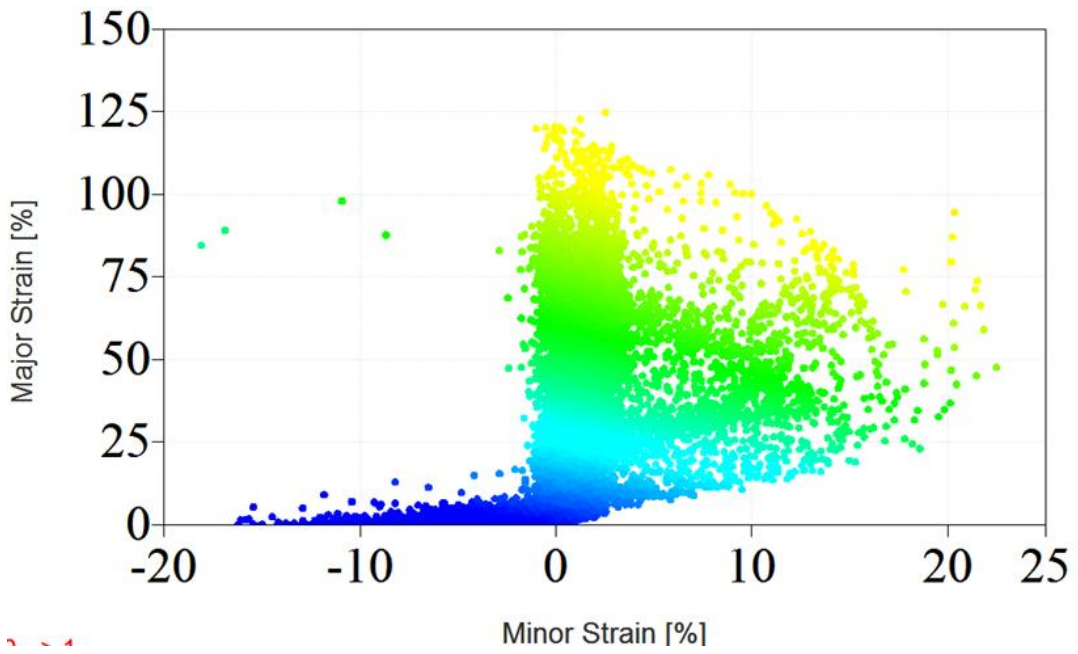
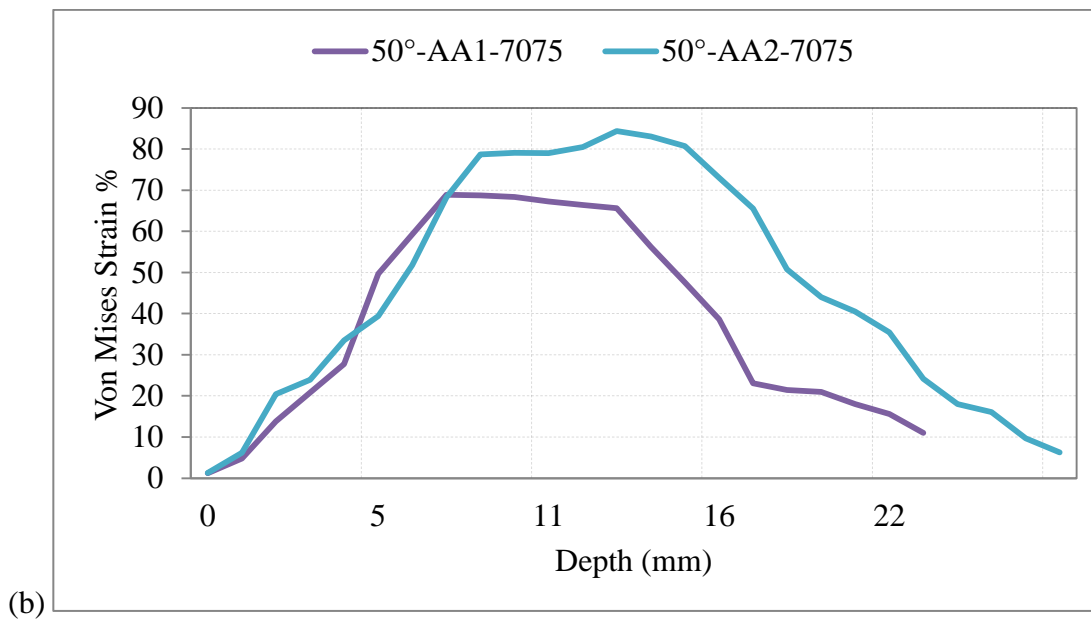
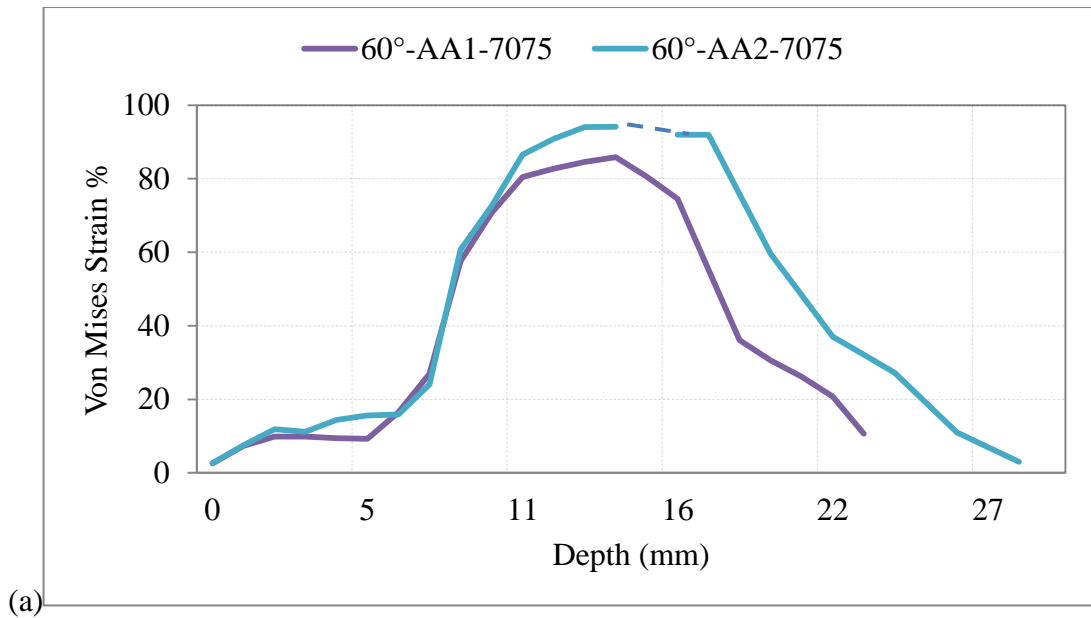
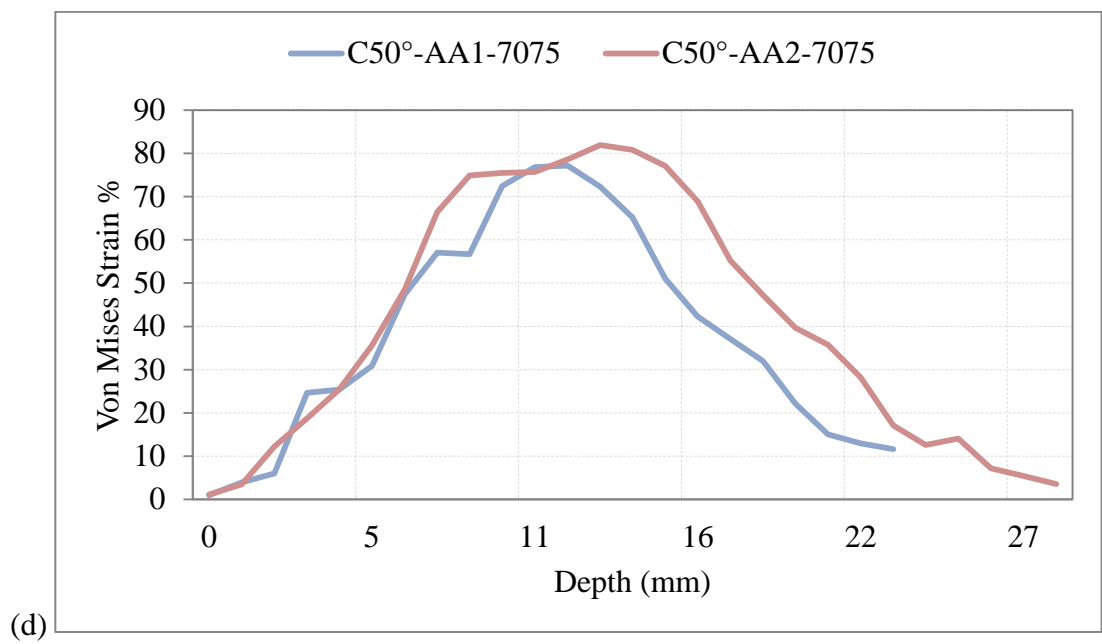
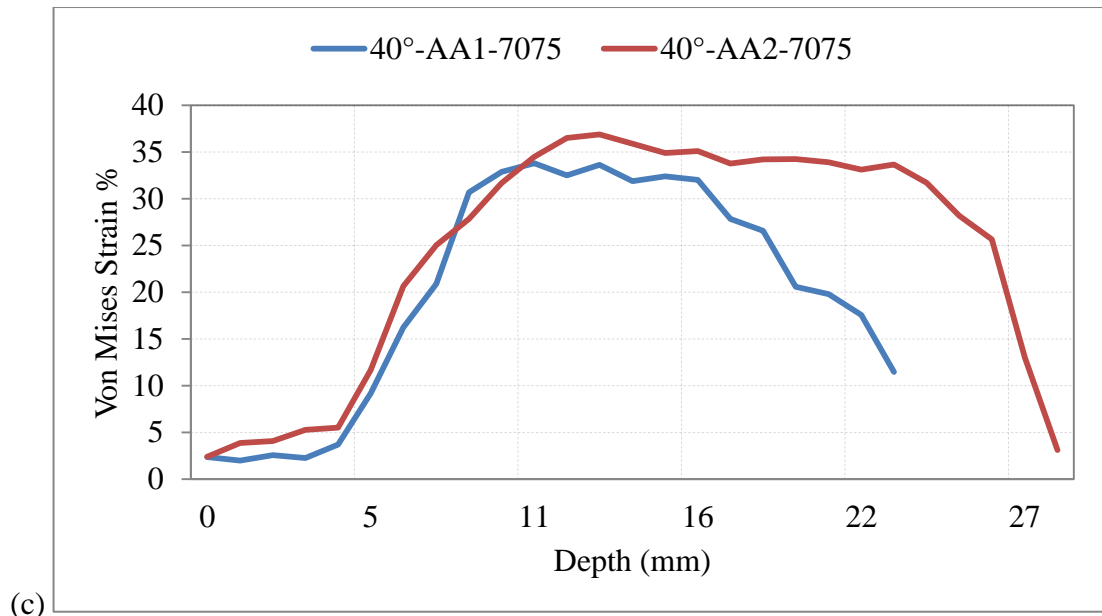


Figure 11-79 Major and minor strain graph AA2-2024.





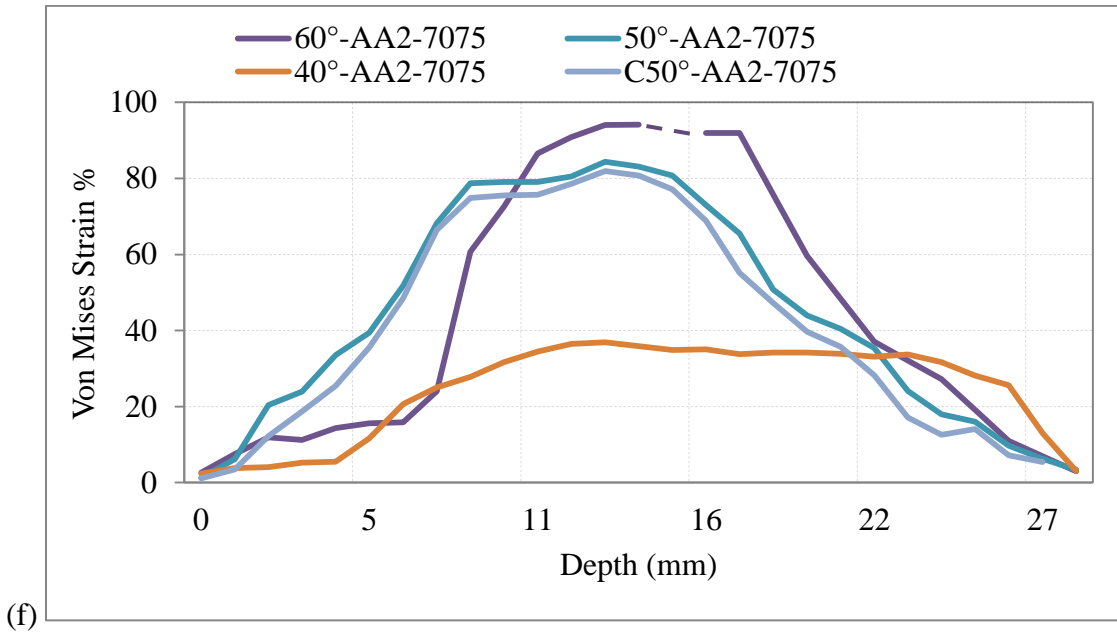
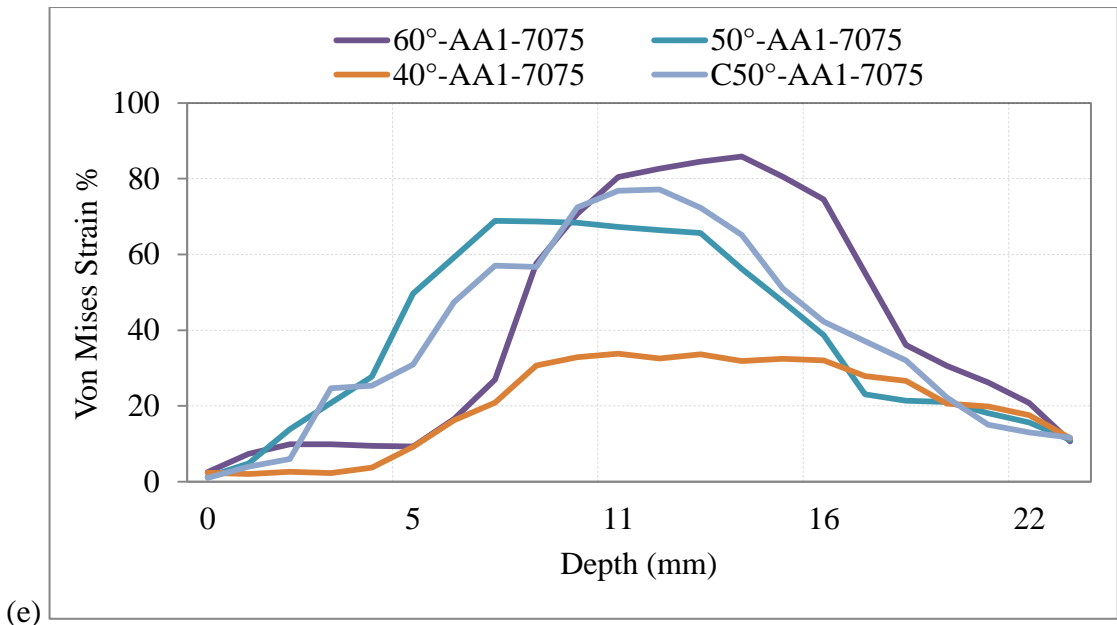


Figure 11-80 Von Mises Strain% vs Depth AA1-7075 & AA2-7075; (a) 60°, (b) 50°, (c) 40°, (d) c50° (e) Wall angle Comparison AA1-7075, (f) Wall angle Comparison AA2-7075.

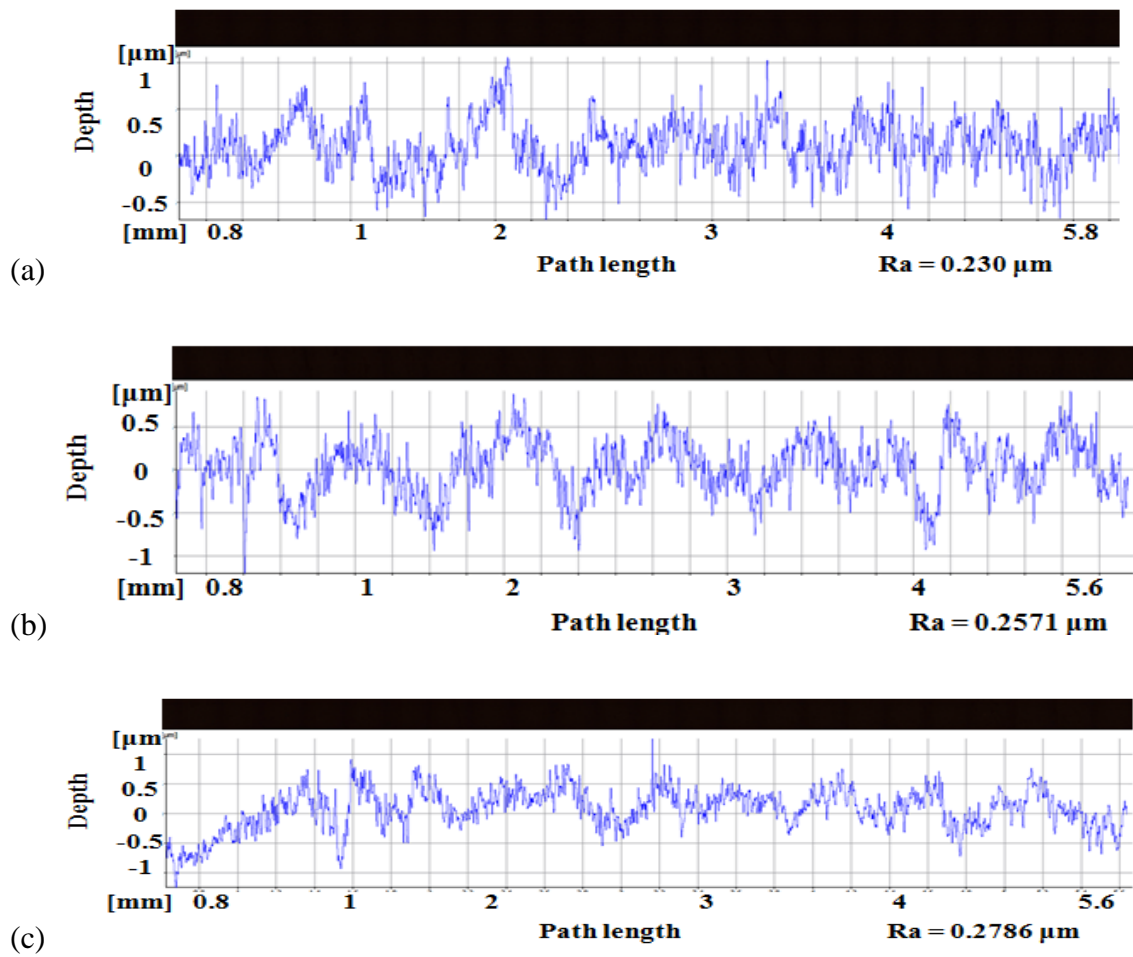


Figure 11-81 Surface roughness profiles of the straight wall feature; (a)  $40^\circ$ , (b)  $50^\circ$ , (c)  $60^\circ$ .



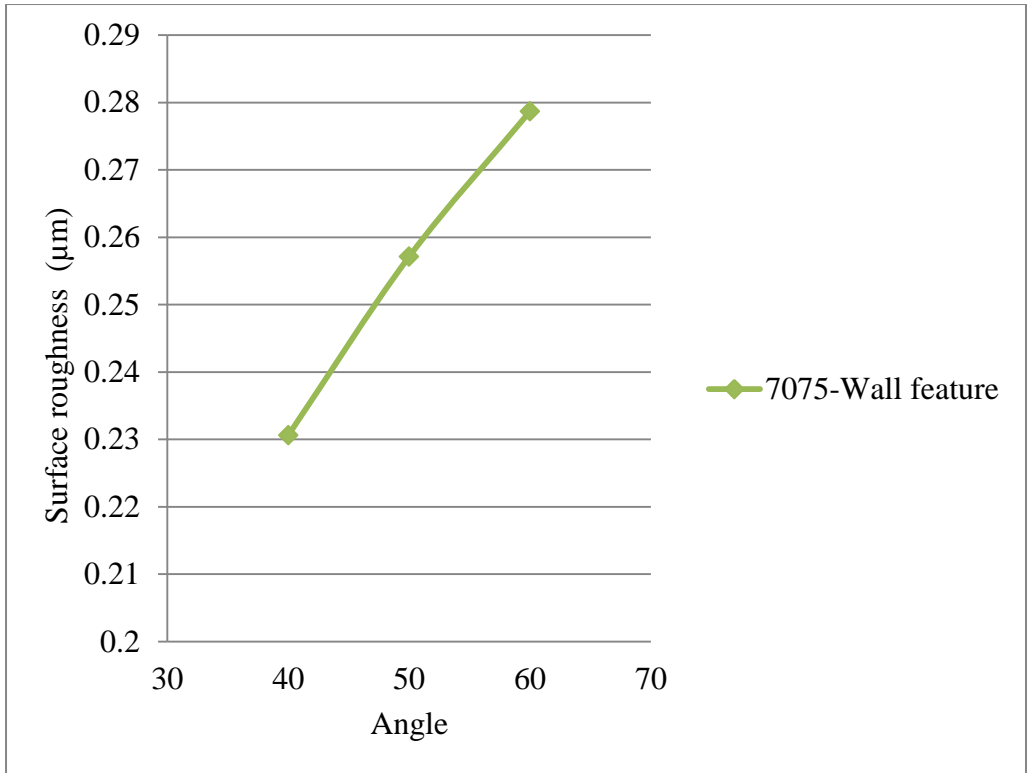


Figure 11-82 Surface roughness- 7075

Table 11-4 Surface roughness- 7075

Surface	Ra (µm)
<b>Wall feature (°)</b>	
40	0.23063
50	0.25713
60	0.27869
<b>Curve feature</b>	
0.30852	

## 12. Appendix E – Hardware, Software & Conclusions

Following are the hardware and software used to perform tests and acquire results. These software and hardware will be mentioned during the text in chapters and are tabulated in Table 12-1 and Table 12-2.

Table 12-1 List of hardware used in the project.

S. No.	Name/Model	Function
1	Zwick/Roell Z150 Material Testing Machine	Screw driven compression, tensile and cyclic loading machine. Used to study the mechanical behavior of metallic materials.
2	Alicona Infinite Focus IFM G4	Used for surface profile form and roughness measurement through digitisation of surface based on focus variation through non-contact optical 3D surface profiling.
3	FEI/Oxford Instruments Quanta 250 FEG SEM	Magnifies up to 1,000,000X , 3nm resolution and is used for structural and chemical analysis of metallographic specimens. Equipped with Scanning Electron Microscope (SEM) and Electron Back-Scatter Diffraction (EBSD). Through SEM microstructure is observed in superior resolution and high magnification. EBSD is used for obtaining crystallographic data of the materials.
4	Olympus GX51 inverted optical microscope	It is used to observe metallographic specimens through optical microscopy at 1000 X magnification.
5	Buehler Vibromet 2 vibratory polisher	It is utilized to acquire high quality exceptional flat surfaces through 7200 cycles per minute horizontal motion on diverse materials for EBSD and SEM applications.
6	Buehler EcoMet 300/AutoMet 300	It is used in automatic or manual modes to prepare high quality polished surfaces motion on diverse materials

	grinder/polisher	for microscopy analysis.
7	Struers Lectro-pol-5 electrolytic polisher	It is an automatic controlled electrolytic etching and polishing machine for metallic components. It has a database with methods for several metals, scanning function to determine parameters, short polishing times, reproducibility of results and built-in safety features.
8	Buehler Abrasimatic 300	It is used to cut large component to extract samples for SEM and EBSD. It has automated and manual cutting.
9	Buehler IsoMet 5000	It is used to cut small component to extract samples for SEM and EBSD. It has automated and manual cutting.
10	GOM ATOS TripleScan III	This is a 3D scanner which uses blue light technology and digitizes geometries to take precise measurements
11	GOM ARAMIS 5M optical 3D deformation system	This system was installed on sheet forming machine. It is a material independent and non-contact measuring system, for dynamically and static loaded specimens. Accurate 3D displacements, surface coordinates and velocities could be acquired through it. It is also used to acquire major and minor strain, thickness reduction and Strain rates.
12	Zwick/Roell BUP 1000 sheet forming machine	This Hydraulically operated testing machine was used to study the formability of sheet metal at room temperature through Nakajima tests.
13	EU Classic Electrolyte Marking Machine	It is used to create high quality electrolytic marks (grids) on metal surfaces through marking process using electrolyte and stencil to perform circular grid analysis.
14	Pillar drill DP-1500G	This is a gear driven drill press which is rigidly designed for heavy drilling.
15	D 300 camera	Used to take images of formed parts with markers to perform circular grid analysis and acquire strain data.

Table 12-2 List of software used in the project.

S. No.	Name	Function
1	Creo and Pro-Mechanica	This 3D software converted conceptual designs into dynamic digital prototypes. Part, assembly, analysis and drawing modules were used.
2	ANSYS	Computer Aided Design software to solve complex structural problems using finite element analysis tools.
3	Solid works	This software creates 3D models.
4	Abaqus	Programs written in C++ or Fortran can be implemented in this is finite element analysis based software.
5	ARGUS	Through this software images of stretched circular grids of the formed components were digitized through image processing. Surface strains and thickness reductions were calculated.
6	ATOS	Through this software 3D scans were digitized into a CAD representation of the actual component and comparison against a nominal CAD model. Thickness and section of profile is also acquired through this software.
7	ARAMIS	This is an optical analysis too that analyses number of images to measure strain, deformation and displacement.
8	Alphacam	This CAD/CAM software is used for generating complicated tool paths for milling and turning machines.
9	Minitab	A statistics based data analysis software used to find trends.

## **13. Appendix F - Work summary**

### **13.1 Summary with respect to aims and objectives**

The aim of this research was to create a process feasibility check model (ISF-FCheck). With the growing importance of ISF coupled with the gap in knowledge, from both the academic and the industrial perspective, it is important to advance understanding of the process and its implementation for different materials and geometries. This need is further compounded by materials and manufacturing issues pertaining to particular industries such as aerospace, automotive and biomedical.

Given this problem, the research was split into different phases. The first phase involved the literature review and the knowledge gap identification. During the second phase, initial scoping experiments were performed on CPTi and the technical problems regarding ISF and data acquisition were understood. The results from phase two are reported in Appendix A. A methodology was proposed in chapter 3. Material testing was done and is described in Appendix B. Design of the equipment and forming a symmetric and asymmetric dome shaped geometries with different tool sizes, which is reported in Appendix C and chapter 4. A Multi-slope geometry with a range of geometric features and manufacturing parameters was studied using SS304L, AA1050H, AA2024 and AA7075. The results from this phase are demonstrated in chapter 5 and Appendix D. Model was validated for a double sided geometry for free form complex shapes and the results were reported in chapter 6.

The research was carried out through experiments using hardware and software discussed in Appendix E. Objective, realist and experimental research paradigm was adopted due to the nature of the research field. To permit generalization studies were carried out for different geometries, materials and manufacturing parameters. The decision to perform these studies was based on the interest of aerospace, automotive and biomedical industry and the research gap.

For each case study, empirical data was collected after forming the sheet metal using hardware and software. As the density of the data was too much, data reduction techniques were applied to plot and cross refer the meaningful data. The data from these formed

components was then presented in the form of graphs, contours, tables and text. The data was reported and analyzed for all the conditions.

From the comparison of these case studies, anomalies and commonalities were identified, providing the knowledge regarding process planning, control and outcomes to acquire objectives of the research. Similar patterns in the outputs of the case studies were discussed and broad insights were generated to help commercialize the ISF process. Following are the the objectives of research

- Through literature review, identify a possible methodology for feasibility assessment.
- Identify and perform experiments to determine the parameter for a feasibility methodology (e.g. different materials, geometries, feedrates, production rate, accuracy, the effect of rolling direction, thickness, surface roughness, strains, microstructure evolution and material properties).
- Analysis of results and detail the feasibility assessment methodology's strengths and limitations.

### **13.2 Chapter wise: Discussion and summary**

During the literature review section (Chapter 2), it was found that there are several advantages of the ISF process for small and medium-sized batches including but not limited to lower cost, usage of conventional CNC machine, accommodate rapid changes. There are certain disadvantages such as low accuracy, low production rate, production equipment and not enough information to implement the process on a commercial level. To cater these disadvantages research has been currently carried out in the areas mentioned above. It is also very important to measure and understand the microstructural evolution due to the ISF process parameters and to understand basic internal mechanics of the process.

Research design, methodology and techniques were discussed in Chapter 3. Based on the literature review and discussion with researchers, a strategy was devised to research high priority areas of the ISF process. Both academic and industrial concerns were targeted while selecting input and output parameters. List of experiments was provided which summarized important parameters and different studies. Limitations of the study were outlined. Hardware and software technology used to perform the experimental tests were tabulated in Appendix E.

Given the problems identified during Appendix A, initial scoping experiments were performed and reported in Chapter 4. These experiments investigated and evaluated mechanical properties together with microstructural evolution of Cp-Ti. It was observed that rolling directions slightly influence the mechanical properties. Thickness was reduced at a localized region of the formed part. For uniform thickness, a better tool path strategy was required. Less springback was observed at higher forming depths, thus it was concluded that better geometries could be attained by deforming the sheet to maximum depth. Elastic recovery controls springback and thickness reduction. Spring back is a linear function with respect to the depth and the strain i.e. greater forming depth will account for greater spring back. The microstructure of Cp-Ti is changed from regular hexagonal to irregular elongated shapes after ISF process is performed. Fracture during ISF process was ductile in nature.

As discussed during literature review, one of the areas researchers are working on is the fixture and tool design for this process discussed in Appendix B. Flexible fixture and rotating tool design for ISF process is a challenge because of highly localized but moving off centered torsional load applied to form the sheet metal. This loading condition can jam the fixture and the tool, thus jeopardize its freedom of movement and stiffness while the part is being formed. Aware of this problem the author created several concepts and evaluated against the design specifications of Incremental Sheet Forming Process. 3D modeling, visualization and finite element analysis and functional prototypes were assessed before manufacturing the flexible fixture with nylon bushes. The results suggested that the Scissors design did not have sufficient lateral (i.e. horizontal) stiffness so consequently a 3 pillars concept with nylon bushes was selected as the final design. Polymer sheet with the industrial heater was used to check the functionality and the large vertical movement of the fixture during ISF process. The rotating tool of different sizes was developed and tested on sheet metal. Following were the findings from this study; tool size selection is highly dependent upon the working area of the sheet and feature size to be manufactured. A larger Tool diameter should be used at the start to give an overall shape of the output geometry and then a finer tool should be used to accommodate finer details and catering local spring-back. Decreasing pitch size result's in better surface roughness. Plane strain condition is dominant regardless of the tool sizes. The surface is smoother for the larger tool compared to the smaller tool for similar operating parameters. Higher local deformation and local stress would be induced in the sheet and the tool for smaller tool size compared to larger one for

similar parameters and thus sheet is more prone to failure. In general formability of the sheet is increased by the tools with bigger diameters. Regardless of the fact that a point load is applied to the sheet at a distance from the center, creating a mixture of bending, tensile and torsional loading both on the sheet and the structure the fixture remained stable, showing no signs of unwanted movement with the Nylon bushes providing sufficient stiffness. Tests were successful and sheets were formed in the shape of the die. After which the fixture and the tool were mounted on a CNC machine and further tests were performed on Aluminum sheet to check rigidity and stiffness of the system under high loading conditions. Spiral tool path was generated with CAM software for tool movement to form the geometry.

Three cases were studied were reported in Chapter 4 for different tool sizes, symmetric and asymmetric geometries. After which results such as thickness reduction, profile changes, major and minor strains and Von Mises strains were acquired from these sheets using circular grid analysis, 3D scanning and other state of the art equipments and techniques. All the parts were formed up to their failing point, despite which significant symmetry and evenness of distribution in the formed parts was achieved. Results such as strain in other regions of the sheet would mean that fixture had moved unevenly while the sheet was being formed. Cheap wooden dies were successfully used to form Aluminum parts. Using polymer or wooden dies would bring down the cost and the time of forming substantially.

After analysis of previous results and literature review, new ideas of geometries were put forward by the author. These geometries were assessed qualitatively and a final geometry was selected, pertaining several wall angles and multiple features. The concept of the shape was sketched and CAD geometry was modeled using software package Creo®. SS 304 L, AA 1050 H, AA 2024 and AA 7075 was used to form this geometry and results were reported in Chapter 5 and Appendix D. Depth of the geometry varied with the material type. An innovative idea of Backsupporting Plate was successfully implemented to increase the accuracy of the components. Results such as thickness reduction, profile changes, major and minor strains and Von Mises strains were acquired from these sheets using circular grid analysis, 3D scanning and other state of the art methods. Influence of these parameters and their interdependence such as wall angle, rolling direction, thickness reduction, surface strain, depth, formability and material properties were discussed. Production rate for the process was successfully increased and higher values of accuracies were achieved.



After checking Multi-slope geometry for several materials and parameters author experimented on double side forming for complicated shapes. A geometry pertaining features on both sides and inspired by the aerospace components was designed. Initial experiments were performed on AA1050H to check this idea and reported in Chapter 6. In contrast to previously studied geometries, this had features on both sides of the sheet metal. Two different strategies were used to form this geometry and their results such as accuracy, thickness, major and minor strains and Von Mises strains were compared. To conclude this discussion, all information was graphically conceptualized in the next section.

Results from all the case studies were analyzed and concluded in chapter 7. The dependency of input parameters to output parameters was discussed and concluded with a table, diagrams and model. These diagrams, table and model can be used as an initial model by the industry to develop new components and help commercialize the ISF process.

### **13.3 Overall conclusions**

- ISF is an emerging sheet metal forming process with great future prospects but needs to be researched more, to be applicable widely in the industry. Thus research aims and objectives, along with experiments were decided based on the knowledge gap through literature review and industrial requirements to commercialize the process.
- Production rate of the process was improved through clamping arrangement and feedrate. Feed rate of the initial experiments was 700mm/min which was increased to 4000mm/min. Due to the lesser force applied in the process; nuts and bolts were replaced with clamps, which reduced lead-time. Time saving through this change was almost equal to the forming time. It was also observed that both these changes had insignificant effect on the final formed part, its resulting properties and features.
- Higher accuracy was successfully achieved on a range of materials such as SS304L, AA7075, AA2024 and AA1050H. Accuracy of the process was increased to less than 1mm through the use of spiral toolpath, toolpath compensation and an innovative backsupporting plate concept. This was done while forming asymmetric shapes with different wall angles and geometric features interacting with each other. Both

increase of the accuracy and the production rate will help commercialization of the process.

- Material properties and sheet thickness play a very important role in the formability of the sheet metal into the required components. Metal sheets having greater thickness and strain hardening coefficient show greater formability.
- Thickness reduction was only observed in the area under the action of the tool. Thus thickness reduction was not uniform either in complete part or through the depth of the formed feature, such as straight wall. It was also observed that in an individual geometric feature thickness was lowest near the middle region and was not strictly following Sin Law as previous research suggested. Saying that, thickness reduction is highly dependent upon wall angle and the depth
- Rolling direction does not have any significant effect on the quality, thickness reduction and surface strains of the formed components.
- Maximum Major and minor strain along with Von Mises strains were at the corner feature of 60° wall. Minor strain is negligible in rest of the component. It's a combination of both major and minor strains due to which the part fractures at the corner feature.
- Surface roughness increases as the wall angle increases. This behavior remains the same for different productions rates, materials and manufacturing parameters.
- During the ISF process, not only wall angle of the formed component is important but also angle between the two features play a vital role. Sheet metal was always cracked at the corner of the 60° wall and curve feature for all the Multi-slope tests due to exceeding strains. Specimens failed along the rolling direction for the dome shaped parts. During asymmetric dome-shaped geometry, component fractured near the support as lesser sheet area is available to get stretched during ISF process. Increase in contact area, availability of the sheet around feature and intelligent toolpath, increases formability of the part.
- Microstructure of the sheet metal is changed from regular structure to the irregular elongated shapes after ISF process is performed. Phase of the material also changes due to the ISF process, so the final specimens will have different material properties at different locations. Fracture during the ISF process was ductile in nature for the tested materials.

- Straight and curve wall features at all angles show behavior analogous to direct loading condition or plane strain condition regardless of the tool or feature size. At the corners, biaxial behavior is observed. Proper planning of geometry can increase accuracy and final quality of the part.
- Inexpensive flexible fixture, rotating tool and wooden or polymer dies can substantially decrease cost of the formed component. This equipment can be used to form a range of materials from polymers to hard metals such as Titanium.
- Tool size selection is highly dependent upon the working area of the sheet and the feature size to be manufactured. A larger Tool diameter should be used at the start to give an overall shape of the output geometry and then a finer tool should be used to accommodate finer details and catering local spring-back. Decreasing pitch size result's in better surface roughness. Plane strain condition is dominant for both tool sizes. Surface is smoother for larger tool compared to smaller tool for similar operating parameters. Higher local deformation and local stress would be induced in the sheet and the tool for smaller tool size, compared to larger one, for similar parameters, thus the sheet is more prone to failure. In general formability of the sheet is increased by tools with bigger diameters.
- Strategy (toolpath, backsupporting plate, tool to diameter ratio, partial or full die) should be selected based upon geometrical feature and the mechanical properties of the specimens.
- The plane strain condition, analogous to tensile tests, prevails in most of the geometric features. The corners however show a biaxial behavior. Limiting value of Strain% can be found through tensile tests or FLC for these conditions. Strain% of location 5, should be lesser than limiting value for a safe useable component.
- Component with features on both sides of the sheet was successfully formed. It was observed that forming the external feature before internal increases the accuracy and reduces sprawling effect. Backsupporting plate should be used to increase accuracy when performing ISF process on both sides of the sheet metal.
- Relationships between different input and output parameters were observed. With the help of this knowledge a conclusive table, qualitative model and Cellular model was introduced. The qualitative model, conclusive table and model can be easily used by the industry to solve ISF problems.

- Objectives of the process such as increasing production rate, accuracy, evaluating formability, microstructural evolution, internal mechanics and dependency of the process parameters upon each other were successfully achieved.
- Cellular model is put forward to graphically conceptualize the forming process. It represents formability not only in terms of the material properties and the geometry (wall angle and depth) but also thickness of the sheet metal.

*The End.*